SERIES IN MATERIALS SCIENCE AND ENGINEERING

CRC Press
Taylor & Francis Group

Flow Batteries

Fundamentals, Technological Advancement and Challenges

Edited by Ram K. Gupta

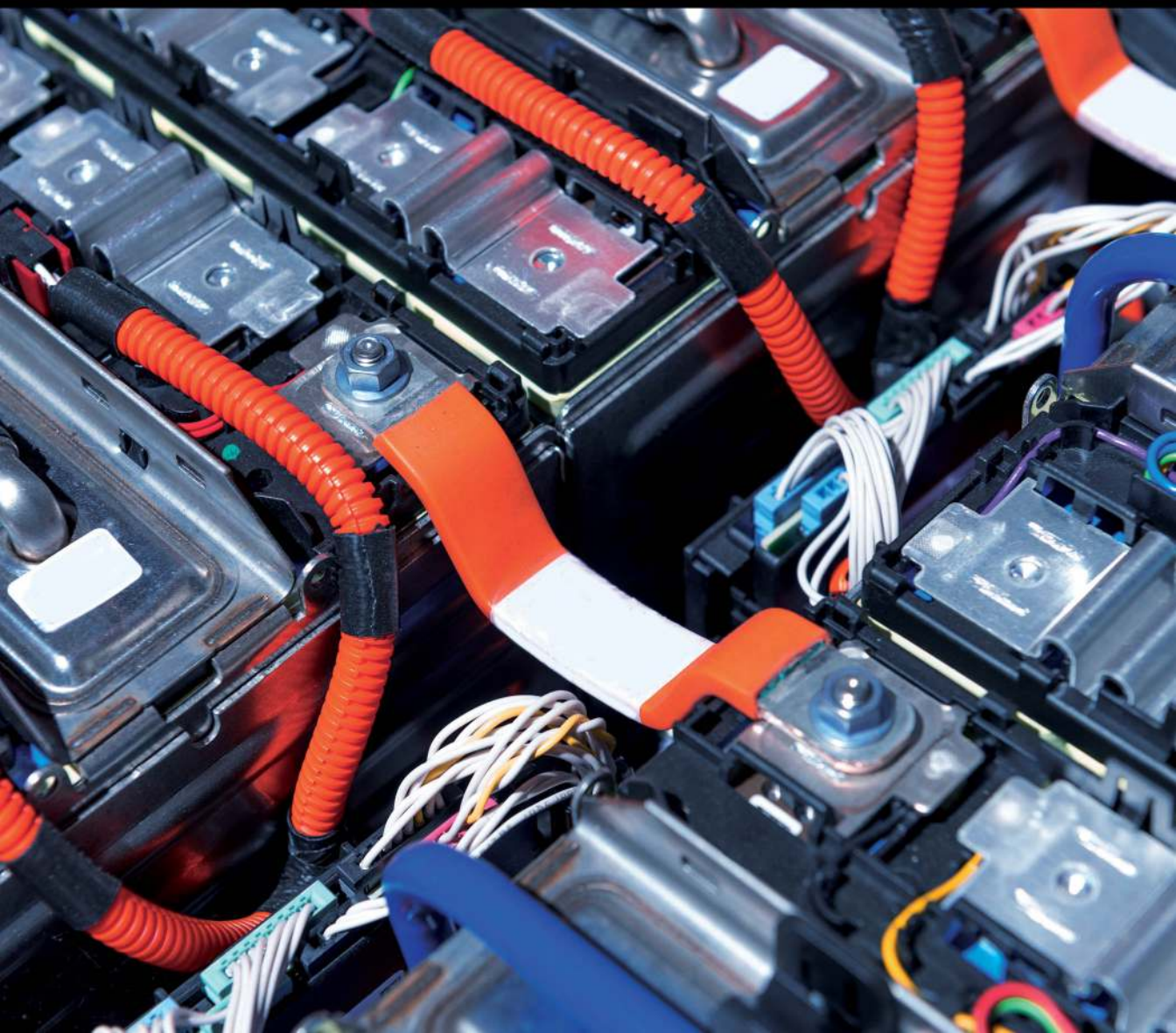

Flow Batteries

Flow Batteries presents a comprehensive examination of this critical energy storage technology at the forefront of renewable energy integration.

Compiling all the major topics in one book, chapters are authored by experts in energy areas, providing state-of-the-art information about flow batteries, their challenges, and applications. Detailed coverage is given to the chemistry and electrochemical characteristics of flow batteries, as well as offering insight into tuning the properties of redox-active materials to improve their electrochemical performances. It provides new directions to scientists, researchers, and students to better understand the principles, technologies, and challenges in flow batteries.

This is a timely resource for students studying materials science and for researchers working in the green energy, materials, and nanotechnology industries.

Ram K. Gupta is a Professor of Chemistry at Pittsburg State University. He is the Associate Vice President for Research Strategy and Advancement at Pittsburg State University. He has been recently named by Stanford University as being among the top 2 percent of research scientists worldwide. Before joining Pittsburg State University, he worked as an Assistant Research Professor at Missouri State University, Springfield, MO, then as a Senior Research Scientist at North Carolina A&T State University, Greensboro, NC. His research spans a range of subjects critical to current and future societal needs including semiconducting materials and devices, biopolymers, flame-retardant polymers, green energy production and storage using nanostructured materials and conducting polymers, electrocatalysts, optoelectronics and photovoltaics devices, organic-inorganic heterojunctions for sensors, nanomagnetism, biocompatible nanofibers for tissue regeneration, scaffold and antibacterial applications, and bio-degradable metallic implants. He has mentored ten Ph.D./Postdoc scholars, 76 MS students, and 58 undergraduate/high school students. He has published over 400 peer-reviewed journal articles (15000+ citations, 67 h-index, 312 i10-index); presented more than 650 national, international, regional presentations; chaired and organized many sessions at national and international meetings; wrote several book chapters (150+); worked as editor for many books (60+) for American Chemical Society, CRC, Springer, Elsevier, etc.; and received several million dollars for research and educational activities from external agencies. He is also serving as editor, associate editor, guest editor, and editorial board member of various journals.

Series in Materials Science and Engineering

The series publishes cutting-edge monographs and foundational textbooks for interdisciplinary materials science and engineering. It is aimed at undergraduate and graduate level students, as well as practicing scientists and engineers. Its purpose is to address the connections between properties, structure, synthesis, processing, characterization, and performance of materials.

Flame Retardant Polymeric Materials, A Handbook
Xin Wang and Yuan Hu

2D Materials for Infrared and Terahertz Detectors
Antoni Rogalski

Fundamentals of Fibre Reinforced Composite Materials
A. R Bunsell. S. Joannes, A. Thionnet

Fundamentals of Low Dimensional Magnets
Edited by Ram K Gupta, Sanjay R Mishra, Tuan Anh Nguyen

Emerging Applications of Low Dimensional Magnets
Edited by Ram K Gupta, Sanjay R Mishra, Tuan Anh Nguyen

Handbook of Silicon Carbide Materials and Devices
Edited by Zhe Chuan Feng

Bioelectronics: Materials, Technologies, and Emerging Applications
Edited by Ram K. Gupta and Anuj Kumar

Advances in 3D Bioprinting
Edited by Roger J. Narayan

Hydrogels: Fundamentals to Advanced Energy Applications
Edited by Ram K. Gupta and Anuj Kumar

Emerging Energy Materials: Applications and Challenges
Edited by Govind Nair, H. Nagabhushana, Nirupama Dhoble and Sanjay J. Dhoble

Handbook of 2D Materials for a Sustainable Future Vol 1
Mangalaraja Ramalinga Viswanathan, Arulraj Arunachalam, Pandiyarajan Thangaraj, and
Edited by Ernesto Chicardi Augusto

Handbook of 2D Materials for a Sustainable Future Vol 2
Edited by Mangalaraja Ramalinga Viswanathan, Arulraj Arunachalam, Arun Thirumurugan and P. Sakthivel

Unravelling the Power of 2D Materials: Revolutionizing Flexible Devices
Edited by Ram K. Gupta

Flow Batteries: Fundamentals, Technological Advancement and Challenges
Edited by Ram K. Gupta

For more information about this series, please visit: https://www.routledge.com/Series-in-Materials-Science-and-Engineering/book-series/TFMATSCIENG

Flow Batteries

Fundamentals, Technological Advancement and Challenges

Edited by
Ram K. Gupta

CRC Press
Taylor & Francis Group
Boca Raton London New York

CRC Press is an imprint of the
Taylor & Francis Group, an **informa** business

Front cover image: Sergii Chernov/Shutterstock

First edition published 2026
by CRC Press
2385 NW Executive Center Drive, Suite 320, Boca Raton FL 33431

and by CRC Press
4 Park Square, Milton Park, Abingdon, Oxon, OX14 4RN

CRC Press is an imprint of Taylor & Francis Group, LLC

ISBN: 978-1-032-81939-6 (hbk)
ISBN: 978-1-032-82812-1 (pbk)
ISBN: 978-1-003-50637-9 (ebk)

DOI: 10.1201/9781003506379

Typeset in Minion
by codeMantra

Contents

Preface

The ever-growing global demand for energy—driven by rapid population growth, industrialization, and the transition toward renewable power—calls for energy storage technologies that are not only high performing but also capable of storing large amounts of energy. While various electrochemical storage systems, such as metal-ion, metal–sulfur, and metal–air batteries, are well suited for portable and lower-scale applications, they fall short when it comes to large-scale energy storage requirements. To achieve reliable integration of renewable energy into the electrical grid and ensure its efficient utilization, there is an urgent need for scalable, safe, and cost-effective storage solutions.

Flow batteries have emerged as one of the most promising candidates to meet this challenge. Their unique design flexibility, potential for long service life, inherent safety characteristics, and suitability for large-scale deployment make them attractive for future energy infrastructure. At the heart of these systems lie high-performance redox-active materials, whose physicochemical properties determine key performance metrics, including cycling stability, solubility, redox potential, energy density, cell voltage, and overall system cost. Advancements in these materials, alongside innovations in battery architecture and engineering, are essential to unlocking the full potential of flow battery technology.

The main objective of this book is to present a comprehensive overview of the fundamentals, recent technological advancements, and existing challenges in the field of flow batteries. It is structured to cover:

- Fundamental principles of redox-active materials and their role in energy storage performance.
- The chemistry, electrochemistry, and engineering aspects of flow battery systems.
- State-of-the-art developments, current limitations, and pathways for innovation.
- Strategies for tuning material properties to enhance electrochemical behavior.
- Perspectives and guidance for researchers, industries, and policymakers engaged in the advancement of flow battery technology.

Each chapter is authored by leading experts from around the world, ensuring both depth and breadth in coverage. This book serves as a valuable resource for students seeking to

understand the principles of flow batteries, for researchers aiming to drive innovation in the field, and for industries exploring scalable solutions to meet the future of sustainable energy storage.

Thank you.

Ram K. Gupta, Ph.D.
Professor, Department of Chemistry
Associate Vice President for Research Strategy and Advancement
Pittsburg State University

Contributors

kalathum Padikkal Abhinav
Department of Physics
School of Advanced Sciences
Vellore Institute of Technology
Vellore, India

Arpana Agrawal
Department of Physics
Prime Minister College of Excellence
Shri Neelkantheshwar Government Post-Graduate College
Khandwa, India

James Friday Amaku
Wastewater Treatment Research Laboratory
Department of Biotechnology and Chemistry
Vaal University of Technology
Vanderbijlpark, South Africa
and
Department of Chemistry
Michael Okpara University of Agriculture
Umudike, Nigeria

Suhrid Sayantha Aniv
Department of Chemistry, Faculty of Science, University of Dhaka, Dhaka 1000, Bangladesh

Noé Arjona
Centro de Investigación y Desarrollo Tecnológico en Electroquímica S.C.
Querétaro, México

Md. Abdul Aziz
Department of Energy Science and Engineering
Daegu Gyeongbuk Institute of Science & Technology (DGIST)
Daegu, The Republic of Korea

Pintu Barman
Department of Physics
Kamrup College
Chamata, India

Barsha Rani Bora
Department of Chemistry
Indian Institute of Technology Guwahati
Kamrup College
Guwahati, India

Denis A. Cabrera-Munguía
Advanced Materials Laboratory
Faculty of Chemical Sciences
Autonomous University of Coahuila
Saltillo, México

Lucía F. Cano-Salazar
Advanced Materials Laboratory
Faculty of Chemical Sciences
Autonomous University of Coahuila
Saltillo, México

Jesús A. Claudio-Rizo
Advanced Materials Laboratory
Faculty of Chemical Sciences
Autonomous University of Coahuila
Saltillo, México

Manoj Kumar Gangwar
Department of Chemistry
University of Allahabad
Prayagraj, India

Hamid Garmestani
Department of Materials Science and Engineering
Georgia Institute of Technology
Atlanta, Georgia

Jesse Greener
Département de Chimie
Université Laval
Québec, Canada

Yinghui Han
College of Resources and Environment
University of Chinese Academy of Sciences
Beijing, China

Xiaotao Hao
School of Physics
Shandong University
Jinan, China

Xinyu Huang
School of Human Settlements and Civil Engineering
Institute of the Building Environment and Sustainability Technology
Xi'an Jiaotong University
Xi'an, China

Md. Mominul Islam
Department of Chemistry, Faculty of Science, University of Dhaka, Dhaka 1000, Bangladesh

Balasubramaniam Jeevanantham
Department of Physics
School of Advanced Sciences
Vellore Institute of Technology
Vellore, India

Nitul Kalita
Department of Chemistry
Indian Institute of Technology Guwahati
Guwahati, India

Dennis Y. C. Leung
Department of Mechanical Engineering
The University of Hong Kong
Hong Kong, China

Michael K. H. Leung
School of Energy and Environment
City University of Hong Kong
Hong Kong, China

Xiang Li
College of New Energy and Electrical Engineering
Hubei University
Wuhan, China

Yuanji Li
School of Human Settlements and Civil Engineering
Institute of the Building Environment and Sustainability Technology
Xi'an Jiaotong University
Xi'an, China

Steven Y. Liang
George W. Woodruff School of Mechanical Engineering
Georgia Institute of Technology
Atlanta, Georgia

Jianwen Liu
College of New Energy and Electrical Engineering
Hubei University
Wuhan, China

Sunil Kumar Baburao Mane
Department of Chemistry
Khaja Bandanawaz University
Kalaburagi, India

Rafael Martínez-Palou
Research Department
Mexican Petroleum Institute
Mexico City, Mexico

Juan J. Mendoza
Advanced Materials Laboratory
Faculty of Chemical Sciences
Autonomous University of Coahuila
Saltillo, México

Runwei Mo
School of Mechanical and Power Engineering
East China University of Science and Technology
Shanghai, China

Mostafa Moslempoor
Department of Chemistry
University of Isfahan
Isfahan, Iran

Fanyana M. Mtunzi
Wastewater Treatment Research Laboratory
Department of Biotechnology and Chemistry
Vaal University of Technology
Vanderbijlpark, South Africa

Navid Nasajpour-Esfahani
Department of Materials Science and Engineering
Georgia Institute of Technology
Atlanta, Georgia

An-Giang Nguyen
College of Engineering and Computer Science
Center for Environmental Intelligence
Vin University
Hanoi, Vietnam

Yang Qu
College of New Energy and Electrical Engineering
Hubei University
Wuhan, China

K. Radhakrishnan
Department of Chemistry
Centre for Material Chemistry
Karpagam Academy of Higher Education
Coimbatore, India

Mohammad Reza Rahimpour
Department of Chemical Engineering
Shiraz University
Shiraz, Iran

Marissa Bailey Reichelscheimer
Department of Materials Science and Engineering
Georgia Institute of Technology
Atlanta, Georgia

Sreenivasan Rijith
Post Graduate and Research Department of Chemistry
Sree Narayana College (Affiliated to University of Kerala)
Thiruvananthapuram, India

Fernando F. Rivera
Centro de Investigación y Desarrollo Tecnológico en Electroquímica S.C.
Querétaro, México

Naghma Shaishta
Department of Chemistry
Khaja Bandanawaz University
Kalaburagi, India

Sangaraju Shanmugam
Department of Energy Science and Engineering
Daegu Gyeongbuk Institute of Science & Technology (DGIST)
Daegu, The Republic of Korea

Esmaeil Sheibani
Department of Chemistry
University of Isfahan
Isfahan, Iran

Mummoorthi Kanagarajan Shobana
Department of Physics
School of Advanced Sciences
Vellore Institute of Technology
Vellore, India

Jyoti Singh
Department of Chemistry
University of Allahabad
Prayagraj, India

Vijayakumari Sasidharan Nair Sumi
Department of Chemistry
Government College
Thiruvananthapuram, India

Athira B. Suresh
Post Graduate and Research Department of Chemistry
Sree Narayana College (Affiliated to University of Kerala)
Thiruvananthapuram, India

Rajadesingu Suriyaprakash
Centre for Research in Environment Sustainability Advocacy and Climate Change (REACH)
SRM Institute of Science and Technology
Kattankulathur, India

Heriberto Díaz Velázquez
Research Department
Mexican Petroleum Institute
Mexico City, Mexico

Rakesh Verma
Department of Chemistry
University of Allahabad
Prayagraj, India

Mohanraj Vinothkannan
Department of Energy Science and Engineering
Daegu Gyeongbuk Institute of Science & Technology (DGIST)
Daegu, The Republic of Korea
and
Centre for Advanced Low Carbon Propulsion Systems (C-ALPS)
Centre for E-Mobility and Clean Growth
Coventry University
Coventry, United Kingdom

Jiarui Wang
Department of Mathematics and Physics
North China Electric Power University
Beijing, China
and
College of Resources and Environment
University of Chinese Academy of Sciences
Beijing, China

Rui Wang
School of Mechanical and Power Engineering
East China University of Science and Technology
Shanghai, China

Wuyang Wang
College of New Energy and Electrical Engineering
Hubei University
Wuhan, China

Yifei Wang
School of Mechanical Engineering and Automation
Harbin Institute of Technology
Shenzhen, China

Ruilin Wu
School of Mechanical and Power Engineering
East China University of Science and Technology
Shanghai, China

Bo Xu
MIIT Key Laboratory of Advanced Display Materials and Devices
School of Materials Science and Engineering
Nanjing University of Science and Technology
Nanjing, China

Yanmei Xu
Department of Mathematics and Physics
North China Electric Power University
Baoding, China

Xiaohu Yang
School of Human Settlements and Civil Engineering
Institute of the Building Environment and Sustainability Technology
Xi'an Jiaotong University
Xi'an, China

Mohammad Zarei-Jelyani
Department of Chemical Engineering
Department of Energy Storage
Institute of Mechanics
Shiraz University
Shiraz, Iran

Mingming Zhang
School of Mechanical Engineering and Automation
Harbin Institute of Technology
Shenzhen, China

CHAPTER 1

Introduction

Naghma Shaishta and Sunil Kumar Baburao Mane

1.1 INTRODUCTION

Energy is probably the most important human necessity for social and economic growth. Today's energy challenges must be addressed because of the depletion of fossil fuels and environmental concerns. The use of renewable energy sources, such as wind and solar power, is expanding as the supply of coal and petroleum becomes increasingly scarce. Rising carbon emissions are the primary driver of global warming and temperature rise, largely resulting from population growth, technological development, and job creation [1]. The fight against resource shortages and global warming is being led by renewable energy sources, notably wind and solar power. They are inaccurate, though, because they rely on the conditions outside. However, solar and wind energy are inherently renewable energy supplies that produce power continuously and arbitrarily. Correctly integrating electricity generated from environmentally friendly sources into the existing power infrastructure is challenging [2].

Distributed generation and renewable energy sources (RESs) are integrated into the grid through energy conservation. Although RES lessens dependency on fossil fuels, supply quality and reliability may be jeopardized due to their intermittent behavior. Storage units help with this by reducing oscillations and providing backup power, increasing customers' energy security [3]. In addition to the intermittent nature of RESs, storage is crucial for maintaining voltage stability and ensuring continuous electricity production. As a result, numerous innovations have been developed, particularly some of the most recent ones, including superconducting magnetic energy, redox flow batteries (RFBs), lithium-ion batteries, and sodium-sulfur batteries [4].

Because there is an increasing demand for intermittent power, battery backup is now essential for the contemporary grid. In addition to serving as generators of electricity, these mechanisms also level out electrical outages and enhance the reliability of the grid generally. To facilitate this shift toward better and more effective energy use, energy storage is essential.

DOI: 10.1201/9781003506379-1

Several types of batteries comprise the electrochemical storage system (ECSS), which stores electrical energy in the form of chemical energy. Rechargeable batteries are a useful tool for energy storage. A significant energy density, ecologically conscious security, and an abundance of resources make reusable aqueous aluminum ion electrolysis an excellent substitute energy storage method. Battery storage units are a viable alternative due to their rapid reaction time, reliable power supply, and flexible position. Determining the ideal battery size that negotiates the benefits (better grid efficiency) with the additional expense is a crucial task [5]. A battery energy storage system (BESS) integrates batteries with facilities and a monitoring platform. Batteries, which are always changing, use layered cells hooked up to the right voltage and current to transform chemical energy into electricity. The generation of electricity and energy storage ability are usually linked in BESS designs. Performance, longevity, operating temperature, and output depth are important variables.

As a result of advancements in battery engineering, deep-cycle batteries like those found in electric vehicles are now able to provide energy capacities of 17–40 MWh and efficiency levels of 70%–80% in power systems [6]. BESS provides flexible deployment, prompt, dependable power, and ecological advantages. The various opportunities provided by various bakery chemistries and cell layouts have sparked current interest in batteries, providing a feasible variety of energy and power densities. The RFBs are those that use two chemical ingredients dissolved in liquids that are pushed across the system on opposite sides of a barrier to create chemical power. Liquids travel in their appropriate areas, and ion transfer takes place across the membrane inside the cell, supported by current flowing through an external circuit. There have been demonstrations of both inorganic and organic FBs, and there are three types of FB designs: membranes, semi-flow, and full flow [7]. Power is retained in the electrolyte of FBs, whereas it is retained in the electrode material of conventional batteries. This is the primary distinction between flow and regular batteries. The FB can be employed as a rechargeable, in which case an electric power source fuels the regrowth of the reducer and oxidant, or as a fuel cell, as well as a charged posolyte.

Boosting the amount of electrolytes kept in the containers of a basic FB is an easy way to boost its energy storage capability. The capacity of the FB system is determined by the electrical connection of the electrochemical cells, which can be made in sequence. One key component of FB systems is the separation of the energy level from the power level. In the electrochemical cell, the electrical and chemical energy that has been accumulated is converted. This is made up of two half-cells divided by an ion-exchange membrane or porous material. In addition to allowing ionic conduction, the barrier keeps the half-cells created electroactive substances from being lost as much, maintaining an elevated Coulombic performance. The half-cell electrodes are the site of the redox reactions that occur throughout charge and discharge. In their most basic form, these electrochemical reactions do not change the electrode materials, which are typically carbon felt.

The distinction between the responses at the negative and positive electrodes is the cell voltage. When a half-cell is being charged, electrons that are liberated at the positive electrode due to the oxidation of its electroactive components are driven to the negative electrode, wherein the reduction of its electroactive component occurs. Upon release, the procedures are reversed. Redox pairs, or chemical compounds capable of reversible

reduction and oxidation, are electroactive substances. Hence, in this chapter, we discuss the history, types, classification, application, challenges, and future perspectives related to RFBs.

1.2 HISTORY OF FBS

RFBs, which are more like rechargeable fuel cells than batteries, have been industrialized since the 1970s. Here are a few significant moments in the development of RFBs: Originally, FBs were made of zinc and bromine ($Zn–Br_2$) [8]. On September 29, 1879, John Doyle filed patent US 224404. In the 1970s, $Zn–Br_2$ batteries, which have a comparatively high specific energy, were tested in electric vehicles. Ti–Fe and Cr–Fe dissolved transition metal ions were the basis for the initial FB, which was shown by Estonian chemist Walther Kangro in Germany during the 1950s [9]. Following preliminary trials utilizing Ti–Fe RFBs, organizations in Japan and other locations, along with NASA, decided to advance Cr–Fe chemistry. The influence of time-dependent content throughout cycling was lessened by the inclusion of blended solutions, which included both chromium and iron components in the posolyte and negolyte.

In 1973, NASA developed the first iron-chromium RFB to be used as a prospective lunar base reserve of energy system. Maria Skyllas-Kazacos of University of New South Wales (UNSW), Sydney, receives a trademark for her vanadium RFB (VRFB) technology (G1 VB). Using dissolved vanadium in a sulfuric acid solution, she demonstrated the first successful All-VRFBs. [10]. Her concept utilized sulfuric acid electrolytes, and in the later part of the 1980s, UNSW licensed patents to companies in Canada, Thailand, and Japan and demonstrated the chemical characteristics of the VRFB. These businesses made varying degrees of progress in their attempts to market the innovation. Later, organic RFBs emerged as a new candidate for storage energy in 2009 [11]. In 2022, Dalin, China, began operating a 400 MWh, 100 MW VFB, which was the largest of its kind at the time [12]. Scientists from all over the globe have been keen on studying RFBs over the past 16 years. They are seen as a strong contender to replace lithium-ion technology.

1.3 DESIGN

The RFB circulates redox-active fluids via an electrochemical cell to produce power, starting in enormous reservoirs. Because of their unique construction, the electrolytes may be electrochemically reduced, which involves accepting electrons, or oxidized, which involves providing electrons. The cathode (catholyte or posolyte) and anode (anolyte or negolyte) are stored in separate tanks of the FB. In the representation of a standard single-cell FB, the anolyte (white) is kept in the tank on the right, and the catholyte (gray) is kept in the tank on the opposite side (Figure 1.1). The electrochemical cell located in the middle of the figure has a helical stream where these electrolytes are pumped. Usually constructed of carbon, the circulation field acts as an amplifier of current, while the electrolytes are reduced and oxidized. Porous carbon electrodes are located next to the circulation domains, optimizing the point that communicates with the liquid electrolyte. There is a spacer located among the porous carbon electrodes. An ion-selective membrane, such as Nafion, usually acts as a barrier [13]. These membranes prohibit the physical mixing of the anolyte and catholyte

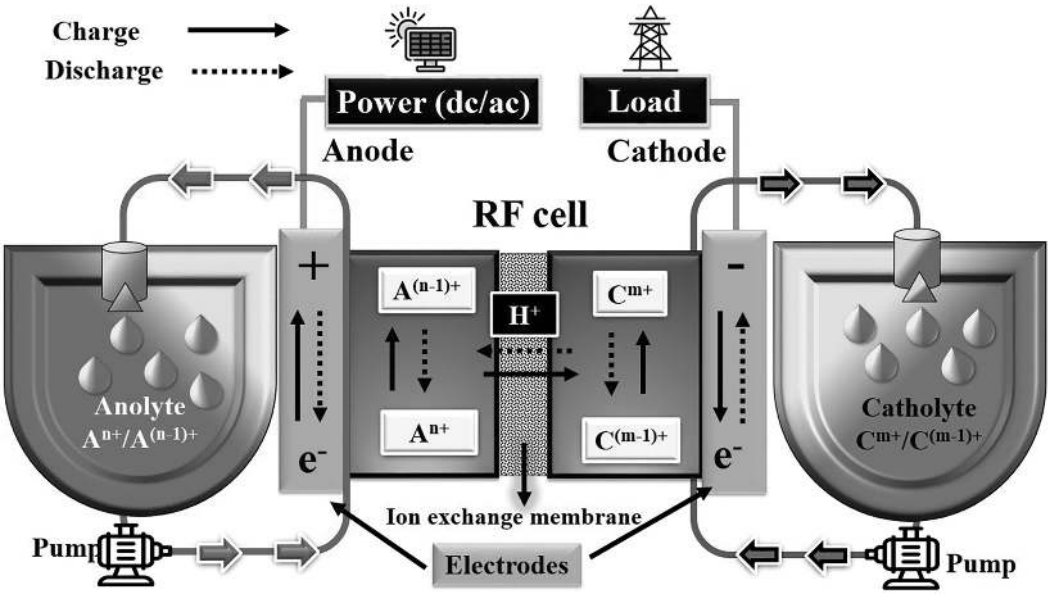

FIGURE 1.1 Representation of electrochemical cells in a single-cell RFB.

as well as the electronic cutting of the opposing carbon electrodes, allowing the passage of inert ions required to charge-balance the electrochemical responses.

1.4 COMPONENTS OF RFBs

The overall RFB consists of three major parts, namely electrolyte, cell tank, and balance of plant (BOP), respectively.

1.4.1 Electrolyte

The charge is carried by the electrolyte, which is stored in a separate tank and requires additional systems to transport it and regulate temperature. The VRFB uses pricey vanadium electrolytes. About 120,000 MT of vanadium were supplied by miners worldwide in 2021; 92% of this was used to produce steel, with 2% going to the VRFB market. The cost of the vanadium electrolyte, which makes up between 30% and 50% of a VRFB's unit cost, is determined by the size of the system as a whole and the amount of time that must be stored. There is an urgent need now for the creation of massive storage facilities of variable green power to satisfy rising energy consumption. To anticipate electrolyte obstruction, Kuperman et al. created an analytical framework for such emulsion electrolytes that have a persistent aqueous-based component and a scattered reactant-rich phase [14]. They demonstrate that the development of a deposited layer along the passageway is a crucial process influencing electrolyte conductivity, highlighting the significance of non-aqueous phase deposition (Figure 1.2a). In both rapid and sustained processes, testing of $Zn–Br_2$ SFB exhibits outstanding concordance with theoretical findings, enabling the extraction of difficult-to-measure characteristics such as the in-situ size of scattered phase droplets.

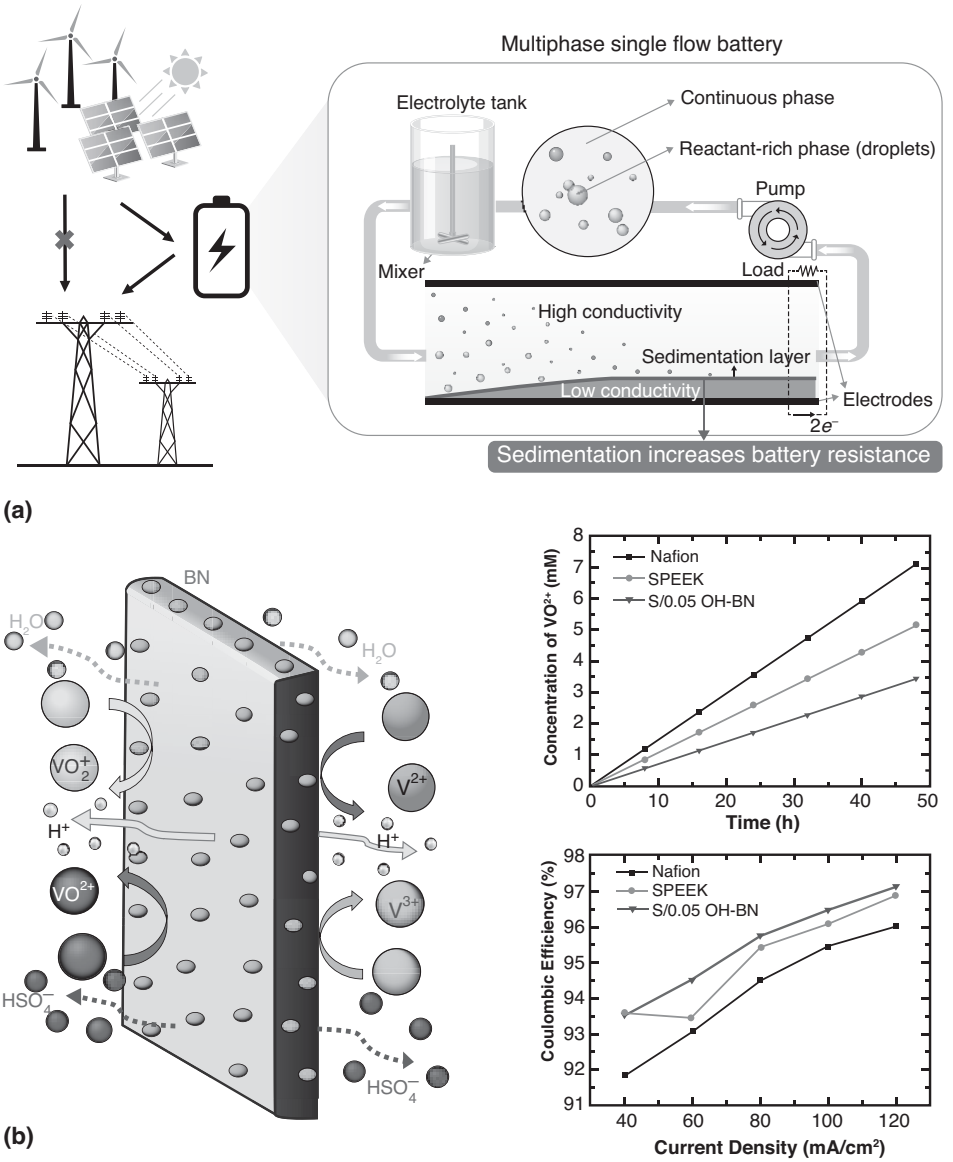

FIGURE 1.2 (a) Representation of effect of flow on electrolyte resistance in SFBs. (Adapted with permission from [14]. Copyright 2024, Elsevier Ltd.) (b) Graphical abstract showing thermochemical and mechanically stable IEM with enhanced specificity for VRFBs. (Adapted with permission from [15]. Copyright 2024, Elsevier Ltd.)

1.4.2 Cell Stack

The cell stack, which consists of multiple essential parts, is also accountable for a sizable amount of the VRFBs' unit cost. The membrane, bipolar plates, electrodes, gaskets, and sealants are all included. The membrane and bipolar plates are the two parts of a VRFB cell stack that are maybe the costliest.

1.4.3 Membrane

The function of membranes is to facilitate the flow of counter ions (such as H^+) while preventing the two electrolytes in an RFB from interacting and meeting one another. The compromise between ionic conductivity and species selectivity is common in membranes. Membranes used in commercial applications range in thickness from 50 to 200 μm. The optimal membrane for an RFB should have strong ionic conductivity and transfer capacity, minimal active species penetration to avoid self-discharge, and chemical resistance against aggressive species. Catalytic ion-exchange membranes (IEMs) are the membranes that are most frequently used in RFBs. IEMs that are cationic might be fluorinated or non-fluorinated.

1.4.4 Ion-Conducting Materials (ICMs)

In FBs, ion-conductive membranes are utilized to transmit charge-carrier ions and divide the redox couples in electrolytes concurrently. Its conductivity and selectivity severely restrict how well RFBs work. A thorough grasp of the connection between membrane structure and ion transport behavior is necessary for future enhancements to ion-conductive membranes (ICM) efficiency. Now, the most widely utilized method for studying ion-conductive membranes is micrology-based, such as scanning electron microscopy (SEM), transmission electron microscopy (TEM), atomic force microscopy (AFM), etc. Over the past couple of decades, these commonly used approaches have aided investigators in depicting the microstructure of ICMs.

The SPEEK (Sulfonated Poly Ether Ether Ketone) membrane supplemented with hydroxylated boron nitride (HBN) is being studied by Myures et al., as a possible proton exchange membrane for VRFBs as a substitute for the costly Nafion membrane [15]. Hydrogen conductance, vanadium permeability, and mechanical, chemical, and thermal durability are the attributes that define SPEEK-based hybrid membranes. The findings demonstrate how the HBN boosts the physicochemical characteristics of SPEEK and increases the endurance and specificity of ions ($52.629 * 10^3$ $S.cm^{-3}.min$). The creation of hydrogen bonds between the hydroxyl moiety of BN and the sulfonic acid group in SPEEK is responsible for the enhanced characteristics (Figure 1.2b).

In the VRFB single-cell efficiency research, the hybrid membrane SPEEK strengthened with 0.05 weight percent of HBN shows a better Coulombic performance of 93.6% (91.8% for Nafion) and a greater self-discharge time of 14.21 hours (11.36 hours for Nafion). An investigation of the cyclic behavior of a hybrid barrier in a VRFB confirms the fundamental, thermal, and chemical resistance of the membrane by demonstrating stable properties across 50 cycles.

1.5 THE EFFECTIVENESS OF FB MEMBRANE

The features of the membrane have an impact on the battery's efficiency. A membrane's exceptionally high selectivity is necessary for the preservation of capacity and Coulombic efficiency (CE), as it must be able to withstand the reactive compounds present in each compartment [16]. An excellent conductivity of the membrane is therefore necessary since, in

the interim, a small reluctance membrane can lessen the ohmic polarization portion of the battery's inner reluctance. The following formulas can be used to assess battery efficiency.

$$\mathrm{CE} = \frac{\text{Discharge Capacity}}{\text{Charge Capacity}} \times 100\%$$

$$\mathrm{EE} = \frac{\text{Discharge Energy}}{\text{Charge Energy}} \times 100\%$$

$$\mathrm{VE} = \frac{\text{Average Discharge Voltage}}{\text{Average Charge Voltage}} \times 100 = \frac{\mathrm{EE}}{\mathrm{CE}} \times 100\%$$

where CE, EE, and VE are Columbic efficiency, energy efficiency, and voltage efficiency, respectively.

According to this formula, a highly selective membrane can raise the CE while reducing reactive material cross-over and capacity degradation. Conversely, a membrane possessing significant conductivity with a minimal area barrier can reduce ohmic polarization, raise average discharge voltage, and lower average charge voltage, ultimately leading to a boost in voltage equivalent to VE. The combination of high VE and high CE can result in an elevated EE, the ultimate metric for assessing battery performance. Consequently, excellent membrane conductivity and specificity are required to attain high battery effectiveness.

Designing the membrane architecture of an ICM can result in good conductivity and specificity. The width, polymer amount, and phase-separation conditions within the standard non-solvent-induced phase separation (NIPS)-made porous membrane can all be changed to modify the membrane shape. Since the ion flow channel is extended in thicker membranes, there is greater susceptibility to reactive chemicals due to a higher area resistance [17].

A membrane with excellent conductivity and choice is anticipated by concentrating selectivity into an extremely thin layer and reducing the role of the remaining membrane components to the barrier. This concept served as the basis for the construction of thin-film composite membranes and two-step phase division, which have been shown to disrupt the compromise impact among ion specificity and conductance of a membrane [18]. To create superior ICMs, nanoporous substances are added to ICMs through the underlying molecular structure engineering of the porous membrane.

1.6 TRADITIONAL OR TYPES OF FBS

The FB is a device that produces electricity from the chemical energy held in the active material. The active ingredients in this device are either added to the system while functioning or kept in the electrolyte. Rather than residing in a cell, at least a single reactant travels through the system in FBs, an example of an electrochemical energy storage device. Their rechargeability is based on the dissolution of two chemical parts in liquids. Energy is retained as the electrode substance in traditional batteries but as the electrolyte in FBs. FBs come in three varieties, namely redox, hybrid, and membraneless. The typical arrangements of VRFB, Zn–Br FB, and Fe–CrFB are presented in Figure 1.3.

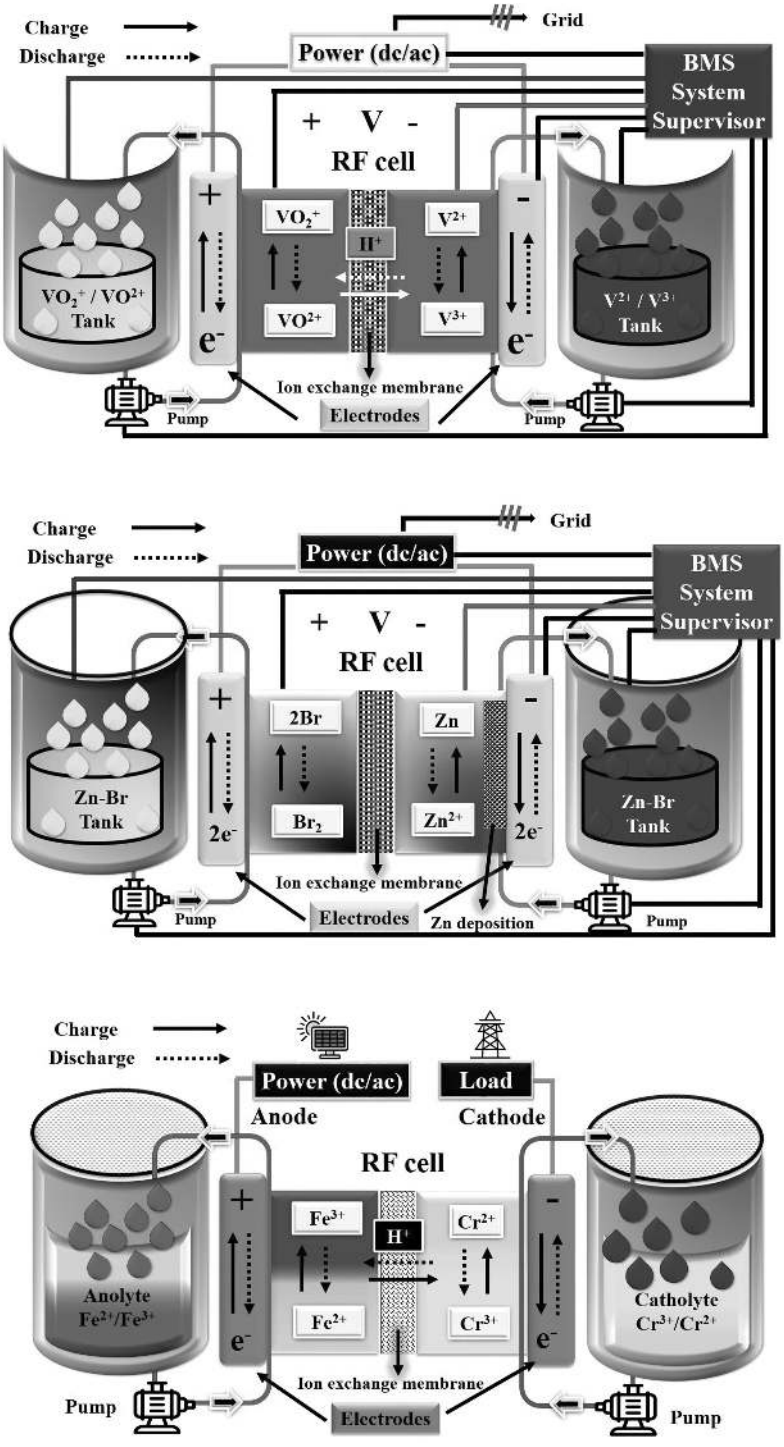

FIGURE 1.3 Typical arrangement of VRFB, Zn–Br FB, and Fe–Cr FB.

1.6.1 Redox Flow Batteries (RFBs)

RFBs are secondary cells that may be recharged, and redox-active species in fluid (liquid or gas) media are used by the redox cell. They resemble fuel cells in addition to traditional batteries since they use heterogeneous electron transfer as opposed to solid-state diffusion. A liquid phase reduction–oxidation reaction is used by RFBs when a liquid electrolyte passes between the electrodes. It is possible to recharge the spent electrolyte by pushing it again through the electrode to the tanks. The primary distinction between fuel cells and batteries is that, in the 1800s, fuel cells were developed to directly generate energy from fuels (and air) through a non-combustion electrochemical mechanism. Rechargeable fuel cells (also known as H_2/O_2), like the unitized regenerative fuel cells (RFCs) in NASA's Helios Prototype, emerged later, specifically in the 1960s and 1990s. Hydrate isomerism, or the equilibrium among electrochemically active Cr^{3+} chloro-complexes and inert hexa-aqua complexes, and hydrogen development on the negode are among the drawbacks of Cr–Fe chemistry. Chelation with amino-ligands can reduce hydrate isomerism; the addition of Pb salts to raise the H_2 overvoltage and Au salts to catalyze the chromium electrode reaction can reduce the formation of hydrogen [19]. The conventional chemical compositions of RFBs consist of vanadium, iron, polysulfide-bromide, and uranium.

1.6.1.1 Vanadium

VRFBs are considered good market competitors since they avoid cross-contamination since they employ vanadium at both electrodes [20]. However, this benefit is outweighed by the restricted solubility of vanadium salts. The benefits of this chemistry comprise the absence of the combining dilution, which is harmful in Cr–Fe RFBs, and four oxidation states within the electrochemical voltage range of the graphite-aqueous acid junction. The near-perfect fit between the voltage range of vanadium redox couples and that of the carbon/aqueous acid junction is more significant for business viability. This leads to an all-time low level of energy by prolonging the life of the inexpensive carbon electrodes and minimizing the effects of side reactions, including H_2 and O_2 evolutions. It also produces a prolonged endurance and multiple-cycle (15,000–20,000) lifespan. Their substantial upfront expenses (caused by membranes, bipolar plates, carbon felts, and vanadium) can be amortized throughout their extended lifespan. The main obstacles are the following: the high cost and low quantity of V_2O_5; the development of hydrogen and oxygen through parasitic processes; and the precipitation of V_2O_5 while cycling.

Vanadium electrolytes, which are 1.6–1.7 M vanadium sulfate dissolved in 2 M sulfuric acid, are utilized as both the catholyte and the anolyte VRFBs. Vanadium exists in four different oxidation states: the V^{2+}/V^{3+} pair functions as a negative electrode, and the V^{5+}/V^{4+} combination is a positive electrode. At the positive electrode, V^{5+} is reduced to produce V^{4+} and water during discharge, producing +1.00 V to the Standard Hydrogen Electrode (SHE). Like this, at a negative electrode with −0.26 V versus SHE, V^{2+} is oxidized to generate V^{3+}. The complete redox reaction involved in VRFBs is shown below.

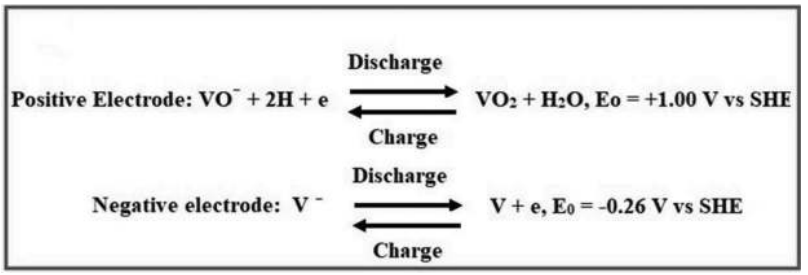

There are potential uses for heteroatom-doped electrodes to increase the durability and effectiveness of VRFBs. Here, Chen et al. combined electrodeposition and high-temperature carbonization with the introduction of protonic acid to synthesize N, P co-doped graphite fiber electrodes with a conductive network configuration in a controlled manner [21]. The H_3PO_4 functions as an additive and H_2SO_4 as an adjuvant. Density functional theory investigations demonstrate that the synergistic impact of N and P creates extra defect patterns and active sites on the electrodes, hence boosting the response rate (Figure 1.4). Moreover, carbon fibers' conductive network topology lowers internal battery impedance and enhances electrode-to-electrode communication. The VRFB performs much better when these tactics are integrated optimally.

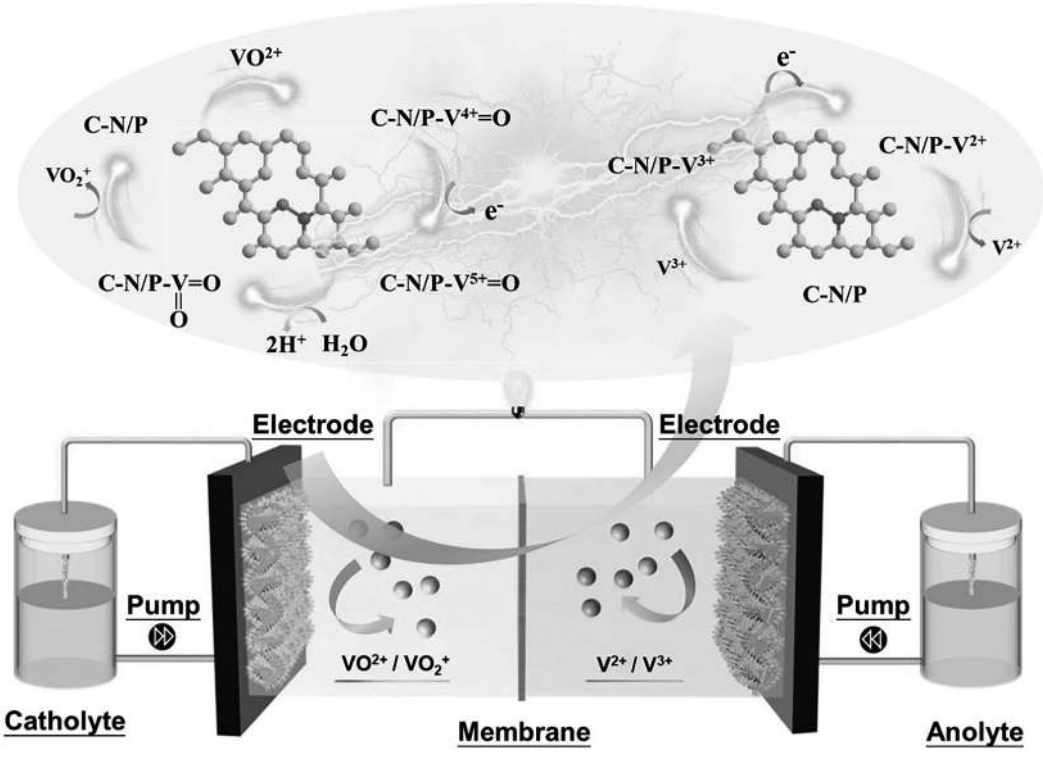

FIGURE 1.4 Application of nitrogen-phosphorus co-doped carbon fiber@graphite felt electrode for high-performance VRFBs. (Adapted with permission from [21]. Copyright 2025, Elsevier Ltd.)

1.6.2 Hybrid

Here, an electrolyte traverses an electrochemical cell with several dissolved electroactive substances present. After that, the electrolyte's chemical energy is transformed into electrical energy. RFCs, another name for Hybrid redox flow batteries (HRFBs), are a kind of electrochemical energy storage device that can offer high energy density for medium- to large-scale electrical energy storage. They are superior to all-liquid RFBs in many ways, such as having a higher energy density, responding more quickly, and not requiring equilibrium charging.

1.6.2.1 Zinc-Polyiodide (ZnI_2)

The energy density of a prototype ZnI_2 FB was found to be 167 Wh/L. About 70 Wh/L is reached by older zinc-bromide cells. Lithium iron phosphate batteries, in contrast, have a 325 Wh/L capacity. Given its lack of acidic electrolytes, nonflammability, and working range of −4°F to 122°F, the ZnI_2 battery is said to be safer than conventional FBs because it doesn't require complex conditioning circuits, which would increase weight and take up storage. One unsolved problem is the accumulation of zinc on the negative electrode, which can penetrate the membrane and decrease productivity. Zn-halide batteries have a low power density due to their inability to function at elevated current densities caused by Zn dendrite development. It may be beneficial to add ethanol to the ZnI battery's electrolyte. The expensive nature of iodide salts, the small area used for Zn accumulation, which lowers the decoupling energy and power, and Zn dendritic development are the disadvantages of Zn/I RFB. As soon as the battery runs completely flat, the electrolyte solution in both tanks is the same: a combination of I^- and Zn^{2+}. One more negative ion, polyiodide (I^{-3}), is stored in a tank that charges. Pumping fluids through the stack, where the liquids combine, allows the battery to generate power. Zn ions undergo a transformation into metallic Zn on the negative side of the stack after passing through a selective membrane underneath the stack [22]. By stabilizing free iodine and generating iodine-bromide ions (I_2Br^-) to free up iodide ions for charge storage, bromide ions (Br^-) are utilized as a complexing substance to boost energy density. In HFBs, 1–1.7 M Zn–Br aqueous solutions are utilized as the anolyte and catholyte. A solid zinc layer placed on a carbon electrode functions as a negative electrode, while bromine dissolved in solution functions as a positive electrode. The voltage produced in relation to SHE and the redox process is shown below.

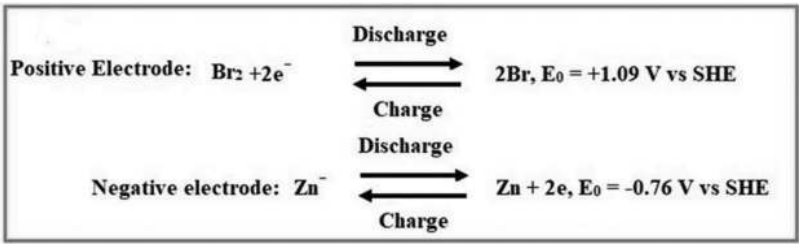

In the case of Fe–Cr FBs, 1 M chromium chloride aqueous solution is used as an anolyte, and ferrous chloride in 2 M hydrochloric acid assists as a catholyte. The voltage produced in relation to SHE and the redox process is shown below.

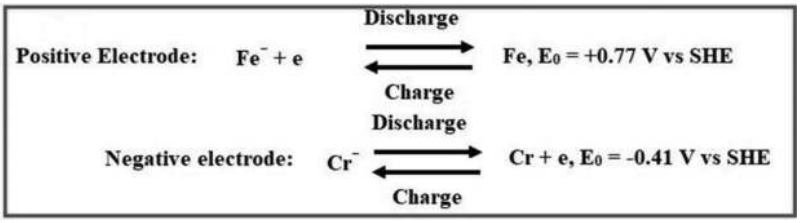

Zinc anode kinetics in an alkaline medium present a lot of opportunities for systems to store electricity because of the minimal redox potential of the $Zn(OH)_4^{2-}/Zn$ redox couple (–1.26 V versus SHE), large capacity, strong stability, two-electron transfer, rapid reversal, affordable price, and eco-friendliness. Without any hesitation, the primary goal for raising the system's energy density is to increase the flow cell's voltage. In this connection, Thamizhselvan et al. show how carefully changing the anolyte from an acidic/neutral to an alkaline state can raise the working cell voltage of a ZnI_2 FB [23]. Surprisingly, the voltage threshold for the ZnI_2 RFB increases dramatically from 1.37 V (neutral) to 1.89 V (alkaline) when the electrolyte is switched from a neutral to an alkaline one (Figure 1.5). Additionally, even at 100 mA cm^{-2}, the improved hybrid ZnI_2 electrolyte significantly increased the RFB's rate competence, displaying a 98% round trip performance and about 46% equivalent energy savings. Conversely, at 20 mA cm^{-2}, the ZnI_2 flow cell achieved an

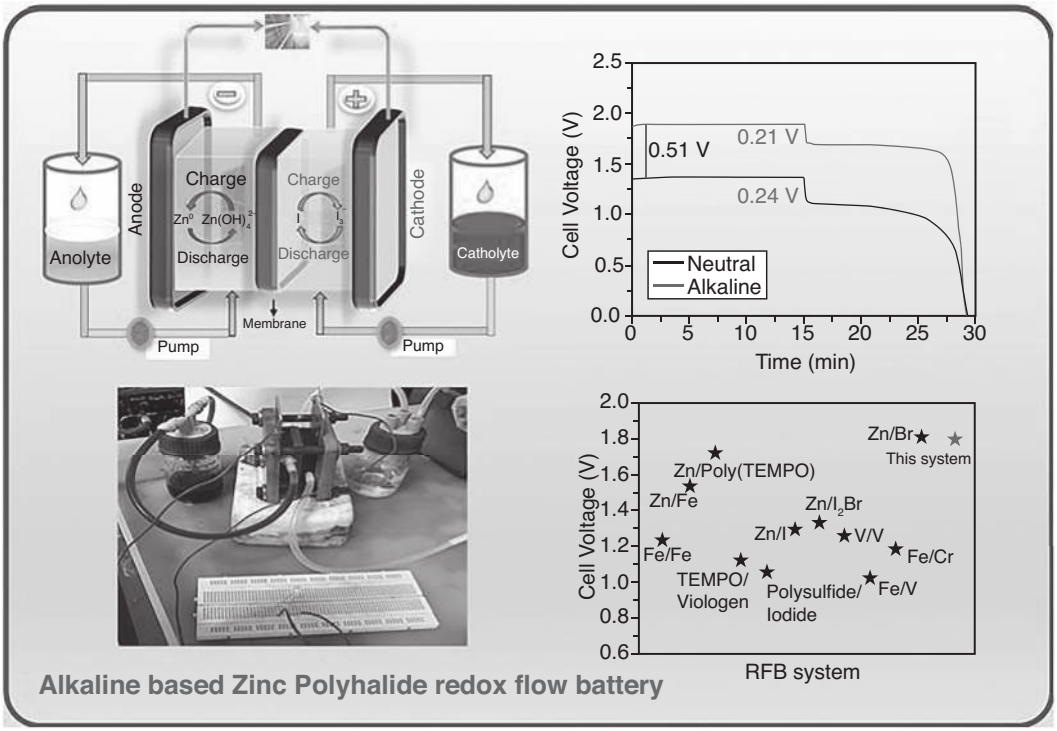

FIGURE 1.5 Schematic diagram with experimental setup and data results for the application of ZnI_2 RFB. (Adapted with permission from [23]. Copyright 2023, Elsevier Ltd.)

optimal value of 96% Coulombic, 83% voltage, and 77% energy utilization at the specified electrolyte environment.

Graphical abstract representing an alkaline-based ZnI_2 with a net cell voltage of 1.8 V, which is 500 mV higher than that of a neutral medium. The cell voltage is carefully increased by converting the anolyte from an acidic or neutral medium to an alkaline one. Furthermore, the ZnI_2 RFB with an alkaline basis operated steadily for 90 cycles at 30 mA cm^{-2}. Tests have also been conducted on 50 cycles at 50 mA cm^{-2}. The highest cyclability ever attained for alkaline-based metal halide RFBs is this reported cycle life. Therefore, when combined with elevated positive redox potential species, an innovative technique that changes the anolyte pH from acid/neutral to alkaline medium provides an effective way to achieve high cell voltage and high energy density in the instrument.

Potential possibilities for energy storage are shown by the S/Fe RFB, which has iron and sulfide as redox-active species in abundance. It has several benefits, such as customizable execution, excellent security, and being inexpensive. However, the volumetric capacity of identified S/Fe RFBs is insufficient to meet industrial needs due to the low solubility threshold of $[Fe(CN)_6]^4$. In this connection, Zou et al. effectively show an alkaline S/Fe RFB that has a high volumetric energy density and enhanced cycling stability made possible by the diverse-ion effect in the catholyte [24]. The concentration of $[Fe(CN)_6]^{4-}$ in a 0.50 M KOH solution reaches 1.52 M at room temperature, which is twice as much as the $K_4[Fe(CN)_6]$ solubility threshold of 0.76 M in deionized water. Theoretically, the volumetric capacity can attain a maximum of 40.74 Ah L^{-1}. The alkaline S/Fe RFB has outstanding results with 1.30 M $[Fe(CN)_6]^{4-}$ in the catholyte. Its extended cycle life of 3,153 hours (more than 4 months), high CE of over 99%, and gradual capacity decline of just 0.0166% each cycle (0.1134% per day) are among its many noteworthy features. Furthermore, the concentrated catholyte exhibits good cycling behavior at elevated temperatures and bigger sizes, confirming the effectiveness of the current approach in enhancing the efficiency of an affordable S/Fe RFB system for real-world uses (Figure 1.6a).

1.6.2.2 Organic RFBs

In contrast to inorganic RFBs like $Zn–Br_2$ and vanadium batteries, the adjustable redox characteristics of their active ingredients are a benefit of organic RFBs. By 2021, organic RFB had not been proven on an industrial basis and had a low endurance [11]. There are two types of organic RFBs: aqueous (AORFBs) with water as a solvent for the electrolyte components and non-aqueous (NAORFBs) with organic solvents. AORFBs and NAORFBs are further subdivided into overall and mixed structures [25]. Whereas the latter employ inorganic materials for both the anode and cathode, the former solely use organic electrode materials. AORFBs offer the safety benefits of water-based electrolytes and have a better business opportunity in bulk energy storage due to their greater conductivity and reduced solvent cost. Alternatively, NAORFBs take substantially fewer resources and offer a much wider voltage range.

A sustainable and safe backup solution for efficiently using renewable power and reducing greenhouse gases from the burning of fossil fuels is the FB. In this study, Zhu et al. show an aqueous colloid FB (ACFB) with well-dispersed colloids made from Prussian blue

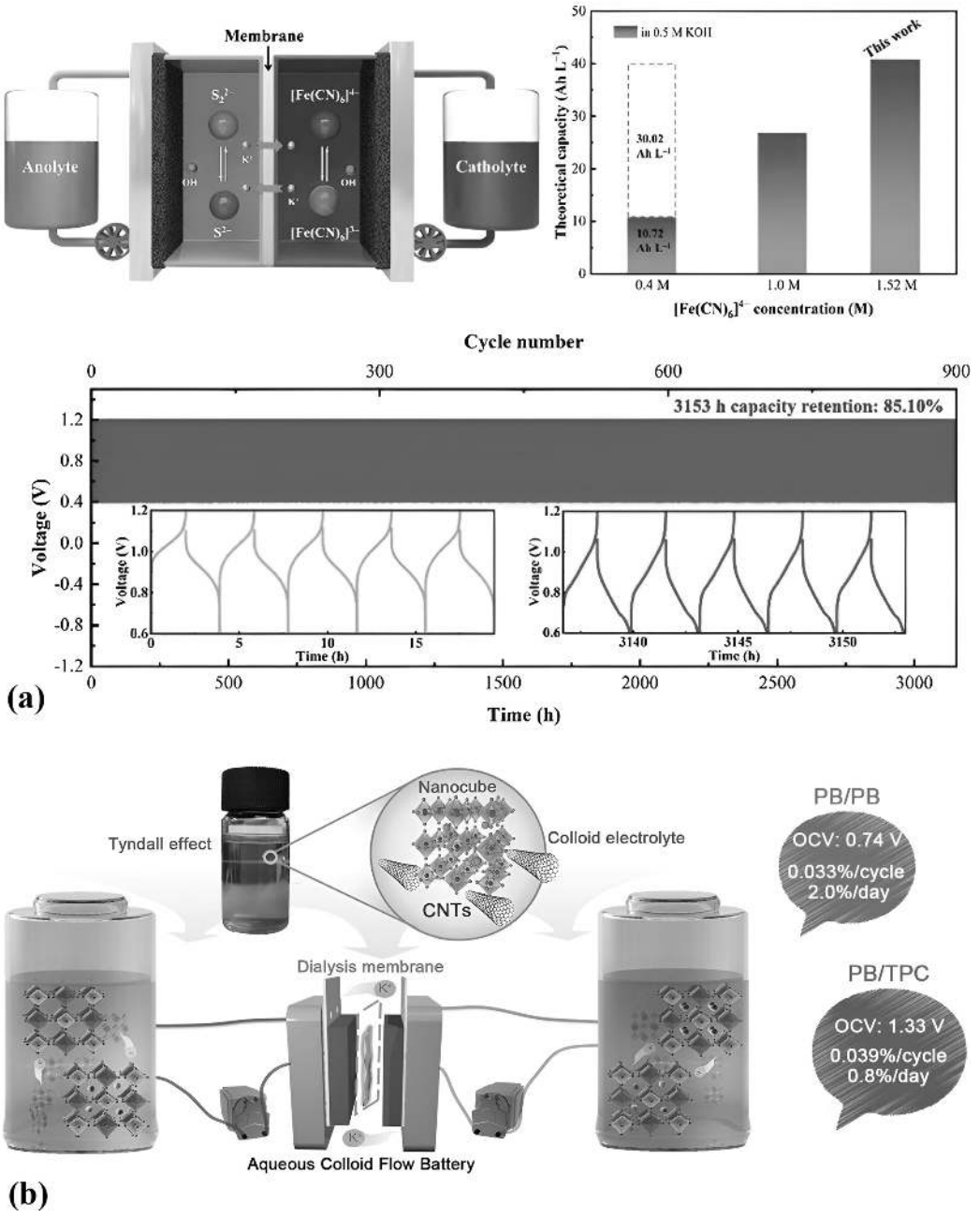

FIGURE 1.6 (a) Application of alkaline S/Fe RFB with high volumetric capacity and long cycle life. (Adapted with permission from [24]. Copyright 2024, Elsevier Ltd.) (b). Representation of cost-effective redox materials derived from Prussian blue. (Adapted with permission from [26]. Copyright 2025, Elsevier Ltd.)

(PB) cubes at the nanoscale to reduce the chemical expense and increase the selected area of different nano redox materials [26]. The created all-PB cell, which uses a cheap dialysis membrane with synthetic PB on both sides, shows an open-circuit voltage (OCV) of

0.74 V by utilizing the two redox pairs of PB. Additionally, the cell using PB as the positive electrolyte shows an OCV of 1.33 V and a capacity fade rate of 0.8%/day or 0.039%/cycle when combined with an organic tetra pyridine macrocycle (Figure 1.6b). Redox-active colloids show promise for dependable and affordable ACFB energy storage because of their long-lasting physicochemical stability and lack of noticeable fundamental alterations even after prolonged cycling.

1.6.3 Membraneless

Laminar movement, whereby two fluids are pushed along a path and perform electrochemical reactions to preserve or discharge energy, is the basis of a membraneless battery [27]. The remedies barely mix as they flow in tandem. The liquids are automatically separated by circulation, so no barrier is needed. Because they are prone to deterioration from constant contact with specific reactants, membranes are frequently the most expensive and unreliable parts of batteries. The usage of hydrogen with a liquid bromine solution is made possible by the lack of a membrane, but when membranes are present, this mixture may trigger problems since it produces hydrobromic acid, which can damage the membrane.

Over a graphite cathode, liquid bromine runs via the passageway, while hydrobromic acid runs beneath a porous anode. Hydrogen gas crosses the anode concurrently. For the first time in a membraneless architecture, chemical responses can be inverted to replenish the battery. An order of magnitude greater than lithium-ion batteries, one such membraneless FB produced a maximum power density of 795 kW/cm^2, threefold that of the other systems was reported [28]. The year 2018 saw the demonstration of a macroscale membraneless RFB that could recharge and recirculate the electrolyte flows. Indistinguishable organic catholyte and hydrophilic anolyte liquids, which demonstrated excellent capacity preservation and Coulombic performance while cycling, served as the foundation for the battery [29].

1.7 CLASSIFICATION OF RFBs

The RFBs are categorized differently based on the redox species they contain and the kind of electrolyte they use. The electrolyte, in which both positive and negative electrolytes flow, is soluble in all active compounds. Since the amount and concentration of the electrolyte may be raised to enhance the potential for storage of the RFBs, this kind is a perfect fit to be employed as a big energy storage technology. Power can be enhanced by boosting the electrode size or by connecting the RFBs in series or parallel. The RFBs can be categorized as aqueous, hybrid, and non-aqueous based on the solvent used in the electrolyte. Aqua (water) is the solvent employed for aqueous RFB, whereas an organic solvent is utilized in non-aqueous RFB. Although aquatic RFBs have a lower energy density than non-aqueous ones due to water's electrochemical potential, which varies depending on pH, they are more secure and affordable than non-aqueous ones. On the other hand, non-aqueous RFBs demonstrated higher power and energy outputs because of the organic solvent's larger potential window, which might exceed 5 V in the case of acetonitrile. The RFBs and traditional secondary batteries are combined to create hybrid RFBs. Their energy density is greater than that of all-liquid RFBs, which means they could be applied to grid-scale energy storage.

1.8 FUTURE PERSPECTIVE

FBs will be essential to the development of RESs in the years to come. Battery backup is necessary for RESs, including solar and wind power, to safeguard extra power produced during peak generation times and discharge it at low-generation times. Because FBs have a high energy storage capacity and a rapid energy release when required, they are perfect for solving this issue. Microgrid systems, which are small-scale energy grids separate from the conventional electrical grid, are another application for FBs. Because they offer a more dependable power supply, microgrids are growing in popularity, particularly in rural or high-risk areas where power outages frequently occur. FBs can also be used in backup power systems to supply electricity in the event of a natural disaster or power outage. The need for lithium in EV batteries will only increase due to the sharp rise in the number of EVs on the road today. To save lithium for electric vehicles, FBs offer a practical substitute for lithium-ion batteries in grid storage. Despite being more obscure than traditional lithium or solid-state batteries, the demand for RFBs is growing as a strong and practical substitute for extended, massive storage of energy. By 2030, these batteries are expected to expand at an average yearly growth rate of 19.9%, which has the potential to revolutionize grid reliability and renewable energy retention. Unsurprisingly, it is anticipated that the international marketplace for this technology will be worth over 700 million euros by 2030.

1.9 CHALLENGES

RFBs have the amazing potential to completely transform massive amounts of energy storage and combine with RESs, but the sector is now addressing several obstacles to ensure their future profitability and maximum impact. The primary one now is the effective modernization of the ways they are produced, which we can infer from the facts provided. Massive manufacturing is still a barrier, despite the relative advancement in processes that include vanadium. It is essential to construct factories capable of producing these batteries at a reasonable cost and with the required level of reliability. Furthermore, scaling up needs to be accomplished without sacrificing the batteries' longevity and productivity, two qualities that are crucial for gaining market acceptability. However, technical improvement is also an option. A further important problem is maintaining RFBs' capacity and performance. Although the energy density of certain existing solutions, like those made from vanadium, is sufficient for programs, all of the aforementioned alternatives must have a boost in energy density to be considered extremely viable in the market. Similar technical advancements are needed for heat control and reducing wasted energy throughout charge and discharge operations. Despite all of this, efforts to maintain affordability continue to be attempted in disciplines like extending the lifespan of services. The incorporation of RFBs into both new and current renewable energy systems is a crucial feature that still faces technological and legal obstacles.

1.10 CONCLUSION

RFBs provide a special, flexible way to satisfy a variety of foreseeable power storage needs. RFBs can be developed for a variety of energy storage as well as power requirements by separating the two concepts of energy and power. RFBs benefit greatly from the

nearly infinite options for electrolyte chemistries, which enable them to maintain their leadership position, whereas other, more conventional chemistries fluctuate in price. Furthermore, RFBs have several important characteristics that may render them more secure compared to other electrochemical energy storage systems. In conclusion, FBs are in an excellent spot to grow in popularity in the coming years due to the demand for extended-period power storage, establishing solar and wind assets, along the desire for more secure, less-flammable energy. In the case of business forecasts, FBs offer an attractive way for microgrid controllers or massive factories to migrate from costly heavy usage to long-duration battery applications as a growing number of energy suppliers move to time-of-use billing models. Nevertheless, FB storage systems remain expensive while having the considerable energy demands needed for utility-scale operations. Most requests are expected in Asia, mainly in China and India. Due to their capacity to be loaded and unloaded without deteriorating, VRFBs are anticipated to be the most widely used kind of FB. The FB market is still a long way from being able to affordably compete with advanced lithium-ion technology. However, they offer an exceptionally lengthy lifespan and long periods of discharge that approach half a day, so as societies and companies become more energy-autonomous, we anticipate seeing them used more frequently in the future.

REFERENCES

1. S. Wali, M. Hannan, P. J. Ker, S. Rahman, K. N. Le, R. Begum, S. Tiong, T. I. Mahlia. Grid-connected lithium-ion battery energy storage system towards sustainable energy: A patent landscape analysis and technology updates. *Journal of Energy Storage*. **2024**, 77, 109986.
2. J. Yuan, Y. Xue, L. Liu, J. Zhang, Y. Xia. Recent development of electrode materials in semi-solid lithium redox flow batteries. *Journal of Energy Storage*. **2024**, 76, 109574.
3. N. M. L. Huq, I. M. Mahbubul, G. Lotif, M. R. Ashrafi, M. Himan. Development and performance analysis of a low-cost redox flow battery. *Processes*. **2024**, 12, 1461.
4. A. Gamal, M. Abdel-Basset, I. M. Hezam, K. M. Sallam, A.M. Alshamrani, I. A. Hameed. A computational sustainable ap-proach for energy storage systems performance evaluation based on spherical-fuzzy MCDM with considering uncertainty. *Energy Report*. **2024**, 11, 1319–1341.
5. E. T. Sayed, A. G. Sayed, A. H. Alami, A. Radwan, A. Mdallal, A. Rezk, M. A. Abdelkareem. Renewable energy and energy storage systems. *Energies*. **2023**, 16, 1415.
6. K. C. Divya, J. Østergaard. Battery energy storage technology for power systems-An overview. *Electric Power Systems Research*. **2009**, 79, 511–520.
7. A. G. Olabi, M. A. Allam, M. A. Abdelkareem, T. D. Deepa, A. H. Alami, Q. Abbas, A. Alkhalidi, E. T. Sayed. Redox flow batteries: Recent development in main components, emerging technologies, diagnostic techniques, large-scale applications, and challenges and barriers. *Batteries*. **2023**, 9, 409.
8. Y. V. Tolmachev. Review-flow batteries from 1879 to 2022 and beyond. *Journal of Electrochemical Society*. **2023**, 170, 030505.
9. W. Kangro, H. Piper. Zur frage der speicherung von elektrischer energie in flüssigkeiten. *Electrochimica Acta*. **1962**, 7, 435–448.
10. E. R. Sum, M. Skyllas-Kazacos. A study of the V(II)/V(III) redox couple for redox flow cell applications. *Journal of Power Sources*. **1985**, 16, 85–95.
11. D. G. Kwabi, Y. Ji, M. J. Aziz, Electrolyte lifetime in aqueous organic redox flow batteries: A critical review. *Chemical Reviews*. **2020**, 120, 6467–6489.

12. N. Lavars. World's largest flow battery connected to the grid in China. New Atlas. 3 October 2022. Retrieved 12 October 2022.
13. S. Maurya, S. H. Shin, Y. Kim, S. H. Moon. A review on recent developments of anion exchange membranes for fuel cell and redox flow batteries. *RSC Advances*. **2015**, 5, 37206–37230.
14. K. Sofia, P. Rewatkar, M. Asarthen, R. Swisa, A. Zigelman. M. E. Suss, A. D. Gat. The impact of flow on electrolyte resistance in single-flow batteries. *Journal of Power Sources*. **2024**, 610, 234687.
15. X. M. Myures. S. Suresh, G. Arthanareeswan. Construction of thermal, chemical and mechanically stable ion exchange membranes with improved ion selectivity for vanadium redox flow batteries applications. *Journal of Power Sources*. **2024**, 591, 233818.
16. Q. Dai, Z. Zhao, M. Shi, C. Deng, H. Zhang, X. Li. Ion conductive membranes for flow batteries: Design and ions transport mechanism. *Journal of Membrane Science*. **2021**, 632, 119355.
17. W. Wei, H. Zhang, X. Li, Zhang, Y. Li, I. Venkelcom. Hydrophobic asymmetric ultrafiltration PVDF membranes: An alternative separation for VFB with excellent stability. *Physical Chemistry Chemical Physics*. **2013**, 15, 1766–1771.
18. M. Shi, Q. Dai, F. Li, T. Li, G. Hou, H. Zhang, X. Li, Membranes with well-defined selective layer regulated by controlled solvent diffusion for high power density flow battery. *Advanced Energy Materials*. **2020**, 10, 2001382.
19. C. Sun, H. Zhang. Review of the development of first-generation redox flow batteries: Iron-chromium system. *ChemSusChem, Chemistry and Sustainability, Energy and Materials*. **2022**, 15, e202101798.
20. A. Fetyan, B. P. Benetho, T. Alkindi, A. Andisetiawan, M. O. Bamgbopa, A. Alhammadi, G. A. El-Nagar. Performance enhancement of vanadium redox flow battery with novel streamlined design: Simulation and experimental validation. *Journal of Energy Storage*. **2024**, 99, 113397.
21. X. Chen, C. Wu, Y. Lv, S. Zhang, Y. Jiang, Z. Feng, L. Wang, Y. Wang, J. Zhu, L. Dai, Z. He. Highly active nitrogen-phosphorus co-doped carbon fiber@graphite felt electrode for high-performance vanadium redox flow battery. *Journal of Colloid and Interface Science*. **2025**, 677, 683–691.
22. G.-M. Weng. Unlocking the capacity of iodide for high-energy-density zinc/polyiodide and lithium/polyiodide redox flow batteries. *Energy & Environmental Science*. **2017**, 10, 735–741.
23. R. Thamizhselvan, R. Naresh, R. Sekar, M. Ulaganathan, V. G. Pol, P. Ragupathy. Redox flow batteries: Pushing the cell voltage limits for sustainable energy storage. *Journal of Energy Storage*. **2023**, 61, 106622.
24. H. Zou, Z. Xu, L. Xiong, J. Wang, H. Fu, J. Cao, M. Ding, X. Wang, C. Jia. An alkaline S/Fe redox flow battery endowed with high volumetric-capacity and long cycle-life. *Journal of Power Sources*. **2024**, 591, 233856.
25. M. O. Bamgbopa, S. H. Yang, A. Saif. The potential of non-aqueous redox flow batteries as fast-charging capable energy storage solutions: Demonstration with an iron–chromium acetylacetonate chemistry. *Journal of Materials Chemistry A*. **2017**, 5 (26), 13457–13468.
26. D. Zhu, L. Li, Y. Ji, P. Wang. Aqueous colloid flow batteries with nano Prussian blue. *Journal of Colloid and Interface Science*. **2025**, 15, 88–97.
27. M. O. Bamgbopa, S. Almheiri, H. Sun. Prospects of recently developed membraneless cell designs for redox flow batteries. *Renewable and Sustainable Energy Reviews*. **2017**, 70, 506–518.
28. W. A. Braff, M. Z. Bazant, C. R. Buie. Membrane-less hydrogen bromine flow battery. *Nature Communications*. **2013**, 4, 2346.
29. M. O. Bamgbopa, Y. S. Horn, R. Hashaikeh, S. Almheiri. Cyclable membraneless redox flow batteries based on immiscible liquid electrolytes: Demonstration with all-iron redox chemistry. *Electrochimica Acta*. **2018**, 267, 41–50.

CHAPTER 2

Fundamentals of Flow Batteries

Kothalam Radhakrishnan and Rajadesingu Suriyaprakash

2.1 INTRODUCTION

Flow batteries represent a distinct class of electrochemical energy storage systems, characterized by their ability to decouple energy storage capacity from power generation. This unique feature arises from their design, where energy is stored in liquid electrolytes that are circulated through electrochemical cells from external tanks. Unlike conventional batteries, where energy is stored in solid-state electrodes, the use of liquid electrolytes in flow batteries allows for a flexible and scalable architecture [1]. This design offers several advantages, including the potential for large-scale energy storage, extended operational lifespan, and enhanced safety. These attributes make flow batteries particularly well-suited for applications such as grid stabilization, renewable energy integration, and load leveling in electricity grids [2].

The concept of flow batteries has evolved significantly since its inception in the 1970s, with the development of the all-vanadium redox flow battery (VRFB) serving as a pioneering achievement in the field. This innovation set the stage for further exploration and refinement of various flow battery chemistries, including zinc-bromine, iron-chromium, and hybrid systems. Each of these chemistries offers unique benefits and poses specific technical challenges, contributing to the diversity of flow battery technologies available today [3]. As the global energy sector increasingly prioritizes sustainability and the integration of renewable energy sources, flow batteries are gaining prominence as a viable solution for long-duration energy storage, capable of addressing the intermittency issues associated with renewable power generation [4].

This chapter explores the fundamental principles underlying flow battery technology, examining the electrochemical mechanisms, system design considerations, and key performance metrics that define their operation. A detailed analysis of the different types of flow batteries will be provided, highlighting their working principles, advantages, and potential applications. Through this comprehensive overview, the chapter aims to provide

DOI: 10.1201/9781003506379-2

a thorough understanding of flow batteries and their critical role in advancing modern energy storage systems, thereby contributing to the ongoing transition toward a more resilient and sustainable energy infrastructure.

2.2 HISTORICAL DEVELOPMENT

The fascinating historical trajectory of flow battery innovation dates back to the early 1900s when there was a pressing need for robust energy storage systems that would be easy to scale and have a higher efficiency. It was during this period that NASA introduced the redox flow battery (RFB), which is the first such battery in space exploration. These batteries made use of vanadium ions in various states of oxidation as their main storage and release mechanisms for energy. This was the dawn of what is today known as one of the most popular flow batteries—VRFB. Over the course of time, this technology took great leaps forward, particularly from the 1970s when scientists began researching other kinds of chemicals and materials. One highlight during this period was zinc-bromine ($Zn\text{-}Br_2$) flow batteries as well as iron-chromium (Fe-Cr) flow batteries. The consequent need for dependable energy storage systems capable of balancing out fluctuations in both power supply and consumption prompted these advancements [5].

The 1980s and 1990s brought further refinement to flow battery designs, focusing on improving energy density, efficiency, and cost-effectiveness. The implementation of membrane technology and the refinement of electrode materials were pivotal in substantially improving the efficiency of flow batteries. During this time, VRFBs gained prominence due to their ability to provide long cycle life and high energy efficiency, making them suitable for large-scale energy storage applications. Entering the 21st century, the demand for renewable energy integration and grid stability propelled the development of next-generation flow batteries. Research efforts expanded to include novel chemistries such as all-vanadium, organic, and metal-air flow batteries. In recent years, flow battery technology has seen a resurgence, with increased investment and research focused on scalability and sustainability. The integration of advanced materials, such as nanomaterials and ionic liquids, has further improved the performance and versatility of flow batteries [6].

2.3 FUNDAMENTALS OF FLOW BATTERIES

2.3.1 Basic Working Principles

Flow batteries are a type of rechargeable battery where energy is stored in liquid electrolytes contained in external tanks, rather than within the battery cell itself. This design differentiates them from conventional batteries, where energy is stored in solid-state materials inside the battery. The fundamental working principle of a flow battery revolves around the continuous circulation of these electrolytes through the electrochemical cell, where energy conversion occurs. The external tanks house the active species in a dissolved form, and the size of these tanks determines the total energy storage capacity of the system, while the power output is dictated by the size of the electrochemical cell [7].

In operation, the electrolyte solutions, often one containing a reducing agent (negative electrolyte) and the other an oxidizing agent (positive electrolyte), are pumped from their

respective storage tanks into the cell. The cell itself comprises electrodes separated by a membrane that allows the selective passage of ions while preventing the mixing of the two electrolytes. During discharge, the electrolytes undergo redox reactions at the electrodes, releasing electrons to the external circuit to provide electrical power. The reverse process occurs during charging, where an external power source drives the redox reactions in the opposite direction, restoring the energy content of the electrolytes [8].

2.3.2 Redox Reactions and Ion Exchange

The fundamental basis of the energy conversion mechanism in flow batteries is inherent in the redox (reduction-oxidation) reactions that take place at the electrodes. The aforementioned reactions entail the exchange of electrons between two species, therefore facilitating the storage and subsequent release of energy. In a typical flow battery, the anode (negative electrode) facilitates the oxidation reaction, where a species loses electrons, while the cathode (positive electrode) supports the reduction reaction, where a species gains electrons.

The ion exchange between the two electrolyte solutions is a crucial aspect of the flow battery's operation. This ion exchange is typically facilitated by an ion-selective membrane or separator, which allows specific ions to pass through while preventing the direct mixing of the two solutions. In the vanadium RFB, vanadium ions in different oxidation states shuttle between the two half-cells through the membrane, maintaining charge balance as electrons move through the external circuit. The effectiveness of this ion-exchange process significantly impacts the efficiency, capacity, and overall performance of the battery [9].

2.3.3 Electrolytes, Membranes, and Electrodes

The choice of electrolytes, membranes, and electrodes is central to the design and performance of flow batteries. Electrolytes in flow batteries are typically aqueous solutions containing redox-active species, such as vanadium, zinc-bromine, or iron-chromium. The concentration of these active species determines the energy density of the battery. Selecting electrolytes with high solubility and stability is crucial for achieving high energy storage capacity and long cycle life. In some advanced designs, nonaqueous or hybrid electrolytes are employed to enhance energy density and operating voltage.

Membranes, also known as separators, play a vital role in allowing ion exchange while preventing the physical mixing of the two electrolytes. These membranes must exhibit high ion conductivity, chemical stability, and low resistance to minimize energy losses. Common materials used for membranes include Nafion and other proton exchange membranes (PEMs), which offer good conductivity and durability but may contribute to the overall cost of the system. Electrodes in flow batteries are typically made of carbon-based materials due to their high conductivity, chemical stability, and surface area, which facilitate efficient redox reactions [10].

2.4 TYPES OF FLOW BATTERIES

Flow batteries are a type of electrochemical energy storage system, where energy is stored in liquid electrolytes that flow through an electrochemical cell, as illustrated in Figure 2.1. The primary types of flow batteries are as follows:

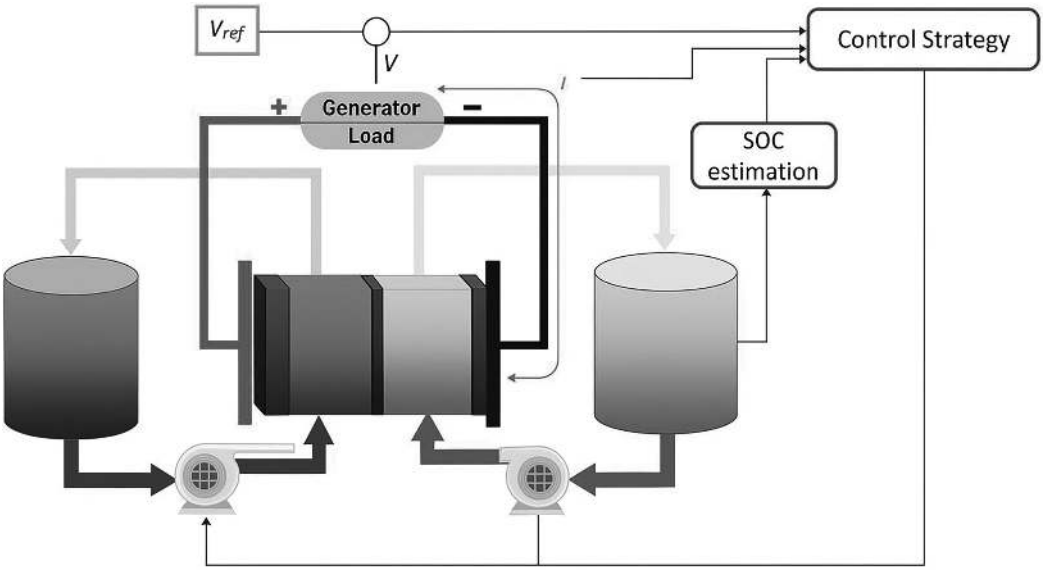

FIGURE 2.1 Graphical abstract for the primary types of flow batteries. (Adapted with permission from [11]. Copyright (2020) MDPI.)

2.4.1 Vanadium Redox Flow Batteries (VRFBs)

Nanomaterials Selection: In VRFBs, nanomaterials play a pivotal role in enhancing performance metrics. Carbon-based nanomaterials, such as graphene and carbon nanotubes, are preferred for their high electrical conductivity, large surface area, and chemical stability, which facilitate efficient electron transfer and increase the electrode's active surface area. Recent advancements include the use of nitrogen-doped graphene and carbon nanofibers, which exhibit superior electrocatalytic properties and reduced overpotentials compared to traditional carbon materials. Titanium-based materials and conductive polymers are also being explored to enhance the stability and conductivity of the electrodes, potentially lowering costs while maintaining high performance [11].

Electrochemical Reactions:

The VRFBs utilize the vanadium redox couples in different oxidation states:

Positive Electrode Reaction : $\left(VO_2^{+}/VO_2^{+4}\right)$ $VO^{2+} + 2H^{+} + 2e^{-} \rightarrow VO^{2+} + 2H_2O$

Negative Electrode Reaction (V^{2+}/V^{3+}): $V^{3+} + e^{-} \rightarrow V^{2+}$

The overall cell reaction can be represented as: $VO^{2+} + V^{2+} + 2H^{+} \rightarrow VO^{2+} + V^{3+} + H_2O$.

These reactions involve vanadium species in sulfuric acid electrolyte, where vanadium ions undergo reduction and oxidation, ensuring high efficiency and energy density [12].

2.4.2 Zinc-Bromine Flow Batteries (Zn-Br)

Nanomaterials Selection: For Zn-Br flow batteries, graphite and carbon felt electrodes are utilized due to their excellent electrical conductivity and chemical stability, which are

crucial for the bromine and zinc redox reactions. Metallic zinc serves as the anode material, while bromine is often incorporated into bromine-doped carbon composites or gel electrolytes to manage bromine's volatility and improve handling. Conductive polymers and nanostructured materials are being researched to enhance the stability and efficiency of the electrolyte system.

Electrochemical reactions: The electrochemical reactions in Zn-Br batteries are as follows:

Negative Electrode Reaction (Zn^{2+}/Zn): $Zn^{2+} + 2e^- \rightarrow Zn$

Positive Electrode Reaction (Br_2/Br^-): $Br_2 + 2e^- \rightarrow 2Br^-$

The overall cell reaction is: $Zn + Br_2 \rightarrow Zn^{2+} + 2Br^-$

These reactions involve zinc dissolution and bromine reduction, which contribute to the battery's high energy density and cycle stability [13].

2.4.3 Iron-Chromium Flow Batteries

Nanomaterials selection: Iron-chromium flow batteries use graphitic and carbon-based electrodes for their good conductivity and stability. Research into iron oxide nanoparticles is focused on leveraging their high surface area and catalytic properties to improve the battery's efficiency. For the electrolyte, iron salts and chromium compounds are used, with advancements aiming at enhancing their solubility and stability. Further research is being conducted on conductive polymers and nanostructured materials to enhance the overall efficiency and durability of the battery module.

Electrochemical reactions: The key electrochemical reactions in iron-chromium batteries are as follows:

Negative Electrode Reaction (Fe^{3+}/Fe^{2+}): $Fe^{3+} + 3e^- \rightarrow Fe^{2+}$

Positive Electrode Reaction : $\left(Cr_2O_2^{2-}/Cr^{3+}\right) Cr_2O_7^{2-} + 14H^+ + 6e^- \rightarrow 2Cr^{3+} + 7H_2O$

The overall cell reaction can be summarized as

$$Fe^{3+} + Cr_2O_7^{2-} + 14H^+ \rightarrow Fe^{2+} + 2Cr^{3+} + 7H_2O.$$

These reactions involve the reduction of chromium and the oxidation of iron, which are facilitated by the flow of electrolytes through the battery [14].

2.4.4 Hybrid Flow Batteries

Nanomaterials selection: Hybrid flow batteries, which combine different redox systems, often use composite electrodes with layered nanomaterials to optimize performance for both redox couples. The use of metal-organic frameworks (MOFs) and nano-sized conductive polymers can enhance both the energy density and power output. Hybrid systems may

integrate materials from different battery types, employing graphene-based composites or nanostructured electrodes to balance performance and cost.

Electrochemical reactions: The electrochemical reactions in hybrid flow batteries depend on the specific combination of redox couples used. For example, if a system combines vanadium and zinc redox couples, the reactions will involve

Vanadium Reaction: $VO^{2+} + 2H^{+} + 2e^{-} \rightarrow VO^{2+} + 2H_2O$

Zinc Reaction: $Zn^{2+} + 2e^{-} \rightarrow Zn$

The overall reaction will be a combination of these reactions, depending on the hybrid design [15].

2.4.5 Organic Flow Batteries

Nanomaterials selection: Organic flow batteries utilize organic redox-active compounds and benefit from graphene oxide and carbon nanomaterials to enhance the stability and conductivity of these compounds. Polymeric materials with high conductivity are used for electrodes. Innovations focus on developing novel organic redox-active compounds such as quinones and viologens to improve the energy density and sustainability of these batteries.

Electrochemical reactions: The electrochemical reactions in organic flow batteries involve the oxidation and reduction of organic molecules. For instance,

Oxidation Reaction: $R–OH \rightarrow R–O^{+} + e^{-}$

Reduction Reaction: $R–O^{+} + e^{-} \rightarrow R–OH$

These reactions depend on the specific organic molecules used, with the goal of optimizing their electrochemical properties for efficient energy storage and conversion [16].

2.5 COMPONENTS OF FLOW BATTERIES

Flow batteries are composed of several essential components that interact intricately to facilitate energy storage and conversion. Each component plays a vital role in determining the overall performance, efficiency, and lifespan of the battery system. Recent literature highlights ongoing advancements and challenges in optimizing these components to enhance flow battery technologies for broader applications. This section delves into the scientific details of these components, integrating insights from recent studies to provide a comprehensive understanding from Figure 2.2 [17].

2.5.1 Electrolyte Tanks and Circulation Systems

In flow batteries, electrolyte tanks are essential for storing liquid electrolytes that facilitate redox reactions. The materials used for these tanks must resist the specific electrolytes employed, such as vanadium-based solutions in VRFBs or zinc-bromine solutions in zinc-bromine flow batteries. Materials like polyethylene, polypropylene, and fluoropolymers are favored for their chemical resistance, mechanical strength, and long-term

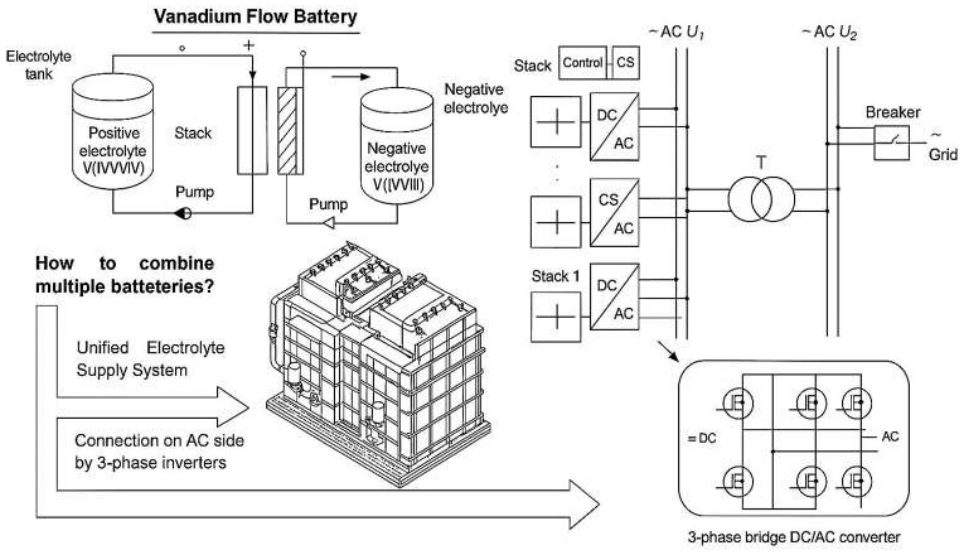

FIGURE 2.2 Schematic representation of the key components in flow batteries. (Adapted with permission from [17]. Copyright (2022) MDPI.)

stability. Recent advancements include modular and scalable tank designs that reduce system footprint while maintaining high storage capacity, making them ideal for decentralized energy storage.

The circulation system ensures continuous electrolyte flow between tanks and flow cells. Proper design of pumps and piping is crucial to prevent issues like cavitation and pressure drops, which can degrade battery performance. Advanced pump technologies have been developed to optimize flow dynamics, reduce energy consumption, and enhance system reliability. Additionally, the integration of smart sensors and control algorithms allows dynamic adjustment of flow rates based on real-time data, improving efficiency and extending battery lifespan [17].

2.5.2 Membranes and Separators

Membranes selectively permit ion passage between electrolyte compartments while preventing reactant mixing, impacting battery efficiency and longevity as illustrated in Figure 2.3. Traditional materials like Nafion are widely used for their ionic conductivity and chemical stability. However, newer membrane materials, such as ion-selective membranes based on sulfonated poly(ether ether ketone), have shown improved proton conductivity and reduced ion crossover in VRFBs, enhancing efficiency and reducing self-discharge. Composite membranes incorporating inorganic fillers also offer better mechanical stability and ion selectivity, extending operational life.

Separators function as physical barriers preventing electrode contact while allowing ion flow. Recent advancements in separator technology focus on improving porosity, wettability, and mechanical strength. Nanostructured separators with tailored pore sizes and surface chemistries have shown improved ion transport and reduced short-circuit

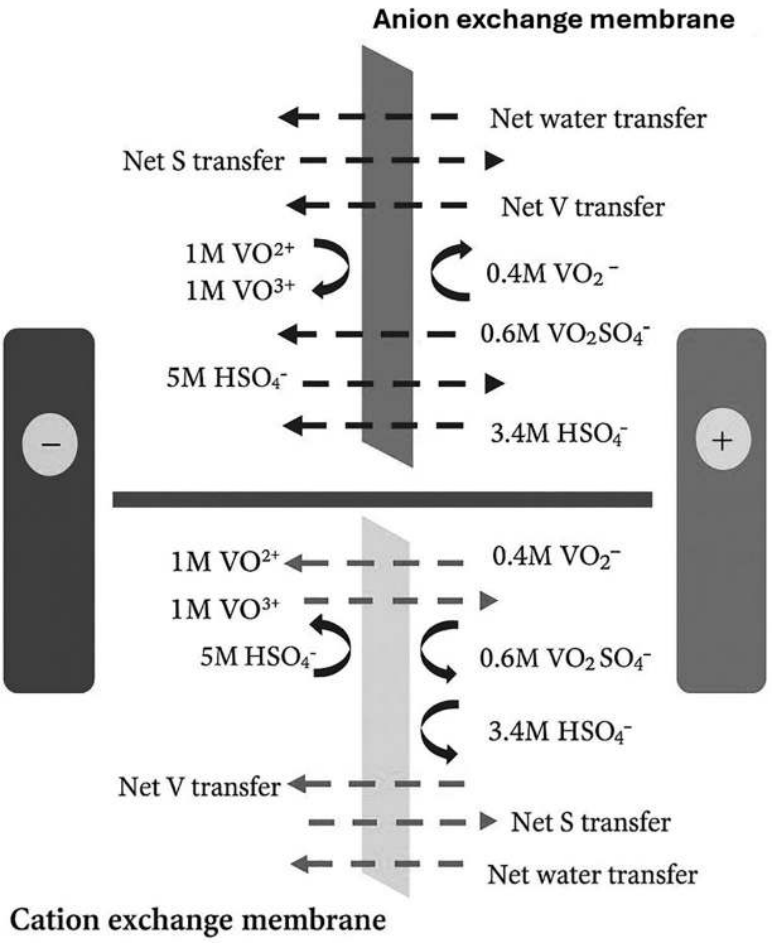

FIGURE 2.3 Schematic illustration of membranes selectively permitting ion passage between electrolyte compartments. (Adapted with permission from [18]. Copyright (2023) MDPI.)

risks. Polyolefin-based separators with surface modifications are now being employed in high-power applications [18].

2.5.3 Electrodes and Current Collectors

Electrodes are where redox reactions occur, making them central to battery operation. Carbon-based materials, like carbon felt and graphite, are commonly used due to their high surface area, conductivity, and chemical stability. Research into functionalizing these materials to enhance catalytic activity has shown promising results. Incorporating metal nanoparticles, such as platinum or palladium, into the carbon matrix increases reaction rates, boosting power density. Nanostructured electrodes with optimized pore structures further improve electrolyte infiltration and ion transport, enhancing electrochemical performance and durability.

Current collectors transmit electrons between electrodes and the external circuit. Common materials include copper, aluminum, and stainless steel, valued for their

electrical conductivity and corrosion resistance. Coating technologies have improved the corrosion resistance of current collectors, particularly in harsh environments like those in zinc-bromine batteries. Additionally, innovative 3D current collectors offer larger surface areas and better electrode contact, reducing resistance and improving overall efficiency [19].

2.5.4 Flow Cells and Stacks

Flow cells are individual electrochemical units where energy conversion occurs. Optimizing flow cell design is crucial for electrolyte flow, electric field distribution, and heat management. Advanced flow field designs, such as interdigitated and serpentine configurations, enhance electrolyte distribution across the electrode surface, improving reaction kinetics and reducing polarization losses. Composite materials with high chemical resistance and mechanical properties help maintain flow cell integrity during prolonged cycling, extending battery life.

Battery stacks, composed of multiple flow cells, scale up voltage or capacity. The design and configuration of stacks are vital for uniform electrolyte flow, effective heat dissipation, and minimal electrical losses. Modular stack designs offer flexibility and scalability, easily adjustable to meet various energy storage needs. Integrated cooling systems have been developed to maintain optimal operating temperatures, preventing thermal degradation and enhancing performance and safety. Advanced computational models now simulate electrochemical and thermal behavior, enabling better design optimization and performance prediction [20].

2.6 WORKING PRINCIPLES OF FLOW BATTERIES

Flow batteries are electrochemical energy storage devices that operate through the reversible redox reactions of active species dissolved in liquid electrolytes. These batteries are uniquely suited for large-scale energy storage applications due to their ability to independently scale power and energy capacity. This section delves into the detailed working principles of flow batteries, covering the intricacies of the charging and discharging processes, electrochemical reactions at the electrodes, ion transport mechanisms within the system, and factors influencing energy conversion efficiency.

2.6.1 Charging and Discharging Processes

Charging process: During charging, electrical energy from an external source, such as the grid or renewable energy systems, is converted into chemical energy stored in the electrolyte solutions. This process involves the oxidation of the active species in one electrolyte and the reduction of the active species in the other, facilitated by an applied voltage across the electrodes.

In a VRFB, the charging process involves the following reactions: At the positive electrode, vanadium ions in the +3 oxidation state (V^{3+}) are oxidized to vanadium ions in the +4 oxidation state (V^{4+}), specifically forming VO^{2+} ions.

$$V^{3+} \rightarrow VO^{2+} + e^{-}$$

Concurrently, at the negative electrode, vanadium ions in the +5 oxidation state (V^{5+}) are reduced to V^{4+} ions.

$$VO^{2+} + 2H^{+} + e^{-} \rightarrow VO^{2+} + H_2O$$

The electrons lost by the V^{3+} ions at the positive electrode travel through an external circuit to the negative electrode, where they are used to reduce the VO_2^{+} ions. Protons (H^{+}) move through the membrane to maintain charge neutrality.

Discharging process: During discharging, the stored chemical energy is converted back into electrical energy. The redox reactions that occurred during charging are reversed.

At the positive electrode, VO^{2+} is reduced back to V^{3+}, releasing an electron.

$$VO^{2+} + 2H^{+} + e^{-} \rightarrow V^{3+} + H_2O$$

At the negative electrode, V^{2+} is oxidized back to V^{3+}, releasing stored energy as the electrons flow through the external circuit.

The flow of electrons generates electricity, while the movement of ions through the membrane ensures the continuation of the redox reactions. This separation of the electrolyte storage from the electrochemical reaction zone is a hallmark of flow battery technology, allowing for flexible scaling of energy capacity by simply increasing the volume of electrolyte [21].

2.6.2 Electrochemical Reactions

Redox reactions: At the core of flow batteries are the reversible oxidation-reduction reactions of the electroactive species in the electrolytes. The efficiency and stability of these reactions are critical to the performance of the battery. The choice of redox couple is fundamental in determining the cell voltage and energy density of the battery. The use of vanadium in all states in VRFBs is advantageous due to its ability to minimize cross-contamination and maintain long-term stability.

In zinc-bromine flow batteries, the reactions involve the below:

- Zinc plating and stripping on the electrode surface during charging and discharging, respectively.

$$Zn^{2+} + 2e^{-} \rightarrow Z\,n$$

- The bromine redox couple, where bromide ions are oxidized to bromine during charging.

$$2Br^{-} \rightarrow Br_2 + 2e^{-}$$

These reactions are highly dependent on the electrode materials and electrolyte composition. Recent research has focused on enhancing reaction kinetics by doping electrodes

with catalysts or optimizing the electrolyte formulation to improve the reversibility and efficiency of these redox processes.

The performance of a flow battery is significantly influenced by the nature of the electrodes, which serve as the sites for the redox reactions. Electrodes in flow batteries typically consist of high-surface-area materials like carbon felts, foams, or graphite composites. The high surface area provides numerous active sites for the redox reactions, increasing the current density and overall efficiency of the battery.

Recent advances include the development of nanostructured electrode materials, such as carbon nanotubes, graphene, and metal oxide nanoparticles, which offer enhanced catalytic activity and improved electron transfer rates. Functionalization of these materials with specific catalysts or conductive polymers can further reduce overpotentials and increase the kinetics of the electrochemical reactions, leading to faster charge and discharge cycles [22].

2.6.3 Ion Transport Mechanisms

Ion transport within the flow battery is essential for maintaining charge balance and sustaining the redox reactions. The movement of ions, typically protons or other cations, occurs through the membrane or separator between the positive and negative electrolyte compartments. The efficiency of ion transport is crucial in determining the internal resistance and overall performance of the battery.

In VRFBs, the PEM plays a critical role in allowing only protons to pass through while preventing the crossover of vanadium ions between the two electrolyte compartments. This selective ion transport is essential for maintaining high coulombic efficiency and minimizing self-discharge.

The development of advanced membranes, such as ion-selective membranes or composite membranes with inorganic fillers, has been a key area of research. These membranes aim to balance ionic conductivity with mechanical stability and chemical resistance, thereby improving the longevity and efficiency of flow batteries.

Membrane and separator function: The membrane or separator not only facilitates ion transport but also prevents the physical mixing of the different electrolyte solutions, which could otherwise lead to short-circuiting or loss of efficiency. The ideal membrane should exhibit high ionic conductivity, low electrical resistance, and excellent chemical stability in the electrolyte environment. The incorporation of silica nanoparticles into a polymer matrix has been shown to increase the membrane's selectivity and reduce crossover, leading to higher energy efficiency and longer battery life [23].

2.6.4 Energy Conversion Efficiency

The energy conversion efficiency of a flow battery is a measure of how effectively it converts the input electrical energy during charging into stored chemical energy and subsequently back into electrical energy during discharging. The overall efficiency is influenced by multiple factors, including voltage efficiency, coulombic efficiency, and energy efficiency.

Voltage efficiency is affected by the overpotentials at the electrodes and the internal resistance of the battery components. Minimizing these losses through better electrode

materials and optimized cell design can significantly improve voltage efficiency. Coulombic efficiency depends on the prevention of side reactions, electrolyte crossover, and the reversibility of the redox reactions. High coulombic efficiency is essential for maximizing the usable energy stored in the battery. Energy efficiency is the product of voltage efficiency and coulombic efficiency and is a critical metric for evaluating the overall performance of the battery. Innovations such as dynamic flow rate control, temperature management, and advanced electrolyte formulations have been shown to enhance energy efficiency in flow batteries.

Recent research has focused on several strategies to enhance the energy conversion efficiency of flow batteries. One approach involves optimizing the flow field design within the flow cells to ensure uniform distribution of the electrolyte and minimize pressure drops. Computational fluid dynamics (CFD) simulations have been employed to model and improve the flow patterns, leading to more efficient operation and reduced energy losses [24].

2.7 PERFORMANCE METRICS OF FLOW BATTERIES

Evaluating flow batteries involves analyzing key metrics such as energy efficiency, power density, cycle life, and cost. These metrics are vital for assessing the effectiveness and economic feasibility of flow batteries in various energy storage applications. Recent advancements in materials and design have enhanced these metrics, leading to more efficient and durable systems.

2.7.1 Energy Efficiency

Energy efficiency, which measures the efficiency of energy conversion during charging and discharging, is a crucial parameter. Recent research has focused on improving both voltage and coulombic efficiency to enhance overall energy efficiency. For instance, novel electrode materials like carbon nanotube-infused electrodes and nanostructured catalysts have been developed to reduce overpotentials and improve voltage efficiency. Additionally, the use of fluorinated ion-exchange membranes in VRFBs has significantly increased coulombic efficiency by minimizing electrolyte crossover [25].

2.7.2 Power Density

Power density, the rate at which a flow battery delivers energy, is critical for applications requiring rapid energy delivery. Innovations in electrode materials, such as 3D-printed electrodes with hierarchical porosity and MOFs, have enhanced power density by increasing active surface area and improving mass transport. Additionally, optimized flow cell designs, like those with improved flow field configurations, have further contributed to higher power densities by enhancing electrolyte distribution and reducing pressure drops [26].

2.7.3 Cycle Life

Cycle life, or the number of charge–discharge cycles a battery can undergo before significant capacity loss, is crucial for long-term viability. Recent advancements have focused on

improving the electrochemical stability of redox-active species and enhancing membrane durability. Stabilizing organic redox couples through chemical modifications has significantly reduced degradation rates, extending the cycle life of organic flow batteries. Additionally, composite membranes that combine the strength of polymers with the chemical resistance of ceramics have proven to be more durable, further extending cycle life [26]. Cost remains a major factor in the deployment of flow batteries, encompassing initial capital, operational, and maintenance costs, as well as the cost per cycle over the battery's lifespan [27].

2.8 APPLICATIONS OF FLOW BATTERIES

Flow batteries are a transformative technology in energy storage, with applications ranging from grid stabilization to industrial energy management. Their long cycle life, flexible energy capacity, and high efficiency make them ideal for modern energy systems [28].

2.8.1 Grid-Scale Energy Storage

Flow batteries, particularly VRFBs, are increasingly used in grid-scale energy storage due to their ability to store large amounts of energy for extended periods. They stabilize power grids by balancing the fluctuations caused by renewable energy sources, providing essential ancillary services like frequency regulation and voltage support. Recent advancements in membrane technology and electrolyte optimization have improved ionic conductivity and reduced crossover, enhancing VRFB performance and making them more competitive with lithium-ion batteries. For instance, optimizing electrolyte composition has increased VRFB energy efficiency to over 80%.

2.8.2 Renewable Energy Integration

Flow batteries play a crucial role in integrating renewable energy sources into the power grid by storing excess energy generated during high-output periods and releasing it during low-output periods, mitigating the intermittency of renewables. This function is vital for a consistent energy supply and reducing fossil fuel reliance. A 250 MW/1,000 MWh VRFB system in California, integrated with a solar power plant, has effectively reduced curtailment and improved solar energy utilization. Similarly, flow batteries integrated with offshore wind farms in Europe have shown potential to reduce storage costs and enhance grid reliability [29].

2.8.3 Peak Shaving and Load Leveling

Flow batteries are effective in peak shaving and load leveling, helping to manage demand–supply balance on the grid. By storing energy during off-peak periods and discharging it during peak demand, they reduce grid strain and lower electricity costs, benefiting industrial and commercial users facing high demand charges. A 20 MWh VRFB in a German manufacturing facility reduced peak demand by 20%, leading to significant cost savings. Flow batteries are also being explored for data centers, providing reliable backup power and improving energy management during grid disturbances.

2.8.4 Microgrid and Off-Grid Systems

Flow batteries are gaining popularity in microgrid and off-grid systems, particularly in remote or underserved regions with limited or no access to the main electricity grid. They provide stable and reliable power, enabling the deployment of renewable energy systems in areas otherwise reliant on diesel generators. A microgrid in a remote Indian village powered by a VRFB system provided 24/7 electricity to over 500 households, demonstrating the potential of flow batteries to support sustainable development. In sub-Saharan Africa, flow batteries have been integrated into microgrids to power health clinics and schools, ensuring reliable electricity for essential services.

2.9 RECENT ADVANCES AND RESEARCH TRENDS

The continuous evolution of flow battery technology is fueled by the pressing need for more efficient, cost-effective, and sustainable energy storage solutions. Recent research has unveiled significant advancements in materials science, system optimization, and environmental sustainability, which are driving the development of next-generation flow batteries. This section elaborates on these advancements and trends, integrating insights from recent literature [30,31].

2.9.1 Electrode and Membrane Developments

High-performance membranes: Recent literature underscores the importance of membrane advancements in flow batteries, particularly in reducing ion crossover and enhancing chemical stability. Innovations in ion-exchange membranes, especially those utilizing advanced polymers like perfluorosulfonic acid (PFSA) and polybenzimidazole (PBI), have resulted in membranes with superior ion selectivity and mechanical strength. The PFSA-based membrane exhibited a 50% reduction in vanadium ion crossover, significantly enhancing the coulombic efficiency and cycle stability of the VRFB [32].

3D-Printed electrodes: The application of 3D printing technology in fabricating flow battery electrodes has led to the creation of complex geometries that optimize fluid dynamics and increase electrode surface area. The printed lattice electrodes enhanced mass transport and reduced pressure drop within the flow battery system. This advancement resulted in a 30% increase in power density and a 20% improvement in energy efficiency compared to conventional planar electrodes [33].

2.9.2 System Optimization and Integration

Advanced system design: System optimization, particularly through computational modeling and simulation, is a growing area of research aimed at improving the overall architecture and integration of flow batteries. CFD and multi-physics simulations are being utilized to optimize flow fields, cell designs, and stack configurations. The CFD was used to design an optimized flow field for a VRFB, which reduced pressure drop by 35% and improved electrolyte distribution uniformity, thereby enhancing overall system performance [34].

Hybrid systems: Hybrid flow batteries that combine traditional flow battery technology with other energy storage systems, such as supercapacitors or solid-state batteries, are

emerging as a promising area of research. These hybrid systems aim to leverage the high energy density of solid-state batteries and the long cycle life of flow batteries. The hybrid flow battery system integrates a lithium-ion battery with a vanadium RFB. This system demonstrated superior energy efficiency and operational flexibility, making it suitable for grid-scale applications and renewable energy integration [35].

2.9.3 Cost Reduction Strategies

Manufacturing innovations: Reducing the cost of flow battery components through manufacturing innovations is critical for their widespread adoption. Recent efforts have focused on developing automated production techniques, such as roll-to-roll processing for membranes and electrode materials, which significantly reduce labor and material costs. The advancements could lower the cost of VRFB systems by up to 40% within the next decade, making them more competitive with other energy storage technologies like lithium-ion batteries [36].

Scaling up production: Scaling up the production of flow battery components is essential for achieving cost reductions and meeting growing demand. Large-scale manufacturing facilities are being developed, benefiting from economies of scale. Additionally, strategic partnerships between academia and industry are accelerating the commercialization of new technologies. The collaboration between a leading VRFB manufacturer and a national research laboratory resulted in a new high-throughput production line that significantly reduced the cost of membranes and electrode materials.

2.9.4 Environmental Sustainability

The adoption of green chemistry principles is increasingly guiding the development of environmentally sustainable flow batteries. Recent research has focused on the use of nontoxic, biodegradable electrolytes and the recycling of battery materials at the end of their life cycle. The iron-based electrolytes, which are abundant and environmentally benign, are used in iron-chromium flow batteries. The study concluded that these electrolytes could achieve similar performance to vanadium-based systems while significantly reducing environmental impact [37].

Life cycle assessment (LCA) is a crucial tool for evaluating the environmental impact of flow batteries from production to disposal. Recent LCAs have provided valuable insights into the carbon footprint, resource consumption, and waste generation associated with different flow battery chemistries. For instance, an LCA of a VRFB system found that recycling vanadium could reduce the overall environmental impact by 30%, making flow batteries a more sustainable option for large-scale energy storage [38].

2.10 CONCLUSION

Flow batteries provide a flexible and durable energy storage system with notable benefits such as scalability, extended cycle life, and the capacity to autonomously adjust energy and power levels. This chapter provided an overview of the basic principles of many types of flow batteries, including VRFBs, zinc-bromine flow batteries, iron-chromium flow batteries, and the developing organic and hybrid flow batteries. It emphasized their distinct

features and uses. Crucial elements like electrolyte tanks, membranes, electrodes, and flow cells were examined, with a focus on their contributions to the efficiency of the system. The operational concepts, encompassing electrochemical reactions and ion transport mechanisms, were elucidated to demonstrate the functioning of these systems and their attainment of high energy conversion efficiency. An overview was provided on the many uses of flow batteries, ranging from large-scale storage in power grids to integration with renewable energy and industrial applications. Current research initiatives prioritize advancements in materials, breakthroughs in electrodes and membranes, optimization of systems, and measures to reduce costs, all of which contribute to improved performance and sustainability. Flow batteries are positioned to have a substantial impact on the future of energy storage, facilitating a shift toward more environmentally efficient and robust energy systems.

REFERENCES

1. C. Zhang, Z. Yuan, X. Li, Designing better flow batteries: An overview on fifty years research. *ACS Energy Lett*. 9 (2024) 3456–3473.
2. L. Trahey, F. R. Brushett, N. P. Balsara, G. Ceder, L. Cheng, Y.-M. Chiang, N. T. Hahn, B. J. Ingram, S. D. Minteer, J. S. Moore, K. T. Mueller, L. F. Nazar, K. A. Persson, D. J. Siegel, K. Xu, K. R. Zavadil, V. Srinivasan, G. W. Crabtree, Energy storage emerging: A perspective from the joint center for energy storage research. *Proc. Natl. Acad. Sci. U.S.A*. 117 (2020) 12550–12557.
3. M. Shoaib, P. Vallayil, N. Jaiswal, P. Iyapazham Vaigunda Suba, S. Sankararaman, K. Ramanujam, V. Thangadurai, Advances in redox flow batteries – A comprehensive review on inorganic and organic electrolytes and engineering perspectives. *Adv. Energy Mater.* 14 (2024) 2400721.
4. H. Ajibade, C.O. Ujah, K.C. Nnakwo, D.V.V. Kallon, Improvement in battery technologies as panacea for renewable energy crisis. *Discov. Appl. Sci*. 6 (2024) 374.
5. G.P. Rajarathnam, A.M. Vassallo, *The Zinc/Bromine Flow Battery*. Springer Singapore, Singapore, 2016.
6. J.-N. Liu, C.-X. Zhao, J. Wang, D. Ren, B.-Q. Li, Q. Zhang, A brief history of zinc–air batteries: 140 years of epic adventures. *Energy Environ. Sci*. 15 (2022) 4542–4553.
7. A.Z. Weber, M.M. Mench, J.P. Meyers, P.N. Ross, J.T. Gostick, Q. Liu, Redox flow batteries: A review. *J. Appl. Electrochem*. 41 (2011) 1137–1164.
8. T. Nguyen, R.F. Savinell, Flow batteries. *Electrochem. Soc. Interface* 19 (2010) 54–56.
9. Y. Wang, A. Mu, W. Wang, B. Yang, J. Wang, A review of capacity decay studies of all-vanadium redox flow batteries: Mechanism and state estimation. *ChemSusChem* 17 (2024) e202301787.
10. K.K. Jana, S.J. Lue, A. Huang, J.F. Soesanto, K. Tung, Separator membranes for high energy-density batteries. *ChemBioEng Rev*. 5 (2018) 346–371.
11. A. Clemente, R. Costa-Castelló, Redox flow batteries: A literature review oriented to automatic control. *Energies* 13 (2020) 4514.
12. Á. Cunha, J. Martins, N. Rodrigues, F.P. Brito, Vanadium redox flow batteries: a technology review: Vanadium redox flow batteries: A technology review. *Int. J. Energy Res*. 39 (2015) 889–918.
13. M.C. Wu, T.S. Zhao, L. Wei, H.R. Jiang, R.H. Zhang, Improved electrolyte for zinc-bromine flow batteries. *J. Power Sources* 384 (2018) 232–239.
14. H. Zhang, C. Sun, Iron–chromium flow battery, in: C. Roth, J. Noack, M. Skyllas-Kazacos (Eds.), *Flow Batteries*, 1st ed., Wiley, 2023: pp. 741–763.

15. Y. Zhang, J. Cao, Z. Chen, J. Xu, C. Yu, An organic-based aqueous hybrid flow battery with high power and long cycle life: a tetrapyridophenazine/ferrocyanide system. *J. Mater. Chem. A* 8 (2020) 6874–6881.
16. J. Cao, J. Tian, J. Xu, Y. Wang, Organic flow batteries: Recent progress and perspectives. *Energy Fuels* 34 (2020) 13384–13411.
17. A. Loskutov, A. Kurkin, I. Kuzmin, I. Lipuzhin, Ways to ensure parallel operation of vanadium flow batteries to create high power energy storage systems. *Batteries* 8 (2022) 120.
18. A.G. Olabi, M.A. Allam, M.A. Abdelkareem, T.D. Deepa, A.H. Alami, Q. Abbas, A. Alkhalidi, E.T. Sayed, Redox flow batteries: Recent development in main components, emerging technologies, diagnostic techniques, large-scale applications, and challenges and barriers. *Batteries* 9 (2023) 409.
19. G.L. Soloveichik, Flow batteries: Current status and trends. *Chem. Rev.* 115 (2015) 11533–11558.
20. Z. He, Y. Lv, T. Zhang, Y. Zhu, L. Dai, S. Yao, W. Zhu, L. Wang, Electrode materials for vanadium redox flow batteries: Intrinsic treatment and introducing catalyst. *Chem. Eng. J.* 427 (2022) 131680.
21. M. Park, J. Ryu, J. Cho, Nanostructured electrocatalysts for all-vanadium redox flow batteries. *Chem. Asian J.* 10 (2015) 2096–2110.
22. K. Lourenssen, J. Williams, F. Ahmadpour, R. Clemmer, S. Tasnim, Vanadium redox flow batteries: A comprehensive review. *J. Energy Storage* 25 (2019) 100844.
23. A. Khor, P. Leung, M.R. Mohamed, C. Flox, Q. Xu, L. An, R.G.A. Wills, J.R. Morante, A.A. Shah, Review of zinc-based hybrid flow batteries: From fundamentals to applications. *Mater. Today Energy* 8 (2018) 80–108.
24. Z. Huang, A. Mu, L. Wu, H. Wang, Vanadium redox flow batteries: Flow field design and flow rate optimization. *J. Energy Storage* 45 (2022) 103526.
25. Y. Yao, J. Lei, Y. Shi, F. Ai, Y.-C. Lu, Assessment methods and performance metrics for redox flow batteries. *Nat Energy* 6 (2021) 582–588.
26. Z. Huang, A. Mu, L. Wu, H. Wang, Y. Zhang, Electrolyte flow optimization and performance metrics analysis of vanadium redox flow battery for large-scale stationary energy storage. *Int. J. Hydrogen Energy* 46 (2021) 31952–31962.
27. M. Han, W. Sun, W. Hu, Y. Liu, J. Chen, C. Zhang, J. Li, Emerging polyoxometalate clusters-based redox flow batteries: Performance metrics, application prospects, and development strategies. *Energy Storage Mater.* 71 (2024) 103576.
28. P. Alotto, M. Guarnieri, F. Moro, Redox flow batteries for the storage of renewable energy: A review. *Renew. Sustain. Energy Rev.* 29 (2014) 325–335.
29. S.H. Qazi, D.V. Bozalakov, L. Vandevelde, Frequency and power shaving controller for grid-connected vanadium redox flow batteries for improved energy storage systems. *Front. Energy Res.* 12 (2024) 1393728.
30. D. Reber, S.R. Jarvis, M.P. Marshak, Beyond energy density: Flow battery design driven by safety and location. *Energy Adv.* 2 (2023) 1357–1365. https://doi.org/10.1039/D3YA00208J.
31. N. Poli, C. Bonaldo, M. Moretto, M. Guarnieri, Techno-economic assessment of future vanadium flow batteries based on real device/market parameters. *Appl. Energy* 362 (2024) 122954.
32. R.G. Charles, M.L. Davies, P. Douglas, I.L. Hallin, I. Mabbett, Sustainable energy storage for solar home systems in rural Sub-Saharan Africa – A comparative examination of lifecycle aspects of battery technologies for circular economy, with emphasis on the South African context. *Energy* 166 (2019) 1207–1215.
33. W. Wang, Q. Luo, B. Li, X. Wei, L. Li, Z. Yang, Recent progress in redox flow battery research and development. *Adv. Funct. Mater.* 23 (2013) 970–986.
34. L. Su, J.A. Kowalski, K.J. Carroll, F.R. Brushett, Recent developments and trends in redox flow batteries, in: Z. Zhang, S. S. Zhang (Eds.), *Rechargeable Batteries*, Springer International Publishing, Cham, 2015: pp. 673–712.

35. A. Adeniran, A. Bates, N. Schuppert, A. Menon, S. Park, Recent advances in aqueous redox flow battery research. *J. Energy Storage* 56 (2022) 106000.
36. A. Asif, R. Singh, Further cost reduction of battery manufacturing. *Batteries* 3 (2017) 17. https://doi.org/10.3390/batteries3020017.
37. A. Dinesh, M.S. Anantha, M.S. Santosh, M.G. Priya, K. Venkatesh, K.S. Yogesh Kumar, M.S. Raghu, H.B. Muralidhara, Improved performance of iron-based redox flow batteries using WO3 nanoparticles decorated graphite felt electrode. *Ceramics Int*. 47 (2021) 10250–10260.
38. M. AlShafi, Y. Bicer, Life cycle assessment of compressed air, vanadium redox flow battery, and molten salt systems for renewable energy storage. *Energy Rep*. 7 (2021) 7090–7105.

CHAPTER 3

Materials and Chemicals of Flow Batteries

Jesús A. Claudio-Rizo, Denis A. Cabrera-Munguía, Lucía F. Cano-Salazar, and Juan J. Mendoza

3.1 INTRODUCTION

Flow batteries consist of one or more electrochemical cells that enable efficient electricity generation and storage (Figure 3.1). They have a significant impact on technologies related to power grids, renewable energy, electric vehicles, and public transport due to their versatility and ease of industrial application [1]. The core of a flow battery is the electrochemical cell, where electrons are shuttled between species through an electrolyte in a redox system. The spontaneity of this process depends on the reduction potential, which defines the electron-donating or -accepting capacity of redox pairs [2].

The performance and efficiency of a flow battery depend on its design and the materials used, including redox-active species, electrolyte systems (aqueous, nonaqueous, or organic), separators, and pumps. Transition metals like vanadium, zinc, iron, and cobalt are commonly employed for their stable redox states. Vanadium offers high resistance to cross-contamination and redox stability but is limited by cost and mining constraints [3]. Zinc and iron exhibit excellent redox reversibility but face solubility challenges [4]. Cobalt provides high energy density and redox stability, but its toxicity and extraction complexities must be considered [5].

Organic molecules, such as quinones and anthraquinones, are also used in flow batteries. Their conjugated electronic systems enable stable redox reactions and biodegradability, making them suitable for sustainable energy. However, their thermal degradability requires attention, and structural modifications are often necessary to enhance performance [6]. Nanomaterials, including metal nanoparticles and carbon-based derivatives like graphene, have improved flow battery efficiency. They enhance the catalytic surface

DOI: 10.1201/9781003506379-3

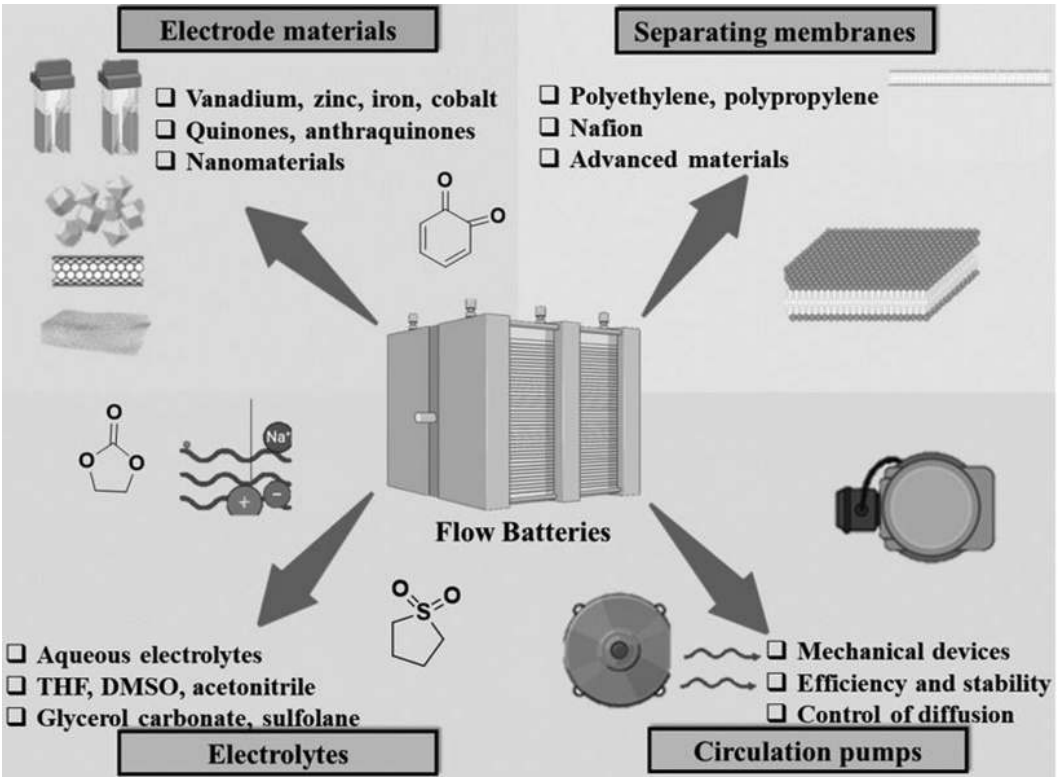

FIGURE 3.1 General schematic showing the materials and chemicals used in the construction of flow batteries.

area and thermal stability, advancing the design of high-performance batteries [7]. The diffusion of electrons between redox species depends on the electrolyte. Aqueous electrolytes, with ions like sodium, chloride, and sulfate, facilitate immediate electron transfer but are limited by solubility and temperature constraints [8]. Organic solvents, such as tetrahydrofuran (THF) and dimethyl sulfoxide (DMSO), address these issues but pose flammability and environmental concerns [9]. Lithium-ion flow batteries offer high efficiency and compatibility with metallic lithium but require organic support electrolytes to stabilize its reactivity [10].

Separating membranes are critical in flow batteries, facilitating ion exchange and electron transfer. Synthetic polymers like polyethylene and Nafion are common but suffer from low ionic conductivity over time. Enhancing these materials with carbon nanotubes or graphene improves performance. Alternative materials, such as ionic polymers and ceramic membranes, offer superior thermal and mechanical properties, boosting functionality [11]. Circulation pumps maintain the flow of charged electrolytes, optimizing redox reactions, temperature control, and diffusion [12]. In this chapter, materials and chemicals for flow battery design are comprehensively analyzed, providing insights for advancing flow battery technologies.

3.2 ELECTROLYTES AND ELECTRODES USED IN FLOW BATTERIES

Electrodes and electrolytes are crucial to the efficiency of flow batteries, directly influencing energy storage and conversion. Electrodes facilitate electrochemical reactions, with material composition and surface area significantly impacting performance, capacity, and lifespan. Electrolytes, as liquid ion conduits, connect electrodes and enable charge transfer, with their composition determining the temperature range, stability, and energy density of the system [13].

The choice of eutectic medium also affects active compounds, cycle life, and charge/discharge efficiency, making the optimization of these components essential for advancing flow battery technology and scaling up energy storage systems (ESSs) [14].

Flow battery systems typically include half-cells and anion exchange membranes (AEMs), with separate electrolyte reservoirs circulating during charge and discharge cycles [15]. These design elements are critical for efficient operation and are illustrated in Figure 3.2, which highlights the basic structure of flow batteries.

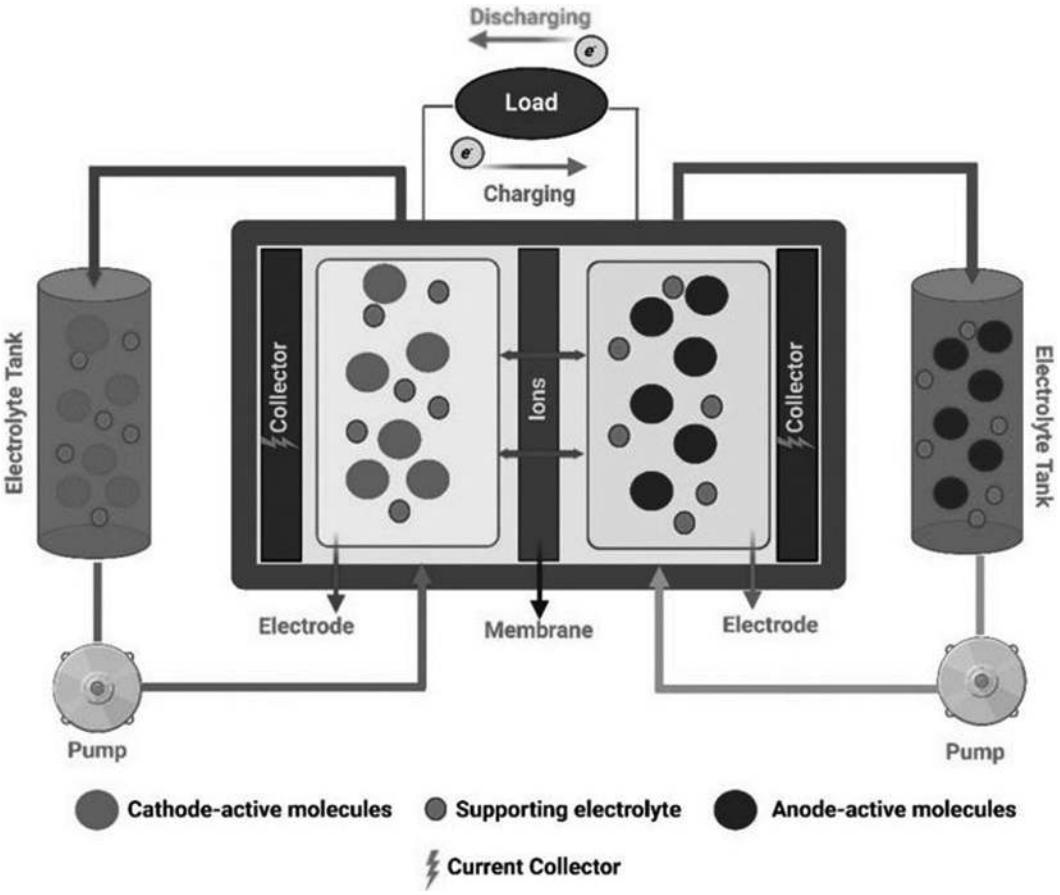

FIGURE 3.2 Diagram of a conventional flow battery.

As previously highlighted in Figure 3.2, electrodes and electrolytes make the most fundamental and crucial part of a flow battery system. In this section, the main materials for constructing electrodes are examined, and the most widely used and recent potential electrolytes are pointed out.

3.2.1 Electrodes

In flow batteries, the electrochemical reactions at electrodes are critical for energy conversion and storage. Electrode materials significantly influence reaction kinetics, charge transport rates, and system efficiency. Ideal electrodes require high electrical conductivity, chemical stability, and resistance to degradation. Surface area and morphology also affect energy and power density [16]. Advances in electrode materials and design are essential to improve charge/discharge rates, cycle life, and operational stability, driving flow battery technology toward enhanced energy storage solutions.

Carbon-based electrodes, such as carbon paper, carbon cloth, graphite felt, and carbon felt, are preferred due to their high conductivity, porous structure, and corrosion resistance [17]. However, pure carbon materials exhibit limitations like low specific surface area and activity. Modifications to enhance electrochemical activity and hydraulic permeability are crucial for large-scale application and commercialization [17]. Table 3.1 summarizes electrode materials, modifications, synthesis techniques, and their impact on energy efficiency.

Vanadium redox flow batteries (VRFBs) are recognized for their ecological, economic, and performance advantages, largely due to their stable, recyclable vanadium electrolyte and long-lasting components, minimizing environmental impact [18]. Redox reactions (V(III)/V(II) and V(II)/V(III)) occur at the negative electrode during charging and discharging. Carbon composites are widely used as electrode materials, but their basic properties often limit performance, requiring modifications to enhance efficiency [19]. Graphite oxidation during charging highlights the need for improved materials to increase cycle life and stability [20].

Current efforts focus on improving both positive and negative electrodes to boost electrochemical activity and suppress unwanted reactions, such as hydrogen evolution. This is essential for enhancing cycle life and supporting renewable energy integration.

Organic molecules, including quinones and anthraquinones, also show promise due to their redox stability and water solubility, benefiting green energy technologies. However, structural modifications are needed to address their thermal degradability for long-term use [6].

3.2.2 Electrolytes

An electrolyte, a compound that dissociates into ions in solution or molten form, facilitates ion transfer between electrodes in electrochemical cells, playing a critical role in ion transport, energy conversion, and system efficiency [21]. Among redox flow batteries (RFBs), VRFBs are the most advanced and commercially viable. Unlike other RFBs like Zn-Br and Fe-Cr systems, VRFBs utilize vanadium in multiple oxidation states, addressing cross-contamination issues [22].

TABLE 3.1 Types of Electrodes Described in the Literature, Fabrication Methods, and Efficiency

Electrode Type (Negative/Positive)	Synthesis Method	Energy Efficiency (%)
Nitrited TiO_2 carbon felt (negative)	Hydrothermal process	70
Titanium nitrite coated graphite felt (negative)	Hydrothermal method and nitridation reaction	77.4
Titanium carbide-decorated graphite felt (negative)	Hydrothermal synthesis and carbothermal	76
ZrO_2 nanoparticle embedded carbon nanofibers (negative)	Electrospinning technique	73.3
MnO_2 nanosheet array-decorated carbon paper (negative)	Controllable redox deposition method	66.4
TiO_2 modified graphite felt (negative)	Thermal treatment	71.2
Graphene deposited carbon felt (CF) (positive)	Solution coating method	85
3D graphene-nanowall-decorated carbon felts (positive)	In situ microwave plasma enhanced chemical vapor deposition method	90
Graphite felt/MnO_2 composite electrodes (positive)	Hydrothermal process	80
$TiNb_2O_7$ nanoparticle-decorated graphite felt (positive)	Solvothermal method	79.1
Binary $NiCoO_2$-modified graphite felt (positive)	Hydrothermal and calcination process	73.2
SO_3H-functionalized carbon paper (positive)	Exfoliation	80.8
N and O co-functionalized graphite felt (positive)	Impregnation of urea or melamine and chemical vapor deposition	74
Biomass-derived electrode (positive)	Pyrolysis process	86.3
Water-activated graphite felt (positive)	Water activation method in tube furnace	83
CO_2-activated graphite felt (positive)	Direct treatment in a CO_2 atmosphere at a high temperature	84

Source: Adapted with permission from ref [47], Copyright The Authors, some rights reserved; exclusive licensee Wiley Online Library. Distributed under a Creative Commons Attribution License 4.0 (CC BY) [47].

The VRFB structure comprises two electrolyte tanks. At the positive electrode, VO_2^+ and VO_2^+ undergo reactions between vanadium's +4 and +5 oxidation states, while at the negative electrode, V^{3+} reacts with V^{2+}. Equations (3.1) and (3.2) describe these electrode reactions, with Equation (3.3) representing the net system reaction [22]. This design ensures high efficiency and stability, making VRFBs a leading technology for scalable energy storage. Figure 3.3 illustrates the basic structure of a VRFB.

$$\text{Positive}: VO^{2+} + 2H^+ + e^- \leftrightarrow VO_2^+ + H_2O \quad E_0 = 1.00\,\text{V} \tag{3.1}$$

$$\text{Negative}: V^{3+} + e^- \leftrightarrow V^{2+} \quad E_0 = -0.25\,\text{V} \tag{3.2}$$

$$\text{Net}: VO^{2+} + H_2O + V^{3+} \leftrightarrow VO_2^+ + 2H^+ + V^{2+} \quad E_0 = 1.25\,\text{V} \tag{3.3}$$

If vanadium with an oxidation state of +3 is included in the positive electrolyte, this species is oxidized to vanadium +4 prior to the oxidation of V(IV) to V(V) during charging.

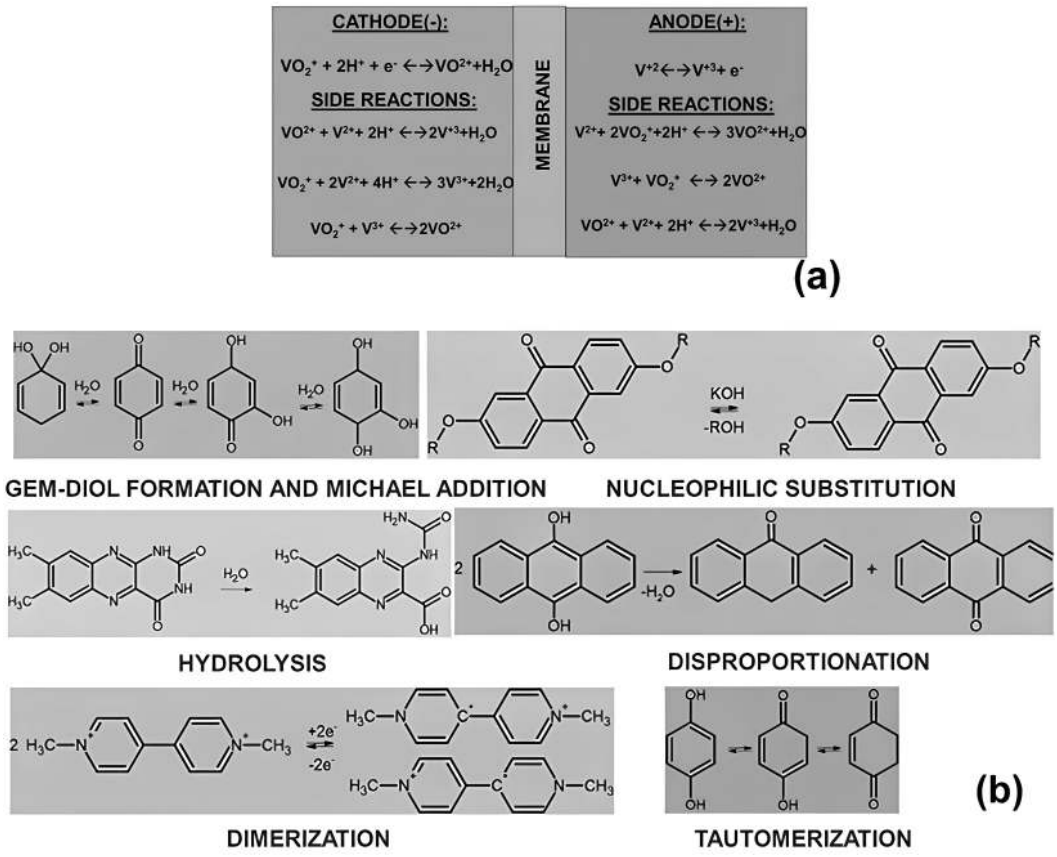

FIGURE 3.3 (a) Crossover reactions in VRFBs and (b) Degradation reaction in organic flow batteries.

Similarly, in the negative electrolyte, V(IV) is reduced to the V(III) species during the charging process before further reduction from V(III) to V(II). This process is described in Equation (3.4).

$$VO^{2+} + 2H^+ \; e^- \leftrightarrow V^{3+} + H_2O \quad E_0 = 0.34\,V \tag{3.4}$$

Usually, the positive electrolyte contains vanadium IV and V in sulfuric acid, and the negative electrolyte consists of vanadium II and III in sulfuric acid, which is the most practiced procedure of VRFBs [23].

Electrolytes play a vital role in ESSs and commercialization, with recent advancements enabling the use of various vanadium compounds effectively. Ionic liquids (ILs) have garnered attention due to their superior electrochemical performance compared to organic electrolytes, finding applications in flow batteries and ESSs for solar and thermal energy [15]. Unlike traditional sulfuric acid-based electrolytes in RFBs, ILs offer reduced corrosion risks and enhanced stability, addressing the limitations of organic and aqueous systems [15,24].

RFBs rely on the harmonious operation of electrodes and electrolytes, as failure often arises from component interdependencies rather than individual breakdowns [21,25]. Alternatives such as organic solvents (e.g., THF, DMSO, and sulfolane) enhance electron transfer kinetics but pose fire risks and require stringent stability assessments [9]. Lithium-ion flow batteries represent a significant advancement, featuring improved energy conversion, stability, and efficiency. However, their reliance on reactive metallic lithium and strong organic solvents necessitates careful handling to prevent chemical reactivity [10].

Despite progress in electrode and electrolyte development, further innovations are essential to enhance efficiency and promote environmentally sustainable ESSs, aligning with the goals of renewable energy adoption and technological advancement.

3.3 ELECTRODE REACTIONS INVOLVED IN FLOW BATTERIES

RFBs use electrolytes, the catholyte and anolyte, which circulate between tanks and cell stacks. An ion-exchange membrane, typically Nafion, facilitates ion transport—commonly hydronium ions—between electrolytes to maintain charge neutrality [26]. Unlike electrolytes, anodic and cathodic electrodes do not participate directly in electrochemical reactions, contributing to their longer lifespan. Common electrode materials include carbon, graphite, graphene, metals, and metal oxides, which can be modified to enhance electrocatalytic performance [26,27].

The electrolyte solution typically consists of redox-active solutes dissolved in a primary solvent, usually water or an organic solvent (Table 3.2) [27]. Factors that degrade electrolytes and impair battery performance include precipitation of active species, ion crossover, and contamination by fine particles or by-products [27,28]. Side reactions, such as water splitting into oxygen and hydrogen, can alter pH levels, damage active species, and lead to CO_2 formation from carbon electrodes [28].

Addressing these degradation mechanisms is critical for improving the performance and longevity of RFBs. Advances in electrode and electrolyte stability, along with mitigation strategies for side reactions, are essential for the continued development and commercialization of this energy storage technology.

3.3.1 Inorganic Electrodes

3.3.1.1 VRFBs

VRFBs can achieve up to 20,000 cycles with 80% efficiency due to their operation in highly acidic environments [28]. Vanadium species dissolve in sulfuric acid but form chlorine gas in hydrochloric acid. A critical operating temperature range of 10°C–40°C prevents precipitation at low temperatures and instability of VO^{2+} at high temperatures [27]. Advantages include low capital costs, minimal electrolyte contamination, and suitability for renewable energy integration and electric vehicle charging [27]. However, challenges include high acidity, expensive vanadium, poor thermal stability, V_2O_5 hill formation, and vanadium crossover (Figure 3.3) [28,29].

TABLE 3.2 Redox Reactions Involve in Flow Batteries

Cathode	Anode	Theoretical	Solvent	Ref.
$VO_2^+ + 2H^+ + e^- \leftrightarrow VO^{2+} + H_2O$	$V^{+2} \leftrightarrow V^{+3} + e^-$	1.25	Acid	[29]
$PbO_2 + 4H^+ + 2e^- \leftrightarrow Pb^{2+} + 2H_2O$	$Pb \leftrightarrow Pb^{2+} + 2e^-$	1.59	Acid	[27]
$2Ce^{4+} + 2e^- \leftrightarrow 2Ce^{3+}$	$Zn \leftrightarrow Zn^{2+} + 2e^-$	2.41	Acid/neutral	[27]
$MnO_2 + 4H^+ + 2e^- \leftrightarrow Mn^{2+} + 2H_2O$	$Zn \leftrightarrow Zn^{2+} + 2e^-$	2.30	Acid	[27]
$I_2 + 2e^- \leftrightarrow 2I^-$	$Zn + 4OH^- \leftrightarrow Zn(OH)_4^{2-} + 2e$-	1.88	Alkaline	[27]
$Br_2 + 2e^- \leftrightarrow 2Br^-$	$Zn \leftrightarrow Zn^{2+} + 2e^-$	1.84	Acid/neutral	[27]
$2Fe(CN)_6^{3-} + 2e^- \leftrightarrow 2Fe(CN)_6^{4-}$	$Zn + 4OH^- \leftrightarrow Zn(OH)_4^{2-} + 2e^-$	1.73	Alkaline	[27]
$O_2 + 2H_2O + 4e^- \leftrightarrow 4OH^-$	$2Zn + 8OH^- \leftrightarrow 2Zn(OH)_4^{2-} + 4e^-$	1.66	Alkaline	[27]
$2Fe^{3+} + 2e^- \leftrightarrow 2Fe^{2+}$	$Zn \leftrightarrow Zn^{2+} + 2e^-$	1.53	Acid/neutral	[27]
$2Fe(CN)_6^{3-} + 2e \leftrightarrow 2Fe(CN)_6^{4-}$	$Zn + 4Br^- \leftrightarrow ZnBr_4^{2-} + 2e^-$	1.32	Neutral	[27]
$Fe^{3+} + e^- \leftrightarrow Fe^{2+}$	$Cr^{2+} \leftrightarrow Cr^{3+}$	1.18	Acid	[30]
$3Br^- \leftrightarrow Br_3^- + 2e^-$	$2S_2^{2-} \leftrightarrow S_4^{2-} + 2e^-$	1.35	Acid	[30]
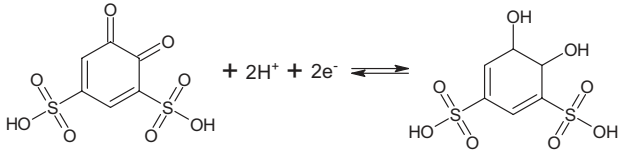	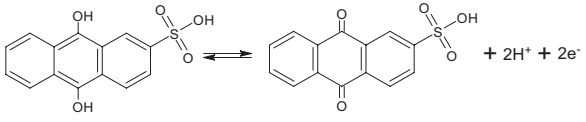	0.76	Acid	[31]
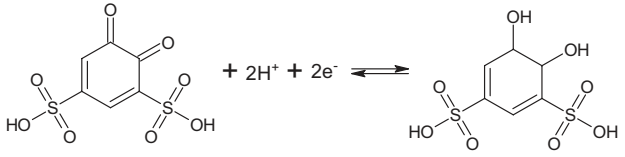	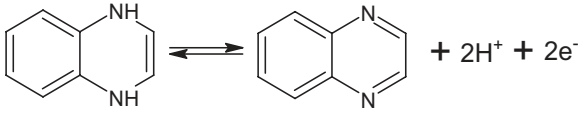	1.35	Acid	[31]
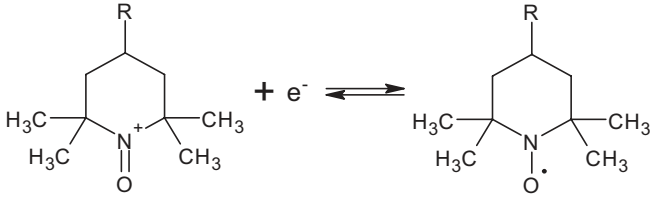	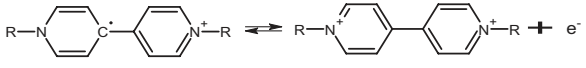	1.20	Neutral	[48]

3.3.1.2 Lead Flow Batteries

Lead flow batteries bypass membranes, using Pb^{2+} species generated during redox reactions. Metal lead (Pb^0) and insoluble PbO_2 plate onto electrodes in an electrolyte with dissolved Pb^{2+} ions [27,30]. Challenges include PbO_2 plating issues, Pb dendrites, and side reactions. Additionally, the acidic environment produces oxygen and hydrogen, leading to cracking, peeling, and corrosion of deposits [31].

3.3.1.3 Zinc-Based Batteries

3.3.1.3.1 Zinc-Cerium In zinc-cerium batteries, zinc chloride forms part of the anolyte, whereas cerium methanesulfonate, soluble in methanesulfonic acid, forms part of the catholyte. The theoretical voltage claimed is 2.5 V, but the values have been reported to be less than 2.0 V in discharge tests [30]. A high-level concentration of acids maintains a reasonable Ce^{4+} solubility but decreases Ce^{3+} solubility. Zinc plating and stripping are inhibited, for instance, by the lead oxide additives, but there is a limit on energy density imposed by the solubility of Ce salts, and therefore, new Ce-based electrolytes are required [27].

3.3.1.3.2 Zinc-Manganese The combination of Zn and MnO_2 forms redox pathways using manganese (II) acetylacetonate ($Mn(acac)_2$) as the electrolyte, which has many advantages, such as high cost-effectiveness, good reversible activity, and stability in neutral media, which helps reduce the formation of Zn dendrites. However, an acidic medium is the best for Mn^{2+} species for stability reasons. Further research needs to be directed at devising other redox pairs with enhanced hydrophilic nature and electrical conductivity [27].

3.3.1.3.3 Zinc-Iodine $Zn(OH)_4^{2-}/Zn$ and I^-/I_3^- demonstrate a potential difference of 1.88 V (Table 3.2). Specifically, to stabilize I_2 and give rise to I^-, bromide ions (Br^-) form I_2Br. More work is required to achieve stable I_2 electrolytes [27].

3.3.1.3.4 Zinc-Bromine This battery records an operating voltage of about 1.84 V with good reversible charge and low charge cost. Energy density and rate of kinetic reactions can be enhanced by using a high concentration of bromine (Br_2) and bromide ions. Nevertheless, the toxicity of bromine, corrosive by-products of HBr, and low energy efficiency, besides short cycle life. Further improvement in efficiency and less material and operational expenses is required [27,30,31].

3.3.1.3.5 Zinc-Iron Zinc-iron batteries are versatile because they can be used in neutral, basic, or acidic electrolytes. In a neutral system, $ZnCl_2/ZnBr_2$ and $K_3Fe(CN)_6$ are used, thereby providing low cost, no corrosion, and fair energy density (1.32 V, Table 3.2). However, crossover phenomena deserve attention. In acidic medium, Zn/Zn^{2+} and Fe/Fe^{3+} pairs are utilized, but zinc promotes the evolution reaction of hydrogen, while the iron compounds used are not stable. It is necessary to look for appropriate inhibitors or active materials to prevent the degradation of Zn-Fe batteries [27].

3.3.1.3.6 Zinc-Air Zinc-air batteries usually have a standard potential of 1.6 V, though they operate in a potential range of 1.0 V–1.4 V. These are inexpensive and nonhazardous but have a short cycle life primarily due to zinc plating as well as dendrite growth due to the high activity of the oxygen species developed from the superoxide radicals and other pathways toward this. The development of electrocatalysts for efficient oxygen reduction reaction constitutes great hurdles to this [27].

3.3.1.4 Iron-Chromium

As for iron-chromium auxiliary cells, the catholyte contains Fe^{2+}/Fe^{3+}, and the anolyte contains Cr^{2+}/Cr^{3+} and hydrochloric acid as a supporting material. On carbon or graphite electrodes, the iron redox couple is pretty much reversible, while the chromium redox couple, on the other hand, is more complicated as it requires the use of electrocatalysts such as bismuth and necessitates the addition of ethylenediaminetetraacetic acid to complex Cr^{+5} [30,31].

3.3.1.5 Bromine-Polysulfide

Sodium bromide is the catholyte, while sodium polysulfide is the anolyte. These electrolytes are low-budget as well as quite soluble in water. While all active species are anions, a cation-exchange membrane is required in order to avoid crossover with sodium ions acting as the charge carrier through the membrane. Operating voltage range is 1.7–2.1 V with carbon/polyolefin composite electrodes. Shortcomings include low screening, crossover, precipitation of sulfur species, and formation of H_2S and Br_2, among other limitations [30].

3.3.2 Organic Electrodes

3.3.2.1 VRFBs

Organic batteries, using organic polymer binders between iron-based electrodes, provide solutions to high manufacturing costs, crossover, and impact resistance. Vanadium batteries, however, have low energy density compared to typical batteries. While X-ray lithography is time-consuming for fabrication, S, P, and P-based polymers are suitable for bending electronics [28,29]. Power in such systems depends on factors like the quantity of electrons, voltage, and active species [27]. Electrodes in aqueous electrolytes have a potential range of 1.5–1.8 V, whereas organic solvents can support voltages up to 5 V [26]. Organic solvents, however, suffer from poor solubility of active materials, leading to safety and power density issues. Functionalizing solvents with hydrophilic groups like hydroxyl, quaternary ammonium, and sulfonates improves solubility [26]. Organic electrolytic systems include ferrocyanide/ferrocene, quinones, viologens, and 2,2,6,6-tetramethylpiperidin-1-oxyl (TEMPO) derivatives [28].

3.3.2.2 Quinone-Based Compounds

Quinone compounds, like 1,2-benzoquinone-3,5-disulfonic acid (BQDS), are tunable and can store one or two electrons. However, BQDS degrades in aqueous media via Michael addition reactions [27].

3.3.2.3 Anthraquinone Derivatives

Anthraquinones are poorly soluble in organic solvents, but solubility can be improved with oligoether or ionic chains [27].

3.3.2.4 Viologen Derivatives

Methyl viologen and 4-OH-TEMPO show good cycling performance but may precipitate. Polyethylene glycol functionalization improves solubility, efficiency, and cyclability [27].

3.3.2.5 Other Derivatives

Phenazine derivatives are stable with reduced potential, azobenzene has good charge–discharge properties, and nitrobenzene offers high energy density but with potential stability challenges [27]. Benzothiadiazole and benzotriazole derivatives, with low reduction potentials, are also promising [27]. Redox activity in organic molecules can be hindered by reactions like Michael addition, hydrolysis, and disproportionation [29].

3.4 SEPARATING MEMBRANES AND CIRCULATING PUMPS FOR FLOW BATTERIES

Flow batteries are secondary batteries designed for energy storage, using redox couples in liquid electrolytes transported to electrodes. A key component is the membrane, or separator, which allows ion flow between cell stacks while preventing transverse electrolyte flow and electron passage. Catalysts are stored in isolated tanks, and electrolytes circulate with pumps during redox reactions inside the cell [32,33].

Typically made of polymer materials, the ion-exchange membrane provides mechanical support between the anode and cathode, preventing unwanted reactions while permitting necessary ion flow (e.g., H^+, SO_4^{2-}) for battery function. These membranes require high ion permeability, selectivity, good proton conductivity, and resistance to chemical and thermal degradation for capacity retention. Additionally, mechanical strength is needed to withstand pump pressures and temperature ranges. Cost remains a key challenge for commercial viability (Figure 3.4). Cation-exchange membranes (CEMs), AEMs, and amphoteric ion-exchange membranes (AIEMs) are commonly used, along with porous and composite membranes for specific needs [32].

3.4.1 Ion-Exchange Membranes

Ion-exchange membranes are formed by cross-linking polymer chains to provide mechanical stability and prevent dissolution in water. These membranes consist of fixed ionic groups with counterions that maintain electrical neutrality through ion exchange. For CEMs, such as Nafion, a fluoropolymer with ether-based side chains and sulfonic acid end groups is commonly used in flow batteries, especially all-vanadium systems. However, Nafion's high permeability to vanadium ions has led to the development of alternative materials, including modified perfluorinated and non-perfluorinated hydrocarbon membranes. Research has shown that Nafion membrane thickness (50–175 μm) impacts efficacy in VRFBs. Thicker membranes improve vanadium insulation and Coulombic efficiency, while thinner membranes reduce area resistance and improve performance at

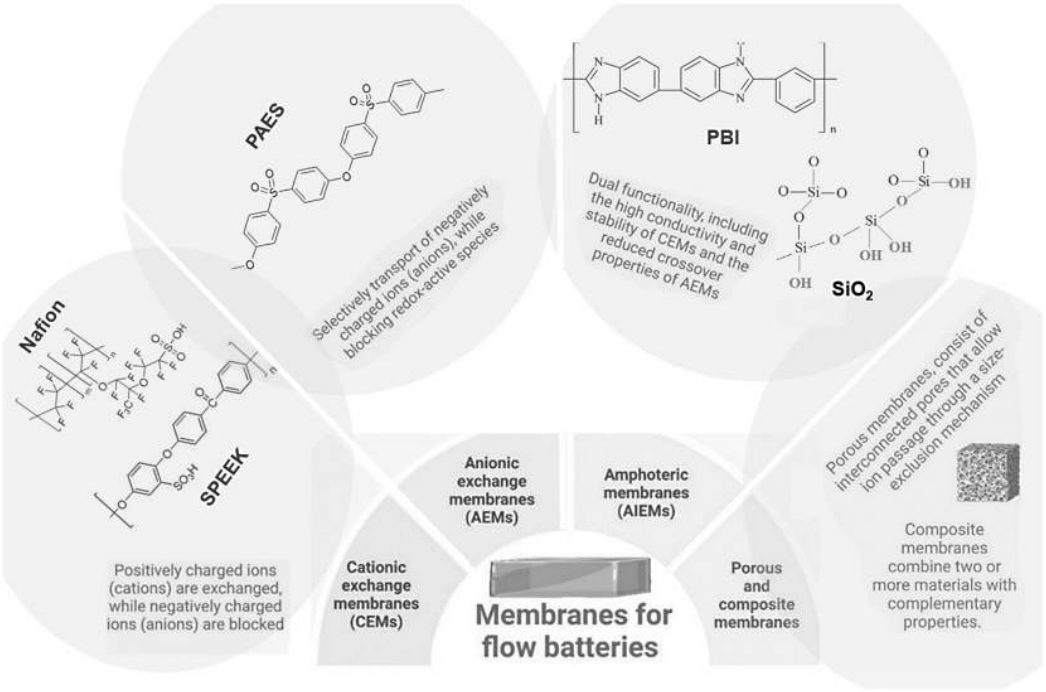

FIGURE 3.4 Classification of membranes for flow batteries.

high current densities. Nafion membranes of 125 μm thickness are optimal for energy and electrolyte efficiency at current densities of 120–240 mA cm^{-2} [33,34]. Optimization of Nafion includes modifications with interfacial chemical modifiers, sol-gel treatments, and layer-by-layer (LbL) deposition of poly(ethylene imine) [35,36]. Non-perfluorinated membranes, made from hydrocarbon polymers, offer cost-effective, environmentally friendly alternatives with superior ion selectivity, oxidation resistance, and mechanical stability [37]. For instance, aromatic polymers, including membranes with polyphenylsulfone, sulfonated polyether ether ketone (SPEEK), and sulfonated polyethersulfone, have much improved thermal and chemical stability and excellent mechanical properties [38,39]. New alternatives such as sulfonated polyimide membranes and poly[2,2′-(m-phenylene)-5,5′-b ibenzimidazole] (PBI) appear to be promising due to low crossover rates of active species, high chemical resistance, and good thermal and mechanical stability [40].

Another type of ion-exchange membrane, AEMs, is also applied in flow batteries. Unlike CEMs, where hydroxide or chloride ions may dominate diffusion, AEMs pass only certain types of ions, which are negatively charged, such as OH^- or Cl^-, and do not allow redox-active species to pass. AEMs are usually preferred in aqueous organic systems because of their higher selectivity and lower cost compared to CEMs [39]. In VRFB applications, AEMs employ Donnan exclusion to keep out positively charged vanadium ions, thus minimizing their migration [34]. The appropriate AEMs for a flow battery must be such that they allow high ionic conduction of anions, minimal leakage of active species

to avoid self-discharge in the cell, excellent durability against acids and oxidizing agents such as VO_2^+, and excellent mechanical strength to withstand wear and tear. Quaternary ammonium-functionalized common ion-exchange membranes whose backbone is hydrocarbon polymers such as poly(phenylene oxide) (PPO), poly(arylene sulfide) (PAS), poly(arylene ether) (PAE), or poly(arylene ether sulfone) (PAES) are known to improve ion selectivity [34,41].

In the case of, for instance, G.J. Hwang and other groups, it has been presented that commercial AEMs and CEMs are used as membrane separators in VRFBs with evaluated membranes and vanadium ion barriers [42]. The results indicated that ionic conductivities were, for the most part, lower than those of Nafion 117; however, it was indicated that NEPEM115 (Nafion-based) membranes were more helpful under certain conditions. In another study, it was qualitatively concluded that the AEMs, when used alongside standard CEMs such as Nafion 211 and 212, performed worse in chemical and electrochemical tests, but there was electrolyte leakage due to high water uptake [43]. Such membrane development attempts to develop AEMs have some advantages. The discharge of CEMs, of course, would be critical in any application. However, AEMs also have disadvantages, such as degradation of functional cationic groups, causing their lifetime to be shorter compared to that of CEMs. Some efforts on polymer modifications and improved steric hindrance are still active to make them less vulnerable to oxidation in order to increase their stability.

AIEMs, it is claimed, do not suffer from the drawbacks of both cation and AEMs by having high ion conductivity and mechanical stability as well as low ion crossover. Therefore, the dual functional properties mean decreased permeability to V^{5+}, HSO_4^-, and SO_4^{2-}, among others, which in effect means reduced spontaneous discharge or self-discharge of the device and improved efficiency and stability of flow batteries. Nafion and SPEEK membranes with anion exchange immobilized copolymerized D-L-lysine are some examples of AIEMs. Hydrophobic polysulfone chains were introduced into SPEEK to reduce the amount of hydrophilic area and provide anionic characteristics by imidazole functional groups [44]. There is another method of using a membrane that has been modified by an ion with an anionic structure, for instance, the chloromethylated poly(phthalazinone ether sulfone ketone) CMMPESK with quaternary ammonium groups, which has great membrane mechanical and chemical stability, performing better than Nafion 117 [45]. In general, three distinct groups of AIEMs are defined: polymer blends with special ionic groups, single polymers modified with both cationic and anionic sides, or multilayer construction by LbL assembly [32,33,39].

3.4.2 Membranes with Porous Structure and Composite Membrane

Porous and composite membranes have become the best proportionate replacement for the usually used polymeric ion-exchange membrane that is perfluorinated. Also, unlike the dense networks that are often provided, porous membranes do have pores with a network that can transport ions due to size exclusion. The ion conductivity of such membranes is often a function of membrane thickness, its hydrophilic nature, and also pore size, among other factors, where this aspect favors thicker as well as more hydrophilic, larger pores

[32,35]. In the case of VRFBs, neutral protons and vanadium ions can be separated when a porous membrane is used because their diameters are not identical. So as to increase ion selectivity, especially for very small specific ion-selective membranes, concentration is made on prepared and designed morphology and pore size about 50–500 Å in diameter [46]. But this also leads to poor ion selectivity and high permeability due to large pore sizes, hence the reason for the need for the use of nanoporous membranes. Furthermore, few researchers indicate a critical pore size for the ion conductive membranes around 5 nm that was found to be optimal for both ion conductivity and ion crossover ratio. Therefore, notwithstanding these results, the modification of porous membranes in order to obtain high voltage efficiencies at increased current densities is yet a great problem among the membranes that requires changes to preserve CE.

Blending two or more different materials that compensate for each other's drawbacks leads to the creation of composite membranes, which is yet another effective approach. The first method involves forming hydrogen bond interactions by mixing ion-conducting polymer materials with low ionic materials and/or organic polymers that have low ionic conductivity. Or use, as an example, first the thin ion-exchange layer that is applied to the porous support layer to solve the existing problem. The impact that production techniques such as dip coating, spin coating, and plasma polymerization [32,39] have on the making of composite membranes is very high. Further, such interactions have a practical significance in the optimization of ion-selective membranes for batteries and solutions to minimize the gas crossover and improve the ionic conductivity. Another usefulness of polymer doping is reducing the permeability of active materials through the membrane, enhancing ionic conductivity, and elevating thermal, dimensional, and oxidative stability. Table 3.3 contains other selected examples of membranes available in the literature, which include ion-exchange membranes, porous membranes, and composite membranes employed in flow batteries.

In many flow batteries, membranes are therefore an integral part, yet some designs do not incorporate membranes, such as certain flow batteries equipped with gas diffusion electrodes or other designs with two solid electrodes. These include membrane-discretionary approaches using immiscible redox electrolytes, which self-separate into two liquid phases, and the oil–water-type interfaces that thermal gels provide, while preventing the mass and ionic transport of the redox chemicals to the interface.

3.4.3 Circulating Pumps

The recirculation pumps power the electrolytes in and out of the storage tanks, as pointed out earlier. Electrolyte circulation is also required to distribute the electrolytes inside the electrochemical reactors (usually composed of cell stacks), which in turn allows the reaction of electrical energy to chemical energy in charge and discharge cycles by providing suitable valences to the electroactive species [33]. The type of pump features is determined by the pumping conditions in the flow battery system, among which the centrifugal ones are the most preferable, being rather effective and safe. But there are peristaltic and

TABLE 3.3 Examples of Ion Exchange, Porous and Composite Membranes for Flow Batteries

Type of Membrane	Membrane ID	Full Name	Classification	Refs.
Perfluorinated	Nafion 112 and 115	Sulfonated tetrafluoroethylene	CEMs	[35]
Perfluorinated	N/FC	Sulfonated tetrafluoroethylene/ fluorocarbon surfactant (potassium nonafluoro-1-butanesulfonate)	CEMs	[36]
Non-perfluorinated aromatic backbone	SPEEK/FCB-3	Sulfonated polyether ether ketone/ functionalized carbon black	CEMs	[40,49]
Non-perfluorinated	AF1-HNN5–50-X, AF1-HNN8–50-X	Commercial membranes from Aemion™	AEMs	[43]
Poly aryl ether	Polysulfone/SPEEK	Imidazolium-functionalized polysulfone/poly (ether ether ketone)	AIEMs	[44]
Sulfonated polyimide	PBI/SIO_2	Polybenzimidazole/silice	Porous	[50]

diaphragm ones that also fit very well into the application, especially for those who require a more accurate flow of the electrolyte or need to deal with the thicker gel-like or liquid electrolytes.

Primary considerations for the design of the circulating pumps include the employment of nonconductive, chemically stable, and noncorrosive materials that will not deteriorate in the submerged conditions, even when in contact with the electrolytes. Besides, these pumps should ensure a steady flow of the electrolyte, ensure that the designed pressure level within the system is achieved, and do so with as little power usage as possible for the better efficiency and performance of the flow battery system. Efficient operation of flow batteries depends on correct and regular selection and management of the circulating pumps because they determine the stability, capacity, and lifetime of the ESS.

3.5 CONCLUSIONS AND PERSPECTIVES

In flow batteries, materials range from electrode construction materials such as transition metals and conjugated organic molecules (quinones and anthraquinones) to advanced metal-ceramics or nanoparticles designed to enhance electrical current generation. Electrolytes, including aqueous and organic types, improve electron diffusion, facilitating efficient electron transfer between electrodes. These solutions often contain inorganic ions, organic solvents like THF, DMF, and DMSO, and organic carbonates with low electrochemical degradation. Separator membranes, typically made from synthetic polymeric materials like Nafion or fluorocarbon polymers for ion or cation exchange, are often reinforced with inorganic materials such as graphene and activated carbon. Corrosion-resistant circulation pumps regulate electrolyte flow within the battery, ensuring optimal energy generation. However, for flow batteries to be fully utilized in energy applications—whether in transportation, industrial, or domestic energy supply—further improvements in materials and chemicals are needed. Economically effective flow batteries must be developed to ensure long-term practical use in these sectors.

REFERENCES

1. P. Arévalo-Cid, P. Dias, A. Mendes, J. Azevedo, Redox flow batteries: A new frontier on energy storage, *Sustain. Energy Fuels* 5, 2021, 5366–5419.
2. P. Linnik, V. Osadchyi, N. Osadcha, R. Linnik, Redox potential as an important characteristic of the chemical and biological state of surface waters (review), *Chem. Ecol.* 39, 2023, 640–672.
3. K. Lourenssen, J. Williams, F. Ahmadpour, R. Clemmer, S. Tasnim, Vanadium redox flow batteries: A comprehensive review, *J. Energy Storage* 25, 2019, 100844.
4. H. Zhang, C. Sun, M. Ge, Review of the research Status of cost-effective zinc–iron redox flow batteries, *Batteries* 8, 2022, 202.
5. N. Kocyigit, M. Gencten, M. Sahin, Y. Sahin, Chrome and cobalt-based novel electrolyte systems for redox flow batteries, *Int. J. Energy Res.* 44, 2020, 8014–8023.
6. P. Symons, Quinones for redox flow batteries, *Curr. Opin. Electrochem.* 29, 2021, 100759.
7. R. Zhang, H. Zhou, P. Sun, Q. Ma, M. Lu, H. Su, W. Yang, Q. Xu, Research progress on nanoparticles applied in redox flow batteries, *Battery Energy* 1, 2022, 20220023.
8. C.G. Cannon, P.A.A. Klusener, N.P. Brandon, A.R.J. Kucernak, Aqueous redox flow batteries: Small organic molecules for the positive electrolyte species, *ChemSusChem* 16, 2023, e202300303.
9. J. Ma, S. Rong, Y. Cai, T. Wang, Z. Han, Y. Ji, Aqueous organic redox-targeting flow batteries with advanced solid materials: Current status and future perspective, *Sustainability* 15, 2023, 15635.
10. Y. Matsuda, M. Morita, Organic electrolyte solutions for rechargeable lithium batteries, *J. Power Sources* 20, 1987, 273–278.
11. L. Gubler, Membranes and separators for redox flow batteries, *Curr. Opin. Electrochem.* 18, 2019, 31–36.
12. C. Zhang, Z. Yuan, X. Li, Designing better flow batteries: An overview on fifty years' research, *ACS Energy Lett.* 9, 2024, 3456–3473.
13. J. Li, M. Al-Yasiri, H. Pham, J. Park, Redox flow batteries, In Sabu Thomas, Didier Rouxel, Nandakumar Kalarikkal, Bicy Kottathodi and Hanna J. Maria (eds), *Advanced Materials for Battery Separators*, Elsevier, 2024, pp. 327–347.
14. S. Sagadevan, M.R. Johan, A.R. Marlinda, O. Akbarzadeh, K. Pandian, M.M. Shahid, F. Mohammad, J. Podder, Background of energy storage, In Mohammad Khalid, Numan Arshid, Nirmala Grace (eds), *Advances in Supercapacitor and Supercapattery: Innovations in Energy Storage Devices*, Elsevier, 2020, pp. 1–26.
15. V.M. Ortiz-Martínez, L. Gómez-Coma, G. Pérez, A. Ortiz, I. Ortiz, The roles of ionic liquids as new electrolytes in redox flow batteries, *Sep. Purif. Technol.* 252, 2020, 117436.
16. S. Aberoumand, P. Woodfield, B. Shabani, D.V. Dao, Advances in electrode and electrolyte improvements in vanadium redox flow batteries with a focus on the nanofluidic electrolyte approach, *Phys. Rep.* 881, 2020, 1–49.
17. R. Wang, Y. Li, Carbon electrodes improving electrochemical activity and enhancing mass and charge transports in aqueous flow battery: Status and perspective, *Energy Storage Mater.* 31, 2020, 230–251.
18. Z. He, Y. Lv, T. Zhang, Y. Zhu, L. Dai, S. Yao, W. Zhu, L. Wang, Electrode materials for vanadium redox flow batteries: Intrinsic treatment and introducing catalyst, *Chem. Eng. J.* 427, 2022, 131680.
19. J. Vázquez-Galván, C. Flox, J.R. Jervis, A.B. Jorge, P.R. Shearing, J.R. Morante, High-power nitrided TiO_2 carbon felt as the negative electrode for all-vanadium redox flow batteries, *Carbon* 148, 2019, 91–104.
20. A. Parasuraman, T.M. Lim, C. Menictas, M. Skyllas-Kazacos, Review of material research and development for vanadium redox flow battery applications, *Electrochim. Acta* 101, 2013, 27–40.

21. Y.S. Meng, V. Srinivasan, K. Xu, Designing better electrolytes, *Science* 378, 2022, 3750.
22. C. Choi, S. Kim, R. Kim, Y. Choi, S. Kim, H.Y. Jung, J.H. Yang, H.T. Kim, A review of vanadium electrolytes for vanadium redox flow batteries, *Renew. Sustain. Energy Rev.* 69, 2017, 263–274.
23. M. Skyllas-Kazacos, F. Grossmith, Efficient vanadium redox flow cell, *JES*. 134, 1987, 2950–2953.
24. Y. Toshimitsu, Y. Katayama, T. Miura, Electrode reactions of ruthenium–bipyridine complex in amide-type ionic liquids, *Electrochim. Acta* 82, 2012, 43–47.
25. K. Xu, Li-ion battery electrolytes, *Nat. Energy* 6, 2021, 763.
26. Y. Liu, Y. Niu, X. Ouyang, C. Guo, P. Han, R. Zhou, A. Heydari, Y. Zhou, O. Ikkala, G.A. Tigranovich, C. Xu, Q. Xu, Progress of organic, inorganic redox flow battery and mechanism of electrode reaction, *Nano Res. Energy* 2, 2023, e9120081.
27. M. Shoaib, P. Vallayil, N. Jaiswal, P.I.V. Suba, S. Sankararaman, K. Ramanujam, V. Thangadurai, Advances in redox flow batteries – A comprehensive review on inorganic and organic electrolytes and engineering perspectives, *Adv. Energy Mater.* 14, 2024, 2400721.
28. L. Briot, M. Petit, Q. Cacciuttolo, M.C. Pera, Aging phenomena and their modelling in aqueous organic redox flow batteries: A review, *J. Power Sources* 536, 2022, 231427.
29. D.G. Kwabi, Y. Ji, M.J. Aziz, Electrolyte lifetime in aqueous organic redox flow batteries: A critical review, *Chem. Rev.* 120, 2020, 6467–6489.
30. A.Z. Weber, M.M. Mench, J.P. Meyers, P.N. Ross, J.T. Gostick, Q. Liu, Redox flow batteries: A review, *J. Appl. Electrochem*. 41, 2011, 1137–1164.
31. G.L. Soloveichik, Flow batteries: Current status and trends, *Chem. Rev.* 115, 2015, 11533–11558.
32. W. Wang, Q. Luo, B. Li, X. Wei, L. Li, Z. Yang, Recent progress in redox flow battery research and development, *Adv. Funct. Mater.* 23, 2013, 970–986.
33. L.F. Arenas, F.C. Walsh, C.P. de León, General aspects and fundamentals of flow batteries, In Christina Roth, Jens Noack, Maria Skyllas-Kazacos (eds), *Flow Batteries: From Fundamentals to Applications*, 2023, pp. 69–97.
34. C.H.L. Tempelman, J.F. Jacobs, R.M. Balzer, V. Degirmenci, Membranes for all vanadium redox flow batteries, *J. Energy Storage* 32, 2020, 101754.
35. B. Jiang, L. Wu, L. Yu, X. Qiu, J. Xi, A comparative study of Nafion series membranes for vanadium redox flow batteries, *J. Membr. Sci*. 510, 2016, 18–26.
36. X. Teng, J. Dai, J. Su, G. Yin, Modification of Nafion membrane using fluorocarbon surfactant for all vanadium redox flow battery, *J. Membr. Sci*. 476, 2015, 20–29.
37. J. Grosse Austing, C. Nunes Kirchner, L. Komsiyska, G. Wittstock, Layer-by-layer modification of Nafion membranes for increased life-time and efficiency of vanadium/air redox flow batteries, *J. Membr. Sci*. 510, 2016, 259–269.
38. S. Jerzy, Z. Yang, P. Wiecí, J. Kacprzy´nska, K. Kacprzy´nska-Gołacka, M.T. Tsehaye, R.A. Tufa, R. Berhane, F. Deboli, K.A. Gebru, S. Velizarov, Modified membranes for redox flow batteries—A review, *Membranes* 13, 2023, 777.
39. A. Ashok, A. Kumar, A comprehensive review of metal-based redox flow batteries: Progress and perspectives, *GCLR* 17, 2024, 1.
40. X. Lou, B. Lu, M. He, Y. Yu, X. Zhu, F. Peng, C. Qin, M. Ding, C. Jia, Functionalized carbon black modified sulfonated polyether ether ketone membrane for highly stable vanadium redox flow battery, *J. Membr. Sci*. 63, 2022, 120015.
41. S.L. Huang, H.F. Yu, Y.S. Lin, Modification of Nafion® membrane via a sol-gel route for vanadium redox flow energy storage battery applications, *J. Chem*. 2017, 2017, 4590952.
42. G.J. Hwang, S.W. Kim, D.M. In, D.Y. Lee, C.H. Ryu, Application of the commercial ion exchange membranes in the all-vanadium redox flow battery, *J. Ind. Eng. Chem*. 60, 2018, 360–365.
43. E. Lallo, A. Khataee, R.W. Lindström, Vanadium redox flow battery using AemionTM anion exchange membranes, *Process* 10, 2022, 270.

44. X. Yan, C. Zhang, Y. Dai, W. Zheng, X. Ruan, G. He. A novel imidazolium-based amphoteric membrane for high-performance vanadium redox flow battery, *J. Membr. Sci*. 544, 2017, 98–107.
45. X.G. Jian, C. Yan, H.M. Zhang, S.H. Zhang, C. Liu, P. Zhao, Synthesis and characterization of quaternized poly(phthalazinone ether sulfone ketone) for anion-exchange membrane, *Chin. Chem. Lett*. 18, 2007, 1269–1272.
46. P. Arora, Z. Zhang, Battery separators, *Chem. Rev*. 104, 2004, 4419–4462.
47. M. Gencten, Y. Sahin, A critical review on progress of the electrode materials of vanadium redox flow battery, *Int. J. Energy Res*. 44, 2020, 7903–7923.
48. P. Leung, A.A. Shah, L. Sanz, C. Flox, J.R. Morante, Q. Xu, M.R. Mohamed, C. Ponce de León, F.C. Walsh, Recent developments in organic redox flow batteries: A critical review, *J. Power Sources* 360, 2017, 243–283.
49. J. Li, Q. Zhang, S. Peng, D. Zhang, X. Yan, X. Wu, X. Gong, Q. Wang, G. He, Electrospinning fiberization of carbon nanotube hybrid sulfonated poly (ether ether ketone) ion conductive membranes for a vanadium redox flow battery, *J. Membr. Sci*. 583, 2019, 93–102.
50. X. Che, H. Zhao, X. Ren, D. Zhang, H. Wei, J. Liu, X. Zhang, J. Yang, Porous polybenzimidazole membranes with high ion selectivity for the vanadium redox flow battery, *J. Membr. Sci*. 611, 2020, 118359.

CHAPTER 4

Materials for Flow Battery

Chemical Structures, Compositions, and Chemistries

Suhrid Sayantha Aniv and Md. Mominul Islam

4.1 INTRODUCTION

The technology of flow batteries is critically important as a large-scale energy storage system that plays a phenomenal role in the expansion of renewable energy. Flow batteries convert chemical energy directly to electrical energy from electroactive materials. Since the first proposal of the flow batteries in the early 1880s, the development has undergone many drastic iterations [1]. The highlighted attraction of this technology is due to the design flexibility, high scalability, and decoupling of energy, which have resolved issues like discontinuity, instability, and uncontrollability of renewable energy. This development has led to the transfer of higher numbers of electrons and eventually increased cell potential that is unparalleled in other battery alternatives [2]. Depending on the configuration and phases of redox reactions, they are categorized into different types (Figure 4.1). However, recent iterations of these batteries mostly contain the redox-active chemicals in a liquid electrolyte, ultimately known as redox flow batteries (RFBs) [3]. The redox reactions in RFBs take place in fluids, and hence, a large amount of solvent is needed for the dissolution of the redox species. Besides the assembly of different components, the functionality involving the efficiency, cyclability, and stability of flow batteries is completely laid on the inherent properties of electrode materials, the chemistries of redox species storing charges, and the electrolytic media supporting the efficient charging–discharging cycles [3]. The environmental friendliness and capital and operational costs of RFBs, which may be well-suited by exploring and learning the chemistries of materials, are the main concerns in designing practical flow batteries. This chapter focuses on the materials used in different phases, their fundamental structures, and the associated chemistries involving the materials and the component variations. Attention is also given to the prospects and future direction of research on promising materials of RFBs.

DOI: 10.1201/9781003506379-4

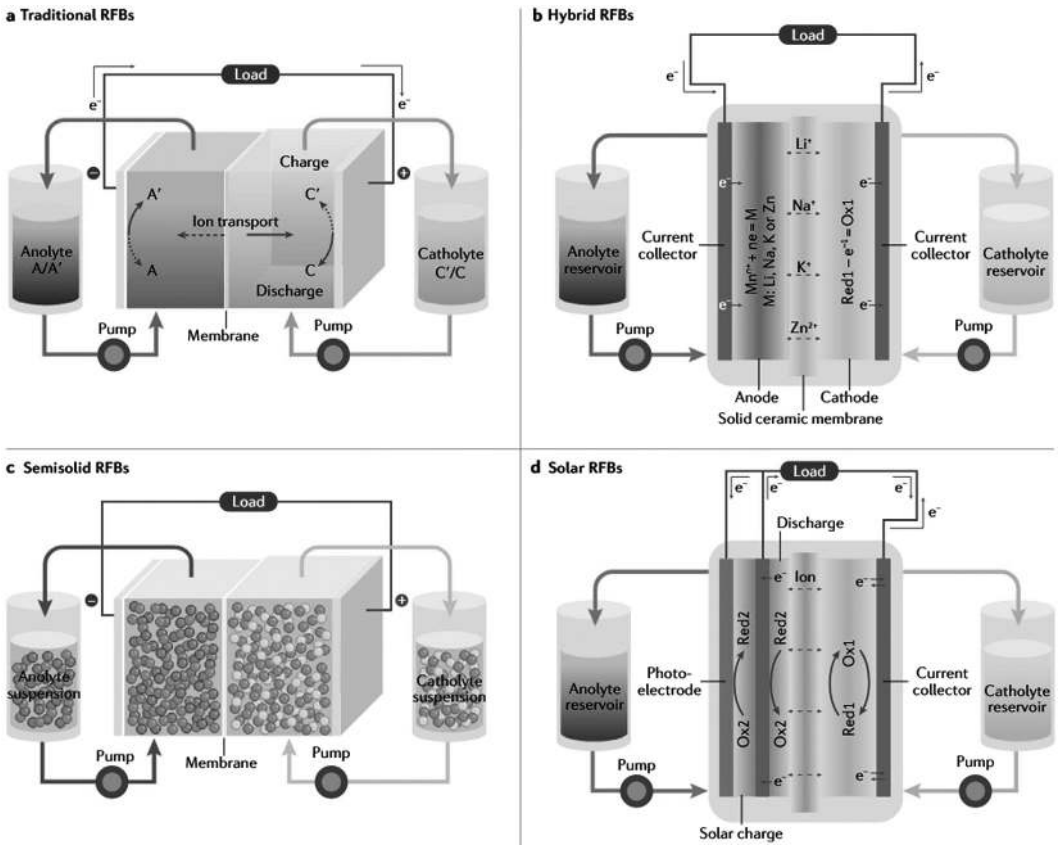

FIGURE 4.1 (a) A typical RFB with redox species in liquid electrolytes, (b) a hybrid RFB with different metal electrodes and appropriate electrolytes, (c) a semisolid RFB with solid species and carbon black suspended in liquid electrolytes, and (d) a solar RFB with a photoelectrode. (Adapted with permission from [4], Copyright 2022, Nature.)

4.2 STRUCTURAL AND FUNCTIONAL COMPONENTS

4.2.1 Common Structural Features

The working principle of RFBs is distinctly different from that of conventional and Li-ion batteries. Structurally, the RFBs comprise various components, including electrodes, bipolar plates, current collectors, energy-bearing redox couples, electrolytes for dissolving redox-active materials, an ion-conductive membrane, and two external tanks [4], as schematically depicted in Figure 4.1. RFBs store electrical energy in these redox couples with distinct redox potentials dissolved or suspended in the external electrolyte tanks. The tanks containing negative and positive electrolytes are called the anolyte (negolyte) and catholyte (posolyte), respectively [5]. A cell stack containing a pair of porous carbon electrodes is separated by an ion-conductive membrane with high charge-carrier selectivity. The redox reactions occur on this stack, where the electrolytes are circulated by pumps to flow through the electrodes. The separator membrane, being high charge-carrier selective, helps to balance the charge transfer during charging and discharging [5]. The scaling of

the capacity is dependent on the available charges stored in the electrolyte tank, while the rate of charge transfer reactions determines the output of RFBs. This unique configuration enables design flexibility in the architecture of the RFBs, and various versions of the flow batteries are seen in practice [1].

4.2.2 Classifications of Flow Battery

The continuous pursuit of better flow batteries has led to the development of better battery chemistries, contemporary designs, and state-of-the-art materials that have helped to leap beyond conventional RFBs [6]. They have the advantage of design flexibility that helps the integration of other concepts into the flow system, such as metal deposition/dissolution [7], photoelectrochemical reactions [8], and solid intercalation chemistry [9]. These integrated combinations are adapted to the flow batteries, called hybrid RFBs, to increase energy density and metal deposition chemistry with low redox potentials and high capacity (Figure 4.1b) [4]. Figure 4.2 depicts the overall types of RFB systems. Depending on electrolytes, RFBs are broadly categorized into aqueous and nonaqueous systems [4]. Most of the studies are with aqueous systems. Nonaqueous RFBs, including conventional systems, ionic liquid (IL), and deep eutectic solvent (DES), are efficient electrolytes with a wider operating potential window [10].

Inorganic-based RFBs are mostly made of alkali metal salts due to their high theoretical capacitances and low redox potentials. Traditional aqueous alkali metal-based RFBs have limited working potential due to the corrosion of the metals. This can be minimized by using organic (nonaqueous) electrolytes [2]. Suspension-based RFBs (Figure 4.1c) are a considerably new concept featuring the usual flow characteristics. The energy density is enhanced by suspending high-energy-dense solid active powders and conductive additives, where $LiCoO_2$, $LiFePO_4$, $LiMn_2O_4$, and $Li_4Ti_5O_{12}$ are widely explored [2,4]. The structure of the suspension comprises a solvation complex that is formed by surrounding the solute species with a concentric shell of solvent species. This approach breaks through the solubility limit, and the redox chemistries are broadened to a wide range of flowable solid electroactive species [11]. Taking advantage of the design flexibility of RFBs,

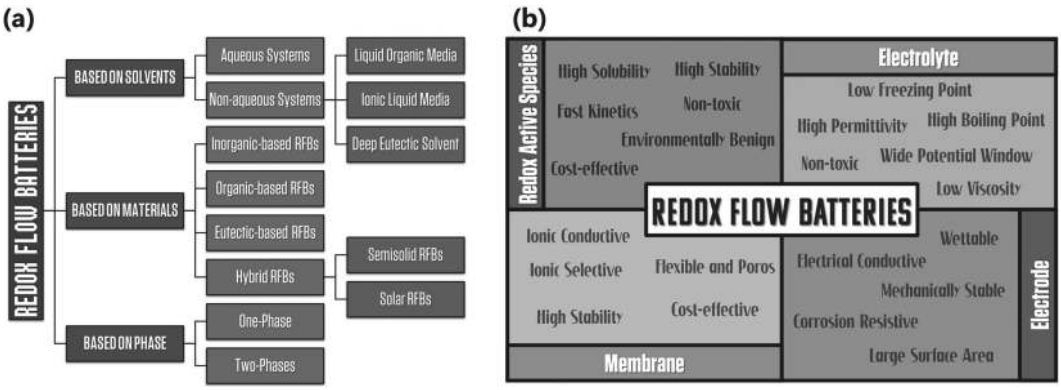

FIGURE 4.2 (a) Overall classifications of RFBs and (b) characteristics of the materials required for RFBs.

the semiconductor photoelectrode has been integrated into the technology, named solar RFBs [12] (Figure 4.1d). The general architecture of solar RFBs has one photoelectrode that absorbs solar energy to generate photoexcited carriers for the reactions of redox species [4]. Photoelectrodes with narrow band gap energy are remarkably effective since more photons can be harvested.

4.2.3 Design Philosophy of RFBs

The performance matrices of RFBs depend on the intrinsic properties of the materials used in the aforementioned components (Figure 4.2b). Out of different features, the performance of advanced RFBs is essentially governed by the four main components:

- The capacitance is dependent on the solubility and charge transfer numbers of the redox-active materials.
- The cell potential is governed by the potential difference between the active materials used in the cathode and anode, as usual in other electrical energy storage systems.
- Reaction kinetics of active species, structure of electrodes, and ionic conductivity of membranes affect the current density.
- Efficiency, cycle life, and stack cost are governed by all functional components of RFBs.

The materials of RFBs should have the following basic characteristics [2,4]: (1) high solubility (concentration ≥ 1.0 M), (2) reversible redox activity and stability, (3) fast kinetics with a long lifetime, (4) scalable synthesis with low cost, and (5) environmental sustainability with recycling of the resources. Like the redox-active materials, the electrolytes featured in RFBs should maintain special properties for providing an optimized performance [4,6], namely, low freezing and high boiling points, a wide working potential window, lower solvent viscosity for higher ionic conductivity, higher relative permittivity facilitating higher solubility, and a nontoxic and eco-friendly nature.

The membrane materials with (1) high ionic selectivity, (2) high ionic conductivity for the reduction of ohmic polarization, (3) high chemical stability, (4) cost-effectiveness, and (5) mechanical properties, like flexibility and porosity, are the choice of designers. The electrodes, also complying with performance, require characteristics, including high electrical conductivity, high mechanical stability, a large surface area with active sites, resistivity against corrosion, and wetting behavior while designing advanced RFBs [2,6].

4.3 MATERIAL ARCHITECTURE OF FLOW BATTERIES

The nutshell of the indispensable features of different components of RFBs is highlighted in Figure 4.2. The detailed knowledge of their underlying structural features as described below is important in fabricating practically applicable RFBs. The main concern for developing materials used for large-scale applications is their chemistries along with other factors, including redox potential, solubility, electrochemical reversibility, cost, availability, and toxicity.

4.3.1 Active Redox Species

4.3.1.1 Inorganic Active Species

Early development of the chemistries of RFBs has been truly focused on inorganic materials, as they offer good chemical and thermal stabilities with the capability of rebalancing after crossover and fast reaction kinetics in aqueous solutions. The most used active species in the RFB systems usually have simple electrode reactions with reversibility, high volumetric current densities with faradaic efficiency, and a potential window of the redox couple within the decomposition range of the electrolytes. Ions with high oxygen affinity or containing oxygen, for example, MnO_4^-, Cr^{3+} are avoided for simplifying hydrogen management. However, materials with multiple oxidation states are advantageous for significant energy storage [13].

Vanadium ions in different oxidation states (V^{2+}, V^{3+}, V^{4+}, and V^{5+}) are one of the most popular inorganic materials that are used in RFB systems since they have high energy density, good reversibility, and long cycle life. All-vanadium RFB (VFB) and mixed acid vanadium RFBs are also popular. The potential membrane crossover and high cost prevent the proper potential of the material [14]. Iron and chromium ions have higher theoretical energy density and potential for improved membrane selectivity; as a result, they have been used at the same time in iron-chromium RFBs (ICBs) for two one-electron redox couples Fe^{2+}/Fe^{3+} as catholyte and Cr^{2+}/Cr^{3+} in hydrochloric acid solution as anolyte. However, the kinetics of the anodic reaction is slow, restricting the practical implementation of ICBs [15]. By substituting the Cr^{2+}/Cr^{3+} anolyte with a V^{2+}/V^{3+} redox couple, an iron-vanadium RFB (IVB) system has been established. This substituted vanadium anode showed the ability to overcome the sluggish kinetics of the chromium system, elevating energy efficiency (EE) without any catalyst loading at ambient conditions [16]. Zinc RFBs can decouple energy and power storage, along with their potential for long cycle life and minimal maintenance, making them an attractive choice for grid-scale applications. Zinc and bromine ions bring the advantages of high energy density, good reversibility, and lower cost, but challenges like bromine vaporization, corrosiveness, and zinc dendrite formation remain to raise concerns for the developments [13].

Polyoxometalates (POMs) are a structurally diverse class of compounds ideal for redox-active materials in RFBs. These compounds consist of d^0 metal-centered polyhedra linked by oxygen atoms at their vertices. POMs are highly suitable for energy storage due to their ability to undergo reversible multi-electron redox processes, for example, vanadium-modified polyoxotungstate, A-α-$K_6HSiV_3W_{12}O_{40}$, and so on. The aqueous RFB system shows higher coulombic efficiencies (CEs), while the nonaqueous system operates at a higher voltage [17].

4.3.1.2 Organic Active Species

Metal complexes and organometallic compounds belong to this group, offering the metal center and chelating ligands for the necessary redox reaction of RFBs. Organic electroactive species have features like lower cost, better solubility, tunable redox properties, and crossover transport via the introduction of various substituents [15]. Some important standards are required to maintain while designing redox-active organic molecules, such as the good distribution of redox centers (i.e., C, N, O, S) in the molecular structure to

stabilize the radical, chemical, and thermal stability under operating potentials, and the formation of conjugated or resonance structures in any electrolytes, whereas the addition of electron-donating groups to form organic radicals or the introduction of functional groups with high steric hindrance in nonaqueous electrolytes [4].

In battery formulation, they can be used in both aqueous and nonaqueous systems. The aqueous electrolytic RFB systems use hydrophilic functional groups like hydroxyl, quaternary ammonium, and sulfonate-based groups that improve the solubility of the organic active materials [18]. On the contrary, there are two groups of redox pairs in nonaqueous organic RFBs: metal-based and metal-free redox pairs. Among the metals, V is still the attractive one due to its variable oxidation states, offering multiple faradic reactions as expressed later (Table 4.4).

Monodentate ligands such as dimethyl sulfoxide and *N*,*N*-dimethylformamide (DMF) are mostly used. Double-oxygen (acetylacetone (acac), hexafluroacetylacetone, dipivaloylmethane), double-nitrogen (2,2′-bipyridine (bpy)), and double-sulfur (maleonitriledithiolene) are the common bidentate ligands used in RFBs. However, acac and bpy are the most frequently used because they are the simplest, forming strong coordination bonds with many transition metals. The electron transfer in metal-free redox pairs involves the formation of stable radicals by losing or gaining electrons, developing the redox potential of the pair [10]. Metal-free redox species, that is, organic molecules, usually involve ILs or DES. However, the quinone/hydroquinone redox couple can undergo a fast two-electron reaction in aqueous solution [15]. The potential of quinone/hydroquinone varies from –0.80 V to +0.87 V via changing their molecular structures and solution acidity. These redox couples can be used as active materials for both aqueous catholyte and anolyte in RFBs [21].

4.3.1.3 Highly Soluble Species

Designing inorganic molecules with high solubility can be achieved through routine methods like pH tuning or species screening. Heavy metal ions are soluble at low pH levels but precipitate as insoluble hydroxides if pH is increased. Therefore, most RFBs are operated in concentrated acidic conditions, ensuring the maximum solubility of the inorganic species [1]. Employing low-melting liquid redox species directly without using additional solvents can be an innovative way to mimic the high solubility of the active material. Mixing solid redox species with certain supporting salts can lead to the formation of liquid eutectics, another feasible way to achieve high concentration [2].

Solubilizing organic molecules in an aqueous system requires a higher polarity with hydrophilic functional groups and local structure asymmetry of substituted functional groups. Nonaqueous systems also follow similar principles [4]. The dielectric and dissociation constants of metal-organic complexes with nonaqueous solvents should be higher because the lower value of these two constants leads to lower electrolyte conductivity compared to aqueous systems. However, implementing supporting electrolytes such as tetraalkylammonium salts can mitigate this problem [15].

4.3.2 Designing Electrolytes

Electrolytes are the most important components of advanced RFBs since the overall performance of RFBs is truly dictated by the electrolytes. Indeed, the reaction kinetics of a

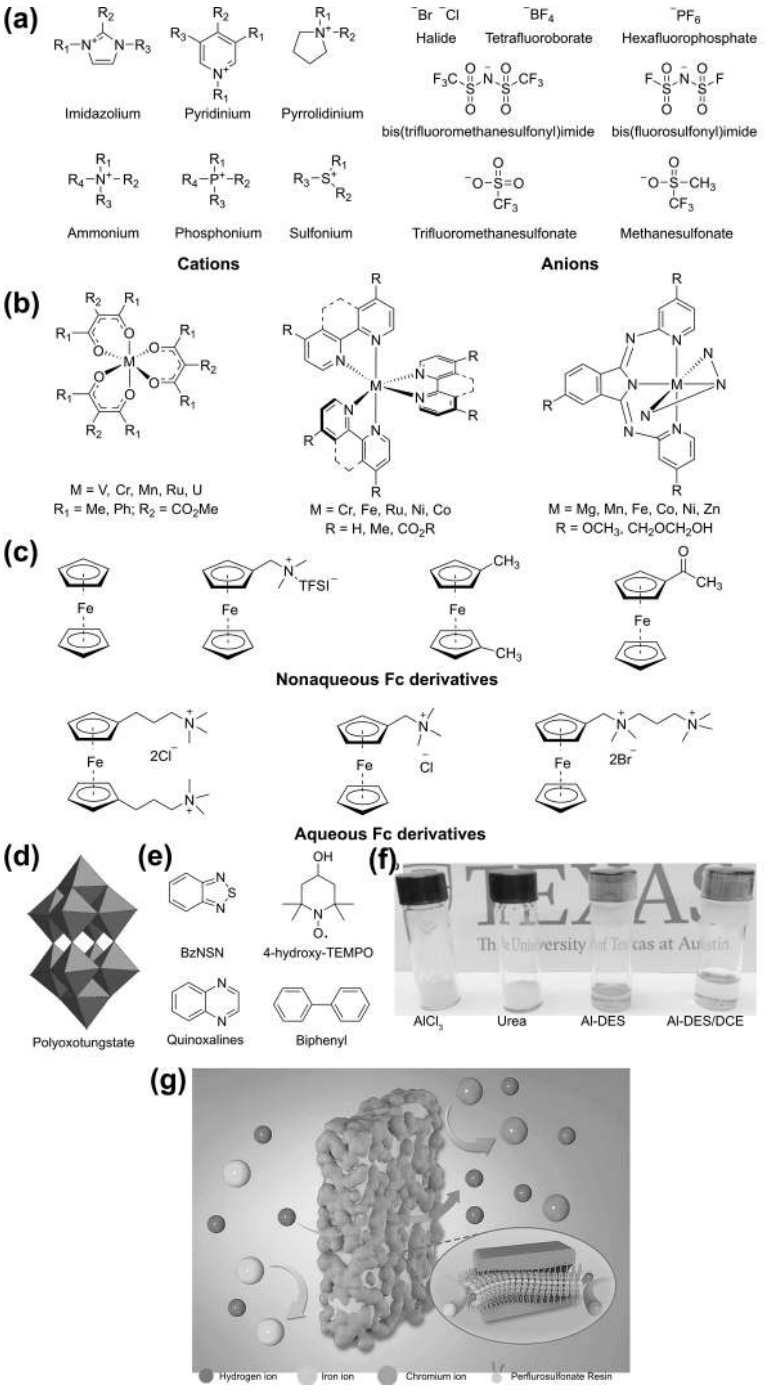

FIGURE 4.3 Chemical structures of (a) commonly used ILs, (b) metal-ligand complexes, (c) metallocene-based redox species, (d) polyoxotungstate, and (e) redox-active molecules with polymeric and low molecular weights. (f) Images of the Al-DES/DCE system. (Adapted with permission from [19], Copyright 2017, Wiley.) (g) Transmission mechanism of a composite membrane. (Adapted with permission from [20], Copyright 2022, MDPI.)

material is the inherent property of redox species, but the electrolyte composition plays a vital role in the performance of RFBs (see Table 4.1). The redox species and solvent must have stable interactions to maximize solubility, ensuring the longevity of the flow battery systems [27]. The high concentration of the redox species facilitates achieving high theoretical energy density, but it might undesirably increase the viscosity of the fluid and hence decrease the ionic conductivity and cell performance [6]. In this regard, the temperature window is another key parameter for the performance of the flow battery. The wider temperature window of the electrolytes will ensure the best performance out of RFBs.

4.3.2.1 Aqueous Electrolytes

The early development of RFBs was focused on inorganic materials; the aforementioned aqueous electrolyte systems were a go-to choice. Aqueous flow battery systems have features like higher power density, lower electrolyte resistance, better safety, lower cost, and better environmental friendliness [21]. However, the working potential of aqueous RFBs is heavily constrained by the water splitting.

VFBs use vanadium sulfate redox active species in sulfuric acid electrolyte, where V^{2+}/V^{3+} is anolyte and V^{5+}/V^{4+} is catholyte [27]. The concentration of V^{5+} (vanadate ion) varies from 5.0 M down to 2.0 M between the temperature windows of 25°C–50°C. On the contrary, V^{4+} (vanadyl ion) loses its mobility as the electrolyte concentration increases. Therefore, the sulfate-chloride-mixed electrolytes are used to enhance the solubility of vanadium up to 2.5 M. Similarly, the mixed salts of a ratio of 1:1 of VBr_3 and VBr_4 in aqueous HBr as an electrolyte help to increase the vanadium concentration to 4.0 M [32]. Since the redox potential of the metal ions is affected by chelation, the kinetics of ICB can also be improved by implementing Fe diethylenetriaminepentaacetic acid (FeDTPA) and Cr 1,3-diaminopropanetetraacetic acid (CrPDTA) containing electrolytes (Figure 4.4c). The addition of indium chloride ($InCl_3$) to the electrolyte of ICB is another way of increasing the performance. In^{3+} ions effectively inhibit the hydrogen evolution reaction (HER), accelerating the kinetics of Fe^{2+}/Fe^{3+} and Cr^{3+}/Cr^{2+} redox reactions (Figure 4.4d) [18].

A high-concentration aqueous solution of polysulfide halide is a popular option as a redox-active material. Bromine and iodine are used as catholytes in the form of polybromide and polyiodide anions. However, compared to the toxicity of bromine, iodine is a better choice that also comes with a high volumetric capacity of electrolytes and fast kinetics.

TABLE 4.1 Commonly Used Electrolytes in RFBs

Redox System	Electrolyte/Solvent	Cell Potential V	Current Density mA cm^{-2}	References
All-vanadium	Sulfuric acid	1.60	10–30	[22]
Vanadium-bromine	Aqueous HBr + HCl	1.40	20	[23]
Zinc-bromine	$ZnBr_2$ in Br_2 + KCl	1.60	15	[24]
Zinc-cerium	ZnO in methane sulfonic acid	2.45	50	[24]
Iron-chromium	Aqueous HCl	1.18	21.5	[24]
Bromine-polysulfide	NaBr in Br_2 + Na_2S	2.10	40	[25]
$[Ru(acac)_3]$	Acetonitrile	1.76	0.28	[26]

As an example, KI (6.0 M) and K_2S_2 (3.0 M) are used in polysulfide-iodide RFB systems as electrolytes. High electrolyte concentration results in high conductivity, fast kinetics, and high volumetric capacity of electrolytes in the aforementioned polysulfide-based RFBs [21].

4.3.2.2 Nonaqueous Electrolytes

Despite all the benefits of aqueous flow battery systems, the main culprit restraining their performance is the working potential window, which is limited by HER and oxygen evolution reaction (OER). Table 4.2 depicts the features of nonaqueous solvents used in the RFB system. Nonaqueous electrolytes have become attractive choices, as not only can the working potential window be increased, but they also have advantages over the range of temperature window, cell voltage, and energy density compared to the aqueous RFBs. The tailoring nature of organic solvents, the superior characteristics of ILs, or the rational screening of eutectic solvents give an edge over aqueous RFBs, broadening the spectrum of applications.

4.3.2.2.1 Organic Molecular Solvents Acetonitrile, tetrahydrofuran, γ-valerolactone, dichloromethane, 1-propanol, acetone, propylene carbonate, *N*-methyl-2-pyrrolidone, DMF, toluene, hexane, methanol, ethanol, etc., are some of the extensive list of nonaqueous electrolytes used in RFBs. Tetrahydrofuran and 1-propanol have a total temperature

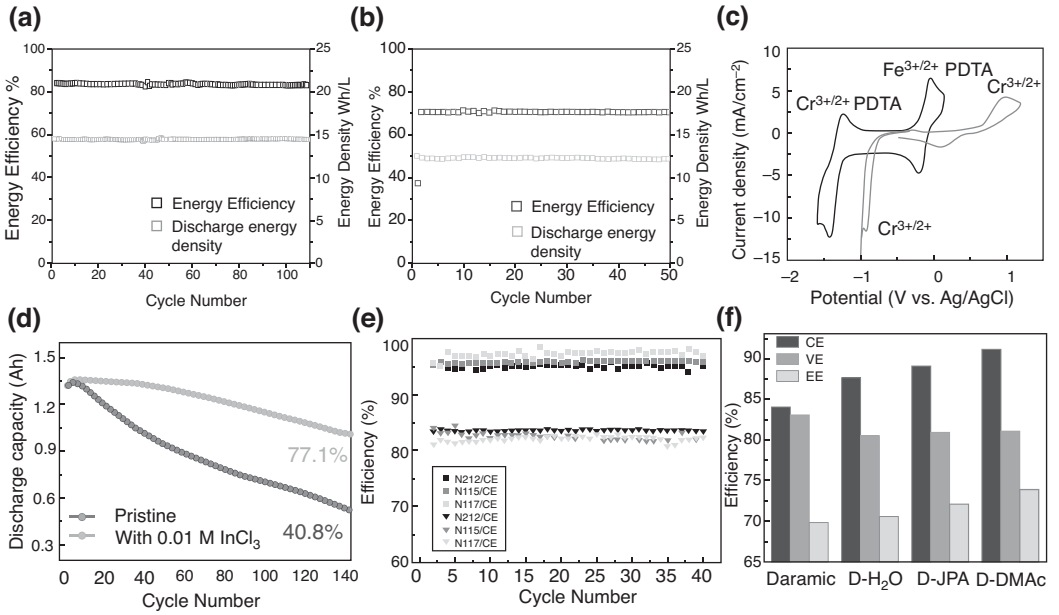

FIGURE 4.4 Cyclic performance of IVB using (a) Nafion 212 and (b) Daramic at 50 mA cm^{-2}. (Adapted with permission from [28], Copyright 2012, Wiley.) (c) CVs of $CrCl_3/FeCl_2$ and CrPDTA/FeDTPA at 100 mV s^{-1}. (Adapted with permission from [29], Copyright 2020, ACS.) (d) Discharge capacity curves of ICB. (Adapted with permission from [30], Copyright 2021, Elsevier.) (e) EE and CE profiles of ICBs assembled with three membranes. (Adapted with permission from [31], Copyright 2019, Wiley.) (f) CEs, voltaic efficiencies (VE), and EEs of membranes assembled ICBs at 80 mA cm^{-2}. (Adapted with permission from [20], Copyright 2022, MDPI.)

TABLE 4.2 Features of Nonaqueous Solvents for RFBs [33]

	T_f	T_b	Temperature Window		E_{red}	E_{ox}	Potential Window
Electrolyte	**°C**	**°C**	**°C**	ε_r	**V vs SHE**	**V vs SHE**	**V**
Nitromethane	−29	101	130	36.7	−1.0	2.9	3.9
γ-Valerolactone	−31	208	239	42.0	−2.8	5.4	8.2
Methoxyacetonitrile	−35	120	155	36.0	−2.5	3.2	5.7
γ-Butyrolactone	−43	204	247	39.1	−2.8	5.4	8.2
Acetonitrile	−44	82	126	35.9	−2.6	3.5	6.1
Trimethyl phosphate	−46	197	243	21.0	−2.7	3.7	6.4
Propylene carbonate	−49	242	291	64.9	−2.8	3.8	6.6
Nitroethane	−90	115	205	28.0	−1.1	3.2	4.5
3-Methoxypropionitrile	−57	165	222	36.0	−2.5	3.3	5.8

T_f: freezing point; T_b: boiling point; ε_r: relative permittivity of pure solvent and data.

window of 174°C and 223°C, respectively; hence, their suitability for the development of nonaqueous RFBs. Acetonitrile and γ-valerolactone have a wide potential window of ca. 6.1 V and 8.2 V, respectively. Dichloromethane has low viscosity with low relative permittivity, whereas DMF has high viscosity and relative permittivity [10]. All these organic solvents need to be harmless; therefore, toxicity and flammability are two valid parameters for devising RFBs. The lower value of vapor pressure signifies a lower possibility of solvent intake, reducing the toxicity and flammability [10].

The first nonaqueous RFBs had ruthenium complex-based systems as active species, such as $[Ru(bpy)_3]^{2+}/[Ru(bpy)_3]^{3+}$ complexes [34] and $Ru(acac)_3$-based systems [35]. The electrolyte is composed of acetonitrile and tetraethylammonium tetrafluoroborate $\left(\left[TEA^+\right]\left[BF_4^-\right]\right)$, where the latter plays the role of supporting electrolyte. A nonaqueous RFB utilizing $[Co(bpy)_3]^{+}/[Co(bpy)_3]^{2+}$ (anolyte) and $[Fe(bpy)_3]^{2+}/[Fe(bpy)_3]^{3+}$ (catholyte) redox couples in a 0.5 M solution of $\left[TEA^+\right]\left[BF_4^-\right]$ in propylene carbonate and carbon-coated Ni-FeCrAl and Cu metal foam electrodes exhibited a practical operating voltage of >2.1 V and an EE of 85% with no loss of efficiency over 300 cycles [35].

4.3.2.2.2 Ionic Liquids ILs are another choice of material for any kind of electrochemical charge storage device. Organic molecular solvents have poor ionic conductivity and cyclic stability compared to mixed media. Inadequate ionic conductivity and mediocre cyclic stability of organic supporting electrolyte systems necessitate overcoming [10]. ILs generally have a wide electrochemical window, high ionic conductivity, and better thermal stability, making them suitable for high-temperature applications [36]. In addition, ILs offer some other great advantages, including enhancing cyclic stability, diffusion and conductivity, solubility of active species, etc., as supporting electrolytes [34]. Some of the common anions of ILs (see Figure 4.3) include tetrafluoroborate $\left(BF_4^-\right)$, bis(trifluoromethanesulfonyl) imide ($TFSI^-$), and hexafluorophosphate $\left(PF_6^-\right)$. Quaternary ammonium-based cations, such as tetrabutylammonium (TBA^+), tetraethylammonium (TEA^+), and 1-ethyl-3-methylimidazolium ($EMIm^+$) of ILs, have been used as supporting electrolytes of RFBs.

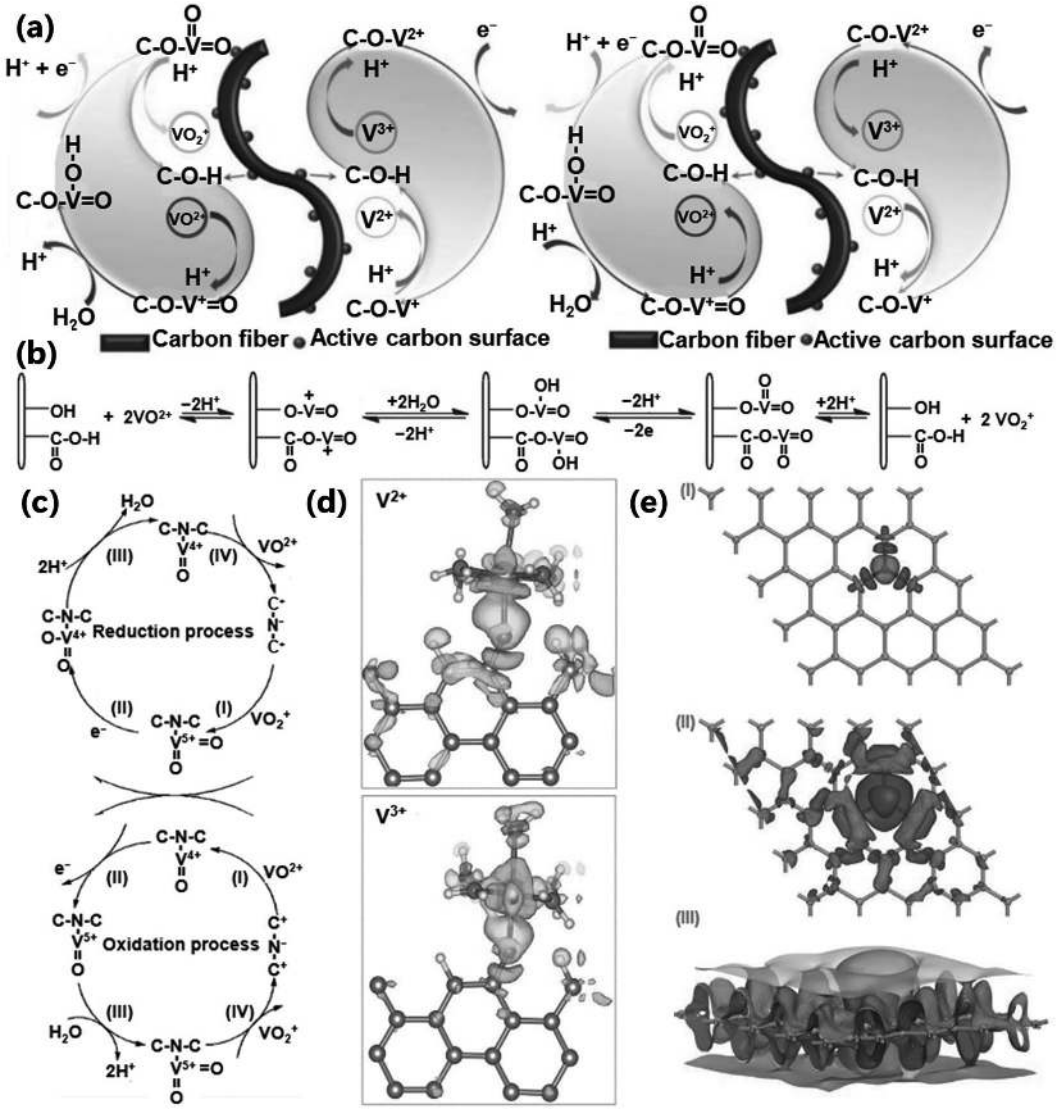

FIGURE 4.5 (a) Mechanisms of the redox reaction during the charging–discharging process. (Adapted with permission from [38], Copyright 2020, Elsevier.) Reactions occurring on the (b) O-doped (Adapted with permission from [39], Copyright 2013, Elsevier), and (c) N-doped electrode surfaces of VFB systems. (Adapted with permission from [40], Copyright 2013, ACS.) (d) Electron density difference maps of the inner-sphere structure of the V^{2+}/V^{3+} species (light grey- and dark grey parts represent the rise and fall of the electron density, respectively). (Adapted with permission from [41], Copyright 2017, RSC Publishing.) (e) Visualized electron density model of N-doped graphene and the structure where the carbon atom has been replaced by a nitrogen atom, with the isosurfaces (grey represents charge concentration and black represents charge depletion). (Adapted with permission from [42], Copyright 2016, Elsevier.)

TABLE 4.3 Constructions and Performances of Different Advanced RBFs

Redox System	Electrolyte/Solvent	Membrane	Electrode	Cell Potential V	Current Density mA cm^{-2}	CE %	VE %	EE %	Ref.
All-vanadium	Sulfuric acid	Nafion 115	Graphite felt	1.6	10–30	97		77	[22,43]
Vanadium-bromine	Aqueous HBr + HCl	Nafion 112	Carbon or graphite felt	1.4	20	74 (overall)			[23]
Zinc-bromine	$ZnBr_2$ in Br_2 + KCl	Microporous membrane	Carbon paper	1.6	15	95	86	78	[24,44]
Bromine-polysulfide	NaBr in Br_2 + Na_2S	Nafion 115 or 117	Activated carbon/ polyolefin pressed	2.1	40	77 (overall)			[24]
Zinc-cerium	ZnO in methane sulfonic acid	Nafion	Carbon plastic anode, platinized titanium mesh cathode	2.45	50	98			[24]
Iron-chromium	Aqueous HCl	Ion exchange membrane	Carbon felt	1.18	21	95	84	81	[24,45]
$[Ru(acac)_3]$	Acetonitrile	Undivided flow-through reactor	Graphite felt	1.76	0.28	5 (overall)			[26]
Benzophenone/DBB	Acetonitrile + $[TEA^+]$ $[TFSI^-]$			2.95	1	97	46	44	[46]
Quinoxaline derivatives/DBMMB	Propylene carbonate + $LiBF_4$	Nafion 117		2.4	0.06	70		37	[47]

4.3.2.2.3 Eutectic Media ILs might have a very wide potential window, but they are very expensive. This limitation can be overcome by featuring DESs in the RFB systems. DESs are an emerging material for designing RFBs with appealing features like low cost, high concentration of active species, nonflammability, potential biodegradability, and multi-electron transfer reactions. DESs are typically formed by mixing Lewis or Brønsted acids and bases at room temperature [2]. DESs and ILs share similarities, with anionic and cationic species having an asymmetric spatial configuration and delocalized charge, reducing lattice energy and lowering freezing points. The broad design space of DES-based electrolytes and their properties can be adjusted by rational screening of eutectic components or functional additives [6]. Their narrow potential window and high viscosity limit their widespread application; however, they have tailor-crafting ability, better ionic conductivity, and environmental friendliness.

4.3.3 Membranes or Separators

In RFBs, the membranes separate the cathode and anode compartments to prevent the mixing of the electrolytes while allowing the transport of charged ions (like H^+ and SO_4^{2-}) to complete the circuit. The properties of ideal membranes in RFBs should include good mechanical stability, low cost, less crossing of active substances, and high ionic conductivity. The thickness of the membrane also has some influence on the performance. Thicker membranes have a relatively low permeability of active species and a high discharge capacity decay rate, resulting in a decrease in CE (Figure 4.4e) [18]. Membranes are broadly divided into two main categories: dense (e.g., Nafion) or porous (e.g., Daramic) [4,27]. While the separators can be mechanistically classified into four groups, such as mesoporous separators, ionic exchange membranes, hybrid membranes, and solid ionic conductors [13]. Depending on the ion exchange property, they are also classified as cation exchange, anion exchange, and zwitterion exchange.

The perfluoropolymer Nafion is the most used membrane in VFBs. However, the high cost and ion migration problem have shifted the application to crosslinked polyvinylpyrrolidone and polysulfone semi-interpenetrating polymers as separators [18]. IVBs using Nafion 212 and Daramic microporous membranes displayed a significant capacity retention (Figure 4.4a and b), attributable to the fact that there is no proton generation and gas production in the redox and side reactions, respectively. Recent developments in sulfonated poly(ether ether ketone) and zeolite membranes are also gaining popularity for ICBs. Overall, composite membranes are more effective and efficient in ICBs than intrinsic ones like Daramic (Figure 4.4f) [18]. Hydrocarbon-based membranes and separators are usually used for ICBs and IVBs due to the less corrosive active materials. This sensible choice significantly reduces the capital cost of the systems [27].

4.3.4 Material and Design for Electrodes

RFBs commonly use a concentrated acidic and corrosive environment that restricts the choice of electrode materials. Noble metal-based electrodes can be used, but the increase in cost remains an obstacle. Superior chemical stability, higher electrical conductivity, and large surface areas of porous carbon materials (carbon paper, graphite felts) placed them

on the most wanted list of electrode materials [37]. Surface treatments, coatings, and deposition of electrocatalysts are modification techniques that can elevate the electrochemical activity, wettability, number of active sites, and electron conductivity of carbon-based electrodes [1].

Doping the electrode surface is a method of increasing the activity and efficiency. Thermal treatment in the graphite felt can activate the electrode by the sorption of oxygen atoms, offering a material with faster electron transfer through the surface. N-doped electrodes also exhibit increased electrochemical activity with relatively lower inner resistance and higher efficiency. The importance of the role of these surface modifications is calculated by electron density difference mapping, DFT, and projected density of states calculations (Figure 4.5d and e) [18]. These calculations also play a vital role in determining the reaction mechanism on the surface of the electrode, depicted in Figure 4.5.

Studies on diffusion, sorption dynamics, viscosity, thermal conductivity, structural stability, and reaction mechanisms of various species and events assist in designing efficient RFBs. The simulation study helps to reduce costs and has high security and precision, demonstrating how the internal connection among the reactants impacts the kinetic, thermal, structural, and chemical properties (Table 4.3) [18]

4.4 CHEMISTRIES OF FLOW BATTERIES

The working principle of RFBs is like that of any other energy storage device. This can be surmised as a chemical reaction between two redox couples that results from the combination of two corresponding half-reactions from the two chambers and can generally be expressed by Equations (4.1)–(4.3) [13]:

$$\text{Anode}: \quad A^{x} \rightleftharpoons A^{x+z} + z\, e^{-} \quad \phi_A \tag{4.1}$$

$$\text{Cathode}: \quad C^{y} + z\, e^{-} \rightleftharpoons C^{y-z} \quad \phi_C \tag{4.2}$$

$$\text{Cell}: \quad A^{x} + C^{y} \rightleftharpoons A^{x+z} + C^{y-z} \quad \phi_Z = \phi_C - \phi_A \tag{4.3}$$

The half-cell reactions taking place at the interface between the electrode and the electrolyte can be divided into two groups [13]:

i. **Outer sphere reactions:** The charge is forced to tunnel through the solvation shell of the redox-active species. The kinetics of these reactions do not depend on the state of the surface of the electrodes.

ii. **Inner-sphere reactions:** These reactions involve specific interactions of the electrode surface. The kinetics of the redox couples highly depend on the state of the electrode surface, which is extremely fast compared to the outer sphere reactions by several orders of magnitude.

However, some examples of half-cell reactions with corresponding cell potential are represented in Table 4.4. In the next consecutive sections, the redox chemistries of different RFBs are detailed.

4.4.1 Aqueous Systems

The aqueous VFB systems involve the redox reactions of V3+/V2+ and V4+/V5+ as expressed by Equations (4.4)–(4.6). The cross-transport of the active ions is controlled by separating the two redox couples with membranes. However, the energy conversions take place by changing vanadium valence states through electrode reactions [51,26]:

$$\text{Anode}: \quad V^{3+} + e^- \rightleftharpoons V^{2+} \quad \phi_A = -0.25\,V \tag{4.4}$$

$$\text{Cathode}: VO^{2+} + H_2O \rightleftharpoons VO_2{}^+ + 2H^+ + e^- \quad \phi_C = +1.00\ V \tag{4.5}$$

$$\text{Cell}: \quad VO^{2+} + V^{3+} + H_2O \rightleftharpoons VO_2{}^+ + V^{2+} + 2H^+ \quad \phi_Z = 1.25\,V \tag{4.6}$$

The chemistry of ICBs is somewhat controlled by the ion-selective membranes that only allow protons and chloride ions to pass. ICBs have some flaws, like the low standard potential of Cr^{3+}/Cr^{2+} (Equations 4.7–4.9) and hydrogen evolution tendencies, but they are cost-effective and have higher cell potentials [27,52].

$$\text{Anode}: \quad Cr^{3+} + e^- \rightleftharpoons Cr^{2+} \quad \phi_A = -0.42\ V \tag{4.7}$$

TABLE 4.4 Cell Reactions and Potentials of Different RFBs

RFB Type	Half-Reactions	Cell Potential V	Ref.
Fe-V	Anode: $V^{3+} + e^- \rightleftharpoons V^{2+}$ Cathode: $Fe^{2+} \rightleftharpoons Fe^{3+} + e^-$	1.02	[27]
Zn-Ce	Anode: $Zn(CH_3SO_3)_2 + 2H^+ + 2e^- \rightleftharpoons Zn + 2CH_3SO_3H$ Cathode: $2Ce(CH_3SO_3)_3 + 2CH_3SO_3H \rightleftharpoons 2Ce(CH_3SO_3)_3 + 2H^+ + 2e^-$	2.40	[48]
Ni-Fe(bpy) complexes	Anode: $\left[Ni(bpy)_3\right]^{2+} + 2e^- \rightleftharpoons \left[Ni(bpy)_3\right]$ Cathode: $\left[Fe(bpy)_3\right]^{2+} \rightleftharpoons \left[Fe(bpy)_3\right]^{3+} + e^-$	2.30	[13]
V(acac) complex	Anode: $\left[V(acac)_3\right] + e^- \rightleftharpoons \left[V(acac)_3\right]^-$ Cathode: $\left[V(acac)_3\right] \rightleftharpoons \left[V(acac)_3\right]^+ + e^-$	2.18	[13]
Cr(acac) complex	Anode: $\left[Cr(acac)_3\right] + e^- \rightleftharpoons \left[Cr(acac)_3\right]^-$ Cathode: $\left[Cr(acac)_3\right] \rightleftharpoons \left[Cr(acac)_3\right]^+ + e^-$	3.40	[49]
Fe-Zn DES	Anode: $[ZnCl_4]^{2-} + 2e^- \rightleftharpoons Zn\,(s) + 4Cl^-$ Cathode: $2[FeCl_4]^- + 2e^- \rightleftharpoons 2[FeCl_4]^{2-}$	—	[50]

$$\text{Cathode}: \quad Fe^{2+} \rightleftharpoons Fe^{3+} + e^- \quad \phi_C = +0.77\ \text{V} \tag{4.8}$$

$$\text{Cell}: \quad Cr^{3+} + Fe^{2+} \rightleftharpoons Cr^{2+} + Fe^{3+} \quad \phi_Z = 1.19\ \text{V} \tag{4.9}$$

The addition of vanadium in IVBs has been found to boost the slow kinetics of Cr^{3+}/Cr^{2+} and the problem of HER, as well as thermal stability [28,53]. Polysulfide-based flow batteries usually employ bromine/bromide, chlorine/chloride, or iodine/iodide catholyte and polysulfides/sulfide as anolytes [25,54]. A usual standard cell voltage of 1.33 V is gained via the redox reactions as Equations (4.10)–(4.12) [13]:

$$\text{Anode}: \quad 2Na^+ + xNa_2S_{x+1} + 2e^- \rightleftharpoons (x+1)Na_2S_x \quad x = 1-4 \quad \phi_A = -0.27\ \text{V} \tag{4.10}$$

$$\text{Cathode}: \quad 2NaBr \rightleftharpoons Br_2 + 2Na^+ + 2e^- \quad \phi_C = +1.06\ \text{V} \tag{4.11}$$

$$\text{Cell}: \quad 2Na^+ + xNa_2S_{x+1} + 2NaBr \rightleftharpoons (x+1)Na_2S_x + 2Na^+ + Br_2 \quad \phi_Z = 1.33\ \text{V} \tag{4.12}$$

RFBs based on POMs with three redox pairs can have a current efficiency of over 95%. This high efficiency has been achieved with 20 mM POM in 0.5 M aqueous H_2SO_4 electrolyte with graphite felt electrodes and a Nafion membrane [17].

$$\text{Anode}: \quad \left[SiV_3^{IV}W_9^{VI}O_{40}\right]^{13-} + 3e^- \rightleftharpoons \left[SiV_3^{IV}W_3^{V}W_6^{VI}O_{40}\right]^{13-} \tag{4.13}$$

$$\text{Cathode}: \quad \left[SiV_3^{IV}W_9^{VI}O_{40}\right]^{10-} \rightleftharpoons \left[SiV_3^{V}W_9^{VI}O_{40}\right]^{7-} + 3e^- \tag{4.14}$$

$$\text{Cell}: \quad \left[SiV_3^{IV}W_9^{VI}O_{40}\right]^{13-} + \left[SiV_3^{IV}W_9^{VI}O_{40}\right]^{10-} \rightleftharpoons \left[SiV_3^{IV}W_3^{V}W_6^{VI}O_{40}\right]^{13-} + \left[SiV_3^{V}W_9^{VI}O_{40}\right]^{7-} \tag{4.15}$$

4.4.2 Nonaqueous Systems

Metal ions in nonaqueous systems usually exhibit poor dissolution and incomplete solvation. Therefore, this system is suitable for redox-active organic molecules and metal-ligand complexes (metals of the *d* and *f* series). The scheme for nonaqueous RFBs based on metal complexes remains unchanged between the various metal complexes if there is no change in the metal coordination number. However, it is impossible to exclude a change in coordination during a redox conversion in the battery completely [13]. The general reactions are shown by Equations (4.16) and (4.17):

$$\text{Anode}: \left[\text{ML}_k\right]^x \rightleftharpoons \left[\text{ML}_k\right]^{x+z} + z\ \text{e}^- \tag{4.16}$$

$$\text{Cathode}: \left[\text{ML}_k\right]^y + z\ \text{e}^- \rightleftharpoons \left[\text{ML}_k\right]^{y-z} \tag{4.17}$$

where M is the central atom, for example, Ru, Fe, V, and so on; L represents the ligand, for example, bpy and β-diketonate; k is the number of ligands; z is the number of electrons involved; and x and y indicate the charges of the complexes under consideration.

In designing a metal-coordinated redox agent, the metal center usually dictates the redox potential, and the ligands govern the solution chemistry. RFBs containing ruthenium-bipyridyl complexes were the first of the nonaqueous RFBs with metal-ligand complexes, such as $[\text{Ru(bpy)}_3](\text{BF}_4)_2$. In this case, $\left[\text{TEA}^+\right]\left[\text{BF}_4^-\right]$ dissolved in acetonitrile electrolyte supported the redox reactions expressed by Equations (4.18)–(4.20) [13,27,55].

$$\text{Anode}: \left[\text{Ru}\left(\text{bpy}\right)_3\right]^{2+} + \text{e}^- \rightleftharpoons \left[\text{Ru}\left(\text{bpy}\right)_3\right]^{+} \quad \phi_\text{A} = -1.60\ \text{V vs Ag/Ag}^+ \tag{4.18}$$

$$\text{Cathode}: \left[\text{Ru}\left(\text{bpy}\right)_3\right]^{2+} \rightleftharpoons \left[\text{Ru}\left(\text{bpy}\right)_3\right]^{3+} + \text{e}^- \quad \phi_\text{B} = +1.00\ \text{V vs Ag/Ag}^+ \tag{4.19}$$

$$\text{Cell}: 2\left[\text{Ru}\left(\text{bpy}\right)_3\right]^{2+} \rightleftharpoons \left[\text{Ru}\left(\text{bpy}\right)_3\right]^{3+} + \left[\text{Ru}\left(\text{bpy}\right)_3\right]^{+} \quad \phi_\text{Z} = 2.60\ \text{V} \tag{4.20}$$

Iron- and nickel-bipyridyl complexes showed more stability, wherein $[\text{Fe(bpy)}_3](\text{BF}_4)_2$ as an anolyte and $[\text{Ni(bpy)}_3](\text{BF}_4)_2$ as the catholyte in acetonitrile performed well with a wide cell window of 2.30 V [56,53]. Metal-acetylacetone complexes like (Ru(acac)_3), (V(acac)_3), (Cr(acac)_3), and others are all organic RFBs, showing better chemical stability, higher solubility, and faster kinetics in acetonitrile. RFBs involve neat organic species that could theoretically be available in virtually unlimited quantities. RFB using 2,2,6,6-tetramethyl-1-piperidinyloxy (TEMPO) as catholyte and *N*-methylphthalimide in acetonitrile was one of the first built pure organic RFBs that was inspired by biomimetic principles. NaClO_4 salt was added to increase the conductivity [13].

4.4.3 Chemistries of RFBs in ILs

ILs could simultaneously act as electroactive species and reaction media. Two types of IL, namely (1) metal-containing ILs (metal-ILs) and (2) polymeric ILs (poly-ILs), are used as redox-active species in RFBs. Metal-ILs display redox activity in the cation core, anions, and ligands [34]. A low-cost first-row transition metal cation with a weakly pairing anion is used in metal-ILs containing RFBs. As an example, RFB developed with ferrocene (Fc)-containing ligands and iodide ions into an IL with a metal-coordinated cation, forming $\text{Fe(EA)}_{6-x}(\text{FcEA})_x(\text{OTf})_{2-y}\text{I}_y$, can enhance the capacity by 300%. Another

Cu-based metal-IL, $[Cu(MeCN)_4][Tf_2N]$, with high Cu concentration, can play the roles of both electrolyte and solvent. The metal-IL is a good electroactive species for RFBs, as the developed redox couple Cu^+/Cu and Cu^{2+}/Cu^+ is separated by 0.9 V. The charge density of the RFB can be obtained up to 300 kC L^{-1} with an energy density of 75 W h L^{-1} and 85% CE [57].

Neutral rubrene molecule and rubrene radical anion (Rubrene/Rubrene$^-$) were one of the first proposed poly-IL redox pairs for RFBs of this kind, with a redox potential of −1.9 V and a redox potential of 1.4 V. The short-lived nature of most of the radicals is due to their extreme reactivity. Structurally, the stabilization of radicals can be ensured through molecular engineering with steric crowding, electronic resonance, and/or dimer formation [10]. Other metal-free poly-IL redox species include TEMPO, *N*-methylphthalimide, 1,5-bis(2-(2-(2-methoxyethoxy)ethoxy)ethoxy)anthracene-9,10-dione, 2,5-di-tert-butyl-1,4-bis(2-methoxyethoxy)benzene, and a quinoxaline family [10].

4.4.4 Eutectic Media

DESs assist in mixing metal- and organic-based electroactive materials with appropriate inorganic or organic compounds, like quaternary ammonium salts or hydrogen bond donors (HBDs) [2]. The general formula of DESs can be expressed as $[Cat^+][X^-zY]$, where Cat^+ can be a phosphonium, ammonium, or sulfonium cation, X can be a halide ion, and z refers to the number of Y molecules. The interaction between X^- and other components forms a complex, which is tunable by changing HBDs or adding extra HBDs. A range of transition metals can be incorporated into the DES matrix by mixing anhydrous/hydrated metal halides with urea, such as $AlCl_3$, $ZnCl_2$, and $FeCl_3.6H_2O$ [6].

All-copper DES is one of the first reported DES RFBs, where a mixture of choline chloride and ethylene glycol is combined in a 1:2 molar ratio, known as ethaline. The produced DES benefits from the lowest viscosity and highest conductivity. The reaction mechanism of such an all-copper DES RFB is presented by Equations (4.21) and (4.22) [58]:

$$\text{Anode:}\quad \left[CuCl_3\right]^{2-} + e^- \rightleftharpoons Cu\,(s) + 3Cl^- \tag{4.21}$$

$$\text{Cathode:}\quad \left[CuCl_3\right]^{2-} + Cl^- \rightleftharpoons \left[CuCl_4\right]^{2-} + e^- \tag{4.22}$$

Both metal centers and coordination conditions may govern the redox reactions of DESs. Changing organic salts or HBDs or adding additives might alter the physical properties and tune the coordination environment of metal ions. This implies that DESs also have some tailorable properties. The $AlCl_3$-urea-Fe DES system as anolyte is used to develop Al-halogen RFBs with the half-cell reactions as expressed by Equations (4.23) and (4.24) [19]:

$$\text{Anode:}\quad 2\left[AlCl_2(\text{urea})_n\right]^+ + 3e^- \rightleftharpoons Al + 2n(\text{urea}) + \left[AlCl_4\right]^- \tag{4.23}$$

$$\text{Cathode}: \left[FeCl_4\right]^- + e^- \rightleftharpoons \left[FeCl_4\right]^{2-} \tag{4.24}$$

4.5 CONCLUDING REMARKS

RFBs hold significant promise as a scalable and flexible energy storage solution. Their ability to decouple energy and power storage, along with their potential for long cycle life and minimal maintenance, makes them attractive for grid-scale applications. The efficiency of RFBs can be improved by focusing on developing new redox couples and electrode and electrolyte materials. For instance, using nanomaterials and advanced catalysts can significantly improve reaction kinetics and overall performance. Aqueous RFB systems offer safer and more environmentally friendly options compared to nonaqueous ones, indeed. Nonaqueous RFBs have the advantage of tailoring capability that offers high energy densities but face challenges such as low conductivity and safety concerns. Research should aim to overcome these limitations to make them viable for commercial applications.

The optimization in the cell design and system architecture is also crucial. This can surely ensure better flow field designs, improved membrane materials, and more efficient power management systems. Finding cheaper alternatives to expensive materials like vanadium can drastically reduce costs, leading to lower production costs and increased scalability. VFBs, being the most mature and widely studied RFBs, offer excellent stability and long cycle life, contrary to the inflated cost of vanadium and the relatively low energy density. Developing electrolytes with higher energy densities is a key area of research; as previously mentioned, electrolytes play a significant role in dictating performance. This includes both aqueous and nonaqueous systems that can store more energy per unit volume. The safety issues can be regulated by improving the durability and selectivity of membranes. This includes developing membranes that are resistant to chemical degradation and mechanical stress.

Future technological advancements aim for environmentally friendly and sustainable materials. Therefore, environmentally benign materials are becoming a priority. This includes biodegradable electrolytes and recyclable components. Conducting comprehensive lifecycle analyses to understand and minimize the environmental impact of flow batteries from production to disposal should also be considered for the development of the future. If RFBs can be developed in the same manner, keeping the shortcomings in mind, then RFBs can be ideal for integrating with renewable energy sources in the future. As the technology matures, the market for flow batteries is expected to expand, leading to increased investment and further technological advancements.

REFERENCES

1. Park, M.; Ryu, J.; Wang, W.; Cho, J. Material Design and Engineering of Next-Generation Flow Battery Technologies. *Nat. Rev. Mater.* **2016,** *2* (1), 16080.
2. Ding, Y.; Zhang, C.; Zhang, L.; Zhou, Y.; Yu, G. Pathways to Widespread Applications: Development of Redox Flow Batteries Based on New Chemistries. *Chem.* **2019,** *5* (8), 1964–1987.
3. Nguyen, T.; Savinell, R. F. Flow Batteries. *Electrochem. Soc. Interface* **2010,** *19* (3), 54.

4. Zhang, L.; Feng, R.; Wang, W.; Yu, G. Emerging Chemistries and Molecular Designs for Flow Batteries. *Nat. Rev. Chem.* **2022,** *6* (8), 524–543.
5. Yao, Y.; Lei, J.; Shi, Y.; Ai, F.; Lu, Y.-C. Assessment Methods and Performance Metrics for Redox Flow Batteries. *Nat. Energy* **2021,** *6* (6), 582–588.
6. Zhang, C.; Zhang, L.; Ding, Y.; Peng, S.; Guo, X.; Zhao, Y.; He, G.; Yu, G. Progress and Prospects of Next-Generation Redox Flow Batteries. *Energy Storage Mater.* **2018,** *15*, 324–350.
7. Zhao, Y.; Ding, Y.; Li, Y.; Peng, L.; Ryung Byon, H.; B. Goodenough, J.; Yu, G. A Chemistry and Material Perspective on Lithium Redox Flow Batteries towards High-Density Electrical Energy Storage. *Chem. Soc. Rev.* **2015,** *44* (22), 7968–7996.
8. Li, W.; Jin, S. Design Principles and Developments of Integrated Solar Flow Batteries. *ACC. Chem. Res.* **2020,** *53* (11), 2611–2621.
9. Yan, R.; Wang, Q. Redox-Targeting-Based Flow Batteries for Large-Scale Energy Storage. *Adv. Mater.* **2018,** *30* (47), 1802406.
10. Gong, K.; Fang, Q.; Gu, S.; Yau Li, S. F.; Yan, Y. Nonaqueous Redox-Flow Batteries: Organic Solvents, Supporting Electrolytes, and Redox Pairs. *Energy Environ. Sci.* **2015,** *8* (12), 3515–3530.
11. Duduta, M.; Ho, B.; Wood, V. C.; Limthongkul, P.; Brunini, V. E.; Carter, W. C.; Chiang, Y.-M. Semi-Solid Lithium Rechargeable Flow Battery. *Adv. Energy Mater.* **2011,** *1* (4), 511–516.
12. Li, W.; Zheng, J.; Hu, B.; Fu, H.-C.; Hu, M.; Veyssal, A.; Zhao, Y.; He, J.-H.; Liu, T. L.; Ho-Baillie, A.; Jin, S. High-Performance Solar Flow Battery Powered by a Perovskite/Silicon Tandem Solar Cell. *Nat. Mater.* **2020,** *19* (12), 1326–1331.
13. Noack, J.; Roznyatovskaya, N.; Herr, T.; Fischer, P. The Chemistry of Redox-Flow Batteries. *Angew. Chem. Int. Ed.* **2015,** *54* (34), 9776–9809.
14. Liu, T.; Li, X.; Zhang, H.; Chen, J. Progress on the Electrode Materials towards Vanadium Flow Batteries (VFBs) with Improved Power Density. *J. Energy Chem.* **2018,** *27* (5), 1292–1303.
15. Soloveichik, G. L. Flow Batteries: Current Status and Trends. *Chem. Rev.* **2015,** *115* (20), 11533–11558.
16. Gong, K.; Xu, F.; Grunewald, J. B.; Ma, X.; Zhao, Y.; Gu, S.; Yan, Y. All-Soluble All-Iron Aqueous Redox-Flow Battery. *ACS Energy Lett.* **2016,** *1* (1), 89–93.
17. Pratt III, H. D.; Hudak, N. S.; Fang, X.; Anderson, T. M. A Polyoxometalate Flow Battery. *J. Power Sources* **2013**, *236*, 259–264.
18. Liu, Y.; Niu, Y.; Ouyang, X.; Guo, C.; Han, P.; Zhou, R.; Heydari, A.; Zhou, Y.; Ikkala, O.; Tigranovich, G. A.; Xu, C.; Xu, Q. Progress of Organic, Inorganic Redox Flow Battery and Mechanism of Electrode Reaction. *Nano Res. Energy* **2023,** *2*, e9120081.
19. Zhang, C.; Ding, Y.; Zhang, L.; Wang, X.; Zhao, Y.; Zhang, X.; Yu, G. A Sustainable Redox-Flow Battery with an Aluminum-Based, Deep-Eutectic-Solvent Anolyte. *Angew. Chem. Int. Ed.* **2017,** *56* (26), 7454–7459.
20. Qiao, L.; Liu, S.; Fang, M.; Yang, M.; Ma, X. A Composite Membrane with High Stability and Low Cost Specifically for Iron–Chromium Flow Battery. *Polymers* **2022,** *14* (11), 2245.
21. Liu, W.; Lu, W.; Zhang, H.; Li, X. Aqueous Flow Batteries: Research and Development. *Chem. Eur. J.* **2019,** *25* (7), 1649–1664.
22. Skyllas-Kazacos, M.; Grossmith, F. Efficient Vanadium Redox Flow Cell. *J. Electrochem. Soc.* **1987,** *134* (12), 2950.
23. Skyllas-Kazacos, M. Novel Vanadium Chloride/Polyhalide Redox Flow Battery. *J. Power Sources* **2003,** *124* (1), 299–302.
24. De Leon, C. P.; Frías-Ferrer, A.; González-García, J.; Szánto, D. A.; Walsh, F. C. Redox Flow Cells for Energy Conversion. *J. Power Sources* **2006,** *160* (1)**,** 716–732.
25. Remick, R. J.; Ang, P. G. Electrically Rechargeable Anionically Active Reduction-Oxidation Electrical Storage-Supply System. **1984** (Patent No. US 4485154).
26. Sum, E.; Skyllas-Kazacos, M. A Study of the V (II)/V (III) Redox Couple for Redox Flow Cell Applications. *J. Power Sources* **1985,** *15* (2–3), 179–190.

27. Wang, W.; Luo, Q.; Li, B.; Wei, X.; Li, L.; Yang, Z. Recent Progress in Redox Flow Battery Research and Development. *Adv. Function. Mater.* **2013**, *23* (8), 970–986.
28. Wang, W.; Nie, Z.; Chen, B.; Chen, F.; Luo, Q.; Wei, X.; Xia, G.; Skyllas-Kazacos, M.; Li, L.; Yang, Z. A New Fe/V Redox Flow Battery Using a Sulfuric/Chloric Mixed-Acid Supporting Electrolyte. *Adv. Energy Mater.* **2012,** *2* (4), 487–493.
29. Waters, S. E.; Robb, B. H.; Marshak, M. P. Effect of Chelation on Iron–Chromium Redox Flow Batteries. *ACS Energy Lett.* **2020,** *5* (6)**,** 1758–1762.
30. Wang, S.; Xu, Z.; Wu, X.; Zhao, H.; Zhao, J.; Liu, J.; Yan, C.; Fan, X. Excellent Stability and Electrochemical Performance of the Electrolyte with Indium Ion for Iron–Chromium Flow Battery. *Electrochim. Acta* **2021,** *368*, 137524.
31. Sun, C.; Zhang, H. Investigation of Nafion Series Membranes on the Performance of Iron-Chromium Redox Flow Battery. *Int. J. Energy Res.* **2019,** 3 (14), 8739–8752.
32. Li, L.; Kim, S.; Wang, W.; Vijayakumar, M.; Nie, Z.; Chen, B.; Zhang, J.; Xia, G.; Hu, J.; Graff, G.; Liu, J.; Yang, Z. A Stable Vanadium Redox-Flow Battery with High Energy Density for Large-Scale Energy Storage. *Adv. Energy Mater.***2011,** *1* (3), 394–400.
33. Izutsu, K. *Electrochemistry in Nonaqueous Solutions* **2009**, John Wiley & Sons.
34. Ortiz-Martínez, V. M.; Gómez-Coma, L.; Pérez, G.; Ortiz, A.; Ortiz, I. The Roles of Ionic Liquids as New Electrolytes in Redox Flow Batteries. *Sep. Purif. Technol.* **2020,** *252*, 117436.
35. Chakrabarti, M. H.; Dryfe, R. A. W.; Roberts, E. P. L. Evaluation of Electrolytes for Redox Flow Battery Applications. *Electrochim. Acta* **2007,** *52* (5), 2189–2195.
36. Bajpai, P. Comparison of Deep Eutectic Solvents and Ionic Liquids. *Deep Eutectic Solvents for Pretreatment of Lignocellulosic Biomass* **2021,** Springer: Singapore, pp. 81–87.
37. Park, M.; Ryu, J.; Cho, J. Nanostructured Electrocatalysts for All-Vanadium Redox Flow Batteries. *Chem. Asian J.* **2015,** *10* (10), 2096–2110.
38. Wang, R.; Li, Y. Carbon Electrodes Improving Electrochemical Activity and Enhancing Mass and Charge Transports in Aqueous Flow Battery: Status and Perspective. *Energy Storage Mater.* **2020,** *31*, 230–251.
39. Zhang, W.; Xi, J.; Li, Z.; Zhou, H.; Liu, L.; Wu, Z.; Qiu, X. Electrochemical Activation of Graphite Felt Electrode for VO^{2+}/VO_2^+ Redox Couple Application. *Electrochim. Acta* **2013,** *89*, 429–435.
40. Jin, J.; Fu, X.; Liu, Q.; Liu, Y.; Wei, Z.; Niu, K.; Zhang, J. Identifying the Active Site in Nitrogen-Doped Graphene for the VO^{2+}/VO_2^+ Redox Reaction. *ACS Nano* **2013,** *7* (6), 4764–4773.
41. Jiang, Z.; Klyukin, K.; Alexandrov, V. First-Principles Study of Adsorption–Desorption Kinetics of Aqueous V^{2+}/V^{3+} Redox Species on Graphite in a Vanadium Redox Flow Battery. *Phys. Chem. Chem. Phys.* **2017,** *19* (23), 14897–14901.
42. Ferre-Vilaplana, A.; Herrero, E. Understanding the Chemisorption-Based Activation Mechanism of the Oxygen Reduction Reaction on Nitrogen-Doped Graphitic Materials. *Electrochim. Acta* **2016,** *204*, 245–254.
43. Zhao, Y.; Liu, L.; Qiu, X.; Xi, J. Revealing Sulfuric Acid Concentration Impact on Comprehensive Performance of Vanadium Electrolytes and Flow Batteries. *Electrochim. Acta* **2019,** *303*, 21–31.
44. Suresh, S.; Ulaganathan, M.; Aswathy, R.; Ragupathy, P. Enhancement of Bromine Reversibility Using Chemically Modified Electrodes and Their Applications in Zinc Bromine Hybrid Redox Flow Batteries. *ChemElectroChem* **2018,** *5* (22), 3411–3418.
45. Wang, S.; Xu, Z.; Wu, X.; Zhao, H.; Zhao, J.; Liu, J.; Yan, C.; Fan, X. Analyses and Optimization of Electrolyte Concentration on the Electrochemical Performance of Iron-Chromium Flow Battery. *Appl. Energy* **2020,** *271*, 115252.

46. Wang, X.; Xing, X.; Huo, Y.; Zhao, Y.; Li, Y.; Chen, H. Study of Tetraethylammonium Bis (Trifluoromethylsulfonyl) Imide as a Supporting Electrolyte for an All-Organic Redox Flow Battery Using Benzophenone and 1, 4-Di-Tert-Butyl-2, 5-Dimethoxybenzene as Active Species. *Inter. J. Electrochem. Sci.* **2018,** *13* (7), 6676–6683.
47. Brushett, F. R.; Vaughey, J. T.; Jansen, A. N. An All-Organic Non-Aqueous Lithium-Ion Redox Flow Battery. *Adv. Energy Mater.* **2012,** *2* (11), 1390–1396.
48. Leung, P. K.; Ponce-de-León, C.; Low, C. T. J.; Shah, A. A.; Walsh, F. C. Characterization of a Zinc-Cerium Flow Battery. *J. Power Sources* **2011,** *196* (11), 5174–5185.
49. Liu, Q.; Shinkle, A. A.; Li, Y.; Monroe, C. W.; Thompson, L. T.; Sleightholme, A. E. Non-Aqueous Chromium Acetylacetonate Electrolyte for Redox Flow Batteries. *Electrochem. Commun.* **2010,** *12* (11), 1634–1637.
50. Lloyd, D.; Vainikka, T.; Ronkainen, M.; Kontturi, K. Characterisation and Application of the Fe (II)/Fe (III) Redox Reaction in an Ionic Liquid Analogue. *Electrochim. Acta* **2013,** *109*, 843–851.
51. Chen, D.; Hickner, M. A.; Agar, E.; Kumbur, E. C. Optimizing Membrane Thickness for Vanadium Redox Flow Batteries. *J. Membrane Sci.* **2013,** *437*, 108–113.
52. Gahn, R. F.; Hagedorn, N. H.; Ling, J. S. Single Cell Performance Studies on the Fe/Cr Redox Energy Storage System Using Mixed Reactant Solutions at Elevated Temperature. *Intersoc. Energy Conversion Engr. Conf.* **1983**.
53. Kim, J.-H.; Kim, K. J.; Park, M.-S.; Lee, N. J.; Hwang, U.; Kim, H.; Kim, Y.-J. Development of Metal-Based Electrodes for Non-Aqueous Redox Flow Batteries. *Electrochem. Commun.* **2011,** *13* (9), 997–1000.
54. Price, A.; Bartley, S.; Male, S.; Cooley, G. A Novel Approach to Utility-Scale Energy Storage. *Power Eng.* **1999,** *13* (3), 122–129.
55. Matsuda, Y.; Tanaka, K.; Okada, M.; Takasu, Y.; Morita, M.; Matsumura-Inoue, T. A Rechargeable Redox Battery Utilizing Ruthenium Complexes with Non-Aqueous Organic Electrolyte. *J. Appl. Electrochem.* **1988,** *18* (6), 909–914.
56. Mun, J.; Lee, M.-J.; Park, J.-W.; Oh, D.-J.; Lee, D.-Y.; Doo, S.-G. Non-Aqueous Redox Flow Batteries with Nickel and Iron Tris (2, 2'-Bipyridine) Complex Electrolyte. *Electrochem. Solid-State Lett.* **2012,** *15* (6), A80.
57. Joseph, A.; Sobczak, J.; Żyła, G.; Mathew, S. Ionic Liquid and Ionanofluid-Based Redox Flow Batteries-A Mini Review. *Energies* **2022,** *15* (13), 4545.
58. Lloyd, D.; Vainikka, T.; Kontturi, K. The Development of an All-Copper Hybrid Redox Flow Battery Using Deep Eutectic Solvents. *Electrochim. Acta* **2013,** *100*, 18–23.

CHAPTER 5

Molecular Engineering Strategies for Flow Batteries

Esmaeil Sheibani, Bo Xu, and Mostafa Moslempoor

5.1 INTRODUCTION

For the first time in 1949, the idea of using redox-active material solutions for storing energy was outlined [1]. Various redox systems, such as Br^{-}/Br^{3-}, V^{2+}/V^{3+}, and V^{4+}/V^{5+}, were utilized in the 1970s and later in the 1980s, and the modern all-vanadium-based flow batteries (VFBs) were comprehensively developed [2]. VFB exhibited high efficiency, fewer cross-contaminations, and a long lifetime. Even though VFB occupies a majority of the market in megawatt scales, it encounters troubles such as high cost, limited vanadium sources, poor thermal stability, and corrosion of acidic electrolytes [3]. The inherent variability and intermittency of wind and solar energy [4–18] limit their widespread adoption, making large-scale energy storage facilities necessary. Redox-flow batteries (RFBs) show bright prospects as candidates for large-scale energy storage because of their long operation life, high safety, and decoupled energy from power. The active materials are utilized as energy storage and electrodes for redox reactions, which are designed separately. In contrast to encapsulated, solid-state batteries, the RFBs use redox-active materials dissolved in electrolyte solutions, which are circulated between storage tanks and a cell (Figure 5.1), which performs the energy conversion. The tank volume defines the capacity and the size of the cell and the power capability of the RFB. The energy density of an RFB is determined by the definite electrolyte volume and concentration, the number of transferred electrons, and the cell voltage. The energy density can be calculated using Equation (5.1), where E denotes energy density, n is the number of electrons in the redox reaction, C symbolizes the concentration of electrolytes, F stands for Faraday's constant, V is the voltage of the battery, and μv is the volume factor, which is calculated as $\mu v = 1 +$ (lower electrolyte concentration/higher electrolyte concentration) [19].

DOI: 10.1201/9781003506379-5

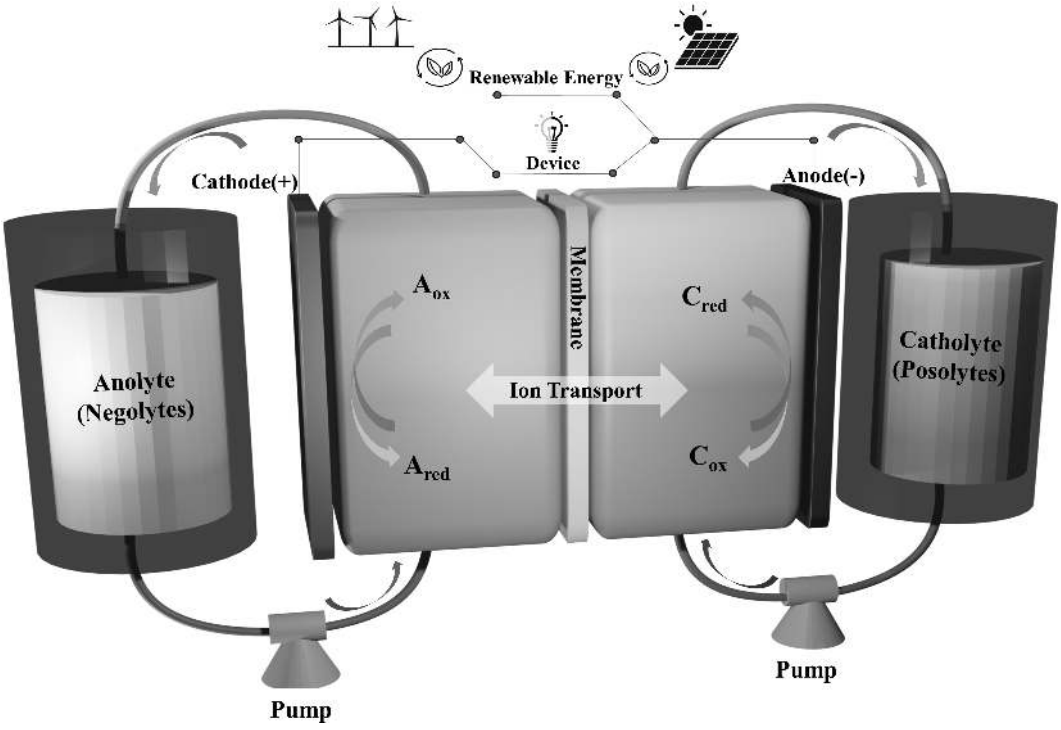

FIGURE 5.1 Schematic of a typical RFB.

$$E = \frac{nCFV}{\mu v} \tag{5.1}$$

Due to the separation of power from energy, RFBs can regulate the volume of the electrolyte reservoirs and electrode surface area autonomously. The RFBs can drive at high power densities and high current due to the high conductivity of supporting electrolytes and fast electrochemical kinetics. Further, it covers safe energy storage technology by developing nonflammable electrolyte materials. Energy storage and release occurred by the redox species having positive and negative active electrochemical roles. In the charging process, the posolyte undertakes oxidation, delivering electrons, while the negolyte undergoes reduction, accepting the electrons, thus saving energy in the form of potential [20]. The reverse reaction happens during discharging, releasing the stored energy as electrical energy.

There are various techniques for enhancing the solubility of redox species. These include attaching hydrophilic units with high polarity and ionization tendency (such as sulfonate, carboxylate, hydroxy, polyethylene glycol, quaternary amine, and phosphate moieties), identifying substitution sites, utilizing supramolecular interactions (such as hydrogen bonding, ionic bonding, ion-induced dipole forces, ion-dipole forces, and Van der Waals dispersion forces), replacing hydrophilic counterions, and employing symmetry-breaking approaches. For example, incorporating sulfonate units not only increases solubility but

also results in high coulombic efficiency and better cycle stability because of the stability of sulfonates. By mimicking traditional batteries, solubilizing additives is another concept to act as a bridge between the aqueous solution and the active mediator through amphiphilic molecules.

Since the battery performance is directly controlled by the intrinsic chemical and physical properties of redox species, inorganic electroactive materials cannot provide an optimistic candidate due to the limitation of the valence change of metal centers. In contrast, organic molecules utilize appealing features like tunable chemical and physical properties, minimal environmental footprint, and low cost, which are more environmentally benign for widespread implementation. Over the last few decades, molecular frameworks as negolytes, like pyridinium, phenazine, and viologen, as well as posolytes, including dialkoxybenzene, nitroxyl radical, phenothiazine, and anthraquinone, have received substantial exploration as potential redox-active materials for energy storage applications. Nonetheless, exceptional properties are held by organic redox molecules, but still, physical and electrochemical properties consisting of low redox potential, poor stability of radicals, solubility, and low ionic conductivity hamper this technology from taking the place of metal or semimetal batteries. Tailoring molecular engineering is capable of paving the way to tackle the above obstacles with significant improvements of high-energy-density RFB, and as indicated in Figure 5.2, it can bring acceptable features. This chapter ubiquitously pondered the most prominent array of organic catholytes (encompassing the dialkoxybenzenes, quinone derivatives, phenothiazines, and nitroxyl radicals) and anolytes (pyridinium and viologen derivatives) for both aqueous and nonaqueous organic RFBs.

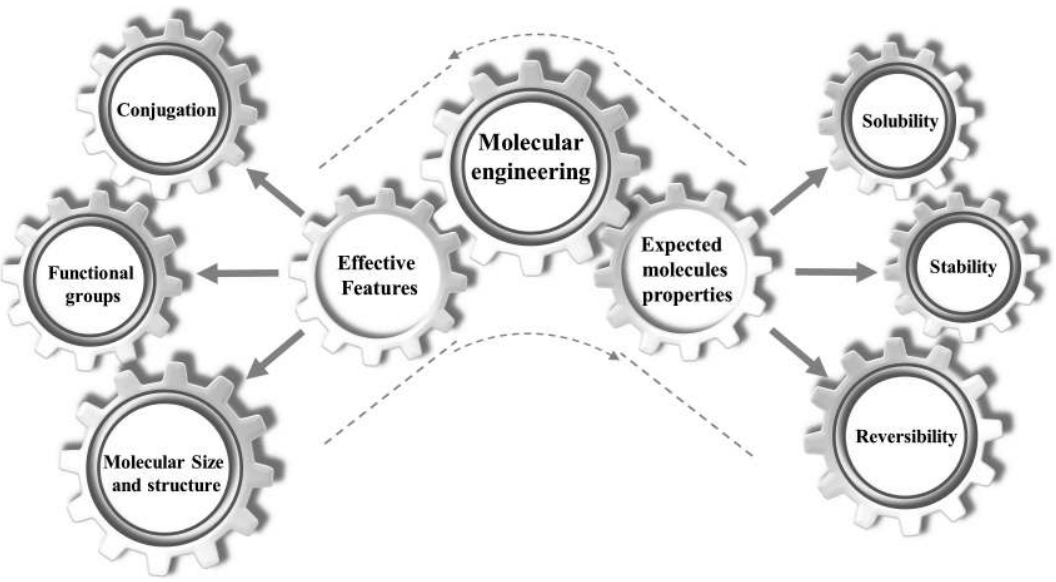

FIGURE 5.2 Effective properties in molecular engineering structures and expected molecules.

5.2 AQUEOUS RFBs

Compared to nonaqueous systems, water is nonflammable and exhibits acceptable ionic conductivity; in addition, it possesses a high dielectric constant and has a large dipole moment, all of which indicate significant potential for future applications. It is essential to realize the limitations of this outstanding technological demand through action and reaction of stability, electrochemical potential, and solubility in redox-active molecules. One of the big disadvantages of aqueous RFBs is low cell voltage (ca. 1.3 V), which sequentially necessitates larger tank volumes to maintain huge amounts of electroactive materials and drives up costs [21]. It is noteworthy that some of the molecular structures utilized in this category of systems are evident in Figure 5.3.

Jin et al. investigated the molecular engineering of phenazine derivative anolytes in alkali conditions coupled with ferrocyanide catholyte [22]. They considered redox potential, solubility, and cycling stability of the phenazine performance through ortho-substituents of the hydroxyl groups in phenazine derivatives. Putting an additional phenyl group to the phenazine core structure has a strong solubilizing effect on compound. The name of compound is benzo[a]hydroxyphenazine-7/8-carboxylic acid (BHPC). The RFB of BHPC at 1.0 M electron concentration displays a greatly improved capacity retention rate of 99.986% cycle^{-1} (99.92% day^{-1}) and stable average energy efficiency (EE) of ~80% for over 1,300 cycles. The other structure, 2-amino-3-hydroxyphenazine, exhibits inferior solubility because of intramolecular hydrogen bonds between the hydroxyl anion and the adjacent amino group. The oxidation potential of 2,2′,6,6′-tetramethylpiperidine-1-oxyl (TEMPO) to its corresponding oxoammonium salt TEMPO$^+$ strongly depends on the substituent in the 4-position. Specifically, robust electron-withdrawing moieties increase the redox potential, which in turn benefits

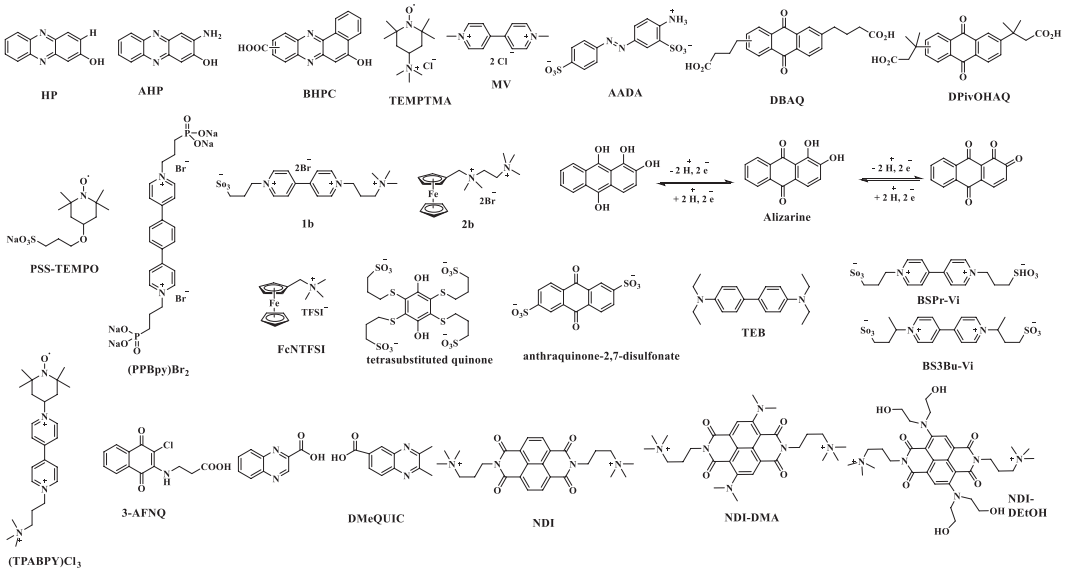

FIGURE 5.3 Chemical structures of various molecules for aqueous RFBs based on different building blocks.

the cell voltage and energy density of the battery. Schubert and coworkers propose a battery from cost-effective and high solubility in natural pH, which utilizes the viologen derivative N,N′-dimethyl-4,4′-bipyridinium dichloride (MV) and highly soluble N,N′,N″-2,2′,6,6′-hep tamethylpiperidinyl oxy-4-ammonium chloride (TEMPTMA) as redox-active compounds [23]. The made-up cell applying these electrolyte solutions releases cell parameters, including a voltage of 1.4 V, energy density of 38 Wh L^{-1}, and capacity of 54 Ah L^{-1}. For this reason, the trimethylammonium chloride group $\left(-N(CH_3)_3^+ Cl^-\right)$, as a strong electron-withdrawing group with high solubility, was introduced along with the chloride ion to act as a charge carrier inside the electrolyte solution for increasing electrical conductivity.

Yu and coworkers decorated azobenzene-based molecules with hydrophilic functional groups (amino and sulfonic), and 4-amino-1,1′-azobenzene-3,4′-disulfonic acid monosodium salt (AADA) was synthesized [24]. Further, urea, as the hydrotropic agent, was added to the electrolyte to increase solubility through anisotropic hydrogen bond interactions. The target asymmetric configuration encompasses favorable intermolecular hydrogen bonds, resulting in the solubility enhancement from near zero to 2 M concentrations in an alkali condition. The UV–Vis spectra and electrochemical analysis proved that the azobenzene redox mediator exhibits good stability and electrochemical reversibility in aqueous electrolytes (Figure 5.4a). It is consistent with the ^{13}CNMR (Figure 5.4b) spectrum, which

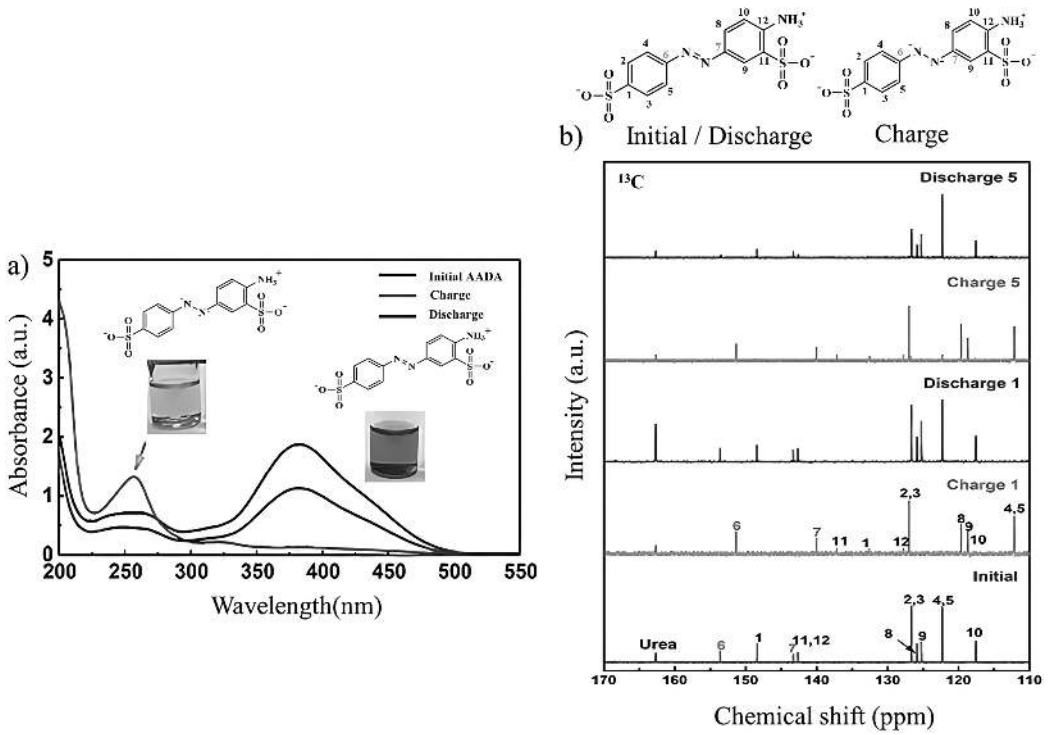

FIGURE 5.4 (a) UV/Vis spectra of the AADA anolyte at different redox states. (b)^{13}C NMR spectra of the anolyte in D_2O. The anolyte solution consists of 0.5 M AADA and urea dissolved in a 2 M NaOH solution. (Adapted with permission from [24], Copyright 2020, WILEY.)

shows large chemical shifts to the high field in the reduced AADA structure, particularly the C4 and C5, due to the ortho position of –N=N– in the benzene ring. After the discharge cycle, the initial ^{13}C NMR spectrum of the AADA-based anolyte appeared again.

The fabricated RFB based on 0.1 M AADA anolyte paired with the ferro/ferrocyanide catholyte displays long cycling stability with a capacity retention of 99.95% per cycle over 500 cycles with a high columbic efficiency (CE) of 99%. Two redox-active organic molecules based on inexpensive 9,10-dihydroanthracene were synthesized as negolytes, called 4,4′-(9,10-anthraquinone-diyl)dibutanoic acid (DBAQ) and 3,3′-(9,10-anthraquinone-diyl) bis(3-methylbutanoic acid) (DPivOHAQ) [25]. These two water-soluble anthraquinones were synthesized from 9,10-dihydroanthracene by Friedel–Crafts alkylation or acylation and later simple oxidation with chromium oxide with almost quantitative yield. At alkaline pH, coupling with a ferrocyanide posolyte, DBAQ, and DPivOHAQ reveals a voltage cell of 1.0 V and also carries 2 M and 1.4 M electrons with capacity fade rates of 0.0084% per day and 0.014% per day, respectively. Even by regulating the supporting electrolytes to pH 14, DPivOHAQ showed a record low capacity fade rate of <1% per year. It found that the carbon-linked functional groups of DPivOHAQ are chemically stronger than the oxygen-linked side chains in DBEAQ. The authors recognized that the small amount of losing capacity is related to the construction of anthrone, which can be blocked at high pH of the electrolyte and even revert back to the starting material by periodic air exposure to realize very low capacity fade rates. This study disclosed that the molecular lifetimes of anthraquinone-based electrolytes are strongly dependent on the positions of their functional groups and the type of substitution.

As reported, the MV/4-hydroxy-TEMPO couple came across crossover through an anion exchange membrane (AEM) and viologen decomposition. For this reason, Wang et al. reported a pair of aqueous anionic organic molecules based on molecular engineering of viologen and TEMPO, namely (PPBPy)Br_2 and PSS-TEMPO, as anolyte and catholyte, respectively [26]. From a structural point of view, the longer side chain of PSS-TEMPO effectively quenches the interactions between TEMPO radicals by steric hindrance and valuably lightens the contrary influence of the strong electron-withdrawing group on the skeleton stability. On the other hand, the premier stability of (PPBPy)Br_2 was attributed to the strong electrostatic repulsion among molecules of the negative charges and phosphonate steric hindrance, while the phenylene bridge could extend the π-conjugated system and distribute the charges. At neutral conditions, the cell pair displays a high voltage of 1.61 V with exceptionally low penetrance across the cation-exchange membrane and worthy cycling stability. The cell reveals notable electrochemical stability after 1,000 cycles with a capacity decay rate as low as 0.012%/cycle. Remarkably, the highest peak power density of 509 mW cm^{-2} has been realized among all-organic aqueous RFBs reported till now. Furthermore, (PPBPy)Br_2 has a solubility of above 1.10 M in water, and that of PSS-TEMPO is above 2.55 M, corresponding to a volumetric capacity of 29.48 Ah L^{-1} and 68.43 Ah L^{-1} for anolyte and catholyte, respectively. Thus, the theoretical energy density of the (PPBPy)Br_2/PSS-TEMPO aqueous organic redox flow batteries (AORFB) can achieve 33.1 Wh L^{-1}.

Usually, the second reduction process of methyl viologen (MV^{+2}) is not explored thoroughly because MV^0 has a low polarity and consequently causes limited solubility in the

neutral charge state. Liu and colleagues proposed a rational design of viologen compounds by integrating function-oriented organic synthesis with two-electron storage as anode electrolytes to emphasize the art of molecular engineering as a powerful approach for emerging sustainable, greener energy storage systems [27]. Therefore, the methyl groups of MV are replaced with one or two hydrophilic moieties, including propylammonium or propyl sulfonate. The electrochemical reversibility of the second electron reduction was followed by CV. The electrochemical analysis results of two successive electron-transfer reactions displayed a faster diffusion process ($\sim 5 \times 10^{-6}\,cm^2\,s^{-1}$) and reaction kinetics ($>0.38\,cm\ s^{-1}$) than conventional inorganic redox species. In the presence of ferrocene derivatives (such as 2b) as a cathode alternative and viologen derivatives (such as 1b) in neutral electrolytes, the cell performed a power density of 130 mW cm^{-2} and capacity retention of 99.99% per cycle at 60 mA cm^{-2}.

Up to now, several procedures have been reported to exploit the second electron of viologen compounds via molecular engineering perspectives. As declared previously, the high solubility of the doubly reduced species resulted from the attachment of highly hydrophilic pendant ammonium groups to the viologen molecules. The second tactic included the insertion of thiazolo[5,4-d]thiazole (TTz) framework to spread the π-conjugation system and simultaneously functionalize with ammonium hydrophilic groups [28]. Another strategy to manage the insoluble MV^0 generated from the second reduction of MV is propounded via (trifluoromethane)sulfonamide (TFSI) counter anion replacement. Paired with (Ferrocenylmethyl)trimethylammonium bis(trifluoromethanesulfonyl)imide (FcNTFSI) as the catholyte [29], CV experiments were carried out to determine the redox potential and reversibility of both active materials containing 1.0 M LiTFSI in CH_3CN, MVTFSI electrolyte. At 40 mA cm^{-2}, by taking advantage of the conductive LiTFSI/CH_3CN supporting electrolyte and a porous Daramic separator, the battery disposed of more than 68.3% EE together with more than 88% capacity maintenance after 100 cycles. By increasing the current density from 10 to 40 mA cm^{-2}, the coulombic efficiency amplified from 82.8% to 95.2%. At neutral pH, viologen derivatives are one of the prevalent anolytes. In a real state at an alkaline situation, the trace amount of oxygen sped up the breakdown of viologen derivatives due to the cleavage of the N-substituent. So, the presence of dissolved oxygen in the electrolyte makes the irreversible reduction of oxygen happen, whether by electrochemical reaction in the electrodes or automatic charge transfer with reduced active species. In the aftermath, the anolyte does not grasp a full state of charge (SOC) at the end of the charging process, dropping the discharge capacity and dwarfing the energy storage capacity, thus resulting in a faradaic imbalance. Working with cells under argon conditions may be a useful approach to investigate at the research level, but it is not applicable for large-scale (>MWh) applications over long periods (>10 years). To get rid of this unavoidable process, the carbon connected directly to the pyridine core (N atom) must be a secondary carbon to diminish hydroxide attack to the carbon via nucleophilic substitution reactions [30]. In terms of molecular engineering, the addition of an alkyl group at the α-position of the N-substituent could obstruct the attack by stereoelectronic effects and even enhance the stability and solubility of the viologen derivative. The battery cells of both viologen derivatives, 1,1′-Bis(3-sulfonatopropyl)-4,4′-bipyridinium (BSPr-Vi) and

1,1′-Bis(1-methyl-3-sulfonatopropyl)-4,4′-bipyridinium (BS3Bu-Vi) (with steric hindrance on the α-carbon atom), were assessed for 3 days. The capacity fading of 0.45% and 0.15% h^{-1} was achieved, respectively.

As discussed previously, the theory of a symmetric cell architecture has special benefits, like simplicity in design and less worry of crossover. Aziz et al. proposed a symmetric all-anthraquinone aqueous battery with three stable oxidation states in both positive and negative electrodes [31]. During oxidation, the right ortho-hydroquinone group of alizarin is converted into ortho-quinone on the negative side to draw up fused quinone, and in the course of charging, the center para-quinone figure is reduced into para-hydroquinone. The battery disclosed a capacity of 163 mAh g^{-1} at 10°C and a cell voltage of 1.04 V. After 100 cycles with 100% depth of discharge, the alizarin-based symmetric quinone-acid cell retains 45% of its capacity. Since the benzoquinones are reactive electrophiles, they are susceptible to various nucleophiles, such as water, to Michael addition, and even oligomerization. Quinones are attractive objects as organic charge carriers for aqueous redox flow batteries (ARFBs), but their function suffers from inadequate stability under working circumstances. Similar to the other category of organic redox-active compounds, ancillary substitutions have a sturdy impact on the redox potentials. Stahl and colleagues studied a series of water-soluble quinones under acidic aqueous conditions (1 M H_2SO_4) with a redox potential fluctuating from 605 to 885 mV versus NHE [32]. The quinone derivatives are scrutinized as cathodic electrolytes in an aqueous RFB, paired with anthraquinone-2,7-disulfonate as the anodic electrolyte. The results proved that a tetrasubstituted quinone decorated with four sulfonated thioether substituents is the most stable, because the thioether linkage withstands replacement over a long time in aqueous acid at elevated temperature. The cell battery made of all-organic RFB with four sulfonated thioethers and anthraquinone-2,7-disulfonate exhibited a power density of >100 mW cm^{-2} at current densities of 800 mA cm^{-2}.

Through molecular engineering, a series of promising N-substituted benzidine families is explored as water-soluble catholyte applicants with variable redox potentials (0.78–1.01 V vs. standard hydrogen electrode (SHE)). Among benzidine derivatives, N,N,N′,N′-tetraethylbenzidine (TEB) illustrates both good solubility (1.1 M) and high redox potential (0.82 V vs. SHE) [33]. Fortunately, the radical state of TEB is not susceptible to nucleophile attacks, and the pH fluctuation and azopolymerization are suppressed via alkylating the active amine groups. Pairing with $H_4[Si(W_3O_{10})_4]$ anolyte, the battery presented high CE of ~100% over 1,200 cycles and discharge capacity retention of 99.4% per. The cell containing 1.0 M TEB catholyte revealed a stable discharge capacity of 41.8 Ah L^{-1}, along with a CE of 97.2% and EE of 91.2%.

Recently, a bipolar redox-active organic molecule strategy was outlined in a single big molecule via a covalent bonding of TEMPO with viologen moieties to reduce the crossover rate with the size exclusion effect [34]. This feature meets several characteristics, which include the following: (1) 1-(1-oxyl 2,2′,6,6′-tetramethylpiperidin-4-yl)-1′-(3-(trimethylam monio)propyl)-4,4′-bipyridinium trichloride ((TPABPy)Cl_3), which reveals high solubility (1.76 M) owing to highly hydrophilic groups. (2) The electrochemical behavior of (TPABPy) Cl_3 shows two separated highly reversible peaks at −0.56 and 0.76 V, related to the TEMPO

and viologen groups, resulting in a high cell voltage up to 1.32 V. The electronic structure was confirmed during the redox process with DFT calculation and electron paramagnetic resonance analyses. (3) The existence of hydrophilic quaternary ammonium can deliver extra solubility at 1.76 M (TPABPy)Cl_3 solution with reasonable stability and a high capacity of 25 Ah L^{-1} compared to the non-bipolar counterparts. More to the point, the capacity fading can be successfully retrieved by applying the polarity-inversion rebalance strategy to manage the charging species permeating through the membrane. In contrast to the redox-active polymer, this tactic also increases the molecular solubility in the solution and mass transfer rate in the electrode [35]. Mostly, reduced naphthoquinone derivatives tend to tautomerize to ketone forms and lose their redox reversibility due to the kinetics and thermal equilibrium. In addition, the double band conjugation with the quinone functional group is very susceptible to Michael addition in the alkaline medium. To improve the solubility of naphthoquinone in AORFBs with an asymmetric charge distribution, the amino acid group at the 3-position was grafted to the naphthoquinone, and 3-(2-chloro-1,4-naphthoquinon-3-ylamino)propanoic acid (3-AFNQ) was synthesized via biomimetic nature molecular [36]. The amino acid group causing hydrogen bonds with water molecules to augment the aqueous solubility and chloride substitution hinders enol–ketone tautomerization; consequently, great reversibility and good redox kinetics of 3-AFNQ appeared as a negolyte. The RFB demonstrates a 0.39% capacity fade rate per day at high concentration. The AORFBs containing 3-AFNQ with a concentration of 0.5 M displayed a capacity of 23.70 Ah L^{-1}, with a power density of 264 mW cm^{-2} and a capacity retention of 94.3% for over 500 cycles, which is one of the highest among AORFBs based on naphthoquinone derivatives at the corresponding time.

Typically, quinoxaline derivatives show poor chemical stability with capacity fade rates >20%/day. Compared to anthraquinones and phenazines, quinoxaline derivatives have valuable potential to make lower redox potentials and low molecular weights with accepted solubility. Careful molecular structure investigation reveals that the unwanted tautomerization of the reduced form under alkaline conditions is the main reason for the decomposition mechanisms. For this reason, 2,3-dimethylquinoxaline-6-carboxylic acid was completely analyzed with ultraviolet–visible spectroscopy, NMR, mass spectroscopy, and DFT modeling to elucidate the structure with the right place of functional groups to withstand tautomerization, thus leading to quinoxaline-2-carboxylic acid as a commercially available anolyte, while the other detrimental effects like a Michael addition, dimerization, or hydrogenation are not responsible for this huge amount of fading capacity [37]. Another anodic category utilized in neutral AORFBs with great potential is the naphthalene diimide family because of their highly conjugated molecular structure and tolerance of two-electron storage capacity in a two-step, two-electron transfer process. Naturally, when two separate steps of electron transfer occur, it has a detrimental effect on voltage and energy. Generally, the second electron transfer is tougher due to augmented coulombic repulsion and demands a more negative voltage. A new strategy was outlined to tune the redox properties and suppress this hurdle. A novel regional charge buffering strategy was implemented by attaching an electron-donating group to the core-building block of naphthalene diimides, thus following two electron transfers via a single-step redox process

[38]. This strategy increases the electron density of the p-conjugated framework, thereby moderating the rapid changes in charge density of the naphthalene diimide derivatives. Exceptional intrinsic stability was revealed by symmetrical battery testing of NDI-DEtOH with only 0.11% after 11 days. Compared to NDI/FcNCl, AORFBs with NDI-DMe/FcNCl and NDI-DEtOH/FcNCl demonstrated a notable enhancement (40%) in peak power density at 50% SOC. Aqueous RFBs have exhibited strong benefits such as high power, nonflammability, low cost, and several operational ion-selective membranes [39]. Similar to nonaqueous, electro active materials, they demonstrate high chemical diversity and earth-abundant elements.

5.3 NONAQUEOUS RFBs

Owing to the limited cell voltage (<1.3 V), conventional aqueous flow batteries usually indicate low energy density systems (~25 Wh L^{-1}), whereas nonaqueous flow batteries can attain a higher energy density (~50–100 Wh L^{-1}). More pronounced constraint is related to the high freezing temperature of water (≥0°C) that imposes severe limitations on attaining higher energy density in the regions at northern latitudes above 30° with average winter temperatures ranging between −10°C and −40°C [40]. Unlike the aqueous electrolytes, the nonaqueous counterpart extends a broader window of electrochemical stability that supports performance at higher cell voltages (>4 V). Due to the variety of nonaqueous solvents, there is a great selection of available organic redox building blocks. Accompanying these profits, it is promising to decrease the cost of energy and conceivably facilitate high-energy, small-footprint storage devices. In order to provide low energy cost ($100 per usable kWh), it is mandatory to generate high cell voltage (>3 V), high solubility (>0.8 kg kg^{-1}), and high charge capacity (~180 mA h g^{-1}) [41]. According to the capacity definition, it is described as the theoretical amount of charge (in mAh) accumulated per gram of material. The higher intrinsic capacity is obtained by the lower molecular weight. To address this challenge, the molecular "pruning" approach is a practical solution to decipher unclear electron transport mechanisms. Radical cations take part in prevalent reactions such as disproportionation, dimerization, deprotonation, and radical addition to the electrophilic center. A feasible way to overcome the above-mentioned hurdles is through steric protection with correct unit of substitution and accurate location; moreover, tuning the solubility in various types of polar electrolytes is also important.

All-organic nonaqueous RFBs suffer from serious low coulombic efficiency and capacity fade owing to the high permeability of redox-active species across the battery's membrane. Increasing the size of molecular dimensions above the membrane pore-size exclusion is a practical solution to magnify cycle life and efficiency. The oligomer compound was synthesized by displacement reaction between N-ethyl-4,4′-bipyridinium hexafluorophosphate with 1,3-bis(bromomethyl)benzene [42]. In the presence of macromolecular redox-active organics, denoted as 2a in Figure 5.5 (Some molecular structures used in nonaqueous RFBs), with 1.0 M concentration, the rate of active-material permeation at microporous polymer membranes (chemically cross-linking polymer to confine pore swelling in electrolyte) was reduced more than 9,000 (less than 3 μmol cm^{-2} day^{-1}) compared to Celgard separators for compound 2a.

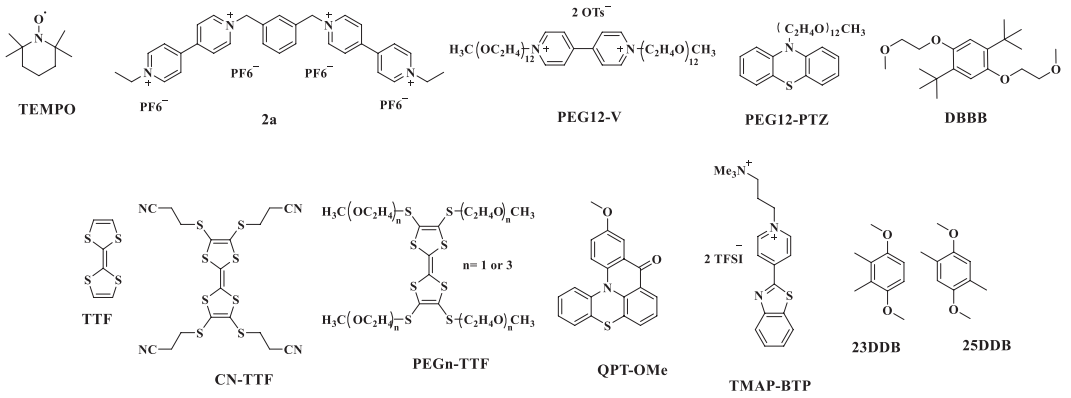

FIGURE 5.5 Chemical structures of various molecules for nonaqueous RFBs.

To achieve this goal, PEGylated phenothiazine and PEGylated viologen are employed as the catholyte and anolyte, respectively [43]. Along with a composite nanoporous aramid nanofiber separator, the cell exhibits distinguished capacity holding of 99.90% per cycle and a coulombic efficiency of 99.7%, while the half-PEGylated and non-PEGylated electrolytes show poorer cyclability because of the crossover of non-PEGylated materials. A series of potential substituted 1,4-dimethoxybenzenes has been comprehensively analyzed to eliminate the bulky substituent groups of 2,5-ditert-butyl-1,4-bis(2-methoxyethoxy)benzene (DBBB) and employed as a successful overcharge protection material [44]. All properties, including solubility, diffusivity, and galvanostatic cycling, were examined to derive that 2,3-dimethyl-1,4-dimethoxybenzene (23DDB) and 2,5-dimethyl-1,4-dimethoxybenzene (25DDB) are considered particularly promising among various derivatives. They found that the methyl groups still can handle both electron-donating and steric hindrance to stabilize the radical cations, while simultaneously achieving electrochemical stability performance as DBBB.

Potash et al. explained in detail the principle benefit of a concept regarding molecules with two redox processes and three states [45]. This approach has the capability to utilize small molecules with suitable flexibility, while the electronic interaction between redox units advocates an extra degree of freedom to tune the cell voltage of symmetric RFB. Bipolar redox-active molecules (BRMs) are an applied strategy to hamper electrolyte crossover and unpredictable side reactions in redox-flow batteries, which can cause electrolyte pollution. In this technique, the redox mediator can either oxidize or reduce reversibly on the half-cell independent reactions via a p-type moiety and an n-type moiety, respectively. Functional group modification of BRMs is a little restricted to bringing favorite redox-active moieties with suitable cell voltage through fused extent conjugation. Moreover, bipolar eutectic mixtures usually create high viscosity that has a detrimental influence on the diffusion rate of active molecules, which in turn leads RFB to work at a relatively low current density. In a research study, symmetrical RFB based on 11-methoxy-9H-quinolino[3,2,1-kl]phenothiazin-9-one, denoted QPT-OMe, containing quaternary ammonium and ketone redox moieties, was fabricated with an appropriate voltage gap of 2.5 V and good electrochemical stability. Strikingly, across a wide sweep rate between 5 and

5,000 mV s^{-1}, both cathodic and anodic peaks persisted very symmetrically [46]. The diffusion coefficient 2.3×10^{-6} $cm^2 s^{-1}$ of QPT-OMe was obtained by a perfect linear relationship of peak current versus the square root of the sweep rate by using the Randles–Sevcik equation. The symmetrical cell containing QPT-OMe as an active material and tetrabutylammonium bis-(trifluoromethylsulfonyl)imide (TBA-TFSI) as a support with equal volumes of 0.1 mL of 0.025 M QPT-OMe in a 0.5 M TBA-TFSI/acetonitrile solution was employed as both catholyte and anolyte, with a porous membrane as a separator. The cell function was scrutinized by UV–Vis spectra in which the anolyte displayed no clear change below 500 nm during a charge/discharge cycle. Whereas the SOC increased from 0% to 100%, a wide adsorption band steadily came into view at 650–850 nm. On the other hand, the catholyte around 425 nm fairly decreased when the SOC increased.

The limited availability of membranes and the crossover of redox materials are presenting severely challenging issues to attain the long-term cyclability of RFBs. To conquer these obstacles, a novel category of pyridinium-based negolytes was introduced. Through connecting benzothiazole into the C_4-position of pyridinium, the π-conjugation structure was broadened; meanwhile, the substitution reaction with nitrogen of pyridine produced a cationic ammonium functional group to increase solubility and suppressed crossover simultaneously, called TMAP-BTP [47]. Besides, the solubility was improved up to ~1.0 M by replacing the counterion from hexafluorophosphate (PF_6^-) or tetrafluoroborate (BF_4^-) to bis(trifluoromethanesulfonyl)imide ($TFSI^-$). From the molecular engineering point of view, these combined approaches generated high stability and enlarged the size of the molecule to inhibit the crossover of the pyridinium negolytes through an AEM. The increased stability originated from the combination of the electron-withdrawing effect and the extended conjugation effect of the benzothiazole group. Moreover, in the presence of tetrabutylammonium bis(trifluoromethanesulfonyl)imide (TBA-TFSI), the solubility of the pyridinium negolyte was raised to ~1 M in acetonitrile. Because of the large structure, the penetrance of $TMAP\text{-}BTP^{2+}$ and $TMAP\text{-}BTP^{+}$ through the AEM became slow (3.64×10^{-9} and 1.44×10^{-8} $cm^2 s^{-1}$, respectively; Figure 5.6a and b). The manufactured cells comprising 0.1 M of dicationic benzothiazolylpyridinium redox electrolytes demonstrated a capacity-fading rate per cycle of 0.0083% for 250 cycles in symmetric RFBs (Figure 5.6c) and 0.08% in full RFBs (Figure 5.6d), including the ammonium-substituted ferrocene as a posolyte for 500 cycles, which is a good sign in the evolutionary development direction.

Notwithstanding incredible growth, the limited solubility hindered higher energy density, parasitic reactions, and cyclability, which has a vital effect on the application of RFBs. Jiang et al. introduced a robust family of redox compounds, tetrathiafulvalenes (TTFs), and dual-type flow batteries, including aqueous and nonaqueous electrolytes in slurry and solution-based RFBs, correspondingly. TTF comprises four cyanoethyl chains (CN-TTF) employed in a suspension state in an aqueous electrolyte, while the cyano group anodically moves the redox potential to a higher cell voltage [48]. The integration of the hydrophobic chains into TTF increased the solubility and destroyed the dimerization of the aromatic core of TTF during the redox reaction concurrently, thus affording higher stability with a capacity retention of 75.8% after 1,000 cycles (99.97% per cycle) (226 h, 9.4 d) at 1.0 M CN-TTF. In addition, poly(ethylene glycol) chains (PEGn-TTF) dissolve in carbonate

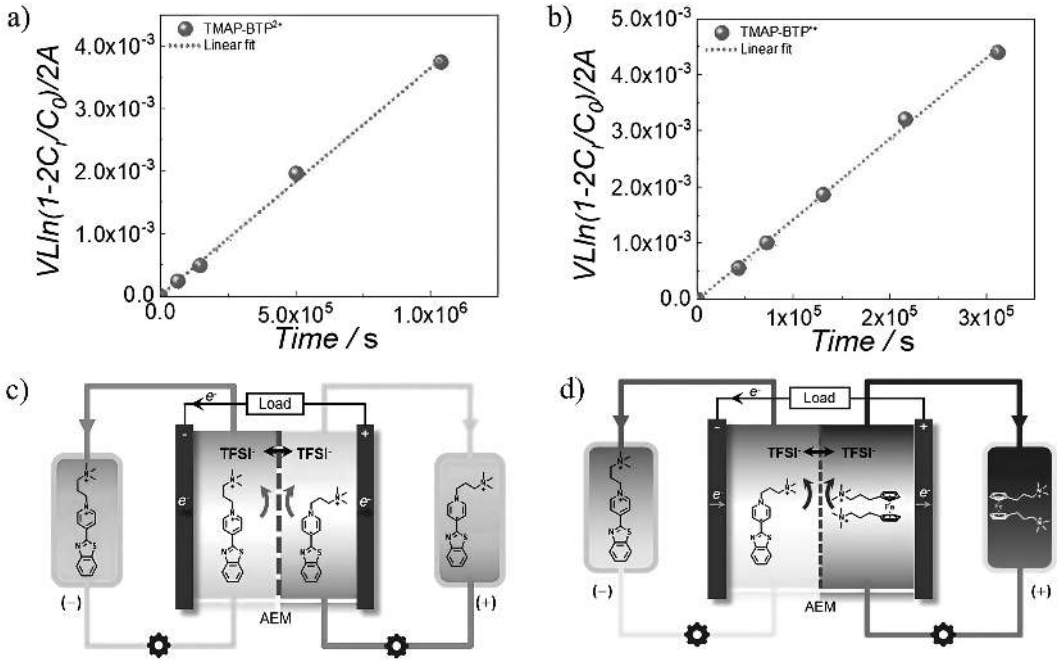

FIGURE 5.6 (a, b) Permeability curves of (a) 50 mM TMAP-BTP^{2+} and (b) 50 mM TMAP-BTP$^{\bullet+}$. Permeability was measured at 3.64×10^{-9} cm^2 s^{-1} and 1.44×10^{-8} cm^2 s^{-1}, respectively. (c) Schematic illustration of a symmetric RFB. (d) Schematic illustration of a full RFB. (Adapted with permission from [47], Copyright 2020, ACS.)

electrolyte with a concentration of 0.5 M (equivalent to 1.0 M electron concentration); when paired with Li as the anode, the battery displays capacity retention of 82.9% with a cell voltage of 3.64 V and a high energy density of 88 W h L^{-1} after 100 cycles (after 18 d, 99.87% per cycle). The electrochemical kinetics of TTF, CN-TTF, and PEG3-TTF (1 mM solution) were deliberated via RDE to specify the diffusion coefficients (D_0) and kinetic rate constant (k_0) by the Koutecký–Levich equation. The diffusion coefficients of all TTF compounds were of the order of 10^{-5} or 10^{-6} cm^2 s^{-1}, which means the attached chains have a negligible impact on the electrochemical kinetics.

Whereas nonaqueous redox flow batteries have appeared as a valuble route of energy storage system, still facing with critical issues that that we dicsscussed above. It has become manifest that molecular engineering strategies to attaching or detaching functional moieties, with their electron-withdrawing or donating groups, sustain a decisive pattern to meticulously tailor the redox potential, solubility, and stability of these organic materials. Furthermore in these molecular respects, the pragmatic features of cost and synthesis duration must be taken seriously.

5.4 CONCLUSION AND OUTLOOK

Yet, the development of organic redox-active materials for RFBs is still in its fancy stage, and further improvement is required to address the critical challenges to increase the volumetric capacity and energy density, and these parameters are much lower than those

of state-of-the-art vanadium RFBs. The solid answer to augment volumetric capacity is happening with high concentration/solubility of the organic active materials. We believe that there is a large space to generate the stable potential window of both aqueous- and nonaqueous-based electrolytes. In addition, the growth of high-performance (ionic conductivity and selectivity) and cost-effective membranes is another critical topic that has to be resolved. Furthermore, the lack of long-term cycling life, including both cycle number and cycle time, must be scrutinized in order to identify a stable redox couple with minimal crossover. Attaching hydrophilic substituents or polar functional groups can ameliorate the solubility of organic molecules, including sulfonic acid, hydroxyl, and ammonium groups. The structure asymmetry created by different substituted positions results in preferential solvation and increased molecular polarity. As a result, the solubility of organic molecules can be effectively improved. In the end, we have provided a complete summary of a diverse range of redox-active organic molecules and comprehensibly analyzed various functional groups on electrochemical behaviors. Moreover, in-depth assessments of the full cell-cycling performances of these redox-active posolytes and negolytes are also discussed.

REFERENCES

1. W. Kangro, Verfahren zur Speicherung von elektrischer Energie, German patent, 914264 (1949).
2. M. Rychcik, M. Skyllas-Kazacos, Characteristics of a new all-vanadium redox flow battery, *Journal of Power Sources*, 22 (1988) 59–67.
3. H. Zhang, W. Lu, X. Li, Progress and perspectives of flow battery technologies, *Electrochemical Energy Reviews*, 2 (2019) 492–506.
4. X. Li, M. Haghshenas, L. Wang, J. Huang, E. Sheibani, S. Yuan, X. Luo, X. Chen, C. Wei, H. Xiang, A multifunctional small-molecule hole-transporting material enables perovskite QLEDs with EQE exceeding 20%, *ACS Energy Letters*, 8 (2023) 1445–1454.
5. B. Xu, E. Sheibani, P. Liu, J. Zhang, H. Tian, N. Vlachopoulos, G. Boschloo, L. Kloo, A. Hagfeldt, L. Sun, Carbazole-based hole-transport materials for efficient solid-state dye-sensitized solar cells and perovskite solar cells, *Advanced Materials*, 26 (2014) 6629–6634.
6. E. Sheibani, B. Xu, *3D Printed Conducting Polymers for Perovskite Light-Emitting Diodes and Solar Cells, 3D Printed Conducting Polymers*, CRC Press, 2025, pp. 104–118.
7. J. Deng, H. Ahangar, Y. Xiao, Y. Luo, X. Cai, Y. Li, D. Wu, L. Yang, E. Sheibani, J. Zhang, Side-group-mediated small molecular interlayer to achieve superior passivation strength and enhanced carrier dynamics for efficient and stable perovskite solar cells, *Advanced Functional Materials*, 34 (2024) 2309484.
8. A. Feda, M. Moslempoor, E. Sheibani, Electron transporting materials based on n-type polymers in inverted perovskite solar cells: A review, *Iranian Journal of Polymer Science and Technology*, 36 (2023) 457–485.
9. E. Sheibani, M. Moslempoor, F. Arami Ghahfarokhi, Hole-transporting materials based on p-type polymers in invert perovskite solar cells, *Iranian Journal of Polymer Science and Technology*, 36 (2023) 107–132.
10. E. Sheibani, L. Yang, J. Zhang, *Conjugated Polymer for Charge Transporting Applications in Solar Cells, Organic Electrodes: Fundamental to Advanced Emerging Applications*, Springer, 2022, pp. 119–135.
11. D. Molina, E. Sheibani, B. Yang, H. Mohammadi, M. Ghiasabadi, B. Xu, J. Suo, B. Carlsen, N. Vlachopoulos, S.M. Zakeeruddin, Molecularly engineered low-cost organic hole-transporting

materials for perovskite solar cells: The substituent effect on non-fused three-dimensional systems, *ACS Applied Energy Materials*, 5 (2022) 3156–3165.
12. L. Lindh, O. Gordivska, S. Persson, H. Michaels, H. Fan, P. Chábera, N.W. Rosemann, A.K. Gupta, I. Benesperi, J. Uhlig, Dye-sensitized solar cells based on Fe N-heterocyclic carbene photosensitizers with improved rod-like push-pull functionality, *Chemical Science*, 12 (2021) 16035–16053.
13. E. Sheibani, L. Yang, J. Zhang, Recent advances in organic hole transporting materials for perovskite solar cells, *Solar RRL*, 4 (2020) 2000461.
14. L. Wang, E. Sheibani, Y. Guo, W. Zhang, Y. Li, P. Liu, B. Xu, L. Kloo, L. Sun, Impact of linking topology on the properties of carbazole-based hole-transport materials and their application in solid-state mesoscopic solar cells, *Solar RRL*, 3 (2019) 1900196.
15. E. Sheibani, M. Heydari, H. Ahangar, H. Mohammadi, H.T. Fard, N. Taghavinia, M. Samadpour, F. Tajabadi, 3D asymmetric carbozole hole transporting materials for perovskite solar cells, *Solar Energy*, 189 (2019) 404–411.
16. M.G. Gatty, S. Pullen, E. Sheibani, H. Tian, S. Ott, L. Hammarström, Direct evidence of catalyst reduction on dye and catalyst co-sensitized NiO photocathodes by mid-infrared transient absorption spectroscopy, *Chemical Science*, 9 (2018) 4983–4991.
17. E. Sheibani, M. Moslempoor, M. Ghiasabadi, Synthesis and application of organic hole transporting materials for perovskite solar cells at doped-free condition, *Applied Chemistry Today*, 19 (2024) 95–110.
18. M. Moslempoor, E. Sheibani, *Semiconducting Fibers for Optoelectronic Devices, Semiconducting Fibers*, CRC Press, 2024, pp. 89–101.
19. B. Hu, C. DeBruler, Z. Rhodes, T.L. Liu, Long-cycling aqueous organic redox flow battery (AORFB) toward sustainable and safe energy storage, *Journal of the American Chemical Society*, 139 (2017) 1207–1214.
20. Y. Ding, C. Zhang, L. Zhang, Y. Zhou, G. Yu, Molecular engineering of organic electroactive materials for redox flow batteries, *Chemical Society Reviews*, 47 (2018) 69–103.
21. D. Chao, S.-Z. Qiao, Toward high-voltage aqueous batteries: Super-or low-concentrated electrolyte?, *Joule*, 4 (2020) 1846–1851.
22. C. Wang, X. Li, B. Yu, Y. Wang, Z. Yang, H. Wang, H. Lin, J. Ma, G. Li, Z. Jin, Molecular design of fused-ring phenazine derivatives for long-cycling alkaline redox flow batteries, *ACS Energy Letters*, 5 (2020) 411–417.
23. T. Janoschka, N. Martin, M.D. Hager, U.S. Schubert, An aqueous redox-flow battery with high capacity and power: The TEMPTMA/MV system, *Angewandte Chemie International Edition*, 55 (2016) 14427–14430.
24. X. Zu, L. Zhang, Y. Qian, C. Zhang, G. Yu, Molecular engineering of azobenzene-based anolytes towards high-capacity aqueous redox flow batteries, *Angewandte Chemie*, 132 (2020) 22347–22354.
25. M. Wu, Y. Jing, A.A. Wong, E.M. Fell, S. Jin, Z. Tang, R.G. Gordon, M.J. Aziz, Extremely stable anthraquinone negolytes synthesized from common precursors, *Chem*, 6 (2020) 1432–1442.
26. M. Gao, M. Salla, Y. Song, Q. Wang, High-power near-neutral aqueous all organic redox flow battery enabled with a pair of anionic redox species, *Angewandte Chemie*, 134 (2022) e202208223.
27. Y. Ding, G. Yu, Molecular engineering enables better organic flow batteries, *Chem*, 3 (2017) 917–919.
28. J. Luo, A. Sam, B. Hu, C. DeBruler, X. Wei, W. Wang, T.L. Liu, Unraveling pH dependent cycling stability of ferricyanide/ferrocyanide in redox flow batteries, *Nano Energy*, 42 (2017) 215–221.
29. B. Hu, T.L. Liu, Two electron utilization of methyl viologen anolyte in nonaqueous organic redox flow battery, *Journal of Energy Chemistry*, 27 (2018) 1326–1332.

30. R. Rubio-Presa, L. Lubián, M. Borlaf, E. Ventosa, R. Sanz, Addressing practical use of viologen-derivatives in redox flow batteries through molecular engineering, *ACS Materials Letters*, 5 (2023) 798–802.
31. L. Tong, Y. Jing, R.G. Gordon, M.J. Aziz, Symmetric all-quinone aqueous battery, *ACS Applied Energy Materials*, 2 (2019) 4016–4021.
32. J.B. Gerken, C.W. Anson, Y. Preger, P.G. Symons, J.D. Genders, Y. Qiu, W. Li, T.W. Root, S.S. Stahl, Comparison of quinone-based catholytes for aqueous redox flow batteries and demonstration of long-term stability with tetrasubstituted quinones, *Advanced Energy Materials*, 10 (2020) 2000340.
33. X. Liu, T. Li, C. Zhang, X. Li, Benzidine derivatives: A class of high redox potential molecules for aqueous organic flow batteries, *Angewandte Chemie*, 135 (2023) e202307796.
34. L. Wang, M. Huang, K. Wan, Z. Fu, Z. Xiang, Z. Liang, Highly soluble TEMPO-viologen bipolar molecule for ultra-stable aqueous redox flow batteries, *Advanced Functional Materials*, 34 (2024) 2310620.
35. E.S. Beh, D. De Porcellinis, R.L. Gracia, K.T. Xia, R.G. Gordon, M.J. Aziz, A neutral pH aqueous organic–organometallic redox flow battery with extremely high capacity retention, *ACS Energy Letters*, 2 (2017) 639–644.
36. Y. Liu, P. Zhang, Z. Wu, G. Ding, X. Song, J. Ma, W. Wang, X.-Z. Wang, Z. Jin, Biomimetic naphthoquinone zwitterion derivative with water-solubilizing amino acid side chain for high-stability aqueous redox flow batteries, *ACS Energy Letters*, 9 (2024) 586–593.
37. S.V. Modak, D. Pert, J.L. Tami, W. Shen, I. Abdullahi, X. Huan, A.J. McNeil, B.R. Goldsmith, D.G. Kwabi, Substituent impact on quinoxaline performance and degradation in redox flow batteries, *Journal of the American Chemical Society*, 146 (2024) 5173–5185.
38. Z. Wang, X. Liu, X. Zhang, H. Zhang, Y. Zhao, Y. Li, H. Yu, G. He, Realizing one-step two-electron transfer of naphthalene diimides via a regional charge buffering strategy for aqueous organic redox flow batteries, *Materials Horizons*, 11 (2024) 1283–1293.
39. C. Zhang, Z. Niu, S. Peng, Y. Ding, L. Zhang, X. Guo, Y. Zhao, G. Yu, Phenothiazine-based organic catholyte for high-capacity and long-life aqueous redox flow batteries, *Advanced Materials*, 31 (2019) 1901052.
40. Z. Liang, R.K. Jha, T.M. Suduwella, N.H. Attanayake, Y. Wang, W. Zhang, C. Cao, A.P. Kaur, J. Landon, S.A. Odom, A prototype of high-performance two-electron non-aqueous organic redox flow battery operated at–40° C, *Journal of Materials Chemistry A*, 10 (2022) 24685–24693.
41. R.M. Darling, K.G. Gallagher, J.A. Kowalski, S. Ha, F.R. Brushett, Pathways to low-cost electrochemical energy storage: A comparison of aqueous and nonaqueous flow batteries, *Energy & Environmental Science*, 7 (2014) 3459–3477.
42. S.E. Doris, A.L. Ward, A. Baskin, P.D. Frischmann, N. Gavvalapalli, E. Chénard, C.S. Sevov, D. Prendergast, J.S. Moore, B.A. Helms, Macromolecular design strategies for preventing active-material crossover in non-aqueous all-organic redox-flow batteries, *Angewandte Chemie*, 129 (2017) 1617–1621.
43. J. Chai, A. Lashgari, X. Wang, C.K. Williams, All-PEGylated redox-active metal-free organic molecules in non-aqueous redox flow battery, *Journal of Materials Chemistry A*, 8 (2020) 15715–15724.
44. J. Huang, L. Su, J.A. Kowalski, J.L. Barton, M. Ferrandon, A.K. Burrell, F.R. Brushett, L. Zhang, A subtractive approach to molecular engineering of dimethoxybenzene-based redox materials for non-aqueous flow batteries, *Journal of Materials Chemistry A*, 3 (2015) 14971–14976.
45. R.A. Potash, J.R. McKone, S. Conte, H.D. Abruna, On the benefits of a symmetric redox flow battery, *Journal of The Electrochemical Society*, 163 (2015) A338.
46. Y. Liu, G. Dai, Y. Chen, R. Wang, H. Li, X. Shi, X. Zhang, Y. Xu, Y. Zhao, Effective design strategy of small bipolar molecules through fused conjugation toward 2.5 V based redox flow batteries, *ACS Energy Letters*, 7 (2022) 1274–1283.

47. S. Ahn, J.H. Jang, J. Kang, M. Na, J. Seo, V. Singh, J.M. Joo, H.R. Byon, Systematic designs of dicationic heteroarylpyridiniums as negolytes for nonaqueous redox flow batteries, *ACS Energy Letters*, 6 (2021) 3390–3397.
48. X. Wang, A. Lashgari, R. Siwakoti, R.K. Gautam, J.J. McGrath, P. Sarkar, G. Naber, J. Chai, J.J. Jiang, Tetrathiafulvalene (TTF) derivatives as catholytes for dual-type redox flow batteries: Molecular engineering enables high energy density and cyclability, *Journal of Materials Chemistry A*, 11 (2023) 19056–19065.

CHAPTER 6

Electrocatalysts for Flow Batteries

Sreenivasan Rijith, Athira B. Suresh, and
Vijayakumari Sasidharan Nair Sumi

6.1 INTRODUCTION

In 2019, the U.S. National Oceanic and Atmospheric Administration (NOAA) reported that it was the hottest July on record globally [1]. The urgency to transition the global economy to a low-carbon economy has become evident. A recent extensive survey by the Pew Research Center revealed that people in many countries consider global climate change a significant threat to their nations [2]. It is clear from an engineering perspective that any renewable energy system will necessitate large-scale energy storage. An effective storage unit must have the capacity to store energy generated from intermittent renewable sources like solar and wind power and release it as needed. Developing efficient energy storage systems will not only improve the performance and reliability of the electrical grid by storing surplus electrical power during low-demand periods and releasing it during peak periods (i.e., load balancing), but it can also be used as a cost-effective solution for peaks at industrial and commercial sites, leading to a substantial reduction in utility expenses. Additionally, it can function as an uninterruptible power supply to supply electrical power to a load in the event of a main power source failure.

Redox flow batteries (RFBs) are considered one of the most promising technologies for electrochemical energy storage devices [3]. Unlike traditional batteries, where the electroactive substances are housed inside the cell and serve as the electrode, in RFBs, the electrochemically active substances for each electrode are dissolved in electrolytes and stored in separate external tanks. These electrolytes are then circulated through the cell containing the electrodes, where the redox reactions take place [4]. Typically, the negative and positive half-cells are housed in separate compartments and are divided by an

DOI: 10.1201/9781003506379-6

ion-exchange membrane to prevent the electroactive substances from crossing over. A schematic of a standard RFB is illustrated in Figure 6.1.

The energy and power of RFBs can be independently scaled up because the active materials are stored in electrolytes rather than internally in the electrodes. The size of the electrodes in the cell controls the power density of RFBs, while the energy density of the battery is determined by the size of the external storage tanks and electrolyte volume. Furthermore, RFBs typically have a longer operational life with less maintenance compared to conventional static batteries because the electroactive species are stored in the electrolyte rather than the electrodes, thus avoiding any chemical or physical changes in the electrode during operation.

The electrodes play a crucial role in the RFBs. They serve as the active sites for the redox reactions within the battery and can influence the kinetics and reversibility of the redox couples involved. Furthermore, the electrode structure can impact concentration and activation overpotentials, directly affecting the battery's voltage efficiency. As a result, extensive research is currently dedicated to developing stable, low-resistance, and cost-effective electrode materials for RFBs. Although RFBs based on various chemistries such as iron-chromium, zinc-bromine, all-vanadium, zinc-cerium, all-iron, polysulfide-bromine, and organic-based species have been suggested, most electrode development studies have

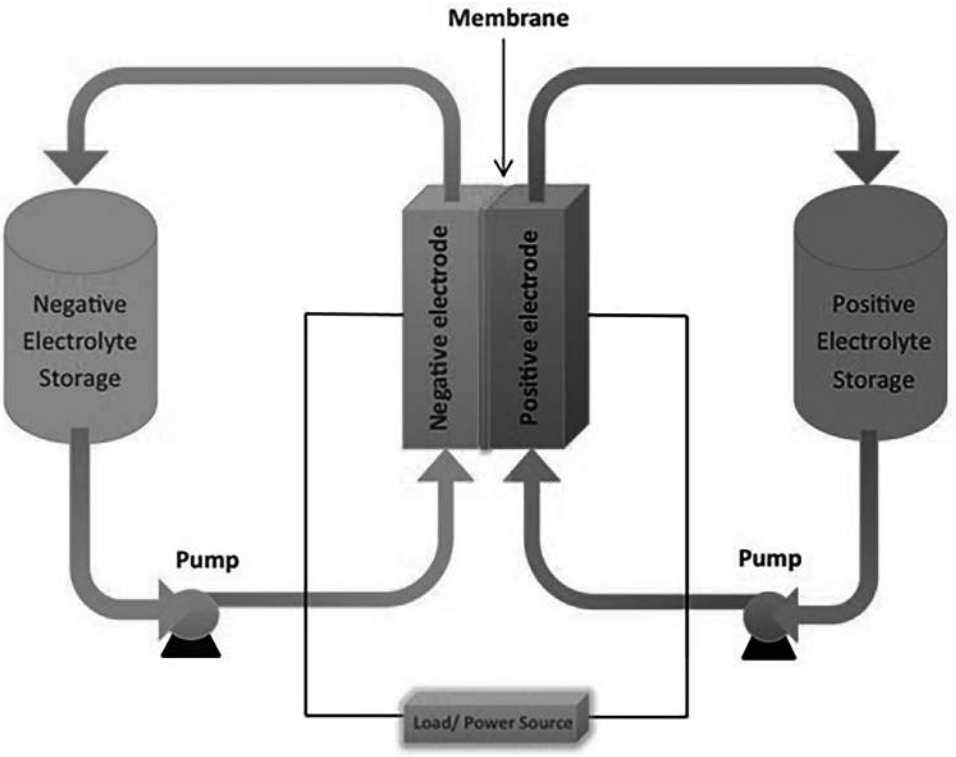

FIGURE 6.1 Schematic representation of a redox flow battery (RFB). (Adapted with permission from [6]. Copyright 2020, Wiley.)

focused on vanadium-based RFBs. All-vanadium RFBs are the most popular due to the use of vanadium species in both half-cells, allowing for regeneration of the solution through recharging or rebalancing the electrolytes in the event of cross-contamination.

In redox reactions, precious metals are considered superior catalysts compared to carbon-based materials [5]. Electrocatalysts made of metal oxides have been considered as promising cost-effective alternatives to precious metals. Therefore, the focus of this chapter is to give a summary of the latest advancements in electrocatalysts made of both metals and metal oxides.

6.2 METHODS FOR MODIFICATION WITH METALS AND METAL OXIDES

A variety of techniques have been used to alter electrodes with metal and metal oxide electrocatalysts for use in RFBs. Modifying electrodes with metal electrocatalysts has been accomplished through different methods, including electrodeposition, impregnation/drying, and direct addition of metal ions into the battery electrolyte. During electrodeposition, the unmodified electrode is placed in an electrolyte containing the desired metal ions, and then an electric current is used to coat the metallic ions onto the electrode. This method offers the advantage of closely controlling the grain size, mass, and thickness of the metal electrocatalyst layer by adjusting the electrodeposition operating parameters, such as deposition time, current, and electrolyte composition. Additionally, the electrodeposition process is easily scalable and does not require any subsequent treatment steps like annealing, making it a simple procedure. However, it has been demonstrated that electrodeposition of nanosized particles has some limitations regarding the achievable morphologies and size ranges [7].

Soaking an unaltered electrode in a water-based solution containing the water-soluble precursor of the desired metal is the process of impregnation. Metal chlorides, sulfates, and nitrates are the most commonly used metal precursors. When the electrode is immersed in the precursor solution, metal-containing substances either stick to the substrate through ion adsorption or exchange ions with components on the substrate. Afterward, the electrode is rinsed and dried to remove excess solvent. Finally, an activation step is carried out to convert the deposited metal compound into an active phase. This typically involves calcination to form a metal oxide and a reduction step to convert the metal oxide into the corresponding metal catalyst. Impregnation is a well-researched and uncomplicated method for modifying electrodes. However, this technique tends to result in low metal loadings on the electrode surface. It is possible to achieve higher metal loadings by skipping the washing step and directly drying the electrode to retain all the precursor on the electrode surface, although the mechanical durability of these catalysts is uncertain.

The electrode is modified with catalysts before the battery is operated in the methods mentioned above. Some studies have taken an approach to directly add the metallic ion of the desired catalyst to the battery's electrolyte to avoid lengthy and complex pretreatment steps. Depending on the electrode potential of the catalyst, the metal may dissolve back into the electrolyte during discharge. The catalyst layer is deposited in situ during battery operation, utilizing part of the current applied to the battery for this purpose instead of charging the vanadium species. As a result, during discharge, part of the output current

comes from the dissolution of the catalyst species. This method, while ingeniously simple, is only suitable for specific types of metal catalysts with standard electrode potentials for deposition close to the electrode potentials of the vanadium redox reactions. One potential drawback of this method is that agglomeration may cause the growth of large catalyst particles on the substrate, which could dislodge and form a suspension of large particles in the electrolyte. Additionally, when the catalyst is introduced as an additive to the electrolyte, its performance will also depend on the ease of deposition/dissolution over repeated charge/discharge cycles of the battery [8].

Previous investigations into metal oxide electrocatalysts have predominantly utilized hydrothermal methods, although the techniques employed for metal catalysts have also been intermittently applied. Using this method, chemical reactions are conducted in a heated autoclave at elevated temperatures and pressures to produce a metal oxide compound [9]. This approach offers the advantage of allowing control over the crystal size, morphology, and composition of the resulting electrocatalyst by adjusting the temperature, pressure, pH, and concentration of the aqueous solution. In certain studies, the hydrothermal process is succeeded by calcination or heat treatment. Classical RFBs utilize a solution-based redox couple recycled through each half-cell to a reservoir, a common strategy being to separate the half-cells by an ion-exchange membrane in a bipolar plate filter-press reactor, while hybrid RFBs combine a solution-based redox couple with an electrode surface/solution electrode reactions [10].

Another technique used for creating metal oxide catalysts for RFBs is electrospinning. This method involves applying an electric field to transform a viscoelastic polymeric liquid into a solid polymeric fiber. When synthesizing metal oxide catalysts, the polymeric liquid contains soluble metal salts. After the electrospinning process, the collected fabric undergoes a calcination step to create the metal oxide compound and eliminate the polymeric template. Electrospinning is a versatile approach for producing fibers and can be adapted to different materials. However, there are some experimental challenges when working with metal oxides. One significant challenge is that mixing the polymeric liquid with metal salts can significantly alter the solution's conductivity, directly impacting the electrospinning process and potentially making it difficult to control fiber thickness.

6.3 METAL ELECTROCATALYSTS

Transition and noble metals are commonly utilized as electrocatalysts because of their high activity, which stems from their electron configuration. The catalytic activity of transition metals is associated with their partially filled d orbital, enabling them to either donate or accept electrons. Metal electrocatalysts, known for their exceptional electrical conductivity, are appealing for application in RFBs. Nevertheless, the high cost of noble and rare-earth metals makes them impractical for large-scale RFBs. Early research efforts focused on substituting carbon-based electrodes with more durable all-metal electrodes, despite the increased expense. Assessments of lead, titanium, platinized titanium, and iridium oxide dimensionally stable anode (DSA) electrodes indicated that platinized titanium and iridium oxide DSA exhibited good reversibility for redox reactions. Further exploration of alternative metal-based catalyst options and cost reduction for electrodes is necessary [11].

6.3.1 Iridium-Based Catalysts

Iridium, a transition metal, is commonly utilized as a catalyst because of its resistance to corrosion and a wide range of oxidation states. It was anticipated that applying iridium to graphite felt (GF) would reduce cell resistance and battery overpotential. However, experiments involving polarization and impedance spectroscopy revealed a 63% decrease in overpotential. The slope of the Warburg impedance was higher in the Ir-modified felt, indicating that the reduced diffusivity was caused by the blockage of felt pores by Ir-containing substances. Charge/discharge experiments demonstrated an approximately 11% improvement in energy efficiency of a bench-scale RFB with Ir-modified positive felt. However, the charge efficiency was lower when using iridium-modified GF at this current density.

In their 2012 study, Tsai et al. utilized graphene instead of GF and adorned it with iridium, discovering that the peak separation for V(IV)/V(V) was smaller when graphene was decorated with iridium. Further investigation is necessary to comprehend the impact of iridium on battery performance [12,13].

6.3.2 Platinum-Based Catalysts

Platinum is a valuable metal known for its ability to resist oxidation and high temperatures, making it useful in various catalytic applications. In an acidic solution, platinum has been utilized as a catalyst for the redox reaction. To improve the reaction, platinum-modified graphite electrodes have been employed. Huang et al. experimented with coating platinum/multiwalled carbon nanotubes (Pt/MWCNTs) on pristine GF and evaluating the electrode's performance for the V(IV)/V(V) and V(III)/V(IV) redox reactions [14]. They observed low energy efficiencies in two types of batteries, attributing the low energy efficiency primarily to poor coulombic efficiencies. Tseng et al. examined the performance of Pt particles deposited on a carbon black catalyst (Pt/C) at different platinum-to-carbon ratios. They discovered that higher storage capacity, voltage efficiency, and current efficiency were achieved with higher Pt loadings [15]. However, current efficiency showed minimal change with any further increase in Pt content, possibly due to its simultaneous enhancement of oxygen evolution. Stabilizers are incorporated during the metal impregnation process to prevent particle aggregation and control their distribution. The polyol process, which utilizes ethylene glycol as a reducing agent and stabilizer, was used for metal deposition. The polyol-based Pt/C catalyst exhibited a 34% reduction in particle size and a more uniform distribution over the electrode surface compared to commercially prepared Pt/C. The polyol-based Pt/C GF electrodes demonstrated a higher voltage efficiency (≈10%) compared to commercial Pt/C electrodes. Further research on the role of electrocatalyst particle size and distribution in enhancing voltage efficiency would be advantageous [16].

6.3.3 Indium-Based Catalysts

Indium, a post-transition metal, has been used in the semiconductor industry to enhance hydrogen evolution overpotential, reducing the hydrogen evolution reaction rate. Indium-modified carbon paper electrodes have shown potential for battery applications, with 6.84 wt% indium deposited through impregnation. The modified electrodes showed increased oxidation and reduction peak currents compared to thermally treated and

as-received carbon papers. The enhanced wettability of the electrode may be influenced by higher hydrophilicity and an enlarged effective surface area. Despite no charge/discharge experiments or stability under electrolyte flow, further research into the performance of this catalyst in an operational RFB would be beneficial [17].

6.3.4 Bismuth-Based Catalysts

Bismuth is a dense, heavy metal commonly used as a catalyst in organic reactions due to its low toxicity and cost-effectiveness. Research indicates that bismuth-modified GFs can be utilized in RFBs to achieve smaller peak separation and higher cathodic and anodic peak current densities, but the electrode's performance in an operational RFB was not assessed. It was determined that an optimal concentration of 0.01 m Bi^{3+} yielded the best results, as higher concentrations caused the formation of large bismuth particles on the GF surface. The redox reactions exhibited significant performance enhancements in the modified GF electrodes compared to bismuth-modified carbon felt electrodes [18].

6.3.5 Antimony-Based Catalysts

Antimony was directly added to the negative electrolyte of an RFB in the form of $SbCl_3$ salt and was deposited onto a polyacrylonitrile (PAN)-based GF electrode during battery charge without complex pretreatment procedures. However, analysis indicated that some antimony particles may persist on the electrode surface after discharge, potentially accumulating over multiple charge–discharge cycles. The catalytic impact of antimony on the reactions was assessed, demonstrating increased catalytic activity and capacitance. A comparison of charge/discharge cycles with and without antimony ions showed a higher discharge capacity and power density in the presence of antimony. Although the performance of the battery with antimony ions in the negative electrolyte was not directly compared with the previously discussed RFB modified with bismuth, the data suggested that bismuth-modified electrodes offered greater efficiencies than antimony-modified electrodes [19].

6.3.6 Tin-Based Catalysts

Mehboob et al. investigated the use of tin as an additive in RFBs. Tin had a significant impact on the electrochemical performance of the battery, especially when included in the negative electrolyte [20]. Adding 0.01 M Sn^{2+} to the negative electrolyte reduced overpotential and improved specific capacity, particularly at higher current densities, resulting in energy efficiency comparable to other additives. However, the addition of Sn^{2+} to the negative electrolyte slightly decreased current efficiency. The presence of Sn^{2+} had a more significant effect on enhancing battery performance when added to the negative side compared to the positive side. The observed improvement when Sn^{2+} was added to the positive electrolyte could be attributed to the crossover of Sn^{2+} from the positive to the negative side, subsequently catalyzing the negative reaction [21].

6.3.7 Copper-Based Catalysts

Copper possesses excellent conductivity for electricity and exhibits catalytic properties, making it an appealing choice for various electrochemical processes. A recent investigation

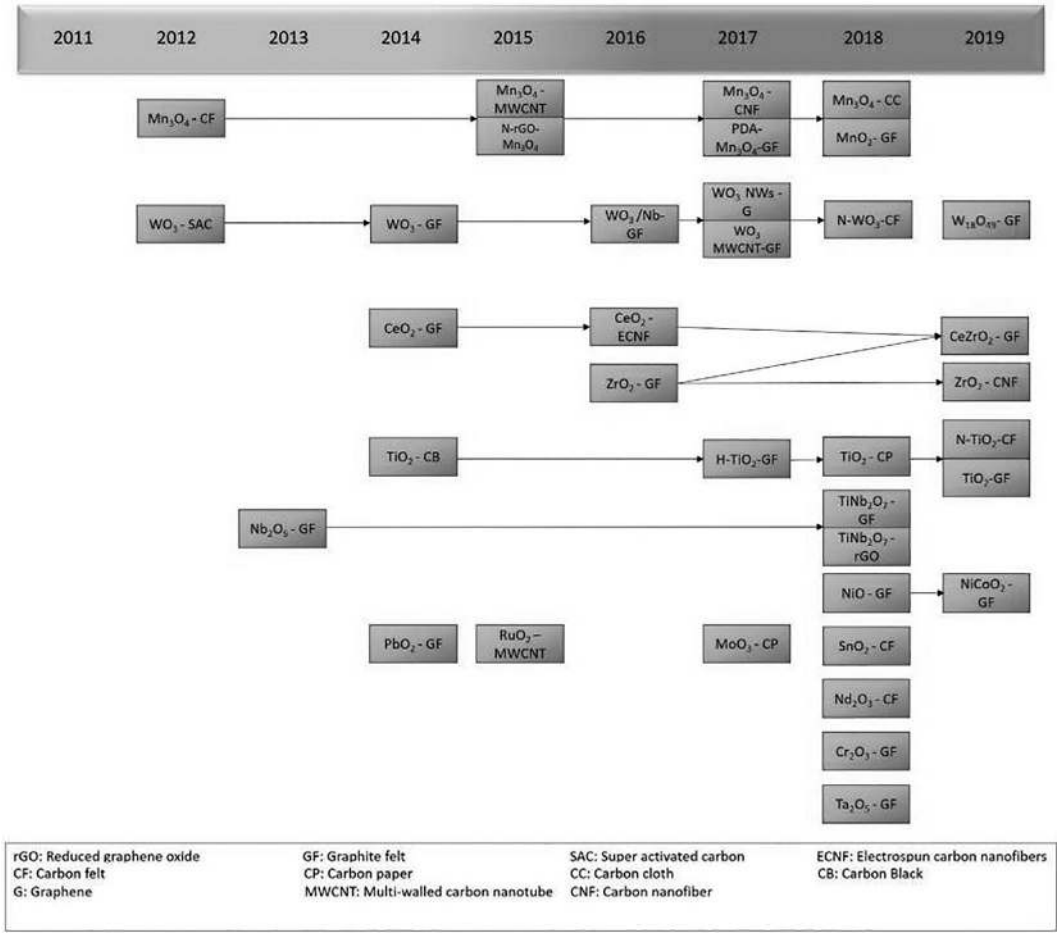

FIGURE 6.2 Historical flowchart for research on metal electrodes and metal electrocatalysts for RFBs. (Adapted with permission from [6]. Copyright 2020, Wiley.)

delved into the impact of copper nanoparticles on enhancing the redox reaction through synchronous metal deposition during charging. Experiments using full cells demonstrated that copper nanoparticles decreased overpotentials and improved energy efficiency in a bench-scale RFB at high current densities. However, a recent analysis found that copper speeds up hydrogen evolution in the negative half-cell, resulting in a loss of capacity. The study also observed a slight decline in charge efficiency, possibly due to the utilization of current by copper deposition during charging. Further research is necessary to comprehend the potential impact of copper on battery charge efficiency and capacity (Figure 6.2) [22].

6.4 METAL OXIDE ELECTROCATALYSTS

Metal oxides are preferred as electrocatalysts because they can function as acid or base sites, promote heterolytic dissociative adsorption, and improve interaction with polar molecules. Transition metal oxides, which consist of transition metal cations and oxygen anions, are especially sought after for specific catalytic processes. They are cost-effective

and durable, making them well-suited for large-scale energy storage systems such as RFBs. Nevertheless, metal oxides face the challenge of low electronic conductivity, which hampers battery performance. To tackle this issue, electrocatalyst supports with high conductivity, such as carbon-based nanomaterials, can be employed. This holds significant promise for RFBs [23].

6.4.1 Mn_3O_4-Based Catalysts

Mn_3O_4 catalysts exhibit electrocatalytic properties for a variety of redox reactions because of their polymorphism and mixed-valence states. They enhance the energy efficiency of RFB systems by using metal oxide-modified electrodes. Mn_3O_4 particles attached to carbon nanotubes demonstrate high electrical conductivity and favorable catalytic effects. By integrating Mn_3O_4 into carbon-based nanofibers, a mechanically flexible, self-supporting electrode with excellent conductivity and catalytic activity is produced. The research investigates the enhancement of Mn_3O_4 catalysts in battery manufacturing. The Mn_3O_4-CNF electrode showed a higher number of active sites and improved electrode kinetics. Nonetheless, the charge efficiency experienced a slight decrease due to side reactions. Ejigu et al. developed an N-rGO-Mn_3O_4 catalyst for RFB systems, maintaining electrode activity even after 2,000 cycles. Additional experiments are necessary to comprehend the role of Mn_3O_4 in enhancing electrode performance [24].

6.4.2 MnO_2-Based Catalysts

Manganese dioxide, a different form of manganese oxide, can be created by oxidizing Mn_3O_4. Similar to Mn_3O_4, MnO_2 is a cost-effective and environmentally friendly metal oxide that acts as a catalyst in various systems. Previous studies on the use of MnO_2-modified graphene foam for supercapacitors have shown that the pH of the solution can control the shape of MnO_2. In the absence of HCl, MnO_2 typically takes on a consistent reticular shape on graphene. However, the introduction of HCl can result in the formation of crumpled flower-like, regular flower-like, or uniform hollow MnO_2 nanotubes, depending on the amount of acid added [25].

6.4.3 PbO_2-Based Catalysts

Compared to most other metal oxide electrocatalysts, such as MnO_2 mentioned earlier, PbO_2 exhibits high electrical conductivity. It is also more affordable than noble metals and resistant to corrosion. The tetragonal β-PbO_2 form is typically used as the anode electrode due to its lower resistivity, which can be achieved through deposition in acidic conditions. On the other hand, the orthorhombic α-PbO_2 form, obtained through deposition from alkaline solutions, is more compact and provides better particle contact and adhesion to most surfaces. Although the potential change in the effective surface area of the electrode upon modification was not explored, larger anodic and cathodic current densities for the redox reactions were observed in the cyclic voltammograms (CVs) conducted on this electrode. A voltage efficiency of 82.4% was achieved at 70 mA cm^{-2} with PbO_2-modified GF, which was moderately higher than the 79.8% achieved using unmodified GF [26].

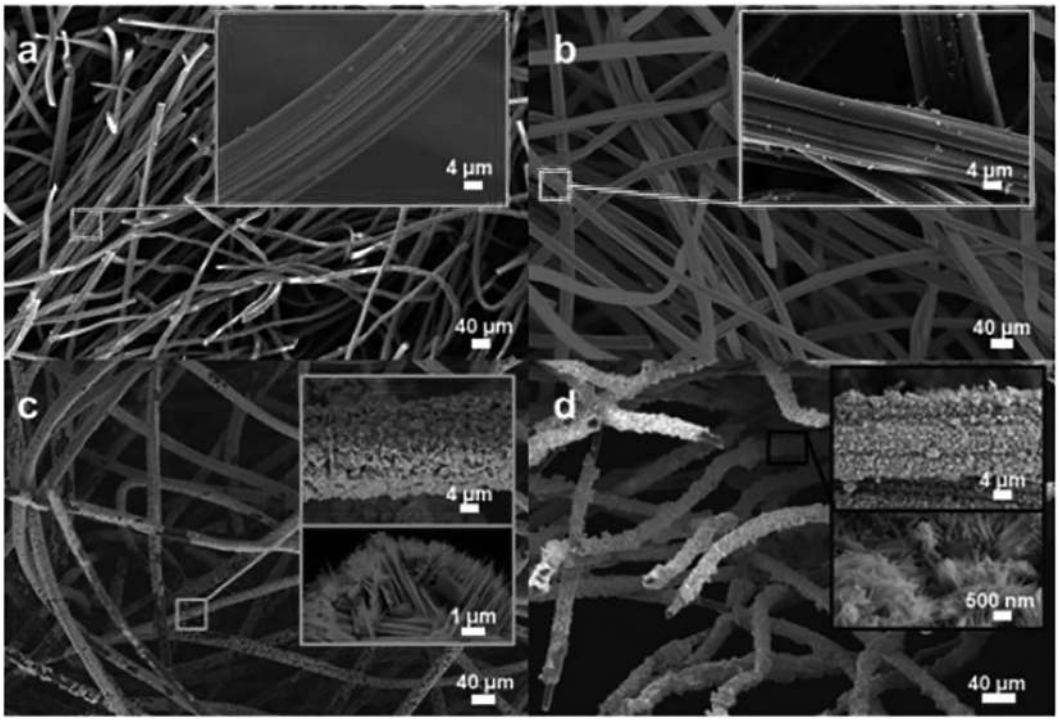

FIGURE 6.3 Morphology of different modified carbon felt electrodes. (a) Heat-treated CF; (b) nitrogen-doped heat-treated CF; (c) WO_3-modified CF; and (d) nitrogen-doped WO_3-modified CF. (Adapted with permission from [6]. Copyright 2020, Wiley.)

6.4.4 WO_3-Based Catalysts

WO_3 exhibits unique optical properties and sensing capabilities as a metal oxide, finding applications in gas sensors, catalysts, and semiconductors. Although it is less expensive than metal-based electrocatalysts, its low conductivity makes it unsuitable for standalone use as an electrode. Yao et al. developed a composite WO_3-superactivated carbon for RFB systems, enhancing redox reactions [27]. Kabtamu et al. studied the enhanced performance of a GF electrode with hexagonal tungsten (h-WO_3) nanowires doped with niobium, achieving an energy efficiency of 65.83% at 160 mA cm^{-2} (Figure 6.3) [28].

He created a 3D graphene sheet foam modified with WO_3 nanowires, establishing a conductive network to support other materials such as metal oxide catalysts. The combination of WO_3 and MWCNTs offered high surface area, beneficial carboxyl groups, and catalytic sites for the RFB system. Hosseini et al. explored modifying carbon felt with nitrogen and WO_3 groups, resulting in modified electrodes with enhanced electrocatalytic activity, increased capacitance, and electrode surface area [29].

6.4.5 CeO_2-Based Catalysts

CeO_2, a naturally occurring compound of cerium, is a widely available rare-earth element that is frequently used as a catalyst in three-way converters to transform carbon

monoxide, hydrocarbons, and nitrogen oxides into harmless byproducts. CeO_2 facilitates the VO_2^+/VO^{2+} redox reaction by providing oxygen vacancies. Research indicates that electrodes modified with CeO_2 exhibit lower peak separation and charge-transfer resistance compared to unmodified substrates. However, modifying substrates with CeO_2 has been found to improve their wettability, as evidenced by contact angle measurements. The electrochemical activity of the electrode was assessed for the V(IV)/V(V) reaction, and it was determined that an electrode containing 0.2 wt% CeO_2\GF was the most effective. Jing et al. proposed the utilization of electrospun carbon nanofibers containing CeO, which boast a large surface area and good conductivity but low hydrophilicity. Introducing CeO_2 as a modification resulted in a more than fourfold increase in the effective surface area of the carbon nanofiber electrode. Nevertheless, the authors concluded that CeO_2 did not display any electrocatalytic activity in the V(IV)/V(V) reaction, and the observed enhancement in the current response of the positive redox reaction on the CeO_2-ECNF electrode was attributed to the significantly higher ECSA [30].

6.4.6 ZrO_2-Based Catalysts

Zirconium dioxide has seen rapid growth as a catalyst for various applications, including ethanol electro-oxidation and the reduction of carboxylic acid to aldehydes. This is due to the abundant oxygen-containing functional groups provided by ZrO_2 and its unsaturated Lewis acid-base Zr^{4+}-O^{2-} pairs. The introduction of zirconium nanoparticles into GF improved the wettability of the electrode surface and resulted in a reduction in separation of the CV peaks, as well as an increase in the peak current densities for both redox reactions on ZrO_2-GF compared to unmodified GF. The characterization of the catalytic activity of ZrO_2 using peak separation and charge-transfer resistance values indicates the necessity for further detailed analysis to determine whether ZrO_2 exhibits catalytic activity toward the vanadium redox reactions, in addition to enhanced wettability. An RFB assembled with ZrO_2-GF as both negative and positive electrodes demonstrated improved voltage and energy efficiencies. To better evaluate the stability of the electrospun electrodes compared to those fabricated via impregnation, battery performance must be directly compared over more cycles and at higher current densities [31].

6.4.7 $CeZrO_2$-Based Catalysts

The performance of mixed cerium–zirconium oxides ($Ce_xZr_{(1-x)}O_2$) on both the negative and positive sides of an RFB was investigated by Yu et al., as the separate incorporation of CeO_2 and ZrO_2 particles was found to have positive effects on RFB performance [32]. This mixed oxide is widely used as a three-way catalyst in the energy field. Incorporating zirconia into the CeO_2 structure is known to decrease its specific surface area. However, ceria–zirconia mixed oxide has been demonstrated to possess a very high oxygen storage capacity, indicating its ability to donate and accept oxygen in a reaction. Similar to previous findings, the incorporation of CeO_2 led to increased electrode wettability. It remains unclear whether the catalysts exhibited catalytic activity toward vanadium redox reactions or if the enhanced battery performance due to modification was solely a result of the improved wettability of the electrode. Nonetheless, the authors proposed a mechanism for

the catalytic reaction. When $CeZrO_2$–GF electrodes were utilized on both the negative and positive sides, the RFB demonstrated higher energy and voltage efficiencies compared to configurations where $CeZrO_2$–GF was used in only one of the half-cells or when using bare GF electrodes. The energy efficiency achieved by an RFB operating with $CeZrO_2$–GF on both sides was similar to the level reported in the previous study with ZrO_2 [33].

6.4.8 TiO_2-Based Catalyst

TiO_2 is an n-type semiconductor that demonstrates excellent stability in both acidic and alkaline environments. It has found use in diverse applications such as solar cells, photocatalysts, and sensors. It enhances the wettability of the catalyst layer and remains chemically stable. Tseng et al. developed a composite material consisting of TiO_2 and carbon black for the negative electrode in an RFB, effectively suppressing hydrogen evolution and exhibiting greater hydrophilicity and wettability compared to an unmodified carbon felt electrode [34]. Vazquez-Galvan et al. cultivated hydrogen-treated rutile, a titanium dioxide polymorph, on GF to be utilized as the negative electrode in RFBs [35]. The hydrogen treatment aimed to create oxygen vacancies in the TiO_2 lattice, resulting in absorption across both UV and visible ranges up to 800 nm. The TiO_2-modified electrode notably inhibited the HER, and the charge efficiency and specific capacity exceeded those achieved in Tseng et al. [34].

6.4.9 Nb_2O_5-Based Catalysts

Nb_2O_5, as a transition metal oxide and an n-type semiconductor, exhibits high stability in acidic aqueous environments. Through the addition of tungsten to the electrolyte in the form of ammonium paratungstate, the researchers successfully facilitated the catalyst's precipitation on the electrode's surface, thereby decreasing agglomeration. Based on their analysis using fast Fourier transform, they hypothesized that the inclusion of ammonium paratungstate resulted in the creation of tungsten-doped Nb_2O_5 single crystal nanorods instead of a mixture of WO_3 and Nb_2O_5 nanorods. The potential enhancement of the surface area due to the modification was not taken into account, and the improved electrochemical performance observed in their CVs was credited to enhanced electrode kinetics. Further investigations are necessary to determine the role of this Nb_2O_5-based catalyst in facilitating the redox reactions [36].

6.4.10 $TiNb_2O_7$-Based Catalysts

Based on previous research, enhancing the electrodes with titanium and niobium-based oxides led to better performance of the RFB. Therefore, Kabtamu et al. proposed utilizing titanium niobium oxide ($TiNb_2O_7$) as a catalyst for this purpose [37]. The structure of ($TiNb_2O_7$) is monoclinic and layered, with Ti^{4+} and Nb^{5+} coordinated to six oxygen atoms to form TiO_6 and NbO_6 groups at edge-sharing and corner-sharing octahedral sites, respectively. Due to $TiNb_2O_7$'s poor electronic conductivity, Kabtamu et al. created an electrode by combining it with GF. The $TiNb_2O_7$-modified GF was specifically assessed for the redox reactions. Modification with the catalyst was found to enhance the wettability of the electrode, as indicated by contact angle measurements. In the absence of reduced graphene

sheets, noticeable aggregation of $TiNb_2O_7$ nanoparticles took place. However, the presence of graphene caused the $TiNb_2O_7$ nanoparticles to attach themselves to the sites provided by rGO, thereby preventing aggregation. Furthermore, the $TiNb_2O_7$ particles acted as a spacer, preventing the restacking of the rGO. The energy efficiency achieved for a single cell assembled with $TiNb_2O_7$-rGO-modified positive and negative electrodes was slightly higher than that previously reported by Kabtamu et al. using $TiNb_2O_7$-modified GF electrodes [37].

6.4.11 NiO-Based Catalysts

Nickel oxide, an inexpensive semiconductor, has been employed as a catalyst for the oxygen evolution reaction. Blends of nanostructured NiO particles with carbon substances improve the poor conductivity of NiO, thereby boosting charge-transfer speeds. The robust bonding between NiO nanoparticles and carbon fibers prevents clumping and preserves a consistent catalyst particle size. NiO-altered GF exhibits greater hydrophilicity compared to unmodified GF, and its resilience has been proven through testing [37].

6.4.12 MoO_3-Based Catalysts

Molybdenum oxide is very stable in acidic solutions and has been utilized as a catalyst in polymer electrolyte fuel cells. MoO_3 possesses an orthorhombic structure and is nonconductive, but it gains conductivity when electrochemically reduced to H_xMoO_3. Moreover, the surface of MoO_3 contains numerous oxygen vacancies and has a high overpotential for oxygen evolution. With these benefits in mind, Cao et al. recommended using this catalyst on both the negative and positive sides of RFBs. In their study, MoO_3 was coated on the carbon paper (CP) electrode. A single-cell RFB that operated with MoO_3-modified CP demonstrated superior performance compared to thermally treated CP. Analysis of the electrode's morphology revealed that the shape of the MoO_3 particles on the CP electrode changed from microflakes to extremely thin nanosheets, and the remaining amount of catalyst decreased after 140 charge/discharge cycles with the MoO_3-modified CP electrode. It was suggested that some of the catalyst had been washed away from the electrode surface. Further investigation is needed to understand the reasons for the transformation of the catalyst surface and the mechanism behind this phenomenon [38].

6.4.13 SnO_2-Based Catalysts

SnO_2, a semiconductor oxide material with a wide band gap and strong resistance to corrosion, is commonly used in catalyst support and energy storage technologies. Mehboob et al. studied the performance of SnO_2 decorated on a carbon felt electrode as both the negative and positive electrodes in RFB systems. They evaluated their CVs using the Randles–Sevick equation and determined the electrode surface area before and after modification based on the slope of a plot of current density versus the square root of the scan rate. This analysis indicated that the modification with SnO_2 had increased the electrode's surface area. As mentioned earlier, this method for calculating the surface area may not be precise, as the Randles–Sevick equation is only suitable for planar electrodes involving semifinite diffusion of the electroactive species and is not suitable for porous electrodes [39].

6.4.14 Nd_2O_3-Based Catalysts

Neodymium is an excellent oxygen binder with low electronegativity and high Nd–O binding strength. Its catalytic activity in vanadium redox reactions is attributed to its higher electrochemical activity. Fetyan et al. proposed a mechanism for Nd_2O_3-CF catalytic activity, which involves forming Lewis acids and Brønsted acids [40,41].

6.4.15 RuO_2-Based Catalysts

Even though it comes with a high price tag, RuO_2 has been extensively utilized as an electrocatalyst, particularly in the oxygen evolution reaction, because of its exceptional stability in acidic conditions. Studies have indicated that the electrochemical properties of ruthenium oxide are influenced by its oxidation and hydration states. Ruthenium dioxide and other tetravalent ruthenium oxides are known to be appropriate materials for electrode components in various electrochemical systems. Furthermore, a comprehensive analysis of the entire battery is necessary. Considering that RuO_2 is more costly than many other metal oxides that have been tested, the battery's performance with RuO_2 must demonstrate a significantly greater improvement compared to the others to justify using this catalyst [42].

6.4.16 Cr_2O_3-Based Catalysts

Chromium(III) oxide is an affordable substance utilized as an electrocatalyst for water splitting and the electroreduction of N_2. Contact angle measurements have verified that modifying the electrode with Cr_2O_3 improves its wettability. Similar to research on other systems, the improvements seen in the half-cell CV experiments (such as lower peak separation and higher peak current density) may be attributed, at least in part, to the increase in the effective surface area of the electrode [43].

6.4.17 Ta_2O_5-Based Catalysts

Tantalum peroxide's stability, corrosion resistance, strong adhesion with substrates, and less toxic and environmentally benign nature make it a valuable component in RFBs. The schematic expression of the vanadium redox flow battery (VFRB) in the presence of Ta_2O_5 nanoparticles on the surface of GF is illustrated in Figure 6.4.

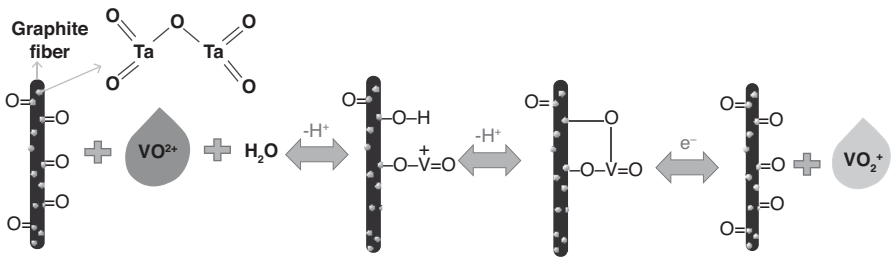

FIGURE 6.4 Schematic Illustration of the mechanism for the VO_2^+/VO^{2+} redox reaction occurring in the presence of Ta_2O_5 nanoparticles on the surface of the GF electrode. (Adapted with permission from [44]. Copyright 2018, American Chemical Society.)

Bayeh et al. enhanced a GF electrode by applying commercial Ta_2O_5 powder, leading to a rise in oxygen-containing functional groups and expanded surface area, which increases the electrochemical activity toward the VO_2^+/VO^{2+} redox reaction [44]. The presence of four Ta=O bonds and two Ta–O bonds in Ta_2O_5 results in an increase in oxygen-containing groups available for charge transfer [44].

6.5 SUMMARY

RFBs show promise as energy storage devices capable of storing energy over extended periods. One approach to reducing costs and enhancing the system's power and energy output involves the development of efficient and cost-effective electrode materials. This review paper presents a comprehensive overview of the metal and metal oxide electrocatalysts designed for redox flow batteries, particularly focusing on all-vanadium RFBs. The paper extracts the performance data of these electrodes used in full-cell experiments to compare charge, voltage, and energy efficiencies. Numerous studies in the literature have concentrated on metal oxide electrodes, such as manganese oxide, due to their lower cost compared to metal-based materials. However, cost-effective metal electrocatalysts like bismuth and copper are also available and have demonstrated significant potential in facilitating redox reactions.

It is important to note that the choice of membrane in the battery has an impact on the charge efficiency of RFBs, as one of the sources of charge loss is the crossover of vanadium species between the positive and negative half-cells, which is influenced by the membrane type. Therefore, comparing the voltage efficiencies of the systems would be more meaningful. It is observed that at higher current densities, the voltage efficiency decreases due to increased ohmic resistance and mass transfer limitations. The top-performing electrode (tested at high current density with good efficiencies) is highlighted in yellow, while materials that offer good efficiencies at lower current densities or lower efficiencies are highlighted in green. Among the metal-based catalysts, the Bi-C electrode operates at the highest current density among these systems and demonstrates a high voltage efficiency. However, further investigation is needed to evaluate the practicality of this electrocatalyst for the negative half-cell of RFBs due to the potential impact of copper in enhancing the hydrogen evolution side reaction and reducing the battery's charge efficiency. More studies are necessary to gain a better understanding of the role of Mn3O4 in enhancing electrode performance and to determine whether its modification solely increases the surface area or exhibits catalytic activity toward the vanadium redox reactions. Furthermore, the long-term adherence of Mn_3O_4 particles to the electrode substrate must be examined through extended battery cycling.

REFERENCES

1. C. Ponce de León, A. Frías-Ferrer, J. González-García, D.A. Szánto, F.C. Walsh, Redox flow cells for energy conversion, *J. Power Sources*. 160 (2006) 716–732. https://doi.org/10.1016/j.jpowsour.2006.02.095.
2. T. Nguyen, R.F. Savinell, Flow batteries, *Electrochem. Soc. Interface*. 19 (2010) 54. https://doi.org/10.1149/2.F06103if.

3. R. Jervis, M.D.R. Kok, J. Montagut, J.T. Gostick, D.J.L. Brett, P.R. Shearing, X-ray nano computed tomography of electrospun fibrous mats as flow battery electrodes, *Energy Technol.* 6 (2018) 2488–2500. https://doi.org/10.1002/ente.201800338.
4. M.D.R. Kok, R. Jervis, D. Brett, P.R. Shearing, J.T. Gostick, Insights into the effect of structural heterogeneity in carbonized electrospun fibrous mats for flow battery electrodes by X-ray tomography, *Small.* 14 (2018) 1–15. https://doi.org/10.1002/smll.201703616.
5. S. Liu, M. Kok, Y. Kim, J.L. Barton, F.R. Brushett, J. Gostick, Evaluation of electrospun fibrous mats targeted for use as flow battery electrodes, *J. Electrochem. Soc.* 164 (2017) A2038–A2048. https://doi.org/10.1149/2.1301709jes.
6. K. Amini, J. Gostick, M.D. Pritzker, Metal and metal oxide electrocatalysts for redox flow batteries, *Adv. Funct. Mater.* 30 (2020). https://doi.org/10.1002/adfm.201910564.
7. A. Parasuraman, T.M. Lim, C. Menictas, M. Skyllas-Kazacos, Review of material research and development for vanadium redox flow battery applications, *Electrochim. Acta.* 101 (2013) 27–40. https://doi.org/10.1016/j.electacta.2012.09.067.
8. S. Ha, K.G. Gallagher, Estimating the system price of redox flow batteries for grid storage, *J. Power Sources.* 296 (2015) 122–132. https://doi.org/10.1016/j.jpowsour.2015.07.004.
9. P. Leung, X. Li, C. Ponce de León, L. Berlouis, C.T.J. Low, F.C. Walsh, Progress in redox flow batteries, remaining challenges and their applications in energy storage, *RSC Adv.* 2 (2012) 10125–10156. https://doi.org/10.1039/C2RA21342G.
10. F.C. Walsh, C. Poncedeléon, L. Berlouis, G. Nikiforidis, L.F. Arenas-Martínez, D. Hodgson, D. Hall, The development of Zn-Ce hybrid redox flow batteries for energy storage and their continuing challenges, *Chempluschem.* 80 (2015) 288–311. https://doi.org/10.1002/cplu.201402103.
11. L.W. Hruska, R.F. Savinell, Investigation of factors affecting performance of the iron-redox battery, *J. Electrochem. Soc.* 128 (1981) 18–25. https://doi.org/10.1149/1.2127366.
12. J. Winsberg, T. Hagemann, T. Janoschka, M.D. Hager, U.S. Schubert, Redox-flow batteries: From metals to organic redox-active materials, *Angew. Chemie - Int. Ed.* 56 (2017) 686–711. https://doi.org/10.1002/anie.201604925.
13. D. Mohanty, Y.H. Wang, Y.C. Tsai, I.M. Hung, Reprint of "Characteristics and electrochemical performance of copper/graphite felt composite electrodes for vanadium redox flow battery," *J. Taiwan Inst. Chem. Eng.* 154 (2024) 105316. https://doi.org/10.1016/j.jtice.2023.105316.
14. R.-H. Huang, C.-H. Sun, T. Tseng, W. Chao, K.-L. Hsueh, F.-S. Shieu, Investigation of active electrodes modified with platinum/multiwalled carbon nanotube for vanadium redox flow battery, *J. Electrochem. Soc.* 159 (2012) A1579–A1586. https://doi.org/10.1149/2.003210jes.
15. T.-M. Tseng, R.-H. Huang, C.-Y. Huang, K.-L. Hsueh, F.-S. Shieu, A kinetic study of the platinum/carbon anode catalyst for vanadium redox flow battery, *J. Electrochem. Soc.* 160 (2013) A690–A696. https://doi.org/10.1149/2.073304jes.
16. P. Leung, T. Martin, M. Liras, A.M. Berenguer, R. Marcilla, A. Shah, L. An, M.A. Anderson, J. Palma, Cyclohexanedione as the negative electrode reaction for aqueous organic redox flow batteries, *Appl. Energy.* 197 (2017) 318–326. https://doi.org/10.1016/j.apenergy.2017.04.023.
17. M. Ulaganathan, V. Aravindan, Q. Yan, S. Madhavi, M. Skyllas-Kazacos, T.M. Lim, Recent advancements in all-vanadium redox flow batteries, *Adv. Mater. Interfaces.* 3 (2016) 1–22. https://doi.org/10.1002/admi.201500309.
18. Y. Ji, J.L. Li, S.F.Y. Li, Synergistic effect of the bifunctional polydopamine–Mn_3O_4 composite electrocatalyst for vanadium redox flow batteries, *J. Mater. Chem. A.* 5 (2017) 15154–15166. https://doi.org/10.1039/C7TA03922K.
19. K.J. Kim, M.-S. Park, Y.-J. Kim, J.H. Kim, S.X. Dou, M. Skyllas-Kazacos, A technology review of electrodes and reaction mechanisms in vanadium redox flow batteries, *J. Mater. Chem. A.* 3 (2015) 16913–16933. https://doi.org/10.1039/C5TA02613J.

20. S. Mehboob, A. Mehmood, J.-Y. Lee, H.-J. Shin, J. Hwang, S. Abbas, H.Y. Ha, Excellent electrocatalytic effects of tin through in situ electrodeposition on the performance of all-vanadium redox flow batteries, *J. Mater. Chem. A*. 5 (2017) 17388–17400. https://doi.org/10.1039/C7TA05657E.
21. D. Dixon, D.J. Babu, J. Langner, M. Bruns, L. Pfaffmann, A. Bhaskar, J.J. Schneider, F. Scheiba, H. Ehrenberg, Effect of oxygen plasma treatment on the electrochemical performance of the rayon and polyacrylonitrile based carbon felt for the vanadium redox flow battery application, *J. Power Sources*. 332 (2016) 240–248. https://doi.org/10.1016/j.jpowsour.2016.09.070.
22. J. Xi, W. Zhang, Z. Li, H. Zhou, L. Liu, Z. Wu, X. Qiu, Effect of electro-oxidation current density on performance of graphite felt electrode for vanadium redox flow battery, *Int. J. Electrochem. Sci*. 8 (2013) 4700–4711. https://doi.org/10.1016/S1452-3981(23)14633-5.
23. Y. Li, J. Parrondo, S. Sankarasubramanian, V. Ramani, Impact of surface carbonyl- and hydroxyl-group concentrations on electrode kinetics in an all-vanadium redox flow battery, *J. Phys. Chem. C*. 123 (2019) 6370–6378. https://doi.org/10.1021/acs.jpcc.8b11874.
24. L. Yue, W. Li, F. Sun, L. Zhao, L. Xing, Highly hydroxylated carbon fibres as electrode materials of all-vanadium redox flow battery, *Carbon N. Y.* 48 (2010) 3079–3090. https://doi.org/10.1016/j.carbon.2010.04.044.
25. P. Han, H. Wang, Z. Liu, X. Chen, W. Ma, J. Yao, Y. Zhu, G. Cui, Graphene oxide nanoplatelets as excellent electrochemical active materials for VO^{2+}/VO^{2+} and V^{2+}/V^{3+} redox couples for a vanadium redox flow battery, *Carbon N. Y.* 49 (2011) 693–700. https://doi.org/10.1016/j.carbon.2010.10.022.
26. X. Wu, H. Xu, L. Lu, H. Zhao, J. Fu, Y. Shen, P. Xu, Y. Dong, PbO_2-modified graphite felt as the positive electrode for an all-vanadium redox flow battery, *J. Power Sources*. 250 (2014) 274–278. https://doi.org/10.1016/j.jpowsour.2013.11.021.
27. C. Yao, H. Zhang, T. Liu, X. Li, Z. Liu, Carbon paper coated with supported tungsten trioxide as novel electrode for all-vanadium flow battery, *J. Power Sources*. 218 (2012) 455–461. https://doi.org/10.1016/j.jpowsour.2012.06.072.
28. D.M. Kabtamu, J.-Y. Chen, Y.-C. Chang, C.-H. Wang, Electrocatalytic activity of Nb-doped hexagonal WO_3 nanowire-modified graphite felt as a positive electrode for vanadium redox flow batteries, *J. Mater. Chem. A*. 4 (2016) 11472–11480. https://doi.org/10.1039/C6TA03936G.
29. Y. Shen, H. Xu, P. Xu, X. Wu, Y. Dong, L. Lu, Electrochemical catalytic activity of tungsten trioxide- modified graphite felt toward VO^{2+}/VO^{2+} redox reaction, *Electrochim. Acta*. 132 (2014) 37–41. https://doi.org/10.1016/j.electacta.2014.03.107.
30. M. Rychcik, M. Skyllas-Kazacos, Characteristics of a new all-vanadium redox flow battery, *J. Power Sources*. 22 (1988) 59–67. https://doi.org/10.1016/0378-7753(88)80005-3.
31. K. Fominykh, J.M. Feckl, J. Sicklinger, M. Döblinger, S. Böcklein, J. Ziegler, L. Peter, J. Rathousky, E.W. Scheidt, T. Bein, D. Fattakhova-Rohlfing, Ultrasmall dispersible crystalline nickel oxide nanoparticles as high-performance catalysts for electrochemical water splitting, *Adv. Funct. Mater.* 24 (2014) 3123–3129. https://doi.org/10.1002/adfm.201303600.
32. L. Yu, F. Lin, W. Xiao, L. Xu, J. Xi, Achieving efficient and inexpensive vanadium flow battery by combining $CexZr_{1-x}O_2$ electrocatalyst and hydrocarbon membrane, *Chem. Eng. J.* 356 (2019) 622–631. https://doi.org/10.1016/j.cej.2018.09.069.
33. H. Zhou, Y. Shen, J. Xi, X. Qiu, L. Chen, ZrO_2-Nanoparticle-modified graphite felt: Bifunctional effects on vanadium flow batteries, *ACS Appl. Mater. Interfaces*. 8 (2016) 15369–15378. https://doi.org/10.1021/acsami.6b03761.
34. T.-M. Tseng, R.-H. Huang, C.-Y. Huang, C.-C. Liu, K.-L. Hsueh, F.-S. Shieu, Carbon felt coated with titanium dioxide/carbon black composite as negative electrode for vanadium redox flow battery, *J. Electrochem. Soc*. 161 (2014) A1132–A1138. https://doi.org/10.1149/2.102406jes.
35. J. Vázquez-Galván, C. Flox, C. Fàbrega, E. Ventosa, A. Parra, T. Andreu, J.R. Morante, Hydrogen-treated rutile TiO_2 shell in graphite-core structure as a negative electrode for high-performance vanadium redox flow batteries, *ChemSusChem*. 10 (2017) 2089–2098. https://doi.org/10.1002/cssc.201700017.

36. Z. Lin, L. Lan, P. Xiao, S. Sun, Y. Li, W. Song, P. Gao, L. Wang, H. Ning, J. Peng, High-mobility thin film transistors with neodymium-substituted indium oxide active layer, *Appl. Phys. Lett.* 107 (2015). https://doi.org/10.1063/1.4931140.
37. E. Tsuji, A. Imanishi, K.I. Fukui, Y. Nakato, Electrocatalytic activity of amorphous RuO_2 electrode for oxygen evolution in an aqueous solution, *Electrochim. Acta*. 56 (2011) 2009–2016. https://doi.org/10.1016/j.electacta.2010.11.062.
38. M. Gong, W. Zhou, M.J. Kenney, R. Kapusta, S. Cowley, Y. Wu, B. Lu, M.C. Lin, D.Y. Wang, J. Yang, B.J. Hwang, H. Dai, Blending Cr_2O_3 into a NiO-Ni electrocatalyst for sustained water splitting, *Angew. Chemie - Int. Ed*. 54 (2015) 11989–11993. https://doi.org/10.1002/anie.201504815.
39. T. Yamamiira, Y. Shiokawa, Y. Ikeda, H. Tomiyasu, Electrochemical investigation of tetravalent uranium β-diketones for active materials of all-uranium redox flow battery, *J. Nucl. Sci. Technol*. 39 (2002) 445–448. https://doi.org/10.1080/00223131.2002.10875503.
40. A. Fetyan, G.A. El-Nagar, I. Derr, P. Kubella, H. Dau, C. Roth, A neodymium oxide nanoparticle-doped carbon felt as promising electrode for vanadium redox flow batteries, *Electrochim. Acta*. 268 (2018) 59–65.
41. T. Yamamura, N. Watanabe, T. Yano, Y. Shiokawa, Electron-transfer kinetics of Np^{3+}/Np^{4+}, NpO^{2+}/NpO_2^{2+}, V^{2+}/V^{3+}, and VO^{2+}/VO^{2+} at carbon electrodes, *J. Electrochem. Soc*. 152 (2005) A830. https://doi.org/10.1149/1.1870794.
42. C.N. Sun, F.M. Delnick, L. Baggetto, G.M. Veith, T.A. Zawodzinski, Hydrogen evolution at the negative electrode of the all-vanadium redox flow batteries, *J. Power Sources*. 248 (2014) 560–564. https://doi.org/10.1016/j.jpowsour.2013.09.125.
43. H. Kaneko, K. Nozaki, Y. Wada, T. Aoki, A. Negishi, M. Kamimoto, Vanadium redox reactions and carbon/a, *Electrochim. Acta*. 36 (1991) 1191–1196.
44. A.W. Bayeh, D.M. Kabtamu, Y.C. Chang, G.C. Chen, H.Y. Chen, G.Y. Lin, T.R. Liu, T.H. Wondimu, K.C. Wang, C.H. Wang, Ta_2O_5-Nanoparticle-modified graphite felt as a high-performance electrode for a vanadium redox flow battery, *ACS Sustain. Chem. Eng.* 6 (2018) 3019–3028. https://doi.org/10.1021/acssuschemeng.7b02752.

CHAPTER 7

Electrolytes for Flow Batteries

Jianwen Liu, Wuyang Wang, Xiang Li, and Yang Qu

7.1 INTRODUCTION OF ELECTROLYTE

As the energy storage medium of a flow battery, the electrolyte is one of the most important materials of a flow battery. The solubility of the electrolyte active substance and the number of gained and lost electrons determine the capacity of the flow battery, and its ionic conductivity also greatly affects the power and efficiency of the battery, and the stability of the electrolyte active substance greatly affects the cycle stability of the battery. Different types of flow battery piles have basically similar structures, but the composition of the electrolyte is completely different. As displayed in Figure 7.1, the positive and negative electrolytes of all-vanadium flow batteries (referred to as "vanadium battery," VFBs) take vanadium ions of different valence states as the active substance, usually sulfuric acid aqueous solution as the solvent, and hydrochloric acid solution as the additive to improve the solubility and stability of vanadium ions. According to the difference of positive and negative active substances, their power density and energy density will be different, and there are many kinds of active substances available in flow batteries, which is also an important feature

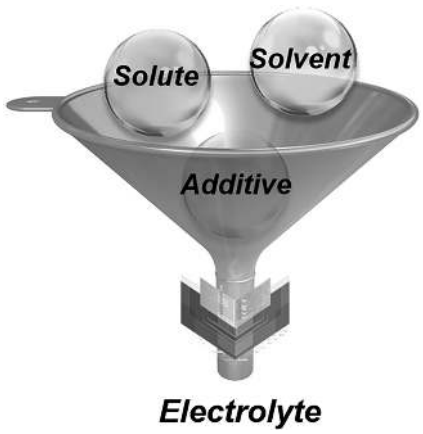

FIGURE 7.1 The composition of the electrolyte for flow batteries.

DOI: 10.1201/9781003506379-7

and advantage of flow batteries. According to the different active substances of electrolytic liquid oxygenation reduction, the most common flow batteries with industrialization prospects are VFBs, iron-based flow batteries (IFBs), and sodium polysulfide/bromine flow batteries (PSBs). This chapter will introduce the above types of flow batteries and electrolytes.

7.2 CLASSIFICATION OF ELECTROLYTE

7.2.1 All-Vanadium Flow Batteries

7.2.1.1 The Operating Principle

VFB, as the most mature flow battery, was first proposed in the 1980s by the Australian scientist Skyllas-Kazacos and his colleagues [1–3]. VFBs have VO^{2+}/VO_2^{+} a positive electrode reaction, V^{2+}/V^{3+} have a negative electrode reaction, and positive and negative electrodes have good electrochemical reversibility. The earliest VFB used sulfuric acid solution with high conductivity as the supporting electrolyte. Later, researchers from the Pacific Northwest Laboratory of the United States proposed the second-generation VFB with a mixed acid system. It is characterized by the use of hydrochloric acid as the supporting electrolyte, which can improve the thermal stability of positive vanadium ions and make it difficult to precipitate vanadium pentoxide due to heat production during the charge–discharge cycle [4].

The standard positive electrode potential of the VFB is 1.0 V, and the standard negative electrode potential is 0.26 V, so the VFB has a higher voltage of 1.26 V. Moreover, since the positive and negative electrodes use the same vanadium element, cross-contamination can be reduced to a certain extent, and the capacity can be restored by mixed re-electrolysis after a long-term cycle. Therefore, the cycle times of VFBs can reach 20,000 times, and the electrolyte can serve for several years or even decades [5, 6]. The energy efficiency is about 80% under the condition of 600 mA cm^{-2}, which has the best comprehensive performance among all flow batteries. In the process of vanadium battery charging and discharging, redox reactions occur in the positive and negative electrodes. A path for H^{+} is formed during the charging and discharging process, which passes through the diaphragm to the negative electrode during the charging process and returns to the positive electrode during the discharge process. The basic principle can be explained in the following Equations (7.1–7.3) and Figure 7.2.

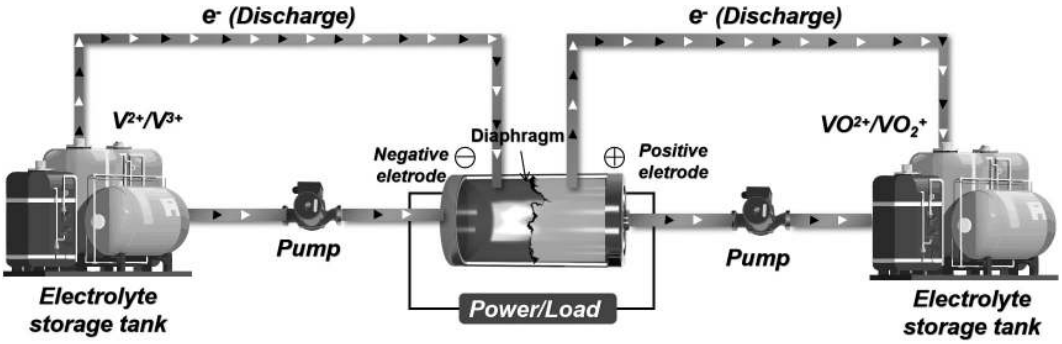

FIGURE 7.2 Charging and discharging schematic diagram of VFB.

$$\text{Positive reaction}: \ VO_2^+ + 2H^+ + e^- \rightarrow VO^{2+} + H_2O \tag{7.1}$$

$$\text{Negative reaction}: \ V^{3+} + e^- \rightarrow V^{2+} \tag{7.2}$$

$$\text{Total battery reaction}: \ VO^{2+} + V^{3+} + H_2O \rightarrow VO_2^+ + 2H^+ + V^{2+} \tag{7.3}$$

7.2.1.2 The Preparation of Electrolyte

The preparation methods of VFB electrolyte mainly include the physical method, chemical method, and electrolysis method [7]. The physical method is to dissolve tetravalent vanadium ion compounds and trivalent vanadium ion compounds directly in water, which has a high raw material cost and cannot be promoted on a large scale. Currently, the industrial preparation of electrolyte mainly uses the chemical method and the electrolysis method, and the chemical method uses a reducing agent to reduce the pentavalent vanadium ion compound to the tetravalent vanadium ion compound.

7.2.1.2.1 Physical Solution Method The physical dissolution method is to dissolve the high-purity $VOSO_4$ directly in the concentrated H_2SO_4 electrolyte, which has been applied in the early vanadium battery research. However, due to the complex preparation process and expensive $VOSO_4$, the concentration of the prepared vanadium battery electrolyte is generally not more than 2 mol L^{-1}. Therefore, this method is not suitable for the large-scale preparation of vanadium battery electrolyte [8].

7.2.1.2.2 Chemical Reduction Method The chemical reduction method is mainly to reduce the high-valent vanadium compound or vanadate solution with sulfuric acid as the electrolyte to the low-valent vanadium solution at high temperature, such as reducing agent oxalic acid to reduce V_2O_5 in the medium to VO^{2+}. The commonly used reducing agents include hydrogen peroxide, formic acid, and hydrazine hydrate, and the chemical reduction method is mainly used for the preparation of electrolytes in the laboratory [9].

7.2.1.2.3 Electrolysis Method Electrolysis is a method suitable for the preparation of a large-scale high-concentration vanadium battery electrolyte, which is to dissolve the V_2O_5 powder in the H_2SO_4 solution of the negative electrode and put the solution of the same concentration in the positive electrode. Through electrolysis, oxygen will be produced in the positive electrode of the electrolytic cell, and at the negative terminal VO_2^+ is reduced to VO^{2+}. The basic mechanism can be demonstrated in the following Equations (7.4) and (7.5):

$$\text{Positive reaction}: \ H_2O \rightarrow 1/2O_2 + 2H^+ + 2e^- \tag{7.4}$$

$$\text{Negative reaction}: \ VO_2^+ + 2H^+ + e^- \rightarrow VO^{2+} + H_2O \tag{7.5}$$

Compared with the chemical reduction method, the electrolyte concentration obtained by the electrolysis method is higher, which is more suitable for the preparation of large-scale vanadium flow batteries. But the electrolysis method also has shortcomings; that is, the electrolytic process is slow, requiring sophisticated equipment and high-purity V_2O_5 when preparing the VFB electrolyte [10].

7.2.1.3 The Existing Problems

Currently, with the application of VFBs, it is found that the electrolyte of VFBs is often unbalanced, and the main reasons include the transmembrane migration of the electrolyte and the side reaction of hydrogen evolution. Electrolyte transmembrane migration will lead to insufficient VO_2^+ in the positive electrode, accumulation of negative V^{3+}, reduce utilization of vanadium ions in electrochemical reactions, and a significant decrease in battery capacity, as displayed in Figure 7.3a [11]. To solve this problem, the positive and negative electrolytes can be mixed regularly. However, when the hydrogen evolution side reaction occurs, it will not only increase the average oxidation state (AOS) of the electrolyte

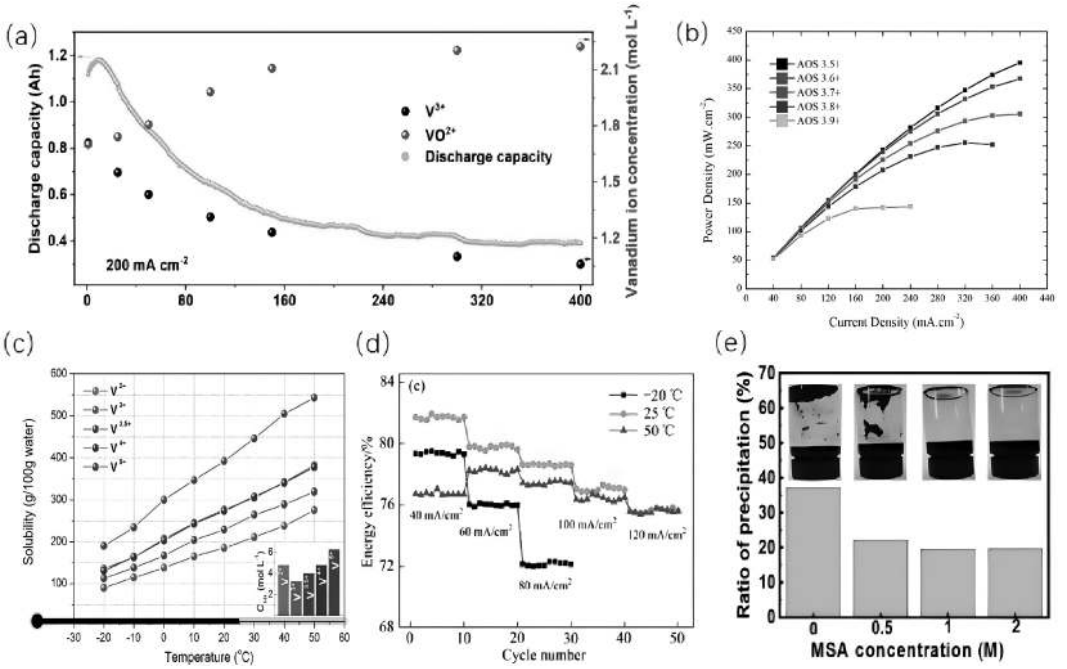

FIGURE 7.3 (a) Change in capacity and concentration of V^{3+} and VO^{2+} with cycle number in VRFB. (Adapted with permission from ref. [11]. Copyright (2023) American Chemical Society.) (b) Discharge power density curves for the flow cells with the electrolytes at different AOSs. (Adapted with permission from ref. [12]. Copyright (2019) Electrochemical Society, Inc.) (c) Impact of temperature on the conductivity of five types of electrolytes. (Adapted with permission from ref. [13]. Copyright (2016) Elsevier.) (d) Change of energy efficiency with cycle number. (Adapted with permission from ref. [14]. Copyright (2019) Central South University Press.) (e) The stability of the electrolyte was tested at 5°C and 40°C. (Adapted with permission from ref. [17]. Copyright (2021) Korean Society of Industrial Engineering Chemistry.)

but also consume current and generate bubbles, which will reduce the active area of the electrode and eventually lead to the deterioration of battery performance. In Figure 7.3b, studies have shown that when the AOS of vanadium battery electrolyte increases from 3.5 to 3.9, the resistance, charge transfer resistance, and mass transfer impedance of the electrolyte increase by 19.3%, 709.0%, and 206.0% respectively, the available power density decreases by more than 40%; and the discharge capacity decreases by 52% relative to the theoretical limit value [12].

7.2.1.4 The Optimization Scheme

Since the stability of different valence vanadium ions in the electrolyte is different in Figure 7.3c, the solubility of V^{2+}, V^{3+} in sulfuric acid solution increases with the increase of temperature. V^{2+} and V^{3+} are easy to precipitate vanadium compounds under low temperature conditions [13]. In particular, V^{3+} is easy to precipitate as $V_2(SO_4)_3$ at low temperatures, while VO^{2+} is easy to precipitate as V_2O_5 at high temperatures, which makes the traditional VFB operate at a narrow temperature range, generally 10°C–40°C.

Sulfuric acid is usually used as the supporting electrolyte for VFB electrolyte. Since sulfuric acid is easy to form long-chain compounds with vanadium ions, it has a certain impact on the electrochemical activity of vanadium ion pairs. Although increasing the concentration of sulfuric acid can improve the thermal stability of vanadium pentavalent electrolyte, it will also increase the viscosity of electrolyte, reduce the rate of ion diffusion, and increase the concentration polarization. As a result, the energy efficiency of the battery is reduced, the power loss of the pump is increased, and the cost of the battery system is correspondingly increased. In addition, the increase in the concentration of sulfuric acid will also reduce the solubility of V^{3+} and generate $V_2(SO_4)_3$ precipitation in the cathode electrolyte. To improve the thermal stability and electrochemical activity of vanadium electrolyte, there are two common ways to optimize the performance of the electrolyte: preparing a new mixed acid support system and introducing suitable additives to the traditional electrolyte.

7.2.1.4.1 Preparation of a New Mixed Acid Support System In addition to the improvement of the performance of the VFB electrolyte based on the traditional sulfuric acid as a support electrolyte, the Pacific Northwest National Laboratory in 2011 developed a mixed acid system of sulfuric acid and hydrochloric acid as a support electrolyte metal vanadium energy storage medium. It is reported that the total concentration of metal vanadium ions in the energy storage medium reaches 2.5 mol L^{-1}, and the energy density of the vanadium energy storage medium increases by about 70% compared with the traditional sulfuric acid system. Meanwhile, the nuclear magnetic resonance test results show that the chloride ions in the mixed acid system can form $VO_2Cl(H_2O)_2$ through complexation, which effectively improves the stability of metal vanadium ions. In addition, through the stability test of different valence metal vanadium ions, the vanadium metal energy storage medium of the mixed acid system can still maintain stability in the solution even if it works in the temperature range of −5°C to 50°C.

However, the electrolyte of the mixed acid system inevitably faces the problem of volatilization of chlorine chloride and release of chlorine gas due to the introduction of chloride ions. Therefore, it is necessary to optimize the concentration composition of the electrolyte of the mixed acid system to eliminate the hidden danger caused by the introduction of chloride ions and further improve the energy density of the electrolyte. From Figure 7.3d, Yang et al. studied the performance optimization of vanadium battery electrolyte based on a sulfuric acid–hydrochloric acid mixed system and found that under the condition of 50°C, when the chloride ion concentration in the electrolyte does not exceed 6.4 mol L^{-1}, volatilization of hydrogen chloride can be effectively avoided and the stability of the electrolyte of the mixed acid system can be ensured. When the concentration of vanadium ion in the electrolyte is 2.2 mol L^{-1}, the concentration of sulfate is 2.75 mol L^{-1}, and the concentration of chloride ion is 5.8 mol L^{-1}, the electrochemical performance of the sulfuric acid–hydrochloric acid mixed acid system electrolyte is the best, and the energy efficiency can reach 77% [14].

7.2.1.4.2 Introduction of Appropriate Additives

7.2.1.4.2.1 Inorganic Solvents Alkali metal salts such as oxalates, sulfates, and phosphates are often used as inorganic additives to improve the thermal stability of V^{5+} electrolyte in VFBs.

Wu et al. used $Na_2C_2O_4$, Na_2SO_4, and K_2SO_4 as additives for VFB electrolyte and found that the electrolyte containing 3% additives had the best stability, and that the appropriate amount of additives could improve the conductivity and electrochemical activity of the electrolyte [15]. Feng et al. added NaH_2PO_4, $NH_4H_2PO_4$, or KH_2PO_4 into the VFB electrolyte as additives and found that the electrolyte with 2%–5% additives had better stability and electrochemical activity, because $H_2PO_4^-$ can combine with the electrolyte to form V–O–P bonds, avoiding the formation of V–O–V bonds [16]. In particular, hydrolysis of $VO(OH)_3$ to V_2O_5 precipitate can be effectively avoided in the pentavalent vanadium ion electrolyte, which effectively improves the stability of different valence vanadium ion electrolytes and significantly improves the life of vanadium battery.

7.2.1.4.2.2 Organic Solvents Surfactants and organics containing functional groups such as –OH and $–NH_2$ are usually used as organic additives in VFB electrolyte to improve the thermal stability and chemical activity of the electrolyte.

Surfactants can be widely used to improve the performance of electrolytes because of their synergistic perturbation, hydrogen bonding, and micellar catalysis. Kim et al. studied the effects of methylsulfonic acid (MSA) as an additive on the thermal stability and electrochemical performance of vanadium battery electrolytes [17]. In Figure 7.3e, the results showed that the concentration of pentavalent vanadium electrolyte with MSA added at 40°C was higher, and MSA could delay the formation of sediments. Electrochemical analysis displayed that MSA could accelerate the diffusion of vanadium ions and the redox reaction rate, improving the energy efficiency and electrolyte utilization rate of VFBs. Some researchers added 1%–5% maleic anhydride, acrylamide, and glycerol to the all-vanadium battery electrolyte, and the stability of the electrolyte was significantly improved. It is concluded that the carboxyl functional group contained in the additive can chelate with vanadium ions in

the electrolyte, and the amino functional group can adsorb vanadium ions in the electrolyte through strong adsorption, and the synergistic effect of the two can effectively prevent the self-polymerization of vanadium ions so as to prevent their precipitation.

7.2.1.4.2.3 Vanadium-Containing Compounds Researchers added a small amount of vanadium tetrasulfide to the vanadium electrolyte of the sulfuric acid system to improve the comprehensive performance of the electrolyte [18]. The results showed that compared with the battery assembled by the traditional electrolyte, the battery capacity increased by more than 11%, the utilization rate increased by more than 6%, and the energy density increased by more than 14% when assembled by the electrolyte with vanadium tetrasulfide. Vanadium tetrasulfide, a member of the transition metal sulfide group, has a one-dimensional chain structure, and two $(S_2)^{2-}$ polymers are connected around each vanadium ion along the c-axis, so it has a relatively higher theoretical capacity [19].

7.2.1.5 Conclusions

Vanadium flow batteries have outstanding advantages in the field of large-scale energy storage, but there are also problems that cannot be ignored. As the carrier of vanadium battery power, the performance of vanadium electrolyte directly affects the storage capacity of vanadium battery, and the cost of vanadium raw material directly affects the cost of the electrolyte (which can account for about 85% of the entire electrolyte cost), thus affecting the cost of vanadium battery. The purity of vanadium also affects the performance of the electrolyte. The high purity of vanadium raw materials is often very costly. The use of low-purity or cheap vanadium to produce high-performance vanadium electrolyte is worth studying. In addition, vanadium battery technology has attracted more and more attention in the field of energy storage applications and commercialization. Thanks to the pioneering work of scholars, vanadium electrolyte technology has been significantly improved and enhanced and is moving in the direction of being denser, more reliable, and more cost-effective.

7.2.2 Iron-Based Flow Batteries

7.2.2.1 The Operating Principle

IFB refers to a flow battery system with Fe^{2+}/Fe^{3+} as a positive redox couple, including all-iron flow batteries and flow battery systems with different positive and negative active substances (such as iron chromium and iron zinc), as exhibited in Figure 7.4.

When operating the IFB, the electrolyte containing active substances flows through the stack from the storage tank, and the active substances undergo electrochemical reaction on the electrode surface to carry out the charging/discharging process. When the battery is charged, its electrode reaction is illustrated by the following Equations (7.6) and (7.7):

$$\text{Positive reaction}: \ Fe^{2+} \rightarrow Fe^{3+} + e^{-} \tag{7.6}$$

$$\text{Negative reaction}: \ X^{m+} + (m-n)e^{-} \rightarrow X^{n+} \tag{7.7}$$

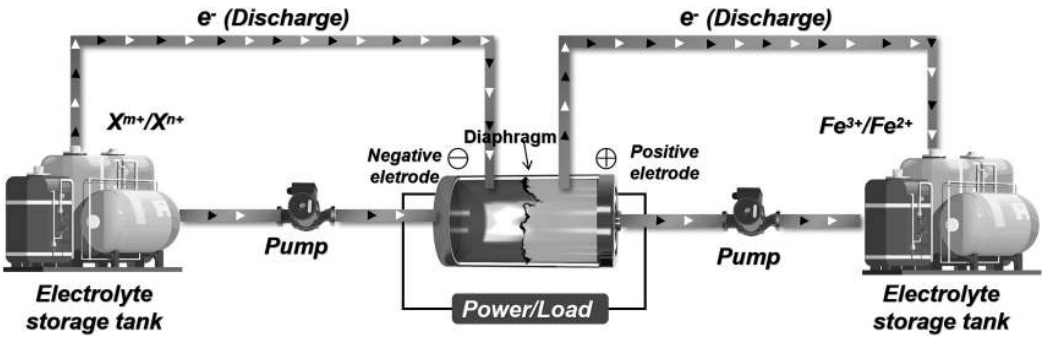

FIGURE 7.4 Charging and discharging schematic diagram of IFB.

When charging, the positive electrode Fe^{2+} loses electrons and is oxidized to Fe^{3+}, and the negative electrode is reduced. Different types of IFBs can be formed by optimizing the negative electrode pairs of flow batteries, and their performance is also different. Among them, the common iron-base flow batteries are iron-chromium flow batteries, iron-titanium flow batteries, iron-vanadium flow batteries, etc., which will be introduced for the more widely used iron-chromium flow batteries and their electrolytes.

7.2.2.2 Aging of the Electrolyte

In the early study of iron-chromium flow battery electrolyte by the National Aeronautics and Space Administration (NASA), researchers took the battery system under the condition of 25°C as the main research object, and the $FeCl_2$/HCl mixed solution and $CrCl_3$/HCl mixed solution were chosen as the positive and negative electrolytes, respectively. There are three complex ions $Cr(H_2O)_6^{3+}$, $Cr(H_2O)_5Cl^{2+}$ and $Cr(H_2O)_4Cl^{2+}$ in the hydrochloric acid aqueous solution of $CrCl_3$, and there is a dynamic equilibrium among the three complex ions, as displayed in Equation (7.8).

$$\left[Cr(H_2O)_4Cl_2\right]Cl\cdot 2H_2O \leftrightarrow \left[Cr(H_2O)_5Cl\right]Cl_2H_2O \leftrightarrow \left[Cr(H_2O)_6\right]Cl_3 \tag{7.8}$$

At room temperature, $Cr(H_2O)_5Cl^{2+}$ and $Cr(H_2O)_4Cl^{2+}$ are easily converted to $Cr(H_2O)_6^{3+}$ with the increase of use time, while $Cr(H_2O)_6^{3+}$ has no electrochemical activity. Therefore, the conversion rate of $Cr(H_2O)_5Cl^{2+}$ to $Cr(H_2O)_6^{3+}$ is relatively slow, but there is a reaction kinetics of Cr^{2+} that can accelerate the conversion of $Cr(H_2O)_5Cl^{2+}$ to $Cr(H_2O)_6^{3+}$ so that the electrochemically active ions in the electrolyte are reduced, and the electrolyte is prone to aging. The charging and discharging ability of the battery with a high degree of aging will change significantly under too high or too low temperature environment and too large or too small a current condition so that the battery performance will decay.

The performance can be improved by promoting the chromium chemical activity of the positive electrolyte at high temperatures (avoiding aging). In addition, large iron-chromium flow battery systems produce heat release during the charge–discharge cycle due to resistance loss and inefficiency, and the heat generated can protect the system at high temperatures. To solve the problem of low utilization rate of electrolyte and attenuation of battery

performance, researchers have proposed that increasing the temperature of electrolyte to 65°C can promote the conversion of $Cr(H_2O)_6^{3+}$ into $Cr(H_2O)_5Cl^{2+}$ so as to solve the problem of aging of electrolyte. However, the increase in temperature may significantly reduce the ion selectivity of the diaphragm and increase the cross-mixing rate of active substances. Therefore, although increasing the temperature of the electrolyte can improve the activity of the electrode reaction, it also brings the risk of cross-contamination [20].

Iron-chromium flow battery electrolyte is a solution containing iron and chromium ions, whose physical and chemical properties directly affect the performance of the battery. Both the electrochemical reaction and the hydrogen evolution reaction (HER) occur at the electrode/electrolyte interface. HER is a parasitic side reaction in the charging process of iron-chromium flow battery, which reduces the stability of the battery. It not only consumes part of the charging current but also reduces the utilization rate of the electrode surface area due to the formation of hydrogen bubbles, thus accelerating the imbalance of charge and discharge and eventually leading to the deterioration of the battery stability during the charge and discharge process [21]. In addition, the production of hydrogen can also lead to a decrease in conductivity, which limits the capacity of iron-chromium flow batteries and even leads to potential safety issues due to the increased concentration of hydrogen in the electrolyte tank.

7.2.2.3 Optimization of the Electrolyte

In view of the aging problem of electrolytes, researchers have found that the electrochemical performance of the battery can be improved by modifying the electrode or electrolyte to a certain extent. Placing chromium(III) acetone redox coupling or other integrated chromium electrolytes in an electrolyte with a low concentration of Cr^{3+} provides a higher voltage and has been found to improve the electrochemical performance of the battery. In the early stage, $FeCl_2$ and $CrCl_3$ were dissolved in HCl solution as positive and negative electrolytes. However, due to the different osmotic pressures on both sides of the ion conduction diaphragm, ions are easy to cross and overlap, which reduces the battery performance. NASA researchers proposed that the positive and negative electrodes use the same mixed electrolyte to ease the cross-stringing of active substances. To obtain an iron-chromium flow battery with better performance, Gao et al. used a mixed electrolyte with the same positive and negative electrodes and investigated the conductivity, viscosity, and electrochemical performance of the electrolyte with different ion concentrations and acid concentrations [22]. The optimal solution of electrolyte composition of iron-chromium flow battery was determined as 1 mol L^{-1} $FeCl_2$, 1 mol L^{-1} $CrCl_3$, and 3 mol L^{-1} HCI. Under these conditions, the synergistic effect of conductivity, electrochemical activity, and transport characteristics of the electrolyte is the best.

As well known, there is a serious deactivation effect of Cr^{3+}/Cr^{2+} electric pair in iron-chromium flow battery; that is, due to the isomerization of Cr^{3+} in aqueous solution, the redox reversibility of Cr^{3+}/Cr^{2+} electric pair becomes worse and worse, which affects the cycle life of the battery. To further improve the battery performance, soluble substances can be dissolved in the electrolyte as additives, which do not participate in the redox reaction during the charge and discharge process but can improve the electrochemical performance

of the electrolyte. Researchers have found that different additives have different effects; adding In^{3+} as an additive to the negative electrolyte will not only inhibit the HER of the negative electrode but also promote the reaction process of Cr^{3+}/Cr^{2+}. In Figure 7.5a–c, adding In^{3+} concentration of 0.01 mol L^{-1} to the electrolyte, the energy efficiency of the battery can reach 77.0% at the current density of 200 mA cm^{-2}. After 140 cycles at the current density of 160 mA cm^{-2}, the capacity retention rate remains 36.3% higher than that without adding electrolyte [23].

In recent years, the electrochemical activity of Cr^{3+}/Cr^{2+} pairs has been improved by changing the complexation between chromium ions and complexants, and the application of neutral solutions as supporting electrolytes has been gradually developed. Complexation changes the electrochemical properties of metal ions by changing their electron transfer kinetics and electrochemical potential. Common complexing agents include ethylenediamine tetraacetic acid (EDTA), diethyltriamine pentaacetic acid (DTPA), and 1,3-propylenediamine tetraacetic acid (PDTA) [24]. Studies have shown that although EDTA can reduce the reduction potential of chromium ions from −0.41 to −0.99 V, the solution is close to neutral pH, and the dynamic coefficient of chromium reduction can be increased to more than 10^5. However, when Cr-EDTA is used as the positive and negative electrolyte solution, the battery has low energy efficiency and is easy to evolve hydrogen,

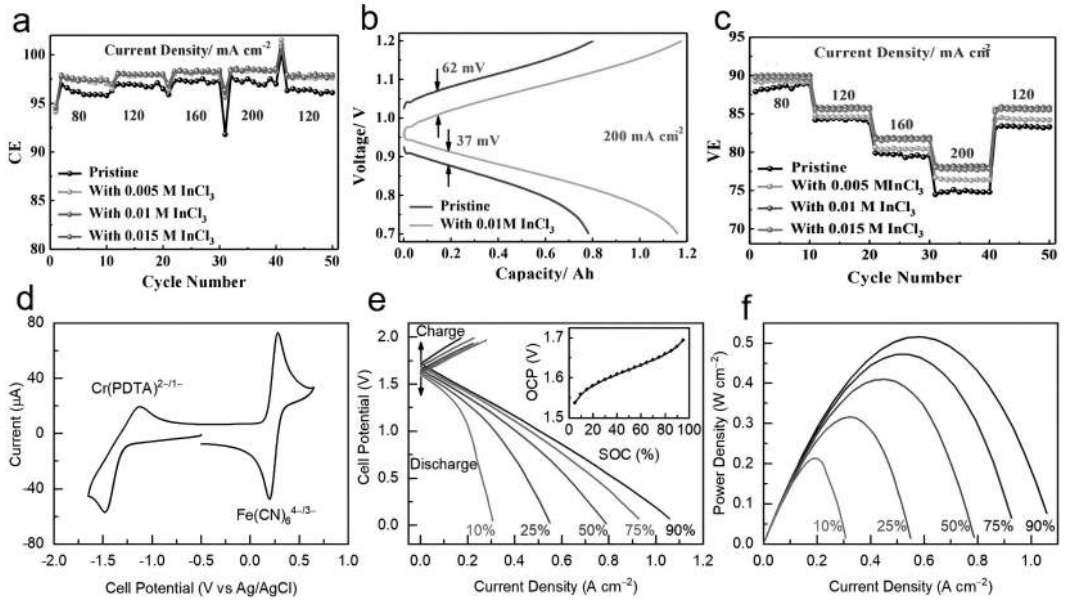

FIGURE 7.5 (a–c) Performance of an iron-chromium redox flow battery with indium ion as anode additive. (Adapted with permission from ref. [23]. Copyright (2020) Elsevier.) (d) CV curves at 100 mV s^{-1} of 5 mM KCrPDTA and 5 mM $K_4Fe(CN)_6$ in 0.125 M KBi (pH = 9) recorded on a glassy carbon working electrode. (e) Polarization curves of an RFB containing 0.4 M CrPDTA in 0.2 M KBi versus 0.3 M $Fe(CN)_6^{4-}$ and 0.45 M $Fe(CN)_6^{3-}$ in 0.025 M KBi at varying SOC. (f) Discharge power density versus current density at varying SOC for the solution. (Adapted with permission from ref. [27]. Copyright (2019) Elsevier.)

which cannot be applied in practice. Through NMR, spectral, and X-ray structural analysis, Ahmad et al. found that the coordination between water and Cr-EDTA could promote water decomposition, resulting in an increase in hydrogen evolution [25]. Therefore, it is proposed that PDTA, whose structure is closer to the octahedron, can be used as a complexing agent to eliminate the coordination with water and inhibit hydrogen evolution.

The chromium ion reduction potential of Cr-PDTA is −1.1 V, which is lower than Cr-EDTA, improving the electrode dynamics of the glass carbon electrode. When used as a negative electrolyte, the battery voltage and performance are increased. At room temperature, when the current density is 0.1 A cm^{-2}, the battery energy efficiency reaches 80%. In addition, the researchers proposed DTPA as a complexing agent molecule to complex Cr^{3+} while changing the supporting electrolyte [26]. In Figure 7.5d–f, the regulated Cr^{3+} changes the size of the molecule, avoids the penetration of the negative electrolyte into the positive electrolyte, and has better diffusion capacity, electrical conductivity, and higher solubility when using an aqueous solution. Although the battery performance of the complex electrolyte is excellent at low current density, the battery performance is poor at high current density [27]. In addition, there are some studies on iron ion complexation, but no large-scale application has been reported.

7.2.2.4 Conclusions

Facing the development needs of the large-scale energy storage field, the development of IFBs provides a more economical choice for large-scale energy storage in view of the high cost of traditional VFBs. From the initial iron-chromium flow battery to the continuous development of the all-iron flow battery, IFB has attracted more and more researchers' attention [28]. Many companies have carried out the demonstration application of iron-chromium flow batteries and zinc-iron flow batteries, and all-iron flow batteries are one of the most important development directions in the future. In the period of rapid development of IFBs, it is still necessary to further strengthen the research and development of key materials, improve the electrode reaction kinetics, solve the problem of hydrogen evolution in the negative electrode, explore new iron complex electric pairs to improve the performance of IFBs, and constantly promote the industrial application of high-power IFBs.

7.2.3 Sodium Polysulfide/Bromine Flow Batteries

7.2.3.1 The Operating Principle

As a typical flow battery, PSB uses sodium polysulfide (Na_2S_x) and sodium bromide (NaBr) aqueous solutions as the negative and positive electrolytes of the battery and the active substance of the battery's electrochemical reaction. PSB was proposed by American scholars Remick and Ang in 1984. Br^- exists mainly as the form of Br_3^- in the positive electrolyte, and elemental sulfur and sulfur ions combined into polysulfide ions exist in the negative electrolyte [29]. The battery uses an anion redox reaction to achieve the conversion of electrical and chemical energy, rather than a cationic reaction. The positive and negative electrolytes of the battery are separated by an ion exchange (conduction) diaphragm, and a pathway is formed by the electromigration of Na^+ between the positive and negative electrolytes during battery charging and discharging, as presented in Figure 7.6.

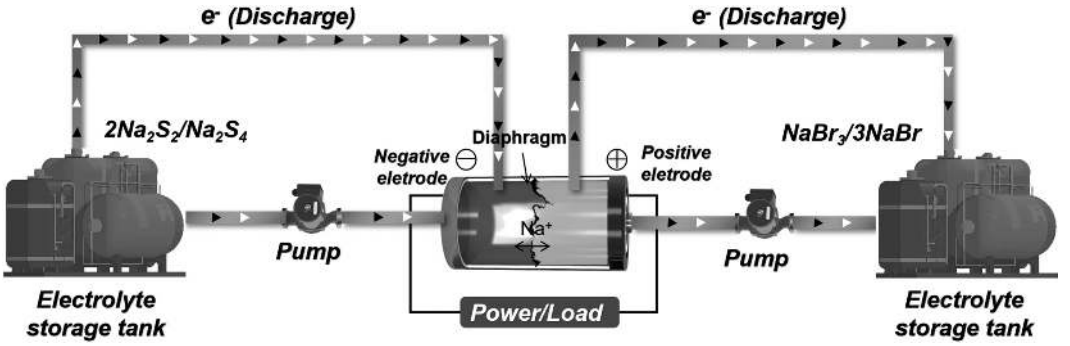

FIGURE 7.6 Charging and discharging schematic diagram of PSB.

The electrode reaction of PSB is explained as follows:

$$\text{Positive reaction}: \ 2\text{NaBr} - 2\text{e}^- \rightarrow \text{Br}_2 + 2\text{Na}^+ \tag{7.9}$$

$$\text{Negative reaction}: \ 2\text{Na}^+ + (x-1)\text{Na}_2S_x + 2\text{e}^- \rightarrow x\text{Na}_2\text{S}_{x-1}\,(x = 2-4) \tag{7.10}$$

$$\text{Total battery reaction}: \ 2\text{NaBr} + (x-1)\text{Na}_2\text{S}_x \rightarrow \text{Br}_2 + x\text{Na}_2\text{S}_{x-1}\,(x = 2-4) \tag{7.11}$$

The standard electrode potential of the positive electrode of the PSB is 1.087 V, and the standard electrode potential of the negative electrode is −0.428 V, so the standard electromotive force of the PSB is 1.515 V. Due to the difference in electrolyte concentration and charging and discharging state, the open circuit voltage of a single battery is generally 1.54–1.60 V.

The PSB was invented by the American Institute of Gas Technology in 1984, but it did not receive much attention from the technology or industry in the following years. In the early 1990s, the British Regenesys Technologies Limited developed three series of battery pack modules with power of 5, 20 and 100 kW. In 1996, Regenesys tested a 1 MW Na_2S_x/Br system at Aberthaw in South Wales, and the results showed that this system could meet the technical, environmental, and safety requirements. In August 2000, Regenesys built the first commercial-scale energy storage peaking demonstration power plant, which was matched with a 680 MW gas turbine power plant. The energy storage system had a capacity of 120 MWh and a maximum output power of 15 MW, which could meet the electricity demand of 10,000 households for 1 day.

In addition to the successful development of the Na_2S_x/Br series energy storage battery pack module by the British Regenesys Company and the initial commercial demonstration operation, there are not many reports on the research and development of Na_2S_x/Br battery technology in other countries in the world. As large-scale energy storage technology has broadened application prospects in the field of power storage, the Dalian Institute of Chemical Physics of the Chinese Academy of Sciences, supported by the Frontier Project of Knowledge Innovation Engineering, has started on the Na_2S_x/Br battery technology

research since 2000. Based on certain progress on electrode materials, stack structure, ion exchange diaphragm selection and modification, sealing materials, and technology, the hundred-watt and kilowatt Na_2S_x/Br energy storage battery packs were developed from 2002 to 2004 [30,31]. In 2005, with the funding of the national "863" program energy field project, the Dalian Institute of Chemical Physics of the Chinese Academy of Sciences (CAS) has made great progress in sodium polysulfide/bromine battery system integration and successfully completed the research and development of a 5 kW Na_2S_x/Br energy storage battery system for the development and demonstration of a larger flow energy storage battery system.

7.2.3.2 The Preparation of Electrolyte

PSBs use Na_2S_x as a negative electrolyte, and there are four main preparation methods: (1) Directly reacting elemental sodium and sulfur in a molten state or organic solvent; (2) the electrochemical synthesis method of middle-temperature sodium-sulfur batteries; (3) sodium sulfide and elemental sulfur reacting in a solvent or molten state; and (4) sodium hydrosulfide and elemental sulfur reacting in organic solvents or in a molten state. When Na_2S_x is prepared by the melting process, the reaction between sodium and sulfur is very violent, and it is easy to cause a fire or explosion. The reaction of sodium hydrosulfide and sulfur in organic solvent or molten state requires the use of hydrogen sulfide gas as the reactant, and the amount of gas is large and difficult to control [32].

There are various equilibria between ions in Na_2S_x solution, which are very sensitive to temperature and pH and directly affect the operational reliability and stability of PSBs. Therefore, it is necessary to study whether the composition and stability of polysulfide ion solution can meet the needs of practical applications. The investigation of polysulfide ion solution equilibrium is mostly confined to the static state, that is, the initial state, and there is no special study on the dynamic change of the charging and discharging process of PSB. Lessner et al. discussed the composition changes of various ions in the electrolyte under different charging and discharging states and the corresponding potential changes [33]. However, all equilibria in the solution were not considered, and the initial ratio and concentration of elemental sulfur were too low, which was not suitable for the application of PSBs. The research team of Zhang from the Dalian Institute of Chemical Physics (CAS) prepared Na_2S_x solution directly at low temperature with different reactant ratios without hydrogen sulfide gas.

7.2.3.3 Conclusions

Compared with other flow batteries, PSB electrolyte is relatively cheap and very suitable for large-scale storage of large capacity, but the real commercialization of PSB still needs to make breakthroughs in high selectivity, low cost, good durability of ion exchange diaphragm materials, high-stability electrode materials, stack structure optimization design and sealing materials and technologies, etc. In particular, breakthroughs are needed in applied basic research in related fields. From the analysis of the situation reported at present, there are still many problems in PSB, mainly concentrated in the following aspects:

1. The active substances in the positive and negative electrolyte solutions are seriously interlinked, resulting in excessive attenuation of the capacity of the energy storage system of the PSB.
2. During the charging process of the PSB energy storage system, side reactions and secondary reactions are complicated. For example, the negative HER, sulfur, or sodium sulfate crystal precipitation has seriously affected the cycle stability of the PSB energy storage system.
3. Strong corrosive bromine and strong irritating bromine in the electrolyte solution pollute the environment and pose safety risks.

7.3 SUMMARY AND OUTLOOK

7.3.1 Summary

With the development of human production and the continuous improvement of living standards, energy demand also increases. Energy on earth is roughly divided into fossil energy (coal, oil, natural gas) and clean renewable energy (wind energy, solar energy, water energy, tidal energy, biomass energy, etc.), and currently, people's demand for electric energy is increasing with the increasing degree of dependence. The traditional energy supply structure dominated by fossil energy, due to its limited resources and environmental problems caused by overuse, prompts people to pay more attention to the development and utilization of renewable energy. However, the uncontrollability and discontinuity problems, such as wind energy and solar energy, cannot meet the social demand for sustainable, stable, and controllable power energy. Therefore, the research on efficient energy storage technology has become particularly important, among which flow battery technology has been widely valued by the industry due to its advantages, such as large energy storage scale, high safety, long charge and discharge cycle life, and recyclable battery materials. As one of the most important materials for flow batteries, the performance of electrolyte has a direct impact on the performance of batteries. In the future, it will be necessary to prepare and develop high-concentration, high-conductivity and high-stability electrolyte [34].

In summary, this chapter introduces the electrolytes of different types of flow batteries (VFB, IFB, PSB). Among them, VFB and IFB are more widely used. The basic principle of the battery, different methods of electrolyte preparation, and common problems and solutions of electrolytes are expounded in detail. It provides a reference for scholars to understand and further study the flow battery-related content.

7.3.2 Outlook

With the rapid development of efficient energy storage technology, flow batteries have received much attention due to their advantages, such as long life and large energy storage scale, but with their wide application, their disadvantages have gradually become prominent. Although the cycle performance of VFBs can meet the needs of industrialization, due to the soaring price of vanadium in recent years, the cost of VFBs has become a limiting factor limiting their further industrialization and promotion [35,36].

Therefore, it is necessary to study how to improve energy efficiency under higher current density and how to reduce the volume and cost of the stack. As for the PSB, owing to sulfur deposition and cross-contamination of positive and negative electrolytes, there are no reports that the energy storage power station has been completed and put into operation. In zinc-based flow batteries, when the metal zinc grows to a certain limit, it will form dendrites. With the progress of the charging process, dendrites continue to grow, which makes it easy to pierce the diaphragm, thereby resulting in the positive and negative electrolyte mixing. The electrolyte mixing can cause a serious battery self-discharge phenomenon, correspondingly affecting the energy efficiency and safety performance of the battery. In the organic flow battery, the solubility and stability of the organic flow battery electrolyte need to be improved because organic matter is the active substance of the flow battery.

In general, research on key materials and components for flow batteries will focus on high-performance, low-cost, durable, and high-concentration, high-stability electrolytes in the future.

REFERENCES

1. G. Tomazic, M. Skyllas-Kazacos, P. T. Moseley, J. Garche. Chapter 17-Redox flow batteries. In *Electrochemical Energy Storage for Renewable Sources and Grid Balancing*, edited by: Patrick T. Moseley and Jürgen Garche, pp. 309–336. Elsevier, 2015.
2. M. Skyllas-Kazacos, J. F. McCann, C. Menictas, M. Skyllgs-Kazacos, T. M. Lim. Chapter 10-Vanadium redox flow batteries (VRBs) for medium and large-scale energy storage. In *Advances in Batteries for Medium and Large Scale Energy Storage*, edited by: Chris Menictas, Maria Skyllas-kazacos and Tuti Mariana Lim, pp. 329–386. Elsevier, 2014.
3. M. Skyllas-Kazacos, C. Menictas, T. Lim, Z. Melhem. Chapter 12-Redox flow batteries for medium to large-scale energy storage. In *Electricity Transmission, Distribution and Storage Systems*, edited by: Ziad Melhem, pp. 398–441. Woodhead, 2013.
4. B. Li, T. Ma, Z. B. Huang, X. Xing, Evaluation of the effect of hydrogen evolution reaction on the performance of all-vanadium redox flow batteries, *Electrochim. Acta* 504 (2024) 144895.
5. P. Loktionov, A. Pustovalova, R. Pichugov, D. Konev, A. Antipov, Quantifying effect of Faradaic imbalance and crossover on capacity fade of vanadium redox flow battery, *Electrochim. Acta* 485 (2024) 144047.
6. M. H. Hossain, N. Abdullah, K. H. Tan, R. Saidur, M. A. M. Radzi, S. Shafie, Evolution of vanadium redox flow battery in electrode, *Chem. Rec.* 1 (2024) e202300092.
7. Y. Guo, J. Huang, J. K. Feng, Research progress in preparation of electrolyte for all-vanadium redox flow battery, *J. Ind. Eng. Chem.* 118 (2023) 33–43.
8. M. Skyllas-Kazacos, Review-highlights of UNSW all-vanadium redox battery development: 1983 to present, *J. Electrochem. Soc.* 169 (2022) 070513.
9. H. Jiang, J. Sun, L. Wei, M. Wu, W. Shyy, T. Zhao, A high power density and long cycle life vanadium redox flow battery, *Energy Storage Mater.* 24 (2020) 529–540.
10. A. Verma, N. Beriwal, Development of economical and highly efficient electrolyte using vanadium pentoxide for vanadium redox flow battery. *Environ. Sci. Pollut. Res.* 29 (2022) 72187–72195.
11. Z. Y. Wang, Z. X. Guo, J. Y. Ren, Y. J. Li, B. Liu, X. Z. Fan, T. S. Zhao, An electrolyte with elevated average valence for suppressing the capacity decay of vanadium redox flow batteries, *ACS Cent. Sci.* 9 (2023) 56–63.

12. M. Nourani, C. R. Dennison, X. F. Jin, F. Q. Liu, E. Agar, Elucidating effects of Faradaic imbalance on vanadium redox flow battery performance: Experimental characterization, *J. Electrochem. Soc*. 166 (2019) A3844–A3851.
13. S. B. Xiao, L. H. Yu, L. T. Wu, L. Liu, X. P. Qiu, J. Y. Xia, Broad temperature adaptability of vanadium redox flow battery Part 1: Electrolyte research, *Electrochim. Acta* 187 (2016) 525–534.
14. Y. D. Yang, Y. M. Zhang, L. Tang, T. Liu, J. Huang, X. Yang, Sulphuric acid-hydrochloric acid mixed acid system performance optimisation of vanadium battery electrolyte, *J. Nonferrous Met*. 31 (2021) 1621–1631.
15. X. W. Wu, Y. H. Xiang, Energy storage materials-foundation and application, B. *Chem. Ind. Press* 25 (2019) 173–174.
16. J. K. Feng, J. W. Wen, Y. N. Xin, A method for enhancing the energy storage efficiency of vanadium battery electrolyte by using vanadium tetrasulfide. CN2022111942699, 2022-09-28.
17. G. Kim, Y. K. Kim, T. Yim, K. Kwon, Effects of methanesulfonic acid on electrolyte for vanadium redox flow batteries, *J. Ind. Eng. Chem*. 99 (2021) 326–333.
18. Y. J. Ye, M. Wu, M. J. Nan, M. L. Fang, M. J. Yang, L. Qiao, X. K. Ma, The influence of inorganic salt additives in the electrolyte on iron-chromium flow batteries at room temperature, *Appl. Energy Mater*. 7 (2024) 4200–4206.
19. A. Okazawa, T. Kakuchi, K. Kawai, M. Okubo, lron-based catholytes for aqueous redox-flow batteries, *Appl. Mater*. 11 (2023) 11.
20. J. Z. Li, C. Wang, R. Wang, C. F. Zhang, G. J. Li, D. Kenneth, S. L. Zhang, Z. P. Guo, Progress and perspectives on iron-based electrode materials for alkali metal-ion batteries: A critical review, *Chem. Soc. Rev*. 53 (2024) 4154–4229.
21. S. E. Waters, C. M. Davis, J. R. Thurston, M. P. Marshak, Maximizing vanadium deployment in redox flow batteries through chelation, *J. Am. Chem. Soc*. 144 (2022) 39.
22. J. X. Gao, K. Lee, K. Amini, R. G. Gordon, A. Betley, M. J. Aziz, A highly soluble lron-based posolyte species with high redox potential for aqueous redox flow batteries advanced functional materials, *Adv. Funct. Mater*. 34 (2023) 11.
23. S. L. Wang, Z. Y. Xu, X. L. Wu, H. Zhao, J. L. Zhao, J. G. Liu, C. W. Yan, X. Z. Fan, Excellent stability and electrochemical performance of the electrolyte with indium ion for iron-chromium flow battery, *Electrochim. Acta*. 368 (2021) 137524.
24. A. Dinesh, S. Oliwera, K. Venkatesh, S. Santosh, G. M. Priya, Inamuddin, M. A. Abdullah, H. B. Muralidhara, Iron-based flow batteries to store renewable energies, *Environ. Chem. Lett*. 16 (2018) 683–694.
25. A. Ahmad, T. A. Aldawood, M. Mansha, S. Ali, M. N. Tahir, M. Khan, I. A. Khan, S. A. Khan, Optimized and cost-effective elemental-sulfur sodium polysulfide/sodium bromide aqueous electrolytes for redox flow batteries, *J. Power Sources* 614 (2024) 235013.
26. S. H. Ge, H. T. Zhou, B. L. Yi, H. M. Zhang, Sodium polysulfide-bromine energy storage battery pack, *Power Suppl. Tech*. 28 (2004) 373–375.
27. B. H. Robb, J. M. Farrell, M. P. Marshak, Chelated chromium electrolyte enabling high-voltage aqueous flow batteries, *Joule* 3 (2019) 2503–2512.
28. H. T. Zhou, H. M. Zhang, P. Zhao, B. L. Yi, Sodium polysulfide/bromine redox flow battery, *Renew. Energy Source* 121 (2005) 62–64.
29. R. J. Remick, P. G. P. Ang, Electrically rechargeable anionically active reduction-oxidation electrical storage-supply system. US4485154, 1984-11-27.
30. L. Li, X. G. Chen, Z. M. Feng, Y. Q. Jiang, L. Dai, J. Zhu, Y. G. Liu, L. Wang, Z. X. He, Recent advances and perspectives of practical modifications of vanadium redox flow battery electrodes, *Green. Chem*. 26 (2024) 6339–6360.
31. W. T. Liu, X. Z. Sun, X. Y. Yan, Gao, Y. H. Zhang, X. Wang, K. Ma, Y. W. Review of energy storage capacitor technology, *Batteries* 10 (2024) 217–230.

32. N. Poli, C. Bonaido, M. Moretto, M. Guarnieri, Techno-economic assessment of future vanadium flow batteries based on real device/market parameters, *Appl. Energy* 12 (2024) 24–29.
33. P. M. Lessner, F. R. McLarnon, E. J. Cairns, *Kinetics and Transport Processes in Aqueous Polysulfide Electrode Reactions: LBL-22399*, Lawrence Berkeley National Laboratory, 1986.
34. L. B. Guo, H. L. Huang, S. Tao, Y. H. Cheng, Inhibition of zinc dendrites in zinc-based flow batteries, *Front. Chem*. 8 (2020) 557.
35. H. Lu, S. Meng, T. He, C. Zhang, J. H. Yang, Recent progress in covalent organic frameworks for rechargeable zinc-based batteries, *Coord. Chem. Rev.* 514 (2024) 215910.
36. B. Lu, K. F. Yu, W. D. Shao, Y. Ji, F. Zhang, Organic redox-active molecules for alkaline aqueous redox flow batteries, *Curr. Opin. Green. Sust*. 47 (2024) 100905.

CHAPTER 8

Advancements in Electrocatalysts

Powering the Future of Flow Battery Technology

Jyoti Singh, An-Giang Nguyen, Manoj Kumar Gangwar, and Rakesh Verma

8.1 INTRODUCTION

Carbon dioxide emissions rise along with global economic growth, disrupting the ecosphere and intensifying the adverse impacts of climate change. Developing a sustainable approach to harnessing electricity from renewable sources like wind and solar power is crucial [1,2]. The implementation of energy storage systems is crucial for facilitating the use of renewable and sustainable sources of energy, as well as enhancing the dependability of electrical grids. These systems are designed to store surplus electrical energy, thereby contributing to the overall efficiency of the grid network [3,4]. The energy that has been stored can subsequently be supplied to end users or power grids on an as-needed basis. It is becoming apparent that the use of rechargeable batteries with electrochemical energy storage based on redox chemistry can address this problem. Redox-flow batteries (RFBs) utilize recirculating liquid electrolytes for energy storage, offering distinct benefits. Their energy density is independent and can vary based on elements like tank size, electrolyte concentration, cell voltage, and the number of cells [5]. Furthermore, their capacity generation capability is influenced by various factors, including electrode dimensions and reaction kinetics [5]. When considering factors like cost, flexibility of the system, rapid response, and safety issues for large-scale applications, RFBs offer significant benefits compared to other battery types, including lead-acid and Li-ion batteries [6]. As a result, it is expected that RFBs will have an increasing presence in the commercial market in the future due to technological advancements. Consequently, it is crucial to comprehend the

DOI: 10.1201/9781003506379-8

redox chemistry and underlying technical principles of flow batteries, as these factors play a key role in their technological success and market adoption [7].

In order to enhance the effectiveness of RFBs, it is crucial to develop electrocatalysts that lower the activation energy of redox reactions and increase reaction kinetics. Nanocatalysts offer several advantages over traditional bulk catalysts, such as an extensive active area, high catalytic activity, and outstanding reaction selectivity. These advantages have resulted in their widespread application across diverse fields, including energy storage, environmental protection, and chemical engineering [8–11]. Among electrocatalysts, metal-based electrocatalysts are known for their high reaction activity and conductivity, while metal compounds are relatively inexpensive and exhibit significant catalytic activity [12,13]. Furthermore, N-doped carbon electrocatalysts are a new technology that reliably shows a large specific surface area and excellent electrical conductivity. This performance is attributed to their distinct structure and composition. The unique design and makeup of this structure create many active sites for redox reactions to occur. Also, N-doped carbon nanomaterials can create a stable conductive network structure that lets RFBs handle large amounts of current [14].

In this chapter, we will primarily concentrate on the advancements in electrocatalysts for aqueous RFBs. We will provide a comprehensive summary of the various types of electrocatalysts that can improve the electrochemical kinetics of commonly used redox-active substances. Finally, this study will present substantive recommendations for the ongoing development and implementation of electrocatalysts in RFBs.

8.2 THE HISTORY OF REDOX-FLOW BATTERIES DEVELOPMENT

A regenerative fuel cell, commonly referred to as an RFB, is a kind of fuel cell that can store electricity by charging it. In 1974, Dr. L. H. Thaller from NASA in the United States introduced the idea of the RFB system [15]. At the same period, a team of researchers in Japan, headed by Nozaki et al. and affiliated with the National Institute of Advanced Industrial Science and Technology, started their fundamental research and development of RFB systems [16]. In 1986, Professor Skyllas-Kazacos from the University of New South Wales in Australia developed the V/V RFB [17]. This invention greatly enhanced the efficiency of RFB systems and opened the door for their practical use.

During the 1980s, Japan faced an issue with the disparity in electricity demand between daytime and nighttime, prompting the development of RFBs as national projects and collaborations between power companies and manufacturers. In 2001, Sumitomo Electric Industries launched a VRFB system [18]. Since then, around 30 projects have been completed, featuring operational systems in factories and universities, along with demonstration systems in national initiatives [19]. In about 2010, the effort to promote renewable energy to address climate change resulted in a rise in the development of energy storage batteries, including RFBs.

The United States Department of Energy has played a significant role in advancing energy storage technologies, particularly in the form of RFBs, by providing substantial financial support as a result of the American Recovery and Reinvestment Act, which was enacted in 2009. Additionally, in June 2010, the International Flow Battery Forum (IFBF),

a prestigious academic society specializing in RFBs, was established in Europe. The annual IFBF conferences have been highly successful, contributing to the increasing number of scientific reports on RFBs, which surpassed 400 in 2014.

8.3 CLASSIFICATION OF REDOX-FLOW BATTERIES

RFBs are typically classified based on the phases of their electrolyte and electrodes, which are depicted in Figure 8.1 as three distinct categories.

8.3.1 The Classical or True Redox-Flow Battery

At the electrodes, no phase change occurs because all electroactive species remain in a soluble form, similar to the process in all-vanadium RFBs. Although the electrodes themselves are inert, they do need to possess efficient electrocatalytic surfaces. Energy is solely stored within the electrolytes. Typical challenges faced in these RFBs include slow reaction kinetics, the unintended blending of half-cell electrolytes, and the volatility of reactants.

8.3.2 The Type-1 Hybrid Redox-Flow Battery

Electrode reactions can involve a change in phase, which allows for the presence of electroactive species in either solid or gas form. The amount of energy that half-cells can store is restricted by how much material can be deposited on the electrodes. Although the practicality of commercial Zn-Br RFB [20] has been demonstrated, these systems may face challenges such as blocked manifolds due to emerging solids or dendrites, edge effects at the electrodes, and complications arising from the flow inlet and outlet [21]. In hybrid systems that incorporate metal deposition, such as Zn-Ce and Zn-Br [22], slow self-discharge may occur due to deposit corrosion.

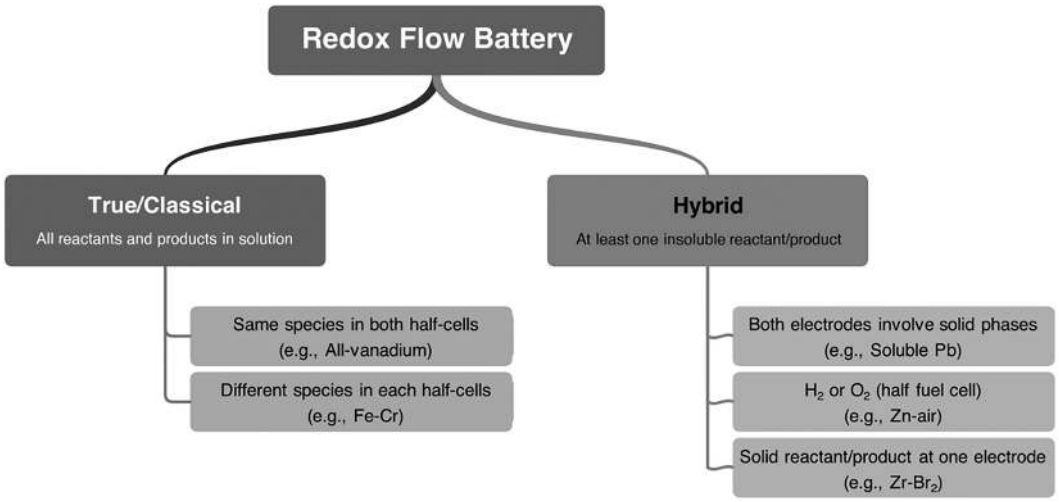

FIGURE 8.1 Classification of redox-flow batteries, illustrating both conventional and hybrid models.

8.3.3 The Type-2 Hybrid Redox-Flow Battery

Phase transitions take place at both electrodes of the cell. The charging and discharging processes of each half-cell reaction cause phase changes at the electrode surfaces. These changes are similar to what happens in a soluble lead RFB [21]. In this system, lead ions in an acidic solution are converted into PbO_2 at the positive electrode during charging, and at the negative electrode, they are transformed into metallic lead. Energy is kept in deposits found in the two electrodes, and the amount of energy that can be stored is restricted by the space between them.

8.4 ESSENTIAL CHARACTERISTICS OF REDOX-FLOW BATTERIES

High-performance RFBs should demonstrate the following essential characteristics:

- **High cell potential:** The unique feature is primarily influenced by the notable voltage difference in the electrode reactions. This factor is essential for the capacity to store energy, with an emphasis on reducing overpotentials and ohmic losses.
- **High cell current:** Achieved by increasing electron-transfer speeds, creating larger electrode surfaces, and eliminating obstacles to mass transport.
- **High energy efficiency:** This involves two main aspects: enhanced current efficiency resulting from rapid kinetics and the avoidance of side reactions, along with improved voltage efficiency.
- **Long operational lifespan:** The materials used for electrodes, membranes, and electrolytes should experience minimal degradation, fouling, or any alterations that lead to capacity decrease over numerous cycles.
- **Practicality:** The substances and materials used should be safe for health, come from sustainable or easily recyclable sources, and be affordable.
- **High energy storage capacity:** The electroactive parts need to be very soluble, ensuring that all oxidation states remain stable while dissolved in the solution.

8.5 BASIC PRINCIPLES OF REDOX-FLOW BATTERIES

RFBs are a type of rechargeable battery that utilize two soluble redox couples to store electrical energy. These batteries consist of basic components such as electrodes, bipolar plates, and membranes, as well as two external tanks. RFBs are categorized according to the active chemical species involved in their reactions. Examples include Fe/Cr, polysulfide/Br_2, Zn/Br_2, quinone/Br_2, and Zn/polyiodide [23,24]. The vanadium redox-flow batteries (VRFBs) stand out as the most developed option among different types of flow batteries [25]. Currently, construction is underway on large-scale commercial VRFBs. VRFBs operate by utilizing vanadium metal in two different oxidation states, one at the positive half-cell and the other at the negative half-cell. Figure 8.2 illustrates the structure and charge and discharge reactions of VRFBs. During discharge, reduction occurs at the cathode and oxidation occurs at the anode, as shown in Equations (8.1)–(8.3) (discharge: charge:) [26].

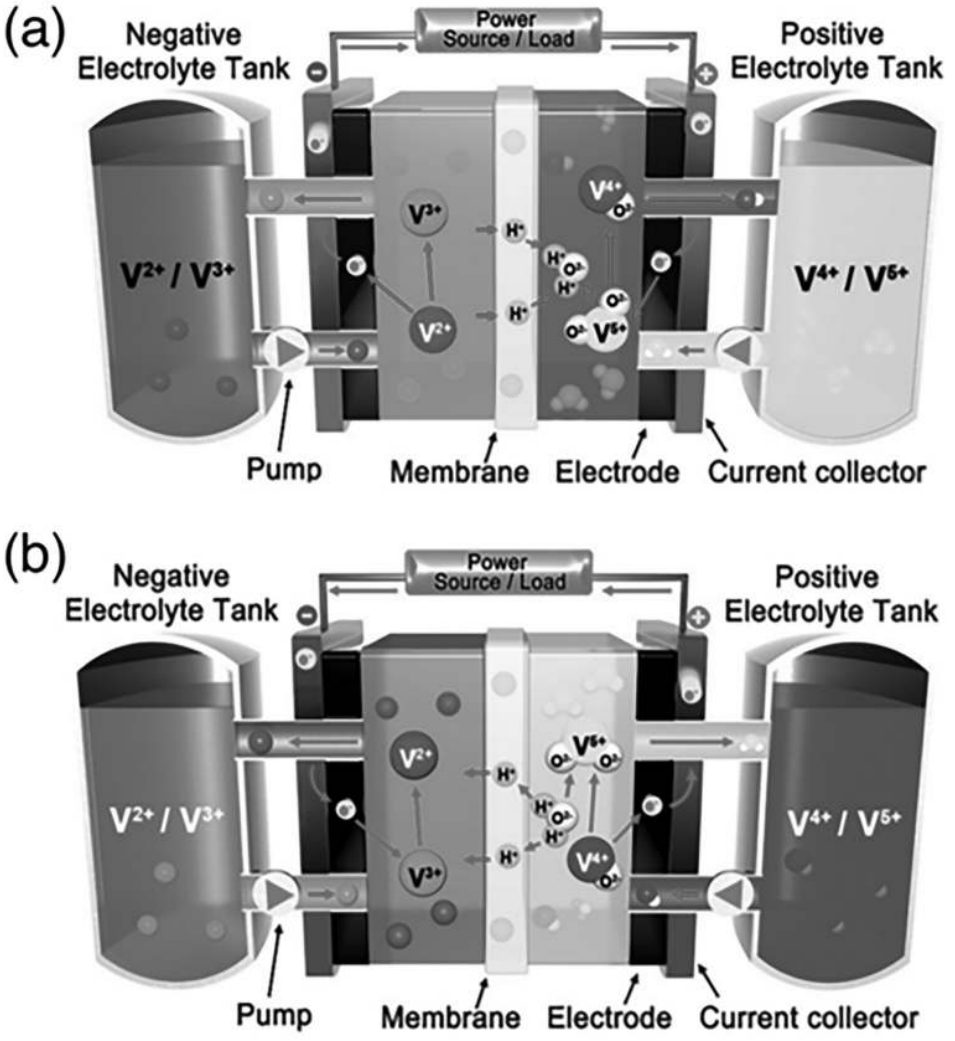

FIGURE 8.2 The diagram illustrates the processes of (a) discharging and (b) charging within the VRFB system, which consists of two primary electrolyte tanks and electrode materials that are separated by a membrane. (Adapted with permission from Reference [27], Copyright 2015 Wiley-VCH.)

While these redox reactions occur, proton ions diffuse across the membrane, and electrons transfer through an external circuit.

Negative electrode:

$$V^{2+} \rightleftarrows V^{3+} + e^- \quad (E^\circ = -0.26 \text{ V vs. SHE}) \tag{8.1}$$

Positive electrode:

$$VO_2^+ + 2H^+ + e^- \rightleftarrows VO^{2+} + H_2O \quad (E^\circ = 1.00 \text{ V vs. SHE}) \tag{8.2}$$

Overall reaction:

$$V^{2+} + VO_2^{+} + 2H^{+} \rightleftarrows VO^{2+} + V^{3+} + H_2O \quad (E^{\circ} = 1.26\ \text{V vs. SHE}) \tag{8.3}$$

For all VRFBs, the standard cell voltage is typically 1.26 V. To determine the cell voltage at a certain temperature, pH, and concentration of vanadium species, the Nernst equation can be employed as

$$E = 1.26 - \frac{RT}{F}\ (V) \tag{8.4}$$

where R stands for the universal gas constant, T stands for absolute temperature, and F stands for the Faraday constant. The movement of vanadium ions across the membrane can take place, leading to self-discharge and the undesired mixing of vanadium species on both sides of the cell [27].

At the negative electrode:

$$V^{2+} + VO^{2+} + 2H^{+} \rightleftarrows 2V^{3+} + H_2O \tag{8.5}$$

$$2V^{2+} + VO^{2+} + 4H^{+} \rightleftarrows 3V^{3+} + 2H_2O \tag{8.6}$$

$$V^{3+} + VO_2^{+} + \rightleftarrows 2VO^{2+} \tag{8.7}$$

At the positive electrode:

$$V^{2+} + 2VO_2^{+} + 2H^{+} \rightleftarrows 3VO^{2+} + H_2O \tag{8.8}$$

$$V^{3+} + VO_2^{+} \rightleftarrows 2VO^{2+} \tag{8.9}$$

$$V^{2+} + VO^{2+} + 2H^{+} \rightleftarrows 2V^{3+} + H_2O \tag{8.10}$$

During the operation, side reactions can occur, including the evolution of hydrogen due to the decomposition of water and the evolution of CO_2 due to the oxidation of carbon-derived electrodes [28]. Battery performance is typically assessed using three measures of efficiency: coulombic efficiency (CE), voltage efficiency (VE), and energy efficiency (EE). Each of these is defined as follows:

$$\text{CE} = \frac{\text{discharge capacity}}{\text{charge capacity}} \times 100\% \tag{8.11}$$

$$\mathrm{VE} = \frac{\text{average discharge voltage}}{\text{average charge voltage}} \times 100\% \tag{8.12}$$

$$\mathrm{EE} = \mathrm{CE} \times \mathrm{VE} \tag{8.13}$$

The VE is impacted by various factors. These include the current density during operation, the ionic conductivity of the membrane, the properties of the electrode materials, the flow rate, and how well the electrolyte is transported. With the rise in current density, the VE typically declines as a result of increased polarization.

Recently, various nanomaterials, both metal- and carbon-based, have been engineered to serve as electrocatalysts aimed at improving the CE and VE of VRFBs.

8.6 METAL-BASED ELECTROCATALYSTS

8.6.1 Metal Electrocatalysts

Metals, particularly those identified as noble or transition metals, are widely employed as electrocatalysts because of their high activity, a property that can be attributed to their outer electron arrangement [29]. Transition metals have catalytic abilities because their d orbitals are partially filled. This feature allows them to either give away or take in electrons. This characteristic has been observed to be a key factor in their catalytic properties [30]. In addition, metal electrocatalysts are appealing materials for RFBs because of their superior electrical conductivity. Moreover, noble metals exhibit a high level of stability and inertness in the highly acidic conditions present in all VRFBs. Unfortunately, many metals, particularly rare-earth and noble metals, are too expensive for use in huge-scale RFBs. Nevertheless, the early study by Rychcik and Skyllas-Kazacos focused on metals because they found that graphite deteriorated greatly under the oxidizing conditions present in the positive half-cell. This degradation resulted in a carbon suspension forming in the positive electrolyte [31]. Therefore, the primary objective at that time was to substitute carbon-derived electrodes with more durable all-metal electrodes, even though they were more expensive. Rychcik and Skyllas-Kazacos evaluated the dimensional stability of anode electrodes constructed from titanium, lead, platinized titanium, and iridium oxide catalysts [31]. In addition, the examination of alternative metal-based catalyst options has been initiated with the aim of reducing costs. The results of this investigation are presented in the forthcoming sections.

8.6.1.1 Iridium-Based Electrocatalysts

Electrocatalysts that use iridium are significant for various applications. These materials play a crucial role in energy conversion processes, including fuel cells and electrolyzers. Iridium-based catalysts are known for their efficiency and stability, making them vital in improving the overall performance of these technologies. Understanding their properties and potential can enhance advancements in clean energy solutions. Iridium, a transition metal that is part of the platinum group, is frequently utilized as a catalyst in both acidic

and alkaline environments. The extensive use of iridium can be attributed to its ability to exist in various oxidation states, ranging from (–3) to (+9), along with its exceptional resistance to corrosion [29]. Previous research conducted by Sun and Skyllas-Kazakos demonstrated the beneficial effect of using Ir^{3+} to modify the V(IV)/V(V) reaction [32]. Following this, Wang and Wang explored how Ir-modified carbon felt electrodes performed in the redox reaction involving V(IV) and V(V) [33]. Ir is known for its excellent conductivity, so adding iridium to graphite felt should lower the cell resistance and battery overpotential significantly. Subsequent tests on polarization and impedance spectroscopy (IES) revealed a 63% reduction in overpotential. The authors suggested that this reduced ability to diffuse was likely due to Ir-containing materials blocking the pores of the felt. However, experiments with charging and discharging using small-scale VRFBs with the Ir-modified positive felt demonstrated an approximately 11% increase in the battery's EE at a current density of 60 mA cm^{-2}. This enhancement is attributed to the increased VE of the battery.

8.6.1.2 Bismuth-Based Electrocatalysts

Bismuth-based electrocatalysts are becoming increasingly important in the area of VRFBs. Its nontoxic and low corrosive properties make it a favored option as a catalyst in organic reactions [34]. Bismuth catalysts are less expensive than those constructed of iridium, platinum, and indium, in addition to the previously listed advantages. These catalysts play a significant role in various energy conversion processes. Researchers are exploring different ways to utilize bismuth-based electrocatalysts to enhance performance and reduce costs, which could lead to more sustainable energy solutions. The ongoing studies in this area aim to better understand how these catalysts work and how they can be optimized for practical applications. Santamara's team initially examined how bismuth (Bi) nanoparticles function as catalysts in both positive and negative vanadium redox reactions through the use of cyclic voltammetry [35,36]. The study focused on the catalytic properties of bismuth (Bi) metal. To produce this metal, bismuth oxide (Bi_2O_3) was heated on graphite fabric at a temperature of 450°C [35]. The electrochemical characteristics of the original graphite felt, the thermally treated variant, and the Bi-modified graphite felt (Bi-MGF) were analyzed through cyclic voltammetry measurements of VO_2^+/VO_2^+ ions used as positive electrodes. The excellent performance was achieved with the Bi-MGF, which displayed enhanced peak current densities for both anodic and cathodic reactions. Additionally, it achieved a reversible voltage difference of 50 mV. These findings indicated a significant enhancement of the charge-transfer rate at the interface between the electrode and electrolyte, thanks to the superior electrical conductivity offered by the Bi nanoparticles.

The same team developed a graphite felt that has Bi nanoparticles embedded in it that function as the VRFBs system's negative electrode. The Bi-MGF demonstrated a reversible reaction (V^{2+} to V^{3+}), with a consistent redox peak current ratio that approaches 1. To evaluate its cyclability, the performance of the Bi-MGF was analyzed through 500 cycles in a CV test. The Bi-modified samples showed no significant changes in the redox peaks. This outcome suggests that the presence of Bi nanoparticles helps maintain the oxygen

groups in carbon felt. Significantly, the scientists suggested a catalytic mechanism that incorporates Bi nanoparticles in the negative electrode of the V^{2+} to V^{3+} system. This mechanism indicates that Bi nanoparticles have the potential to form BiHx as an intermediate compound. As a result, BiHx may play a role in preventing irreversible hydrogen evolution, as demonstrated in Figure 8.3. Li et al. [37] carried out a study on Bi-MGF, where they introduced bismuth to the electrolyte as a soluble $BiCl_3$ salt rather than pretreating the electrode with bismuth particles. As shown in Figure 8.4a, the electrode potential for the Bi^{3+}/Bi reaction is 0.308 volts against the standard hydrogen electrode, indicating that Bi^{3+} can be reduced to its elemental form and deposited on the graphite felt surface before V^{3+} is reduced to V^{2+} during the charging process of the negative half-cell. Notably, the cyclic voltammetry tests revealed that adding Bi^{3+} had little impact on the V(IV)/V(V) redox process, which contradicts findings from a previous study that used a different method to modify the electrode with bismuth.

Researchers from the Pacific Northwest National Laboratory have recently shared findings on vanadium electrolytes that contain bismuth (Bi^{3+}) ions, which are designed for outstanding performance of VRFBs [37]. They managed the amount of $BiCl_3$ additives in a range from 0 to 0.02 M within a 5 M HCl electrolyte that also contained 2 M $VOSO_4$. A small quantity of soluble Bi^{3+} ions can be reduced and deposited onto the negative graphite felt electrode at the same time during the charging process, as shown in Figure 8.4b. In the cyclic voltammograms (CVs), an electrolyte with 0.01 M of Bi^{3+} ions demonstrated enhanced catalytic activity specifically for the redox couple (V^{2+}/V^{3+}) when compared to the electrolyte lacking Bi^{3+} ions, as illustrated in Figure 8.4c. A single flow cell test for VRFBs was conducted by adjusting the Bi^{3+} concentration from 0 to 0.02 M, while the current rates ranged from 50 to 150 mA cm^{-1}. Notably, the addition of 0.01 M Bi^{3+} resulted in the best electrochemical performance, showcasing high stability over 50 cycles and enhanced rate capability at 150 mA cm^{-1}. Several metal nanoparticles demonstrated strong activities in vanadium redox reactions. However, challenges like high costs and limited availability restrict their widespread application as electrocatalysts in VRFBs.

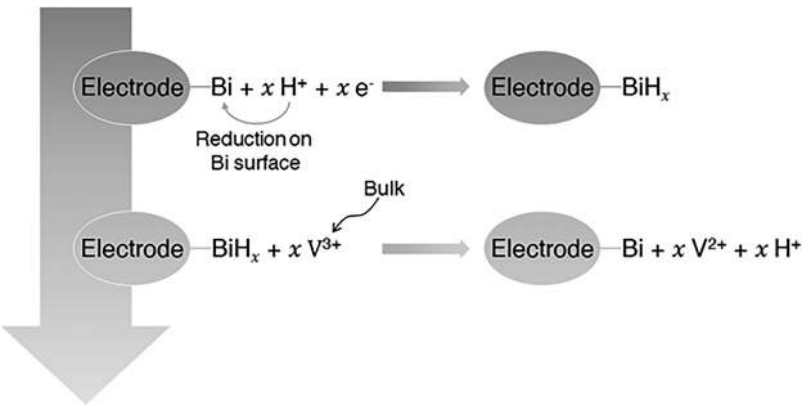

FIGURE 8.3 Proposed mechanism for the V^{2+}/V^{3+} redox reaction occurring on a Bi-modified electrode.

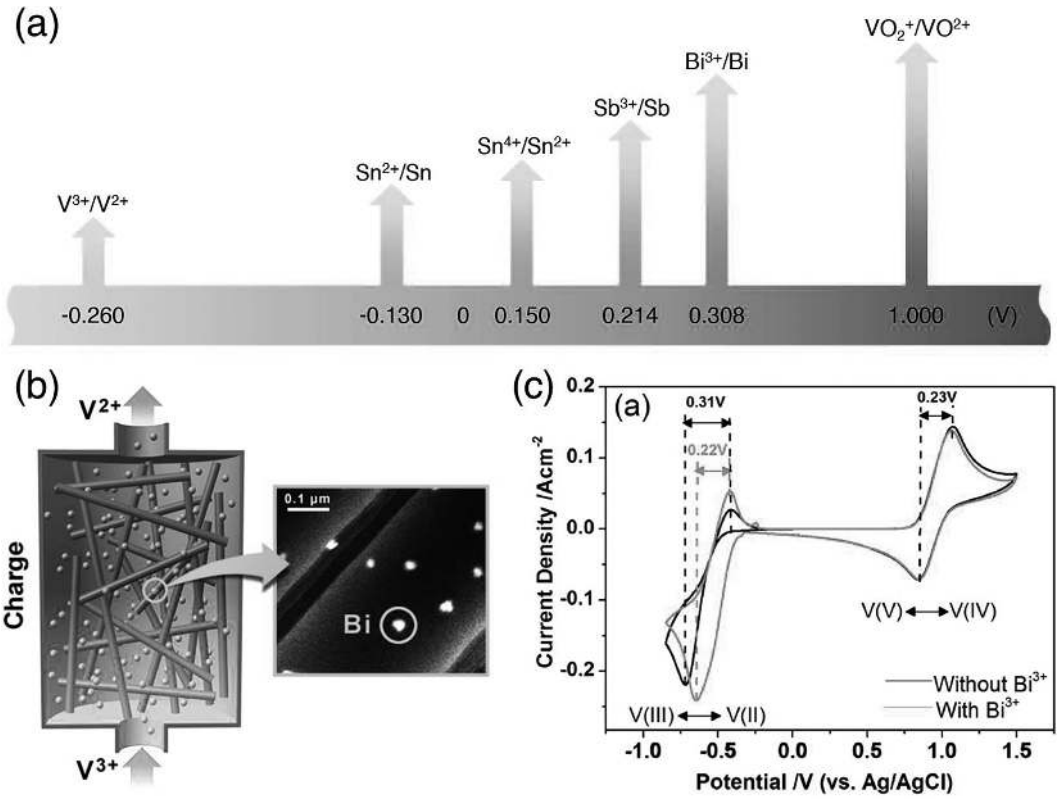

FIGURE 8.4 (a) The electrode potentials compared to the standard hydrogen electrode were analyzed for several redox couples to evaluate their electrocatalytic activity for the V^{2+}/V^{3+} and VO^{2+}/VO_2^+ reactions. (b) A negative electrolyte tank illustration displays the STEM image of Bi nanoparticles after cycling. (Adapted with permission from Reference [37], Copyright 2013 American Chemical Society.) (c) Cyclic voltammograms were recorded using a glassy carbon working electrode in solutions of 2 M $VOSO_4$ and 5 M HCl, both with and without the addition of 0.01 M $BiCl_3$. (Adapted with permission from Reference [37], Copyright 2013 American Chemical Society.)

8.6.2 Metal Oxide Electrocatalysts

Metal oxide electrocatalysts are crucial components in various energy conversion processes. They enhance the efficiency of reactions in fuel cells and batteries, making them essential for advancing clean energy technologies. Various electrocatalysts based on transition metal oxides, including WO_3, IrO_2, PbO_2, Mn_3O_4, and Nb_2O_5, have demonstrated improvements in the catalytic efficiency of vanadium redox couples. These materials are attractive because they are cost-effective and readily available [32,37–40]. In 1987, Skyllas-Kazacos and her research team developed the dimensionally stable anode (DSA) by applying IrO_2 to a titanium electrode. This material, IrO_2, exhibited superior overall overpotentials in VRFBs [37]. Recently, a carbon felt electrode coated with a Mn_3O_4 catalyst was synthesized through a hydrothermal process using a 1 M solution of manganese

acetate $(C_2H_3O_2)_2Mn{\cdot}4H_2O$ [32]. This reaction took place at a temperature of 200°C over a duration of 12 h. The powder X-ray diffraction (XRD) patterns revealed that the Mn_3O_4 crystals have a tetragonal structure. The surface structure of the altered carbon felt was analyzed using scanning electron microscopy, which showed that the Mn_3O_4 nanoparticles were evenly distributed. Furthermore, both the V^{2+}/V^{3+} and VO^{2+}/VO_2^+ redox reactions exhibited higher redox peak currents and an enhanced difference in peak voltage. This suggests that Mn_3O_4 is a promising catalyst for VRFBs. The carbon felt enhanced with Mn_3O_4 in the flow cell demonstrated an EE of approximately 75% under a current density of 40 mA cm^{-2}. Nevertheless, the CE was less than 86%, indicating that it was not operating at its best.

Graphite felt treated with WO_3 has been suggested as an alternative to noble metal catalysts, aimed at improving the electrochemical efficiency of VRFBs. The sample was synthesized using a hydrothermal method, which involved heating $Na_2WO_4{\cdot}2H_2O$ at a temperature exceeding 180°C for a duration of 4 h [39]. WO_3 nanoparticles have been effectively incorporated into the graphite felt. Following the surface treatment, the current density for the VO^{2+}/VO_2^+ reaction peak showed an increase in the CV curves. However, there was no observed reduction in the separation of the peak potentials. In the battery cycling tests, the WO_3-modified graphite felt electrode showed EE of 78.13%, VE of 78.92%, and CE of 99.00% while functioning at a current density of 70 mA cm^{-2}.

Similarly, lead oxide (PbO_2) used on a graphite felt electrode has been recognized as a substitute for expensive metal catalysts. This alternative enhances the electrochemical performance in positive vanadium redox reactions [40]. The pulse deposition technique was used to create a dense and consistently coated PbO_2 catalyst. PbO_2 consists of a combination of two crystallographic phases, referred to as α and β. The CV curve for graphite felt loaded with PbO_2 indicated higher peak current densities for the oxidation and reduction of the redox couples (VO^{2+}/VO_2^+) when compared to the curve of pristine graphite felt. The outcomes of the IES showed a 20% reduction in charge-transfer resistance after PbO_2 was applied to the graphite felt. A flow cell experiment was carried out using PbO_2-modified graphite felt, with the current density gradually increasing from 40 to 80 mA cm^{-2}. The resulting EE, VE, and CE were found to be 78.1%, 78.3%, and 99.7%, respectively. The researchers concluded that the catalytic activity for positive vanadium redox ions was attributed to the uniform distribution of PbO_2 particles on the graphite felt surface.

8.7 CARBON-BASED ELECTROCATALYSTS

8.7.1 Zero-Dimensional Carbon

Zero-dimensional (0-D) carbon refers to a form of carbon material that has no length, width, or height. This unique structure means that the carbon atoms are arranged in a way that is different from other forms of carbon, such as one-dimensional (1-D) or two-dimensional (2-D) materials. The properties of 0-D carbon can lead to various applications, making it an area of significant interest in research and technology. Understanding

its characteristics is essential for advancements in various fields, including electronics and materials science.

Activated carbon is commonly used as a 0-D carbon-based catalyst because it has a large specific surface area and good electrical conductivity and remains stable in acidic conditions. This material features a distinct porous structure that enhances its catalytic activity with reactants [41]. Recently, researchers developed mesoporous activated carbon with a large surface area by carbonizing coconut shells, aiming to boost electrocatalytic activity for vanadium redox ions [42]. The carbon precursor was processed to isolate particles sized between 20 and 30 mesh, then heated to 800°C in a nitrogen and carbon dioxide environment. After being washed with 0.1 M hydrochloric acid and distilled water, the resulting activated carbon sample exhibited a BET-specific surface area of 1652 $m^2 g^{-1}$ and a porosity of around 60%. The scientists indicated that the highly accessible mesoporous structure of the reactive sites enhanced vanadium redox reactions, evidenced by the notable presence of redox peaks (V^{3+} to V^{4+}) and a reduced peak voltage separation. Additionally, an EE of 85% was achieved using the activated carbon-modified carbon paper electrode in a static vanadium redox-flow battery cell setup.

8.7.2 One-Dimensional Carbon

Unlike zero-dimensional carbon nanoparticles, where electron transport occurs through hopping or diffusion mechanisms, one-dimensional nanostructures allow for efficient charge transfer across a continuous network. This phenomenon results in improved electron-transfer speeds and lower contact resistance [43]. Yan and his colleagues have done a lot of research on different electrocatalysts made from carbon nanotubes, such as modified multiwalled carbon nanotubes (MWCNTs) and single-walled carbon nanotubes (SWCNTs) [44,45]. The researchers studied how well SWCNTs function as an electrocatalyst for both positive and negative redox reactions [45]. We refluxed the pristine SWCNTs in an H_2SO_4/HNO_3 solution for six hours to remove impurities and create surface active sites. XPS analysis confirmed that carboxyl functional groups and additional oxygen-containing groups were effectively added to the modified SWCNTs. The increase in the VO^{2+}/VO^{2+} redox current density was more prominent on modified SWCNTs compared to V^{2+}/V^{3+}. This indicates that the positive redox reactions were more sensitive and effective than the negative ones. The greater specific surface area and oxygen functionalities contributed to this enhanced performance.

The same team studied MWCNTs that had been modified with carboxyl or hydroxyl groups to investigate how these changes affect the catalytic activity of vanadium redox pairs [44]. The percentage of hydroxyl and carboxyl MWCNTs that were functionalized was 10.3% (C–OH) and 9.6% (–COOH), respectively. Particularly, as seen in Figure 8.5a, the carboxyl MWCNTs exhibited outstanding electrochemical activity toward VO^{2+}/VO_2^{+} ions. In a static cell test, the carbon felt treated with carboxyl MWCNTs demonstrated impressive efficiencies: 98.6% for CE, 76.1% for VE, and 75.0% for EE at a current density of 70 mA cm^{-2}. The authors suggest that the improved electrochemical performance may stem from the larger surface area of the MWCNTs and their increased oxygen content, as

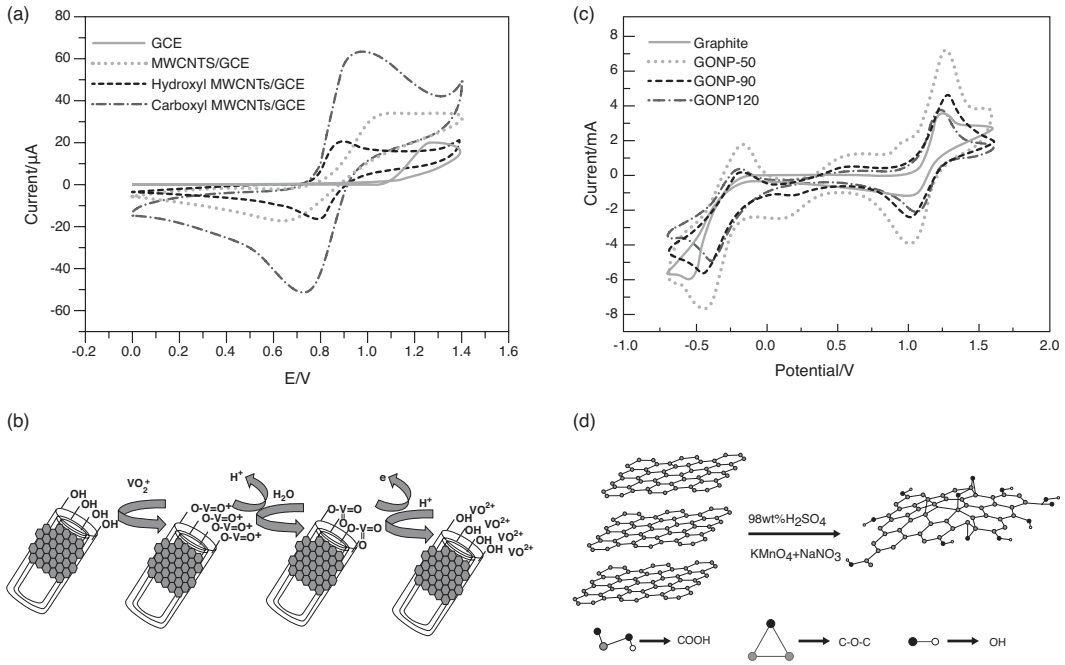

FIGURE 8.5 (a) The cyclic voltammograms (CVs) of glassy carbon electrode modified with bare, hydroxyl, and carboxyl multiwalled carbon nanotubes were recorded at a scan rate of 10 mV s^{-1} in a solution of 0.1 M $VOSO_4$ and 2M H_2SO_4. (b) The suggested redox process involves the hydroxyl-modified multiwalled carbon nanotube on a glassy carbon electrode in relation to the VO^{2+}/VO_2^+ ions. (Adapted with permission from Reference [45], Copyright 2011 Elsevier.) (c) CVs of the pristine graphite and GONP samples were recorded at a scan rate of 10 mV s^{-1} in a solution of 2 M $VOSO_4$ and 2 M H_2SO_4. (Adapted with permission from Reference [47], Copyright 2011 Elsevier.) (d) Diagram showing the steps involved in synthesizing GO nanoplatelets. (Adapted with permission from Reference [47], Copyright 2011 Elsevier.)

illustrated in Figure 8.5b. The larger surface area and higher oxygen levels of MWCNTs enhance their electrochemical performance.

8.7.3 Two-Dimensional Carbon

Two-dimensional carbon is a material that has garnered considerable attention in diverse scientific disciplines. Its distinctive properties render it valuable for numerous applications, ranging from electronics to materials science. The investigation of 2-D carbon presents novel opportunities for innovation and technological advancement. Elucidating its characteristics may lead to significant developments across various industries. Since the 2010s, various graphene-based two-dimensional nanosheets, including carbon nanowalls, graphene oxide (GO), edge-functionalized graphene nanoplatelets (E-GNPs), and reduced graphene oxide (rGO), have received significant attention for their potential as electrocatalysts in VRFBs [46–48]. Initially, graphene oxide nanoplatelets (GONPs) were first introduced as an electrocatalyst in vanadium redox reactions due to the presence of various oxygen groups on their edges and flat surfaces [46]. GONPs were synthesized using a modified Hummer's technique.

As illustrated in Figure 8.5d, the resultant products underwent vacuum drying at different temperatures: 50°C, 90°C, and 120°C for 24 h. Particularly, the GONPs subjected to drying at 50°C exhibited the highest concentrations of functional groups with the names C–OH and –COOH. In comparison to other samples, this one has shown superior electrocatalytic activity for the vanadium redox pairs V^{2+}/V^{3+} and VO^{2+}/VO_2^{+} (Figure 8.5c). However, as the surface oxygen functionalities increased, the electrical conductivity decreased significantly, leading to higher polarization in the cyclic voltammetry results.

GO can have its catalytic activity improved through different reduction methods, which helps achieve better electrical conductivity in graphene. Thermally reduced graphene oxide (TRGO) is produced by heating the GO in a nitrogen environment at temperatures reaching 1,000°C for 1 h. Recent studies have indicated that TRGO demonstrates a tiny overpotential and a rapid electron-transfer rate when interacting with positive vanadium ions. The improved outcome came from the better quality of the graphene structure, which is noted for its excellent electrical conductivity and remaining hydroxyl functional groups [49]. Cho and colleagues recently discovered the active redox sites found in the oxygen functional groups situated between the edges and the basal plane of graphene-based materials [48]. E-GNPs were chosen for their defect-free structure in the basal plane, while the edges contain oxygen defects that serve as active sites for redox reactions. For comparison, rGO was prepared with flaws in the basal plane and edges. As seen in Figure 8.6a, graphite combined with dry ice was ball-milled to create the E-GNPs [49]. The XPS spectra of C 1s indicated a rise in carboxyl functional groups (–COOH) in the E-GNP materials when compared to pure graphite. Additionally, HR-TEM investigation showed a crystalline basal plane along with edge defects in the E-GNPs. These defects enhanced the transfer of electrons and the movement of mass transport. The distinct structure of the E-GNPs enhanced their electrochemical properties for both V^{2+}/V^{3+} and VO^{2+}/VO^{2+} species. This resulted in a smaller peak potential separation and a higher peak current density when compared to rGO. Therefore, the suggested mechanism, shown in Figure 8.6b and c, indicates that edge defects play a crucial role in the adsorption and desorption of vanadium ions. These defects enhance the transport of ions in the E-GNPs.

8.8 CONCLUSIONS AND PERSPECTIVES

RFBs are efficacious energy storage solutions capable of retaining energy for extended durations. To reduce costs and enhance the system's power and energy performance, it is imperative to develop efficient and economically viable electrode materials. This chapter presents a comprehensive examination of electrocatalysts derived from metal, metal oxide, and carbon materials that have been developed for application in RFBs, with a primary focus on all-vanadium RFBs. The majority of catalysts composed of metal and carbon exhibited catalytic activity on vanadium redox reactions occurring in both the positive and negative half-cells.

Nanomaterials based on metals have shown excellent electrical conductivity and reactivity. This leads to reduced polarization and enhances the reversibility of vanadium

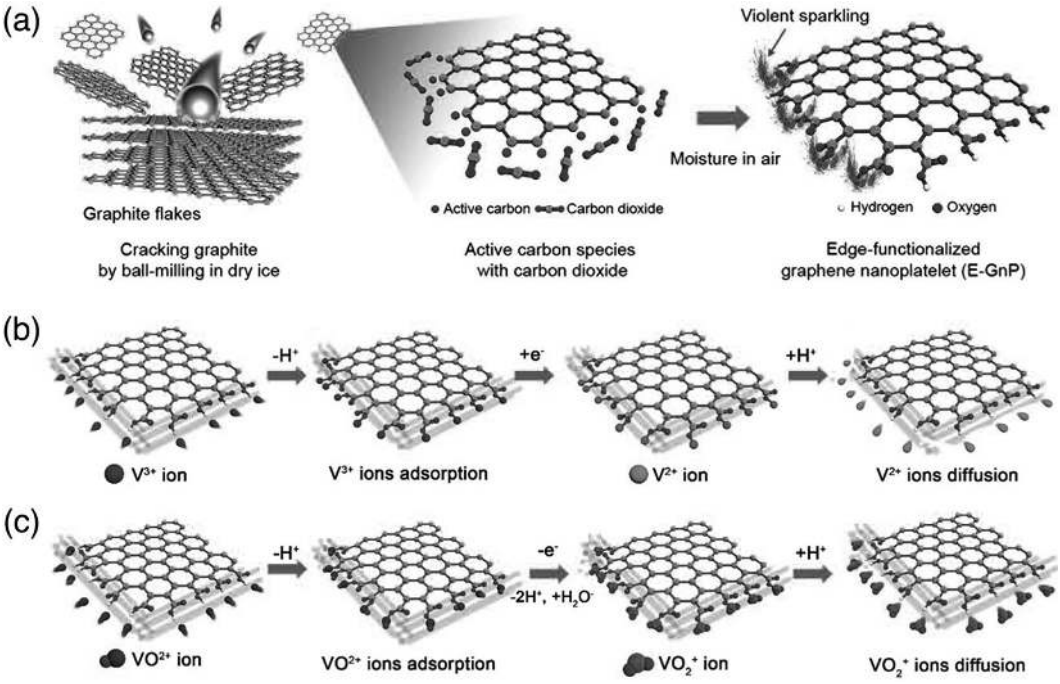

FIGURE 8.6 (a) A schematic illustrating the synthesis of E-GNP. Vanadium redox reactions on the E-GNP electrocatalyst: a proposed catalytic mechanism that displays the ions (b) V^{2+}/V^{3+} and (c) VO^{2+}/VO_2^+. (Adapted with permission from Reference [49], Copyright 2014 Wiley-VCH.)

redox reactions. To reduce hydrogen production on precious metal catalysts, different metal oxides were utilized to minimize the overpotential within the negative half-cell. The durability of these metal-derived catalysts can decline over time when exposed to the strongly acidic conditions found in the vanadium electrolyte. Consequently, metal alloys that exhibit superior corrosion resistance may serve as viable alternatives. Furthermore, new nano-sized metallic alloys are expected to provide enhanced catalytic activity due to their large surface area and superior electrical conductivity. Conversely, carbon-derived nanomaterials of various dimensions have demonstrated unique advantages. These materials can be customized with significant flexibility to achieve a large surface area and a wealth of surface functional groups, including species containing oxygen and nitrogen. Numerous reports indicate that these surface features can serve as direct redox-active sites, promoting the adsorption and desorption of vanadium ions. In addition, many nanostructured carbon materials demonstrate remarkable electrical conductivity, akin to that of metal catalysts. These two characteristics of carbon-derived catalysts greatly enhance vanadium redox reactions, leading to elevated electron-transfer rates and more efficient mass transport kinetics. With the growing need for high-performance energy storage solutions, it is essential to clarify and understand the principle behind the vanadium redox reaction in different electrocatalysts to secure more focus on vanadium redox-flow batteries.

REFERENCES

1. G.L. Soloveichik, Flow batteries: Current status and trends. *Chem. Rev.* 115 (2015) 11533–11558.
2. W. Wang, Q. Luo, B. Li, X. Wei, L. Li, Z. Yang, Recent progress in redox flow battery research and development. *Adv. Funct. Mater.* 23 (2013), 970–986.
3. A.-G. Nguyen, R. Verma, P.N. Didwal, C.-J. Park, Challenges and design strategies for alloy-based anode materials toward high-performance future-generation potassium-ion batteries. *Energy Mater.* 3 (2023), 300030.
4. K. Lin, Q. Chen, M.R. Gerhardt, L. Tong, S.B. Kim, L. Eisenach, A.W. Valle, D. Hardee, R.G. Gordon, M.J. Aziz, M.P. Marshak, Alkaline quinone flow battery. *Science* 349 (2015) 1529–1532.
5. N. Trung, F. S. Robert, Flow batteries. *Electrochem. Soc. Interface* 19 (2010) 54.
6. C. Ponce De León, A. Frías-Ferrer, J. González-García, D.A. Szánto, F.C. Walsh, Redox flow cells for energy conversion. *J. Power Sources* 160 (2006) 716–732.
7. A.G. Olabi, M.A. Allam, M.A. Abdelkareem, T.D. Deepa, A.H. Alami, Q. Abbas, A. Alkhalidi, E.T. Sayed, Redox flow batteries: Recent development in main components, emerging technologies, diagnostic techniques, large-scale applications, and challenges and barriers. *Batteries* 9 (2023) 409.
8. W.-X. Hua, J.-Y. Xia, Z.-H. Hu, H. Li, W. Lv, Q.-H. Yang, Bimetallic compound catalysts with multiple active centers for accelerated polysulfide conversion in Li-S batteries. *J. Electrochem.* 29 (2023) 2217006.
9. R. Verma, P.N. Didwal, H.-S. Ki, G. Cao, C.-J. Park, SnP_3/carbon nanocomposite as an anode material for potassium-ion batteries. *ACS Appl. Mater. Interfaces* 11 (2019) 26976–26984.
10. Y.-J. Zhang, G.-X. Huang, L.R. Winter, J.-J. Chen, L. Tian, S.-C. Mei, Z. Zhang, F. Chen, Z.-Y. Guo, R. Ji, Y.-Z. You, W.-W. Li, X.-W. Liu, H.-Q. Yu, M. Elimelech, Simultaneous nanocatalytic surface activation of pollutants and oxidants for highly efficient water decontamination. *Nat. Commun.* 13 (2022) 3005.
11. Z.-H. Xie, H.-Y. Zhou, C.-S. He, Z.-C. Pan, G. Yao, B. Lai, Synthesis, application and catalytic performance of layered double hydroxide-based catalysts in advanced oxidation processes for wastewater decontamination: A review. *Chem. Eng. J.* 414 (2021) 128713.
12. S. Wang, Z. Xu, X. Wu, H. Zhao, J. Zhao, J. Liu, C. Yan, X. Fan, Excellent stability and electrochemical performance of the electrolyte with indium ion for iron–chromium flow battery. *Electrochim. Acta* 368 (2021) 137524.
13. D.M. Kabtamu, J.-Y. Chen, Y.-C. Chang, C.-H. Wang, Electrocatalytic activity of Nb-doped hexagonal WO_3 nanowire-modified graphite felt as a positive electrode for vanadium redox flow batteries. *J. Mater. Chem. A* 4 (2016) 11472–11480.
14. J. Hu, M. Yue, H. Zhang, Z. Yuan, X. Li, A boron nitride nanosheets composite membrane for a long-life zinc-based flow battery. *Angew. Chem. Int. Ed.* 59 (2020) 6715–6719.
15. L. H. Thaller, Electrically rechargeable redox flow cells. *Proceedings of the 9th IECEC*, NASA Lewis Research Center Cleveland, OH, United States, 1974, pp. 924–928.
16. X. Toshio, Recent development trends of redox flow batteries. *SEI Techn. Rev.* 89 (2019) 5–11.
17. E. Sum, M. Rychcik, M. Skyllas-Kazacos, Investigation of the V(V)/V(IV) system for use in the positive half-cell of a redox battery. *J. Power Sources* 16 (1985) 85–95.
18. M. Shigematsu, Redox flow battery for energy storage. *SEI Techn. Rev.* 73 (2011) 4–13.
19. T. Shigematsu, Development and practical verification of the redox flow battery in SEI. *ECS Trans.* 89 (2019) 5–13.
20. P.C. Butler, P.A. Eidler, P.G. Grimes, S.E. Klassen, R.C. Miles, Zinc/bromine batteries, In: D. Linden, T. B. Reddy (Eds.), *Handbook of Batteries*, McGraw-Hill, 2001, pp. 37.1–37.16.
21. R.G.A. Wills, J. Collins, D. Stratton-Campbell, C.T.J. Low, D. Pletcher, F.C. Walsh, Developments in the soluble lead-acid flow battery. *J. Appl. Electrochem.* 40 (2010) 955–965.

22. P.K. Leung, C. Ponce-de-León, F.J. Recio, P. Herrasti, F.C. Walsh, Corrosion of the zinc negative electrode of zinc–cerium hybrid redox flow batteries in methanesulfonic acid. *J. Appl. Electrochem.* 44 (2014) 1025–1035.
23. M.C. Wu, T.S. Zhao, L. Wei, H.R. Jiang, R.H. Zhang, Improved electrolyte for zinc-bromine flow batteries, *J. Power Sources* 384 (2018) 232–239.
24. M. Skyllas-Kazacos, M.H. Chakrabarti, S.A. Hajimolana, F.S. Mjalli, F.S. Saleem, Progress in flow battery research and development. *J. Electrochem. Soc.* 158 (2011) R55.
25. F.S. Munaiah, F.S. Suresh, S. Dheenadayalan, V.K. Pillai, P. Ragupathy, Comparative electrocatalytic performance of single-walled and multiwalled carbon nanotubes for zinc bromine redox flow batteries. *J. Phys. Chem. C* 118 (2014) 14795–14804.
26. M. Skyllas-Kazacos, M. Rychcik, R.G. Robins, A.G. Fane, M.A. Green, New all-vanadium redox flow cell. *J. Electrochem. Soc.* 133 (1986) 1057–1058.
27. M. Park, J. Ryu, J. Cho, Nanostructured electrocatalysts for all-vanadium redox flow batteries. *Chem. Asian J.* 10 (2015) 2096–2110.
28. A. Tang, J. Bao, M. Skyllas-Kazacos, Thermal modelling of battery configuration and self-discharge reactions in vanadium redox flow battery. *J. Power Sources* 216 (2012) 489–501.
29. A. Venkatalaxmi, B.S. Padmavathi, T. Amaranath, A general solution of unsteady Stokes equations. *Fluid Dyn. Res.* 35 (2004) 229–236.
30. K. Amini, J. Gostick, M.D. Pritzker, Metal and metal oxide electrocatalysts for redox flow batteries. *Adv. Funct. Mater.* 30 (2020) 1910564.
31. M.B. Gawande, R.K. Pandey, R.V. Jayaram, Role of mixed metal oxides in catalysis science—Versatile applications in organic synthesis. *Catal. Sci. Technol.* 2 (2012) 1113–1125.
32. M. Rychcik, M. Skyllas-Kazacos, Evaluation of electrode materials for vanadium redox cell. *J. Power Sources* 19 (1987) 45–54.
33. B. Sun, M. Skyllas-Kazakos, Chemical modification and electrochemical behaviour of graphite fibre in acidic vanadium solution. *Electrochim. Acta* 36 (1991) 513–517.
34. W.H. Wang, X.D. Wang, Investigation of Ir-modified carbon felt as the positive electrode of an all-vanadium redox flow battery. *Electrochim. Acta* 52 (2007) 6755–6762.
35. S. Solyntjes, B. Neumann, H. Stammler, N. Ignat'ev, B. Hoge, Bismuth perfluoroalkylphosphinates: new catalysts for application in organic syntheses. *Chem. Eur. J.* 23 (2017) 1568–1575.
36. Z. González, A. Sánchez, C. Blanco, M. Granda, R. Menéndez, R. Santamaría, Enhanced performance of a Bi-modified graphite felt as the positive electrode of a vanadium redox flow battery. *Electrochem. Commun.* 13 (2011) 1379–1382.
37. B. Li, M. Gu, Z. Nie, Y. Shao, Q. Luo, X. Wei, X. Li, J. Xiao, C. Wang, V. Sprenkle, W. Wang, Bismuth nanoparticle decorating graphite felt as a high-performance electrode for an all-vanadium redox flow battery. *Nano Lett.* 13 (2013) 1330–1335.
38. K.J. Kim, M.-S. Park, J.-H. Kim, U. Hwang, N.J. Lee, G. Jeong, Y.-J. Kim, Novel catalytic effects of Mn_3O_4 for all vanadium redox flow batteries. *Chem. Commun.* 48 (2012) 5455–5457.
39. B. Li, M. Gu, Z. Nie, X. Wei, C. Wang, V. Sprenkle, W. Wang, Nanorod niobium oxide as powerful catalysts for an all-vanadium redox flow battery. *Nano Lett.* 14 (2014) 158–165.
40. Y. Shen, H. Xu, P. Xu, X. Wu, Y. Dong, L. Lu, Electrochemical catalytic activity of tungsten trioxide- modified graphite felt toward VO^{2+}/VO_2^+ redox reaction. *Electrochim. Acta* 132 (2014) 37–41.
41. X. Wu, H. Xu, L. Lu, H. Zhao, J. Fu, Y. Shen, P. Xu, Y. Dong, PbO_2-modified graphite felt as the positive electrode for an all-vanadium redox flow battery. *J. Power Sources* 250 (2014) 274–278.
42. G.J.W. Radford, J. Cox, R.G.A. Wills, F.C. Walsh, Electrochemical characterisation of activated carbon particles used in redox flow battery electrodes. *J. Power Sources* 185 (2008) 1499–1504.
43. M. Ulaganathan, A. Jain, V. Aravindan, S. Jayaraman, W.C. Ling, T.M. Lim, M.P. Srinivasan, Q. Yan, S. Madhavi, Bio-mass derived mesoporous carbon as superior electrode in all vanadium redox flow battery with multicouple reactions. *J. Power Sources* 274 (2015) 846–850.

44. Y. Shen, L. Yan, H. Song, J. Yang, G. Yang, X. Chen, J. Zhou, Z. Yu, S. Yang, A general strategy for the synthesis of carbon nanofibers from solid carbon materials. *Angew. Chem. Int. Ed.* 51 (2012) 12202–12205.
45. W. Li, J. Liu, C. Yan, Multi-walled carbon nanotubes used as an electrode reaction catalyst for VO^{2+}/VO_2^+ for a vanadium redox flow battery. *Carbon* 49 (2011) 3463–3470.
46. W. Li, J. Liu, C. Yan, The electrochemical catalytic activity of single-walled carbon nanotubes towards VO^{2+}/VO_2^+ and V^{3+}/V^{2+} redox pairs for an all-vanadium redox flow battery. *Electrochim. Acta* 79 (2012) 102–108.
47. P. Han, H. Wang, Z. Liu, X. Chen, W. Ma, J. Yao, Y. Zhu, G. Cui, Graphene oxide nanoplatelets as excellent electrochemical active materials for VO^{2+}/VO_2^+ and V^{2+}/V^{3+} redox couples for a vanadium redox flow battery. *Carbon* 49 (2011) 693–700.
48. Z. González, S. Vizireanu, G. Dinescu, C. Blanco, R. Santamaría, Carbon nanowalls thin films as nanostructured electrode materials in vanadium redox flow batteries. *Nano Energy* 1 (2012) 833–839.
49. M. Park, I. Jeon, J. Ryu, J. Baek, J. Cho, Exploration of the effective location of surface oxygen defects in graphene-based electrocatalysts for all-vanadium redox-flow batteries. *Adv. Energy Mater.* 5 (2015) 1401550.

CHAPTER 9

Recent Developments in Membranes for Flow Batteries

Md. Abdul Aziz, Mohanraj Vinothkannan,
and Sangaraju Shanmugam

9.1 INTRODUCTION

Membranes are one of the pivotal components in flow batteries (FBs) that contribute to the cost, performance, and lifetime of FBs [1]. During FB operation, the membrane physically separates the anode and cathode, functionally exchanging charge carriers and minimizing electrolyte cross-mixing. However, it has been analyzed that the membrane contributes approximately 20% of the entire battery cost [2]. It is thus important to prescreen the membrane materials, designs, and synthesis strategies to achieve a rational FB in terms of performance and cost. Up till now, various categories of membranes have been experimentally designed and tested in FBs. They are generally categorized as (1) proton-exchange membrane (PEM), (2) anion-exchange membrane (AEM), (3) amphoteric ion-exchange membrane (AIEM), and porous membrane. However, experimental studies can hardly give comparative investigation and cumulative understanding to identify a better membrane that provides the optimal balance between cost and performance. Considering the time and financial implications, addressing such characteristics by experimental studies may not be comprehensive enough. Several articles have been published to review the efforts to develop various categories of membranes for FB applications. However, few previously published reviews centered on overviewing a specific membrane type in FB. Li et al. [3] attempted to review the applications of various PEMs in FB. On the contrary, Maurya et al. [4] presented an overview devoted only to AEMs for FB. Even though few other reviews collected the efforts on all types of membranes, discussions on ion-transport phenomena, cost, performance evaluations, and progress on the commercialization of membranes were rarely included. Hence, a recent and timely overview of membranes for FB is necessary for knowledge and information updates. In this chapter, we describe the influential factors of membranes in FB applications from the viewpoint at cell level and membrane

DOI: 10.1201/9781003506379-9

levels. Also, summarize the current efforts regarding design and modification of different types of membranes. Finally, new directions in the future research of membranes for next-generation FB are highlighted.

9.2 INFLUENTIAL CHARACTERISTICS OF THE MEMBRANE AT FB LEVEL AND MEMBRANE LEVEL

Membranes, as discussed earlier, are one of the indispensable components of FB, which perform as a medium not only for the exchange of ions but also to preclude the cross-mixing of electrolyte solutions between two half-cells. Thus, creating a membrane that provides excellent performance at FB and membrane levels is paramount. The generally accepted influential characteristics of the membrane at FB and membrane levels are discussed in this section, as illustrated in Figure 9.1.

9.2.1 FB Level

9.2.1.1 Polarization Curve

A polarization curve measures voltage decay with respect to current density in an FB, illustrating the relationship between output voltage and applied current density. It also identifies three main losses: activation, ohmic, and mass transport. Due to the slow reaction kinetics of electrodes, activation loss occurs at low current densities. Ohmic loss, from resistance to electron and ion flow, arises at medium current densities. Mass transport loss, dominant at high current densities, results from inadequate reactant supply to electrodes. Efforts to reduce these losses include advanced electrode materials, minimized electrode distances, and higher electrolyte concentrations, with ion-conductive membranes offering partial mitigation by enhancing conductivity and reducing crossover. However, it is worth noting that the shape of the polarization curve may not give detailed information on FB. To quantify the polarization curve, FB is typically charged to a state of charge (SOC) of around 50%–100% [5]. Afterward, the curve can be obtained by recording voltage drop as a function of current density to demonstrate the relationship between these two parameters. Generally, while operating at 20–100 mA cm^{-2}, the FB equipped with a Nafion membrane

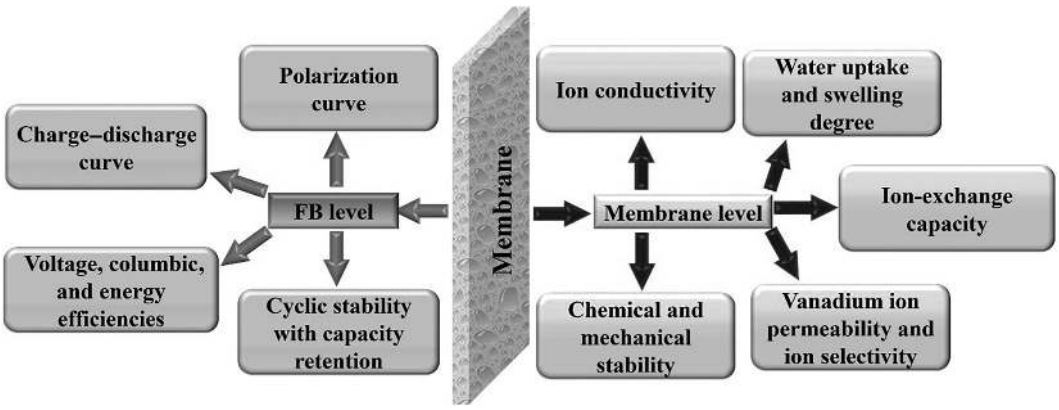

FIGURE 9.1 Schematic illustration of influential factors of membranes at FB and membrane levels.

can attain a voltage plateau of about 1.35–1.5 V during charging and a voltage plateau of around 1.35–1.1 V during discharging [6].

9.2.1.2 Charge–Discharge Curve

The charge–discharge curve is another critical indicator to evaluate the membrane activity at the FB level. The charge–discharge curve is quantified at a constant current density of FB to scrutinize the cell's power generation and energy storage capacity. In the charge–discharge curve, the discharge capacities and charge–discharge pattern of FB are actual results for evaluating performance. While the discharge capacity reveals the maximum quantity of electricity the FB can provide, the charge–discharge pattern indicates the charge and discharge voltages of FB. An ideal membrane is required to afford an FB with low charge voltage, high discharge voltage, and stable charge–discharge capacity. In an FB, the charge–discharge curve is generally quantified with a battery tester at a current density from 20 to 100 mA cm^{-2} with a voltage range of 0.7–1.7 V.

9.2.1.3 Voltage, Columbic, and Energy Efficiencies

Apart from the charge–discharge curve, the three essential factors such as voltage, columbic, and energy efficiencies, are frequently used to determine the performance of FB. The voltage efficiency (VE) refers to the losses in overpotential during the charging and discharging process of FB. In contrast, columbic efficiency (CE) is a performance indicator that estimates the ratio between discharge and charge capacity FB [7]. It is revealed that high VE can be attained when there is superior ion conductivity through the membrane, which further reduces the internal resistance of the overall cell. On the other hand, the CE is solely credited to the vanadium-ion permeability of the membrane and the capacity retention ability of the cell. Energy efficiency (EE), which is commonly obtained by multiplying the VE with CE, precisely demonstrates the overall performance of the FB system. These three efficiencies of FB can be calculated using the corresponding Equations (9.1 9.3) shown below.

$$\mathrm{VE}\,(\%) = \left[\frac{\text{Discharge voltage}}{\text{Charge voltage}}\right] \times 100 \tag{9.1}$$

$$\mathrm{CE}\,(\%) = \left[\frac{\text{Discharge capacity}}{\text{Charge capacity}}\right] \times 100 \tag{9.2}$$

$$\mathrm{EE}\,(\%) = \mathrm{VE} \times \mathrm{CE} \tag{9.3}$$

9.2.1.4 Cyclic stability with Capacity Retention

The cyclic stability with capacity retention of FB is a direct indicator of the durability of the membrane. Although the cyclic stability of FB does not solely rely on membrane

durability, the membrane still plays a crucial role in determining the cyclic stability of cells. The cyclic stability of FB is generally quantified using the same battery tester used for charging–discharging tests while mainly focusing on measuring the stability in cell performance after long-term operation [8]. This measurement is performed by repeatedly charging and discharging the FB to quantify its capacity retention ability, which is computed from the capacity difference between the first and last discharge cycles. A result with many cycles and high-capacity retention of FB indicates good long-term durability and high vanadium-ion resistivity of the membrane.

9.2.2 Membrane Level

While performance indicators of the membrane at the FB level (discussed in Section 9.2.1) provide a comprehensive understanding of the influence of the membrane on FB performance, it is also important to investigate the performance indicators at the membrane level. Generally, ion conductivity, water uptake capacity, swelling degree, ion-exchange capacity, vanadium-ion permeability, ion selectivity, and chemical stability are the essential performance indicators of the membrane at the membrane level [9].

9.2.2.1 Ion Conductivity

The ion-conductivity measurement, which demonstrates the charge-carrier ability of the membrane, is thus considered a paramount performance indicator of the membrane with low ion conductivity, causes high internal resistance, and reduces the FB performance, particularly at high discharge current density. By contrast, a membrane with high ion conductivity can facilitate the charge-carrier exchange between anode and cathode, resulting in high FB performance. There are two measurements generally used to measure the ion conductivity of a membrane: (1) in-pane and (2) through-plane [10]. In-plane ion conductivity of the membrane was quantified using a four-point Bekktech cell coupled with an electrochemical impedance analyzer and gas accessory. To measure conductivity, a sheet of membrane was placed across four platinum probes in the Bekktech cell, and then the cell was placed in thermo-controlled humid chamber. Specific voltage was applied through two electrodes (working and counter electrodes), and resistance of ion flow in the membrane was measured by the remaining two electrodes (sense and reference electrodes). The resistance (R) of the membrane can be varied based on the thickness (T) and width (W) of the membrane and the temperature and relative humidity of the cell. L is the distance between the electrodes. The following formula was exploited to calculate the in-plane conductivity ($\sigma\|$, Siemens per centimeter (S cm^{-1})) of the membrane.

$$\sigma \| \left(\text{mS cm}^{-1} \right) = \frac{L}{\text{RTW}} \tag{9.4}$$

To evaluate through-plane ion conductivity, a membrane specimen was sandwiched between two platinum electrodes. The resistance value is evaluated based on the frequency intercept of impedance with the real axis. The following formula was employed to calculate the through-plane conductivity ($\sigma \perp$, (S cm^{-1})) of the membrane [11].

$$\sigma \perp \left(\text{mS cm}^{-1}\right) = \frac{T}{AR} \tag{9.5}$$

where T represents the thickness of the membrane, A refers to the exposed area of the electrode to the membrane, and R indicates the resistance of the membrane. Many researchers widely use in-pane measurement among these two methods because through-plane conductivity is more challenging to quantify. Meanwhile, it is worth mentioning that several researchers performed the ion-conductivity measurement of the membrane in H_2SO_4 or $VOSO_4$ medium to realize the actual scenario of FB [12,13]. Considering real FB operating conditions, evaluating membrane ion conductivity under the $VOSO_4$ medium would provide important information relevant to membranes used in the FB system. Thus, to confirm the suitability of membranes to be used in FB, such membranes must exhibit reasonable ion conductivity under H_2SO_4 or $VOSO_4$ medium.

9.2.2.2 Water Uptake and Swelling Degree

The optimized water uptake capacity of the membrane is of significant importance to balance its dimensional stability and ion conductivity. Water molecules in the membrane help dissociate the ions from the fixed ion-exchange groups ($-SO_3H$, $-NH_2$, $-N+OH^-$), thereby facilitating ion conductivity. However, excessive water uptake could cause swelling and consequently decrease the dimensional stability of the membrane. Considering the environment of aqueous electrolytes in FB, water uptake and consequent swelling play an essential role in the activity of the membrane applied in FB. Hence, the water uptake and swelling degree measurements should be considered when evaluating the suitability of the membrane for FB. Typically, water uptake and swelling degree of membranes are determined by quantifying the changes in weight, area, and thickness of membranes before and after hydrated states. Following Equations (9.6) and (9.7) were exploited to compute the water uptake and swelling degree of membranes [14].

$$\text{Water uptake}\,(\%) = \left[\frac{\text{weight of wet membrane} - \text{weight of dry membrane}}{\text{weight of dry membrane}}\right] \times 100 \tag{9.6}$$

$$\text{Swelling degree}\,(\%) = \left[\frac{\text{Volume of wet membrane} - \text{volume of dry membrane}}{\text{volume of dry membrane}}\right] \times 100 \tag{9.7}$$

9.2.2.3 Ion-Exchange Capacity

Similar to water uptake properties, the ion-exchange capacity (IEC) of the membrane is another paramount factor to be high to obtain high FB performance. IEC is a direct indicator of the number of ionizable groups in the membrane. IEC of membrane is typically measured by the conventional titration method, as reported in literature [15,16]. In general, different aqueous solutions are being used to calculate the IEC of PEM and AEM. For IEC measurement of PEM, the mostly used aqueous solutions are NaOH and NaCl. In this

case, PEM was soaked in the desired concentration and volume of NaCl solution for 24 h to replace H^+ ions with Na^+ ions. Afterward, the obtained solution is titrated against the desired concentration of NaOH using phenolphthalein as an indicator. IEC of PEM was computed according to the following Equations.

$$\text{IEC}\left(\text{meq}\cdot\text{g}^{-1}\right)=\frac{\text{Volume of NaOH consumed}\times\text{Concentration of NaOH}}{\text{Weight of dry membrane sample}} \tag{9.8}$$

In contrast, $AgNO_3$ and $NaNO_3$ solutions are widely employed to quantify the IEC of AEM. In this method, AEM is first soaked into the desired volume and concentration of $NaNO_3$ solution for 48 h to completely discharge Cl^- ions from AEM. Afterward, the $AgNO_3$ solution is exploited to titrate the discharged Cl^- ions. IEC of AEM was computed using the Equation given below [17,18].

$$\text{IEC}\left(\text{meq}\cdot\text{g}^{-1}\right)=\frac{\text{Volume of AgNO}_3\text{ consumed}\times\text{Concentration of AgNO}_3}{\text{Weight of dry membrane sample}} \tag{9.9}$$

9.2.2.4 Vanadium-Ion Permeability and Ion Selectivity

Since the crossover of vanadium ions (V^{2+}, V^{3+}, V^{4+}, and V^{5+}) through the membrane is considered a key drawback, it may lead to several critical issues, such as membrane fouling, self-discharge, and low cyclic durability of FB [19]. During the operation of FB, the crossover of various species, including protons, water, and vanadium ions, through the membrane usually occurs. In the case of vanadium ions, the crossover of V^{2+} and V^{3+} occurs from the anode to the cathode, while the crossover of V^{4+} and V^{5+} occurs from the cathode to the anode [20]. Thus, measurement of vanadium-ion permeability through the membrane is usually conducted prior to applying the membrane in FB. Over the past years, many researchers performed vanadium-ion crossover measurements using the electrolyte comprising only V^{4+} ions, owing to the stability of V^{4+} ions in the open air. The V^{4+} ion permeability through membrane is typically evaluated using a two-compartment (A and B) diffusion cell. In the cell, A compartment is filled with 1 M $VOSO_4$ and 2 M H_2SO_4, while the B compartment is filled with 1 M $MgSO_4$ and 2 M H_2SO_4. The membrane was used to divide these two compartments physically. The solutions in both compartments were stirred continuously, and the aliquot sample was taken at regular intervals from the B compartment [21,22]. The concentration of crossover V^{4+} ion was determined using Ultraviolet-visible spectrometer. The following Equation was utilized to determine the rate of V^{4+} diffusion (P_0).

$$P_0=-\frac{V_B l}{2At}\ln\frac{A_0-0}{(A_0-B)-B}=-\frac{V_B l}{2At}\ln\frac{A_0}{A_0-2B}=-\frac{V_B l}{2At}\ln\frac{1}{1-2x_B} \tag{9.10}$$

where V_B refers to the volume of both cells, l refers to the thickness of the membrane, t denotes the reaction time, A_0 represents the initial absorbance of solution A, B indicates the absorbance of solution B, and $^{x}{}_{B}$ denotes the concentration of crossover of V^{4+} ions to B side normalized by the initial concentration compartment A.

Ion selectivity (S) was evaluated from the obtained values of proton conductivity (σ) and V^{4+} ion permeability (P_0) using the Equation (9.11) [23].

$$S = \frac{\sigma}{P_0} \tag{9.11}$$

9.2.2.5 Chemical and Mechanical Stability

Since the membrane used in FB is always in contact with a highly oxidizing electrolyte solution, it may lead to chemical degradation of the membrane and thereby limit the cyclical durability of FB [24]. Besides this, the membrane frequently experiences strong mechanical pressure because it is kept in the middle of the FB stack. Altogether, these deleterious factors cause tears, perforations, and cracks on the membrane surface, leading to failure in the cyclical durability of FB. Therefore, it is essential for membranes used in FB to possess high chemical and mechanical stabilities to maximize the long-term cyclical durability of FB [25,26]. Two methods commonly evaluate the chemical stability of membranes: one is the ex situ method, and another is the in situ method. In the first (ex situ) approach, a dry membrane sample was weighed and soaked in 0.1 M V^{5+} solution. During membrane oxidation, V^{5+} ions (yellow color) turn into V^{4+} ions (blue color). The concentration of V^{4+} ions in solution was quantified with Ultraviolet absorption spectroscopy and computed based on Beer-Lambert's law. The chemical stability of the membrane was estimated by V^{4+} ion concentration in solution with the following Equation (9.12) [27].

$$\text{Reduction rate}\,(\%) = \left[\frac{\text{Final concentration of } V^{4+}}{\text{Initial concentration of } V^{5+}}\right] \times 100 \tag{9.12}$$

Moreover, the chemical stability of the membrane can also be calculated from the weight difference in the membrane before and after immersing in 0.1 M V^{5+} solution as follows.

$$\text{Weight loss}\,(\%) = \left[\frac{W_b - W_a}{W_b}\right] \times 100 \tag{9.13}$$

where W_b and W_a are weights of the membrane before and after the chemical stability test, respectively.

In the second (in situ) approach, the membrane was tested under FB working conditions. The IEC, areal resistance, vanadium permeability, and cell performance are quantified periodically before and after charging–discharging cycles. Any changes in the aforementioned characteristics (caused by chemical degradation) help to evaluate the chemical stability of membranes.

To study the mechanical stability of the membrane, the universal testing machine (UTM) was generally exploited. The test has been usually conducted to measure both tensile strength and elongation at the break of membranes under dry and wet states. High tensile strength and elongation at break under dry and wet states demonstrate a membrane with good mechanical stability. For example, the widely exploited Nafion has been reported to have a tensile strength of 14–24 MPa and elongation of 170%–250% under dry

and wet states. Hence, this could be a standard for assessing the mechanical properties of other membranes used in FBs.

9.3 CLASSIFICATIONS OF MEMBRANES

As mentioned earlier, different membrane types have been used to benefit from FB in terms of performance, cost, and durability. Based on their functional groups, these membranes can be classified into PEM, AEM, AIEM, and porous membranes (Figure 9.2). The essential FB properties of each type of membrane are described in detail in the following sections.

9.3.1 Proton-Exchange Membranes

PEM is the most studied, developed, and extensively used membrane in FB. In PEM, the negatively charged species ($-COO^-$, $-SO_3^-$, $-PO_3^{2-}$, $-C_6H_4O^-$, and $-PO_3H^-$) are usually attached to the polymer skeleton and facilitate the proton transport (as shown in Figure 9.2a) through the membrane. Besides this, PEM allows the transfer of water as well as vanadium ions (in the case of vanadium redox FB) from anode to cathode during battery cycling, owing to the higher diffusion rate of V^{2+}, V^{3+}, and water compared to V^{4+} and V^{5+} ions. As a result, V^{2+} and V^{3+} ions in the negative electrolyte are poorly utilized, resulting in rapid capacity decay and high overpotential during charging–discharging of FB. Numerous efforts have been made to improve the ion conductivity and reduce electrolyte diffusivity across the PEM. The following section covers preparation strategies adopted,

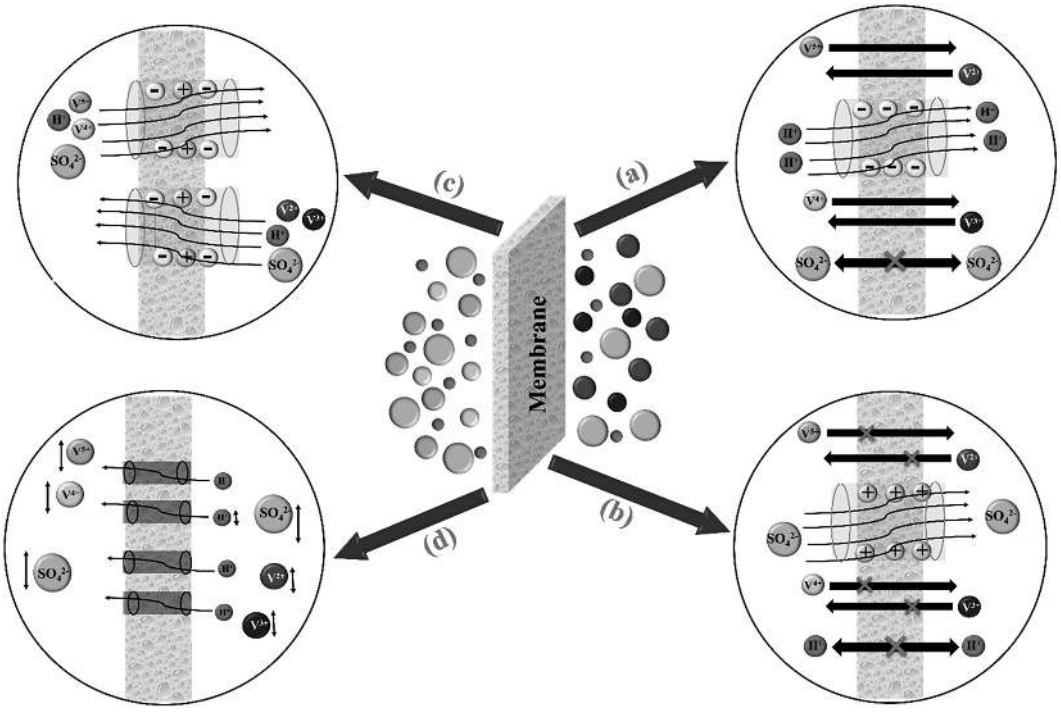

FIGURE 9.2 Schematic illustration of ion transport through (a) PEM, (b) AEM, (c) AIEM, and (d) porous membrane.

and significant insights achieved on corresponding efforts. Reed et al. [28] assembled 1 kW FB with various Nafion membranes and investigated its performance at different current densities. They reported that thin Nafion-212 and Nafion-211 membranes would be a great choice compared to thick Nafion-115 membranes when considering the performance and cost of FB. On the contrary, Jiang et al. [29] reported that as the thickness of the membrane increases, the permeability of vanadium ions decreases, but the areal resistance of the membrane increases. Hence, the obtained CE and EE of FB are inversely proportional to each other. On the other side, the significance of blending polymers or inorganic filler is to suppress the vanadium-ion permeability of the Nafion membrane by generating tortuous pathways across the membrane. Such Nafion composite membrane exhibited relatively lower vanadium crossover and excellent CE in FB than the bare Nafion membrane. Aziz et al. introduced a porous ZrO_2 nanotube (ZrNT) into Nafion to fabricate a composite membrane for FB [20]. The –OH in ZrNT increases the composite membrane's water absorption and proton conductivity, whereas the tubular structure of ZrNT partly blocks the $–SO_3H$ groups in Nafion and serves as a barrier for vanadium diffusion. Consequently, Nafion/ZrNT showed high durability, capacity retention, CE, VE, and EE during FB operation, which was a few times better than the Nafion-117 membrane.

Even though Nafion and its hybrid membranes can provide reasonable FB performance, their price has dramatically hindered the commercial adoption of FB. To reduce the cost of PEM without losing chemical stability, various hydrocarbon membranes, such as sulfonated poly (ether ether ketone) (SPEEK), sulfonated poly (arylene ether ketone) (SPAEK), sulfonated poly (phenylene sulfide sulfone) (SPSS), polybenzimidazole (PBI), sulfonated poly (imide), sulfonated poly (ether sulfone), and sulfonated poly (arylene thioether), have been established and studied for FB applications. Yu et al. [30] fabricated a polydopamine coated carbon nanotube (CNT@PDA)/SPEEK membrane and used it as the membrane in FB. The mechanical strength, proton conductivity, and vanadium barrier property of CNT@PDA/SPEEK were improved via acid–base interaction between $–NH_2$ of CNT@PDA and $–SO_3H$ groups of SPEEK. Consequently, the FB assembled with CNT@PDA/SPEEK membrane exhibited the VE and EE of 85.1% and 83.6%, respectively, which were higher than that of FB equipped with Nafion-115 membrane (VE: 82.5% and EE: 77.4%). Phosphotungstic acid coupled graphene oxide (PWA-mGO) was integrated with SPAEK to reduce vanadium diffusion as well as boost the ion conductivity of SPAEK (Figure 9.3a) [31]. As shown in surface morphology (Figure 9.3b), the pores of the SPAEK surface were effectively blocked by PWA-mGO, so the SPAEK/PW-mGO membrane showed a high proton conductivity (71 mS cm^{-1}), low vanadium permeability (0.28×10^{-7} $cm^2 min^{-1}$), and outstanding ion selectivity of 2.5×10^6 S min cm^{-3} (Figure 9.3c). Branchi et al. [32] synthesized the SPSS membrane using thioether-containing ionomers to enhance the stability of the SPSS membrane during FB application. SPSS membrane showed excellent proton conductivity and vanadium-ion permeability, leading to an outstanding ion selectivity compared to SPEEK and Nafion-115 membranes. They reported that the SPSS membrane contains less freezable water than the nonfreezable one; hence, the lower the vanadium-ion crossover could be achieved. Furthermore, the SPSS membrane revealed no significant change even after 30 days in VO_2^+ solution, indicating higher dimensional and oxidative stability

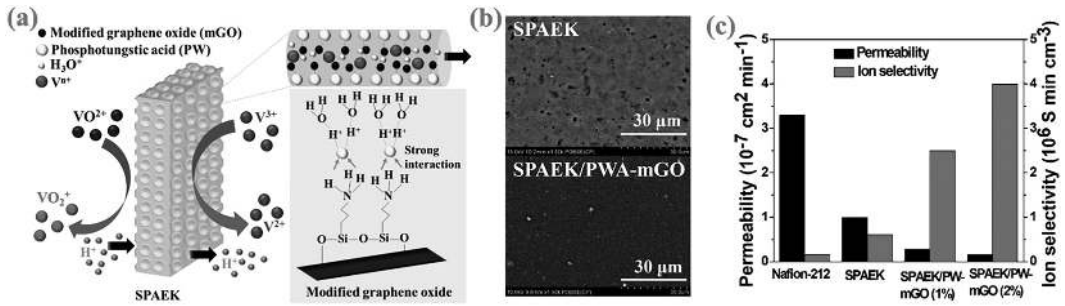

FIGURE 9.3 (a) Schematic illustration of proton diffusion and vanadium-ion barrier across SPAEK/PWA-mGO membrane, (b) FE-SEM images of bare SPAEK and composite membrane, and (c) vanadium-ion permeability and ion selectivity of membranes. (Adapted with permission from reference [31]. Copyright the Authors, some rights reserved; exclusive licensee [Royal Society of Chemistry]. Distributed under a Creative Commons Attribution-Non Commercial 3.0 Unported License.)

of the SPSS membrane relative to the bare SPEEK membrane. The FB polarization curve was also quantified at 100% SOC. Compared to Nafion and SPEEK membranes, the SPSS exhibited higher power output.

9.3.2 Anion-Exchange Membranes

AEM is another type of membrane that gained considerable attention for FB applications because of its high ion selectivity. Unlike PEMs, AEMs are made up of fixed cationic groups ($–NR_2H^+$, $–NR^{3+}$, SR^{2+}, and $–NH^{3+}$) on the polymer skeletons to selectively restrict the vanadium ions via the Donnan exclusion effect (as displayed in Figure 9.2b), which in turn leads to high CE of FB. As a result, AEMs have been widely studied as potential alternatives to state-of-the-art Nafion and other PEMs. However, poor ion conductivity and chemical stability are the major concerns associated with AEMs. Many research efforts have been devoted to the development of potential AEMs for FB through the fabrication and investigations of various materials, including poly (phenylene), poly (fluorenyl ether), quaternized poly (phthalazinone ether ketone), poly (arylene ether sulfone), polysulfone, etc. The selective AEMs with prominent FB performance were discussed in detail as follows.

Ren et al. [33] synthesized a blend membrane composed of quaternized polysulfone (QAPSF) and polyvinylidene fluoride (PVDF), wherein the mechanical strength of blend membranes increased with increasing the mass ratio of PVDF. The fabricated QAPSF/PVDF (20%) membranes showed reasonable water uptake, swelling degree, IEC, and lower vanadium-ion permeability. Furthermore, the membrane exhibited an impressive EE of 91.12% at 40 mA cm^{-2} and an outstanding CE of 99.29% at 80 mA cm^{-2}, which are 3.33% and 4.89% higher than the Nafion-115 membrane at identical current density, respectively. Wang et al. [34] demonstrate a new type of poly(terphenylene) membranes with superior anion conductivity as well as chemical stability in FB. While the polymer backbone and cation-tethered alkyl chains varied, the prepared membranes demonstrated an extremely lower vanadium-ion permeability and high conductivity. The FB with poly

(terphenylene) AEM showed higher CE and EE values at the current density of 20 mA cm^{-2}, which are 2% and 5% higher when compared to Nafion-212 under the same current density. Shukla et al. [35] coupled the quaternized GO with poly(ether sulfone) (PS-DTQG) using 1,4-diazabicyclo[2,2,2]octane (DABCO) (Figure 9.4a), which provides high proton conductivity as well as good stabilities under acidic/oxidative environment owing to the bulky nature of quaternized GO. The PS-DTQG membrane showed 32.46% water uptake, 2.14 meq g^{-1} IEC, 6.06×10^{-2} S cm^{-1} ionic conductivity, and 18.93×10^{5} S min cm^{-3} selectivity. The FB assembled with PS-DTQG-5 AEM displayed outstanding efficiencies (CE: 98.06%, EE: 76.4%, and VE: 78.0%) at 60 mA cm^{-2}, which are better than those of the Nafion-117 membrane (Figure 9.4b).

9.3.3 Amphoteric Ion-Exchange Membranes

So far, various materials and fabrication strategies have been developed to enhance the utilization of PEMs and AEMs in FB. However, some inevitable drawbacks of those membranes have also been pointed out. For example, PEMs usually suffer from high vanadium permeability, whereas the AEM is associated with low ion conductivity. Hence, to attain a membrane that combines the beneficial properties (i.e., high ion conductivity and restricted vanadium permeability) of both PEM and AEM, the concept of grafting both anionic and cationic functional groups onto the polymer skeleton has been suggested and named AIEM (Figure 9.2c). Various materials, such as modified Nafion, PVDF, and polyether, were explored as AIEM for FB. Some of these materials were discussed in detail in the following sections.

The Nafion membrane generally has high chemical stability and ion conductivity, but it is hard to introduce the zwitterionic groups into the Nafion matrix to prepare AIEM.

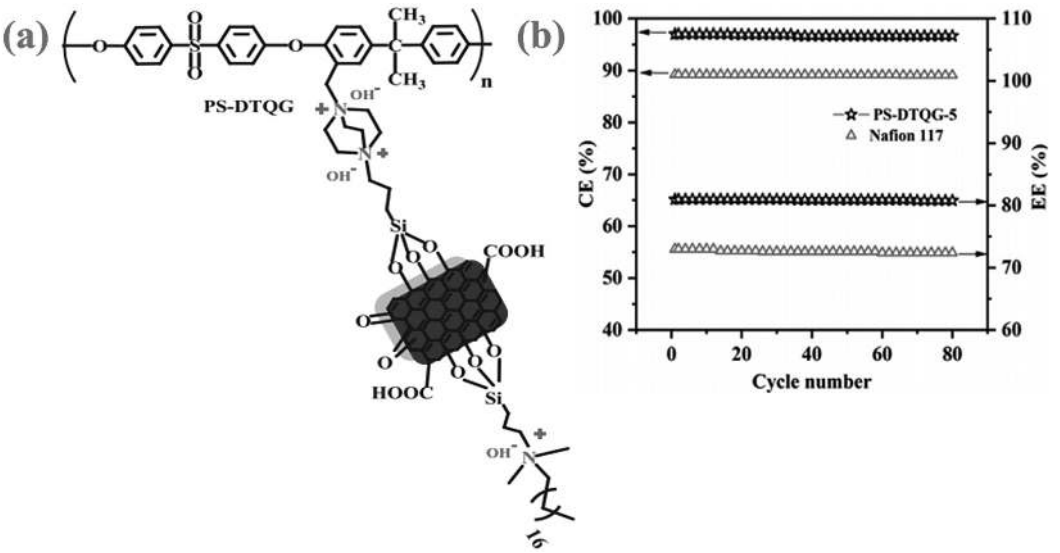

FIGURE 9.4 (a) Chemical structure and (b) FB efficiencies of PS-DTQG/quaternized GO membrane at 60 mA cm^{-2}. (Adapted with permission from reference [35]. Copyright © 2019 Elsevier B.V.)

However, Dai et al. [36] successfully grafted the zwitterion ($-NR_3^+$ and $-SO_3^-$) in Nafion-115 (Nafion-115-g-PSBMA) via surface-initiated atom transfer radical polymerization (Figure 9.5a). While compared to bare Nafion-115, whose surface is smooth and even, the Nafion-115-g-PSBMA showed white particles on its surface. The $-NR_3^+$ and $-SO_3^-$ groups in Nafion-115-g-PSBMA allowed both anion and cations through the membrane and afforded comparable ion conductivity with Nafion-115. Nevertheless, the VO^{2+} permeability of the Nafion-115-g-PSBMA membrane is less than half of the Nafion-115 membrane. Subsequently, the Nafion-115-g-PSBMA membrane delivered a high discharge capacity compared to the Nafion-115 membrane. Moreover, the Nafion-115-g-PSBMA membrane exhibited CE above 96.2% with no decay after 100 charge–discharge cycles (Figure 9.5b). PVDF has been grafted with styrene and dimethyl aminoethyl methacrylate (DMAEMA) via a γ-irradiation process by Hu et al. [37]. A new kind of AIEM was synthesized through subsequent sulfonation and protonation processes. It was found that FB with this AIEM maintained an open-circuit voltage (OCV) of 1.2 V after 68 h, which was much longer compared to that of the Nafion-1117 membrane. Yan et al. [38] fabricated the AIEM by blending SPEEK with imidazolium-functionalized polysulfone (ImPSf) via the solution casting method and utilized it in FB. The SPEEK/ImPSf membrane demonstrated high performance even at high current density (i.e., 200 mA cm^{-2}) and attained a CE of 97.5% and EE of 77.3%, both of which are higher than those of Nafion-212 (CE: 92.4% and EE: 73.4%). Similarly, Liu et al. [39] prepared the AIEM by blending SPEEK with quaternized poly(ether imide) (QAPEI) by a solution casting approach. In the FB test, the SPEEK/QAPEI membrane improved CE and EE with bare SPEEK and Nafion-115 membranes. Furthermore, the SPEEK/QAPEI membrane had a stable performance up to 100 cycles without significant decay in EE.

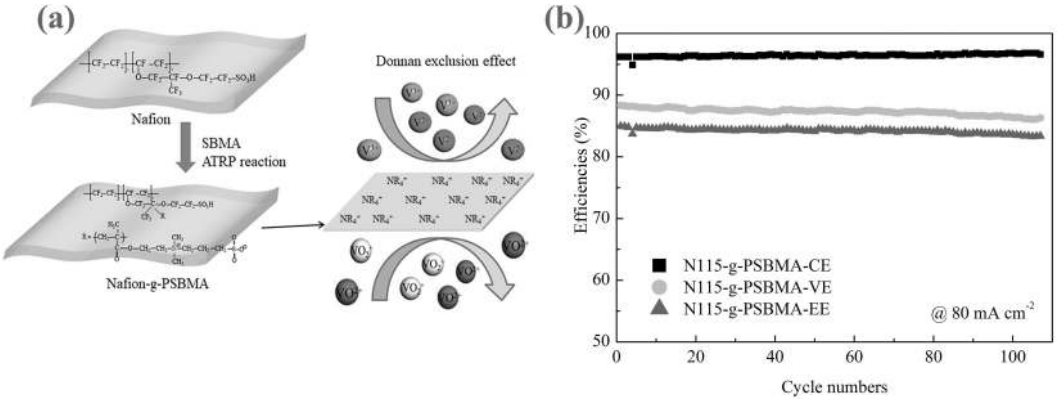

FIGURE 9.5 (a) Schematic representation of preparation and ion-conduction mechanism through Nafion-115-g-PSBMA membrane and (b) FB efficiencies of Nafion-115-g-PSBMA membrane at 80 mA cm^{-2}. (Adapted with permission from reference [36]. Copyright © 2018 Elsevier B.V.)

9.3.4 Porous Membranes

Although PEM, AEM, and AIEM have been proposed and developed for FB applications, their high cost and complex synthetic protocols still hamper their extensive usage in FB. The porous membranes, inspired by the idea of distinguishing protons and other ions via the size exclusion effect, have received great attention and investigation. An ideal porous membrane needs well-defined ion-conducting channels that promote a quick exchange of protons while hampering the exchange of other ions, thereby delivering high FB efficiencies. The general working principle of the porous membrane, when exploited in FB, is displayed in Figure 9.2d. Apart from conventional membranes, porous membranes have high chemical stability because of the absence of ion-conducting groups. Researchers have used several materials, including porous glass, PVDF, PBI, PES, polyacrylonitrile, etc., to prepare porous membranes. However, the charged porous membranes have mostly received significant attention when considering noncharged porous membranes, owing to their outstanding combination of ion conductivity and selectivity. Nevertheless, their stability is relatively insufficient to maintain the durability of FB. Therefore, introducing internal crosslinking frameworks on sponge-like would be a great choice to improve membrane stability. Zhao et al. [40] synthesized a charged porous membrane of chloromethylated polysulfone (CMPSF)-butane by crosslinking, where the crosslinking segments are susceptible to developing hydrophilic-hydrophobic phase separation. Combining with excellent morphological properties, the CMPSF-butane membrane showed a superior FB cyclic performance of CE (99%) and EE (87.1%) at 80 mA cm^{-2} current density. Furthermore, a remarkable durability of 4000 FB charge–discharge cycles without notable performance decay, indicating a great potential of CMPSF-butane membrane for FB application. Zhao et al. [41] also synthesized a porous membrane containing partial pendant hydrophilic trimethylamine (TMA) groups with flexible crosslinking networks, where the hydronium ions or proton can easily migrate through the pores (Figure 9.6a). Cross-sectional FE-SEM

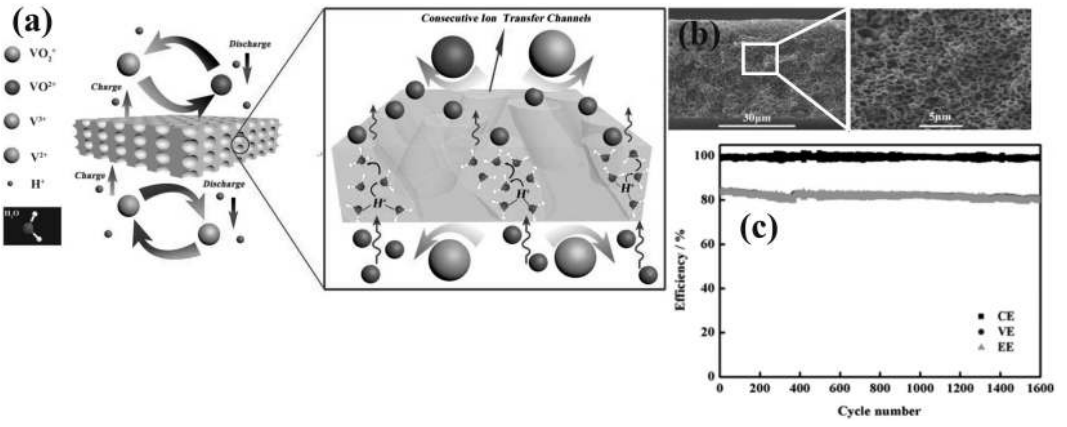

FIGURE 9.6 (a) Schematic of proton conductivity and vanadium barrier property through porous membrane, (b) FE-SEM images of porous membranes, and (c) FB efficiencies of porous membranes over 1,500 cycles at 160 mA cm^{-2}. (Adapted with permission from reference [41]. Copyright © 2018 Elsevier B.V.)

images of porous membranes indicate that an interconnected porous network across the membrane (Figure 9.6b). Owing to the high ion selectivity and superior stability, the FB equipped with a porous membrane showed a stable CE (<99%) and VE (<80%) of over 1500 charge–discharge cycles even at a higher current density of 160 mA cm^{-2} (Figure 9.6c). Zhou et al. [42] prepared a porous SPES (PSPES) membrane with ultrahigh ion selectivity via ionic-liquid (IL) induced phase separation. The PSPES showed excellent single-cell performance when applied in FB. The CE and EE of the cell with PSPES (IL-30) membrane reached 98.75% and 84.13%, respectively, at 100 mA cm^{-2}. It is comparable with Nafion-212. Moreover, the estimated capital cost of the PSPES (IL-30) membrane would be lower than that of Nafion-212.

9.4 CONCLUSION AND FUTURE PERSPECTIVES

FB holds immense potential to revolutionize renewable energy storage by mitigating the intermittency of solar and wind energy. At the heart of this technology lies the membrane—a critical component dictating overall performance. While significant progress has been made in developing and modifying membranes, challenges persist in balancing cost, stability, and scalability for industrial deployment.

Future advancements must address key properties such as ion conductivity, vanadiumion resistance, and chemical and mechanical stability. Alternatives to Nafion, including fluorinated and hydrocarbon-based PEMs, have shown promise but require further refinement to overcome limitations like chemical degradation and low proton conductivity. Similarly, innovative approaches are needed to optimize alternative membranes like AEMs, AIEMs, and porous membranes, which face synthesis complexity and ion-transport challenges.

Innovative strategies such as filler incorporation, chemical crosslinking, and pore-size tuning are essential to advance membrane technology. These efforts will pave the way for cost-effective, high-performance, and durable membranes that meet the stringent demands of real-world applications. The ongoing research and collaborative efforts in this domain promise to unlock the full potential of FB technology, positioning it as a cornerstone of sustainable energy systems and a key enabler in the global transition to a renewable energy future.

REFERENCES

1. J. Ran, L. Wu, Y. He, Z. Yang, Y. Wang, C. Jiang, L. Ge, E. Bakangura, T. Xu, Ion exchange membranes: New developments and applications, *Journal of Membrane Science*, 522 (2017) 267–291.
2. Y.K. Zeng, T.S. Zhao, L. An, X.L. Zhou, L. Wei, A comparative study of all-vanadium and iron-chromium redox flow batteries for large-scale energy storage, *Journal of Power Sources*, 300 (2015) 438–443.
3. X. Li, H. Zhang, Z. Mai, H. Zhang, I. Vankelecom, Ion exchange membranes for vanadium redox flow battery (VRB) applications, *Energy & Environmental Science*, 4 (2011) 1147–1160.
4. S. Maurya, S.-H. Shin, Y. Kim, S.-H. Moon, A review on recent developments of anion exchange membranes for fuel cells and redox flow batteries, *RSC Advances*, 5 (2015) 37206–37230.

5. H.R. Jiang, W. Shyy, M.C. Wu, L. Wei, T.S. Zhao, Highly active, bi-functional and metal-free B4C-nanoparticle-modified graphite felt electrodes for vanadium redox flow batteries, *Journal of Power Sources*, 365 (2017) 34–42.
6. A.B. Shah, X. Zhou, P. Brezovec, D. Markiewicz, Y.L. Joo, Conductive membrane coatings for high-rate vanadium redox flow batteries, *ACS Omega*, 3 (2018) 1856–1863.
7. M. Skyllas-Kazacos, C. Menictas, T. Lim, 12-Redox flow batteries for medium- to large-scale energy storage, in: Z. Melhem (Ed.) *Electricity Transmission, Distribution and Storage Systems*, Woodhead Publishing, 2013, pp. 398–441.
8. P.C. Ghimire, A. Bhattarai, T.M. Lim, N. Wai, M. Skyllas-Kazacos, Q. Yan, In-situ tools used in vanadium redox flow battery research—Review, *Batteries*, 7 (2021) 53.
9. T.Y. Son, K.S. Im, H.N. Jung, S.Y. Nam, Blended anion exchange membranes for vanadium redox flow batteries, *Polymers*, 13 (2021) 2827.
10. S. Ryu, J.-H. Kim, J.-Y. Lee, S.-H. Moon, Investigation of the effects of electric fields on the nanostructure of Nafion and its proton conductivity, *Journal of Materials Chemistry A*, 6 (2018) 20836–20843.
11. J.-H. Fang, Chapter 7-Polyimide proton exchange membranes, in: S.-Y. Yang (Ed.) *Advanced Polyimide Materials*, Elsevier, 2018, pp. 323–383.
12. R.B. Moore, C.R. Martin, Chemical and morphological properties of solution-cast perfluorosulfonate ionomers, *Macromolecules*, 21 (1988) 1334–1339.
13. J. Saqib, I.H. Aljundi, Membrane fouling and modification using surface treatment and layer-by-layer assembly of polyelectrolytes: State-of-the-art review, *Journal of Water Process Engineering*, 11 (2016) 68–87.
14. L. Cao, L. Kong, L. Kong, X. Zhang, H. Shi, Novel sulfonated polyimide/zwitterionic polymer-functionalized graphene oxide hybrid membranes for vanadium redox flow battery, *Journal of Power Sources*, 299 (2015) 255–264.
15. S.C. Chieng, M. Kazacos, M. Skyllas-Kazacos, Preparation and evaluation of composite membrane for vanadium redox battery applications, *Journal of Power Sources*, 39 (1992) 11–19.
16. S.S. He, C.W. Frank, Facilitating hydroxide transport in anion exchange membranes via hydrophilic grafts, *Journal of Materials Chemistry A*, 2 (2014) 16489–16497.
17. S. Maurya, S.-H. Shin, K.-W. Sung, S.-H. Moon, Anion exchange membrane prepared from simultaneous polymerization and quaternization of 4-vinyl pyridine for non-aqueous vanadium redox flow battery applications, *Journal of Power Sources*, 255 (2014) 325–334.
18. S. Zhang, C. Yin, D. Xing, D. Yang, X. Jian, Preparation of chloromethylated/quaternized poly(phthalazinone ether ketone) anion exchange membrane materials for vanadium redox flow battery applications, *Journal of Membrane Science*, 363 (2010) 243–249.
19. J. Xi, Z. Wu, X. Teng, Y. Zhao, L. Chen, X. Qiu, Self-assembled polyelectrolyte multilayer modified Nafion membrane with suppressed vanadium ion crossover for vanadium redox flow batteries, *Journal of Materials Chemistry*, 18 (2008) 1232–1238.
20. M.A. Aziz, S. Shanmugam, Zirconium oxide nanotube–Nafion composite as high performance membrane for all vanadium redox flow battery, *Journal of Power Sources*, 337 (2017) 36–44.
21. T. Mohammadi, M. Skyllas-Kazacos, Characterisation of novel composite membrane for redox flow battery applications, *Journal of Membrane Science*, 98 (1995) 77–87.
22. J. Ye, X. Lou, C. Wu, S. Wu, M. Ding, L. Sun, C. Jia, Ion selectivity and stability enhancement of SPEEK/lignin membrane for vanadium redox flow battery: The degree of sulfonation effect, *Frontiers in Chemistry*, 6 (2018) 549.
23. Y. Lei, B.W. Zhang, Z.H. Zhang, B.F. Bai, T.S. Zhao, An improved model of ion selective adsorption in membrane and its application in vanadium redox flow batteries, *Applied Energy*, 215 (2018) 591–601.
24. Y. Park, D. Kim, Chemical stability enhancement of Nafion membrane by impregnation of a novel organic ·OH radical scavenger, 3,4-dihydroxy-cinnamic acid, *Journal of Membrane Science*, 566 (2018) 1–7.

25. T. Mohammadi, M.S. Kazacos, Evaluation of the chemical stability of some membranes in vanadium solution, *Journal of Applied Electrochemistry*, 27 (1997) 153–160.
26. S. Kim, T.B. Tighe, B. Schwenzer, J. Yan, J. Zhang, J. Liu, Z. Yang, M.A. Hickner, Chemical and mechanical degradation of sulfonated poly(sulfone) membranes in vanadium redox flow batteries, *Journal of Applied Electrochemistry*, 41 (2011) 1201–1213.
27. E. Wiedemann, A. Heintz, R.N. Lichtenthaler, Transport properties of vanadium ions in cation exchange membranes: Determination of diffusion coefficients using a dialysis cell, *Journal of Membrane Science*, 141 (1998) 215–221.
28. D. Reed, E. Thomsen, W. Wang, Z. Nie, B. Li, X. Wei, B. Koeppel, V. Sprenkle, Performance of Nafion® N115, Nafion® NR-212, and Nafion® NR-211 in a 1 kW class all vanadium mixed acid redox flow battery, *Journal of Power Sources*, 285 (2015) 425–430.
29. B. Jiang, L. Wu, L. Yu, X. Qiu, J. Xi, A comparative study of Nafion series membranes for vanadium redox flow batteries, *Journal of Membrane Science*, 510 (2016) 18–26.
30. L. Yu, F. Lin, W. Xiao, D. Luo, J. Xi, CNT@polydopamine embedded mixed matrix membranes for high-rate and long-life vanadium flow batteries, *Journal of Membrane Science*, 549 (2018) 411–419.
31. M.A. Aziz, K. Oh, S. Shanmugam, A sulfonated poly(arylene ether ketone)/polyoxometalate–graphene oxide composite: A highly ion selective membrane for all vanadium redox flow batteries, *Chemical Communications*, 53 (2017) 917–920.
32. M. Branchi, M. Gigli, B. Mecheri, D. De Porcellinis, S. Licoccia, A. D'Epifanio, Poly(phenylene sulfide sulfone) based membranes with improved stability for vanadium redox flow batteries, *Journal of Materials Chemistry A*, 5 (2017) 18845–18853.
33. J. Ren, Y. Dong, J. Dai, H. Hu, Y. Zhu, X. Teng, A novel chloromethylated/quaternized poly(sulfone)/poly(vinylidene fluoride) anion exchange membrane with ultra-low vanadium permeability for all vanadium redox flow battery, *Journal of Membrane Science*, 544 (2017) 186–194.
34. T. Wang, J.Y. Jeon, J. Han, J.H. Kim, C. Bae, S. Kim, Poly(terphenylene) anion exchange membranes with high conductivity and low vanadium permeability for vanadium redox flow batteries (VRFBs), *Journal of Membrane Science*, 598 (2020) 117665.
35. G. Shukla, V.K. Shahi, Amine functionalized graphene oxide containing C16 chain grafted with poly(ether sulfone) by DABCO coupling: Anion exchange membrane for vanadium redox flow battery, *Journal of Membrane Science*, 575 (2019) 109–117.
36. J. Dai, Y. Dong, C. Yu, Y. Liu, X. Teng, A novel Nafion-g-PSBMA membrane prepared by grafting zwitterionic SBMA onto Nafion via SI-ATRP for vanadium redox flow battery application, *Journal of Membrane Science*, 554 (2018) 324–330.
37. G. Hu, Y. Wang, J. Ma, J. Qiu, J. Peng, J. Li, M. Zhai, A novel amphoteric ion exchange membrane synthesized by radiation-induced grafting α-methylstyrene and N,N-dimethylaminoethyl methacrylate for vanadium redox flow battery application, *Journal of Membrane Science*, 407–408 (2012) 184–192.
38. X. Yan, C. Zhang, Y. Dai, W. Zheng, X. Ruan, G. He, A novel imidazolium-based amphoteric membrane for high-performance vanadium redox flow battery, *Journal of Membrane Science*, 544 (2017) 98–107.
39. S. Liu, L. Wang, D. Li, B. Liu, J. Wang, Y. Song, Novel amphoteric ion exchange membranes by blending sulfonated poly(ether ether ketone)/quaternized poly(ether imide) for vanadium redox flow battery applications, *Journal of Materials Chemistry A*, 3 (2015) 17590–17597.
40. Z. Yuyue, W. Lu, Z. Yuan, L. Qiao, X. Li, H. Zhang, Advanced charged porous membranes with flexible internal crosslinking structures for vanadium flow batteries, *Journal of Materials Chemistry A*, 5 (2017) 6193–6199.
41. Y. Zhao, H. Zhang, C. Xiao, L. Qiao, Q. Fu, X. Li, Highly selective charged porous membranes with improved ion conductivity, *Nano Energy*, 48 (2018) 353–360.
42. X. Zhou, R. Xue, Y. Zhong, Y. Zhang, F. Jiang, Asymmetric porous membranes with ultra-high ion selectivity for vanadium redox flow batteries, *Journal of Membrane Science*, 595 (2020) 117614.

CHAPTER 10

Microfluidic Flow Batteries

Yifei Wang, Mingming Zhang, Michael K. H. Leung, and Dennis Y. C. Leung

10.1 INTRODUCTION

The widespread implementation of renewable energy instead of traditional fossil energy is the major trend of energy transition in the 21st century, such as solar, wind and geothermal energy. Consequently, large-scale energy storage is indispensable for these renewable energies due to their intermittency, among which electrochemical energy storage is well known for its high energy efficiency and modular capacity. For instance, secondary batteries can achieve round-trip efficiency as high as 90%, whose storage capacity can also be flexibly adjusted by modular scaling up. However, since the active material is stored in solid-state electrodes of conventional batteries, the power density is inevitably increased along with the storage capacity, which brings extra cost. Alternatively, if the active material is stored in the flowing electrolyte, namely the redox flow battery (RFB), the improvement of storage capacity can be achieved by scaling up the electrolyte storage tank, which is a much more cost-efficient choice [1].

Despite the appealing feature of "power density–storage capacity" independence, current RFBs still encounter several technical and economic problems. Among them, the membrane separator is highly associated with the high capital cost as well as poor cycling lifetime. The ion-selective membrane accounts for 20%–40% of the total cost in a flow battery system [2], while the membrane fouling problem during flow battery operation significantly affects the battery lifetime [3]. To tackle these membrane-related issues, membraneless RFBs have been proposed in recent years, which can be classified into two main types as shown in Figure 10.1, including the microfluidic RFB (μRFB) and the immiscible RFB. The μRFB utilizes a microchannel for electrolyte delivery, leading to laminar flows with low Reynolds number (Figure 10.1a). In this manner, the anolyte and catholyte will not mix convectively, while only an ultrathin mixing layer exists at the flow interface due to slow diffusion. On the other hand, the immiscible RFB utilizes two electrolytes that will naturally stratify, so that the dissolved active species in each electrolyte will not mix with each other (Figure 10.1b). Owing to space constraints, this chapter will focus on

DOI: 10.1201/9781003506379-10

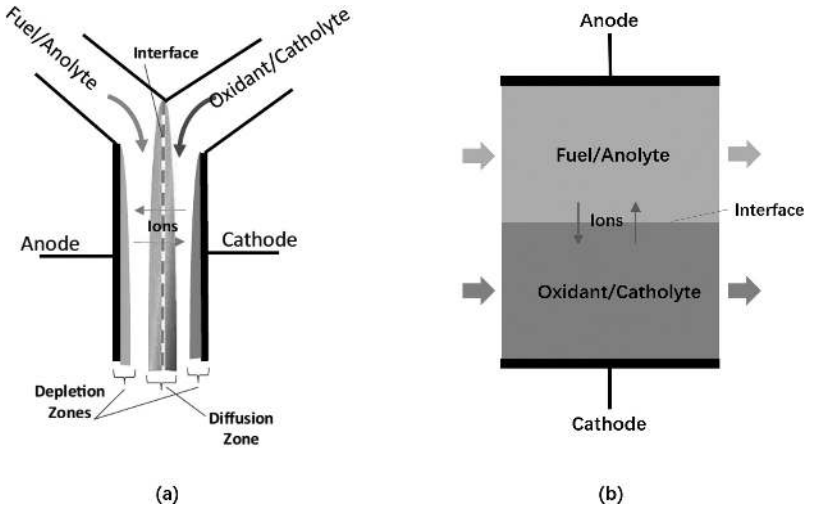

FIGURE 10.1 Schematic diagram of two types of membraneless RFB: (a) The microfluidic RFB. (Adapted with permission from [2], Copyright 2017, Elsevier) and (b) the immiscible RFB.

the introduction of μRFB only, including the mainstream all-vanadium μRFB and other μRFBs with different redox species. As for the immiscible RFB, readers may refer to a recent review paper authored by Li et al. [4]

10.2 ALL-VANADIUM μRFB

The first μRFB prototype proposed by Ferrigno et al. [5] in 2002 was based on all vanadium species. In their work, a Y-shaped microchannel was adopted for delivering the V^{2+} anolyte and V^{5+} catholyte with H_2SO_4 as supporting electrolyte, and graphite was utilized as both electrodes. A peak power density of 38 mW cm^{-2} was achieved at a flow rate of 1,500 μL min^{-1}, but the fuel utilization was only 0.1% due to the high flow rate. Afterward, tremendous works have been conducted on all-vanadium μRFBs.

10.2.1 Experimental Studies

The graphite electrode in the work of Ferrigno et al. [5] had a 2D reaction surface. To improve this, Kjeang et al. [6] employed porous carbon paper as electrodes, which had a much higher surface area due to its 78% porosity. With a flow rate of 1,000 μL min^{-1}, an improved power density of 70 mW cm^{-2} was reported, but the fuel utilization at this high flow rate was also quite low. When a much smaller flow rate of 1 μL min^{-1} was adopted, the fuel utilization could be improved to 55%, but the peak power density was sacrificed. This trade-off between power density and fuel utilization is a well-known dilemma in all microfluidic-based cells. In addition to the carbon paper electrode, Kjeang et al. [7] also developed a μRFB with multiple graphite rods as electrode, which were placed uniformly as an array inside the anolyte and catholyte. Due to the 2D reaction surface, the power density of 35 mW cm^{-2} was not very outstanding, but the fuel utilization was improved to 78% at 30 μL min^{-1}, which was mainly attributed to the sufficient contact between electrode and

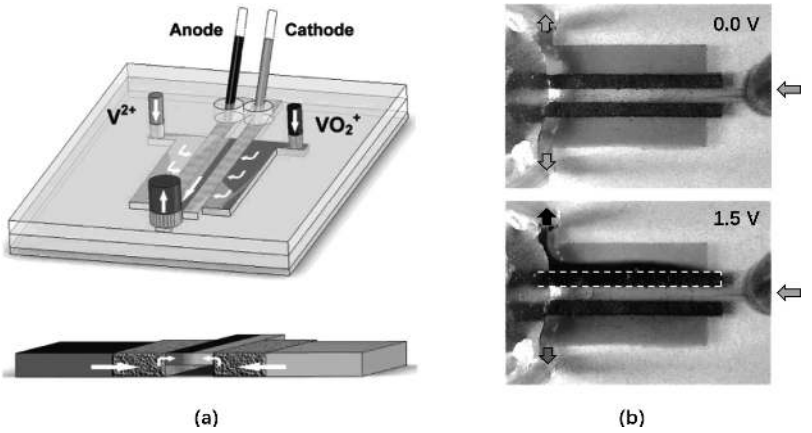

FIGURE 10.2 The milestone all-vanadium μRFB with flow-through electrodes and orthogonal electrolyte flow: (a) Cell structure and (b) battery recharge demonstration. (Adapted with permission from [8], Copyright 2008, ACS.)

electrolyte throughout the whole microchannel. Furthermore, they have proposed a milestone cell architecture with flow-through electrodes and orthogonal electrolyte flow [8]. As shown in Figure 10.2a, the anolyte and catholyte flow face to face rather than side by side, penetrating the porous electrodes and meeting with each other in the middle channel and finally evacuating through the common outlet. Benefited from the much-improved reaction surface area, the peak power density was improved to 120 mW cm^{-2} at 300 μL min^{-1}. The fuel utilization was also improved to 94% at 1 μL min^{-1}. Furthermore, by pumping the waste electrolyte (V^{3+} and V^{4+}) back from outlet to inlets and applying a voltage higher than OCV to the electrodes, the regeneration of anolyte and catholyte was successfully demonstrated in their work (Figure 10.2b), proving the rechargeability of a μRFB based on vanadium species.

Salloum et al. [9] also proposed a counter-flow μRFB with flow-through electrodes based on a cross-shape channel, in which the anolyte and catholyte flow face to face and meet at the middle point (Figure 10.3a). To fully avoid mixing, a third electrolyte of sulfuric acid was injected at the middle point, separating the anolyte/catholyte and guiding them to their corresponding outlets. However, the power density was only 5 mW cm^{-2} at 300 μL min^{-1}, which was probably due to the higher ionic resistance between electrodes in their cell design. The fuel utilization of 24.9% at 50 μL min^{-1} was also not very high due to the low cell performance. Nevertheless, the idea of third electrolyte separation is very advantageous for reactant recycling, which can fully avoid reactant mixing in long-term operation.

The long carbon paper electrode in μRFB may cause high ohmic resistance when only one end is used for external connection, especially for the section away from that end. To solve this issue, Lee et al. [10] proposed the utilization of a thin-film Au current collector beneath the whole carbon paper electrode, providing a fast track for electrons. In this manner, the peak power density was improved from 37.6 to 47.1 mW cm^{-2} at 10 μL min^{-1} and from 52 to 93 mW cm^{-2} at 300 μL min^{-1}, proving the effectiveness of this method. The cell ohmic resistance was also found to decrease from 24.5 to 16.6 Ω, which was the main reason behind this performance improvement. To better implement the charge and discharge of the μRFB,

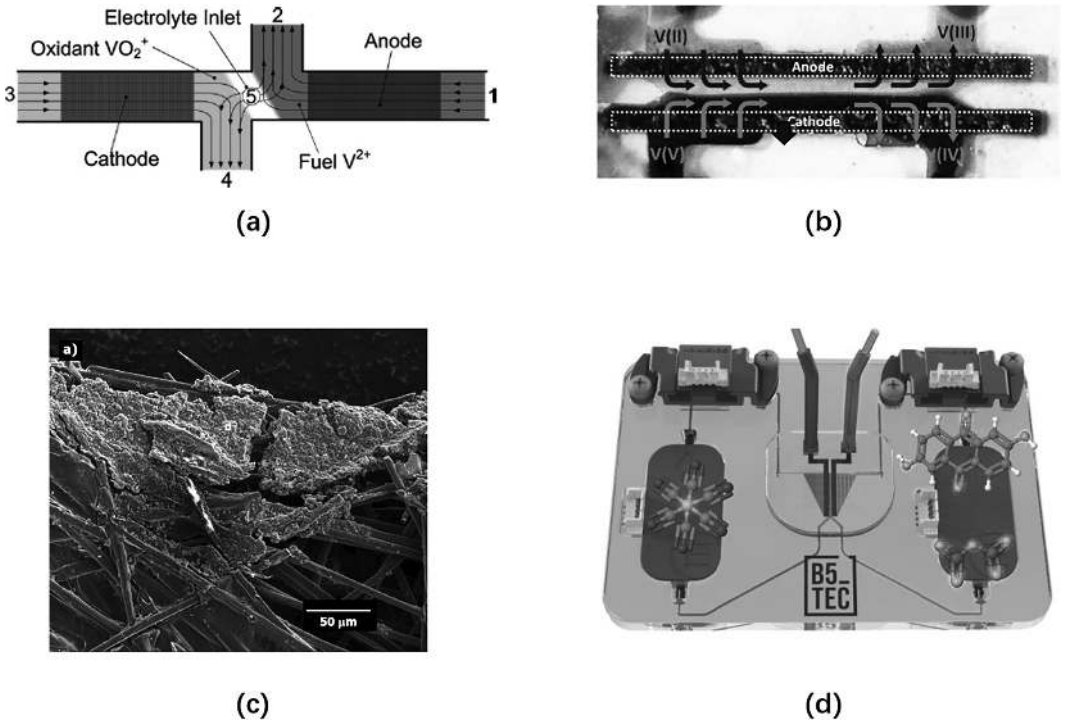

FIGURE 10.3 Structural, material, and system innovations for the all-vanadium μRFB: (a) Counter-flow cell with third electrolyte (Adapted with permission from [9], Copyright 2010, Elsevier), (b) dual-pass cell (Adapted with permission from [11], Copyright 2013, RSC), (c) in-operando deposition of CNT into flow-through electrodes (Adapted with permission [14], Copyright 2017, Elsevier), and (d) Closed-loop electrolyte recirculation battery system. (Adapted with permission [18], Copyright 2024, Wiley.)

Lee et al. [11] developed a dual-pass cell architecture with two inlets and two outlets. As shown in Figure 10.3b, the anolyte or catholyte would penetrate the carbon paper electrode twice, first from the inlet to the middle channel and second from the middle channel to the outlet, leading to a symmetric cell structure. When discharged at 10 μL min^{-1}, a very high power density of 300 mW cm^{-2} was reported. Moreover, when the discharged electrolyte was flowed backward, the anolyte and catholyte were regenerated at 1.7 V, which could be discharged again at 1 V. However, the round-trip efficiency was only 20%, which needed to be improved significantly compared with membrane-based RFBs. By adopting carbon aerogel as flow-through electrodes instead of conventional carbon paper, Lee et al. [12] also proposed a concept of nanofluidic RFB, in which the electrolyte formed nanofluids when it passed through the nanoscale pores (less than 50 nm) of this novel electrode. Benefited from its 2,000 times higher surface area, the nanofluidic RFB achieved much better performance than the μRFB at the high-voltage region (i.e. activation-controlled region). However, the ohmic resistance of carbon aerogel was four times higher than the carbon paper, leading to lower cell performance at the low-voltage region (i.e. ohmic-controlled region).

To study the feasibility of electrolyte recirculation for μRFB, Goulet et al. [13] compared two different cell structures, one with a single outlet and the other with double outlets,

while the electrode length was kept the same. It was found that the double-outlet μRFB could achieve 20% higher power output than the single-outlet μRFB, which was mainly due to its doubled linear flow rate when penetrating the porous electrode. However, such a double-outlet design would also lead to asymmetric crossover between anolyte and catholyte, so that the degradation rate during electrolyte recirculation was doubled (8%) compared with the single-outlet cell (4%). They have further proposed a novel method of in-operando deposition in order to improve the power density of all-vanadium μRFB [14]. In this method, carbon nanotube (CNT) was suspended in the redox electrolyte, which was flowed through the carbon paper electrode during battery operation and deposited dynamically into the porous electrode (Figure 10.3c). This could not only increase the reaction surface but also improve the local convective flow rate inside the electrode, leading to a power density as high as 2,010 mW cm^{-2}. However, the long-term durability of such a high performance was not investigated, which warrants further study considering the physical attachment of CNT only without any binder.

To get rid of external pumping for such a small power source, Zhang et al. [15] investigated the feasibility of using an evaporation pump to deliver the electrolyte. By using ethyl acetate as evaporation solvent at the outlet of the μRFB, a constant passive flow rate from 11 to 60 μL min^{-1} could be obtained, and the best cell performance was achieved at 60 μL min^{-1}, providing a power density of 10.2 mW cm^{-2}. However, such a unidirectional pump is not able to support recirculation or recharge missions. Kim et al. [16] also developed a pumpless μRFB by using the osmosis-driven electrolyte flow. At the outlet, a semipermeable membrane was added, which had waste electrolyte on one side and polyethylene glycol solution on the other side. In this manner, water in the waste electrolyte would be continuously absorbed into the polyethylene glycol solution, leading to a passive flow rate of 0.79–3.34 μL min^{-1}. However, the power density was only 0.3 mW cm^{-2}, which was mainly due to the low flow rate that brought a significant crossover effect.

In real applications, the all-vanadium μRFB should be in closed-loop operation with electrolyte recirculation, considering the high toxicity of vanadium species. Poblete et al. [17] developed a closed-loop system using piezoelectric micropumps and micro flowmeters to realize electrolyte recirculation (Figure 10.3d). At the outlet, micro flow cuvettes were added and connected to optical fibers, so that the ratio between V^{3+} and VO^{2+} could be determined by a UV-vis spectrophotometer. Using this micro system, they have investigated the effect of electrolyte flow rate, reactor internal resistance and potential side reactions on the electrolyte preconditioning process (i.e., from original V^{3+} and VO^{2+} mixture solution to V^{3+} anolyte and VO^{2+} catholyte). They have also studied other redox species in this closed-loop system, such as the alkaline quinone [18].

10.2.2 Modeling Studies

Compared with experimental investigation, the modeling study of the all-vanadium μRFB is also a hot research area, which can better reveal its working mechanism under different cell structures and operation conditions.

Early studies mainly focused on developing modeling methods and determining key input parameters. As shown in Figure 10.4a, Krishnamurthy et al. [19] first developed

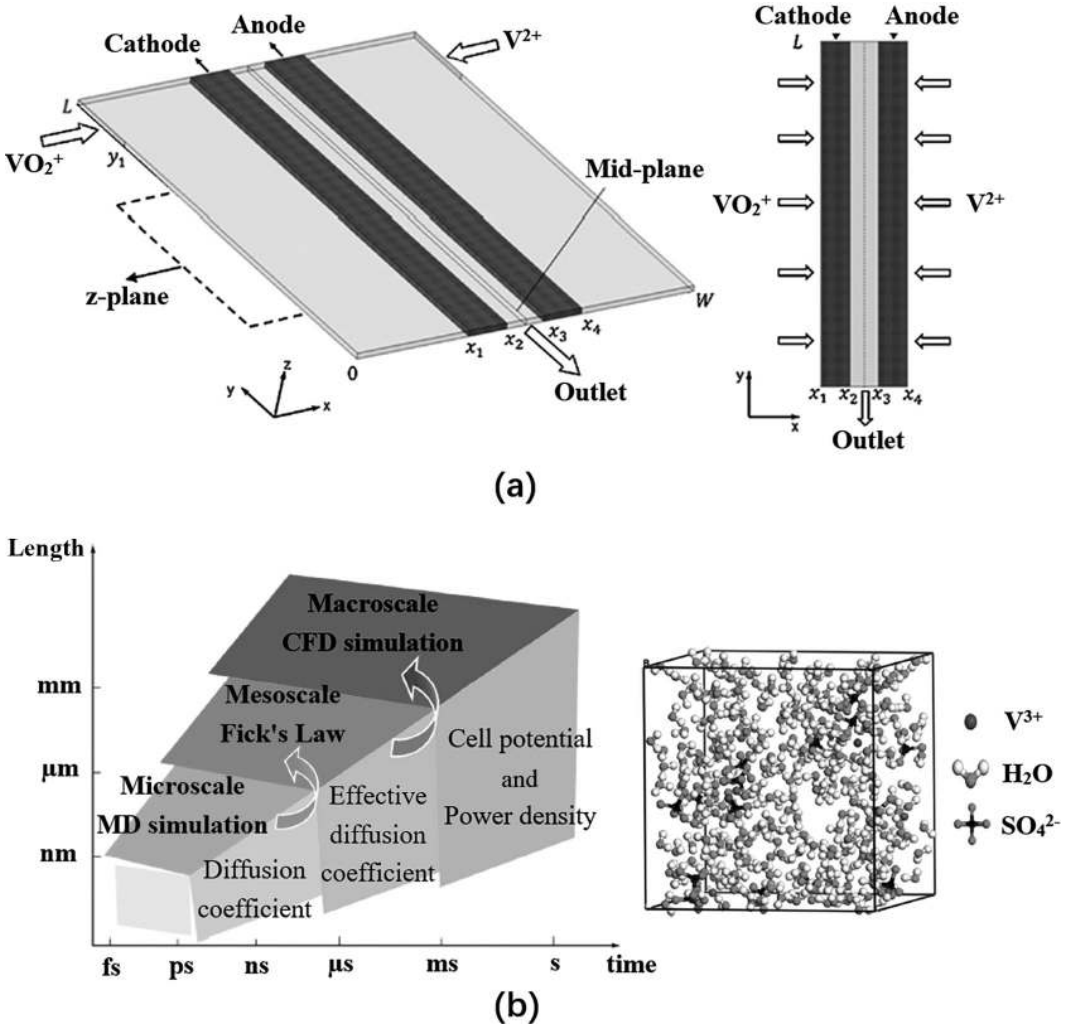

FIGURE 10.4 Two different modeling methods for the all-vanadium μRFB single cell: (a) Conventional multiphysics model with diffusion coefficient obtained from experimental testing (Adapted with permission from [19], Copyright 2011, Elsevier) and (b) hierarchical multiscale model with diffusion coefficient obtained from molecular dynamics. (Adapted with permission from [21], Copyright 2014, Elsevier.)

an all-vanadium μRFB model with flow-through electrodes. With several simplification assumptions, such as isothermal, steady-state, incompressible fluid and without gravity, a multiphysics model coupling fluid flow, mass transport, and electrochemical kinetics was successfully built and validated against experimental data. Through this model, the upper limits of fuel utilization and power density were predicted, namely 77% and 193 mW cm^{-2} for their cell structure and operation condition. Moreover, the effect of reactant crossover could be neglected, probably due to the small diffusion coefficient of vanadium ions. To make the model more accurate, Lee et al. [20] investigated the electrochemical characteristics of vanadium redox reactions on three different carbon electrode materials. Half-cell

electrochemical impedance spectroscopy was used to determine the ohmic resistance, a Tafel plot was used to determine the key kinetic parameters such as the rate constant and charge transfer coefficient, while cyclic voltammetry was used to determine the reversibility of the redox reactions. With the input of these updated parameters, the accuracy of the all-vanadium μRFB model was evidently improved. Furthermore, Yu et al. [21] developed a hierarchical multiscale model for the all-vanadium μRFB as shown in Figure 10.4b, which included the microscale molecular dynamic simulation to calculate the diffusion coefficient of ions, the mesoscale computing of effective diffusion coefficient inside the porous electrode based on Fick's law, and finally the macroscale multiphysics coupling among fluid flow, mass transport, and electrochemical kinetics. It was confirmed that such a multiscale model could predict the battery performance more accurately than conventional models.

For μRFBs with counter-flow electrolytes and flow-through electrodes, the overall ohmic resistance could be very large due to long ion transport path as well as low through-plane electrode conductivity, leading to poor battery performance. To tackle this issue, Li et al. [22] proposed a partial modification method in which the exchange current density was increased by 10 times at the electrode region near the middle channel. In this manner, more reaction took place at this modified region, which had lower ionic resistance, leading to improved battery performance. In another work, they have also proposed a trapezoidal electrode design that had a larger cross-sectional area near the channel middle and a smaller cross-sectional area away from it [23]. Consequently, the overall ionic resistance could be reduced as well, leading to improved power density compared with conventional rectangular electrodes. Furthermore, they have developed a novel multilayer electrode design, in which five layers of carbon paper were stacked together with the inner layer deposited with Pt catalyst to increase its exchange current density [24]. Similarly, the power density could be improved by five times compared with the bare carbon paper electrode without Pt loading. To better utilize the hourglass cross-sectional shape of the mixing layer, Wu et al. [25] proposed the utilization of arc-shaped electrodes in all-vanadium μRFB. Modeling results revealed that arc-shaped electrodes could further compress the hourglass mixing layer to the channel middle, preventing reactant crossover while reducing the ionic resistance. Both the convective mass transport inside the channel and the diffusive mass transport on electrode surface were enhanced, leading to improved power output and fuel utilization for the μRFB. To sum up, the part of electrode close to middle channel is the prime location for redox reaction, whose reaction kinetics or surface area should be increased as much as possible.

To better understand the flow-through electrode, Li et al. [26] have compared the influence of its key kinetic parameters (i.e., reaction rate constant and charge transfer coefficient) and structural parameters (i.e., porosity and specific surface area). It was found that the anode suffered from more overpotential loss than the cathode, in which the mass transfer loss was the major reason. Consequently, modifying the structural parameters of electrodes could provide more significant improvement to the battery performance than the kinetic parameters. As for fuel utilization, the effect of kinetic optimization was also limited due to mass transfer limitation, while the structural optimization of porous electrode was more effective in achieving high fuel utilization [27]. In addition to these

parameters, they have also studied the effect of electrode conductivity and its top-view geometry [28]. It was found that increasing the electrode conductivity solely was not very effective in improving the battery performance. Alternatively, optimizing the top-view aspect ratio of electrode could improve both absolute current and current density at the same time, of which the optimal ratio was determined to be 2:6. Furthermore, considering the different diffusivity and reaction kinetics of V^{2+} and V^{5+}, they have developed an unsymmetrical μRFB with different electrode lengths and electrolyte flow rates between anode and cathode [29]. When the flow rate or reactant concentration was low, longer electrodes would be preferred to sustain the output current, of which the cathode length could be shorter than the anode length. Moreover, the catholyte flow rate could also be reduced to half without sacrificing the battery performance evidently, leading to significant reduction of catholyte consumption.

Besides flow-through electrodes, the performance of all-vanadium μRFB can be influenced by many factors. To distinguish their significance, Li et al. [30] developed a dimensionless model for the all-vanadium μRFB, based on which a statistical multiparametric sensitivity analysis was conducted. It was found that the equilibrium potential and charge transfer coefficient were strong influencing factors; the reactant concentration, specific surface area, electrolyte conductivity, mass transport coefficient, and electrode porosity were moderate influencing factors, and the flow rate, exchange current density, electrode conductivity, and diffusion coefficient were weak influencing factors. Moreover, they have studied the position and property of the current collector on the battery performance [31]. Due to the nonuniform distribution of electrolyte flow rate inside the porous electrode, it was more appropriate to locate the current collector at the high-flow-rate region such as the downstream of the electrode, which could lead to a 61% higher power density. The thickness, conductivity, and external wire positioning of the current collector were also found to influence the battery performance. Furthermore, they have investigated the effect of inlet geometry design, including the inlet reservoir size, the inlet size, and the inlet position [32]. Modeling results indicated that the inlet reservoir size could be greatly minimized to improve device energy density without sacrificing battery performance. On the other hand, the inlet size had limited influence on battery performance, especially at high-flow-rate conditions. As for the inlet position, it was better to be located close to the current collector.

The above-mentioned modeling works mainly focus on single-cell optimization with a single pass of electrolyte, while practical applications of μRFB require electrolyte recirculation in a closed loop as shown in Figure 10.5a, which will bring new issues other than power density and fuel utilization, such as the capacity loss due to reactant crossover as shown in Figure 10.5b. Ibanez et al. [33] studied the effect of diffusive mixing and self-discharge reaction on the crossover rate of an all-vanadium μRFB. Due to the lack of information on the self-discharge reaction rate, two limiting cases were investigated, including infinitely slow reaction and infinitely fast reaction. In spite of the different ion distribution patterns in these two cases, the loss of charged vanadium ions was found to be controlled by diffusion. To alleviate this crossover effect and therefore capacity degradation, Heras et al. [34] studied the deflection of the mixing layer in the all-vanadium μRFB, as well

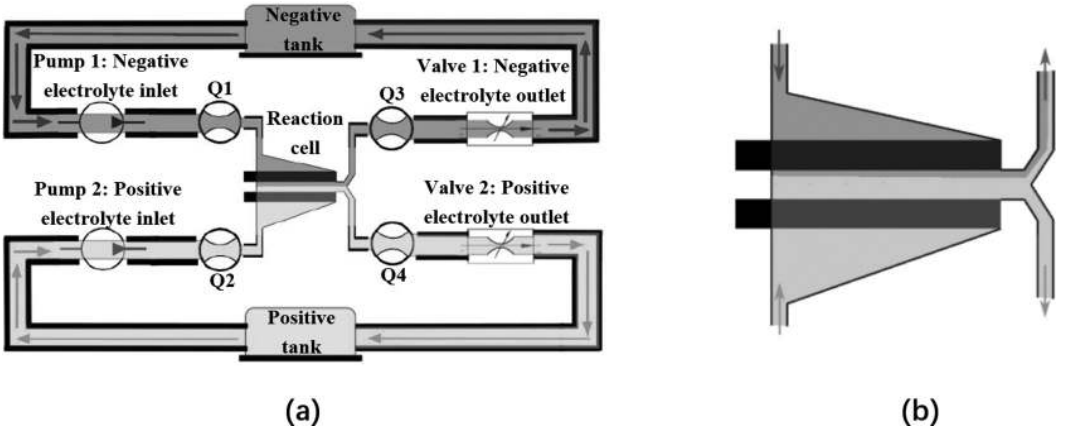

FIGURE 10.5 A closed-loop all-vanadium μRFB system includes the cell, tanks, pumps, valves, and flowmeters: (a) System schematic diagram and (b) reactant crossover due to flow rate mismatch. (Adapted with permission from [35], Copyright 2023, IEEE.)

as the potential strategy that can control this phenomenon. The variation of electrolyte viscosity according to different states of charge was also considered in order to make the model more realistic, and the infinitely slow reaction of self-discharge was assumed. Due to pressure perturbation and hydraulic asymmetry, a large mixing rate would occur in the reactant tank. To avoid this, flow rate regulating valves were added to the channel outlet, and different valve control strategies were studied to reduce the mixing rate. Furthermore, Quiros et al. [35] studied the adaptive modeling of an all-vanadium μRFB system and the associated closed-loop control strategy. The input parameters were determined by a gray-box modeling technique, while real-time correction factors were added as well to adapt the model to the real situation. Based on this model, an incremental state optimal control strategy was proposed for the μRFB system, which could improve its microfluidic response and therefore battery performance. They have also developed an electric model to study the influence of fluid dynamics on the battery's steady-state power, transient power dynamics and mixing and self-discharge losses [36]. Modeling results were well validated by experimental data, proving the effectiveness of this electric model on predicting the influence of fluid dynamics to a μRFB system.

10.2.3 Stacking Studies

Considering the fact that a μRFB single cell can only provide mW-level power output due to its small size, it is inevitable to develop μRFB stacks with multiple single cells connected in series/parallel. This will, however, bring many new issues such as shunt current loss, complex water management and single-cell performance mismatch, which will lead to great loss of stacking efficiency if not handled properly.

Salloum et al. [37] first developed a two-cell μRFB stack connected in parallel with a common flow channel as shown in Figure 10.6a. A third electrolyte was also utilized to better separate the anolyte and catholyte at the outlet of each single cell. At the flow rate of 500 μL min^{-1} (anolyte and catholyte) and 50 μL min^{-1} (third electrolyte), the μRFB stack

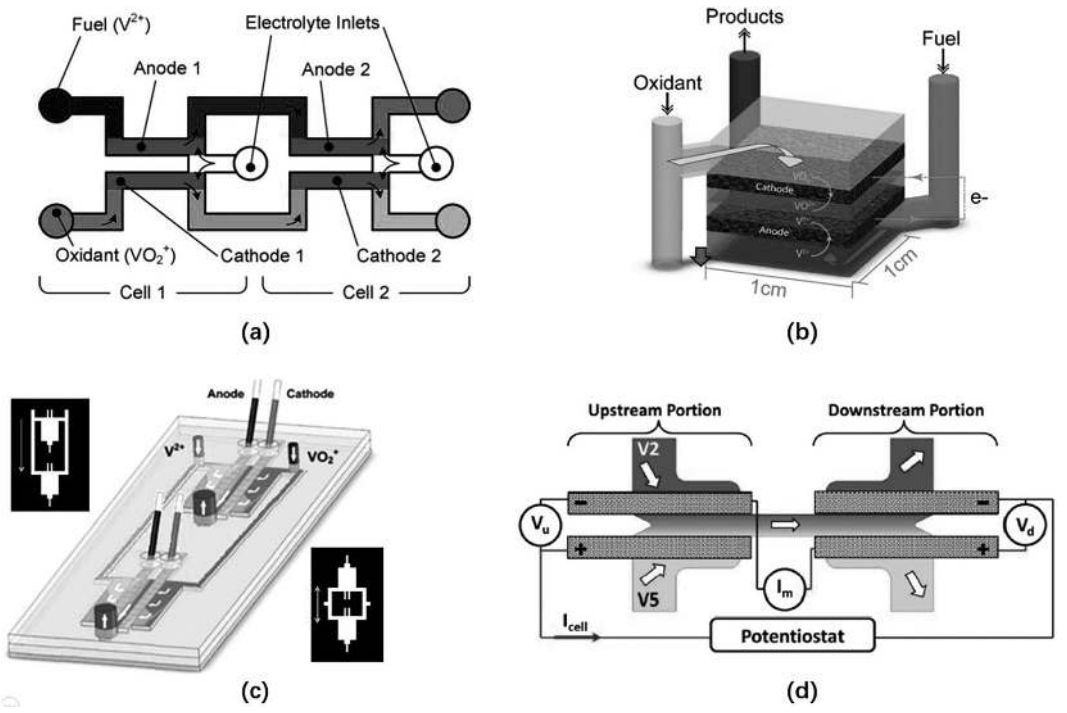

FIGURE 10.6 Different stack designs for the all-vanadium μRFB: (a) A two-cell stack with common flow channel and third electrolyte separation (Adapted with permission from [37], Copyright 2011, Elsevier), (b) a plate-frame single cell structure for vertical stacking (Adapted with permission [38], Copyright 2011, Elsevier), (c) a two-cell stack with independent flow channel, nonsymmetric design in top left corner, and symmetric design in bottom right corner (Adapted with permission from [39], Copyright 2013, ASME), and (d) illustration of cross cell and shunt current in a two-cell stack connected in series with common flow channel. (Adapted with permission [40], Copyright 2015, ECS.)

power was more than doubled compared to that of the single cell, and the fuel utilization was improved from 6% to 11%, proving the effectiveness of this stacking method. However, the downstream cell would suffer from insufficient reactant supply in this stack design, which is especially the case for a large-scale stack with more single cells. The third electrolyte will also dilute the anolyte and catholyte, reducing the performance of downstream cells.

To mimic the stacking of proton exchange membrane fuel cell (PEMFC), Moore et al. [38] developed a vertical μRFB architecture as shown in Figure 10.6b, in which the two flow-through electrodes were placed on the top and bottom of the middle channel, while the corresponding electrolytes flowed face to face in the vertical direction. At 50 μL min^{-1}, the peak power density reached 5.8 mW cm^{-2}, which was much lower than previous works. This could be attributed to the enlarged electrode area that might bring severe flow nonuniformity. The effect of electrode thickness was also studied, and a larger thickness benefited both the power output and the fuel utilization. Finally, a two-cell stack was successfully demonstrated.

Ho et al. [39] proposed a two-cell μRFB stack connected in series with independent flow channels as shown in Figure 10.6c. At the common inlet, the electrolyte was separated into

two brunch flows and entered the two single cells independently, which finally flowed out from their respective outlets. Based on the relative location of the single cells, both non-symmetric unilateral and symmetric bilateral designs were fabricated and tested, of which the latter design achieved much better performance. This was probably because the symmetric bilateral design could lead to more uniform brunch flows for the two single cells due to its even flow resistance.

Ibrahim et al. [40] studied the effect of shunt current generation in a two-cell μRFB stack connected in series with common flow channel. As shown in Figure 10.6d, the anode of upstream cell and the cathode of downstream cell would form a cross cell when they were connected, which was always in short-circuit state and generated shunt current. This would not only lower down the stack OCV but also consume reactants without electricity output, reducing the stack power output and fuel utilization at the same time. To alleviate this loss, it was recommended to increase the flow resistance between the single cells in order to increase the ionic resistance of the cross cell. They have also studied the two-cell μRFB stack connected in parallel with common flow channel [41]. This time, the shunt current no longer existed since electrodes with the same polarity were connected, so that no cross cell was formed. However, the downstream cell still suffered from lower performance due to reactant consumption as well as crossover.

10.3 OTHER μRFBS

10.3.1 All-Copper μRFB

In addition to electric recharge that consumes electricity, some RFBs can be thermally recharged by using waste heat, leading to thermally regenerative RFBs. Among them, the thermally regenerative ammonia RFB has attracted wide attention, in which the following reactions take place during battery discharge:

$$\text{Anode}: \text{Cu}_{(s)} + 4\text{NH}_{3(aq)} \rightarrow \text{Cu}\left(\text{NH}_3\right)_{4(aq)}^{2+} + 2\text{e}^- \left(E^0 = 0.04\ \text{V}\right) \tag{10.1}$$

$$\text{Cathode}: \text{Cu}_{(aq)}^{2+} + 2\text{e}^- \rightarrow \text{Cu}_{(s)} \left(E^0 = 0.34\ \text{V}\right) \tag{10.2}$$

After discharge, the NH_3 can be regenerated from used anolyte by waste heat absorption, which will be dissolved back to form fresh anolyte for the next discharge. Therefore, this kind of battery can also be termed as all-copper RFB.

To lower down the device cost, Vicari et al. [42] first proposed the all-copper μRFB that utilized a laminar electrolyte instead of an expensive polymer membrane. Using Cu as electrodes, $Cu(NO_3)_2 + NH_4NO_3$ as catholyte, and $Cu(NO_3)_2 + NH_4NO_3 + NH_4OH$ as anolyte, a peak power density of 7.34 mW cm^{-2} was achieved at 50°C, which was even higher than conventional membrane-based batteries operated under batch mode. Nevertheless, the voltage output was intrinsically restricted by redox chemistry, which requires a series connection of multiple single cells in real applications. Shi et al. [43] also adopted this all-copper chemistry to develop a thermally regenerative ammonia battery without a

membrane. Specifically, considering the lower density of NH_4OH than $Cu(NO_3)_2$ and NH_4NO_3, a higher concentration of it will accumulate in the upper part of anolyte, leading to severe NH_4OH crossover. To tackle this issue, an upward anode was proposed to alleviate the crossover extent, leading to 4% higher power density than the conventional level anode. Furthermore, when coupled with a tapered channel, a much-improved power density of 5.5 mW cm^{-2} could be achieved at room temperature.

To avoid external pumping, a fiber-based all-copper μRFB was also developed by Jiang et al. [44], in which capillary and gravity forces were utilized to transport electrolyte passively through the porous fiber microchannel. With braided carbon fibers as electrode, $NH_4Br+CuBr_2$ as catholyte, $NH_4Br+CuBr+NH_4OH$ as anolyte, and a third electrolyte of NH_4Br, this pumpless μRFB could provide a power density as high as 24.9 mW cm^{-2} at room temperature, which was much higher than previous pump-based counterparts. This improvement might be attributed to the variation of redox chemistry in this work.

10.3.2 H_2-Br_2 μRFB

A H_2-Br_2 RFB utilizes H_2 gas in the anode, dissolved Br_2 in the cathode, and a HBr solution as a supporting electrolyte, which has many advantages such as rapid reaction kinetics, low reactant cost, and high electrolyte conductivity. As shown by the equations given below, the theoretical OCV reaches 1.09 V, guaranteeing a high power density.

$$\text{Anode}: H_{2(\text{gas})} \rightarrow 2H^+ + 2e^- \left(E^0 = 0\ \text{V}\right) \tag{10.3}$$

$$\text{Cathode}: Br_{2(\text{aq})} + 2e^- \rightarrow 2Br^- \left(E^0 = 1.09\ \text{V}\right) \tag{10.4}$$

Braff et al. [45] first developed a H_2-Br_2 μRFB with gas diffusion anode based on Pt catalyst and flow-over cathode based on graphite material. Using 25 sccm H_2 as fuel and 5M Br_2 as oxidant, the μRFB could deliver a power density of 800 mW cm^{-2} at room temperature, which was benefited from the high reaction kinetics as well as high ionic conductivity of the 3M HBr electrolyte. Furthermore, a round-trip efficiency as high as 92% was obtained at 25% of the peak power density.

To further improve the battery performance and to suppress Br_2 crossover, Suss et al. [46] employed a flow-through cathode to better utilize the Br_2, and a nanoporous separator was also added on cathode surface to minimize Br_2 crossover. With this structural modification, the power density was improved to 925 mW cm^{-2} with 3M Br_2, and the current density also exceeded 3 A cm^{-2}. Alfisi et al. [47] further analyzed the loss mechanism of this type of μRFB by breaking down different resistances during battery operation. By developing an equivalent RC circuit for the battery and fitting it to electrochemical impedance spectroscopy results, key resistance values could be distinguished from each other. It was found that the major reason for voltage loss originated from the porous cathode, accounting for more than 50% of the total resistance. Second, ionic resistance from the electrolyte

accounted for 25% of the total resistance. These results can provide valuable directions for the further optimization of H_2-Br_2 μRFB.

10.3.3 Organic μRFB

Recently, RFBs using organic redox species have been proposed and received wide research interests, which is mainly because of their great abundance, tunable properties, and environmental friendliness. Based on the reaction species, it can be divided into all-organic RFBs and half-organic RFBs; while based on the solvent type, it can be divided into aqueous RFBs and nonaqueous RFBs.

Karakurt et al. [48] first developed an all-organic μRFB using 2,6-DHAQ and ferro/ferricyanide as redox pair. The battery was fabricated based on a flexible PDMS substrate, which was targeted for wearable applications such as wristwatch. However, the necessity of external pumping and bulky electrolyte storage were huge obstacles to this mission. With laser-induced graphene electrodes, 0.1 M reactants, and 1 M KOH as supporting electrolyte, the battery could provide a peak power density of 0.75 mW cm^{-2}, which was much lower than those obtained by inorganic μRFBs. To understand the in-depth reaction mechanism of all-organic μRFBs, Park et al. [49] developed a transparent μRFB using 9-fluorenone and 5,10-bis(2-methoxyethyl)-5,10-dihydrophenazine (BMEPZ) as redox pair. Benefited from the distinct color change of BMEPZ in different charge states, the charge and mass transfer process could be observed visually by manipulating the current density and flow rate, respectively, leading to direct elucidation of the electrokinetic phenomena. Furthermore, by redesigning the conventional electrode into a tapered shape, the battery performance could be enhanced.

Marschewski et al. [50] developed a half-organic μRFB with anthraquinone/iron redox pair. To improve mass transport in the laminar flow regime, herringbone-shaped flow promotors were added on the bottom of the channel below the above electrodes, which could increase the convective transport of reaction species to the corresponding electrode surface. Benefited from this chaotic mixing effect, the battery limiting current was more than doubled, leading to much-improved battery performance. Chaabene et al. [51] further developed a half-organic μRFB using 1-ethyl-3-methylimidazolium bis(trifluoromethylsulfonyl) imide as supporting electrolyte and quinone/iron chloride as redox pair. Nevertheless, due to the limited solubility of reactants in this ionic liquid supporting electrolyte, the peak power density only reached 0.04 mW cm^{-2}, which might be further improved by using flow-through porous electrodes.

10.4 TECHNICAL CHALLENGES

The major advantage of μRFB technology lies in the elimination of a membrane separator, resulting in cost reduction. By leveraging laminar flow characteristics, the anolyte and catholyte can be naturally separated. However, this advantage comes with a price, including limitation on single-cell dimensions, trade-off between power output and efficiency, and the potential for diffusive mixing over time.

In order to sustain a low Reynolds number, the characteristic length of flow channel is limited to submillimeter scale, which also restricts the electrode size inside. In this manner,

the power output of a single cell is generally less than 1 W, which is insufficient for most applications. To solve this problem, stacking multiple single cells together is believed to be the right way, which can not only improve the total power but also manipulate the voltage output by series connection. However, this will first of all lead to very complex water management since every single cell will need at least two flow inputs. In fact, only two-cell μRFB stacks have been developed in literature, while μRFB stacks with more single cells are not studied yet. To feed these single cells at the same time, a manifold flow can be divided into multiple brunch flows via a flow distributor. At the outlet, all used electrolytes will be collected into one manifold flow again via a flow collector. In this manner, the water management can be greatly simplified. The second issue associated with μRFB stack is the uneven single-cell performance that will deteriorate the stacking efficiency. Due to limited fabrication precision, the single cells may have slight structural differences with each other, especially for their tiny electrodes. On the other hand, the operation conditions of the single cell may also differ from each other, such as the uneven electrolyte flow rate. This issue can only be alleviated by improving the fabrication precision. Furthermore, if a series connection is applied among single cells, the third issue of shunt current generation can greatly impair the stack performance. Due to the inevitable ionic connection, when the anode of one cell and the cathode of another cell is connected, a short-circuited cross cell will be formed, leading to significant shunt current loss inside the stack. This issue can be solved by a multilayer stacking strategy, in which the single cells are connected in parallel only in each layer, while different layers are connected in series without ionic connection. Alternatively, a voltage booster can be adopted to elevate the stack voltage output, so that no series connection is needed any more.

The trade-off between power and efficiency is another technical challenge for μRFBs. To ensure sufficient reactant supply and therefore high power output, the electrolyte flow rate should be high; while to ensure sufficient reactant utilization and therefore high energy efficiency, the electrolyte flow rate should be low. This dilemma in flow rate selection has puzzled μRFB researchers for a long time. To tackle this, flow-through electrodes have been utilized instead of flow-over electrodes, which can reach out to the bulky electrolyte and alleviate the fuel depletion effect at low flow rates. Nevertheless, the battery performance is still poorer than that at a high flow rate, and the flow-through electrode also brings new issues, such as poor ohmic resistance and elevated flow resistance. Another solution to this problem is to add flow promotors inside the channel, inducing local chaotic flows to guide the unreacted reactant onto the electrode surface at high flow rates. However, this may have a negative effect on the flow stability and impair the anolyte–catholyte interface especially under external disturbance. Third, an extra supporting electrolyte can be used to separate the anolyte and catholyte, compressing them into a thin layer near the anode and cathode surface, respectively, so that the utilization efficiency can be improved. This is, however, at the price of more complex water management, which is especially the case for large-scale μRFB stacks.

The third technical challenge for μRFBs is the accumulated diffusive mixing of anolyte and catholyte. In spite of the slow diffusive mixing at their interface, the accumulated reactant crossover is not negligible after long-term operation, which may lead to electrolyte

degradation and impair the battery lifetime. For the all-vanadium μRFB, this problem is less severe since the same reactant species are used in anolyte and catholyte. In this manner, the crossovered vanadium ion can be turned back to the desired valence after battery charging. As for μRFBs with different types of reactants in anolyte and catholyte, this problem is quite serious. To tackle this, a microporous separator can be added between the anolyte and catholyte, which can greatly lower down the reactant crossover. Unlike the ion exchange membrane separator, the microporous separator is a low-cost material, which physically impedes the diffusive mixing of reactants. Nevertheless, this will also increase the ionic resistance of the μRFB, reducing its power output ability. Alternatively, a redox pair with different phases can be adopted, such as the H_2-Br_2 μRFB, in which the dissolved Br_2 in the electrolyte will not mix with the gaseous H_2 outside the flow channel at all.

10.5 CONCLUSION AND FUTURE OUTLOOK

This chapter provides a detailed introduction to a unique type of RFB that utilizes two microfluidic electrolytes for reactant delivery without the need for an ion exchange membrane separator. This design significantly reduces device cost. The laminar characteristic of microfluidics results in the formation of only an ultrathin diffusive mixing layer at the electrolyte interface, ensuring the smooth operation of this microfluidic RFB. Over the past two decades, great efforts have been made in this specific area, among which most works are focused on the classic all-vanadium μRFB. Both experimental and numerical studies have been implemented on the battery material, structure, and system, aiming to improve its power output, fuel utilization, and application potential. In addition to this, μRFB with other redox species has also been investigated in recent years, such as the all-copper, H_2-Br_2, and organic μRFBs, while the difference among their performances can be quite large due to different reaction kinetics. In general, the development of μRFB is still in its early stage, with several technical challenges unsolved.

Due to the small single-cell dimension, the stacking of μRFB is inevitable in order to output an applicable power. However, only two-cell μRFB stacks have been investigated to date, while the water management issue and internal loss problem of large-scale μRFB stacks are not studied yet, which warrants in-depth investigation in the future. With such efforts, the application potential of μRFB for renewable energy storage can be better demonstrated rather than single-cell prototypes in the laboratory. Second, more advanced electrode materials and cell structures should be proposed to break the notorious trade-off between power output and energy efficiency, resulting in a suitable electrolyte flow rate that can balance the convective and diffusive mass transport at the electrode surface. Third, the rechargeability of μRFBs should be studied other than their discharge performance only, which is frequently neglected in existing works. This is probably because of the accumulated reactant crossover after the long-term battery operation, leading to poor cycling performance and lifetime. To address these challenges, readers can explore both the selection of reaction species and the optimization of cell structure for μRFB technology. In conclusion, there remains significant potential for future research of μRFB technology, aiming at overcoming the technical challenges mentioned above and bringing this technology closer to commercial viability.

REFERENCES

1. Iwakiri I, Antunes T, Almeida H, Sousa JP, Figueira RB, Mendes A. Redox flow batteries: Materials, design and prospects. *Energies*. 2021;14:5643.
2. Bamgbopa MO, Almheiri S, Sun H. Prospects of recently developed membraneless cell designs for redox flow batteries. *Renewable and Sustainable Energy Reviews*. 2017;70:506–18.
3. Gao M, Salla M, Zhang F, Zhi Y, Wang Q. Membrane fouling in aqueous redox flow batteries. *Journal of Power Sources*. 2022;527:231180.
4. Li X, Qin Z, Deng Y, Wu Z, Hu W. Development and challenges of biphasic membrane-less redox batteries. *Advanced Science*. 2022;9:2105468.
5. Ferrigno R, Stroock AD, Clark TD, Mayer M, Whitesides GM. Membraneless vanadium redox fuel cell using laminar flow. *Journal of the American Chemical Society*. 2002;124:12930–1.
6. Kjeang E, Proctor BT, Brolo AG, Harrington DA, Djilali N, Sinton D. High-performance microfluidic vanadium redox fuel cell. *Electrochimica Acta*. 2007;52:4942–6.
7. Kjeang E, McKechnie J, Sinton D, Djilali N. Planar and three-dimensional microfluidic fuel cell architectures based on graphite rod electrodes. *Journal of Power Sources*. 2007;168:379–90.
8. Kjeang E, Michel R, Harrington DA, Djilali N, Sinton D. A microfluidic fuel cell with flow-through porous electrodes. *Journal of the American Chemical Society*. 2008;130:4000–6.
9. Salloum KS, Posner JD. Counter flow membraneless microfluidic fuel cell. *Journal of Power Sources*. 2010;195:6941–4.
10. Lee JW, Kjeang E. Chip-embedded thin film current collector for microfluidic fuel cells. *International Journal of Hydrogen Energy*. 2012;37:9359–67.
11. Lee JW, Goulet M-A, Kjeang E. Microfluidic redox battery. *Lab on a Chip*. 2013;13:2504–7.
12. Lee JW, Kjeang E. Nanofluidic fuel cell. *Journal of Power Sources*. 2013;242:472–7.
13. Goulet M-A, Kjeang E. Reactant recirculation in electrochemical co-laminar flow cells. *Electrochimica Acta*. 2014;140:217–24.
14. Goulet M-A, Ibrahim OA, Kim WH, Kjeang E. Maximizing the power density of aqueous electrochemical flow cells with in operando deposition. *Journal of Power Sources*. 2017;339:80–5.
15. Zhang Q, Li H, Liu X, Zhao W, Zong C, Gai H. A self-driven miniaturized liquid fuel cell. *Chemical Communications*. 2016;52:12068–71.
16. Kim S-H, Kim K, Go M, Park JY. Stand-alone external power-free microfluidic fuel cell system harnessing osmotic pump for long-term operation. *Journal of Micromechanics and Microengineering*. 2018;28:125005.
17. Oraá-Poblete B, Perez-Antolin D, Maurice AA, Palma J, Kjeang E, Quintero AE. Preconditioning operation of membraneless vanadium micro redox flow batteries. *Batteries & Supercaps*. 2024;7:e202300367.
18. Torres MJ, Hervas-Ortega J, Oraá-Poblete B, de Quirós AB, Maurice AA, Perez-Antolin D, et al. Membraneless micro redox flow battery: From vanadium to alkaline quinone. *Batteries & Supercaps*. 2024;7:e202400331.
19. Krishnamurthy D, Johansson EO, Lee JW, Kjeang E. Computational modeling of microfluidic fuel cells with flow-through porous electrodes. *Journal of Power Sources*. 2011;196:10019–31.
20. Lee JW, Hong JK, Kjeang E. Electrochemical characteristics of vanadium redox reactions on porous carbon electrodes for microfluidic fuel cell applications. *Electrochimica Acta*. 2012;83:430–8.
21. Yu Y, Zuo Y, Zuo C, Liu X, Liu Z. A hierarchical multiscale model for microfluidic fuel cells with porous electrodes. *Electrochimica Acta*. 2014;116:237–43.
22. Li L, Zheng K, Ni M, Leung MK, Xuan J. Partial modification of flow-through porous electrodes in microfluidic fuel cell. *Energy*. 2015;88:563–71.
23. Li L, Ling L, Xie Y, Shan S, Bei S, Zheng K, et al. Counter-flow microfluidic fuel cell with trapezoidal electrodes. *Sustainable Energy Technologies and Assessments*. 2023;56:103005.

24. Li L, Nikiforidis G, Leung MK, Daoud WA. Vanadium microfluidic fuel cell with novel multi-layer flow-through porous electrodes: Model, simulations and experiments. *Applied Energy*. 2016;177:729–39.
25. Wu B, Wu Q, Xu X, Dong G, Zhang M, Leung DY, et al. Microfluidic fuel cell with arc-shaped electrodes to adapt to its mixing zone, a simulation study. *Applied Energy*. 2024;376:124177.
26. Li L, Xu Q, Wang H, Bei S, Shen S, He Y, et al. Boost performance of porous electrode for microfluidic fuel cells: Electrochemical modification or structure optimization? *International Journal of Energy Research*. 2022;46:3324–34.
27. Li L, Ling L, Xie Y, Shan S, Bei S, Sun Y, et al. Achieving high fuel utilization for microfluidic fuel cell under high flow rate operation. *Sustainable Energy Technologies and Assessments*. 2022;54:102869.
28. Li L, Bei S, Xu Q, Zheng K, Zheng Y. Role of electrical resistance and geometry of porous electrodes in the performance of microfluidic fuel cells. *International Journal of Energy Research*. 2018;42:1277–86.
29. Li L, Wang H, Bei S, Li Y, Sun Y, Zheng K, et al. Unsymmetrical design and operation in counter-flow microfluidic fuel cell: A prospective study. *Energy*. 2023;262:125581.
30. Li L, Fan W, Xuan J, Leung MK. Dimensionless parametric sensitivity analysis of microfluidic fuel cell with flow-through porous electrodes. *Electrochimica Acta*. 2016;187:636–45.
31. Li L, Fan W, Xuan J, Leung MK, Zheng K, She Y. Optimal design of current collectors for microfluidic fuel cell with flow-through porous electrodes: Model and experiment. *Applied Energy*. 2017;206:413–24.
32. Li L, Xie Y, Shan S, Ling L, Bei S, Zheng K, et al. Optimal design of reactant delivery system in microfluidic fuel cell with porous electrodes. *International Journal of Energy Research*. 2022;46:15535–46.
33. Ibáñez SE, Quintero AE, García-Salaberri PA, Vera M. Effects of the diffusive mixing and self-discharge reactions in microfluidic membraneless vanadium redox flow batteries. *International Journal of Heat and Mass Transfer*. 2021;170:121022.
34. de las Heras M, Quintero AE, Maurice AA, Vera M, Ibáñez SE. Deflection and control of the mixing region in membraneless vanadium micro redox flow batteries: Modeling and experimental validation. *International Journal of Heat and Mass Transfer*. 2024;232:125921.
35. De Quirós AB, Quintero A, Francés A, Uceda J. Adaptive microfluidic modeling of a membraneless micro redox flow battery using extended kalman filter. *IEEE Access*. 2023;11:100207–17.
36. De Quirós AB, Quintero AE, Francés A, Maurice AA, Uceda J. Electrical model of a membraneless micro redox flow battery—Fluid dynamics influence. *IEEE Access*. 2023;11:46132–43.
37. Salloum KS, Posner JD. A membraneless microfluidic fuel cell stack. *Journal of Power Sources*. 2011;196:1229–34.
38. Moore S, Sinton D, Erickson D. A plate-frame flow-through microfluidic fuel cell stack. *Journal of Power Sources*. 2011;196:9481–7.
39. Ho B, Kjeang E. Planar multiplexing of microfluidic fuel cells. *Journal of Fluids Engineering*. 2013;135:021304.
40. Ibrahim OA, Goulet M-A, Kjeang E. Microfluidic electrochemical cell array in series: Effect of shunt current. *Journal of the Electrochemical Society*. 2015;162:F639.
41. Ibrahim OA, Goulet M-A, Kjeang E. In-situ characterization of symmetric dual-pass architecture of microfluidic co-laminar flow cells. *Electrochimica Acta*. 2016;187:277–85.
42. Vicari F, Galia A, Scialdone O. Development of a membrane-less microfluidic thermally regenerative ammonia battery. *Energy*. 2021;225:120221.
43. Shi Y, Li Y, Zhang L, Li J, Fu Q, Zhu X, et al. Development of a membrane-less microfluidic thermally regenerative ammonia-based battery towards small-scale low-grade thermal energy recovery. *Applied Energy*. 2022;326:119976.

44. Jiang Q, Shi Y, An Y, Zhang L, Li J, Zhu X, et al. A low-cost self-pumping membraneless thermally regenerative flow battery for small-scale waste heat recovery. *Industrial & Engineering Chemistry Research*. 2024;63: 8860–67.
45. Braff WA, Bazant MZ, Buie CR. Membrane-less hydrogen bromine flow battery. *Nature Communications*. 2013;4:2346.
46. Suss ME, Conforti K, Gilson L, Buie CR, Bazant MZ. Membraneless flow battery leveraging flow-through heterogeneous porous media for improved power density and reduced crossover. *RSC Advances*. 2016;6:100209–13.
47. Alfisi D, Shocron AN, Gloukhovski R, Vermaas DA, Suss ME. Resistance breakdown of a membraneless hydrogen–bromine redox flow battery. *ACS Sustainable Chemistry & Engineering*. 2022;10:12985–92.
48. Karakurt I, Elwood J, Li X, Beker L, Sweet E, Cai W, et al. Membraneless microfluidic redox battery for wearable electronics applications. *2017 19th International Conference on Solid-State Sensors, Actuators and Microsystems (TRANSDUCERS)*, Kaohsiung, Taiwan, China. IEEE; 2017. pp. 1820–3.
49. Park H, Kwon G, Lee H, Lee K, Park SY, Kwon JE, et al. In operando visualization of redox flow battery in membrane-free microfluidic platform. *Proceedings of the National Academy of Sciences*. 2022;119:e2114947119.
50. Marschewski J, Ruch P, Ebejer N, Kanan OH, Lhermitte G, Cabrol Q, et al. On the mass transfer performance enhancement of membraneless redox flow cells with mixing promoters. *International Journal of Heat and Mass Transfer*. 2017;106:884–94.
51. Chaabene N, Ngo K, Turmine M, Vivier V. Ionic liquid redox flow membraneless battery in microfluidic system. *Journal of Energy Storage*. 2023;57:106270.

CHAPTER 11

Performance Evaluation and Modeling of Flow Batteries

Noé Arjona and Fernando F. Rivera

11.1 INTRODUCTION TO FLOW BATTERIES

Redox flow batteries (RFBs), named as flow batteries, are electrochemical energy devices that convert the chemical of a certain chemical species employed as fuel into electrical energy. Contrary to traditional Li-ion batteries, RFBs are designed mostly for grid energy storage. Thus, RFBs are designed for high-power and high-energy systems. In addition, the number of cells and the size of electrodes dictate power, while the energy depends on the electrolyte volume and the utilized fuel or redox pair [1]. Notably, bipolar plates, flow distribution, and textural properties like electrode porosity also influence the performance. The typical redox pairs in RFBs include (1) aqueous fuels like vanadium species dissolved in an aqueous electrolyte, (2) solid fuels like the lead and Zn electrode RFBs, and (3) hybrids, where the species is in the electrolyte and the electrode. The battery components are (1) the bipolar plates with the flow channels, (2) the electrodes, (3) the ion exchange membrane, (4) the current collectors, (5) the stack, and (6) the reservoirs and pumps (Figure 11.1a).

11.2 FUNDAMENTALS ON THE OPERATION OF REDOX FLOW BATTERIES

The discharge process involves the pumping of the active species from the reservoir to the positive electrode to undergo the electrochemical oxidation, releasing electrons, where the flow of electrons is called electricity. The electrons pass to the negative electrode to undergo the electrochemical reduction process. In vanadium RFBs, the VO_2^+/VO^{2+} species are found in the anodic reservoir, and the V^{2+}/V^{3+} species in the cathodic reservoir [2]. The charge process is inverse to the discharge, and in this process, the active anodic and cathodic species are recovered by applying energy to the system. Rechargeable batteries, which are similar to RFBs, are characterized to be conducted by passive flows, and thus, no pumps are required. Typically, rechargeable batteries like Li-ion, Li-air, and Zn-air display different challenges [3] and, in some cases, are attributed to the absence of an active flow like

DOI: 10.1201/9781003506379-11

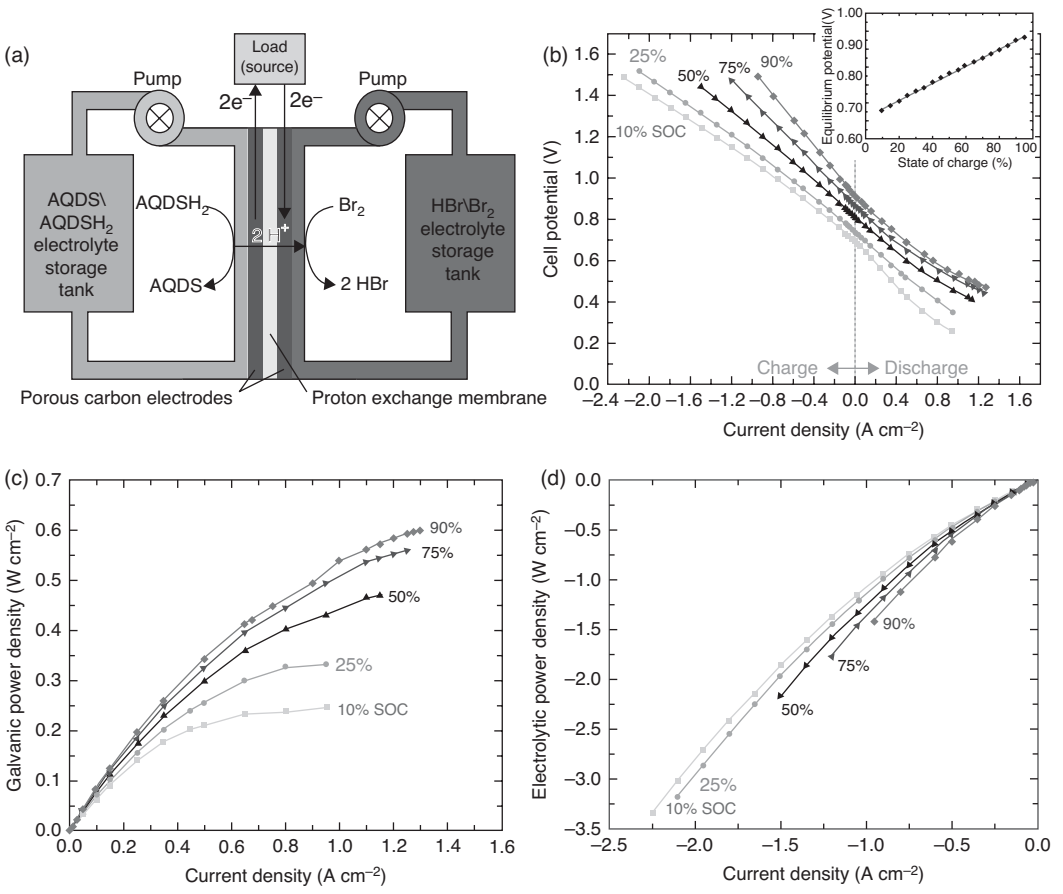

FIGURE 11.1 (a) Schematic representation of an RFB based on a metal-free organic-inorganic aqueous flow battery, (b) charge and discharge curves at different SoC, (c) galvanic power density, and (d) electrolytic power density. (Reproduced with permission from [6], Copyright (2014), Nature.)

in RFBs. Some examples include the formation of dendrites during charge, self-discharge, the formation of undesired precipitates, and electrode passivation. Consequently, the RFBs typically present higher round-trip efficiencies than these rechargeable batteries, and hence, their better usage for grid energy applications. The depth of discharge (DoD) is another fundamental aspect in which RFBs better operate than the above-mentioned rechargeable batteries [4]. The DoD consists of the depth in the amount of charge (amperes-hours) removed from the battery divided by the nominal capacity (Equation 11.1) [5]:

$$\mathrm{DoD} = \frac{\text{Amount of removed charge}}{\text{Maximum available amount of charge (C)}} \cdot 100\% \tag{11.1}$$

And, the DoD is also expressed as (Equation 11.2):

$$\mathrm{DoD} = 100\% - \mathrm{SoC} \tag{11.2}$$

SoC is related to the state of charge (available amount of charge in the battery) at a specific point, and it is expressed in percentage (Equation 11.3) [5]. The SoC indicates how much the battery can still be under-functioning before it needs charge. The DoD is the opposite, measuring the amount of charge that has been used up in the battery.

$$\mathrm{SoC} = \frac{\text{Actually available amount of charge}}{\text{Maximum available amount of charge (C)}} \cdot 100\% \tag{11.3}$$

11.3 PERFORMANCE EVALUATION

In RFBs, performance evaluation is carried out electrochemically using a Potentiostat/Galvanostat, a cycler, a DC electronic load for discharge tests, or a DC power regulator for electrolytic tests. The typical tests involve the discharge and charge curves at different SoC or DoD (Figure 11.1b), the obtaining of the resulting power density curves for discharge (Figure 11.1c), and the nongalvanic power density curve (Figure 11.1d).

The discharge curve has two important components: the cell voltage (V) and the current density (A cm^{-2} or mA cm^{-2}). The open-circuit voltage (OCV) is that in which the net current density is zero, and this voltage is related to the equilibrium potential of the half-cell reactions. Thus, this is the highest voltage achieved by the battery from the electrode–electrolyte configuration. When a current density is demanded, the cell voltage will decrease from the OCV because it will drive electrical work. Thus, the increase of the current density results in a decrease of the cell voltage as is observed in Figure 11.1b. Also, higher cell voltages and current densities will be obtained when the SoC is near 100% (fully charged). In the case of the charging process, the current density increases with the rise of the applied potential (Figure 11.1d), and the current density will be higher when the SoC is near the fully discharge as is observed in the figure. Apart from the SoC, two aspects are required from the development of new batteries: (1) to obtain batteries with the highest cell voltage to improve the battery performance and (2) to obtain batteries where the maximum current density can be achieved at lower overpotentials. These two aspects are better interpreted in the scheme presented in Figure 11.2.

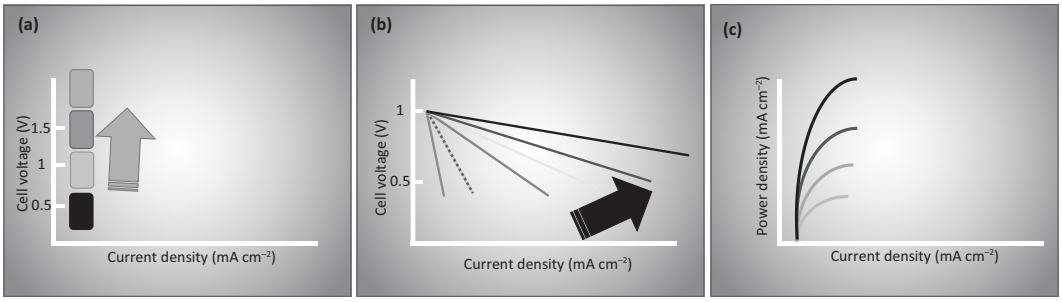

FIGURE 11.2 Schematic representation of aspects looked at in the development of new RFBs: (a) the increase of the cell voltage, (b) the increase of the current density as well as the overpotentials to achieve those values, and (c) the increase of the power density by the previous strategies.

The increase of the cell voltage rises the power density (W cm^{-2}) since it can be calculated from (Equation 11.4):

$$\mathrm{W}\left(\mathrm{W\ or\ mWcm^{-2}}\right) = \mathrm{Voltage\ (V)} \cdot \mathrm{current\ density}\left(\mathrm{A\ or\ mA\ cm^{-2}}\right) \tag{11.4}$$

In the case of the current density, as observed in the equation, its increase also improves the performance. However, as above-mentioned, the ideal scenario is that in which the current density is increased and the overpotential to achieve those improved values is the lowest possible (Figure 11.2b), and it results from the decrease of the three main resistances: (1) the polarization resistances coming from the energetic barriers to start the reaction, (2) the ohmic resistances that result from the electrode resistances, electrode separation resistances, current collector resistances, among others, and (3) mass transport resistances from the difficulty to transport active species from bulk to the interface. And, in consequence, the power density will increase (Figure 11.2c).

In order to increase the power density (Figure 11.2c), other engineering aspects like varying the flow rate, the anolyte-to-catholyte flow ratio, the working temperature, and the fuel and oxidant concentration are typically investigated. Beyond the activity evaluation, in RFB durability is a major concern. Thus, typical durability evaluation tests involve galvanostatic charge–discharge (GCD) curves (Figure 11.3a), capacity retention tests during discharge cycles (Figure 11.3b), and efficiency from similar tests (Figure 11.3c). The major functionality as a function of time or cycles the better rechargeability, and it can also be expressed in terms of capacity retention (Figure 11.3b), round-trip efficiency (also known as voltage efficiency VE, Figure 11.3c), coulombic efficiency (CE), and energy efficiency (EE).

The capacity retention is determined by (Equation 11.5):

$$\text{Capacity retention} = \frac{Q_f}{Q_i} \cdot 100\% \tag{11.5}$$

where C_i is the initial capacity and C_f is the final capacity. It is worth mentioning that C_f in this case is the capacity at each cycle after the first. And, the capacity is determined by (Equation 11.6):

$$Q_{spec} = \frac{\mathrm{current\ (mA\ or\ A)} \cdot \mathrm{service\ time\ (h)}}{\mathrm{volume\ (L)}} \tag{11.6}$$

where the current is those observed during the discharge cycle, the service time is in which the battery is discharged until achieving the cut-off voltage, and the volume is that passed during the service time. The capacity retention is hence obtained from the data in Figure 11.3a as well as the round-trip efficiency, which is obtained from (Equation 11.7):

$$\text{Round-trip efficiency} = \frac{E_{\text{discharge}}}{E_{\text{charge}}} \cdot 100\% \tag{11.7}$$

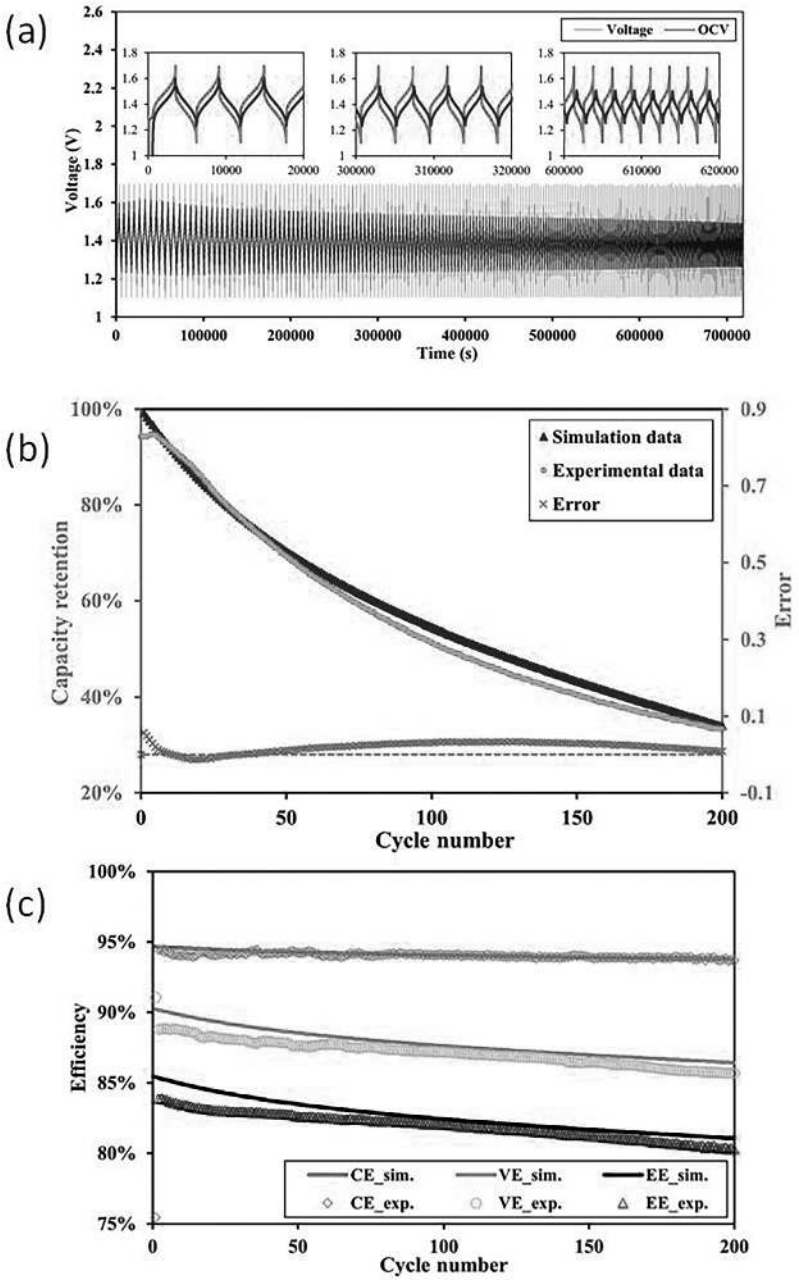

FIGURE 11.3 Typical tests performed on redox flow batteries: (a) galvanostatic charge/discharge (GCD) cycles, (b) capacity retention, and (c) efficiency tests with cycling. (Reproduced with permission from [7], Copyright (2024), Elsevier.)

And, this equation is determined for each cycle, while the CE is obtained as:

$$\mathrm{CE} = \frac{i_{\mathrm{discharge}}}{i_{\mathrm{charge}}} \cdot 100\% \tag{11.8}$$

And, the EE is obtained as:

$$\mathrm{EE} = \frac{E_{\mathrm{discharge}} \cdot i_{\mathrm{discharge}}}{E_{\mathrm{charge}} \cdot i_{\mathrm{charge}}} \cdot 100\% \tag{11.9}$$

And, as observed in Figure 11.3c, the research is addressed to obtain redox flow batteries (RFBs) with the highest round-trip efficiencies as a function of cycling and the highest coulombic and energy efficiencies.

11.4 MODELING AND DESIGN OF REDOX FLOW CELLS

RFBs, and particularly all-vanadium redox flow batteries (VRFBs), have been recognized as one of the most realistic candidates among electrochemical technologies for energy storage in the range of several kW/kWh to tens of MW/MWh [8–10]. However, their actual benefits at these scales are yet to be determined due to a lack of engineering studies and certain implementation challenges of these devices. In conventional batteries, such as lithium-based systems, the charge is stored within the cell as active material adhered to an electrode matrix [11]. This utilizes the electrochemical intercalation phenomenon that degrades the specialized electrode materials, leading to the early replacement of such devices. This issue can be significantly mitigated in RFBs since the charge transfer reactions that occur in systems do not require intrinsic electrode material reactions. Instead, they generally employ conventional fast charge transfer reactions at the electrolyte–solution interface. Nevertheless, RFBs face different challenges and obstacles like:

- The study of materials comprising the entire battery assembly; these aspects include, in addition to the synthesis of critical materials for its operation (such as electrodes, types of electrolyte, and ion exchange membranes), the selection of materials for use in the frames for fixing the electrodes in channels and flow distributors, current collectors, the selection of bidimensional or porous electrodes, among others [12,13].
- The capability and optimization of cell operation since the development of RFB technology must consider flow distribution (which can decrease or increase the concentration overpotential), optimization of electrode size, electrolyte flow rate, stack design, among others. Research and development are needed to determine the criteria for choosing the advanced design of flow batteries based on hydrodynamics and electrochemical engineering to improve their performance [12,13].
- The development of mathematical models and their solutions using detailed computational techniques to describe stationary and transient operations in such devices [10,13].
- Commercial implementation is limited because the electrolyte components of this battery are generally expensive in most cases (as in the VRFB cell). Additionally, for aqueous and nonaqueous electrolyte RFBs, the development of cost-effective and selective ion-conductive membranes with high conductivity and long life is of great importance. Therefore, technical-economic studies are needed to evaluate the economic viability of such systems.

Each of these challenges has an important effect on the cell potential obtained in the device; hence, it is convenient to understand the contributions of the mentioned components in the cell potential and its characteristics. Because of the high operative costs of these systems, the large number of experiments required to improve the understanding of these contributions, and the several coupled phenomena in its operation, modular numerical modeling becomes an important tool to describe several important issues for the application of these systems at different scales, such as fine aspects of the charge transfer mechanisms, the influence of the operational parameters in the performance of the battery, identification of cell potential contributions, and the most important drops, among others.

According to Huang et al. [14], three main approaches have been explored, consisting of the evaluation of equivalent circuit models, solving the governing equations that describe the computational fluid dynamics (CFD) coupled to the chemical and electrical aspects, and simple kinetic models. These approaches are summarized in Figure 11.4, in which the main parameters required for each approach are described, emphasizing that depending on the type of modeling, different kinds of parameters are required (e.g. for equivalent circuits, physical and operational parameters are essential; for simple kinetic model, characteristics of the cell also employed; and CFD employs physical properties of the electrolytes). In this chapter, the most employed equivalent circuits and CFD models are considered to be reviewed.

11.4.1 Cell Potential Contributions and Characteristics

As was mentioned earlier, RFBs are galvanic-type electrochemical devices, but their operation differs from conventional electrochemical energy storage devices such as fuel cells and secondary batteries. Also, the difference between the electrode potentials of the positive and negative redox pairs causes charge transfer electrochemical reactions at the electrodes, and thus, the energy generated by this electrode potential difference could be captured by an external electrical load.

In this way, the cell potential associated with maximum energy generation is expressed as (for the VRFB example):

$$E_{cell} = E_{\frac{VO_2^+}{VO^{2+}}} - E_{\frac{V^{2+}}{V^{3+}}} \tag{11.10}$$

$$E_{\frac{VO_2^+}{VO^{2+}}} = E^\circ + \frac{RT}{nF}\ln\frac{C_{VO_2^+}C^2{}_{H^+}}{C_{VO^{2+}}} \quad \left(\text{positive electrode}\right) \tag{11.11}$$

$$E_{\frac{V^{2+}}{V^{3+}}} = E^\circ + \frac{RT}{nF}\ln\frac{C_{V^{2+}}}{C_{V^{3+}}} \quad \text{(negative electrode)} \tag{11.12}$$

where E is the thermodynamic potential of the component indicated by the subscript, C_i is the concentration of electroactive species, and R, T, F, and n are thermodynamic parameters. From the Nernst equation (Equations 11.10 and 11.11), it is clear that the cell potential depends on the concentration of species. Additionally, this thermodynamic cell potential

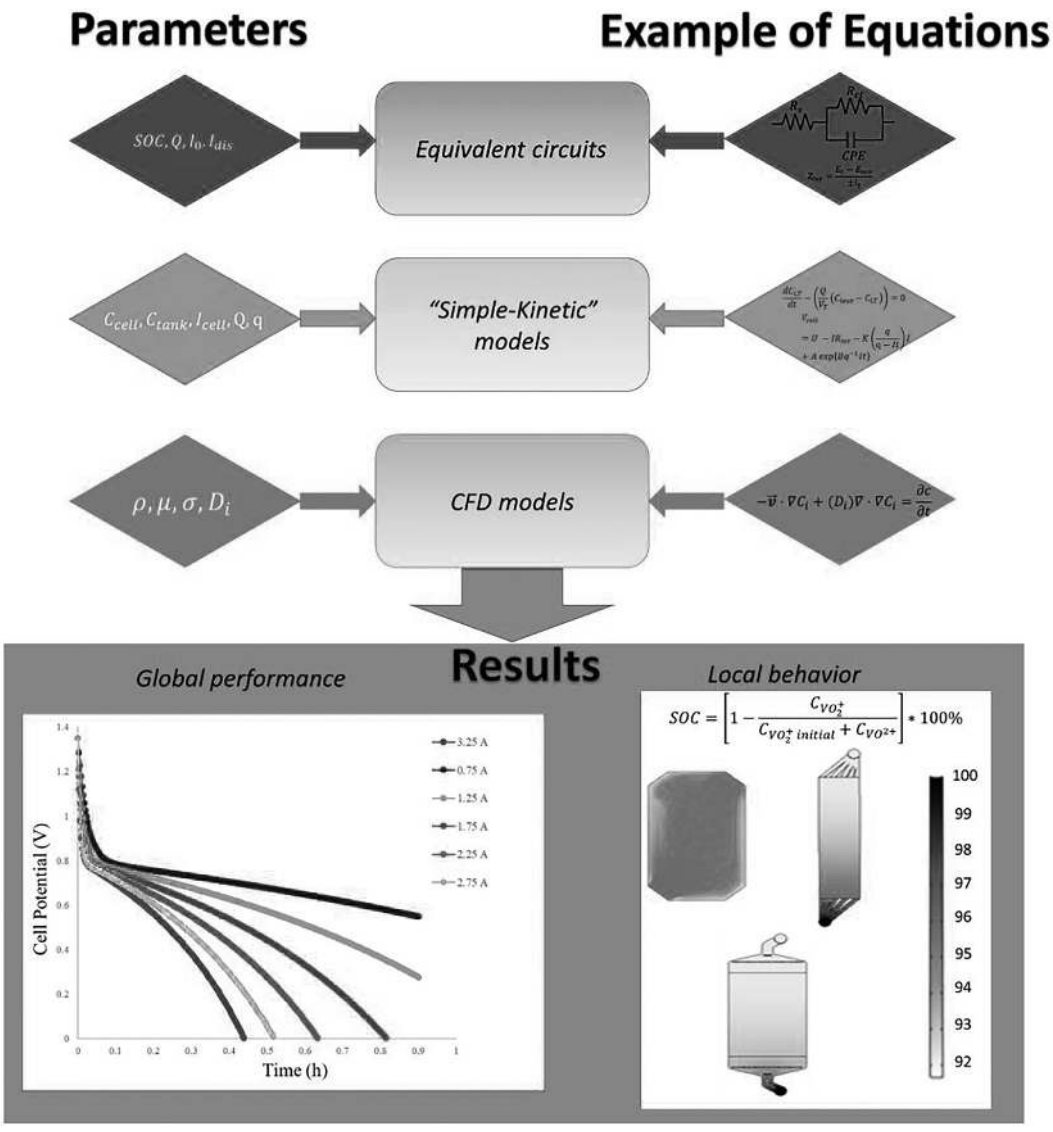

FIGURE 11.4 Schematic of different modular modeling employed to evaluate the engineering aspects of the redox flow cells.

has energy losses mainly due to the ohmic drop of the cell electrolyte and separator, the activation energy of the electrode materials, and the concentration overpotentials near the membrane, according to the following equation:

$$V_{\text{cell}} = (E_c - E_a) - (\eta_{\text{cat}} + IR_{\text{cir.cat}}) + IR_{\text{c. cat}} + IR_{\text{sep}} + IR_{\text{c.anod}} + (\eta_{anod} + IR_{\text{circ.anod}}) \quad (11.13)$$

where η refers to the sum of activation and concentration overpotentials at both the cathode and anode, R is the total resistance of the indicated component, and I is the system's discharge current. Research and development in RFB have succeeded due to

the need for large- and medium-scale energy storage devices for renewable sources [15], peak shaving, and frequency regulation.

Despite their technical advantages, RFB systems are considered a high-capital-cost technology because the electrolytes (e.g., vanadium) and ion exchange membranes remain expensive. Furthermore, the solubility of the most common redox species restricts the maximum energy density of these devices (for example, 1 L of 1 M vanadyl sulfate electrolyte can only achieve a theoretical energy density of 30 Wh dm^{-3}). Due to the solubility and price limitations of metals, the cost of storage capacity for an all-vanadium RFB is around 150–2,500 USD/kWh. The United States Department of Energy has set the competitive cost for all-vanadium and aqueous RFB in general at less than 150 USD/kWh (which is attractive compared to the 400 USD/kWh for Li-based batteries for stationary applications). Thus, efforts have been directed toward reducing the storage capacity costs for vanadium RFB since one of the first reports on this battery was published [12], which reported a power density of 48 mW cm^{-2}. Results reported in these studies do not represent a realistic advancement in RFB technology. Since solubility and material development limit the costs of storage capacity, other battery elements must be studied to reduce the capital costs of RFBs and increase their power density. Therefore, it is necessary to identify some key aspects and indicators that help reduce contributions to potential drop, described in Equation (11.13), and these generally lie in the reliability of the reactor design used as an RFB flow cell, as will be discussed later.

Some works have explored the solving and modeling of battery systems with (Equation 11.13), obtaining parameters from circuit equivalent models or data from experimental tests (for example in Li-ion batteries [16]). In the field of RFBs, Zhang et al. [17] explored the approach of modeling a VRFB by equivalent circuits, taking into account the resistance of all components in the redox battery, the hydraulic energy consumption by pumping of electrolyte, and voltage losses by electrical components. The solving of the equivalent circuit equation was fitted with experimental data by the least square error method to obtain the parameters of the model, reproducing the charge and discharge curves precisely. On the other hand, Bhattacharjee et al. [18] employed an equivalent circuit model modified in comparison to the traditional Randles circuit, to take into account the effects of initial cell temperature, obtaining some parameters from a 1 kW VRFB system instead of obtaining by circuit fitting. By solving the proposed model, the parameters obtained at a 1kW system predict accurately the behavior of a 125 kW system, and the flow rate could also be optimized. Additionally, one example of a "kinetic-simple model" to calculate the cell potential is presented by Li et al. [19] and Clemente et al. [20], which evaluates different RFB systems to contribute to the techno-economical analysis of this kind of battery.

Despite the circuit equivalent and simple models giving a good enough approximation to predict and analyze the behavior of the RFB system, the design of RFBs that achieve high energy storage efficiencies faces challenges in the engineering description of these cells, like the fluid distribution within a cell and its role in reducing concentration overpotential, the use of different electrode geometry configurations (two dimensional or three dimensional), as well as their electrical connection (monopolar or bipolar), among others.

11.4.1.1 Engineering Aspects

As previously mentioned, the engineering aspects implicit in the development of RFB systems become critical topics in the study of batteries containing aqueous electrolytes, such as vanadium and other soluble organic and inorganic redox pairs. Recently, in the field of engineering aspects of RFB systems, the most relevant studies have been reported by the research group of Frank C. Walsh [7,8,13]. It has been concluded that the main attribute of a conventional RFB is the ability to separate power and capacity when both redox pairs are in the aqueous phase. Thus, if an increase in energy storage capacity is required, it is achieved by simply using larger volumes of electrolytes, which is desirable for scaling this technology to grid-level power generation.

Significant studies emphasizing the in-depth analysis of the electrochemical engineering aspects of RFBs were reported by Arenas et al. [21], considering a cerium-based RFB system. Despite the treatment of several and interesting aspects in these references, the analysis of engineering features must consider flow distribution (which can decrease or increase concentration overpotential), optimization of electrode size and electrolyte flow rate, design of stack, among others. Additionally, in engineering studies for redox flow cells using other chemical components in the electrolyte, [22], it was examined the performance of a zinc-cerium RFB for different electrode geometries mentioned earlier demonstrated that using 3D electrodes improves the overall cell voltage performance at different discharge rates by increasing the surface area and volumetric mass transport coefficient (reducing concentration overpotential). This could also improve hydrodynamics, ohmic drops, and potential distribution within the cell; however, only global measurements were taken. For this reason, to elucidate the influence of geometrical and operational parameters on the performance of an RFB, from a phenomenological point of view, fluid dynamics and solving governing equations of mass and electrical transport are crucial tools to understand such phenomenology and designing different types of RFBs.

11.4.2 Dynamic of Fluids and Simulations

Since equivalent circuit and simple kinetic models do not take into account some local phenomena that affect the performance of RFBs, other methodologies are required to address critical design factors such as pressure drop, mass transfer coefficients (flux resistance of electroactive species to the electrode surface), and the effect of local concentration distribution on SOC in different zones across the RFB. The use of CFD is progressively adopted as a tool for analyzing the phenomenological aspects of hydrodynamic electrochemical systems, such as flow reactors [23]. In the field of RFBs, the employment of CFD tools allows analyzing the hydrodynamics in serpentine or interdigitated flow channel geometries [24], which ensure good mass transfer rates and, for this reason, have been traditionally used for PEMFC fuel cells. When evaluating different flow channel geometries in RFB systems, the pressure drop generally varies intrinsically because the viscous dissipation of energy from inertial forces depends on the spatial position. Thus, to compare the suitability between different flow geometries, pressure drop and power-based efficiency [25], given by Equation (11.14), are used as figures of merit to select the most acceptable design for RFB systems.

$$\psi_{\text{power}} = \frac{P_{\text{net}}}{P_{\text{total}}} \tag{11.14}$$

where P_{total} is the total power required by the overall RFB system, and P_{net} is the intrinsic or theoretical net output power of the studied device (excluding energy losses from electrolyte pumping, circuit resistance, and other components). For example, Xu et al. [25] studied the flow field to reduce mass transfer resistance to acceptable pressure drops through a numerical study of different flow distributor geometries. Serpentine, parallel, and rectangular distributors were tested. Pressure drops of around 5,000 Pa were reported for serpentine and square geometries, but power-based efficiency was favored in the serpentine geometry. With these values, the maximum power-based efficiency was 83.5% for the serpentine geometry.

For the implementation of these reactor technologies, an important step is the modeling of experimental data characterization, using known techniques for reactor evaluation such as DTR curves [26], pressure drops [27], and flow visualization through experimental and computational tools (mathematical simulation or via CFD) [28]. This methodology could help to find reactor designs that diminish the pressure drop and improve the fluidodynamics and flow distribution across the electrode. For example, Macdonald and Darling [29] studied hydrodynamics in interdigitated and serpentine flow distribution channels using CFD numerical simulations, employing models based on Darcy's law to determine the velocity field (3D models of free and porous flow) and the pressure drop with 2D models based on solving the Laplace equation coupled to a resistance network. The model predictions suggest that increasing the thickness of the flow channel and the porous electrode helped to homogenize fluid distribution in the two distributors (which is consistent with studies conducted in other electrochemical reactors [30]).

The proposal of new designs of flow channels is also an interesting field in the modeling of RFB. Since the use of three-dimensional electrodes is considered in these new designs, approaches employing the Navier-Stokes equations, coupling with effective properties and velocity calculations (Darcy-Brinkman scheme). Generally, The proposed geometries with 3D electrodes exhibited good flow distribution with a higher average electrolyte velocity within the electrode, which should improve the mass transport rate in the RFB, with a slight influence of the channel geometries, like parallel plates, rectangular, trapezoidal among others [27,31,32].

Recently Lopéz-Maldonado et al. [33] proposed a methodology to perform a local validation of the velocity magnitude profiles data obtained by CFD, in different flow channel designs. This methodology consisted of the use of optical flow and neural networks to analyze images of flow visualization tests, which is an essential tool to characterize the flow dynamics inside the flow channels of electrochemical reactors. The digital image treatment describes adequately the velocity profiles generated by CFD (as is shown in Figure 11.5), elucidating different phenomenology involved when designs with different flow distributors at the inlet are used. This tool appears to be interesting to evaluate the fluid dynamics in RFBs and to achieve rigorous validation.

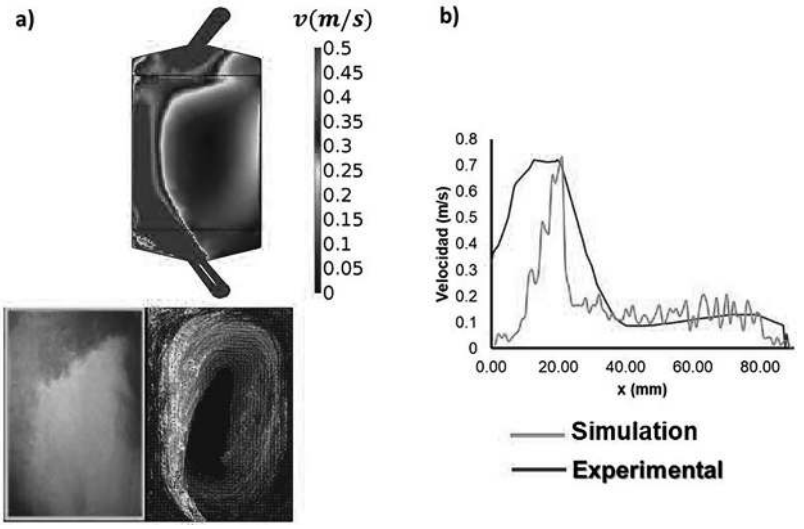

FIGURE 11.5 Calculated and experimental fluid distribution in an electrochemical reactor flow channel. (a) CFD calculation of velocity field by a CFD model based on Navier-Stokes equations approach, and experimental visualization of fluid pattern, (b) comparison of theoretical and experimental velocity profiles obtained, by CFD and digital image treatment in the flow channel, respectively.

11.4.3 Species Transport and Potential Distribution

The effect of the flow field also could impact the distribution of chemical species in the battery, which affects its instantaneous SOC and the concentration overpotential. In this way, it is needed the proposal of models based on CFD and coupling of the mass transport governing equations, for describing the distribution of electroactive species in the positive and negative compartments. This approach has gained traction thanks to the development of computers with the necessary resources, enabling this type of analysis to be performed within a reasonable time. In this context, there is an extensive number of studies that take into account electrochemical aspects, as described in [10].

For example, Messagi et al. [34] described a 3D multiphysics model that coupled flow equations in the porous electrode medium with the conservation equations of the species involved in the operation of a VRFB. Both theoretical and experimental results indicated that the serpentine configuration showed better charge and discharge performance compared to the interdigitated configurations (which seems contradictory to studies suggesting that interdigitated flow channels provide greater uniformity [32]). However, these configurations exhibited higher pressure drops and less homogeneous concentration distributions. Gurieff et al. [35] conducted a study using a similar modeling approach but evaluated a novel fluid distributor using static mixers, which reduced concentration overpotential and pressure drop. León et al. [36] used models based on fluid dynamics (free and porous media equations) and electrochemical species transport (diffusion-convection) to describe fluid dispersion, mass transport, and the state of charge in a Vanadium-Cerium cell with graphite felt electrodes, separated from the membrane by a plastic spacer. Additionally, the

mathematical model only describes a secondary potential distribution, where the surface concentration effect is not strongly coupled.

It is important to note that these proposed multiphysics models are not systematic, where the equations describe the phenomena in the RFB more accurately, other models do not describe the effect of important variables such as the fluid velocity passing through the battery, or the contribution of different fluid fields concerning the discharge rates of these batteries. This is because typically a flow or discharge rate condition is selected to validate power and/or cell potential curves against time at the selected flow rate. Additionally, since the models are uncoupled or weakly coupled from a mathematical perspective, they do not provide interesting information about the role of battery design in its figures of merit (current efficiency, EE, pressure drop factor, etc.). This is because they do not report an explicit dependence of the electric potential on concentration decay and SOC dynamics, which is, of course, one of the most critical parameters in RFB performance. The use of these approaches has led to significant discrepancies regarding which data should be used to validate the proposed models. In some cases, charge and discharge potential curves against time are used; in others, only polarization curves or simple fluid visualization tests, which are not contrasted with battery performance. For this reason, it is necessary to solve the strongly coupled model that would first require the use of intrinsic input parameters (such as residence time or the standard heterogeneous reaction constant, which is generally evaluated for the most common redox pairs) to quantify the resistance due to concentration overpotential and effectively elucidate the effect of concentration decay and state of charge on power loss due to activation and concentration overpotential effects [37].

Another aspect of modeling that has been overlooked and requires further work is the potential distribution across the interelectrode space of RFBs (since ohmic drop represents a significant contribution to energy loss in galvanic systems). In this regard, most of the cited reports use monopolar electrodes, attempting to use bipolar electrodes. In specialized references, the cell potential distribution modeling only assumes that it depends on the disappearance of the active species during charge and discharge within the VRFB, ignoring the strong coupling between the effective surface concentration of the electrode and the electrolyte potential, as well as the influence of kinetic properties on the potential distribution in the 3D solid electrode matrix. In this sense, it is worth noting that in porous electrodes, the charge balance between the liquid electrolyte and the porous matrix must be satisfied according to the following equation [38]:

$$\nabla \cdot j_m + \nabla \cdot j_s = 0 \tag{11.15}$$

where j_m is the current passing through the solid phase or electric current, and j_s is the current passing through the electrolyte solution or ionic current. This equation indicates that the electric charge passing through the solid matrix must be compensated by the same charge leaving the liquid phase but with an opposite sign. This postulate is related to the charge balance between the two phases. In this case, the potential drop in the electrolyte will depend not only on the ohmic drop between electrodes but

also on the reaction rate at the electrode–electrolyte interface. For a quasi-reversible electrochemical reaction, the following applies:

$$\nabla \cdot j_s = -k\nabla^2 \phi_s = j_{\text{kin}} \tag{11.16}$$

$$j_{\text{kin}} = nFk^0 C_i^0 \left[\exp\left(\frac{(1-\alpha)F}{RT}(\eta) \right) + \exp\left(\frac{-\alpha F}{RT}(\eta) \right) \right] \tag{11.17}$$

$$\eta = \phi_m - \phi_s - E_{ocp} \tag{11.18}$$

where k^0 is the standard heterogeneous rate constant, α is the charge transfer coefficient, η is the activation overpotential, ϕ_m and ϕ_s are the potentials in the solid and electrolyte phases, respectively, and j_{kin} is the current due to charge transfer. Here, the equilibrium potential E_{ocp} is given by the Nernst equation for the redox pair. Combining Equation (11.9) with Equation (11.8) yields a system of Poisson-type equations that describe the interaction between the metal potential and the solution potential. Schematics of the expected potential distribution in these kinds of systems are shown in Figure 11.6a.

Solving this system of equations first describes that, due to the conductivity difference between the porous matrix and the electrolyte, the activation overpotential will not remain constant (as postulated by various models in the literature), but it will vary with the electrode size and the charge–discharge rate, as shown in Figure 11.6b, provoking a poor ionic current pass through the porous electrode. This was systematically studied by Bhadra and Haverkort [39], through the derivation of semi-analytical models to describe the tertiary current and potential distribution and to optimize the channel thickness and volumetric surface area to enhance the energetic efficiency of flow-through and interdigitated devices. This is useful in grid-scale applications since the optimization of such parameters could compensate for the energy losses by pressure drop.

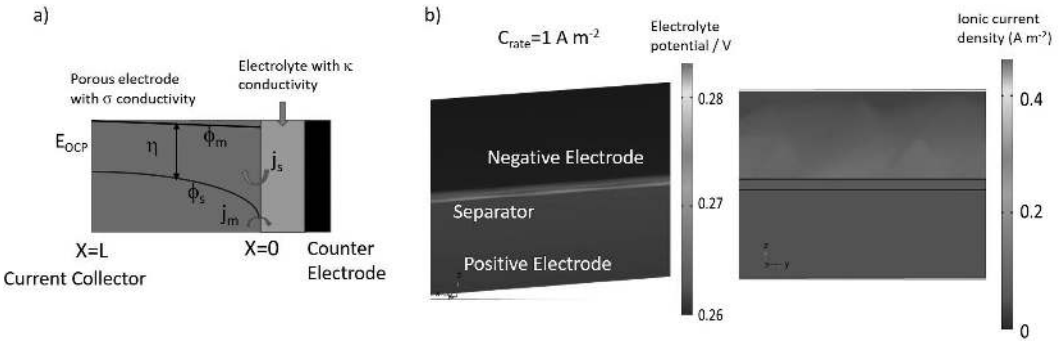

FIGURE 11.6 Schematics of potential distributions presented in 3-D electrodes employed in RFB. (a) Scheme of a model of potential and current distribution described by Equations (11.15)–(11.18) and (b) results obtained by the numerical solving of such model.

11.5 CONCLUSIONS

To achieve competitive performance in RFB devices from the operational point of view, the diminishing of some important contributions like the resistances due to polarization, ohmic, and mass transport effects must be treated to achieve competitive performance in grid applications. Modular numerical modeling has demonstrated its use as an important tool to understand and identify the factors in the diminishing of these resistances at different scales, since the experimental determination of such factors could be expensive, especially at bench and grid scales. The use of global models like the equivalent circuits and simple kinetic models is effective in understanding and determining the resistance values for different voltage losses, determination of pumping energy consumption, and resistance of electrical components. On the other hand, the CFD models are important in the investigation of the parameters that impact the performance from a phenomenological point of view. Three important topics, which must be described by the solution of governing differential equations of the phenomena in the RFB, are fluid dynamics, chemical species, and potential distribution, which are critical engineering aspects to the development of RFB devices. Despite several works have been made efforts to overcome these challenges, further investigation will be needed in the modular modeling of these batteries.

11.6 PERSPECTIVES

Despite the circuit equivalent and simple models giving a good enough approximation to predict and analyze the behavior of the RFB system, the design of RFBs that achieve high energy storage efficiencies faces challenges in the engineering description of these cells, which can be addressed by the use of this approach, like the flow distribution inside the cell, the implications in the use of 3-D porous electrodes, and local distribution of active species.

REFERENCES

1. G. Lota, M. Graś-Ligocka, L. Kolanowski, K. Lota, Flow batteries: recent advancement and challenges, in R. Gupta (eds) *Handbook of Energy Materials*, Springer, Singapore, 2022.
2. E. Sánchez-Díez, E. Ventosa, M. Guarnieri, A. Trovo, C. Flox, R. Marcilla, F. Soavi, P. Mazur, E. Aranzabe, R. Ferret, Redox flow batteries: Status and perspective towards sustainable stationary energy storage, *J. Power Sources* 481 (2024) 228804.
3. T. Wang, T. Yang, D. Luo, M. Fowler, A. Yu, Z. Chen, High-energy-density solid-state metal–air batteries: Progress, challenges, and perspectives, *Small* 20 (2024) 2309306.
4. M. Skyllas-Kazacos, M. H. Chakrabarti, S. A. Hajimolana, F. S. Mjalli, M. Saleem, Progress in flow battery research and development, *J. Electrochem. Soc.* 158 (2011) R55.
5. E. Karden, Secondary batteries lead-acid-systems| automotive batteries: new developments, in J. Garche (eds) *Encyclopedia of Electrochemical Power Sources*, Elsevier, 2009.
6. B. Huskinson, M. P. Marshak, C. Suh, S. Er, M. R. Gerhardt, C. J. Galvin, X. Chen, A. Aspuru-Guzik, R. G. Gordon, M. J. Aziz, A metal-free organic–inorganic aqueous flow battery, *Nature* 505 (2014) 195–198.
7. W.-J. Zou, Y.-B. Kim, S. Jung, Capacity fade prediction for vanadium redox flow batteries during long-term operations, *Appl. Energy* 356 (2024) 122329.
8. P. Leung, X. Li, C. Ponce de Leon, L. Berlouis, C.T.J. Low, F.C. Walsh, Progress in redox flow batteries, remaining challenges and their applications in energy storage, *RSC Adv.* 2 (2012) 10125–10156.

9. C. Ponce de Leon, A. Frias-Ferrer, J. Gonzalez-Garcia, D.A. Szanto, F.C. Walsh, Redox flow cells for energy conversion, *J. Power Sources* 160 (2006) 716–732.
10. Z. Huang, A. Mu, L. Wu, B. Yang, Y. Qian, J. Wang, Comprehensive analysis of critical issues in all-vanadium redox flow battery, *ACS Sustainable Chem. Eng.* 10 (2022) 7786–7810.
11. G.L. Soloveichik, Flow batteries: Current status and trends, *Chem. Rev.* 115 (2015) 11533–11558.
12. P. Leung, A.A. Shah, L. Sanz, C. Flox, J.R. Morante, Q. Xu, M.R. Mohamed, C. Ponce de León, F.C. Walsh, Recent developments in organic redox flow batteries: A critical review, *J. Power Sources* 360 (2017) 243–283.
13. L.F. Arenas, C. Ponce de León, F.C. Walsh, Redox flow batteries for energy storage: Their promise, achievements and challenges, *Curr. Opin. Electrochem*. 16 (2019) 117–126.
14. Z. Huang, A. Mu, L. Wu, H. Wang, Vanadium redox flow batteries: Flow field design and flow rate optimization, *J. Energy Storage* 45 (2022) 103526.
15. M. Aneke, M. Wang, Energy storage technologies and real life applications – A state of the art review, *Appl. Energy* 179 (2016) 350–377.
16. M.T. Castro, J.D. Ocon, Development of chemistry-specific battery energy storage system models using combined multiphysics and reduced order modeling, *J. Energ. Storage* 54 (2022) 105305.
17. Y. Zhang, J. Zhao, P. Wang, M. Skyllas-Kazacos, B. Xiong, R. Badrinarayanan, A comprehensive equivalent circuit model of all-vanadium redox flow battery for power system analysis, *J. Power Sources* 290 (2015) 14–24.
18. A. Bhattacharjee, A. Roy, N. Banerjee, S. Patra, H. Saha, Precision dynamic equivalent circuit model of a Vanadium Redox Flow Battery and determination of circuit parameters for its optimal performance in renewable energy applications, *J. Power Sources* 396 (2018) 506–518.
19. Z. Li, X. Fang, L. Cheng, X. Wei, L. Zhang, Techno-economic analysis of non-aqueous hybrid redox flow batteries, *J. Power Sources* 536 (2022) 231493.
20. A. Clemente, A. Cecilia, R. Costa-Castelló, Online state of charge estimation for a vanadium redox flow battery with unequal flow rates, *J. Energ. Storage* 60 (2023) 106503.
21. L.F. Arenas, C. Ponce de León, F.C. Walsh, Engineering aspects of the design, construction and performance of modular redox flow batteries for energy storage, *J. Energy Storage* 11 (2017) 119–153.
22. L.F. Arenas, C. Ponce de León, F.C. Walsh, Mass transport and active area of porous Pt/Ti electrodes for the Zn-Ce redox flow battery determined from limiting current measurements, *Electrochim. Acta* 221 (2016) 154–166.
23. A. Frías-Ferrer, I. Tudela, O. Louisnard, V. Sáez, M.D. Esclapez, M.I. Díez-García, P. Bonete, J. González-García, Optimized design of an electrochemical filter-press reactor using CFD methods, *Chem. Eng. J.* 69 (1–3) (2011) 270–281.
24. R. Gundlapalli, A. Bhattarai, R. Ranjan, P.C. Ghimire, X.M. Yeo, N.A.B. Zainudin, N. Wai, F. Mahlendorf, A. Jasincuk, H. Thorsten, Characterization and scale-up of serpentine and interdigitated flow fields for application in commercial vanadium redox flow batteries, *J. Power Sources* 542 (2022) 231812.
25. Q. Xu, T.S. Zhao, P.K. Leung, Numerical investigations of flow field designs for vanadium redox flow batteries, *Appl. Energy* 105 (2013) 47–56.
26. F. F. Rivera, L. Castañeda, P. E. Hidalgo, G. Orozco, Study of hydrodynamics at AsahiTM prototype electrochemical flow reactor, using computational fluid dynamics and experimental characterization techniques, *Electrochim. Acta* 245 (2017) 107–117.
27. F. F. Rivera, B. Miranda-Alcántara, G. Orozco, C. Ponce de León, L. F. Arenas, Pressure drop analysis on the positive half-cell of a cerium redox flow battery using computational fluid dynamics: Mathematical and modelling aspects of porous media, *Front. Chem. Sci. Eng.* 15 (2) (2021) 399–409.
28. F. F. Rivera, T. Pérez, L. F. Castañeda, J. L. Nava, Mathematical modeling and simulation of electrochemical reactors: A critical review, *Chem. Eng. Sci.* 239 (2021) 116622.

29. M. Macdonald, R.M. Darling, Comparing velocities and pressures in redox flow batteries with interdigitated and serpentine channels. *AIChE J*. 65 (2019) 16553.
30. A. Rodríguez, F.F. Rivera, G. Orozco, G. Carreño, F. Castañeda, Analysis of inlet and gap effect in hydrodynamics and mass transport performance of a multipurpose electrochemical reactor: CFD simulation and experimental validation, *Electrochim. Acta* 282 (2018) 520–532.
31. R. Cervantes-Alcalá, M. Miranda-Hernández, Flow distribution and mass transport analysis in cell geometries for redox flow batteries through computational fluid dynamics, *J. Appl. Electrochem*. 48 (11) (2018) 1243–1254.
32. M. Yue, J. Yan, H. Zhang, Q. Zheng, X. Li, The crucial role of parallel and interdigitated flow channels in a trapezoid flow battery, *J. Power Sources* 512 (2021) 230497.
33. J.T. López-Maldonado, S. Salazar-Colores, S. Piedra, F.F. Rivera, Effect of flow distributor configuration on the hydrodynamics in a multipurpose flow electrochemical reactor: Numerical analysis and experimental characterization employing digital image treatment, *Ind. Eng. Chem. Res*. 62 (2023) 3327–3337.
34. M. Messaggi, C. Gambaro, A. Casalegno, M. Zago, Development of innovative flow fields in a vanadium redox flow battery: Design of channel obstructions with the aid of 3D computational fluid dynamic model and experimental validation through locally-resolved polarization curves, *J. Power Sources* 526 (2022) 231155.
35. N. Gurieff, D.F. Keogh, M. Baldry, V. Timchenko, D. Green, I. Koskinen, C. Menictas, Mass transport optimization for redox flow battery design, *Appl. Sci*. 10 (2020) 2801.
36. M.I. León, L.F. Arenas, F.C. Walsh, J.L. Nava, Simulation of a vanadium-cerium redox flow battery incorporating graphite felt electrodes, *J. Electroanal. Chem*. 903 (2021) 115847.
37. V. Boovaragavan, A. Basha, A novel approach for computing tertiary current distributions based on simplifying assumptions, *J. Appl. Electrochem*. 36 (2006) 745–757.
38. J.W. Haverkort, A theoretical analysis of the optimal electrode thickness and porosity, *Electrochim. Acta* 295 (2019) 846–860.
39. A. Bhadra, J.W. Haverkort, The optimal electrode pore size and channel width in electrochemical flow cells, *J. Power Sources* 579 (2023) 233240.

CHAPTER 12

Flow Battery Dynamics

Analyzing Performance and Modeling

Barsha Rani Bora, Nitul Kalita, and Pintu Barman

12.1 INTRODUCTION

Flow batteries hold significant potential for large-scale energy storage, especially for intermittent power sources such as solar and wind farms, due to their unique advantages like location independence, scalability, and versatility. Effective performance evaluation and modeling are critical for advancing flow battery technology and overcoming the technical barriers that hinder widespread commercialization. The most utilized method for evaluating flow battery performance is the charging–discharging test. Recently, polarization and power density curves, commonly used for fuel cells, have also been employed in flow battery performance evaluation. However, while these curves provide beneficial information regarding voltage losses (voltage efficiency, VE), they are inadequate for comprehensive assessment as they do not account for coulombic efficiency (CE), energy efficiency (EE), utilization of electrolyte (UE), and capacity stability [1–3]. These parameters are critical for a thorough evaluation during the charging–discharging process, making the charging–discharging test the optimal method for flow battery performance evaluation. Although polarization curves can offer a rough performance evaluation, they fail to capture the critical factors necessary for an accurate assessment of flow batteries. In parallel, mathematical modeling and simulation play essential roles in understanding the complex electrochemical and transport behaviors within flow batteries. These tools are invaluable for predicting and improving cell performance across different system designs. A comprehensive study of state-of-the-art flow batteries reveals the physical and chemical processes involved, alongside the governing equations for the transport of mass, momentum, heat, and charge, as well as the electrochemical reactions in porous-medium models. Advanced simulation techniques, such as lattice Boltzmann method, molecular dynamics, density function simulations, and stack-level network models, further enhance the understanding and optimization of flow batteries [4]. This chapter aims to provide an in-depth analysis of

DOI: 10.1201/9781003506379-12

performance evaluation methods and modeling approaches for flow batteries, highlighting the current state of research and future directions for this promising technology.

12.2 BATTERY CONSTRUCTION AND ELECTROLYTE SYSTEM

The basic construction of flow batteries involves several essential components, including a membrane, electrodes, frames, and current collectors. Using the vanadium flow battery (VFB) as an example, we can illustrate this setup. The membrane, typically made of Nafion due to its high ionic conductivity and chemical stability, separates the positive and negative electrolyte solutions. Carbon felt electrodes, known for their substantial geometric surface area, are installed within frames that also function as seals, defining the battery's active area. These frames, filled with electrodes and the membrane, are then mounted between current collectors, often composed of graphite plates, ensuring efficient electron transfer. Proper compression of the electrode material is achieved using suitable gaskets, which help maintain the battery's integrity and performance. In the VFB, separate solutions containing vanadium ions in different oxidation states are utilized as the positive and negative electrolytes, facilitating the redox reactions necessary for energy storage and release [5].

12.3 PERFORMANCE EVALUATION OF FLOW BATTERIES

Flow batteries are promising for large-scale energy storage due to their long cycle life, high efficiency, and reliability. Various types, such as all-vanadium, iron-chromium, bromine-polysulfide, and zinc-bromine, have been developed, with ongoing research focused on material innovation and structural optimization. Reliable performance evaluation is essential, typically conducted through charge–discharge tests that measure four key characteristics: CE, VE, EE, and UE. Capacity fading, indicated by plotting UE against cycle number, reflects the battery's stability over time [6],

Polarization and power density curves, traditionally used in fuel cell evaluations, have recently been applied to flow batteries to improve performance by reducing polarization and increasing peak power density. Polarization curves reveal voltage loss mechanisms by displaying output voltage at specific current densities, while power density curves offer additional insights by linking voltage to current density. Although these methods have improved battery performance, their effectiveness for comprehensive flow battery evaluation still needs further investigation [7].

12.3.1 Charging–Discharging Performance

A typical plot of charging and discharging voltage versus time, as shown in Figure 12.1, provides a fundamental description of battery performance during the charging–discharging process. In Figure 12.1a, an increase in charging voltage and a decrease in discharging voltage, accompanied by reduced charging–discharging time, are observed with increasing current densities. This is primarily due to increased voltage losses at higher current densities. Based on the aforementioned definitions, the relative CE, VE, and UE for batteries can be roughly determined from this charge–discharge curve. These efficiencies are calculated

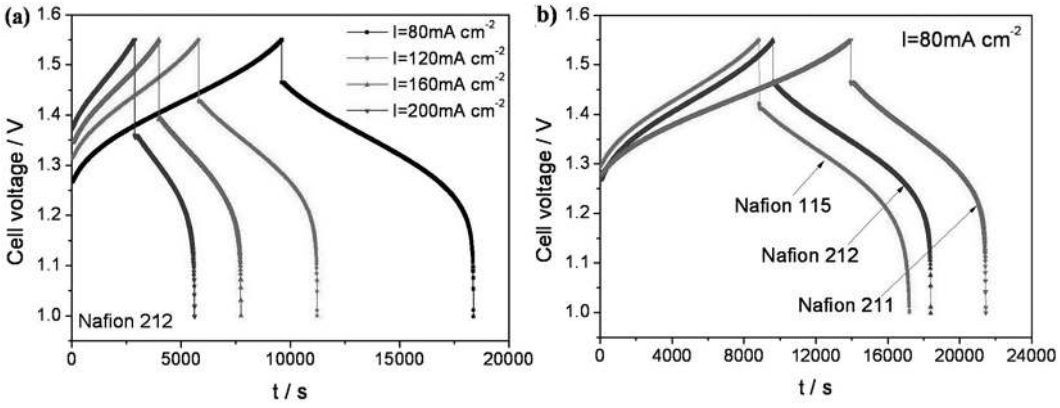

FIGURE 12.1 (a) Charging–discharging voltage curves at different current densities for Nafion 212, (b) Charging–discharging voltage curves of different membranes at the current density of 80 mA cm^{-2}. (Adapted with permission from [8], Copyright (2014), Elsevier.)

by the ratio of discharging time to charging time, the ratio of average discharging voltage to charging voltage, and the discharging time, respectively. Figure 12.1a illustrates the charge–discharge curve of a VFB, displaying the charging and discharging voltage curves for different current densities using Nafion 212. Figure 12.1b shows the charging and discharging voltage curves of different membranes at a current density of 80 mA cm^{-2} [8].

12.3.1.1 Coulombic Efficiency

Calculating the CE of flow batteries from a charge–discharge curve involves analyzing the total charge supplied during charging and the total charge extracted during discharging. CE is a measure of how effectively a battery converts charge input during charging to charge output during discharging. The key parameters needed from the charge–discharge curve include the charging current (I_{charge}), the charging time (t_{charge}), the discharging current ($I_{discharge}$), and the discharging time ($t_{discharge}$) [9].

The first step is to calculate the total charge supplied during the charging process, denoted as Q_{charge}. This is done using the formula,

$$Q_{\text{charge}} = I_{\text{charge}} \times t_{\text{charge}} \tag{12.1}$$

This equation accounts for the electrical charge introduced into the battery over the charging period. Similarly, the total charge extracted during the discharging process, $Q_{discharge}$, is calculated using,

$$Q_{\text{discharge}} = I_{\text{discharge}} \times t_{\text{discharge}} \tag{12.2}$$

This reflects the amount of electrical charge the battery releases during the discharging period. CE is then determined by the ratio of the total charge extracted during discharging

to the total charge supplied during charging, and it is expressed as a percentage. The formula for CE is,

$$\mathrm{CE} = \frac{Q_{\mathrm{discharge}}}{Q_{\mathrm{Charge}}} \times 100\% \tag{12.3}$$

By substituting the earlier expressions for Q_{charge} and $Q_{discharge}$, the formula becomes:

$$\mathrm{CE} = \frac{I_{\mathrm{discharge}} \times t_{\mathrm{discharge}}}{I_{\mathrm{charge}} \times t_{\mathrm{charge}}} \times 100\% \tag{12.4}$$

12.3.1.2 Voltage efficiency

VE in flow batteries is the ratio of average discharging voltage to charging voltage, reflecting energy losses from internal resistance and inefficiencies like activation and concentration overpotentials. It is calculated by analyzing the voltage profiles during charge–discharge cycles.

To begin, identify the average charging voltage (V_{charge}) and the average discharging voltage ($V_{discharge}$) from the charge–discharge curve. These values are typically obtained by averaging the voltage over the entire charging and discharging periods. The average charging voltage can be calculated using [10],

$$V_{\mathrm{charge}} = \frac{1}{t_{\mathrm{charge}}} \int_0^{t_{\mathrm{charge}}} V_{\mathrm{charge}}(t)\, dt \tag{12.5}$$

where V_{charge} is the instantaneous voltage at time t during the charging period. Similarly, the average discharging voltage is given by,

$$V_{\mathrm{discharge}} = \frac{1}{t_{\mathrm{discharge}}} \int_0^{t_{\mathrm{discharge}}} V_{\mathrm{discharge}}(t) dt \tag{12.6}$$

where $V_{discharge}$ is the instantaneous voltage at time t during the discharging period.

Once the average voltages are determined, VE is calculated as the ratio of the average discharging voltage to the average charging voltage, expressed as a percentage,

$$\mathrm{VE} = \frac{V_{\mathrm{discharge}}}{V_{\mathrm{charge}}} \times 100\% \tag{12.7}$$

VE in flow batteries can be improved by reducing cell resistance and using high-conductivity, electroactive electrode materials with a large surface area [11]. Graphite felt electrodes, known for their high surface area, are often used, and pretreating them enhances wettability and electrochemical activity by adding surface functional groups [12].

12.3.1.3 Energy Efficiency

EE in flow batteries measures the overall efficiency of converting electrical energy during charging and discharging. It is the product of CE and VE, considering both the charge–discharge process and voltage profiles [13].

$$\mathrm{EE} = \mathrm{CE} \times \mathrm{VE} \times 100\% \tag{12.8}$$

Maintaining high CE involves minimizing side reactions and self-discharge rates through optimized electrolyte composition, electrode materials, and operational parameters. Ongoing research enhances these factors, boosting overall EE in flow batteries.

12.3.2 Performance Parameters Obtained from Polarization Curve

Typical testing of modifications to redox flow batteries (RFBs) involves charge–discharge cycling to assess voltage, charge, and power efficiency. However, these cycling experiments do not directly reveal the specific mechanisms responsible for efficiency losses in RFBs. In contrast, polarization curves, commonly used in fuel cell studies, are effective tools for analyzing the losses within a cell. When combined with cell resistance measurements, polarization curves provide a clear method for identifying the primary limitations affecting performance [14].

In fuel cells, polarization curves highlight key losses: kinetic activation polarization from slow charge transfer at low current densities, ohmic polarization from ionic and electrical resistance, and concentration polarization at higher current densities due to limited mass transport. These losses overlap and affect overall efficiency but dominate in different regions of the curve, which is shown in Figure 12.2 [15].

- **Activation loss:** Activation loss, or activation overpotential, arises from slow electrochemical reaction kinetics at the electrode surfaces, particularly at low current densities. It depends on catalyst type, amount, temperature, and electrode surface area. Effective catalysts, like platinum, reduce activation loss by enhancing reaction rates, leading to a steep initial voltage drop on the polarization curve at low current densities [16].
- **Ohmic loss:** Ohmic loss, or ohmic overpotential, results from resistance to ion flow in the electrolyte and electron flow in the electrodes and cell components. It is proportional to current density and influenced by the conductivity of the electrolyte, electrode materials, and contact resistances. Represented as a linear segment in the midregion of the polarization curve, reducing ohmic losses involves enhancing conductivity and ensuring good component contact [17].
- **Transport loss:** Transport loss, or concentration polarization, occurs when reactant supply to reaction sites is insufficient at high current densities, leading to a steep voltage drop on the polarization curve. This loss is due to limited reactant flow rates,

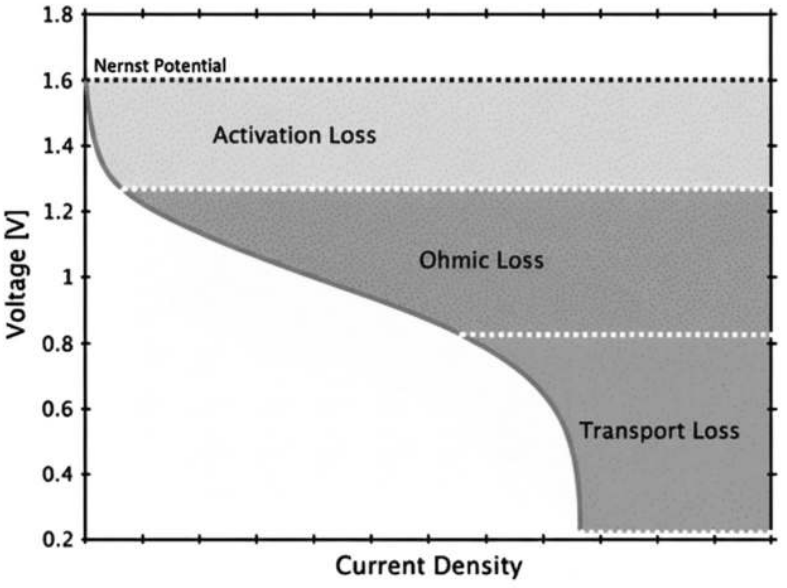

FIGURE 12.2 Generalized polarization curve for a RFB indicating the dominant source of overpotential in each region. (Adapted with permission from [15], Copyright (2011), Springer.)

poor diffusion through electrode materials, and reactant depletion. Improving mass transport involves optimizing flow field design, increasing reactant flow rates, and enhancing electrode material porosity [17].

12.3.3 Electrode Performance Parameter

Cyclic voltammetry (CV) is a vital technique used to assess the reaction kinetics of redox couples and evaluate the performance of electrodes in flow batteries. For instance, in a vanadium redox flow battery (VRFB), CV can provide detailed insights into the electrode's behavior. The CV curves typically show two distinct potential regions: the negative potential region, which corresponds to the V^{2+}/V^{3+} redox reaction, and the positive potential region, which pertains to the VO_2^+/VO_2^+ redox reaction [18].

In one study, the CV curves were compared for standard sulfuric acid electrolyte and a mixed acid electrolyte containing 6 M chloride ions. It was observed that the mixed electrolyte exhibited a higher peak current for the vanadium redox reactions, indicating enhanced reaction kinetics as shown in Figure 12.3a. This improvement is attributed to the superior fluidity of the mixed electrolyte although the reaction voltage for the redox couples in the mixed solution increased slightly compared to the standard sulfuric acid solution. Despite this, there was no significant difference in electrochemical reversibility between the two types of electrolytes.

Further investigation into the electrode performance revealed notable differences between carbon paper electrodes and those coated with biomass-derived activated carbon

(AC). The CV curves for AC-coated carbon paper displayed clear peaks for the V^{3+}/VO_2^+ redox couple, highlighting the superior catalytic activity of the AC coating that has been depicted in Figure 12.3b.

Studies on electrode compression in VRFBs have shown that optimizing the compression ratio can enhance performance. Park et al. [20] identified an optimal compression ratio for carbon felt electrodes, while Oh et al. [21] used simulations to analyze its impact on charging and discharging. Yoon et al. [22] investigated flow distribution related to electrode porosity. Increasing compression improves electron transfer and discharge performance, especially at high current densities, but excessive compression can reduce porosity, hinder electrolyte flow, and increase pumping losses. EE improves with up to 20% compression but declines beyond this point due to impaired electrolyte transport.

Optimizing the compression ratio of carbon felt electrodes can substantially enhance VRFB performance without additional costs, demonstrating the importance of electrode design and configuration in the overall efficiency of flow batteries. Figure 12.4 illustrating these findings provide visual confirmation of the trends discussed, underscoring the critical balance between electron transfer and electrolyte flow in determining battery performance.

12.3.4 Electrolyte Performance Parameter

Electrolyte flow characteristics are critical to redox flow battery performance, affecting reactant supply and participation in redox reactions. Uniform flow ensures even current density, while nonuniform flow degrades performance. The flow rate must be optimized;

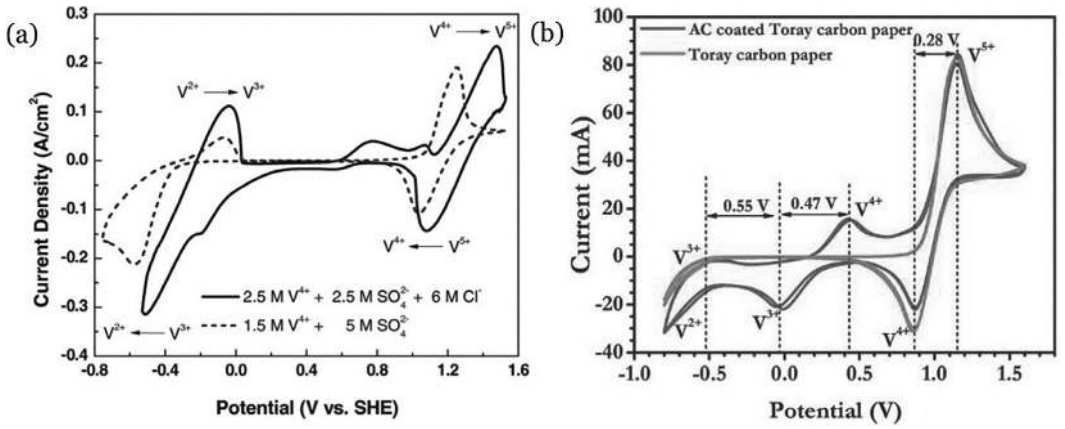

FIGURE 12.3 (a) Cyclic voltammograms recorded on a graphite felt electrode for both a standard sulfate VRFB electrolyte (comprising 1.5 M V^{4+} and 5.0 M SO_4^{2-}) and a mixed electrolyte solution (containing 2.5 M V^{4+}, 2.5 M SO_4^{2-}, and 6 M Cl^-) at a scan rate of 0.5 mV s^{-1}. (Adapted with permission from Reference [18], Copyright (2011), Wiley); (b) Cyclic voltammograms of Toray carbon sheets, both with and without mesoporous AC loading, in 4 M H_2SO_4 solutions containing 1.7 M $V^{3,5+}$, recorded at a scan rate of 5 mV s^{-1}. (Adapted with permission [19], Copyright (2015), Elsevier.)

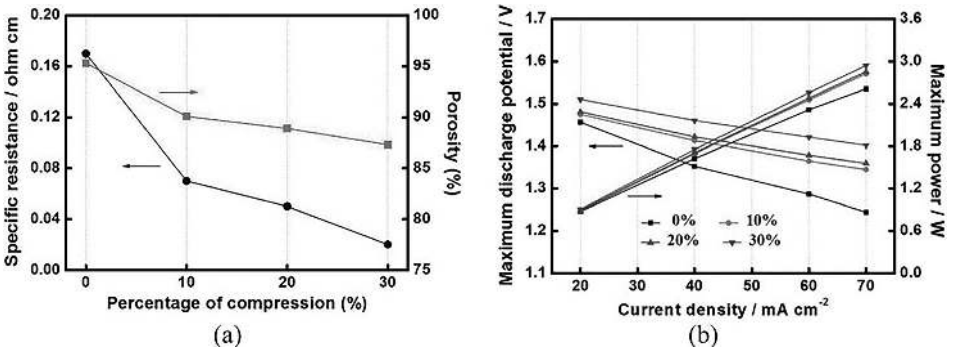

FIGURE 12.4 (a) Graph showing the relationship between specific resistance, porosity, and the compression percentage for FA-30A carbon felt electrodes. (b) Polarization curves of VRFB cells with electrodes compressed to different extents. (Adapted with permission from [20], Copyright (2014), Elsevier.)

too low underutilizes the electrolyte, while too high increases pumping losses, reducing efficiency [23]. The theoretical flow rate can be calculated as follows.

$$Q_{\text{theo}} = \frac{I}{n \times F \times C \times \text{SOC}_{\text{min}}} \tag{12.9}$$

where "I" represents the current, "n" denotes the number of electrons involved in the reaction (1 for vanadium flow batteries), "C" is the total concentration of metal ion in each reservoir (concentration of vanadium for VRFB), and "SOC_{min}" is the minimum state of charge, typically set at 20%.

The stoichiometric number, λ, is defined as the ratio of the actual flow rate to the theoretical flow rate. As illustrated in Figure 12.5, an increase in the stoichiometric number leads to a longer charge–discharge cycle time. This extension can be attributed to the increased capacity of the redox flow battery, indicating that the battery can store more energy.

12.3.4.1 Limiting Current Density

Limiting current density is a crucial metric for assessing the performance of flow batteries. A higher current density facilitates rapid electrochemical reactions and shortens charging time. Newman et al. [25] proposed the following model to describe limiting current density,

$$i_{\text{lim}} = 0.9783 \frac{nFDc}{L} \int_0^L \left(\frac{U_f}{hDX} \right)^{1/3} dX \tag{12.10}$$

The limiting current density of an electrolyte flowing between a flat plate and an electrode, as described by Newman's model (Figure 12.6a), is influenced by several factors: the number of electrons transferred (n), the diffusion coefficient (D), the bulk electrolyte

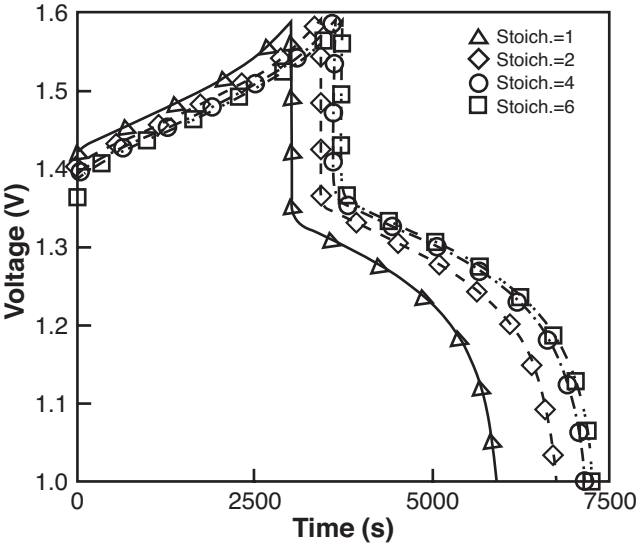

FIGURE 12.5 Variation of charge–discharge curve with various flow rates at 75 mA cm^{-2} of current density. Adapted with permission from [24], Copyright (2018), Elsevier.

concentration (c), the length of the flow channel (L), the average electrolyte flow velocity (u_f), and the distance between the electrode and the flat plate (h). As depicted in Figure 12.6b, the electrolyte flow evolves from an entrance profile to a fully developed one. Due to the porous electrode's low permeability, the flow velocity within it is significantly lower than in the flow channel. This limited penetration of electrolyte into the porous electrode impacts reactant availability and, subsequently, cell performance. As shown in Figure 12.6c, Newman's model assumes no electrolyte penetration into the electrode surface. The maximum current density, which is dominated by the stoichiometric availability of reactant in the porous electrode, is illustrated in Figure 12.6d and can be expressed in the corresponding equation below,

$$i_{\max} = \frac{nFcQ_p}{A} \tag{12.11}$$

The volumetric flow of electrolyte reactant penetrating through the interface between the flow channel and the porous electrode is denoted as Q_p, while A represents the cross-sectional area of the porous electrode perpendicular to the current direction. The entrance flow rate for a "flow-by" type system is higher than that of a "flow-through" type. Increasing the entrance flow rate enhances the penetration of electrolyte into the porous electrode by reducing the diffusion boundary layer, which in turn increases the maximum current density as described by the aforementioned equation. Ke et al. [26] have demonstrated the behavior of VRFB discharge polarization curves under varying flow field and flow rate conditions.

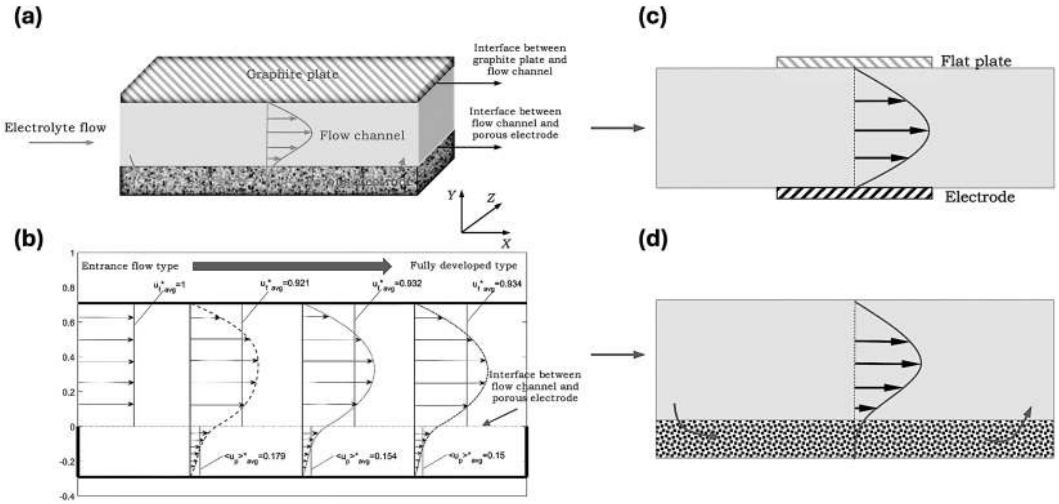

FIGURE 12.6 (a) Schematic of electrolyte flow through a single flow channel and across the porous electrode in RFBs. (b) Two-dimensional flow distributions within the layered flow channel-porous electrode system. (c) Scenario where current density is limited by the diffusion boundary layer between a flat plate and an electrode, preventing electrolyte reactant penetration. (d) Scenario where current density is limited by the stoichiometric availability of electrolyte reactants penetrating the porous electrode from the flow channel. (Adapted with permission from [26], Copyright (2018), Royal Society of Chemistry.)

12.4 MODELING OF FLOW BATTERIES

Flow batteries are ideal for large-scale energy storage but faces commercialization challenges requiring advanced modeling. This chapter reviews flow battery technologies, focusing on electrochemical and transport behaviors, key governing equations, and advanced modeling techniques like lattice Boltzmann and molecular dynamics.

12.4.1 Porous-Medium Models

Porous-medium models in flow batteries simulate the complex interactions within the porous electrodes, capturing the transport of fluids, ions, and heat. These models are critical for understanding how the porous structure influences overall battery performance.

12.4.1.1 Governing Equations

The governing equations for porous-medium models describe the transport properties, including fluid flow, mass transfer, and electrochemical reactions. These equations help in deriving key parameters that are essential for accurate modeling and optimization of flow batteries.

12.4.1.1.1 Assumption and Simplification Here are the common simplifications and assumptions used to streamline the process of solving numerical models,

1. Side reactions, including oxygen and hydrogen evolutions, are ignored.
2. The entire domain is under isothermal conditions.
3. The membrane is considered impermeable to all species and ions except protons.
4. Ionic interactions within the electrolyte are disregarded in the transport analysis.

12.4.1.1.2 Conservation Equations for Fluid Flow The macroscopic superficial velocity of the electrolyte, within the porous electrode can be described using Darcy's law [27],

$$\frac{m}{K}\vec{u} = -p \tag{12.12}$$

Here, n represents the kinematic viscosity, K is the permeability coefficient, and p denotes pressure. The permeability of a porous medium depends on the properties of the material.

The liquid pressure is determined using an overall mass balance as follows,

$$\nabla \cdot \vec{u} = 0 \tag{12.13}$$

Combining Equations (12.12) and (12.13), we can obtain,

$$-\frac{K}{\nu\rho}^{2} p = 0 \tag{12.14}$$

In practical operations, when the SOC exceeds 0.85, side reactions are likely to occur [28]. If these side reactions, particularly oxygen evolution at the positive electrode and hydrogen evolution at the negative electrode during charging, are considered, the flow equations need to be reformulated as follows,

$$\overrightarrow{u_l} = -K\frac{k_{rl}}{\mu_l}\nabla p_l\left(\text{liquid phase}\right) \tag{12.15}$$

$$\overrightarrow{u_g} = -K\frac{k_{rg}}{\mu_g}\nabla p_g\left(\text{liquid phase}\right) \tag{12.16}$$

Here, the subscripts 'l' and 'g' denote the properties of the liquid and gas phases, respectively. The term k_r refers to the relative permeability of a phase, which depends solely on phase saturation.

12.4.1.1.3 Conservation Equations for Mass Transport The transport equation for ion i within the electrolyte is given as,

$$\frac{\partial C_i}{\partial t} = \nabla \cdot \left(D_i^{\text{eff}} \nabla C_i \right) + \frac{Fz_i}{RT} \nabla \cdot \left(D_i^{\text{eff}} C_i \nabla \phi_S \right) - \nabla \cdot \left(\vec{u} C_i \right) + S_i \tag{12.17}$$

where D_i^{eff} represents the effective diffusivity of species i within the porous electrode, and S_i represents the source term arising from chemical or electrochemical reactions. The effective diffusivity is a combination of stagnant and dispersion diffusivity, formulated as follows [29,30],

$$D_i^{\text{eff}} = (0.6 \sim 0.8) D_i + 0.1\ d_p u \tag{12.18}$$

Or

$$\frac{D^{\text{eff}}}{D} = \varepsilon^{1.1} (1 + 1.46 \times 10^{-3} Pe^2) \tag{12.19}$$

where D_i denotes the intrinsic diffusivity of species i, and d_p stands for pore diameter.

The rate at which reactants (or products) are transferred to (or from) the pore walls within the electrode's pore space can be characterized as,

$$N_i = k_m \left(c_i - c_i^s \right) \tag{12.20}$$

Here, c_i^s denotes the concentration at the pore wall, c_i represents the concentration in the bulk of the pore space, and k_m is the local mass transport coefficient. The coefficient k_m is influenced by the pore wall morphology, the properties of the electrolyte, and the local electrolyte velocity.

12.4.1.1.4 Conservation Equations for Heat Transport The balance of energy considers convective heat transfer, heat conduction, and heat generated by electrochemical reactions and Joule heating. To simplify, the temperature is presumed to be uniform across the solid and liquid phases in the electrodes. The balance of energy is expressed as follows [31],

$$\frac{\partial}{\partial t} \left(\overline{\rho C_p} T \right) + \nabla . \left(\vec{u} \overline{\rho C_p} T \right) = \overline{\lambda} \nabla^2 T + \sum_k Q_k \tag{12.21}$$

where $\overline{\rho C_p}$ represents the volume-averaged thermal capacity, $\overline{\lambda}$ denotes the volume-averaged thermal conductivity, and Q_k is the source term.

It is crucial to note that the second simplification and assumption mentioned in Section 12.4.1.1 is only applicable when both the flow rate and the reservoir are adequately large. If not, the isothermal condition cannot be sustained, and the thermal effects throughout operation must be considered.

12.4.1.2 Determinations of Transport Properties

The interactions between transport of mass, heat transfer, fluid flow, and the kinetics of electrochemical process in a flow battery are closely interconnected. Critical factors, including the permeability of the porous electrode, effective ion diffusivities in both the membrane and porous electrode, electrolyte viscosity, and ionic interaction coefficients, play a substantial role in these interrelated processes and affect the overall performance of the RFBs.

12.4.1.2.1 Transport Properties in Porous Electrodes In flow batteries, porous materials serve as electrodes where electrochemical reactions occur, with reactants passing through the pores and reacting on the surfaces. The reaction rate is influenced by the specific surface area of the pores, while flow resistance is determined by pore size distribution and electrode permeability. Permeability, a critical factor for modeling flow in porous media, depends on pore size and tortuosity and can be perceived as the effective channel cross-section for fluid flow.

Various methods, including Ergun-like relationships and numerical simulations, have been used to determine permeability, though practical implementation remains challenging. Numerical simulations offer an alternative, accounting for fine-scale heterogeneities, in terms of effective permeability, becoming relevant when the averaging scale is large relative to heterogeneity. However, equivalent permeability varies with flow conditions in smaller averaging scales. Numerical methods by White and Horne [31] and Durlofsky [32] provide approaches to determining equivalent permeability tensors but have limitations.

Accurate determination of effective diffusivity in porous electrodes is essential for effective modeling. The Bruggemann correction [33] is commonly used but overlooks structural differences in porous materials. Experimental methods, such as UV/V spectroscopic measurements, often ignore dispersion effects. Carrigy et al. [34] addressed this through a 'diffusion bridge' configuration, while Xu and Zhao [4] used electrochemical methods to determine effective diffusivity in VRFBs. They found that at low flow rates, dispersion effects were minimal, but at higher rates, dispersion became significant, suggesting that enhancing vanadium ion diffusivity could improve cell performance at the same flow rate.

12.4.1.2.2 Ions Transport Properties through Membranes Nearly all rechargeable batteries experiences loss of energy capacity after extended charge–discharge cycles. One of the primary causes of this decay is 'self-discharge,' particularly the ions crossover through the membrane. The crossover flux can be described as,

$$\overrightarrow{N_{i,\,\mathrm{mem}}} = -D_{i,\mathrm{mem}}^{\mathrm{eff}} \nabla c_i - F z_i c_i \frac{D_{i,\,\mathrm{mem}}^{\mathrm{eff}}}{RT} \nabla \phi_{\mathrm{mem}} - \frac{K_{\mathrm{mem}}}{\nu M_i} \nabla p \tag{12.22}$$

In the above expression, the right-hand side includes three terms: diffusion flux, migration flux, and convection flux, each indicated by the subscript '*mem*' to denote membrane-related properties. The diffusion rate is driven by the gradient of concentration across the membrane, the rate of migration is influenced by the electric field, and the convection rate is affected by the difference in pressure.

12.4.1.2.3 Transport Properties of Electrolytes In the conventional flow batteries, the transport properties of electrolytes, including ion mobility and diffusion, significantly influence the system's performance. Variations in ion concentration during charge–discharge cycles affect electrolyte viscosity, impacting flow dynamics and pressure drop.

12.4.1.2.3.1 The Variation of Electrolyte Viscosity with SOC In flow batteries, the electrolyte viscosity is crucial for determining both the pressure drop across the electrode and the local velocity. In flow batteries, the electrolyte concentration periodically fluctuates with SOC during charge–discharge cycles, leading to variations in electrolyte viscosity. For instance, in a VRFB, changes in the concentrations of V^{2+}, VO^{2+}, V^{3+}, VO^{2+}, and H^{+} ions during charging illustrate this effect.

Hu et al. were the first to use the semi-ideal hydration model and Eyring's absolute rate theory to examine the mixing behavior of electrolyte viscosities under isopiestic equilibrium. Their method estimates the mixed electrolyte viscosity by using the viscosities of binary solutions (i-H_2O). Eyring's theory allows the viscosity of an electrolyte solution to be calculated as follows,

$$\ln \nu_{\text{mix}} = \sum_i \chi_i \ln \nu_i^{\text{pure}} + \chi_w \ln \nu_w^{\text{pure}} + \frac{1}{RT} \nabla G^{\neq} \tag{12.23}$$

where ν represents the kinematic viscosity, and χ_i is the mole fraction.

$$\chi_i = \frac{m_i}{\left(\left(1000/M_w\right) + \sum_{i=1}^{n} m_i\right)} \tag{12.24}$$

where m_i is the molality in mol/kg, and $\nabla G^{\neq}$ represents the molar excess activation free energy.

$$\nabla G^{\neq} = \beta RT \sum z_i \chi_i \ln a_i \tag{12.25}$$

where β is a unique constant for nonideal solutions specific to the system, and z_i and a_i are the stoichiometric coefficient and activity of the component, respectively.

12.4.1.2.3.2 Ionic Interactions in Electrolytes The frequently used Nernst-Planck equation in its fundamental structure often neglects ionic interactions by disregarding cross-coefficients. However, experimental data indicate that these coefficients can be quite significant, particularly in concentrated electrolytes, making it necessary to include ionic interactions for a more accurate representation. The flux term N_i encompasses both the individual movement of ion i and its interactions with other ions and can be constructed as follows:

$$\overrightarrow{N_i} = -D_i^{\text{eff}} \nabla c_i - F z_i c_i \frac{D_i^{\text{eff}}}{RT} \nabla \phi_s + \vec{u} c_i - \sum_{k=1,\, k \neq i}^{n} L_{ik} \nabla \mu_k \tag{12.26}$$

The terms represented on the right-hand side correspond to different flux contributions: diffusion, migration, convection, and ionic interaction, in that order. Here, μ_k refers to the chemical potential of ion k, while L_{ik} represents the cross-coefficient that indicates the drag on species i caused by the thermodynamic force from ion k. The resulting transport equation for ion "i" is then expressed as follows:

$$\frac{\partial c_i}{\partial t} = \nabla . \left(D_i^{\text{eff}} \nabla c_i \right) + \frac{F z_i}{RT} \nabla . \left(D_i^{\text{eff}} c_i \nabla \phi_s \right) - \nabla . \left(\vec{u} c_i \right) + \nabla . \left(\sum_{k=1,\, k \neq i}^{n} L_{ik} \nabla \mu_k \right) + S_i \tag{12.27}$$

where S_i represents the source term arising from electrochemical or chemical reactions.

The cross-coefficient L_{ik} is challenging to determine. To address this, an additional variable r_i is introduced to encapsulate the contribution of all cross-coefficients to the flux density N_i,

$$r_i = \nabla \cdot \left(\sum_{k=1,\, k \neq i}^{n} L_{ik} \nabla \mu_k \right) \tag{12.28}$$

The variables r_i are measured by minimizing their magnitude under a specific constraint condition.

12.4.2 Lattice Boltzmann Method

The lattice Boltzmann method is a discrete numerical approach based on the Boltzmann equation, where the primary focus is on the distribution of particle velocity function. The distribution function for particle velocity evolved using an update equation, which subsequently allows the calculation of macroscopic quantities such as density and velocity. The lattice Boltzmann method has acquired popularity for investigating transport phenomena within porous media. For instance, Cheng and Hao [35] used the multiphase free-energy lattice Boltzmann method to simulate wettability effects on liquid transport in porous carbon paper, revealing its significant impact on water saturation in two-phase flow. Additionally, the lattice Boltzmann method has been employed to simulate in-plane and through-plane permeability in anisotropic porous materials and random porous media. Van Doormaal et al. [36] used lattice Boltzmann method with a Monte Carlo method to determine permeability, finding that fiber arrangement significantly affects porous layer permeability. Kolyukhin and Espedal [37] improved computational efficiency by simulating effective permeability with double randomization Monte Carlo method. More recently, Qiu et al., Bevilacqua et al., and Zhang et al. [38–40] utilized X-ray computed tomography to model electrolyte flow in a VRFB, combining lattice Boltzmann method for pore-scale

flow with the finite volume method for species and charge transport, providing insights into the structure-property-performance relationship in flow batteries.

12.4.3 Molecular Dynamics and Density Function Simulations

To grasp the chemistry behind flow batteries, molecular and atomic simulations such as density functional theory and molecular dynamics are often employed. Yang and Vijayakumar et al. used MD modeling to identify the V^{5+} species as $[VO_2(H_2O)_3]^+$, a finding initially observed experimentally by Mohammadi s et al. [41]. They observed that this complex loses stability at high temperatures, leading to V^{5+} precipitation because of the deprotonation of the penta-coordinated vanadium ion. At high concentration of acid, this deprotonation can be prevented, stabilizing the V^{5+} solution. Recently, the same researchers used nuclear magnetic resonance spectroscopy and DFT modeling to examine the structure of V^{3+} in vanadium chloride and sulfate mixtures. Their study indicated that counter anions like sulfate and chloride significantly impact the stability of the V^{3+} electrolyte, with precipitation reactions influenced by the vanadium-to-proton ratio and solution temperature. While molecular and atomic simulations are important for understanding material structures, they do not predict macroscopic behavior. Therefore, integrating these methods with macroscopic models is recommended for comprehensive flow battery analysis.

12.4.4 Stack-Level Network Models

To effectively model flow battery systems for control and monitoring, simplified models are crucial because of the complexity of detailed transport processes and electrochemical kinetics. These models, known as stack- or unit-level network models, focus on cell performance and system efficiency rather than detailed variable distributions. Common assumptions include uniform electrolyte concentrations, continuous stirred tank reactor behavior for cells and tanks, and constant cell resistance. Shah et al. [42] developed a unit model for all VRFBs that addresses voltage loss, electrode kinetics, and electrolyte recirculation, linking performance metrics like charge/discharge time and state of charge (SOC) to system properties with high accuracy in practical simulations.

Xu and Zhao [4] proposed a power-based efficiency metric to evaluate flow field designs, finding that serpentine flow fields offer higher energy-based and round-trip efficiency compared to parallel fields. Tang et al. [43] developed a 3D model for VRBs with interdigitated flow channels, identifying flow rate and channel dimensions as critical factors for performance optimization. Scamman and Roberts [44] utilized a utility-scale model to forecast the performance of a large-scale PSB storage plant, recommending electrolyte flow rate and current density ranges for economic viability. Addressing shunt currents, which can divert current away from intended paths, Xing and Zhang [45] analyzed losses in VRFBs and suggested reducing series-wound cells and improving manifold and channel resistance. Codina et al. [46] examined shunt currents in Cr/Fe flow batteries, highlighting the impact of hydraulic interconnection length and assembly current on EE.

Tang et al. [43] created a network model to explore how temperature changes affect a VRFB stack. Their model features a configuration of nineteen cells and two cylindrical

tanks for the electrolyte. It encompasses energy balance equations for both the electrolyte tanks and the battery stack, which can be represented by the following equations:

$$\frac{\partial}{\partial t}\left(\rho V_s C_p T_s\right) = Q_+ C_p \rho\left(T_+ - T_s\right) + Q_- C_p \rho\left(T_- - T_s\right) + I^2 R \tag{12.29}$$

$$\frac{\partial}{\partial t}\left(\rho V_+ C_p T_+\right) = Q_+ C_p \rho\left(T_s - T_+\right) + U_+ A_+ \left(T_{\text{air}} - T_+\right) \tag{12.30}$$

$$\frac{\partial}{\partial t}\left(\rho V_- C_p T_-\right) = Q_- C_p \rho\left(T_s - T_-\right) + U_- A_- \left(T_{\text{air}} - T_-\right) \tag{12.31}$$

The model proposed by Tang and Skyllas-Kazacos includes variables such as temperatures of the stack electrolyte (T_s), positive and negative electrolytes in tanks (T^+ and T^-), ambient air temperature (T_{air}), volumes of the stack, and electrolytes (V_s, V^+, and V^-). It also considers flow rates (Q^+ and Q^-), and heat transfer characteristics and surface area of the tanks (U^+, U^-, A^+, and A^-). The study shows that electrolyte temperatures in the stack and tanks are affected by the current, flow rates, ambient temperature, and heat from cell resistance.

12.5 OVERVIEW AND FUTURE DIRECTIONS

Flow batteries offer an optimal balance of EE, cost-effectiveness, and cycle life, making them a focal point of research for many years. This chapter reviewed the key governing equations related to mass, momentum, heat, charge transport, and electrochemical reactions, alongside discussions on porous-medium models, Lattice Boltzmann methods, molecular dynamics, density function simulations, and stack-level network models.

To advance modeling technologies beyond common simplifications, future efforts should focus on a few key areas:

1. A deeper understanding of redox reaction kinetics on porous electrode surfaces, moving beyond simplified overall reactions to detailed, step-by-step descriptions.
2. Sensitivity analysis to identify parameters with the most significant impact on performance of flow batteries.
3. Detailed investigation of heat and mass transfer in full-scale flow battery stacks, aiding in optimizing stack structures and temperature control.
4. Multiscale modeling that integrates macro and microscale physicochemical processes for a comprehensive understanding.

These advancements in modeling, paired with experimental diagnostics, will enhance the understanding of transport and electrochemical processes, leading to optimized designs, improved operational strategies, and reduced costs, thus accelerating the global adoption of flow battery technologies.

REFERENCES

1. M. Kim, G. Zhang, S. Jang, S. Lee, Z. Suo, S. M. Kim, Fatigue-Resistant Polymer Electrolyte Membranes for Fuel Cells. *Adv Mater*, **2024**, *36*, 2308288.
2. Y. Luo, K. Li, Y. Hu, T. Chen, J. Hu, J. Feng, J. Feng, Boosting the Performance of Low-Platinum Fuel Cells via a Hierarchical and Interconnected Porous Carbon Support. *ACS Appl Mater Interfaces*, **2024**, 16, 4811–4817.
3. D. Siegmund, S. Metz, V. Peinecke, T. E. Warner, C. Cremers, A. Grevé, T. Smolinka, D. Segets, U. P. Apfel, Crossing the Valley of Death: From Fundamental to Applied Research in Electrolysis. *JACS Au*, **2021**, 1, 527–535.
4. Q. Xu, T. S. Zhao, Fundamental Models for Flow Batteries. *Prog Energy Combust Sci*, **2015**, 49, 40–58.
5. Z. Huang, A. Mu, L. Wu, B. Yang, Y. Qian, J. Wang, Comprehensive Analysis of Critical Issues in All-Vanadium Redox Flow Battery. *ACS Sustain Chem Eng*, **2022**, 10, 7786–7810.
6. K. Amini, J. Gostick, M. D. Pritzker, Metal and Metal Oxide Electrocatalysts for Redox Flow Batteries. *Adv Funct Mater*, **2020**, 30, 1910564.
7. O. Nolte, I. A. Volodin, C. Stolze, M. D. Hager, U. S. Schubert, Trust Is Good, Control Is Better: A Review on Monitoring and Characterization Techniques for Flow Battery Electrolytes. *Mater Horizons*, **2021**, 8, 1866–1925.
8. Q. Zheng, F. Xing, X. Li, T. Liu, Q. Lai, G. Ning, H. Zhang, Investigation on the Performance Evaluation Method of Flow Batteries. *J Power Sources*, **2014**, 266, 145–149.
9. H. D. Yoo, Y. Liang, Y. Li, Y. Yao, High Areal Capacity Hybrid Magnesium-Lithium-Ion Battery with 99.9% Coulombic Efficiency for Large-Scale Energy Storage. *ACS Appl Mater Interfaces*, **2015**, 7, 7001–7007.
10. K. Likit-Anurak, K. Uthaichana, K. Punyawudho, Y. Khunatorn, The Performance and Efficiency of Organic Electrolyte Redox Flow Battery Prototype. *Energy Procedia*, **2017**, 118, 54–62.
11. Y. Huang, L. Zhi, R. Bi, Z. Yuan, X. Li, Perspectives on Zinc-Based Flow Batteries. *Fundam Res*, **2024**. https://doi.org/10.1016/j.fmre.2024.06.002
12. E. Ventosa, O. Amedu, W. Schuhmann, Aqueous Mixed-Cation Semi-Solid Hybrid-Flow Batteries. *ACS Appl Energy Mater*, **2018**, 1, 5158–5162.
13. S. Zhao, T. Liu, Y. Zuo, M. Wei, J. Wang, Z. Shao, D. Y. C. Leung, T. Zhao, M. Ni, High-Power-Density and High-Energy-Efficiency Zinc-Air Flow Battery System for Long-Duration Energy Storage. *Chem Eng J*, **2023**, 470, 144091.
14. J. Sun, Z. Guo, L. Pan, X. Fan, L. Wei, T. Zhao, Redox Flow Batteries and Their Stack-Scale Flow Fields. *Carbon Neutrality*, **2023**, 2, 1–33.
15. D. Aaron, Z. Tang, A. W. Papandrew, T. A. Zawodzinski, Polarization Curve Analysis of All-Vanadium Redox Flow Batteries. *J Appl Electrochem*, **2011**, 41, 1175–1182.
16. Z. Li, Z. Zheng, L. Xu, X. Lu, A Review of the Applications of Fuel Cells in Microgrids: Opportunities and Challenges. *BMC Energy*, **2019**, 1, 1–24.
17. M. Jouin, R. Gouriveau, D. Hissel, M. C. Péra, N. Zerhouni, Prognostics and Health Management of PEMFC - State of the Art and Remaining Challenges. *Int J Hydrogen Energy*, **2013**, 38, 15307–15317.
18. L. Li, S. Kim, W. Wang, M. Vijaykumar, Z. Nie, B. Chen, J. Zhang, G. Xia, J. Hu, G. Graph, J. Liu, Z. Yang, A Stable Vanadium Redox-Flow Battery with High Energy Density for Large-Scale Energy Storage. *Adv Energy Mater*, **2011**, 1, 394–400.
19. M. Ulaganathan, A. Jain, V. Aravindan, S. Jayaraman, W. C. Ling, T. M. Lim, M. P. Srinivasan, Q. Yan, S. Madhavi, Bio-Mass Derived Mesoporous Carbon as Superior Electrode in All Vanadium Redox Flow Battery with Multicouple Reactions. *J Power Sources*, **2015**, 274, 846–850.

20. S. K. Park, J. Shim, J. H. Yang, C. S. Jin, B. S. Lee, Y. S. Lee, K. H. Shin, J. D. Jeon, The Influence of Compressed Carbon Felt Electrodes on the Performance of a Vanadium Redox Flow Battery. *Electrochim Acta*, **2014**, 116, 447–452.
21. K. Oh, S. Won, H. Ju, Numerical Study of the Effects of Carbon Felt Electrode Compression in All-Vanadium Redox Flow Batteries. *Electrochim Acta*, **2015**, 181, 13–23.
22. S. J. Yoon, S. Kim, D. K. Kim, Optimization of Local Porosity in the Electrode as an Advanced Channel for All-Vanadium Redox Flow Battery. *Energy*, **2019**, 172, 26–35.
23. A. Karrech, K. Regenauer-Lieb, F. Abbassi, Vanadium Flow Batteries at Variable Flow Rates. *J Energy Storage*, **2022**, 45, 103623.
24. D. K. Kim, S. J. Yoon, J. Lee, S. Kim, Parametric Study and Flow Rate Optimization of All-Vanadium Redox Flow Batteries. *Appl Energy*, **2018**, 228, 891–901.
25. J. Newman, K. E. Thomas-Alyea, *Electrochemical Systems*, 3rd ed. Hoboken: Wiley; **2004**. 647 p.
26. X. Ke, J. M. Prahl, J. I. D. Alexander, J. S. Wainright, T. A. Zawodzinski, R. F. Savinell, Rechargeable Redox Flow Batteries: Flow Fields, Stacks and Design Considerations. *Chem Soc Rev*, **2018**, 47, 8721–8743.
27. H. Al-Fetlawi, A. A. Shah, F. C. Walsh, Modelling the Effects of Oxygen Evolution in the All-Vanadium Redox Flow Battery. *Electrochim Acta*, **2010**, 55, 3192–3205.
28. A. Amiri, K. Vafai, Transient Analysis of Incompressible Flow through a Packed Bed. *Int J Heat Mass Transfer*, **1998**, 41, 4259–4279.
29. Q. Xu, T. S. Zhao, Determination of the Mass-Transport Properties of Vanadium Ions through the Porous Electrodes of Vanadium Redox Flow Batteries. *Phys Chem Chem Phys*, **2013**, 15, 10841–10848.
30. H. Al-Fetlawi, A. A. Shah, F. C. Walsh, Non-Isothermal Modelling of the All-Vanadium Redox Flow Battery. *Electrochim Acta*, **2009**, 55, 78–89.
31. C. D. White, R. N. Horne, Computing Absolute Transmissibility in the Presence of Fine-Scale Heterogeneity. *SPE Reservoir Simulation Conference*, SPE–16011, San Antonio, Texas, February **1987**.
32. L. J. Durlofsky, Numerical Calculation of Equivalent Grid Block Permeability Tensors for Heterogeneous Porous Media. *Water Resour Res*, **1991**, 27, 699–708.
33. M. W. Verbrugge, R. F. Hill, Ion and Solvent Transport in Ion-Exchange Membranes: I. A Macrohomogeneous Mathematical Model. *J Electrochem Soc*, **1990**, 137, 886.
34. N. B. Carrigy, L. M. Pant, S. Mitra, M. Secanell, Knudsen Diffusivity and Permeability of PEMFC Microporous Coated Gas Diffusion Layers for Different Polytetrafluoroethylene Loadings. *J Electrochem Soc*, **2013**, 160, F81.
35. L. Hao, P. Cheng, Lattice Boltzmann Simulations of Anisotropic Permeabilities in Carbon Paper Gas Diffusion Layers. *J Power Sources*, **2009**, 186, 104–114.
36. M. A. Doormaal, J. G. Pharoah, Determination of Permeability in Fibrous Porous Media Using the Lattice Boltzmann Method with Application to PEM Fuel Cells. *Int J Numer Methods Fluids*, **2009**, 59, 75–89.
37. D. Kolyukhin, M. Espedal, Numerical Calculation of Effective Permeability by Double Randomization Monte Carlo Method. *Int J Numer Anal Model*, **2010**, 7, 607–618.
38. G. Qiu, A. S. Joshi, C. R. Dennison, K. W. Knehr, E. C. Kumbur, Y. Sun, 3-D Pore-Scale Resolved Model for Coupled Species/Charge/Fluid Transport in a Vanadium Redox Flow Battery. *Electrochim Acta*, **2012**, 64, 46–64.
39. N. Bevilacqua, L. Eifert, R. Banerjee, K. Koble, T. Farago, M. Zuber, A. Bazylak, R. Zeis, Visualization of electrolyte flow in vanadium redox flow batteries using synchrotron X-ray radiography and tomography – Impact of electrolyte species and electrode compression. *J Power Sources*, **2019**, 439, 227071

40. D. Zhang, Q. Cai, O. O. Taiwo, V. Yufit, N. P. Brandon, S. Gu, The effect of wetting area in carbon paper electrode on the performance of vanadium redox flow batteries: A three-dimensional lattice Boltzmann study. *Electrochim. Acta*, **2018**, 283, 1806.
41. T. Mohammadi, S. C. Chieng, M. S. Kazacos, Water Transport Study across Commercial Ion Exchange Membranes in the Vanadium Redox Flow Battery. *J Membr Sci*, **1997**, 133, 151–159.
42. A. A. Shah, R. Tangirala, R. Singh, R. G. A. Wills, F. C. A. Walsh, Dynamic Unit Cell Model for the All-Vanadium Flow Battery. *J Electrochem Soc*, **2011**, 158, A671.
43. A. Tang, J. Bao, M. S. Kazacos, Thermal Modelling of Battery Configuration and Self-Discharge Reactions in Vanadium Redox Flow Battery. *J Power Sources*, **2012**, 216, 489–501.
44. D. P. Scamman, G. W. Reade, E. P. L. Roberts, Numerical Modelling of a Bromide-Polysulphide Redox Flow Battery. Part 2: Evaluation of a Utility-Scale System. *J Power Sources*, **2009**, 189, 1231–1239.
45. F. Xing, H. Zhang, X. Ma, Shunt Current Loss of the Vanadium Redox Flow Battery. *J Power Sources*, **2011**, 196, 10753–10757.
46. G. Codina, A. Aldaz, Scale-up Studies of an Fe/Cr Redox Flow Battery Based on Shunt Current Analysis. *J Appl Electrochem*, **1992**, 22, 668–674.

CHAPTER 13

Flowing Power

Innovations in Alkaline Batteries

Rafael Martínez-Palou and Heriberto Díaz Velázquez

13.1 INTRODUCTION

Due to recent advances in renewable energies such as solar and wind, the need for efficient, long-life energy storage technologies has been magnified. In this context, alkaline flow batteries (AFBs) emerge as a promising and highly advantageous solution compared to conventional rechargeable batteries [1].

Redox flow batteries have attracted much attention from researchers as a promising technology for practical energy storage because of their attractive features, such as safety, long life, and scalability [2]. On the other hand, redox flow batteries are a very useful type of flow battery for long-duration discharges, as the energy-storing species are held in liquid form in external compartments separate from the power generation stack; this allows the energy and power ratings to be scaled independently and consequently achieve a very high energy-to-power ratio [3].

Within the rechargeable battery family, AFBs stand out for their ability to respond quickly to changes in demand, which guarantees their efficiency [4]. Thus, AFBs have aroused great interest, given their high potential for stationary energy storage.

As a type of rechargeable battery that falls under the flow batteries category, AFBs store energy in two electrolytic reservoirs [5]. These reservoirs are pumped through a reactor to generate electricity. Their external energy storage in tanks sets them apart from conventional batteries, which allows for scalability and potentially longer discharge times [6].

An alkaline flow battery is a rechargeable electrochemical storage system that operates in an alkaline environment, typically using an alkaline electrolyte such as potassium hydroxide (KOH) or sodium hydroxide (NaOH). Flow batteries are unique because they store energy in liquid electrolytes stored in external reservoirs and pumped through a cell stack where electrochemical reactions occur. This design allows decoupling of power (which

DOI: 10.1201/9781003506379-13

depends on the cell stack) from energy capacity (which depends on the size of the tanks), making flow batteries particularly suitable for large-scale energy storage applications.

13.2 BRIEF HISTORY OF AFBs

In the 1970s, the concept of flow batteries emerged during the energy crisis, with researchers looking for efficient ways to store and deliver energy. Flow batteries generally involve two liquid electrolytes that flow through a cell stack, where electrochemical reactions occur to store and release energy. In 1979, the first prototype of an alkaline zinc-iron flow battery was reported with a potential of 1.74 V [7].

In the 1980s, AFBs began to gain attention. The technology uses alkaline electrolytes, typically containing hydroxides like KOH or NaOH. This was an alternative to acidic electrolytes used in other types of flow batteries, such as vanadium redox flow batteries. The alkaline approach was appealing because it promised lower costs and reduced corrosion, which are significant issues in other battery chemistries.

In the 1990s, researchers focused on improving the performance and efficiency of AFBs.

During this time, several attempts have been made to optimize electrolyte composition and membrane technology to increase energy density, reduce adverse reactions, and extend battery lifetime.

In the 2000s, interest in renewable energy and grid storage applications increased, leading to increased efforts in developing flow batteries, including alkaline batteries. Several companies and research groups explored AFBs as a potential solution for storing energy from intermittent renewable sources like solar and wind [8].

At this stage, research on developing alkaline-based organic redox flow batteries was intensified. The expensive vanadium that had been the metal of choice for the commercialization of flux batteries is replaced by easily synthesized metal-free organic compounds. Organic compounds are generally much cheaper than metallic compounds. They can be chemically modified by functionalization, which allows their solubility to be altered and their voltage, rate capability, and energy density to be improved [9].

Advances in materials science and electrochemical engineering led to significant improvements in the performance and reliability of AFBs between the years 2010 and 2020. Innovations in membrane technology and novel catalysts helped address some limitations of earlier designs.

At present, AFBs remain an area of active research, particularly for large-scale energy storage applications. While they are less commercially widespread than other types of flow batteries, ongoing research aims to make them more competitive. The technology particularly appeals to applications requiring long-duration energy storage and scalability [10].

13.3 COMPONENTS OF AFBs

Like standard redox flow batteries, the main components of AFBs are two electrodes [11] and two electrolytes (positive and negative) separated by an ion exchange membrane [12], which is nothing more than a separator that allows the passage of ions while keeping the oxidation and reduction reactions separate. Electrical energy is stored as chemical energy in electroactive species dissolved in an alkaline medium.

The electrolytes are supplied through two compartments containing the active species dissolved in a basic medium, usually containing KOH or NaOH. The electrolyte solutions are stored in external tanks and are pumped through the cell stack during operation. This design allows for easy scaling of the battery's energy capacity by simply increasing the size of the tanks.

The electrolyte solutions are stored in external tanks and are pumped through the cell stack during operation. This design allows for easy scaling of the battery's energy capacity by simply increasing the size of the tanks.

13.3.1 Electrodes

The electrodes in AFBs are typically made from materials like carbon-based composites, metal oxides, or nickel-based alloys. These materials are chosen for their ability to withstand the highly alkaline environment normally created by the KOH electrolyte.

The electrodes have been improved to enhance their performance by strengthening electrical conductivity and enhancing mass and charge transports in an aqueous flow battery, including oxygen (i.e., hydroxyl and carboxylic functional groups on the electrode surfaces), nitrogen, and non-metallic elements (boron, phosphorus, sulfur, and halogens) doped electrode; metal-modified carbon fiber; graphene and graphene oxide electrodes, like Ta_2O_5, TiN, and WO_3, noble metals as carbon-supported Pt, Pd, or Au nanoparticle-modified electrodes and other metals such as Zn, Ni, Fe, Co, Bi, Sb, and Ag and metal oxides (TiO_2, CoO, PbO_2, and Cr_2O_3) as positive electrodes (anodes) [13]. Another strategy to improve the electrode's performance is to increase the electroactive sites by decorating nanostructures and etching pores on the electrode surface.

The electrolyte flow allows the system to store and release energy. By changing the electrolyte, the system can be recharged and used several times (Figure 13.1).

AFBs can withstand thousands of charge and discharge cycles, making them suitable for long-term energy storage applications such as renewable energy integration

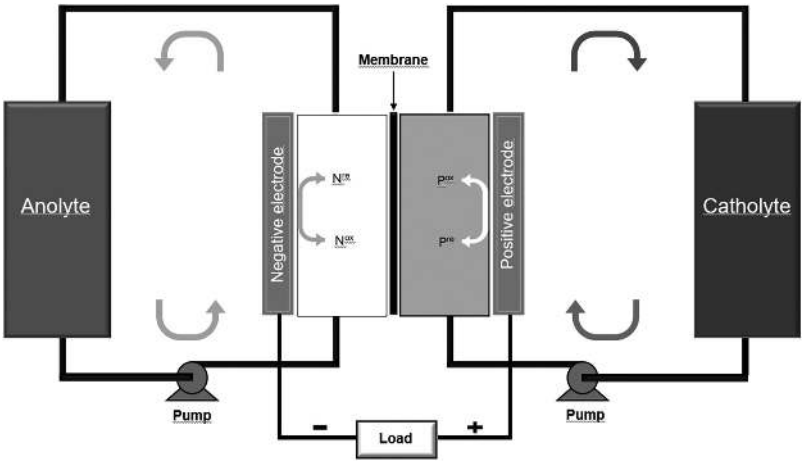

FIGURE 13.1 Scheme of AFBs.

and grid stabilization. The capacity of AFBs can be quickly increased by adding more electrolyte solutions [14].

13.3.2 Electroactive Species in AFBs

In AFBs, electroactive species are the chemical compounds that undergo redox (reduction-oxidation) reactions during operation. In the case of redox compounds, electroactive species are chemical compounds that undergo redox reactions (reduction and oxidation) during their operation. These species are important because their redox reactions store and release energy. The choice of active species determines the energy density, efficiency, stability, and overall battery performance. The choice of active species depends on factors such as redox potential, stability in alkaline environments, and cost-effectiveness.

Electroactive species can be classified as catholyte (positive electrolyte) and anolyte (negative electrolyte), depending on whether they are part of the battery's positive or negative compartment. Electroactive species can be inorganic or organic.

13.3.3 Catholytes

A typical catholyte for AFBs is the inorganic electroactive species from $K_4Fe(CN)_6$ ($Fe(CN)_6^{3-}/Fe(CN)_6^{4-}$). Due to its cost, availability, and low toxicity, $K_4Fe(CN)_6$, a common food additive, has been the option par excellence for the active species of the positive electrode; however, this compound has the disadvantage that its solubility in the basic medium is low. This is the main factor that AFBs have a lower energy density than other battery technologies, which can make energy storage systems take up more space.

Recently, novel alternatives have been proposed to address this limitation; for example, Páez et al. studied energy storage in commercial $Ni(OH)_2$ electrodes confined in the positive reservoir, whereby the $K_4Fe(CN)_6$ dissolved in the electrolyte acts not only as an electroactive species but also as a charge carrier between the current collector and the $Ni(OH)_2$ solid particles located in an external reservoir. To demonstrate the versatility of this innovation, the authors tested the concept in three systems: Zn-$K_4Fe(CN)_6$, anthraquinone-$K_4Fe(CN)_6$, and alkaline phenazine-$K_4Fe(CN)_6$ flow cell, the latter showing the best results with an energy density of 16 Wh L_{total}^{-1} and capacity retention of 99.9% per cycle and 98.7% per day during 100 cycles [15]. Organic species such as TEMPO derivatives, ferrocene, and benzoquinone derivatives have also been used as catholytes for aqueous organic flow batteries [16].

13.3.4 Anolytes

In an alkaline flow battery, the active species for the negative compartment (anolyte) typically involves a redox couple that can effectively operate in an alkaline environment. These active species are chosen based on their electrochemical reversibility, stability in alkaline media, and cost-effectiveness.

Some metals, such as zinc [12], iron [13–15], and vanadium redox couples, can also be used as active species for the negative compartment. Zinc/Zincate ($Zn/Zn(OH)_4^{2-}$).

Zinc is commonly used as an active species in the negative compartment due to its high energy density and good electrochemical properties in alkaline solutions. The oxidation of zinc forms zincate ions in the electrolyte. Iron can also be used in AFBs, where Fe(II) is oxidized to Fe(III) in the negative compartment. Vanadium can exist in multiple oxidation states, making it a versatile option. The V(II)/V(III) redox couple can be used in the negative compartment in an alkaline flow battery [17].

Organic molecules are used as electroactive species in the negative compartment. They can operate in alkaline conditions and provide a sustainable alternative to metal-based systems, including TEMPO (2,2,6,6-Tetramethylpiperidine-1-oxyl) [18,19], quinone [20], anthraquinone [20,21], benzoquinone [13], vitamin B derivative [22], all oxazine [21], and phenazine derivatives [22]

Figure 13.2 shows the chemical structures of some organic systems and polymers that have been used as active species (catholytes or anolytes) in organic redox flow batteries [23].

Different polymers have also been employed as electrolytes in AFBs or electrochemical energy storage applications [24–26]. Polymers with π-conjugated backbones and

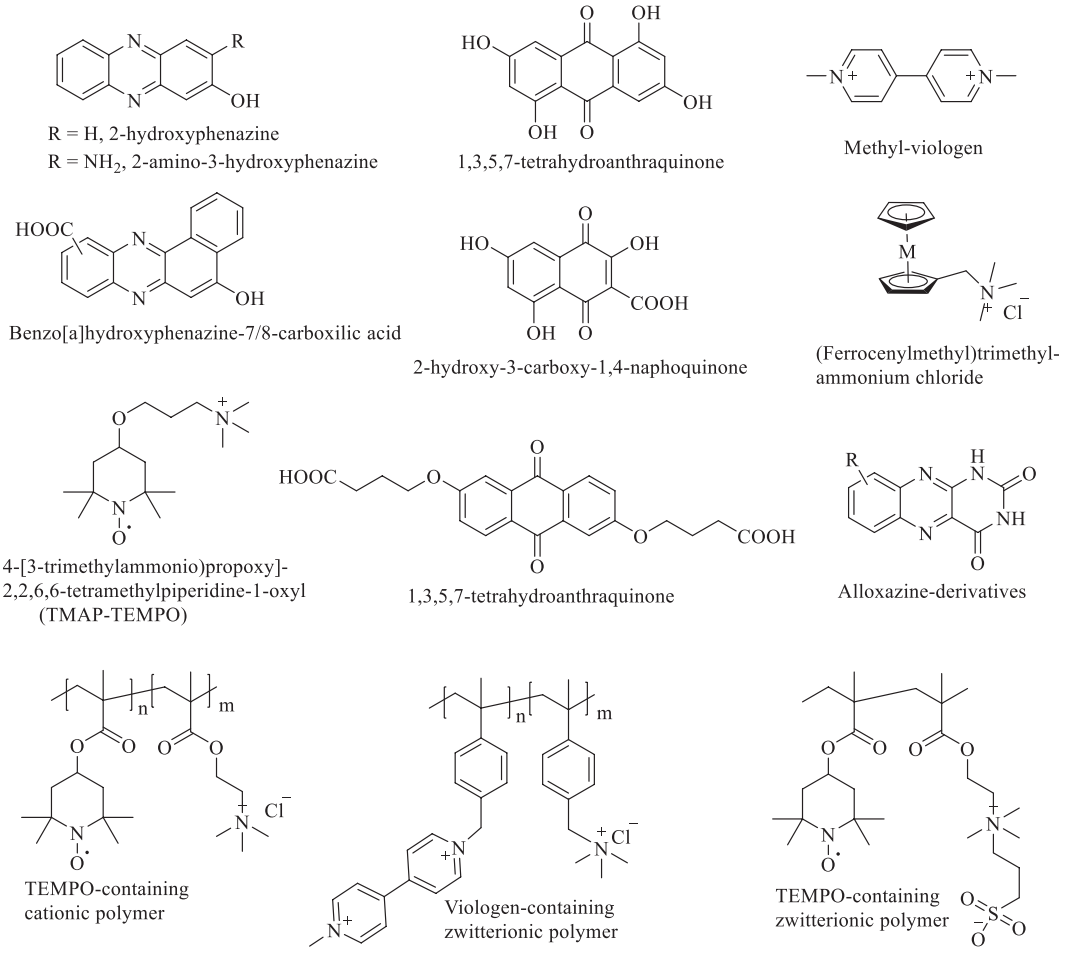

FIGURE 13.2 Structure of some organic electrolytes.

electrochemically active groups are especially useful for use in electrochemical energy storage because they combine the properties of redox kinetics, electronic conductance, and chemical stability. For example, redox-active poly(6-(1H-pyrrol-1-yl)quinoxaline) (PPyQx) has been used as a novel organic anode material for aqueous hybrid flow batteries. The π-conjugated PPyQX polymer containing the redox-active quinoxaline pendant group showed an equilibrium potential at 0.79 V (vs SHE) in strong alkaline aqueous electrolytes. It was studied as an anode material by pairing with a $K_4Fe(CN)_6$ catholyte for aqueous alkaline hybrid flow batteries, which exhibits a considerable open-circuit potential, excellent rate performance, eminent coulombic efficiency, and good cycle stability [25].

Deep eutectic solvents (DES) and ionic liquids have also been investigated as electrolytes [27].

13.3.5 Membranes for AFBs

A membrane or separator is often used to physically separate the anolyte (negative electrolyte) and catholyte (positive electrolyte) compartments while allowing the selective passage of ions to maintain charge balance during operation.

Initially designed for proton transport in fuel cells, Nafion membranes have been the membrane par excellence for cation transport in alkaline RFB [28]; however, these membranes are very expensive for large-scale networked storage systems such as AFBs [29]. Hydrocarbon-based anion exchange membranes in alkaline media could soon be an alternative to Nafion series membranes in AFBs.

Hydrocarbon-based anion exchange membranes in alkaline media could be an alternative to Nafion series membranes in AFBs [30]. In this sense, anion exchange membranes have been investigated with a wide variety of polymers, such as poly (vinyl benzyl chloride), polyimide, polybenzimidazole, and polysulfone with various cationic functional groups to improve their stability. However, these membranes still present significant limitations in withstanding severe alkaline conditions [31].

Xia et al. presented a cost-competitive and stable polysulfide-air hybrid alkaline redox flow battery. A flow cell design with a double-membrane structure mitigates the sulfur crossover problem. They combined manganese/carbon catalyzed air electrodes with sulfided Ni foam polysulfide electrodes, the redox flow battery, whereby the AFB achieved a maximum power density of 5.8 mW cm^{-2} at 50% state of charge and 55°C and an average round-trip energy efficiency of 40% over 80 cycles at 1 mA cm^{-2}, concluding that the double-membrane structure adds greater flexibility and better design options for polysulfide-based AFBs (Figure 13.3) [32].

Great efforts have also been made to develop highly efficient and stable membranes for the zinc-iron flow battery. The membrane for AFBs must satisfy the needs of high ionic conductivity and high selectivity for $Fe(CN)_6^{3-}$ ion, coupled with stability in alkaline media to ensure a long lifetime, which continues to be a challenge in current research (Figure 13.4) [33]. In this sense, Yang, Zhang, and Zhu recently published a work studying a high-performance, stable anion exchange membrane for alkaline zinc-iron flow battery applications. They designed a series of polyethylene glycol-poly(vinylbenzyl

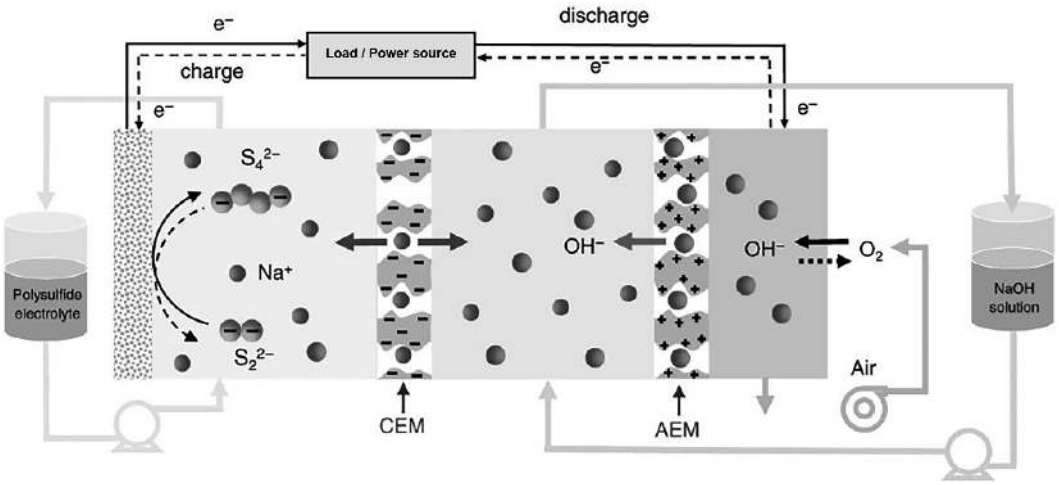

FIGURE 13.3 Redox Flow Battery is based on a stable polysulfide-air hybrid alkaline redox flow battery. (CEM: cathode exchange membrane; AEM: cathode exchange membrane). (Adapted with permission from ref. [32]. Copyright. The Authors, some rights reserved; exclusive licensee [Springer Nature]. Distributed under a Creative Commons Attribution License 4.0 (CC BY) https://creativecommons.org/licenses/by/4.0/.)

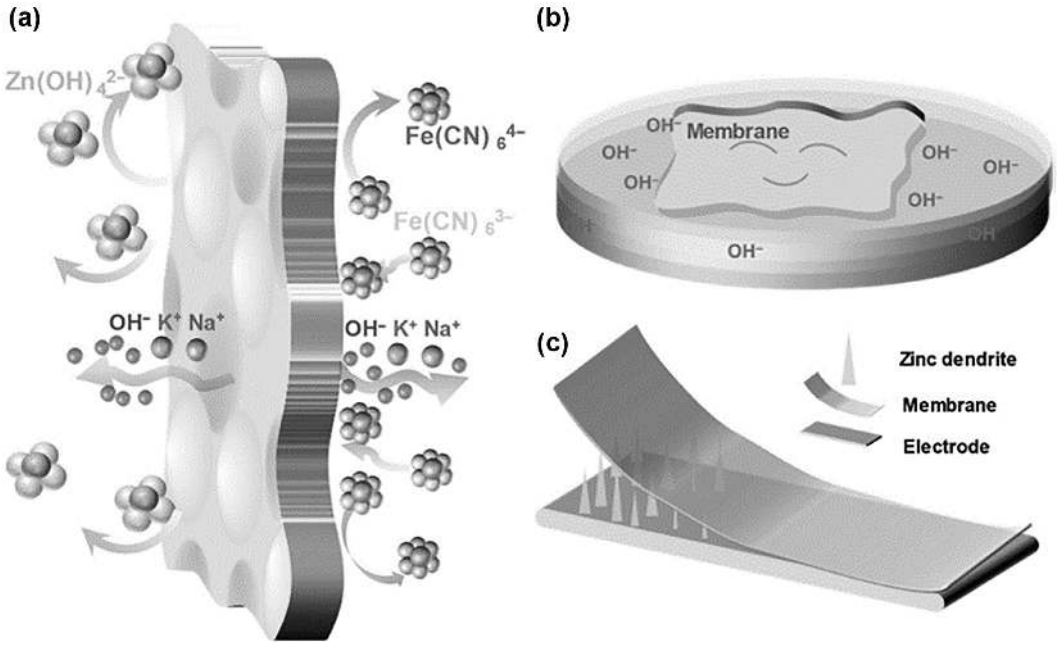

FIGURE 13.4 Schematic presentation of the principles of a membrane for Zn-Fe AFBs. (Adapted with permission from ref. [33]. Copyright. The authors, some rights reserved; exclusive licensee KeIa Publishing. Distributed under a Creative Commons Attribution License 4.0 (CC BY) https://creativecommons.org/licenses/by/4.0/.)

tetramethylimidazolium)-based anion exchange membranes, and the tetramethyl imidazolium cationic group was utilized for its excellent chemical stability in alkaline media [34].

13.4 ADVANTAGES OF AFBs

The most essential advantages of AFBs concerning other flow batteries can be summarized as follows:

The electrolytes used in AFBs are non-flammable, which makes them advantageous to those used in other batteries. This greatly reduces the risk of fire or explosion, an extremely important safety advantage, especially in large-scale installations.

AFBs have notorious thermal stability, which increases the battery's overall safety. The chemical reactions in an AFB occur at room temperature, and the system is designed to effectively regulate heat, reducing the risk of thermal runaway in other types of batteries, such as lithium-ion batteries.

Safety: AFBs have key safety features that distinguish them from other chemical batteries. They typically use aqueous alkaline electrolytes, usually KOH. The electrolytes used in AFBs are non-flammable, which makes them advantageous to those used in other batteries. They greatly reduce the risk of fire or explosion, an extremely important safety advantage, especially in large-scale installations.

AFBs have notorious thermal stability, which increases the battery's overall safety. The chemical reactions in an AFB occur at room temperature, and the system is designed to effectively regulate heat, reducing the risk of thermal runaway in other types of batteries, such as lithium-ion batteries.

The flow battery design separates the reactants and electrolytes into an external reservoir, further enhancing safety by reducing the potential for unwanted chemical reactions.

Scalability: Scalability is critical when considering the potential for widespread use of AFBs, especially for grid-scale energy storage. By increasing the volume of electrolytes, the energy storage capacity can be easily increased.

The scalability of AFBs is a key feature that makes them adaptable to various applications. Their modularity allows for easy scaling up or down by adjusting the size of the electrolyte reservoirs and the number of cells. This adaptability ranges from small-scale residential storage to large-scale grid support. Additionally, the possibility of stacking cells and increasing tank size further enhances their scalability.

Longevity: AFBs are known for their long service life. They can typically withstand thousands or tens of thousands of charge and discharge cycles without significant degradation. This makes them well-suited for applications that require frequent cycling, such as grid stabilization or renewable energy integration.

Unlike batteries based on solid-state electrodes, which can degrade over time due to volume changes during cycling, AFBs experience minimal physical changes in their components. The liquid electrolyte and flow-based operation contribute to this minimal degradation, extending battery life.

AFBs are easier to maintain than other battery types. Components such as pumps, membranes, and electrolyte tanks can be repaired or replaced without replacing the entire battery system.

AFBs typically allow a considerable depth of discharge (DoD) without significantly affecting their service life. This contrasts with other batteries, where frequent deep discharges can shorten battery life.

AFB's performance tends to be consistent over time, with minimal capacity loss. This consistency is vital for applications that need reliable long-term energy storage.

The chemical stability of the electrolyte and the absence of side reactions that can consume the active materials contribute to the long operating life of AFBs. Proper management of electrolyte concentration and pH can further increase longevity.

Sustainability: The materials used in AFBs are generally non-toxic and environmentally friendly. This reduces the risks associated with leaks or spills, making these batteries safer for both users and the environment. Developing sustainable and environmentally friendly electrode and electrolyte materials is a growing area of research, aligning with global trends toward greener technologies.

Flexibility: Power and energy capacity can be sized independently, allowing versatile applications. Unlike pumped hydro or compressed air energy storage, AFBs are not limited by geography, making them more flexible in deployment across various locations. AFBs can be integrated into existing grid infrastructure, but scaling them up will require significant investment in supporting infrastructure, including tanks, pumps, and controllers.

Low cost: The use of abundant and relatively inexpensive materials allows the preparation of relatively low-cost batteries, which, together with their longevity, favors the development of cost-effective batteries. AFBs also have the potential for lower operational and maintenance costs compared to other battery technologies, which supports long-term scalability.

AFBs outperform other types of batteries in terms of capacity. This is particularly true when you factor in long-term operating and maintenance costs.

13.5 CHALLENGES

Also, the development of AFBs still faces significant challenges, so it is necessary to continue research into the development of prototypes that can overcome the limitations that persist and that can be summarized in the following aspects:

Membrane degradation is a significant issue in AFB development, particularly in highly alkaline environments. This degradation can lead to a reduction in battery efficiency and lifespan. However, the potential for cost-effective and durable membranes that can resist degradation and facilitate efficient ion transfer offers hope for the future of AFB development.

Electrolyte management is a crucial aspect of AFB operation. The handling and circulation of liquid electrolytes present challenges in system design and maintenance. Over time, these electrolytes can degrade, leading to a decrease in performance. To maintain performance, regular maintenance and effective electrolyte management are required, underscoring the importance of your role in AFB operation.

In some AFB designs, ion crossover may occur between the two electrolyte solutions across the membrane, resulting in efficiency losses and possible mixing of the electrolytes. This can reduce battery efficiency and require careful management.

Energy density: AFBs tend to have lower energy density than other battery technologies, such as lithium-ion and sodium-ion batteries, which can make energy storage systems take up more space. This limitation is a concern in applications where space is a concern. However, this is less of an issue for stationary storage solutions, where space constraints are minimal.

Electrode stability: Maintaining the long-term stability of electrode materials in an alkaline environment can be difficult, and corrosion can be a major challenge. Electrodes must resist corrosion to maintain structural integrity and electrochemical activity over time. Certain metal oxides and new materials with high chemical stability could solve this problem.

Advanced coatings or treatments should also be applied to the electrode surface to improve its surface stability. Some electrode materials can develop a passivation layer during operation, which can protect the electrode from further degradation but, in turn, hinder its performance by blocking active sites. Another factor contributing to lower efficiency is electrode polarization, which causes voltage losses during operation. Current limitations of electrode materials and designs continue to affect overall performance (lower round-trip efficiency).

AFB performance: The performance of AFBs can degrade over time, especially at high temperatures [35]. AFBs can degrade over time, and this degradation can affect their performance, efficiency, and lifetime. The degradation mechanisms of AFBs depend on several factors, such as the materials used, the operating conditions, and the nature of the electrochemical reactions. The main factors influencing this degradation process are chemical changes of the electrolyte due to side reactions, contamination, or concentration imbalances. For example, KOH electrolytes can react with carbon dioxide in the air to form potassium carbonate, which can reduce the efficiency of the electrolyte and alter its conductivity. The change in pH can affect the electrodes' stability and the battery's efficiency.

Conversely, impurities introduced during operation, such as from electrode materials or external sources, can degrade the electrolyte. This contamination can reduce the ionic conductivity and affect the battery's performance. As previously discussed, the performance of AFBs is also affected by electrode degradation (corrosion or passivation) and membrane degradation.

Table 13.1 shows a comparative analysis between AFBs and other types of flow batteries, such as vanadium, zinc-bromine, iron-chromium, and organic flow batteries, which are discussed in detail in this book in Chapters 10, 11, and 12, respectively.

The comparative refers to the most conventional mode known for each battery type since AFBs include vanadium, zinc-bromine, iron-chromium, and organic electrolytes.

TABLE 13.1 Comparative Analysis Between AFBs and Other Types of Flow Batteries

Feature	AFB	Vanadium Flow Battery	Zinc-Bromine Flow Battery	Iron-Chromium Flow Battery	Organic Flow Battery
Electrolyte	Alkaline solutions	Vanadium in different oxidation states	Zinc and bromide dissolved in water	Iron and chromium dissolved in acid	Organic compounds dissolved in aqueous and non-aqueous solutions
Energy density (Wh/L)	Moderate	Moderate to high	Moderate	Low	Moderate
Energy efficiency (%)	Moderate	75–85	60–75	65–75	70–80
Charge cycles (cycle life)	High	Very high	Moderate	Moderate	High (varies by chemistry)
Material cost	Low	High	Moderate	Moderate	High (dependent on electrolyte)
Safety	High	High	Moderate	Moderate	Low to moderate
Main application	Large-scale energy storage	Large-scale energy storage	Large-scale energy storage	Industrial applications	Grid storage, renewable integration
Technological maturity	Moderate	High	Moderate	Low	Low to moderate
Advantages	Low cost, high safety	High efficiency, long cycle life	Moderate cost, reasonable energy density	Abundant materials, low cost	Renewable materials, customizable chemistries
Disadvantages	Lower efficiency	High cost, dependency on vanadium	Leakage risks, lower efficiency	Low efficiency, limited cycle life	Emerging technology, stability challenges

In summary, we can say that all flow batteries have their pros and cons; in the case of AFBs, their main advantages are their low cost and safety, but with moderate efficiency. Vanadium batteries are the most studied and have a high efficiency and long life cycle but are expensive. On the other hand, although they are costly, zinc-bromine flow batteries show a balance between cost and energy density.

Iron-chromium flow batteries use abundant and inexpensive materials, but their efficiency and lifetime are lower. Organic flow batteries offer flexibility regarding the use of renewable materials and customizable chemistries, but as an emerging technology, they face problems associated with a lack of maturity and stability.

13.6 RECENT ADVANCES IN AFBS

Recent research on AFBs has focused on improving material stability, electrolyte management, energy density, and system efficiency. Advances in electrode materials and membrane technology are essential areas of development that will enable AFBs to become more competitive with other energy storage technologies.

AFBs contribute to a greener future by using water-based electrolytes, a more environmentally friendly option than other batteries that rely on hazardous materials [35]. This eco-conscious design is another reason these batteries are gaining popularity in various applications such as large-scale energy storage, balancing supply and demand on the grid, storage of excess energy from renewable sources such as solar and wind, and use in backup power in case of outages [36].

For the sustainable application of AFBs, designing high-performance active species based on low-cost and environmentally friendly compounds is vital. Therefore, creating new organic species with high solubility, stability, and low toxicity is currently a high-priority issue.

In recent years, alkaline cell prototypes have been developed showing ultra-high voltage and energy density, with high soluble catholytes, very high Columbus efficiency, and electrolytes with high solubility and stability in alkaline medium, among other findings. However, this type of battery has not yet achieved large-scale commercialization, as in the case of all-vanadium batteries. Hence, the research work continues to be arduous in the search for greater efficiency, which is the weakest point of this type of battery.

AFBs have fast response times, making them ideal for applications requiring promptness, such as grid stabilization and frequency regulation. You can be confident in their ability to meet energy demands promptly and efficiently [15].

Some recent research works in the development of AFBs are summarized in Table 13.2.

13.7 CURRENT STATUS AND FUTURE PROSPECTS

AFBs are still in the development and demonstration phase, with several pilot projects and small-scale deployments. Due to their potentially long lifetime, long-term reliability, and relatively low cost, they are seen as a promising grid-scale energy storage technology.

Today, AFBs have some limitations, such as lower energy density than other battery technologies, which can make energy storage systems take up more space. In addition, their performance can degrade over time, especially at high temperatures. Improving the round-trip efficiency of AFBs is crucial for their economic viability on a large scale.

Nie et al. recently reported a rechargeable aqueous alkaline zinc–sulfur flow battery comprising environmental materials zinc and sulfur as negative and positive active species, which showed excellent performance [48].

Future research is expected to focus on further improving efficiency, reducing the cost of materials, and scaling up the technology for broader commercial use. Ongoing efforts aim to enhance the catalytic activity of electrode materials while reducing costs. Innovations like nano-engineered surfaces, hybrid materials, and advanced manufacturing techniques are being explored.

Supportive policies and regulations can accelerate the scaling of AFBs by providing incentives for research, development, and deployment. As the demand for renewable energy storage increases, the scalability of AFBs will be driven by their ability to meet market needs cost-effectively.

Ongoing research and development are essential for improving the performance, cost-effectiveness, and scalability of AFBs. Breakthroughs in materials science, system design, and manufacturing processes will play a key role in making AFBs a competitive option for large-scale energy storage.

TABLE 13.2 Some Recent Research Works Related to the Development of AFBs

AFB Type	Electroactive Species (Redox Pair)	Topic of Research	Relevant Results	References
Alkaline redox aqueous Zn-Fe flow battery	$Fe(CN)_6^{3-}/Fe(CN)_6^{4-}$ $Zn(OH)_4^{2-}/Zn$ redox	Cost evaluation and sensitivity analysis	DOE's cost target of \$150 kWh^{-1} was obtained. High current densities were shown to have little impact on capital cost.	[37]
Alkaline organic redox flow batteries (AORFB)	Anthraquinone-ferro/ferricyanide; $Fe(CN)_6^{3-}/Fe(CN)_6^{4-}$	Steady-state 3D modeling and simulation	A computational 3D model was developed for the study of AORFB. The flow pattern obtained with the model that includes the inlet and outlet collectors in AORFB notably affected the spatial concentration distribution of 2,6-$DHAQ^{2-}$ and $[Fe(CN_6)]^{3-}$	[38]
Alkaline redox aqueous Zn-Fe flow battery	$Fe(CN)_6^{3-}/Fe(CN)_6^{4-}$; $Zn(OH)_4^{2-}/Zn$	Anion exchange membrane (AEM) design	A simple synthesis method was developed to obtain AEMs with high stability. The membrane was obtained from a partial imidazolium-substituted poly(vinyl benzyl chloride) polymer and a polyethylene glycol (PEG) additive.	[39]
Fe-Mn	$[(TEA)Fe–O–Fe(TEA)]^{3-/4-}$; $MnO_4^{-/2-}$	Development of AFB, a novel inorganic system with low cost and high solubility.	Constant current cycling tests were performed at ±41 mA cm^{-2} over 800 h (400 cycles) with an apparent Coulombic efficiency of 100%. The voltage efficiency (VE) gradually decreased from ~75.3% to ~61.4%.	[40]
Aqueous organic flow batteries	Naphthoquinone dimmer (NQD) NQD; AgCl/Ag	Molecular engineering of a naphthoquinone dimer 2,2′-bis(3-hydroxy 1,4-naphthoquinone) as a high, reversible negative-compartment active material.	Naphthoquinone dimerization is a promising synthetic strategy for improving the performance of quinone-based flow batteries. This organic flow battery displayed a theoretical volumetric capacity of 53.6 Ah/L (2 M electrons).	[41]
Alkaline quinone flow batteries	4,40-((9,10-anthraquinone-2,6-diyl)dioxy) dibutyrate (2,6-DBEAQ); $Fe(CN)_6^{3-}/Fe(CN)_6^{4-}$	Development of alkaline quinone batteries that are more soluble and stable at very high pH levels.	Functionalized 2,6-dihydroxyanthraquinone with highly alkali-soluble carboxylate groups gave 2,6-DBEAQ, which was six times more soluble than its precursor. This battery can operate at a pH as low as 12 while maintaining an open-circuit voltage of over 1 V.	[42]

(*continued*)

TABLE 13.2 (Continued) Some Recent Research Works Related to the Development of AFBs

AFB Type	Electroactive Species (Redox Pair)	Topic of Research	Relevant Results	References
All-iron inorganic flow battery	Fe_3O_4/Fe; $Fe(CN)_6^{3-}$/$Fe(CN)_6^{4-}$	Develop inexpensive all-iron redox chemistries for large-scale energy storage.	The coulombic efficiency reaches 99%. The developed battery has a meager material cost (22 kW h^{-1}). An inorganic all-iron alkaline battery was developed in a single static cell configuration. The stack exhibited an equilibrium potential of 1.2 V with an energy efficiency of 76%.	[43]
Alkaline Zn-Mg aqueous flow battery	$Zn(OH)_4^{2-}$/Zn and MnO^{4-}/MnO_4^{2-}	Development of an alkaline flow battery with ultra-high voltage and energy density.	$NaMnO_4$ is highly solubilized (3.92 M) in alkaline conditions, so it significantly influenced the catholyte's performance. The Zn-Mn redox system achieved a maximum energy density of 208 Wh L-1 and a power density of 644 mW cm^{-2}. The Zn-Mn flow battery was stable for over 5,000 cycles and 80% efficient.	[44]
Hybrid alkaline-based $ZnBr_2$ redox flow battery.	$Zn(OH)_4^{2-}$/Zn; $2Br^-/Br_2$	Increasing cell voltage through tailoring the pH of aqueous Zn-Br_2 AFB.	An exceptional voltage of AFB based on metal halide was obtained by switching the electrolyte environment from a neutral to an alkaline medium.	[45]
Phenazine derivative (PD) organic flow battery	(7,8-dihydroxyphenazine-2-sulfonic acid (DHPS); $Fe(CN)_6^{3-}$/$Fe(CN)_6^{4-}$	A biomimetic high-capacity anolyte for aqueous organic redox flow batteries.	A high reversible anolyte capacity of 67 Ah L^{-1} indicates a 90% material utilization, offered an excellent capacity retention of 99.98% per cycle over 500 cycles. Near-saturation concentration exhibits an operating voltage of 1.4 V.	[21]
Alkaline Zn-based flow battery	Zn/Zn^{2+}; $Fe(CN)_6^{3-}$/$Fe(CN)_6^{4-}$	Improved Zn electrode stability and performance with the use of ionic liquids.	The morphological evolution of zinc electrodes was controlled using ionic liquids, 1-ethyl-3-methylimidazolium acetate, and 1-propylsulfonic-3-methylimidazolium tosylate. The reversible change in the zinc electrode morphology improved electrode performance.	[46]
Organic phenazine-derivative AFBs	(PD); $Fe(CN)_6^{3-}$/$Fe(CN)_6^{4-}$ PD: 2- hydroxyphenazine (HP), 2-amino-3-hydroxyphenazine (AHP), and benzo[a]hydroxyphenazine-7/8-carboxylic acid (BHPC)	Design of novel high-performance phenazine-derived anolytes.	Introducing an additional phenyl group adjacent to the hydroxyl group in the structure of phenazine and a carboxyl group, a much-improved capacity retention rate of 99.98% cycle-1 (99.92% day^{-1}) and a stable average energy efficiency of ~80% over more than 1300 cycles were achieved.	[47]

REFERENCES

1. N. A. Sepulveda, J. D. Jenkins, A. Edington, D. S. Mallapragada, R. K. Lester, The design space for long-duration energy storage in decarbonized power systems, *Nat. Energy* 6 (2021) 506–516.
2. B. Hu, H. Li, H. Fan, J. Song, A long-lifetime aqueous organic redox flow battery utilizing multi-redox anolyte, *Energy Storage Mater.* 59 (2023) 102789.
3. M. H. Chakrabarti, S. A. Hajimolana, F. S. Mjalli, M. Saleem, I. Mustafa, Redox flow battery for energy storage, *Arab. J. Sci. Eng.* 38 (2013) 723–739.
4. Z. Yang, J. Zhang, M. C. W. Kintner-Meyer, X. Lu, D. Choi, J. P. Lemmon, J. Liu, Electrochemical energy storage for green grid, *Chem. Rev.* 111 (2011) 3577–3613.
5. J. Li, Z. Xu, M. Wu, Halogen enabled aqueous flow cells for large-scale energy storage: Current status and perspectives, *J. Power Sources* 581 (2023) 233477.
6. Z. Zhu, T. Jiang, M. Ali, Y. Meng, Y. Jin, Y. Cui, W. Chen, Rechargeable batteries for grid scale energy storage, *Chem. Rev.* 122 (2022) 16610–16751.
7. G. B. Adams, R. P. Hollandsworth, B. D. Webber, Rechargeable alkaline zinc/ferricyanide battery, Final report, 29 September 1978–28 September 1979. [35 mA/cm/sup 2/, 4. 5 kW/m/sup 2/]. (1979).
8. T. Nguyen, R. F. Savinell, Flow batteries, *Electrochem. Soc. Interface* 19 (2010) 54–56.
9. D. R. Chang, Y. Kim, S. Jung, Comprehensive study of the performance of alkaline organic redox flow batteries as large-scale energy storage systems, *Int. J. Energy Res.* 43 (2019) 4449–4458.
10. B. Lu, K. Yu, W. Shao, Y. Ji, F. Zhang, Organic redox-active molecules for alkaline aqueous redox flow batteries, *Curr. Opin. Green Sustain. Chem*. 47 (2024) 100905.
11. L. Zhou, J. Xie, D. Xu, Y. Yu, X. Gao, X. Lu, Recent advances and challenges of anodes for aqueous alkaline batteries, *Energy Chem*. 5 (2023) 100102.
12. M. G. Marino, Anion exchange membranes for fuel cells and flow batteries : Transport and stability of model systems, PhD Thesis, Stuttgart University, Max-Planck Institute (2015).
13. R. Wang, Y. Li, Carbon electrodes improving electrochemical activity and enhancing mass and charge transports in aqueous flow battery: Status and perspective, *Energy Storage Mater.* 31 (2020) 230–251.
14. Z. Yang, L. Tong, D. P. Tabor, E. S. Beh, M.-A. Goulet, D. De Porcellinis, A. Aspuru-Guzik, R. G. Gordon, M. J. Aziz: Flow batteries: Alkaline benzoquinone aqueous flow battery for large-scale storage of electrical energy, *Adv. Energy Mater.* 8 (2018) 1870034.
15. T. Páez, A. Martínez-Cuezva, J. Palma, E. Ventosa, Mediated alkaline flow batteries: From fundamentals to application, *ACS Appl. Energy Mater.* 2 (2019) 8328–8336.
16. T. Janoschka, N. Martin, M. D. Hager, U. S. Schubert, An aqueous redox-flow battery with high capacity and power: The TEMPTMA/MV system, *Angew. Chemie Int. Ed.* 55 (2016) 14427–14430.
17. M. Shoaib, P. Vallayil, N. Jaiswal, P. Iyapazham, V. Suba, S. Sankararaman, K. Ramanujam, V. Thangadurai, M. Shoaib, P. Iyapazham, V. Thangadurai, P. Vallayil, N. Jaiswal, S. Sankararaman, K. Ramanujam, Advances in redox flow batteries – A comprehensive review on inorganic and organic electrolytes and engineering perspectives, *Adv. Energy Mater.* 14 (2024) 2400721.
18. S. Deshmukh, R. Thamizhselvan, K. Mariyappan, M. Kathiresan, M. Ulaganathan, P. Ragupathy, Hybrid aqueous alkaline zinc/TEMPO flow battery, a sustainable high voltage green energy storage device, *J. Electrochem. Soc.* 170 (2023) 050522.
19. K. Lin, Q. Chen, M. R. Gerhardt, L. Tong, S. B. Kim, L. Eisenach, A. W. Valle, D. Hardee, R. G. Gordon, M. J. Aziz, M. P. Marshak, Alkaline quinone flow battery, *Science* 1979 (2015) 1–8.

20. K. Lin, R. Gómez-Bombarelli, E. S. Beh, L. Tong, Q. Chen, A. Valle, A. Aspuru-Guzik, M. J. Aziz, R. G. Gordon, A redox-flow battery with an alloxazine-based organic electrolyte, *Nat. Energy* 1 (2016) 16102.
21. A. Hollas, X. Wei, V. Murugesan, Z. Nie, B. Li, D. Reed, J. Liu, V. Sprenkle, W. Wang, A biomimetic high-capacity phenazine-based anolyte for aqueous organic redox flow batteries, *Nat. Energy* 3 (2018) 508–514.
22. C. Zhang, X. Li, Perspective on organic flow batteries for large-scale energy storage. *Curr. Opin. Electrochem*. 30 (2021) 100836.
23. Y. Liu, Q. Chen, P. Sun, Y. Li, Z. Yang, T. Xu, Organic electrolytes for aqueous organic flow batteries, *Mater. Today Energy* 20 (2021) 100634.
24. J. Cao, F. Ding, H. Chen, H. Wang, W. Wang, Z. Chen, J. Xu, A new redox-active conjugated polymer containing anthraquinone pendants as anode material for aqueous all-organic hybrid-flow battery, *J. Power Sources* 423 (2019) 316–322.
25. B. Wang, Y. Zhang, Y. Zhu, Y. M. Shen, W. Wang, Z. Chen, J. Cao, J. Xu, Redox-active poly(6-(1H-pyrrol-1-yl)quinoxaline) as a novel organic anode material for aqueous hybrid flow batteries, *J. Power Sources* 451 (2020) 227788.
26. T. Hagemann, M. Strumpf, E. Schröter, C. Stolze, M. Grube, I. Nischang, M. D. Hager, U. S. Schubert, (2,2,6,6-Tetramethylpiperidin-1-yl)oxyl-containing zwitterionic polymer as catholyte species for high-capacity aqueous polymer redox flow batteries, *Chem. Mater.* 31 (2019) 7987–7999.
27. A. Sharma, R. Sharma, R. C. Thakur, L. Singh, An overview of deep eutectic solvents: Alternative for organic electrolytes, aqueous systems & ionic liquids for electrochemical energy storage, *J. Energy Chem*. 82 (2023) 592–626.
28. Y. H. Wan, J. Sun, Q. P. Jian, X. Z. Fan, T. S. Zhao, A Nafion/polybenzimidazole composite membrane with consecutive proton-conducting pathways for aqueous redox flow batteries, *J. Mater. Chem. A* 10 (2022) 13021–13030.
29. Q. Luo, H. Zhang, J. Chen, P. Qian, Y. Zhai, Modification of Nafion membrane using interfacial polymerization for vanadium redox flow battery applications, *J. Memb. Sci*. 311 (2008) 98–103.
30. G. Merle, M. Wessling, K. Nijmeijer, Anion exchange membranes for alkaline fuel cells: A review, *J. Memb. Sci*. 377 (2011) 1–35.
31. Z. Li, Z. Jiang, H. Tian, S. Wang, B. Zhang, Y. Cao, G. He, Z. Li, H. Wu, Preparing alkaline anion exchange membrane with enhanced hydroxide conductivity via blending imidazolium-functionalized and sulfonated poly(ether ether ketone), *J. Power Sources* 288 (2015) 384–392.
32. Y. Xia, M. Ouyang, V. Yufit, R. Tan, A. Regoutz, A. Wang, W. Mao, B. Chakrabarti, A. Kavei, Q. Song, A. R. Kucernak, N. P. Brandon, A cost-effective alkaline polysulfide-air redox flow battery enabled by a dual-membrane cell architecture, *Nat. Commun*. 13 (2022) 1–13.
33. L. Zhi, Z. Yuan, X. Li, Recent development and prospect of membranes for alkaline zinc-iron flow battery, *Adv. Memb*. 2 (2022) 100029.
34. R. Yang, S. Zhang, Y. Zhu, A high performance, stable anion exchange membrane for alkaline redox flow batteries, *J. Power Sources* 594 (2024) 233974.
35. Z. Zhao, X. Liu, M. Zhang, L. Zhang, C. Zhang, X. Li, G. Yu, Development of flow battery technologies using the principles of sustainable chemistry. *Chem. Soc. Rev*. 52 (2023) 6031–6074.
36. D. Qiu, B. Li, C. Zhao, J. Dang, G. Chen, H. Qiu, H. Miao, A review on zinc electrodes in alkaline electrolyte: Current challenges and optimization strategies, *Energy Storage Mater*. 61 (2023) 102903.
37. Z. Chen, Y. Liu, W. Yu, Q. He, M. Ni, S. Yang, S. Zhang, P. Tan, Cost evaluation and sensitivity analysis of the alkaline zinc-iron flow battery system for large-scale energy storage applications, *J. Energy Storage* 44 (2021) 103327.

38. G. Aparicio-Mauricio, L. Jiménez-Lima, E. P. Rivero, M. R. Cruz-Díaz, 3D modeling and simulation of an alkaline flow battery considering the tertiary current distribution on the electrodes: Anthraquinone-ferro/ferricyanide as organic electroactive species, *J. Power Sources* 582 (2023) 233533.
39. L. Briot, M. Petit, Q. Cacciuttolo, M. C. Pera, Aging phenomena and their modelling in aqueous organic redox flow batteries: A review, *J. Power Sources* 536 (2022) 231427.
40. X. Shen, C. Kellamis, V. Tam, N. Sinclair, J. Wainright, R. Savinell, An all-soluble Fe/Mn-based alkaline redox flow battery system, *ACS Appl. Mater. Interfaces* 16 (2024) 18686–18692.
41. L. Tong, M.-A. Goulet, D. P. Tabor, E. F. Kerr, D. De Porcellinis, E. M. Fell, A. Aspuru-Guzik, R. G. Gordon, M. J. Aziz, Harvard, J. A. Paulson, Molecular engineering of an alkaline naphthoquinone flow battery, *ACS Energy Lett*. 4 (2019) 1880–1887.
42. D. G. Kwabi, K. Lin, Y. Ji, E. F. Kerr, M. A. Goulet, D. De Porcellinis, D. P. Tabor, D. A. Pollack, A. Aspuru-Guzik, R. G. Gordon, M. J. Aziz, Alkaline quinone flow battery with long lifetime at pH 12, *Joule* 2 (2018) 1894–1906.
43. L. Wei, M. C. Wu, T. S. Zhao, Y. K. Zeng, Y. X. Ren, An aqueous alkaline battery consisting of inexpensive all-iron redox chemistries for large-scale energy storage, *Appl. Energy* 215 (2018) 98–105.
44. W. Xiang, M. Yang, M. Ding, X. Chen, J. Liu, G. Zhou, C. Jia, G. I. N. Waterhouse, Alkaline Zn-Mn aqueous flow batteries with ultrahigh voltage and energy density, *Energy Storage Mater.* 61 (2023) 102894.
45. R. Thamizhselvan, R. Naresh, M. Ulaganathan, V. G. Pol, P. Ragupathy, Achieving exceptional cell voltage (2.34 V) through tailoring pH of aqueous Zn-Br2 redox flow battery for potential large-scale energy storage, *Electrochim. Acta* 441 (2023) 141799.
46. T. Mao, J. Dai, M. Xin, D. Zeng, Z. Xie, Alkaline zinc-based flow battery: Chemical stability, morphological evolution, and performance of zinc electrode with ionic liquid, *Front. Mater. Sci.* 18 (2024) 1–9.
47. C. Wang, X. Li, B. Yu, Y. Wang, Z. Yang, H. Wang, H. Lin, J. Ma, G. Li, Z. Jin, Molecular design of fused-ring phenazine derivatives for long-cycling alkaline redox flow batteries, *ACS Energy Lett*. 5 (2020) 411–417.
48. R. Nie, Y. Nie, J. Wu, L. Yu, L. Liu, J. Xi, An aqueous alkaline zinc–sulfur flow battery, *Chem. Commun*. 60 (2024) 2946–2949.

CHAPTER 14

Alkaline Flow Batteries

Rui Wang, Ruilin Wu, and Runwei Mo

14.1 INTRODUCTION

Energy plays a decisive role in the development of human civilization and is a matter of national livelihood and national security, as well as an important factor for human survival and development. Its importance for promoting economic and social progress and improving the quality of life of the people is self-evident. Population growth and social development are accompanied by an increasing demand for energy [1]. Traditional fossil energy is non-renewable from a human perspective, and it is difficult to meet the needs of long-term survival and development, and at the same time, the wide application of fossil energy has exacerbated the greenhouse effect, haze, acid rain, and other environmental pollution problems. In view of the increasingly tight supply of fossil energy, there is an urgent need to develop renewable energy sources and long-life large-scale energy storage systems to cope with the mismatch between grid demand and the intermittent supply of renewable energy sources [2]. In order to achieve carbon neutrality goals and reduce dependence on fossil energy sources, widespread and sustainable deployment of renewable energy sources is crucial, and energy storage devices are seen as one of the highly promising solutions in this process [3]. Since sustainable clean energy sources, represented by wind, hydro, tidal, and solar energy, are dependent on external factors such as seasons and weather, they exhibit discontinuity and instability and are difficult to integrate directly into the grid [4]. Therefore, it has become a more sensible approach to use suitable energy storage methods to utilize technology to store sustainable clean energy and output the energy in a controlled manner when needed.

Energy storage technology, as a technology that cleverly converts and stores energy in different forms and releases it when needed, is not only a core driving force in the modern energy system; an important technology and basic device to support the new electric power system; but also a key to promoting the green energy transition, enhancing energy resilience to cope with extreme climate events, building a strong defense for energy security, supporting the high-quality development of energy, and realizing the goals of global climate governance. The key to achieving global climate governance goals. Energy storage

DOI: 10.1201/9781003506379-14

can significantly improve the stability and reliability of the power system, optimize power quality, and, at the same time, serve as an emergency backup power source to ensure that the power grid can maintain a stable level of power output under any circumstances. The diversity of energy storage technology is reflected in its classification, mainly including mechanical energy storage, electrical energy storage, electrochemical energy storage, thermal energy storage, chemical energy storage, and other types. Among them, mechanical energy storage, with its simple structure, high technological maturity, low construction costs, easy maintenance, and other advantages, is widely used in the form of pump energy storage, compressed air energy storage, and flywheel energy storage to provide a flexible energy regulation scheme for the system. Electric energy storage is known for its long life, high efficiency, and cyclic stability, especially supercapacitor and superconducting energy storage technology, showing a new direction for future energy storage technology. And electrochemical energy storage, as a star technology in the energy revolution, has a particularly promising development prospect [5]. In the electrochemical energy storage system, the electrical energy generated by renewable energy is converted into chemical energy in the charging process and released in the discharging process, which covers a variety of technological routes from traditional lead-acid batteries to advanced lithium-ion batteries, flow batteries, etc., which not only have high energy density and fast response capability but also show significant advantages in scalability, maintenance cost, and service life. In particular, redox flow batteries (RFBs) are regarded as the preferred option for building large-scale grid-level energy storage systems due to their unique design concepts, which enable efficient conversion and long-term storage of energy. Among many electrochemical energy storage technologies, alkaline flow batteries have gradually stood out due to their high safety, significant cost-effectiveness, environmental friendliness, and potential for large-scale applications. Han et al. [6] further confirmed the excellent performance and wide application prospects of alkaline flow batteries as a new type of electrochemical energy storage device by comprehensively evaluating several electrochemical energy storage technologies in terms of their relevant parameters, such as energy efficiency (EE), energy density, cycle life, energy storage cost, performance, and the prospect of wide application. The continuous progress and innovation of this technology are leading the field of electrochemical energy storage to move forward in the direction of greater efficiency, economy, and environmental protection, contributing to the profound change of global energy structure and the positive response to climate change.

The core of the RFB, as a cutting-edge high-efficiency energy storage technology, lies in the ingenious use of a positive and negative electrolyte system with separate cycles. This process profoundly embodies the delicate balance of chemical reduction and oxidation reactions. A typical flow battery architecture is built around a core electrochemical cell, consisting of two tanks and a flow-through electrolyte solution containing redox substances, in which the electrolyte solution is circulated back and forth between the various components of the electrochemical cell through a precisely regulated pump system [7]. The electrochemical cell consists of two electrodes and a separator, which not only serves as a bridge for ion transfer, allowing charge-carrying ions to travel freely, but is also a solid barrier that effectively prevents the crossing of redox substances, thus ensuring the orderly

progression of the chemical reactions within the cell. Redox substances, separators, and high-performance electrodes; these three together constitute the key to the performance of the liquid flow battery. The conversion between electrical and chemical energy relies on the active materials in the positive and negative electrolytes through reversible redox reactions (i.e., valence changes). As shown in Figure 14.1, during charging, electrons are released from the high chemical potential state on the positive side of the battery through oxidation reactions. After the electrons move through the external circuit to do useful work, the electrons are accepted at the positive side of the battery in a lower chemical potential state through a reduction reaction. The direction of current during discharge is opposite to the direction of the chemical reaction [8].

In comprehensively evaluating the electrochemical performance of RFBs, several major evaluation criteria should be considered: energy density, which measures the ability of the battery to store energy; power density, which reflects the rate at which the battery releases energy in a short period of time; Coulombic efficiency (CE), which evaluates the losses during charge transfer; voltage efficiency (VE) and EE, which evaluate the efficiency performance of the battery from the perspectives of voltage conversion and overall energy conversion, respectively; and durability, which is an important yardstick to measure the long-term operational stability of the battery. VE and EE evaluate the efficiency of the battery from the perspective of voltage conversion and overall energy

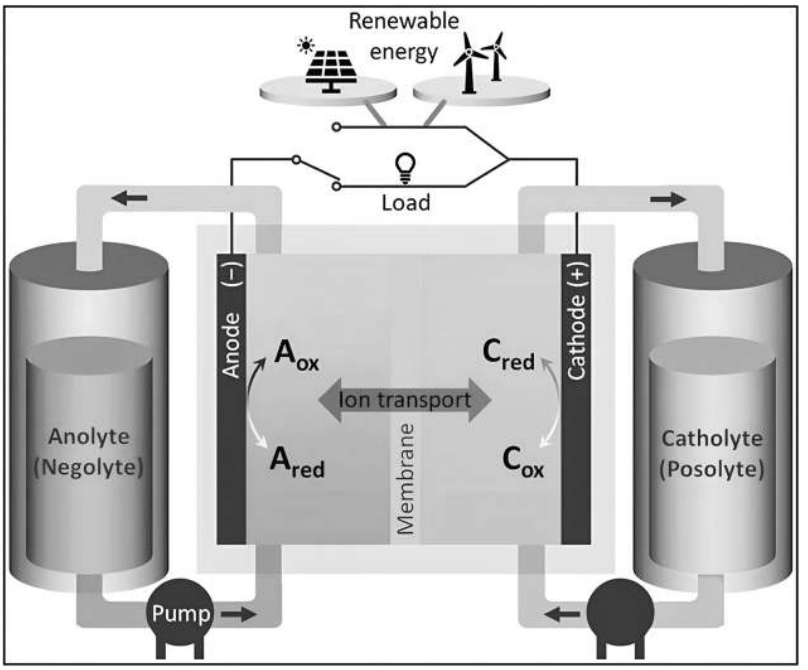

FIGURE 14.1 Schematic diagram of a liquid flow battery [8]. (Adapted with permission from [8]. Copyright the Authors, some rights reserved; exclusive licensee AIP Publishing. This is an open-access article distributed under the terms of the Creative Commons Attribution (CC BY) license, which permits unrestricted use.)

conversion, respectively. The comprehensive consideration of these evaluation criteria lays a solid theoretical foundation and practical guidance for the wide application of RFBs in the field of energy storage [9].

Compared with traditional solid-state batteries, RFBs show remarkable innovation in design. The electrolyte solutions for the positive and negative electrodes are not stored directly inside the battery but are cleverly placed in external tanks. These solutions are efficiently transported to the reaction chamber inside the battery for redox reactions through a sophisticated pumping system and piping network. This unique design eliminates the risk of electrolyte leakage and contamination; furthermore, the core advantage of the flow battery is that the active ingredient exists in the electrolyte in a dissolved state, rather than being embedded in the electrode material as in conventional batteries. This shift not only avoids performance degradation caused by aging or structural changes in the electrode material over time but also ensures the continued stability of battery performance. It is also worth mentioning that the liquid flow battery has achieved a high degree of independence and flexibility in the design of energy density and power density. Specifically, the size of energy density mainly depends on the concentration and volume of active materials in the electrolyte, which provides a direct path to improve the energy storage capacity of the battery. Power density, on the other hand, is influenced by the characteristics of the electrode materials, the fluidity of the electrolyte, and the overall design of the battery, which allows the battery to be adjusted in terms of output power. It is this unique configurability that allows the flow battery to easily respond to diverse energy storage needs. The capacity of a flow battery system can be expanded by simply increasing the volume of electrolyte or increasing the number of cell stacks. This excellent scalability makes flow batteries ideal for large-scale energy storage applications, including, but not limited to, regulation of smart grids, grid-connected storage of renewable energy, and energy supply for electric vehicle charging stations.

Since the 1970s, liquid battery technology has successfully crossed the barriers from basic research to technology application demonstration and has become a key force in promoting the transformation and upgrading of the whole chain of the energy industry—production, conversion, transmission, storage, and consumption. It has not only laid a solid technical support for building a green, low-carbon, safe, and efficient national energy system. In recent years, with the continuous innovation of technology, a variety of new types of liquid current battery energy storage technology systems have emerged. Although the performance of liquid current batteries has met the stringent standards of large-scale energy storage, their economic feasibility is still the main bottleneck that restricts their large-scale promotion. Based on the difference of active materials, liquid power batteries can be subdivided into two categories: inorganic and organic. Further, based on the difference between the electrodes and the solution state on both sides, inorganic liquid flow batteries can be divided into all-liquid inorganic aqueous systems and inorganic hybrid liquid flow batteries. The positive and negative redox pairs of the inorganic system liquid flow battery are inorganic, which have better stability. At present, the energy storage technology represented by all-vanadium liquid flow batteries is booming, but its high cost and relatively low energy density are still problems that need to be solved. In view of

the continuous growth of global demand for green energy, the development of alternative water-based RFBs with lower cost and better performance has become an urgent need, which will bring new breakthroughs and opportunities in the field of energy storage.

Zinc- and iron-based flow battery systems with zinc and iron metal as the anode active components have demonstrated multiple advantages: easy availability of energy storage materials, significant cost-effectiveness, and high energy density, which make them show great potential for application in distributed energy storage and user-side energy storage markets [10]. As an integral part of the flow battery, the electrolyte not only assumes the key functions of energy storage and conductivity but also serves as a medium for the efficient conversion of electrical energy to chemical energy [11]. Based on the difference in the pH value of the electrolyte, the flow battery system is subdivided into an alkaline flow battery system and a neutral (weakly acidic) flow battery system. Among them, alkaline flow batteries stand out for their low cost, excellent safety and stability, as well as theoretically high energy density, and have become a new energy storage technology that has attracted much attention and great research value in the field of electrochemical energy storage.

14.2 WORKING MECHANISM OF ALKALINE FLOW BATTERY

The working mechanism of an alkaline flow battery mainly involves the reaction of an ion-shortening dry cell in the electrolyte, the core of which lies in the electrochemical reaction that occurs at the positive and negative electrodes. In a typical alkaline flow battery system, the application of electric current induces the dissociation of the electrolyte, generating charged ions, which then trigger a redox reaction between the anode and cathode to realize the transfer of electric charge across the electrodes. Specifically, the active material on the anode side undergoes an oxidation process that releases electrons to the external circuit, which are then transferred to the cathode to participate in the reduction reaction on the cathode side. During this process, chemical energy is captured and stored by an electrochemical process, which can subsequently be reversed to electrical energy through a discharge process as required. During charging, the electrical energy provided by the external power supply drives the redox reaction at the positive and negative electrodes, storing the energy in the form of chemical bonds in the electrolyte; during discharging, these chemical energies are released and converted into electrical energy output through the flow of electrons between the electrodes [12].

A distinctive feature of alkaline flow batteries is the use of an electrolyte recycling mechanism in which the electrolyte (i.e., alkaline solution) is circulated between an external storage tank and the battery stack via a pumping system. This design gives the battery system the ability to flexibly adjust the amount of electrolyte to quickly respond to charging and discharging needs while facilitating electrolyte maintenance and replacement. The flow of electrolyte not only accelerates the rate of electrochemical reaction but also promotes the uniform distribution of heat, optimizing the thermal management of the battery system. To avoid the risk of a short-circuit caused by direct contact between the positive and negative electrolytes, alkaline flow batteries have a built-in selective diaphragm, which allows the penetration of charged ions and effectively blocks the direct migration of electrons and other components of the electrolyte, ensuring stable battery

operation. When evaluating the electrochemical performance of alkaline RFBs, redox substances, diaphragms, and electrode materials constitute three key elements. Key performance indicators cover energy density, power density, CE, VE, EE, and lifetime. The theoretical energy density depends on the number of electrons involved in the reaction, the effective concentration of redox species, and the operating voltage. Therefore, strategies to enhance energy density include enhancing the solubility of redox species, lowering the oxidation potential of the anode electrolyte, and raising the reduction potential of the cathode electrolyte to maintain a high operating voltage. Unlike energy density, power density is mainly determined by factors such as operating voltage, kinetics of redox species, electrode surface area, etc. CE and VE are also important indices for evaluating the performance of alkaline flow batteries, in which CE is used to evaluate the selectivity of the cation or anion membrane separator, and VE calculates the ratio of the average discharge voltage to the average charging voltage at a constant current, and the difference of these average values is caused by overpotential. Selection of redox species with fast kinetics and low viscosity, electrolytes with high ionic conductivity, collectors with good electrical conductivity, and suitable flow channel design will help to reduce the overpotential of alkaline flow batteries and achieve high energy density. The durability of alkaline flow batteries is determined by the stability of redox species, membranes, and electrodes. In addition, if the alkaline flow battery can be equipped with a fully reversible anode/cathode pair, a highly selective and stable diaphragm against cross-contamination, and electrode materials with excellent corrosion resistance, it is expected to achieve long-life operation of the system.

14.2.1 Alkaline Zinc-Based Flow Battery

Zinc is the most active metal that can be electrodeposited from aqueous electrolytes, and the large number of electrons transferred involved in its electrochemical reaction process endows it with the ability to achieve excellent energy conversion and high-density power output [13]. In the field of flow batteries, the application of zinc as an anode material is particularly noteworthy, as it not only possesses high unit voltage and energy density but also becomes a leader in decentralized energy storage solutions due to its low cost and the stability it exhibits in air and aqueous solution environments [14]. Compared to neutral zinc-based flow batteries, alkaline zinc-based flow batteries stand out with their unique anode electrolyte, alkaline zinc-based electrolyte ($Zn(OH)_4^{2-}$), which has a redox potential compared to the neutral environment of Zn^{2+} is more negative [8], thus promoting more efficient electrochemical reactions. In addition, the conductivity of alkaline electrolytes is usually higher than that of neutral electrolytes, coupled with the fact that the migration rate of OH^- ions is much higher than that of K^+ or Na^+. Together, these two factors enable alkaline zinc-based flow batteries to carry higher operating current densities and thus achieve higher power density output.

Since the concept first emerged in the 1970s, zinc-based flow battery technology has undergone significant development, and through continuous innovation and diversified coupling of anode reactions, alkaline flow battery systems such as zinc-iron, zinc-bromine, and zinc-iodine, as well as alkaline zinc-based flow battery variants such as zinc-nickel,

zinc-air, zinc-cerium, zinc-vanadium, zinc-manganese, and so forth, based on different anode reactants, have been derived [15].

The core of alkaline zinc-based flow batteries lies in the storage and release of charge through an electrolyte consisting of zinc and a positive active substance, relying on the electrodeposition of zinc in a flowing electrolyte as a negative reaction. The operating principle is based on the electrochemical deposition and dissolution process of zinc in an alkaline electrolyte, whereby zinc ions are combined with different cathode actives in an alkaline environment to form a recyclable zinc plate structure. The electrolyte of such batteries usually consists of a high concentration of strong bases (e.g., KOH, NaOH, LiOH) with zinc salts, which not only provide the necessary alkaline environment but also facilitate the efficient conduct of electrochemical reactions. As shown in Figure 14.2, the whole working process can be divided into four main steps: charging, storing, releasing, and recharging. During the charging process, an external DC power supply drives the zinc ions from the anode side across the ion exchange membrane to the cathode side, where they combine with electrons to form zinc metal and are deposited at the cathode; at the same time, the active substances in the cathode electrolyte undergo a corresponding change and are attached to the anode. When charging is completed, the system enters the storage stage, zinc ions and active substances carrying positive and negative charges flow freely in the electrolyte and enter the anode and cathode electrolyte through the ion exchange membrane to store charge energy;

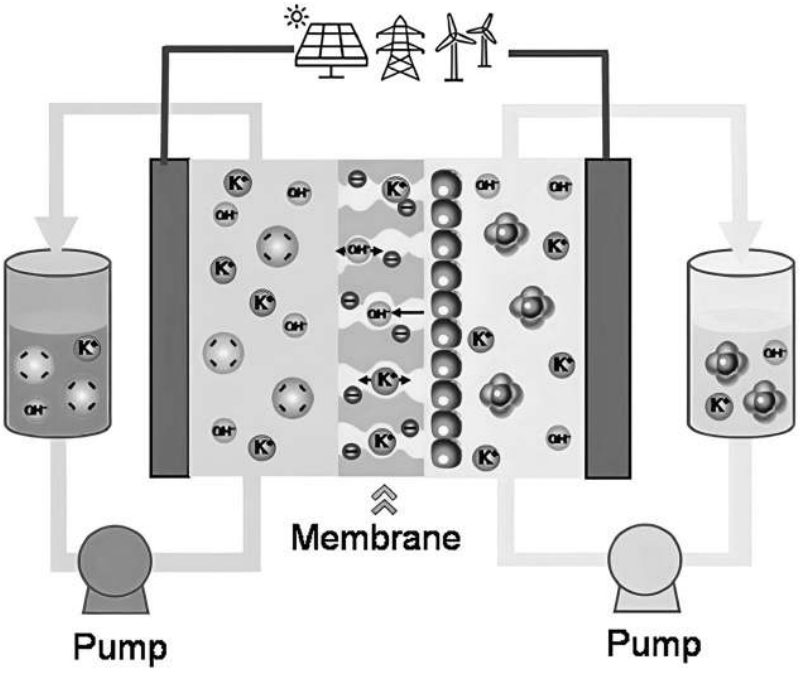

FIGURE 14.2 Working principle of zinc-based flow battery [16]. (Adapted with permission from [16]. Copyright the Authors, some rights reserved; exclusive licensee Springer Nature. Distributed under a Creative Commons Attribution License 4.0 (CC BY)

when it is necessary to release the stored charge, the electrolyte is guided back to the battery stack, and the zinc ions and the active substances migrate between the anode and cathode to form an electric current through the external circuit to complete the energy conversion [15]. Finally, through the recharging operation, the alkaline zinc-based flow battery can repeat the storage and release of charge to achieve the sustainable use of energy.

The specific chemical reactions of an alkaline zinc-based flow battery are as follows:

$$\text{Negative charging}: \mathrm{Zn(OH)_4^{2-}} + 2\mathrm{e^-} \leftrightarrow \mathrm{Zn} + 4\mathrm{OH^-} \tag{14.1}$$

$$\text{Positive discharge}: C^{m^+} - e^- \leftrightarrow C^{(m+1)^+} \tag{14.2}$$

$$\text{Total reaction}: \mathrm{Zn(OH)_4^{2-}} + 2C^{m+} \leftrightarrow \mathrm{Zn} + 2C^{(m+1)^+} + 4\mathrm{OH^-} \tag{14.3}$$

14.2.2 Alkaline Iron-Based Flow Battery

Despite the significant breakthroughs in the research of new organic flow batteries, however, the high cost of their active components and organic solvents still constitutes a major burden on the cost of the electrolyte in water-based flow batteries, which hinders the development of large-scale commercial applications [17], and iron, as one of the most abundant metallic elements in the earth, is a very ideal source of active substances for flow batteries because of its low cost, non-toxicity, and environmentally friendly characteristics. Ideal source of active material for flow batteries. In the pursuit of cost-effective large-scale energy storage solutions, alkaline iron-based flow batteries, with their advantages of low-cost materials, high iron content, and non-toxicity of the system, show great cost-effectiveness and resource potential, which is a perfect fit for the future needs of large-scale energy storage in power grids. Iron-based liquid flow battery refers to the liquid flow battery system with Fe^{2+}/Fe^{3+} as the positive redox electric pair, including all-iron liquid flow batteries as well as liquid flow battery systems with different positive and negative active substances (e.g., ZnFe [18], FeCr [19]). When the iron-based flow battery operates, the electrolyte rich in active substances circulates in the electrochemical chamber, triggering an electrochemical reaction on the electrode surface to realize the charging and discharging cycle. When the battery is charging, the electrode reaction is as follows:

$$\text{Positive pole}: \mathrm{Fe^{2+}} = \mathrm{Fe^{3+}} + \mathrm{e^-} \tag{14.4}$$

$$\text{Negative}: X^{m+} + (m-n)e^- = X^{n+} \tag{14.5}$$

During charging, Fe^{2+} ions at the positive electrode release electrons and are oxidized to Fe^{3+}, while the negative electrode undergoes a corresponding reduction process.

Different types of iron-based liquid flow batteries can be constituted by the preferred selection of the negative electrode pair of the liquid flow battery, and their performance varies.

In all-iron flow batteries, the iron-based chemical exhibits excellent chemical compatibility with the aqueous electrolyte, and the presence of highly soluble $FeCl_2$ as the active species in both half-cells further confers a non-cross-contamination property to the alkaline all-iron flow battery system [20]. The two half-cells of the all-iron liquid flow battery use inexpensive and abundantly available ferric chloride, the electrical energy is stored in the form of chemical energy, and the electrolyte usually consists of metal salt ions. As shown in Figure 14.3, the positive and negative electrolytes of the all-iron flow battery are distributed in two tanks, and the electrolyte for the positive electrode is a mixture of ferrous chloride and ferric chloride. Its flow power is provided by a pump system [21]. In the all-iron redox flow cell operation, different valence states of iron are used for the positive and negative electrodes, and the electrolyte in the external tanks is transported by a pump with piping to the internal reaction chamber of the cell for the (2.1) half-cell reaction. The positive electrode process is designed for solid-state deposition and dissolution of iron, while the negative electrode relies on carbon-based materials for redox conversion [22].

$$\text{Positive electrode}(\text{electroplating}): 2Fe^{2+} \leftrightarrow Fe^{3+} + 2e^{-} + 0.77\,V \tag{14.6}$$

$$\text{Negative}(\text{redox}): Fe^{2+} + 2e^{-} \leftrightarrow Fe^{0} + 0.44\,V \tag{14.7}$$

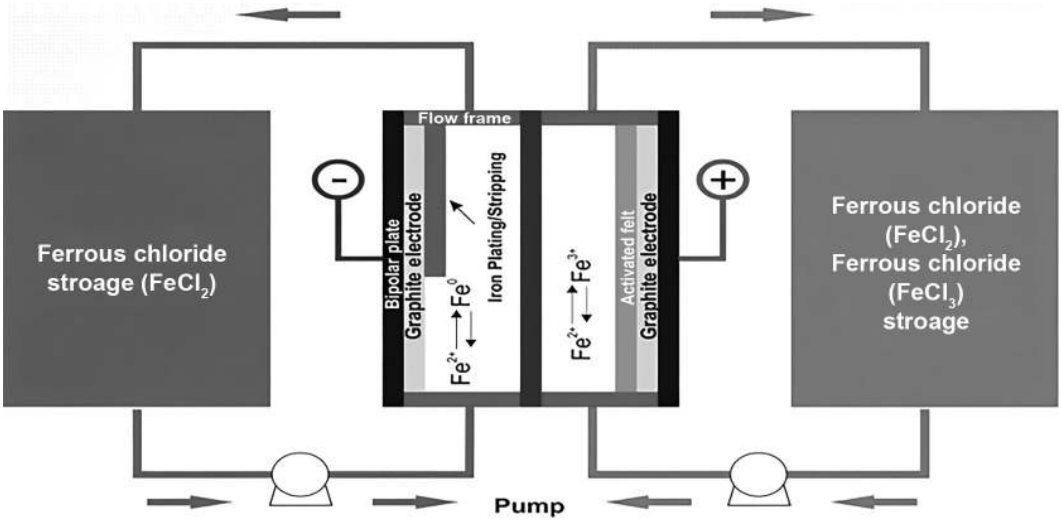

FIGURE 14.3 Schematic diagram of an all-iron flow battery [12]. (Adapted with permission from [12]. Copyright the Authors, some rights reserved; exclusive licensee Springer Nature. Distributed under a Creative Commons Attribution License 4.0 (CC BY)

$$\text{Total reaction}: 3Fe^{2+} \leftrightarrow Fe^{0} + 2Fe^{3+} + 1.21\,V \tag{14.8}$$

In an alkaline iron-based hybrid flow battery, Fe_3O_4 or FeOOH, the compound of iron, is used as the negative electrode of the battery, which is sequentially reduced to $Fe(OH)_2$ and singlet iron during the charging process, and the inverse reaction occurs during the discharge process:

$$Fe_3O_4 + 4H_2O + 2e^- \rightleftharpoons 3Fe(OH)_2 + 2OH^- \tag{14.9}$$

$$FeOOH + H_2O + e^- \rightleftharpoons Fe(OH)_2 + OH^- \tag{14.10}$$

$$Fe(OH)_2 + 2e^- \rightleftharpoons Fe + 2OH^- \quad E_0 = 0.877\,V \tag{14.11}$$

The oxidation of Fe to form $Fe(OH)_2$ may be the reaction of OH^- ion adsorption and the soluble intermediate $HFeO_2^-$

$$Fe + OH^- \rightleftharpoons \left[Fe(OH)\right]_{ad} + e^- \tag{14.12}$$

$$\left[Fe(OH)\right]_{ad} + OH^- \rightleftharpoons Fe(OH)_2 + e^- \tag{14.13}$$

$$\left[Fe(OH)\right]_{ad} + 2OH^- \rightleftharpoons HFeO_2^- + H_2O + e^- \tag{14.14}$$

$$HFeO_2^- + H_2O \rightleftharpoons Fe(OH)_2 + OH^- \tag{14.15}$$

Parameters affecting the cell performance of alkaline iron-based flow batteries include self-discharge of electrodes, wettability and hydrophilicity, pH change of electrolyte, and hydrogen precipitation reaction (HER) during plating [23].

14.3 ADVANCES IN ALKALINE FLOW BATTERIES

14.3.1 Alkaline Zinc-Based Flow Batteries

14.3.1.1 Alkaline Zinc-Based Flow Battery Development Bottleneck and Improvement

Although alkaline zinc-based flow batteries have the advantages of high discharge voltage, large capacity, and cost-controllable materials, their development has been limited by the growth of irregular zinc dendrites as a bottleneck. Zinc dendrites are the biggest bottleneck in the development of zinc-based liquid current batteries. The fundamental reason is

that zinc ions in the charging and discharging process, the dissolution and deposition of their behavior have a random uncertainty. The electrode material in the multiple charging and discharging has a surface charge distribution that is not uniform [24], and the charge aggregation area will induce more ions to deposit, resulting in the macroscopic deposition of zinc ions produced by the dendritic shape of the growth of macro-deposits. The disordered growth of zinc dendrites will puncture the diaphragm, resulting in structural short-circuiting of the flow battery and a self-discharge phenomenon, which will bring about safety problems that cannot be ignored.

14.3.1.2 Research Progress of Alkaline Zinc-Based Liquid Current Battery Electrolyte

As one of the core components of the liquid current battery, the comprehensive performance of the electrolyte plays a crucial role in the overall performance of the battery. The irregular concentration gradient of zinc ions in the electrolyte is one of the possible causes of the disordered growth of zinc dendrites. By improving the performance of the anode electrolyte in zinc-based flow batteries, the negative impact of zinc dendrites on the stability of the battery can be avoided. The addition of soluble salts to the electrolyte is one of the effective ways to address the formation of zinc dendrites, and the presence of additives can help the deposition of zinc ions to be denser and more uniform. Components traditionally used as additives include mercury, cadmium, lead, or their oxides, and these heavy metals and their oxides are mostly added to the electrolyte in the form of soluble hydroxide salts. As an alternative addition, acid radical salts containing elements such as bismuth, calcium, magnesium, indium, tin, and tungsten have also been shown to be effective [25,26]. However, the use of such high concentrations of additives can also reduce the utilization of the active substance and thus affect the electrochemical performance. Previous studies by Yuan et al. have shown that low concentrations of tin ions can have a significant effect on the improved morphology of zinc deposition at concentrations as low as 1.44 mM [27].

Organic additives possess a wealth of physicochemical properties and have received increasing attention in recent years, with common organic additives including polyvinyl alcohol, polyethylene glycol (PEG), polyethyleneimine (PEI), quaternary ammonium salts, polytetrafluoroethylene (PTFE), and cellulose [28–34].

14.3.1.3 Progress of Ion Exchange Membrane for Alkaline Zinc-Based Flow Battery

The traditional zinc-based liquid flow batteries mostly use perfluorosulfonic acid proton exchange membranes (Nafion membranes), which have excellent mechanical properties as well as excellent chemical stability, but the lower ion selectivity as well as low conductivity and high cost have become the bottlenecks restricting their further development. Theoretically, the ion selectivity of the membrane can be improved by adjusting the size and connectivity of the micropores on the membrane, but the membrane preparation process is often extremely complex, which makes the surface micromorphology of the membrane uncertain and leads to various microdefects. For this reason, the emergence of porous and non-fluorinated membranes has made it possible to control the cost of membranes. Anion-exchange membranes based on hydrocarbon polymeric materials such as sulfone and polyether ether ketone have been extensively studied in alkaline flow batteries

[35]. Polymeric membranes have shown a high degree of suitability for flow batteries, for example, sulfonated polyimide, sulfonated polysulfone, sulfonated poly(ether ketone), sulfonated poly(fluorenyl ether ketone), polypropylene, and composite membranes of them [36]. Among them, SPEEK has received much attention because of its low cost, high ion selectivity, and simple fabrication process [37]. However, these polymer membranes generally exhibit poor stability to hydroxides, and the hydrocarbon polymer backbone is prone to stripping from effective anion-exchange groups after receiving corrosion by alkaline groups for a long period of time. Therefore, the development of alkaline-stabilized membranes with high ionic conductivity is important for alkaline flow batteries. In addition to alkaline stability, another key to the membrane in alkaline zinc-based flow batteries is high mechanical strength. The membrane with high mechanical strength can effectively counteract the damage caused by zinc dendrites, thus achieving stable operation of the flow battery.

14.3.1.4 Research Progress of Electrode Materials for Alkaline Zinc-Based Flow Batteries

In alkaline zinc-based flow batteries, the zinc electrode has defects such as zinc dendrite, mechanical deformation, hydrogen precipitation, and so on, resulting in a short cycle life of the battery in general. Common alkaline zinc-based batteries include alkaline zinc-nickel flow batteries, alkaline zinc-iodine flow batteries, alkaline zinc-air flow batteries, and so on. Electrode materials, as a crucial part, play a decisive role in the overall performance, and the electrode materials should have a high specific surface area, a good chemical suitability for the electrolyte, a high electrical conductivity, an excellent electrochemical activity, and mechanical stability. The limitations of zinc electrodes can be addressed in alkaline zinc-based liquid flow batteries by the design of zinc anode nanostructuring. Carbon materials, which have excellent electrochemical stability and provide excellent conductivity for the electrode as a whole, have been widely used in various liquid flow battery systems. Therefore, various methods of carbon-based electrode material modification have been widely reported [38].

14.3.2 Advances in Alkaline Iron-Based Flow Batteries

14.3.2.1 Bottlenecks and Improvements in the Development of Alkaline Iron-Based Hybrid Flow Batteries

In alkaline environments, an unavoidable problem of iron-based flow batteries is the passivation of electrodes and hydrogen precipitation as a side reaction during the charging process, while during the discharge process, due to the low solubility of iron hydroxide, it will adhere to the low-conductivity hydroxide film on the surface of the electrodes, which will make it difficult for the active material to participate in the electrode reaction after many cycles, resulting in electrode passivation and the decay of multiplicative performance, which can greatly influence the charge-discharge response.

In order to inhibit the hydrogen precipitation reaction, a feasible method is to add additives to the electrolyte. The molecules of the introduced additives will be adsorbed on the surface of the electrode and compete with the hydrogen ions for the reduction sites, thus inhibiting the generation of hydrogen, and in addition, the deposits on the surface of the

electrode after the additives are involved in the redox process will increase the overall overpotential of the surface of the electrode, thus inhibiting the rate of hydrogen precipitation reaction [11,19,39].

14.3.2.2 Alkaline All-Iron Flow Battery

Alkaline all-iron flow batteries with redox couples of iron complexes as active materials are considered to be promising for research due to the advantages of the low cost of iron electrolyte and flexibility in power and capacity design, etc. Among the iron complexes, iron-triethanolamine performs well with excellent relative negative potential and excellent electrochemical kinetics, as seen in many reports. For example, Yan et al. [40] proposed an all-liquid all-iron liquid flow battery by coupling an iron-triethanolamine (TEA) redox pair and an iron-cyanide redox pair in an alkaline aqueous system. However, iron complexes such as Fe-triethanolamine lack cyclic stability in strongly alkaline environments, and higher pH values can lead to byproduct competition, such as the reduction of singlet iron [41,42]. Liu [43] proposed a relatively stable alkaline all-iron liquid flow battery on this basis by coupling $[Fe(CN)_6]^{3-}/[Fe(CN)_6]^{4-}$ redox coupling with iron/ferrous gluconate in conjunction with redox electrocoupling, achieving a high solubility of the complex (1.2 mol L^{-1}), high redox kinetic processes, and good stabilization properties in alkaline environments. The high stability of the ferric gluconate complex originates from the stable six-coordinated iron species, which makes a stable alkaline all-iron flow battery possible. The calculated system has a feasible low cost ($76.11 per kWh) as well as an efficient cycling performance, and this work will provide a solid foundation for the application of alkaline all-iron flow batteries in energy storage engineering.

14.4 CONCLUSIONS AND PERSPECTIVES

In this chapter, the development history, basic structure and principle, current development status, and problems to be solved of alkaline flow batteries are described in detail. Alkaline zinc-based flow batteries have developed various systems such as zinc-iron, zinc-nickel, zinc-iodine, zinc-air, and so on by virtue of zinc's own unique advantages of high discharge voltage and high energy density. At present, there have been a small number of distributed energy storage projects based on alkaline zinc-based liquid current batteries that have achieved certain commercialization benefits. However, the dendritic problem of zinc-based batteries has been the biggest bottleneck limiting their development, and in-depth research is needed to solve the zinc dendritic problem from aspects including modification of the electrolyte, development of low-resistance and high-selectivity ionic films, and modification of electrode materials. Alkaline iron-based liquid current batteries, on the other hand, have also gained extensive research and shown great commercial potential, relying on the characteristics of iron's wide range of low-cost sources and environmental friendliness. Alkaline iron-based flow batteries have problems such as hydrogen precipitation and electrode passivation and need to focus on the development of feasible and highly stable iron complex systems and efficient long-life ionic membranes.

In summary, alkaline flow batteries are currently in a rapidly changing stage of development, new materials and new structural innovations are driving the development of

alkaline flow batteries in the direction of safer, more stable, reliable, and low cost, although there is still a long way to go before large-scale commercial applications, but with the increasing demand for energy storage, it is believed that the existing problems can be properly resolved. All in all, the prospect of alkaline flow batteries in energy storage is worth looking forward to.

REFERENCES

1. C. Zhang, L. Zhang, Y. Ding, S. Peng, X. Guo, Y. Zhao, G. He, G. Yu, Progress and prospects of next-generation redox flow batteries, *Energy Storage Materials*. 15 (2018) 324–350.
2. H. Zhang, W. Lu, X. Li, Progress and perspectives of flow battery technologies, *Electrochemical Energy Reviews*. 2 (2019) 492–506.
3. L. Zhi, C. Liao, P. Xu, F. Sun, C. Yuan, F. Fan, G. Li, Z. Yuan, X. Li, An artificial bridge between the anode and the anolyte enabled by an organic ligand for sustainable zinc-based flow batteries, *Energy & Environmental Science*. 17 (2024) 717–726.
4. J. Winsberg, T. Hagemann, T. Janoschka, M. D. Hager, U. S. Schubert, Redox-flow batteries: From metals to organic redox-active materials, *Angewandte Chemie International Edition*. 56 (2017) 686–711.
5. R. Nie, Y. Nie, J. Wu, L. Yu, L. Liu, J. Xi, An aqueous alkaline zinc–sulfur flow battery, *Chemical Communications*. 60 (2024) 2946–2949.
6. Z. Yuan, Y. Yin, C. Xie, H. Zhang, Y. Yao, X. Li, Advanced materials for zinc-based flow battery: Development and challenge, *Advanced Materials*. 31 (2019) 1902025.
7. P. Xu, Z. Yuan, X. Li, Progress on zinc-based flow batteries, *Chinese Science Bulletin*. 69 (2024) 3110–3121.
8. A. Okazawa, T. Kakuchi, K. Kawai, M. Okubo, Iron-based catholytes for aqueous redox-flow batteries, *APL Materials*. 11 (2023) 110901.
9. Z. Hou, X. Chen, J. Liu, Z. Huang, Y. Chen, M. Zhou, W. Liu, H. Zhou, Towards a high efficiency and low-cost aqueous redox flow battery: A short review, *Journal of Power Sources*. 601 (2024) 234242.
10. Y. Song, H. Yan, H. Hao, Z. Liu, C. Yan, A. Tang, Simultaneous regulation of solvation shell and oriented deposition toward a highly reversible Fe anode for all-iron flow batteries, *Small*. 18 (2022) 2204356.
11. J. Yang, H. Yan, Q. A. Zhang, Y. Song, Y. Li, A. Tang, A universal additive design strategy to modulate solvation structure and hydrogen bond network toward highly reversible Fe anode for low-temperature all-iron flow batteries, *Small*. 20 (2024) 2307354.
12. A. Dinesh, S. Olivera, K. Venkatesh, M. S. Santosh, M. G. Priya, Inamuddin, A. M. Asiri, H. B. Muralidhara, Iron-based flow batteries to store renewable energies, *Environmental Chemistry Letters*. 16 (2018) 683–694.
13. A. Dinesh, M. S. Anantha, M. S. Santosh, M. G. Priya, K. Venkatesh, K. S. Yogesh Kumar, M. S. Raghu, H. B. Muralidhara, Improved performance of iron-based redox flow batteries using WO_3 nanoparticles decorated graphite felt electrode, *Ceramics International*. 47 (2021) 10250–10260.
14. M. Daniel, N. P. Byron, C. M. Krowne, Harnessing redox flow batteries for industrial applications: Opportunities and future directions, *Journal of Power Sources*. 591 (2024) 233889.
15. C. Duan, H. Lu, D. Zhang, Z. Zhu, Y. Qin, X. Yuan, Y. Jin, Uniform redistribution of Zn^{2+} flux induced by remodeling the solvated structure to form zincophilic interfaces via sodium alginate electrolyte additive, *Chemical Engineering Journal*. 487 (2024) 150413.
16. Z. Yuan, X. Li, Perspective of alkaline zinc-based flow batteries, *Science China Chemistry*. 67 (2022) 260–275.

17. M. Shin, S. Park, K. Hyun, Y. Kwon, Spectroscopic and electrochemical analyses elucidating capacity degradation mechanism of iron-ligand complex and air in all iron aqueous redox flow batteries, *Chemical Engineering Journal*. 471 (2023) 144682.
18. J. Chullipparambil Balakrishnan, M. Pulikkotti Peter, D. Davis Kombarakaran, J. Ambadan Kunjilona, J. Vadakkan Thomas, Improvement in the performance of an Fe/FeII electrode in an all-iron redox flow battery by the addition of ZnII ions, *ChemistrySelect*. 7 (2022) e202201222.
19. Y. Song, H. Yan, Z. Cong, J. Yang, Y. Li, A. Tang, Surface engineered carbon felt toward highly reversible Fe anode for all-iron flow batteries, *Chemical Engineering Journal*. 487 (2024) 150592.
20. Y. Bai, B. Cai, L. Wang, Y. Gao, X. Li, X. Yang, W. Lü, Aqueous hybrid iron-ion battery capacitors with ultra-long cycle life, *Chemical Engineering Journal*. 487 (2024) 150586.
21. J. Jiang, J. Liu, Iron anode-based aqueous electrochemical energy storage devices: Recent advances and future perspectives, *Interdisciplinary Materials*. 1 (2022) 116–139.
22. S. Belongia, X. Wang, X. Zhang, Progresses and perspectives of all-iron aqueous redox flow batteries, *Advanced Functional Materials*. 34 (2024) 2302077.
23. Y. Song, K. Zhang, X. Li, C. Yan, Q. Liu, A. Tang, Tuning the ferrous coordination structure enables a highly reversible Fe anode for long-life all-iron flow batteries, *Journal of Materials Chemistry A*. 9 (2021) 26354–26361.
24. Y. Cui, Y. He, W. Yu, Y. Ma, Z. Zhao, J. Yu, P. Tan, Revealing the Zn electrodeposition process behind the voltage profile, *Journal of Power Sources*. 601 (2024) 234294.
25. Q. Nian, X. Zhang, Y. Feng, S. Liu, T. Sun, S. Zheng, X. Ren, Z. Tao, D. Zhang, J. Chen, Designing electrolyte structure to suppress hydrogen evolution reaction in aqueous batteries, *ACS Energy Letters*. 6 (2021) 2174–2180.
26. Y.-H. Wen, J. Cheng, L. Zhang, X. Yan, Y.-S. Yang, The inhibition of the spongy electrocrystallization of zinc from doped flowing alkaline zincate solutions, *Journal of Power Sources*. 193 (2009) 890–894.
27. Y. F. Yuan, J. P. Tu, H. M. Wu, S. F. Wang, W. K. Zhang, H. Huang, Effects of stannous ions on the electrochemical performance of the alkaline zinc electrode, *Journal of Applied Electrochemistry*. 37 (2006) 249–253.
28. J.-M. Assafrei, G. Yusibova, K. Ping, H.-M. Piirsoo, A. Tamm, M. Käärik, J. Leis, J. Aruväli, V. Grozovski, E. Lust, N. Kongi, Maximizing the performance of aqueous zinc-air/iodide hybrid batteries through electrolyte composition optimization, *Journal of Energy Storage*. 74 (2023) 109528.
29. H. Park, G. Park, S. Kumar, H. Yoon, J. Baek, T. Tamulevičius, S. Tamulevičius, H.-J. Kim, Synergistic effect of electrolyte additives on the suppression of dendrite growth in a flowless membraneless Zn–Br_2 battery, *Journal of Power Sources*. 580 (2023) 233212.
30. L. Zhi, T. Li, X. Liu, Z. Yuan, X. Li, Functional complexed zincate ions enable dendrite-free long cycle alkaline zinc-based flow batteries, *Nano Energy*. 102 (2022) 107697.
31. B. Liu, X. Yuan, Y. Li, Colossal capacity loss during calendar aging of Zn battery chemistries, *ACS Energy Letters*. 8 (2023) 3820–3828.
32. D. Yang, J. Li, C. Liu, W. Xing, J. Zhu, Design strategy and comprehensive performance assessment towards Zn anode for alkaline rechargeable batteries, *Journal of Energy Chemistry*. 82 (2023) 122–138.
33. R. Ling, Z. Zhu, K. Peng, J. Fang, W. Zou, Q. Li, Y. Liu, Q. Zhu, N. Lin, T. Xu, Z. Yang, Dual-function electrolyte additive design for long life alkaline zinc flow batteries, *Advanced Materials*. 36 (2024) 2404834.
34. X. Liu, H. Du, J. Gao, Z. Shen, T. Sun, Z. a. Tan, F. Chu, Design of a cobweb bionic flow field for organic redox flow battery, *Journal of Power Sources*. 591 (2024) 233848.
35. D. Chen, C. Kang, W. Duan, Z. Yuan, X. Li, A non-ionic membrane with high performance for alkaline zinc-iron flow battery, *Journal of Membrane Science*. 618 (2021) 118585.

36. L. Tong, M.-A. Goulet, D. P. Tabor, E. F. Kerr, D. De Porcellinis, E. M. Fell, A. Aspuru-Guzik, R. G. Gordon, M. J. Aziz, Molecular engineering of an alkaline naphthoquinone flow battery, *ACS Energy Letters*. 4 (2019) 1880–1887.
37. Z. Yuan, Y. Duan, H. Zhang, X. Li, H. Zhang, I. Vankelecom, Advanced porous membranes with ultra-high selectivity and stability for vanadium flow batteries, *Energy & Environmental Science*. 9 (2016) 441–447.
38. C. Xie, H. Zhang, W. Xu, W. Wang, X. Li, A long cycle life, self-healing zinc–iodine flow battery with high power density, *Angewandte Chemie International Edition*. 57 (2018) 11171–11176.
39. A. Ramadas, A. Dinesh, M. S. Anantha, M. Rani, K. Venkatesh, J. M. Patil, C. B. Mohan, H. B. Muralidhara, K. Y. Kumar, Functionalized graphene-MoO2 frameworks: An efficient electrocatalyst for iron-based redox flow battery and supercapacitor application with enhanced electrochemical performances, *Journal of Physics and Chemistry of Solids*. 171 (2022) 110990.
40. K. Gong, F. Xu, J. B. Grunewald, X. Ma, Y. Zhao, S. Gu, Y. Yan, All-soluble all-iron aqueous redox-flow battery, *ACS Energy Letters*. 1 (2016) 89–93.
41. A. Lê, D. Floner, T. Roisnel, O. Cador, L. Chancelier, F. Geneste, Highly soluble Fe(III)-triethanolamine complex relevant for redox flow batteries, *Electrochimica Acta*. 301 (2019) 472–477.
42. M. Shin, C. Noh, Y. Chung, Y. Kwon, All iron aqueous redox flow batteries using organometallic complexes consisting of iron and 3-[bis (2-hydroxyethyl)amino]-2-hydroxypropanesulfonic acid ligand and ferrocyanide as redox couple, *Chemical Engineering Journal*. 398 (2020) 125631.
43. X. Liu, T. Li, Z. Yuan, X. Li, Low-cost all-iron flow battery with high performance towards long-duration energy storage, *Journal of Energy Chemistry*. 73 (2022) 445–451.

CHAPTER 15

Vanadium Redox Flow Batteries

Mohammad Zarei-Jelyani and Mohammad Reza Rahimpour

15.1 INTRODUCTION

Renewable energies are widely acknowledged for their crucial contribution to reducing carbon emissions in the global energy industry [1,2]. Solar and wind energy sources are introduced as crucial players in constructing a future that is more sustainable [3,4]. As reported by the International Energy Agency, it is anticipated that by 2040, there will be a 60% rise in the worldwide demand for energy derived from renewable sources, particularly wind and solar photovoltaic energy [5].

However, sources of renewable energy often lack a consistent and rapid supply due to their naturally fluctuating characteristics. This results in an instability of the power grid [6]. Therefore, it is crucial to develop an efficient energy storage system (ESS). The strategy intends to enable the integration of intermittent renewable sources into the electrical grid by storing the generated energy and releasing it as needed, despite their fluctuating and unpredictable nature. Consequently, it is feasible to generate energy during periods of low demand, when the price is lower, and then utilize it during times when demand surpasses generation capacity [7].

Numerous factors must be considered to design an ESS. The technology should satisfy requirements including energy efficiency, long lifetime, cost-effectiveness, reliability, scalability, substantial capacity for storage, minimal response time, and safety [8,9]. Within this particular context, electrochemical systems represent a superior choice between energy storage technologies, primarily owing to their high performance and adaptability in meeting the vital requirements. Redox flow batteries (RFBs) have garnered significant interest for their use in ESSs. They are known for their adaptable design, outstanding efficiency, and extended lifetime [10]. RFBs are composed of rechargeable batteries, where conversions of energy take place via reversible electrochemical processes involving two redox pairs. Pumps link two key parts of this battery type: a series of stacked cells that conduct

DOI: 10.1201/9781003506379-15

electrochemical processes and external reservoirs that store electrolytes [11]. Vanadium redox flow batteries (VRFBs) are considered the most promising technology for the storage of energy on a large scale among the existing RFBs [12]. Their function is to utilize four distinct oxidation states of vanadium ions, which produce two separate redox pairs known as catholyte and anolyte. This ensures that only vanadium is an active species on both sides. The employment of vanadium as the sole active element is primarily associated with a decrease in contamination issues within the electrolytes, resulting in an elongation of the battery's lifespan as well as the maintenance of the solubility of the species without undergoing a change in phase [13].

As the viability of utilizing VRFBs has grown, researchers have conducted a wide range of studies in recent years. Recent investigations focus on developing the system according to the basic mechanism provided by the Skyllas-Kazacos group in the late 1980s [14]. Since then, extensive studies have been conducted with the goal of advancing the technical development of VRFBs. Numerous recent studies have examined the mechanism of batteries as a whole and the particular technologies associated with components of VRFB systems [8].

15.2 FUNDAMENTAL FEATURES AND OPERATIONAL PRINCIPLES

The negative half-cell of a VRFB contains the pair V^{2+}/V^{3+}, whereas the positive half-cell includes the pair VO^{2+}(or V^{4+})/VO_2^+ (or V^{5+}). The system has two exterior reservoirs designed for storing redox electrolytic pairs. The electrolytes from these reservoirs are pumped for circulation individually through the associated half-cells, in which the reaction takes place on inert electrodes [15]. The system consists of two half-cells, each containing a bipolar plate and an electrode. These half-cells are separated via an ion-exchange membrane, whose function is to avoid the mixing of electrolytes while still allowing for ion exchange. This membrane ensures that charge neutrality exists between the electrolytes. The two half-cells combine to create an electrochemical flow cell, which is the basic unit of a VRFB system (Figure 15.1) [13].

During the charging process, VO^{2+} ions undergo oxidation to form VO_2^+ on the positive side, resulting in the release of electrons and H^+ ions. On the negative side, V^{3+} ions are reduced to V^{2+} ions as they react with electrons, which flow throughout the external circuit [16]. The various vanadium ions present in the cell can be distinguished by their respective colors. These include V^{2+} (violet), V^{3+} (green), VO^{2+} (blue), and VO_2^+ (light-yellow) [17].

A cell stack assembly is formed by combining numerous individual cells. The cells have connections through a bipolar design arrangement, which serves as the fundamental module for a VRFB system, providing increased potential. Maintaining physical separation of the reagents, this module connects electrically the positive electrode of one cell to the negative electrode of a neighboring cell [5]. The obtained potential difference is equal to the sum of each single cell potential. VRFBs use numerous stacks arranged in matrices to enable greater applications [18].

VRFB's design is completely associated with operating issues, including efficiency and system performance, in order to fulfill its intended function of energy storage. The design of the VRFB justifies the separation of its primary parts, namely the stack and

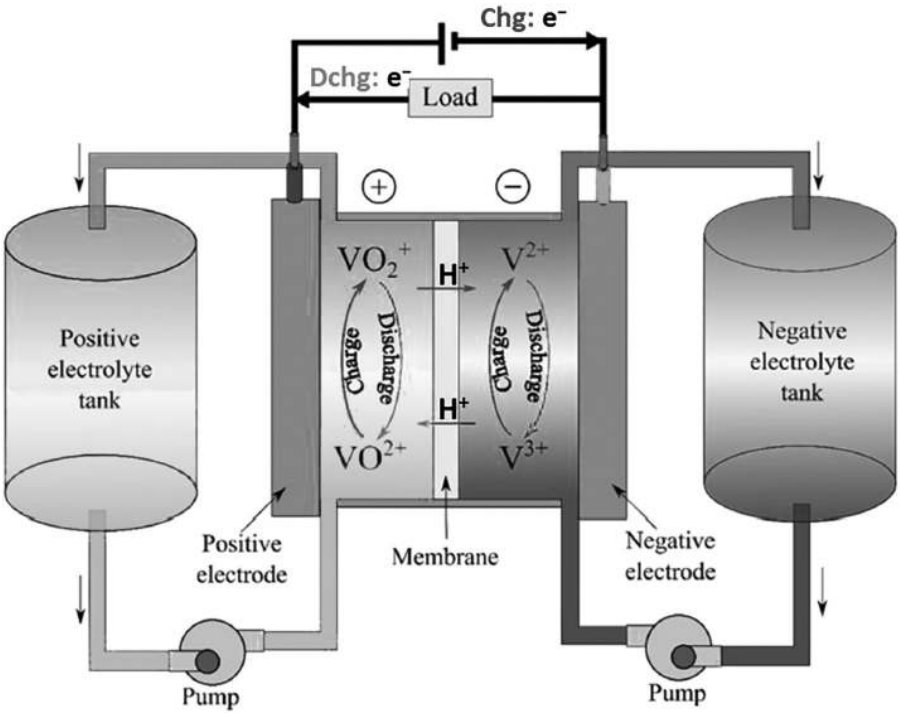

FIGURE 15.1 A schematic of a vanadium redox flow battery. (Adapted with permission from [5], Copyright (2024), Elsevier.)

storage reservoirs, to allow for independent scaling of stored energy (kWh) and power (kW or MW) [19].

15.3 KEY CELLULAR COMPONENTS OF A VRFB

15.3.1 Electrolyte

15.3.1.1 Overall Features

Volume and concentration of the electrolyte have a direct effect on the energy density and capacity of a VRFB because of its role as a medium of energy storage. Electrolyte liquids support vanadium active soluble species, which enable electrochemical reactions and provide ionic conductivity. The electrolyte is a crucial component of a VRFB as well as an expensive portion [20]. The selection of the supporting electrolyte requires consideration of factors such as high stability and solubility, economical cost, reasonable electrochemical performance, and a wide potential range for operation [21], as these factors significantly impact its performance. As a result, it is critical to ensure the electrolyte's solubility and stability in order to improve VRFB performance and overall lifespan [22].

A variety of acids, including H_2SO_4, HCl, methanesulfonic acid, a combination of these, or an organic electrolyte such as vanadium acetylacetonate, can be employed as supporting electrolytes in VRFBs [5]. An earlier study looked at the effects of various

concentrations of vanadium compounds (VCl_3, V_2O_5, and $VOSO_4$) in supporting electrolytes, including HCl, NaOH, and H_2SO_4 [14]. However, the use of VCl_3 and HCl together proved inappropriate since it produced chlorine gas. Additionally, the V_2O_5 limited solubility in acids led to the selection of a vanadyl sulfate solution and a supporting electrolyte of sulfuric acid for both electrolytes. Subsequently, techniques for preparing electrolytes using V_2O_5 were devised [7].

15.3.1.2 Electrochemical Reactions

The process begins with filling the positive electrolyte tank with a V(IV) solution and adding a V(III) solution to the negative electrolyte tank, as illustrated in Figure 15.1. When the electricity is applied to the positive and negative electrodes, the V(IV) ions in the positive electrolyte undergo oxidation to V(V) ions. Simultaneously, the V(III) ions are reduced to produce V(II) ions in the negative electrolyte [23]. Research has revealed that the reaction between V(II) and V(III) and species in the negative electrolyte is the primary factor that restricts the performance of VRFBs [24,25]. The reactions on the positive side, the negative side, and the cell's overall reaction through VRFB charging are shown in Equations (15.1), (15.2), and (15.3), respectively, along with their related redox potentials [26,27].

Positive side reaction:

$$VO^{2+} + H_2O \rightarrow VO_2^{+} + 2H^{+} + e^{-} \quad E^0 = +1.004 \text{ V vs. SHE} \tag{15.1}$$

Negative side reaction:

$$V^{3+} + e^{-} \rightarrow V^{2+} \quad E^0 = -0.255 \text{ V vs. SHE} \tag{15.2}$$

Overall reaction:

$$VO^{2+} + H_2O + V^{3+} \rightarrow VO_2^{+} + V^{2+} + 2H^{+} \quad E^0 = +1.259 \text{ V vs. SHE} \tag{15.3}$$

According to Equation (15.3), the standard cell open circuit voltage (OCV) is about 1.26 V. But in actual cell conditions, with a 50% state of charge (SOC), the OCV is 1.4 V [28], since, as stated by Knehr & Kumbur [29], both Donnan's potential and proton activities have to be taken into account.

Currently, commercialized electrolytes in VRFBs are being produced with a 1:1 molar ratio of species V(IV) and V(III). These electrolytes undergo a pre-loading procedure that converts the combination into its positive and negative forms in separate reservoirs [30]. Equation (15.4) includes the reaction that describes this process, also known as the reaction of cross-contamination, because this reaction happens whenever vanadium ions cross the membrane, which splits the two half-cells [31].

$$VO^{2+} + 2H^{+} + e^{-} \rightarrow V^{3+} + H_2O \quad E^0 = +0.337 \text{ V vs. SHE} \tag{15.4}$$

There is an elevated activation energy and negative potential requirement for the reaction between the species V(IV) and V(III) (Equation 15.4). It is probable that the V(IV) formation in the positive electrolyte will continue by first forming V(V), which will subsequently interact with V(III) [32].

15.3.1.3 Electrolyte Imbalance and Its Regeneration

An electrolyte imbalance, which results from cross-contamination of electrolytes as well as side reactions, has an obvious effect on VRFB performance by decreasing its capacity. The unequal quantities of reduced and oxidized vanadium species cause the imbalance, as explained by Roznyatovskaya et al. [33]. Therefore, just one half-cell of the VRFB can achieve 100% SOC. This corresponds to the half-cell that contains a limited quantity of active species. Jirabovornwisut & Arpornwichanop [34] emphasize that, based on the underlying source of the imbalance, either the negative or positive half-cells could act as the constraining part of the process. One method to confirm this imbalance of electrolytes in practical application is by assessing the status of health (SOH). The SOH can be utilized to evaluate the level of battery degradation during charge-discharge cycles. Along with the SOC, it is a crucial factor in the energy management of the system [35]. In general, the SOH of the battery is determined by the difference in SOC between the negative and the positive half-cells.

Electrolyte imbalance results in a deviation from the acceptable starting average oxidation state (AOS) for the active species in the negative and positive half-cells. At the beginning, the value of AOS is +3.5, indicating that in positive and negative electrolytes, there exists a balanced distribution of 50% VO^{2+} and 50% V^{3+} ions [36]. The literature has examined the use of UV-vis spectroscopy to determine the species concentration within an anolyte [37]. The distinct colors resulting from the various vanadium oxidation states enable the UV-vis method to be a perfect option for quantifying the concentration of these species in the electrolyte. This allows for the detection of any possible imbalance between the two half-cells, as the species absorb light at various wavelengths within the spectrum [38].

Corcuera & Skyllas-Kazacos introduced two methods to alleviate the effects of electrolyte imbalance and restore electrolyte balance. The two processes involved are (1) remixing the electrolytes and (2) rebalancing through the addition of chemicals to the catholyte. Nevertheless, it is crucial to identify the main source of the imbalance. The first approach is suitable for situations when there is just vanadium ion transfer through the membrane, but the second technique is applicable when this transfer leads to undesired side reactions [34,39]. Furthermore, the process of remixing causes energy loss because electrolytes are mixed and reset to an AOS of +3.5. Additionally, it has been observed that frequent efforts to recover the original VRFB capacity could lead to failures. According to Rudolph et al. [40], the variation in hydrogen concentration within the electrolytes swiftly reverses the first beneficial impact resulting from remixing.

The chemical rebalancing approach developed by Corcuera & Skyllas-Kazacos [39] involves the addition of a chemical reductant or organic substances, like oxalic acid, ethanol, and methanol. Typically, the introduction of these compounds partially converts VO_2^+ to VO^{2+}, restoring a balanced ratio between V^{2+} and VO_2^+. This is necessary because

the V^{2+} species is limited owing to the processes of hydrogen evolution as well as oxidation via air [34,39]. Whitehead & Harrer [41] suggested an alternative approach to rebalance electrolytes using hydrogen. The concept entails recycling the hydrogen that the anolyte produces as a byproduct by introducing it into the catholyte. This is carried out using a catalyst to reduce the VO_2^+ in a similar manner to the technique that employs chemical compounds. Nevertheless, the drawback of employing hydrogen as a reducing agent is the sluggish rate of reaction between VO_2^+ and H_2 [41].

15.3.2 Electrodes

The electrode is a crucial component in VRFBs, as it serves to provide an electrochemically active surface where redox reactions take place between the vanadium ion pairs. Electrolytes contribute to the system's stored energy capacity, whereas the surface area of the electrodes, which is related to the number of cells in the VRFB, identifies the battery power [42,43].

For the selection of an electrode, it is important to meet certain criteria. The electrode should contain a porous, three-dimensional structure that enables the electrolyte to flow through its surface easily. It should also have a large active area to enhance electrochemical activity during redox reactions. Additionally, the electrode should have low electrical resistance and be chemically inert to the redox pairs and supporting electrolyte [11]. The electrode also needs to show electrochemical stability within the potential range of the system and be compatible with low pH environments. Furthermore, the electrode should have high H_2 and O_2 overvoltage as well as excellent electrical conductivity to facilitate rapid charge-transfer steps [43]. Ulaganathan et al. [44] examined the impact of several parameters of the electrode composition on the VRFB's performance. The authors asserted that the electrical resistance corresponds to the ohmic losses that may occur when an electrical current is applied. This has a direct effect on the system voltage and the energy efficiency of VRFB. Overvoltage losses are affected by the electrochemical activity of the electrode material, and it also determines the tension that occurs during the charging and discharging processes. The porosity of the electrode is associated with the pressure drop in the electrolyte flow through the VRFB stack that may lead to energy losses caused by pumping.

Currently, electrodes are mostly composed of carbon fiber as the basis material, often in the form of carbon felt, graphite felt (GF), or carbon paper [31]. GFs are the most popular because they meet many of the main criteria for electrodes, including inexpensive cost, great surface area, high chemical stability, good conductivity, and a broad range of operating potential. But this material's poor kinetic reversibility remains a drawback when utilized to make electrodes [31,45].

15.3.3 Membranes

15.3.3.1 Overall Characteristics

The ion-exchange membrane is a vital component of a VRFB. It functions by separating the active species in the negative and positive half-cells, allowing the transport of ions such as SO_4^{2-}, HSO_4^-, and H^+. This mechanism helps to complete the electronic circuit during the

flow of electric current [46]. The membrane's generation of resistance plays a crucial role in restricting the VRFB power density. This resistance has a significant role in preserving the system's high efficiency within multiple cycles. Membranes account for around 40% of the overall expenses of a VRFB cell stack. Therefore, it is critical to develop advanced designs that offer high quality at a lower cost, making this a crucial factor to consider when selecting the material to use [47].

As stated by Wang et al. [48], the membranes should be stable against the electrolyte within the whole SOC range that the VRFB would experience. This is important due to the acidic composition of the electrolytes and the existence of very oxidizing agents inside them. A suitable membrane should possess excellent ionic conductivity in order to effectively complete the circuit, reduce ohmic losses, and maintain the VRFB voltage efficiency [43]. Another important property of membranes in VRFBs is remarkable ion selectivity. This means that they allow the passage of ions, which are involved in load balancing and completing the circuit, while acting as an obstacle to the active species of vanadium. This barrier prevents self-discharge processes and assists in maximizing coulombic efficiency [49]. An inherent conflict may arise between achieving considerable ion selectivity and maintaining powerful ion conductivity, since an increase in one often results in a reduction in another. Therefore, Wang et al. [50] emphasize the need for achieving an appropriate balance between these two characteristics. However, Ulaganathan et al. [44] state that a rise in ionic conductivity leads to a decrease in the resistance of cells. Nevertheless, they also note that using a thinner membrane might potentially compromise the VRFB's mechanical stability. This further illustrates the necessity of using a membrane, which can provide outstanding performance along with acceptable ionic conductivity.

Primary interferences in species transportation across the membrane directly relate to the chemical structure and properties of the membrane [51]. The penetration of water and vanadium ions across the membrane, among the transport mechanisms that take place in a VRFB, requires high attention due to its influence on VRFB performance and cycle stability [52]. The passage of vanadium ions across the membrane between half-cells and their subsequent interaction with other ions of vanadium leads to a phenomenon known as self-discharge. A crucial criterion in the selection of a membrane for employing in VRFBs is its capability to effectively control the transfer of water across the two half-cells [53]. The reason for this is that it is feasible to prevent the vanadium salt precipitation by using membranes that have optimal water transport characteristics. Nevertheless, if water is selectively transferred from one electrolyte to another across the membrane, one electrolyte is going to accumulate a higher concentration of vanadium, while the other will become more diluted. The extent of this variation depends on the unique characteristics of the membrane as well as the VRFB charge state [54].

15.3.3.2 Membrane Categories for VRFB

Over the years, a wide range of membranes has been designed with the aim of meeting the particular requirements needed for VRFBs. These membranes are typically grouped into two main categories: porous membranes and ion-exchange membranes (IEM). A common way to classify the IEMs is by their surface functional groups; cation exchange membranes

(CEM) and anion exchange membranes (AEM) are IEMs that conduct cations and anions, respectively. Another type of IEM is the amphoteric ion-exchange membrane (AIEM), which is typically constructed to include one selective layer for cations and another for anions [43,55].

Traditionally, the most widely used membrane in VRFB systems has been DuPont's Nafion, which offers superior performance. This membrane is a copolymer composed of sulfonated tetrafluoroethylene. It functions as a transporter of protons and is primarily employed as a membrane in a VRFB. Its main purpose is to support extremely acidic electrolytes and strongly oxidative ions, for instance VO_2^+ [49,56]. Nafion membranes have both excellent chemical stability and strong proton conductivity [57]. However, these membranes have significant drawbacks, including their high cost and limited ion selectivity. Specifically, they have an elevated permeability for vanadium ions, which negatively impacts both the coulombic and energy efficiency of the VRFB system. Moreover, this limits the practical use of this membrane in commercial batteries. When the VRFB operates, it mitigates the phenomenon of vanadium ion crossover, especially in situations with high current density. During such situations, the protons exhibit higher diffusivity compared to metal ions [55]. Nevertheless, Nafion membranes have shown the highest level of prolonged chemical stability [58], making them one of the most widely utilized membranes for VRFBs.

15.4 ADVANCEMENT IN VRFBs

The need for solutions to the challenges of VRFBs has motivated many fields of research in recent years. The objective is to improve energy density and efficiency, which in turn reduces precipitation issues for active species of vanadium. Additionally, efforts are being made to optimize the process by using compounds with catalytic activity to speed up redox processes and improve the VRFB's performance. The investigations have primarily focused on the production of electrolytes, which are critical components of VRFBs, as well as the advancement of electrodes and IEM.

15.4.1 Electrolyte Optimization

The electrolyte not only determines energy density but also restricts VRFB operating variables, such as temperature. In the existence of stabilizing substances, this may lessen or even eliminate the frequent problems caused by the restrictions of vanadium species. Because of this, additives should only be compatible with all vanadium oxidation states; otherwise, the electrolyte may disadvantage one species and favor another. Adding K_2SO_4, which has been reported to be a great stabilizer for VO^{2+} species, may have this effect, leading to a faster rate of VO_2^+ precipitation [8].

Li et al. focused their research on utilizing organic additives for positive electrolytes to manage and enhance VO_2^+ solubility. Following an analysis of mannitol, glucose, fructose, and D-sorbitol, they found that D-sorbitol exhibited the highest electrochemical activity, achieving 81.8% energy efficiency [59]. The observed results are associated with the increased presence of hydroxyl groups (–OH), which react with species V(IV), as well as the increasing number of active sites that promote the redox reactions of the V(IV)/V(V)

pair [7,59]. In contrast, Rahman & Skyllas-Kasacos [60] highlight that inorganic additives outperform organic options, as shown by the findings of experimental investigations. The researchers formulated the additive KS11 by combining 1% by weight of K_3PO_4 with 1% by weight of SHMP ($NaPO_3$). This additive successfully provides the continuous solubility of species V(IV) throughout a temperature window of 5°C–20°C, therefore preventing the V(V) precipitation concentrated in 4 M at 50°C [60].

Zarei-Jelyani et al. performed a comparative investigation on different supporting electrolytes of HCl, H_2SO_4, and combined acids ($HCl+H_2SO_4$) in a VRFB. For the VRFB rate capability test, adding HCl to the H_2SO_4 supporting electrolyte made the capacity almost 10% higher at 60, 80, and 100 mA cm^{-2} current densities. The VRFBs' polarization curves illustrated that reducing the VRFB internal resistance from 10 to 9.5 Ω cm^2 was achieved with the addition of HCl to the H_2SO_4 [61].

In their study, Roznyatovskaya et al. [62] found that introducing phosphoric acid to the catholyte slowed the rate of V (V) precipitation while the temperature was increased to 50°C. Because $VOPO_4$ precipitation is possible at concentrations higher than the additive limit, they adopted it at 0.15 M of phosphate [62].

The research conducted by Wang et al. [63] developed upon prior work of the group and focused on controlling the overall concentration of sulfuric acid and vanadium in order to expand the operational temperature window of VRFB. By examining various concentrations of the species (1.5–3.0 M for H_2SO_4 and 0.44–2.2 M for V), the researchers confirmed the vanadium ion stability in all states of valence at a concentration of 1.5 M in a 2.0 M H_2SO_4 supporting electrolyte throughout a broad temperature range (–25°C to 60°C) in the absence of any additives. The result of this study makes it more economically viable to use by lowering the cost of adding compounds that have an electrolytic stabilization action [63].

Further investigations involve the incorporation of stabilizing and catalytic agents into the anolyte. For instance, Shen et al. [45] examined the application of antimony ions (Sb^{3+}) within the anolyte and observed a 9.6% improvement in energy efficiency from an initial value of 57.5% to 67.1%. The research findings indicate that an optimal concentration of Sb^{3+} (5×10^{-3} M) is necessary to enhance the reaction kinetics of the V(II)/V(III) redox pair, which is often sluggish, and to improve its electrochemical activity [45].

15.4.2 Improving the Electrode Performance

The development of electrodes in VRFBs has grown using two primary approaches: activation and surface modification. The activation strategy uses a variety of treatments, including acidic, thermal, and chemical ones, to enhance the electrode by adding a significant number of functional groups, which in turn increases the active sites. The surface modification approach operates through three mechanisms: (1) enhancing the electrode surface area to create more active sites to support the redox reaction; (2) improving the electrode porosity to boost the hydraulic permeability for facilitation of electrolyte transport and reduction of ion concentration loss as well as power of pumping; and (3) elevating the electric conductivity of the electrode employed to minimize the ohmic resistance [64].

In order to increase the electrode surface area, two common approaches have been employed. The first way involves depositing nanosized materials with a larger surface area onto the electrode surface. The second method involves generating fine porous structures on the electrodes made of carbon [64].

A study conducted by Li et al. [65] examined the impact of Bi nanoparticles on the VRFB performance. At a current density of 150 mA cm^{-2}, their research revealed an 11% increase in energy efficiency when Bi nanoparticles were applied to the electrode surface. The noted improvement may be attributed to the advancement in the kinetics of the vanadium-pair redox process. Jiang et al. [66] investigated the influence of B_4C particles on GF electrodes. An enhancement of 18.8% in energy efficiency was reported at 160 mA cm^{-2} current density. Furthermore, they indicated that the GF electrode developed using B_4C nanoparticles was a unique electrode capable of operating at current densities as high as 320 mA cm^{-2}.

Another investigation conducted by Wei et al. [67] used nanowires of titanium nitride to decorate a GF electrode in a VRFB. A significant improvement of over 15% in round-trip energy efficiency was identified at 300 mA cm^{-2} current density. Additionally, there was a more than 43% increase in electrolyte consumption at this current density. This indicates a greater facilitation of ion transport in charge/discharge cycles.

An immersion-drying approach was used by Loghavi et al. to apply graphene to GF electrodes. Graphene, as a conducting electrocatalyst, has enhanced rate capability and promoted redox processes. The enhanced performance is demonstrated by the higher discharge voltage, energy efficiency, and voltage efficiency in a VRFB cell with the modified electrodes in comparison to the bare electrodes [68]. Zarei-Jelyani et al. conducted the investigation by adding CNTs to the carbon felt electrode and treating it with acid and heat. This made the electrode perfect for use as either a positive or negative electrode in the VRFB. The modified electrode had an exchange current density more than 100 times higher than that of bare carbon felt. It also had a much lower charge-transfer resistance than an untreated one [69].

The process of etching by KOH [70], CO_2 [71], FeOOH [72], NiO [73], and H_2O [74] has been documented to generate nanosized pores on the electrode surface. Considering the etching approach, the desired wettability and surface area were achieved to ensure improved performance of the VRFB. Nevertheless, modification of electrodes is not considered a cost-effective approach due to its need for temperatures of 800°C in an atmosphere of nitrogen or argon.

15.4.3 Membrane Advancements

Recent research aims to address the main challenging aspect of the ion-exchange membrane, which is preserving conductivity and chemical stability. However, a completely solvable scenario is still not achieved through keeping a balance between vanadium ion crossover and proton crossing. This balance is crucial to attaining optimal efficiency [5].

Zeng et al. [75] propose using anionic membranes in VRFBs as possible reducers for crossing vanadium ions as electroactive species. In their assessment of the feasibility of this application, Roh et al. [76] created a poly (phenylene oxide) membrane that facilitated proton transport due to the presence of the OH functional group. The made membrane

also promises an improvement in Donnan's exclusion effect, which is a unique benefit of the study. This leads to 99.5% coulombic efficiency, which is about 6% higher than that of the Nafion membrane.

Che et al. [77] recommended employing porous polybenzimidazole membranes to enhance ion selectivity. They utilized a modeling approach involving SiO_2 and a NaOH-based attack solution. The application of a membrane led to an improvement in coulombic efficiency, as shown by 99.5%, which corresponds to 87.9% energy efficiency.

Furthermore, enhancing the conductivity and selectivity of the membrane may be achieved by certain cationic and anionic groups, along with the use of functional additives like sulfated zirconia prepared for the membranes of VRFBs. Due to their elevated acidity, the S-ZrO_2 particles provide an extremely favorable environment for enhancing proton transfer. In parallel, the additive functions as an obstacle that inhibits the vanadium species migration [78]. Zhang et al. reported achieving a high energy and coulomb efficiency of around 86.78% and 98.89%, respectively, in their experimental investigations using the additive. The S-ZrO_2-modified membrane shows a promising potential to improve the VRFB system, including its capability to retain cycling stability throughout 70 charge-discharge cycles at 100 mA cm^{-2} current density, surpassing the performance of the Nafion membrane [78].

Sun et al. [79] significantly enhanced the performance of sulfonated poly(ether ether) membranes through the use of WO_3 nanoparticles to act as catalyst additives. The researchers discovered a hybrid inorganic-organic membrane consisting of sulfonated poly (ether ether ketone) and 23.6% of the additive. This membrane has a major benefit over the Nafion membrane in terms of ion selectivity, which is around 3.2 times greater [79].

15.5 CONCLUSION

This chapter highlights the technical aspects of VRFBs as a transformative solution for large-scale, grid-integrated energy storage, crucial for managing the variability of renewable energy sources. VRFBs, with their unique utilization of vanadium in multiple oxidation states, offer distinct advantages such as long operational lifetimes, scalable energy and power capacities, and reduced electrolyte contamination risks. However, their practical deployment faces challenges primarily related to electrolyte imbalances, membrane degradation, and the high cost of system components.

The chapter's in-depth analysis of VRFB components—electrolytes, electrodes, and membranes—reveals that electrolyte composition plays a central role in determining energy density and operational stability. Advanced formulations, including mixed-acid and stabilized electrolytes, have been shown to enhance performance across a broad temperature range. Similarly, electrode surface modifications through techniques like nanoparticle deposition and functional group activation have significantly improved charge-transfer kinetics and reduced system resistances, paving the way for higher energy efficiencies. Membrane innovations focused on improving ion selectivity and reducing vanadium ion crossover are critical to enhancing the system's coulombic and energy efficiency. Looking forward, the chapter emphasizes the need for continued research into optimizing these components and developing cost-effective materials to

improve the economic viability of VRFBs. Key areas include enhancing the long-term stability of membranes, developing more efficient electrode architectures, and improving electrolyte formulations to prevent capacity fading and side reactions. By addressing these challenges, VRFBs can become a cornerstone technology for large-scale renewable energy integration, offering a reliable, flexible, and sustainable solution to the global energy storage challenge.

REFERENCES

1. W.J. Ripple, C. Wolf, T.M. Newsome, P. Barnard, W.R. Moomaw, World scientists' warning of a climate emergency, *BioScience* 70 (2020) 8–100.
2. F. Zarei-Jelyani, F. Salahi, M. Zarei-Jelyani, M.R. Rahimpour, Various industrial wastes to energy technologies, in: M. R. Rahimpour (Ed.), *Encyclopedia of Renewable Energy, Sustainability and the Environment* (First Edition), Elsevier, Oxford, 2024, pp. 17–28.
3. M. Zarei-Jelyani, F. Esmaeilzadeh, A semi-empirical and multi-variable model for prediction of capacity loss in lithium-ion batteries: Considering cycling and performance time degradations, *Journal of Power Sources* 602 (2024) 234377.
4. M. Zarei-Jelyani, M. Babaiee, S. Baktashian, R. Eqra, H. Shirani-Faradonbeh, Assessment of the formation process effect on the lithium-ion battery performance at low temperatures, *Journal of Materials Science: Materials in Electronics* 34 (2023) 1890.
5. J.H. Vinco, A.E.E. da Cunha Domingos, D.C.R. Espinosa, J.A.S. Tenório, M.D.P.G. Baltazar, Unfolding the vanadium redox flow batteries: An indeep perspective on its components and current operation challenges, *Journal of Energy Storage* 43 (2021) 103180.
6. M. Zarei-Jelyani, F. Zarei-Jelyani, F. Salahi, M.R. Rahimpour, Wind distributed generation system, in: M. R. Rahimpour (Ed.), *Encyclopedia of Renewable Energy, Sustainability and the Environment* (First Edition), Elsevier, Oxford, 2024, pp. 271–282.
7. C. Choi, S. Kim, R. Kim, Y. Choi, S. Kim, H.-Y. Jung, J.H. Yang, H.-T. Kim, A review of vanadium electrolytes for vanadium redox flow batteries, *Renewable and Sustainable Energy Reviews* 69 (2017) 263–274.
8. K. Lourenssen, J. Williams, F. Ahmadpour, R. Clemmer, S. Tasnim, Vanadium redox flow batteries: A comprehensive review, *Journal of Energy Storage* 25 (2019) 100844.
9. M. Babaiee, S. Baktashian, M. Zarei-Jelyani, R. Eqra, M. Gholami, High-performance natural graphite anode for lithium-ion batteries: Using TiO_2 as an additive, *ChemistrySelect* 7 (2022) e202201510.
10. M. Ding, T. Liu, Y. Zhang, Investigations of the influences of K^+ impurity on the electrolyte for vanadium redox flow battery, *Ionics* 26 (2020) 3415–3423.
11. G. Tomazic, M. Skyllas-Kazacos, Redox flow batteries, in: Patrick T. Moseley and Jürgen Garche (Eds.), *Electrochemical Energy Storage for Renewable Sources and Grid Balancing*, Elsevier, 2015, pp. 309–336.
12. M. Zarei-Jelyani, M.M. Loghavi, M. Babaiee, R. Eqra, The significance of charge and discharge current densities in the performance of vanadium redox flow battery, *Electrochimica Acta* 443 (2023) 141922.
13. L. Arenas, C.P. De León, F. Walsh, Engineering aspects of the design, construction and performance of modular redox flow batteries for energy storage, *Journal of Energy Storage* 11 (2017) 119–153.
14. M. Rychcik, M. Skyllas-Kazacos, Characteristics of a new all-vanadium redox flow battery, *Journal of Power Sources* 22 (1988) 59–67.
15. M.H. Moghim, R. Eqra, M. Babaiee, M. Zarei-Jelyani, M.M. Loghavi, Role of reduced graphene oxide as nano-electrocatalyst in carbon felt electrode of vanadium redox flow battery, *Journal of Electroanalytical Chemistry* 789 (2017) 67–75.

16. M. Zarei-Jelyani, M. Babaiee, A. Ghasemi, R. Eqra, Investigation of hydroxylated carbon felt electrode in vanadium redox flow battery by using optimized supporting electrolyte, *Journal of Renewable Energy and Environment* 3 (2016) 54–59.
17. G. Kear, A.A. Shah, F.C. Walsh, Development of the all-vanadium redox flow battery for energy storage: A review of technological, financial and policy aspects, *International Journal of Energy Research* 36 (2012) 1105–1120.
18. S. Mehboob, G. Ali, H.-J. Shin, J. Hwang, S. Abbas, K.Y. Chung, H.Y. Ha, Enhancing the performance of all-vanadium redox flow batteries by decorating carbon felt electrodes with SnO_2 nanoparticles, *Applied Energy* 229 (2018) 910–921.
19. L. Barelli, G. Bidini, P. Ottaviano, D. Pelosi, Vanadium redox flow batteries application to electric buses propulsion: Performance analysis of hybrid energy storage system, *Journal of Energy Storage* 24 (2019) 100770.
20. J.D. Milshtein, R.M. Darling, J. Drake, M.L. Perry, F.R. Brushett, The critical role of supporting electrolyte selection on flow battery cost, *Journal of The Electrochemical Society* 164 (2017) A3883.
21. S. Peng, N.-F. Wang, X.-J. Wu, S.-Q. Liu, D. Fang, K.-L. Huang, Y.-N. Liu, Vanadium species in CH_3SO_3H and H_2SO_4 mixed acid as the supporting electrolyte for vanadium redox flow battery, *International Journal of Electrochemical Science* 7 (2012) 643–649.
22. C. Ding, H. Zhang, X. Li, T. Liu, F. Xing, Vanadium flow battery for energy storage: Prospects and challenges, *The Journal of Physical Chemistry Letters* 4 (2013) 1281–1294.
23. M.M. Loghavi, M. Zarei-Jelyani, Z. Niknam, M. Babaiee, R. Eqra, Antimony-decorated graphite felt electrode of vanadium redox flow battery in mixed-acid electrolyte: Promoting electrocatalytic and gas-evolution inhibitory properties, *Journal of Electroanalytical Chemistry* 908 (2022) 116090.
24. Y. Wu, R. Holze, Electrocatalysis at electrodes for vanadium redox flow batteries, *Batteries* 4 (2018) 47.
25. J. Friedl, U. Stimming, Determining electron transfer kinetics at porous electrodes, *Electrochimica Acta* 227 (2017) 235–245.
26. G.L. Soloveichik, Flow batteries: Current status and trends, *Chemical Reviews* 115 (2015) 11533–11558.
27. T. Liu, X. Li, H. Zhang, J. Chen, Progress on the electrode materials towards vanadium flow batteries (VFBs) with improved power density, *Journal of Energy Chemistry* 27 (2018) 1292–1303.
28. M. Skyllas-Kazacos, L. Cao, M. Kazacos, N. Kausar, A. Mousa, Vanadium electrolyte studies for the vanadium redox battery—A review, *ChemSusChem* 9 (2016) 1521–1543.
29. K. W. Knehr, E. C. Kumbur, Open circuit voltage of vanadium redox flow batteries: Discrepancy between models and experiments. *Electrochemistry Communications* 13(4) (2011) 342–345. https://doi.org/10.1016/j.elecom.2011.01.020
30. N. Roznyatovskaya, J. Noack, K. Pinkwart, J. Tübke, Aspects of electron transfer processes in vanadium redox-flow batteries, *Current Opinion in Electrochemistry* 19 (2020) 42–48.
31. S. Kim, Vanadium redox flow batteries: Electrochemical engineering, *Energy Storage Devices* 1 (2019) 115.
32. N. Roznyatovskaya, J. Noack, M. Fühl, K. Pinkwart, J. Tübke, Towards an all-vanadium redox-flow battery electrolyte: electrooxidation of V (III) in V (IV)/V (III) redox couple, *Electrochimica Acta* 211 (2016) 926–932.
33. N. Roznyatovskaya, T. Herr, M. Küttinger, M. Fühl, J. Noack, K. Pinkwart, J. Tübke, Detection of capacity imbalance in vanadium electrolyte and its electrochemical regeneration for all-vanadium redox-flow batteries, *Journal of Power Sources* 302 (2016) 79–83.
34. T. Jirabovornwisut, A. Arpornwichanop, A review on the electrolyte imbalance in vanadium redox flow batteries, *International Journal of Hydrogen Energy* 44 (2019) 24485–24509.
35. S. Tong, M.P. Klein, J.W. Park, On-line optimization of battery open circuit voltage for improved state-of-charge and state-of-health estimation, *Journal of Power Sources* 293 (2015) 416–428.

36. K. Beyer, J. Grosse Austing, B. Satola, T. Di Nardo, M. Zobel, C. Agert, Electrolyte imbalance determination of a vanadium redox flow battery by potential-step analysis of the initial charging, *ChemSusChem* 13 (2020) 2066–2071.
37. R.P. Brooker, C.J. Bell, L.J. Bonville, H.R. Kunz, J.M. Fenton, Determining vanadium concentrations using the UV-Vis response method, *Journal of The Electrochemical Society* 162 (2015) A608.
38. Z. Tang, D.S. Aaron, A.B. Papandrew, T.A. Zawodzinski, Monitoring the state of charge of operating vanadium redox flow batteries, *ECS Transactions* 41 (2012) 1.
39. S. Corcuera, M. Skyllas-Kazacos, State-of-charge monitoring and electrolyte rebalancing methods for the vanadium redox flow battery, *European Chemical Bulletin* 1 (2012) 511–519.
40. S. Rudolph, U. Schröder, I. Bayanov, On-line controlled state of charge rebalancing in vanadium redox flow battery, *Journal of Electroanalytical Chemistry* 703 (2013) 29–37.
41. A.H. Whitehead, M. Harrer, Investigation of a method to hinder charge imbalance in the vanadium redox flow battery, *Journal of Power Sources* 230 (2013) 271–276.
42. K.J. Kim, M.-S. Park, Y.-J. Kim, J.H. Kim, S.X. Dou, M. Skyllas-Kazacos, A technology review of electrodes and reaction mechanisms in vanadium redox flow batteries, *Journal of Materials Chemistry A* 3 (2015) 16913–16933.
43. X.Z. Yuan, C. Song, A. Platt, N. Zhao, H. Wang, H. Li, K. Fatih, D. Jang, A review of all-vanadium redox flow battery durability: Degradation mechanisms and mitigation strategies, *International Journal of Energy Research* 43 (2019) 6599–6638.
44. M. Ulaganathan, V. Aravindan, Q. Yan, S. Madhavi, M. Skyllas-Kazacos, T.M. Lim, Recent advancements in all-vanadium redox flow batteries, *Advanced Materials Interfaces* 3 (2016) 1500309.
45. J. Shen, S. Liu, Z. He, L. Shi, Influence of antimony ions in negative electrolyte on the electrochemical performance of vanadium redox flow batteries, *Electrochimica Acta* 151 (2015) 297–305.
46. H. Prifti, A. Parasuraman, S. Winardi, T.M. Lim, M. Skyllas-Kazacos, Membranes for redox flow battery applications, *Membranes* 2(2) (2012) 275–306.
47. T.M. Gur, Review of electrical energy storage technologies, materials and systems: Challenges and prospects for large-scale grid storage, *Energy & Environmental Science* 11 (2018) 2696–2767.
48. W. Wang, Q. Luo, B. Li, X. Wei, L. Li, Z. Yang, Recent progress in redox flow battery research and development, *Advanced Functional Materials* 23 (2013) 970–986.
49. X. Li, H. Zhang, Z. Mai, H. Zhang, I. Vankelecom, Ion exchange membranes for vanadium redox flow battery (VRB) applications, *Energy & Environmental Science* 4 (2011) 1147–1160.
50. Wei Wang, James P. Kizewski, Wentao Duan, Introduction to redox flow batteries, in *Redox Flow Batteries*, CRC Press, 2017, pp. 43–76.
51. E. Agar, K. Knehr, D. Chen, M. Hickner, E. Kumbur, Species transport mechanisms governing capacity loss in vanadium flow batteries: Comparing Nafion® and sulfonated Radel membranes, *Electrochimica Acta* 98 (2013) 66–74.
52. M. Pugach, M. Kondratenko, S. Briola, A. Bischi, Zero dimensional dynamic model of vanadium redox flow battery cell incorporating all modes of vanadium ions crossover, *Applied Energy* 226 (2018) 560–569.
53. T. Sukkar, M. Skyllas-Kazacos, Water transfer behaviour across cation exchange membranes in the vanadium redox battery, *Journal of Membrane Science* 222 (2003) 235–247.
54. B. Schwenzer, J. Zhang, S. Kim, L. Li, J. Liu, Z. Yang, Membrane development for vanadium redox flow batteries, *ChemSusChem* 4 (2011) 1388–1406.
55. R. Ye, D. Henkensmeier, S.J. Yoon, Z. Huang, D.K. Kim, Z. Chang, S. Kim, R. Chen, Redox flow batteries for energy storage: A technology review, *Journal of Electrochemical Energy Conversion and Storage* 15 (2018) 010801.

56. Y. Zhang, J. Li, L. Ma, W. Cai, H. Cheng, Recent developments on alternative proton exchange membranes: Strategies for systematic performance improvement, *Energy Technology* 3 (2015) 675–691.
57. B. Jiang, L. Wu, L. Yu, X. Qiu, J. Xi, A comparative study of Nafion series membranes for vanadium redox flow batteries, *Journal of Membrane Science* 510 (2016) 18–26.
58. X. Wei, Z. Nie, Q. Luo, B. Li, B. Chen, K. Simmons, V. Sprenkle, W. Wang, Nanoporous polytetrafluoroethylene/silica composite separator as a high-performance all-vanadium redox flow battery membrane, *Advanced Energy Materials* 3 (2013) 1215–1220.
59. S. Li, K. Huang, S. Liu, D. Fang, X. Wu, D. Lu, T. Wu, Effect of organic additives on positive electrolyte for vanadium redox battery, *Electrochimica Acta* 56 (2011) 5483–5487.
60. F. Rahman, M. Skyllas-Kazacos, Evaluation of additive formulations to inhibit precipitation of positive electrolyte in vanadium battery, *Journal of Power Sources* 340 (2017) 139–149.
61. M. Zarei-Jelyani, M.M. Loghavi, M. Babaiee, R. Eqra, Comparative analysis of single-acid and mixed-acid systems as supporting electrolyte for vanadium redox flow battery, *Journal of Applied Electrochemistry* 54 (2024) 719–730.
62. N.V. Roznyatovskaya, V.A. Roznyatovsky, C.-C. Höhne, M. Fühl, T. Gerber, M. Küttinger, J. Noack, P. Fischer, K. Pinkwart, J. Tübke, The role of phosphate additive in stabilization of sulphuric-acid-based vanadium (V) electrolyte for all-vanadium redox-flow batteries, *Journal of Power Sources* 363 (2017) 234–243.
63. K. Wang, Y. Zhang, L. Liu, J. Xi, Z. Wu, X. Qiu, Broad temperature adaptability of vanadium redox flow battery-Part 3: The effects of total vanadium concentration and sulfuric acid concentration, *Electrochimica Acta* 259 (2018) 11–19.
64. S. Aberoumand, P. Woodfield, B. Shabani, D.V. Dao, Advances in electrode and electrolyte improvements in vanadium redox flow batteries with a focus on the nanofluidic electrolyte approach, *Physics Reports* 881 (2020) 1–49.
65. B. Li, M. Gu, Z. Nie, Y. Shao, Q. Luo, X. Wei, X. Li, J. Xiao, C. Wang, V. Sprenkle, Bismuth nanoparticle decorating graphite felt as a high-performance electrode for an all-vanadium redox flow battery, *Nano Letters* 13 (2013) 1330–1335.
66. H. Jiang, W. Shyy, M. Wu, L. Wei, T. Zhao, Highly active, bi-functional and metal-free B4C-nanoparticle-modified graphite felt electrodes for vanadium redox flow batteries, *Journal of Power Sources* 365 (2017) 34–42.
67. L. Wei, T. Zhao, L. Zeng, Y. Zeng, H. Jiang, Highly catalytic and stabilized titanium nitride nanowire array-decorated graphite felt electrodes for all vanadium redox flow batteries, *Journal of Power Sources* 341 (2017) 318–326.
68. M.M. Loghavi, M. Zarei-Jelyani, M. Babaiee, Z. Niknam, R. Eqra, Graphene/Nafion ink-impregnated graphite felt for both positive and negative sides of enhanced vanadium redox flow battery, *Journal of Solid State Electrochemistry* 27 (2023) 2237–2250.
69. M. Zarei-Jelyani, S. Rashid-Nadimi, S. Asghari, Treated carbon felt as electrode material in vanadium redox flow batteries: A study of the use of carbon nanotubes as electrocatalyst, *Journal of Solid State Electrochemistry* 21 (2017) 69–79.
70. Z. Zhang, J. Xi, H. Zhou, X. Qiu, KOH etched graphite felt with improved wettability and activity for vanadium flow batteries, *Electrochimica Acta* 218 (2016) 15–23.
71. Y.-C. Chang, J.-Y. Chen, D.M. Kabtamu, G.-Y. Lin, N.-Y. Hsu, Y.-S. Chou, H.-J. Wei, C.-H. Wang, High efficiency of CO_2-activated graphite felt as electrode for vanadium redox flow battery application, *Journal of Power Sources* 364 (2017) 1–8.
72. Y. Liu, Y. Shen, L. Yu, L. Liu, F. Liang, X. Qiu, J. Xi, Holey-engineered electrodes for advanced vanadium flow batteries, *Nano Energy* 43 (2018) 55–62.
73. J.J. Park, J.H. Park, O.O. Park, J.H. Yang, Highly porous graphenated graphite felt electrodes with catalytic defects for high-performance vanadium redox flow batteries produced via NiO/Ni redox reactions, *Carbon* 110 (2016) 17–26.

74. D.M. Kabtamu, J.-Y. Chen, Y.-C. Chang, C.-H. Wang, Water-activated graphite felt as a high-performance electrode for vanadium redox flow batteries, *Journal of Power Sources* 341 (2017) 270–279.
75. L. Zeng, T. Zhao, L. Wei, H. Jiang, M. Wu, Anion exchange membranes for aqueous acid-based redox flow batteries: Current status and challenges, *Applied Energy* 233 (2019) 622–643.
76. S.-H. Roh, M.-H. Lim, T. Sadhasivam, H.-Y. Jung, Investigation on physico-chemical and electrochemical performance of poly (phenylene oxide)-based anion exchange membrane for vanadium redox flow battery systems, *Electrochimica Acta* 325 (2019) 134944.
77. X. Che, H. Zhao, X. Ren, D. Zhang, H. Wei, J. Liu, X. Zhang, J. Yang, Porous polybenzimidazole membranes with high ion selectivity for the vanadium redox flow battery, *Journal of Membrane Science* 611 (2020) 118359.
78. Y. Zhang, X. Zhou, R. Xue, Q. Yu, F. Jiang, Y. Zhong, Proton exchange membranes with ultra-low vanadium ions permeability improved by sulfated zirconia for all vanadium redox flow battery, *International Journal of Hydrogen Energy* 44 (2019) 5997–6006.
79. C. Sun, E. Negro, K. Vezzù, G. Pagot, G. Cavinato, A. Nale, Y.H. Bang, V. Di Noto, Hybrid inorganic-organic proton-conducting membranes based on SPEEK doped with WO3 nanoparticles for application in vanadium redox flow batteries, *Electrochimica Acta* 309 (2019) 311–325.

CHAPTER 16

Zinc-Nickel Flow Batteries

Xinyu Huang, Xiaohu Yang, and Yuanji Li

16.1 INTRODUCTION

Extensive dependence on traditional fossil fuels has led to increased environmental pollution and global warming [1]. About 78% of global electricity generation comes from fossil fuels, while renewables account for only 13% [2]. The world's population is growing at an average annual rate of 0.9%, leading to rapid growth in future energy demand and escalating environmental problems. Therefore, there is an urgent need to reform the existing energy framework and improve the efficiency of the use of renewable resources. In recent years, the use of renewable resources for power generation has become a key strategy to reshape the energy landscape, providing a good solution to reduce fossil fuel consumption and environmental degradation [3]. However, in order to effectively integrate renewable energy generation, operational and management strategies focused on improving the reliability and quality of power supply are imperative. Due to the inherent challenge of providing stable and immediate power from renewable energy sources to meet fluctuating grid demand, the deployment of renewable energy to the grid as a power storage and control method has become the preferred method, hence the emergence of energy storage battery technology [4].

As a novel electrochemical energy storage technology, flow batteries have some unique advantages compared with other energy storage technologies. These advantages include scalability, fast response time, high energy storage capacity, cost-effectiveness, long life, stable operation, high energy efficiency, and no geographical restrictions [5,6]. The unique characteristics of flow batteries highlight their great potential for global development [7]. At present, countries have identified flow batteries as the focus of development initiatives.

In some aspects, compared with traditional redox flow batteries, zinc-nickel flow batteries (ZNFBs) have certain advantages. The design of ZNFBs requires only one electrolyte flow channel and no ion exchange membrane [8,9]. The positive electrode of the battery consists of a porous nickel oxide structure, which acts as an energy carrier, while the negative electrode is composed of an extremely pure zinc plate, providing a simple structural composition. The use of alkaline zincate solution as an electrolyte alleviates the problem of negative dendrite formation to some extent. Although ZNFBs have many advantages,

DOI: 10.1201/9781003506379-16

there are still some problems, such as low energy density, self-discharge, uneven negative electrode deposition (especially zinc dendrite growth and inhibition), and oxygen and hydrogen precipitation [10,11].

As a new type of submerged flow battery, ZNFBs have attracted the attention of researchers due to their scalability, high energy efficiency, and ultra-long life [12]. Its unique design makes it a key branch of flow battery technology and aligns with the evolving needs of future energy storage technologies. However, due to the disadvantages of side reactions, dendrite growth and low energy density, the battery capacity and battery failure are reduced, and it is difficult to use on a large scale [13]. In this study, the interaction mechanism between electrochemical reaction and internal mass transfer was discussed by establishing a multi-physics coupling model, and the influence of electrode structure and side reactions on battery performance is reviewed. The findings of this research furnish a theoretical underpinning for optimizing the structure and mitigating side reactions in ZNFBs, thus fostering their continued industrial progression.

16.2 BASIC PROPERTIES OF ZNFBs

The development and enhancement of the mechanism model for ZNFBs hinge on integrating various physical fields. The essential characteristics and fundamental principles of the battery serve as the groundwork for selecting and refining these governing equations. Although model inaccuracies are persistent, ensuring both model accuracy and computational efficiency is essential, often necessitating underlying assumptions. Additionally, the multitude of fundamental equations utilized in the model are also founded on specific assumptions. It is necessary to verify the validity of the numerical model. To improve the accuracy of the model, it is necessary to determine the model error through the complete experimental process.

16.2.1 Working Principle

Figure 16.1 depicts the structural layout of the ZNFBs stack, illustrating components such as the load, external circuit system, reactor core, electrolyte pump, electrolyte flow pipeline, and electrolyte storage tank.

Consider the battery charging process as a paradigm. Electrical energy generated from renewable sources or surplus grid energy is utilized as the power supply, exerting its influence on the battery liquid collection. The electrolyte is driven into the flow channel by the pump. Subsequently, the electricity is converted into solid zinc at the negative electrode surface, with deposition occurring. Simultaneously, there is a release of $Zn(OH)_4^{2-}$ in the electrolyte. Concomitantly, due to the presence of the hydrogen evolution reaction (HER), hydrogen bubbles precipitate gradually, while OH^- in electrolyte interacts with the positive electrode, generating OH^-, and releasing electrons concurrently. The oxidation reaction leads to oxygen deposition within the porous positive electrode (NiOOH). Finally, the electrolyte exits the ZNFBs stack through the flow channel's upper part, entering an external tank to cycle back to ZNFBs. In contrast, the during discharge process, it follows a similar operational process as the charging reaction. This reversal is attributed to the irreversible nature of the hydrogen-oxygen side reaction. Consequently, the reaction process remains unchanged.

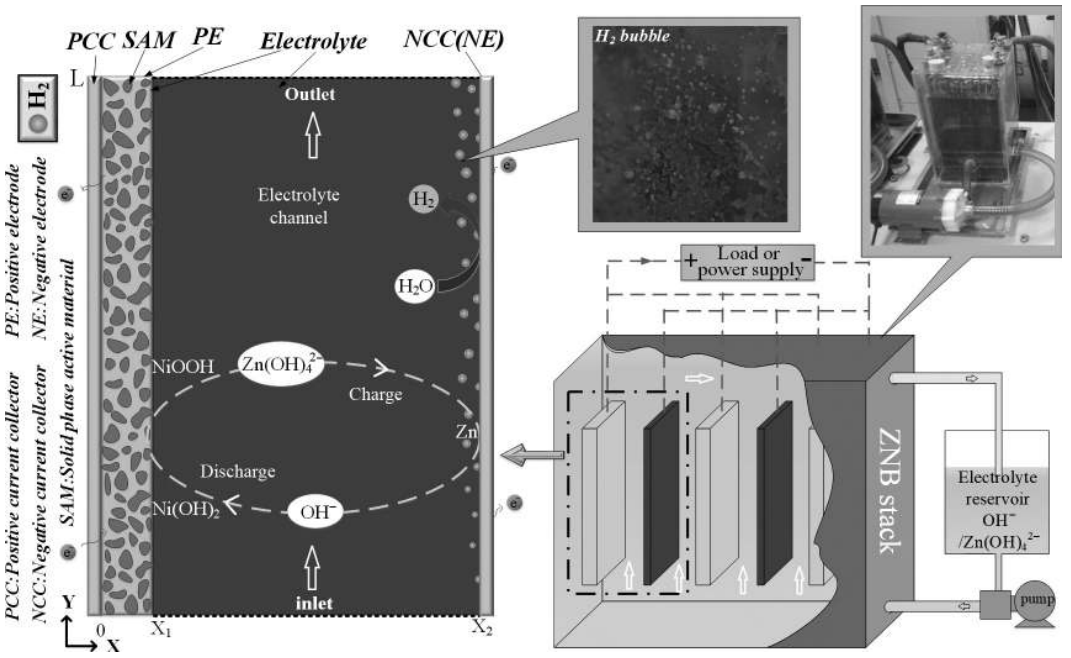

FIGURE 16.1 Structure diagram of ZNFBs stack [5].

Using a single cell within a stack as an illustration, the pertinent electrochemical equations are outlined as follows [14]:

$$\text{Positive}: \quad 2\text{NiOOH} + 2\text{H}_2\text{O} + 2\text{e}^- \rightleftarrows 2\text{Ni}(\text{OH})_2 + 2\text{OH}^- \quad E_0 = 0.490\ \text{V} \tag{16.1}$$

$$\text{Negative}: \quad \text{Zn} + 4\text{OH}^- \rightleftarrows \text{Zn}(\text{OH})_4^{2-} + 2\text{e}^- \quad E_0 = -1.285\ \text{V} \tag{16.2}$$

$$\text{Positive side effect}: \quad 4\text{OH}^- = \text{O}_2 \uparrow + \text{H}_2\text{O} + 4\text{e}^- \quad E_0 = 0.401\ \text{V} \tag{16.3}$$

$$\text{Negative side reaction}: \quad 2\text{H}_2\text{O} + 2\text{e}^- = 2\text{OH}^- + \text{H}_2 \uparrow \quad E_0 = -0.828\ \text{V} \tag{16.4}$$

16.2.2 Source of Hydrogen Evolution and Oxygen Evolution Reaction

The parasitic reaction inside the ZNFB cannot be ignored, which is divided into HER and OER, which has an important influence on the cycle life and efficiency. The evolution of oxygen at the positive electrode of the battery, resulting from the oxidation of hydroxide ions in the alkaline electrolyte conditions into oxygen with simultaneous precipitation, can lead to the detachment of active substances from the nickel oxide electrode. Conversely, in a HER, water is converted to hydrogen by oxidation and OH^- is produced simultaneously. Just as with the oxygen absorption reaction, hydrogen evolution also influences the zinc

deposition process. There is a complex relationship between the pH value of the electrolyte solution and the equilibrium potential of two gas electrodes.

1. From the Nernst equation, the equilibrium potential formula of HER is as follows:

$$E_{e,H_2} = E_{O,H_2} + \frac{RT}{F}\ln\frac{\alpha_{H^+}}{p_{H_2}^{1/2}} \tag{16.5}$$

$$\alpha = p/p_0 \tag{16.6}$$

where α is the activity of the substance, p_0 is the pressure in the standard state (l-atm), and p is the partial pressure.

The relationship between pH value and proton activity:

$$\mathrm{pH} = -\lg\alpha_{H^+} = -\frac{1}{2.303}\ln\alpha_{H^+} \tag{16.7}$$

The equilibrium potential of HER:

$$E_{e,H_2} = E_0 - \frac{2.303RT}{F}\ln\left(PH + \frac{1}{2}\lg p_{H_2}\right) \tag{16.8}$$

2. The equilibrium potential of OER:

$$E_{e,H_2} = E_{o,O_2} + \frac{RT}{4F}\ln\frac{p_{O_2}}{\alpha_{OH^-}^4} \tag{16.9}$$

$$PH = -\lg\alpha_{OH^-} + 14 \tag{16.10}$$

The equilibrium potential of the HER is:

$$E_{e,H_2} = E_{0,O_2} + \frac{RT}{4F}\ln\left(\frac{1}{2}\lg p_{O_2} - 4PH + 56\right) \tag{16.11}$$

Based on the Butler–Volmer equation, the influence mechanism between principal and secondary reactions was revealed to describe the reaction rates of HER and OER. It is expressed as follows:

$$j = j_0^0\left(\frac{c_R^*}{c_R^{0*}}e^{\alpha nF\eta/(RT)} - \frac{c_P^*}{c_P^{0*}}e^{-(1-\alpha)nF\eta/(RT)}\right) \tag{16.12}$$

where the activation overpotential is denoted as η, with surface concentration of products and reactants expressed as c_P^* and c_R^*, respectively. The number of transferred electrons in the electrochemical reaction is represented by n, j_0^0 is the current density in the standard reference state. Given the irreversibility of the HER and OER, $\alpha\ (0<\alpha<1)$ is the transfer coefficient, signifies the effect of reaction interface potential change on these activation energy barriers of forward and reverse reactions.

Due to the high irreversibility of the side reactions of hydrogen evolution and oxygen evolution, the efficiency of the ZNFBs decreases during the charging/discharging process, which is caused by partial current density being consumed. Among them, the battery coulomb efficiency is applied to evaluate the effect of side reactions on the ZNFBs performance, as shown in Equation (16.13):

$$\mathrm{CE} = \frac{\int_0^{t_d} I_d\, dt}{\int_0^{t_c} I_c\, dt} \tag{16.13}$$

where current density is I, the subscripts d and c represent the charging and discharge processes.

16.3 RESEARCH STATUS OF ZNFBs

In 2004, the research group led by Pletcher introduced the concept of a novel flow energy storage battery system – the single-flow full-deposition lead-acid flow battery. Subsequently, numerous researchers conducted studies building on this concept with the emergence of single-flow battery research. The singular-flow batteries have shown remarkable advantages over dual-flow batteries, leading to a significant surge in development through collaborative efforts of scholars worldwide. Various types of single-flow batteries have been explored. Building on this momentum, Cheng et al. [15] proposed the ZNFB system as a single deposition type in 2007, following initial experimental and simulation research. The ZNFB demonstrated favorable features such as system stability, extended service life, straightforward manufacturing processes, and high energy efficiency. This prompted further research on electrode design, battery mechanisms, flow channel optimization, electrolyte solutions, and more. Consequently, the ZNFB evolved into a sophisticated energy storage system. A 100 KWH ZNFB prototype was built based on prior research findings and was deployed in large-scale energy storage demonstrations. This pioneering research positioned the ZNFB at the forefront of international and domestic energy storage development, signifying the direction of flow cell advancement.

16.3.1 Experimental Study

At present, in the relevant experiments of ZNFB, inert materials such as positive electrode NiO and negative electrode nickel foil are used. By using high-concentration ZnO in KOH aqueous solution as an electrolyte, it has a good cost advantage. However, this new type of battery faces the related challenges mentioned earlier, resulting in reduced battery capacity

and efficiency [15,16]. Numerous research studies have been conducted to address these issues, to enhance ZNFB energy density, reduce cyclic charge–discharge energy loss, and advance the ZNFB development.

Zinc deposition in alkaline zincate solution within ZNFBs was investigated by Zhang et al. [17], as demonstrated in Figure 16.2a. Various substrates, including copper, cadmium, and lead, were evaluated through cyclic voltammetry and cathodic polarization. Zinc deposition was carried out under a constant current method, with sediment analysis conducted using SEM. Findings indicated that cadmium substrates outperformed other substrates, demonstrating minimal dendrite formation in flow conditions. Additionally, Zhang et al. [18] explored the dendrite growth on zinc negative electrodes under electrolyte flow. It was observed that the charging current density significantly influenced dendrite formation. Furthermore, through extended charging and discharging experiments on high-capacity batteries, an energy efficiency of 86% and a coulomb efficiency of 96% were achieved.

Cheng et al. [19] examined the impact of zinc ions in the electrolyte on the cycling stability of the nickel oxide electrode in ZNFBs. Their findings indicate that zinc in KOH electrolyte leads to a reduction in the charging voltage and hinders changes in the constant current charging curve over cycles when compared to KOH electrolyte without zinc. Remarkably, the discharge capacity of the electrode remained consistent even after 500 charge–discharge cycles, signifying a substantial enhancement in the cycle performance. Additionally, incorporation of zinc ions into the lattice structure of nickel hydroxide during battery cycling was observed, forming a complex that serves as an additive, preventing phase formation and overcharging. Wen et al. [20] employed current-time techniques of constant potential electrodeposition, scanning electron microscopy, and cyclic testing to assess the effectiveness of lead ions and tetrabutylammonium bromide (TBAB). The results

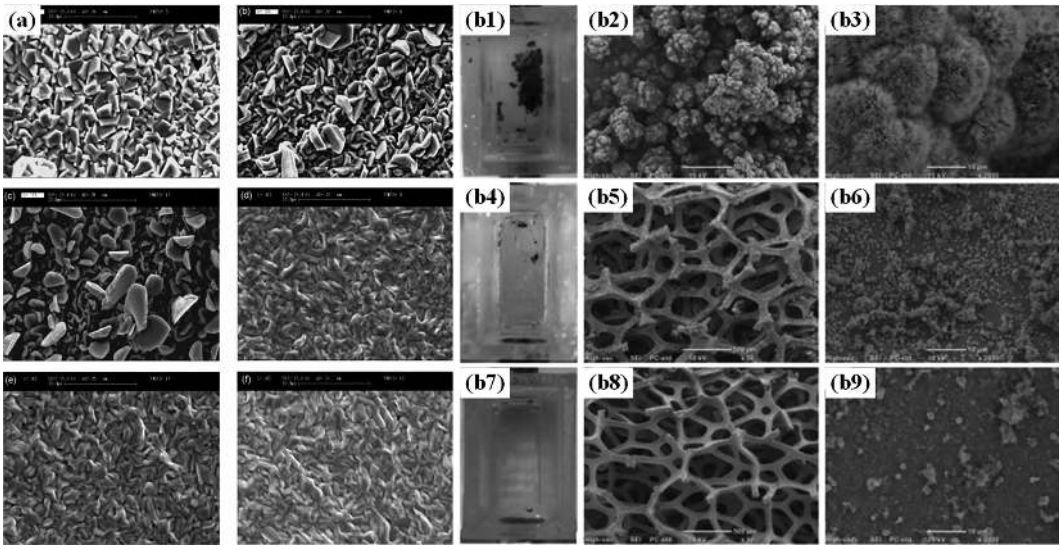

FIGURE 16.2 (a) Surface morphology of deposited zinc in static electrolyte at different current densities [17]; Copyright (2008), Elsevier. (b) SEM images of different battery bottoms [24]. Copyright (2014), Elsevier.

demonstrated that Pb (II) or TBAB effectively suppressed sponge zinc growth in flowing alkaline zincate solution, with the combined addition of Pb (II) and TBAB providing even greater inhibition of sponge zinc growth.

Cheng et al. [21] proposed to improve power density by integrating 3-D porous nickel foam (NF) into ZNFBs. The relationship between potential distribution, working current density, and electrode area is studied experimentally. The results show that the coulomb efficiency is 97.3%, the energy efficiency is 80.1%, and the power density is increased nearly fourfold to 83 W kg^{-1}. Under the condition of high working current density, 3-D porous electrode is more suitable as the negative electrode of ZNFBs. This method provides an effective strategy for improving the power density of ZNFBs. Xing et al. [22] controlled the crystal structure of $Ni(OH)_2$ by adding additives to increase the specific surface area and reduce the aperture. High specific capacitance is generated at different current densities and exhibits excellent cycle durability. In addition, Song et al. [23] evaluated the charging current density, electrolyte flow rate, and zinc deposition surface capacity of ZNFBs through experiments and electrochemical analysis. Their observations on negative dendrite morphology under a microscope revealed that a moderate electrolyte flow rate paired with high current density promotes dense and uniform zinc deposition, effectively enhancing battery charge–discharge capabilities.

The approach devised by Zhang et al. [24] involved altering the negative electrode material from nickel sheet to 2 mm thick NF. The porous nature of the foam material provides a high specific surface area and effective mass transfer structure, causing an escalation in the charge consumed by side reactions alongside increasing electrode thickness. This impact is exemplified in Figure 16.2b by comparing batteries A, B, and C – where battery A employs a nickel sheet negative electrode, battery B involves 1 mm NF, and battery C incorporates 2 mm NF. Transitioning from a nickel negative electrode (at a side reaction charge consumption of 1.3% of battery capacity) to a 2-mm thick NF results in a higher side reaction charge consumption of 3.7% of battery capacity. This notable increase in inside reaction charge consumption diminishes the coulomb efficiency of the negative electrode from 98.7% to 96.3%, aligning it with the positive electrode efficiency. Following the substitution of the nickel sheet anode with NF, the ZNFB exhibits minimal zinc accumulation throughout 400 cycles.

Under constant current density conditions (300 mA cm^{-2}), Cheng et al. [25] researched battery potential distribution of ZNFBs and role of side reactions. Results indicate that the coulomb efficiency initially rises, then declines as current density increases, attributed to the non-uniform distribution of electrode potential and side reactions. With escalating current density, the zinc deposition morphology shifts toward dendritic growth, as shown in Figure 16.3a–f. Figure16.3g displays the overpotential of positive and negative electrodes across various current densities (ranging from 40 to 300 mA cm^{-2}).

Meng et al. [26] have successfully developed a Zn-AILDHs/HC composite material for implementation as the negative electrode in zinc-nickel secondary batteries. Through XRD and SEM analyses, they determined that the composite material exhibited commendable mechanical stability, mitigating significant polarization stemming from structural distortion. Concurrently, electrochemical testing was conducted on the composite, revealing

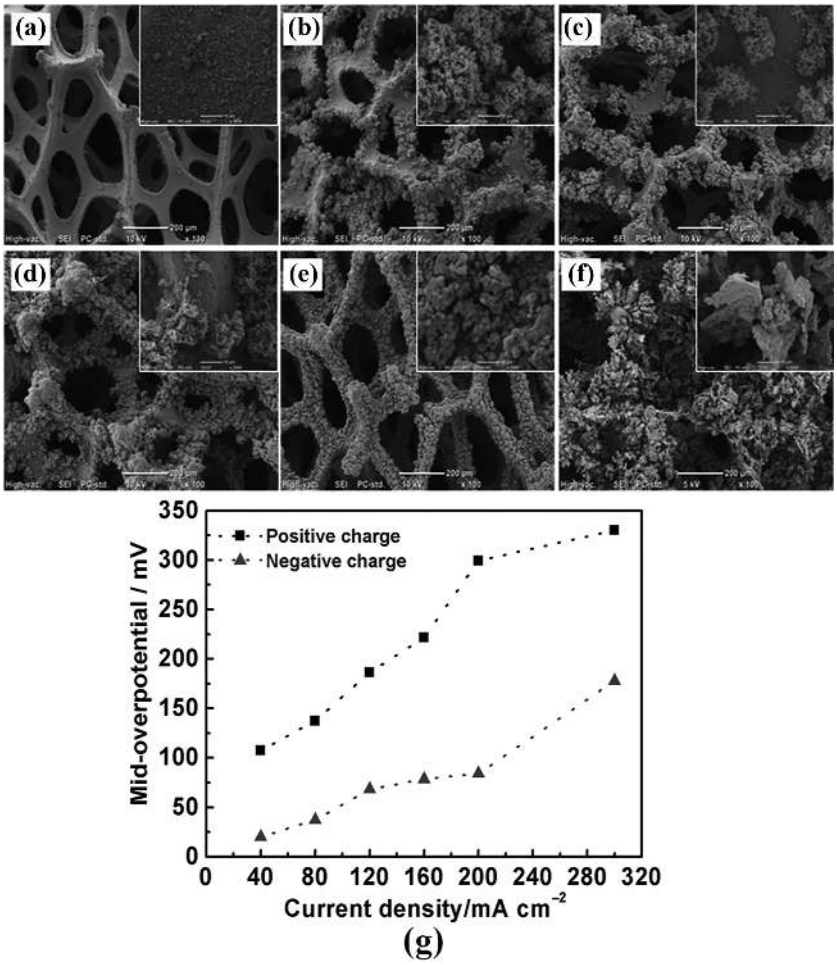

FIGURE 16.3 Zinc electrodeposition morphology of porous nickel foam at different current densities: (a) 40 mA cm^{-2}; (b) 80 mA cm^{-2}; (c) 120 mA cm^{-2}; (d)160 mA cm^{-2};(e) 200 mA cm^{-2}; (f) 300 mA cm^{-2}. (g) Mid-overpotential of positive electrode and negative electrode at various current densities (40 to 300 mA cm^{-2}) [25].

that the hollow carbon sphere served as a conducive conductive substrate, establishing an elaborate internal conductive network to enhance electron transport capacity and conductivity. Moreover, the core-shell structure facilitated electrolyte infiltration, minimizing ion transport pathways to enhance electrochemical reaction rates. In a separate study, Kang et al. [27] investigated nickel-based batteries and devised a NiMoO4@NiCo layered double hydroxide core/shell heterostructure assembled on a nanoarray directly grown on NF as a cathode. Experimental findings demonstrated that the resulting nickel-based battery yielded a surface energy density of 46.7 Wh kg^{-1}, a power density of 720 W kg^{-1} at 1 A g^{-1}, and a high-power density of 5844.5 W kg^{-1} at 10 A g^{-1}. Following 2,000 cycles with a capacity of 6 A g^{-1}, the battery retained 53.2% of its initial capacity, surpassing the performance of other cathode materials with doping additives.

Xiao et al. [28] employed the buffer solution method to fabricate the Mn-doped nickel oxide electrode. Investigations utilizing scanning electron microscopy, specific surface area analysis, and cyclic voltammetry revealed that the crystal particles in the Mn-doped sample were small, with the doped sample exhibiting a larger BET surface area and a mesoporous structure. Notably, the difference between the oxidation peak potential and the reduction peak potential in the Mn-doped samples was minimal. These manganese-doped samples exhibited superior electrochemical characteristics compared to commercially available B-$Ni(OH)_2$. Constant current charging and discharging tests demonstrated that the sample with 18 mol% Mn content displayed the highest specific discharge capacity and optimal cycle stability. In a related study, Li et al. [29] investigated a composite material consisting of cobalt-aluminum layered bimetallic hydroxide and reduced graphene oxide as a cathode additive for nickel-based secondary batteries. A comparison with pure nickel hydroxide and nickel hydroxide cobalt oxide electrodes revealed that the $Ni(OH)_2$ electrode incorporating the additive displayed improved cycle stability and possessed a soft and flexible structure. This modification benefited the electronic conductivity of the electrode, enhanced the electrochemical reversibility of the proton diffusion anode, and facilitated the establishment of a more efficient and stable conductive network. Additionally, it demonstrated higher electrochemical activity and discharge capacity than commercial cobalt oxide.

Drawing from the above experiments, several optimization strategies have emerged to prolong the lifespan and enhance the efficiency of ZNFBs. Despite the beneficial outcomes, the experimental procedures incur high costs, hindering comprehensive analyses of the internal reaction mechanisms and electrochemical phenomena of the battery. Therefore, in order to deeply explore the internal mechanism of the battery, the numerical study of ZNFBs has been gradually advanced.

16.3.2 Numerical Study

During the initial stages, various mathematical simulation models were successively developed by domestic and foreign scholars to investigate the electrochemical reaction and mass transfer mechanisms of porous nickel oxide electrodes in ZNFBs [30,31]. Gu et al. [32] subsequently synthesized prior models and established a comprehensive simulation model for the nickel electrode through their optimized approach. Prior researchers comprehensively modeled the flow behaviors, mass transfer, and electrochemical reactions of ZNFBs across all domains, integrating multiple physical field models using Fluent software to determine the distribution of OH^- and $Zn(OH)_4^{2-}$ ions in both the flow channel and electrode, as well as the voltage drop distribution in the solid and liquid phases of batteries. Subsequently, through Fluent software, the electrolyte flow was analyzed and simulated in various electrode structures to define the flow field distribution within the electrode, facilitating the analysis of ion transport within the internal flow field and the general electrochemical reaction patterns. Nevertheless, due to the simplification of the internal porous structure, the chemical reaction characteristics within the pores were not fully elucidated.

Song et al. [33] built a 3-D model to research the flow field within a battery stack. They assessed the unevenness of the intended flow channel, enhanced the structure of the bottom

and entrance of the channel using the inhomogeneity coefficient, and introduced a novel T-channel pile design. Simulation outcomes demonstrated that the flow field in the stack cell equipped with the T-channel exhibited greater uniformity. Xiao et al. [34] established a comprehensive 3-D steady-state model focusing on mass transfer mechanisms and internal reactions to enhance comprehension of the electrochemical performance of ZNFBs. This model encapsulated mass, momentum, reaction charge, and considered interactions between the anode and cathode, material transport, and electrochemical reactions between the electrodes and electrolytes. The model simulated the internal ion concentration and electrode current density distribution in ZNFB, while also exploring the impacts of channel width and electrolyte flow rate on electrochemical properties. Yao et al. [35] utilized a 2 kW ZNFB modular system as the basis to construct a simulation and analysis model for the energy storage unit for batteries, incorporating unilateral and bilateral liquid supply pipelines as per the design scheme. This model holds significance for the optimization of ZNFB designs. In a related study, Zhao et al. [36] formulated a 3-D stack model grounded on the general conservation law to simulate the distribution of current density and potential within the stack and evaluate the impact of flow rate and inlet concentration on ZNFB stack performance. Simulation results highlighted significant gradients in current density and potential across cell thickness, with the current density gradient predominantly observed in the porous anode and the liquid phase potential gradient mainly located in the bulk electrolyte. Despite within-cell variations, consistency and uniformity were noted across the battery stack.

Yao et al. [37] developed a numerical model for a porous electrode based on the structure of the positive porous electrode in ZNFBs. Utilizing the lattice Boltzmann method, they simulated the flow mass transfer process within the porous electrode. The impacts of varying charging current density, porosity, and electrolyte inlet velocity on electrochemical reactions, flow, and mass transfer within the porous electrode were investigated, focusing on seepage and mass transfer within the pore. This study has some insights to determine the operation law of the physical field in the control porous electrode. In subsequent studies, Liu et al. [38] constructed a ZNFB structure considering porous electrodes through the lattice Boltzmann model, conducted an in-depth study on the dynamics of the charging process of the positive electrode at the pore scale, and explained the changes in the concentration of hydroxide ions and protons during the process. Zhou et al. [39] added the three-dimensional electrode to the three-dimensional transient model of ZNFBs and considered the influence of the electrode on the distribution of chemical and physical properties of the battery. The changes of ion concentration, current density, overpotential, and local charge distribution with time and space during charging are investigated. Furthermore, a three-dimensional transient ZNFB battery model with negative reaction was established [14]. By comparing the calculated results, the side reaction enhanced the activation polarization of the positive electrode, and increased electrolyte flow rate, reduced ambient temperature, and impressed current density were conducive to inhibiting HER.

Based on the three-dimensional transient model of ZNFBs, Huang et al. [40] analyzed the effects of positive and negative electrodes and overall polarization of the battery and compared the effects of the traditional nickel-plated steel strip negative electrode and the porous NF negative electrode on the polarization process. The NF porosity and thickness at different electrolyte flow rates and current densities were preliminarily optimized, and the

response surface method was introduced to further optimize the design in the follow-up study to evaluate the influence of relevant factors on the overall polarization [41].

Utilizing the insights from prior research, a comprehensive three-dimensional transient model of ZNFBs that accounts for side reactions has been effectively developed. This model establishes a groundwork for future investigations into side reactions and the cyclic charge/discharge within battery stacks. The side reactions are recognized to diminish the lifespan and capacity of ZNFBs. To delve deeper into this phenomenon, a mechanism study model focusing on side reactions was created, representing a significant contribution to this area of study. In a related study, Huang et al. [42] established a two-dimensional transient two-phase flow model for ZNFBs considering the side reaction of hydrogen evolution. The mechanism theory of the effect of two-phase flow on battery performance was first proposed. As shown in Figure 16.4, bubble flow promotes ion transfer at the negative interface, effectively reducing concentration and activation polarization loss.

The preceding studies offer valuable insights into comprehending the side reactions of ZNFBs. However, because of significant structural variations and distinct reaction mechanisms among different batteries, it is imperative to establish and advance a multi-physical coupling mechanism analysis model for investigating side reactions in ZNFBs.

Xu et al. [37,43] employed the lattice Boltzmann method (LBM) to devise a mechanism model for the internal mass transfer and electrochemical reactions within the positive electrode of ZNFB. Their analysis delved into the distribution of ion concentration and reaction

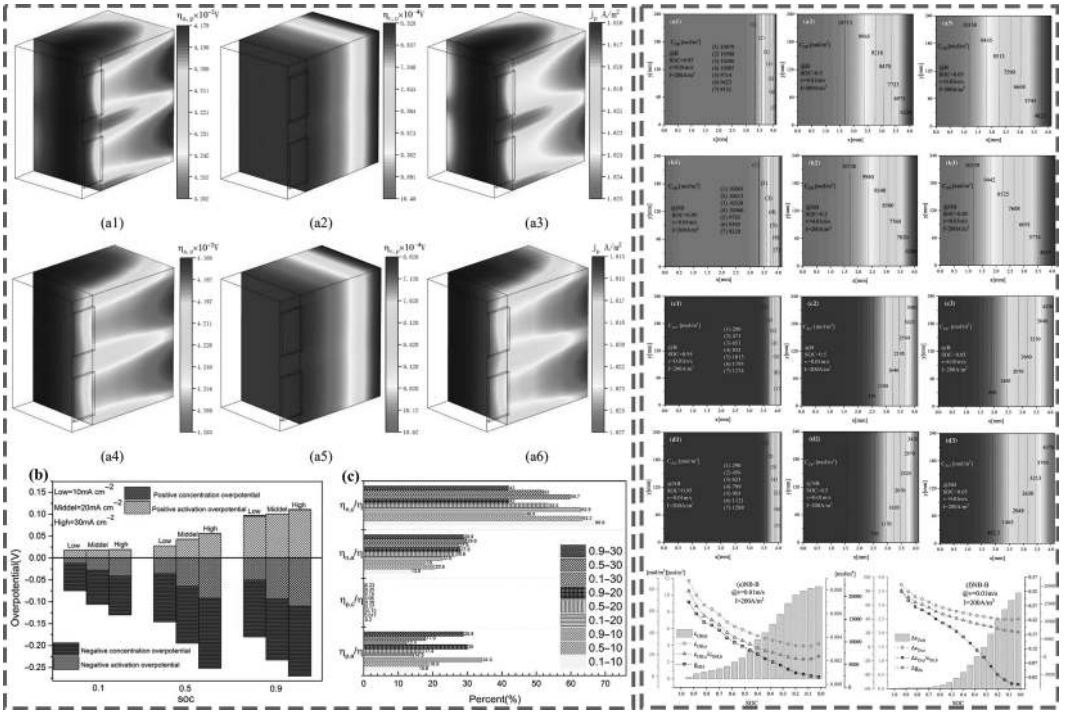

FIGURE 16.4 (a) NS and PC as negative electrode overpotential distribution and ratio; (b) the effect of bubble flow on ion distribution [42]. Copyright (2022), Elsevier.

current density within the battery. Subsequently, leveraging the positive electrode structure of the porous electrode, they formulated a two-dimensional numerical model to explore electrochemical reactions within the porous electrode from the perspective of seepage and mass transfer within the pores. Findings underscored the significant influence of proton concentration on the reaction rate and reaction current density, with hydroxide concentration predominantly impacting overpotential. By using the phase field LBM, Yao et al. [44] established a 2-D ZNFB model that accounted for zinc dendrites. The spatiotemporal distribution of ions and electrons in the battery was analyzed, and the evolution of zinc dendrites was described. The results show that the increase of electrolyte flow rate is conducive to the enhancement of ion diffusion and the decrease of surface ion concentration of the anode. The formation of dendrites can be reduced by adjusting the intensity of anisotropy. Luo et al. [45] reconstructed the microstructure of a porous nickel oxide electrode using the four-structure generator set method and simulated the flow mass transfer and electrochemical reactions within the porous electrode of ZNFB using the LBM method. Their work investigated the electrochemical effects of different porous electrode structures on the interior of ZNFB from the perspective of mass transfer and pore permeability. Findings revealed that varying pore structures affected the diffusion rate of electrolyte ions and influenced the electrochemical reaction. A decrease in porosity and particle size was associated with improved electrolyte ion diffusion and promoted electrochemical reactions. However, increased electrode thickness impeded OH^- ion diffusion and exacerbated concentration polarization, detrimentally impacting battery charging efficiency. Research at the micro- and nano-scales concerning zinc-nickel batteries remains in its nascent stages but holds critical implications for understanding the correlation between internal structure and battery performance.

16.4 OVERVIEW OF LARGE-SCALE PRODUCTION

From its inception in 2006, the ZNFB has seen important advancements in large-scale production both domestically and globally. Notably, enhancements have been made in battery structure, electrode materials, and overall performance. Progress has been achieved in optimizing the structure and size of the stacks, as well as capacity and energy efficiency. However, challenges such as zinc particle shedding and anode surface passivation persist, requiring immediate attention.

The ZNFB has progressed from fundamental technological research and principal validation to small-scale pilot testing. Laboratory principal batteries have demonstrated a cycle life exceeding 10,000 cycles. Currently, three generations of large-scale ZNFB products have been built. Initial generation has been demonstrated and utilized in the State Grid Corporation and two universities in China successfully, showcasing promising operational performance and further development potential [46]. Zhejiang Yuyuan Energy Storage Technology CO., Ltd. has commenced production [47]. Additionally, the production line for the second-generation products is near completion, achieving an energy storage scale of 1 MW·h. Zhangbei National Scenery Storage Demonstration Zone in China has installed a single liquid flow ZNFB system with a total storage capacity of 50 kT·h, composed of 168 200 A·h single batteries in series, demonstrating an energy efficiency of 80%, as depicted in Figure 16.5e. Efforts are underway to optimize and enhance the 300A·h third-generation product, promising a favorable application outlook. Table 16.1 provides an overview of

TABLE 16.1 Comparison of Three Generations of ZNFB Parameters

Product Performance Index	Maximum Cut-off Voltage/V	Minimum Cut-off Voltage/V	Rated Voltage/V	Rated Capacity/ A·h	Electrical Pair/one	Surface Capacity/ $mA{\cdot}h{\cdot}cm^{-2}$	Positive and Negative Plate Size $(W\times L)$/mm	Coulomb Efficiency/%	Cycle Life/ Times	Liquid Supply Mode
First generation	2.05	1.2	1.6	200	15	20	150×180	>90	>10,000	External water pump
Second generation	2.05	1.2	1.6	216	19	20	150×240	>90	>10,000	External water pump
Third generation	2.05	1.2	1.6	300	23	20	150×240	>95	>10,000	Internal micropump
Third-generation improvement	2.05	1.2	1.6	300	23	20	150×240	>95	>10,000	The external electrode drives the spiral frame

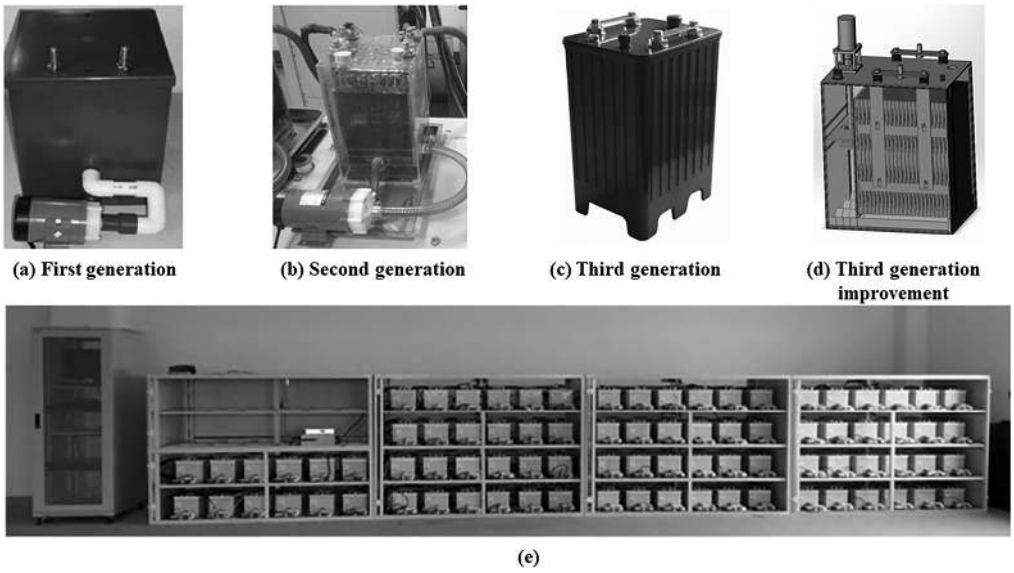

FIGURE 16.5 (a–d) Development process of zinc-nickel flow battery; (e) 50 kWh energy storage system with 168 units of 200 Ah Zn/Ni single-flow redox battery.

the performance parameters of the three generations of products and their enhancements, which have successively increased in capacity. The developmental trajectory of the ZNFB is illustrated in Figure 16.5a–d.

The Energy Institute at City University of New York initiated research on ZNFBs [48], leading to the development of a ZNFB in 2009 and subsequently advancing to a 555 A·h capacity in 2014. Currently, a 25 kW·h energy storage system has been constructed and deployed for large-scale application, involving the connection of 30833 Wh large batteries in series, as illustrated in Figure 16.6a and b. The cycle performance outcomes of a 25 kWh battery at the grid scale are presented in Figure 16.6c, demonstrating a sustained energy efficiency of over 80% for approximately 1,000 cycles. While the commercial application of the ZNFB has not reached the level of advancement seen with the all-vanadium FB, scholars hold optimistic expectations regarding the engineering application potential of ZNFBs. Consequently, a growing body of research is anticipated to concentrate on enhancing ZNFB performance and facilitating large-scale implementation.

16.5 CONCLUSIONS

Although the ZNFB offers high energy density, cost-effectiveness, and safety benefits, certain issues persist that impact battery performance, hindering the commercial application process and warranting further investigation. This paper focuses on summarizing and analyzing the primary challenges, influencing factors, and potential solutions associated with the ZNFB. Additionally, it briefly outlines the current modeling status and engineering applications of the battery system. To drive the future development of ZNFBs, this paper presents the following conclusions and outlook:

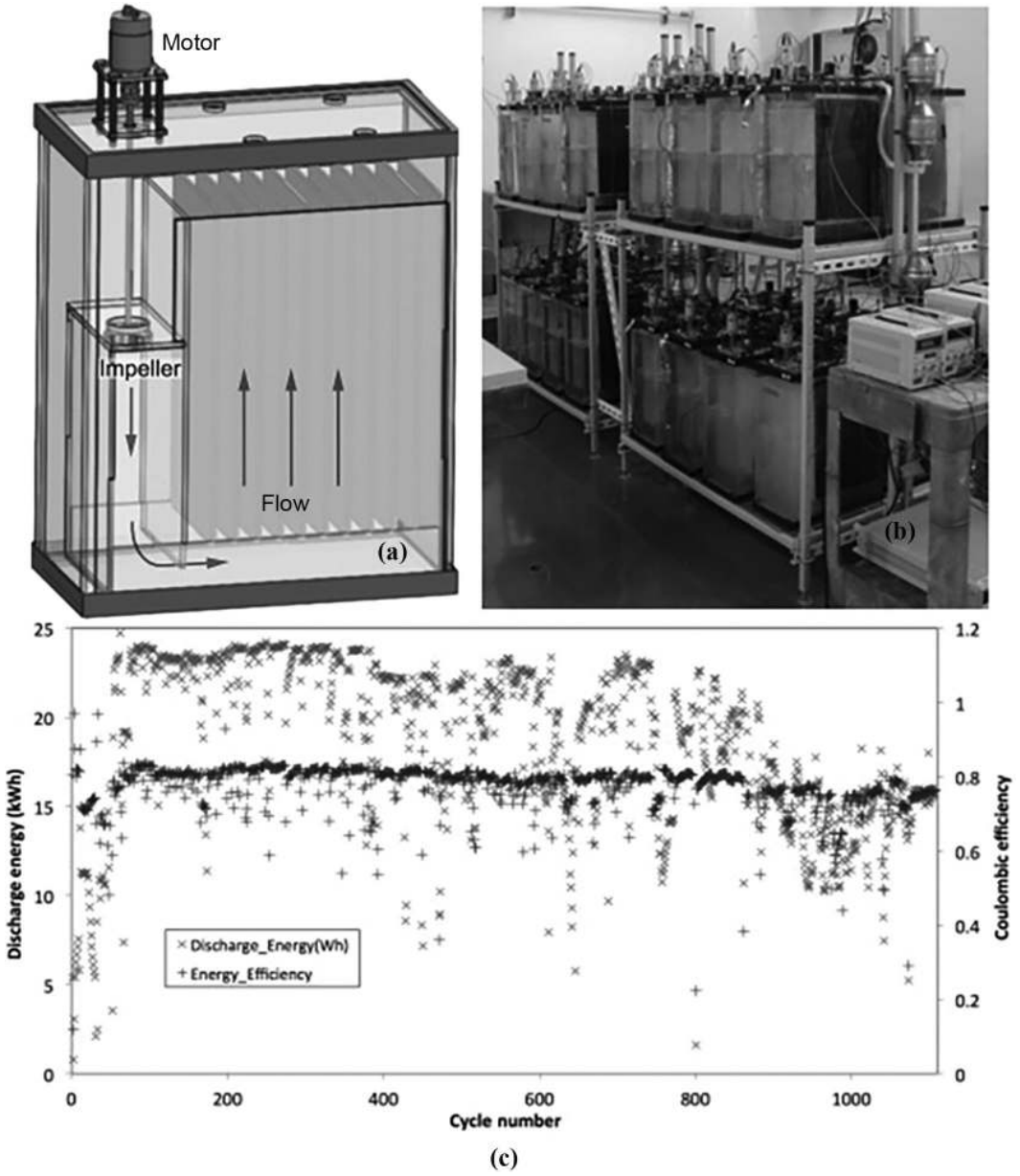

FIGURE 16.6 (a) Structure diagram of 555 Ah battery; (b) grid scale 25 KWH battery photo; (c) cycle performance of 25 kW·h zinc-nickel flow battery [48]. Copyright (2014), Elsevier.

1. Understanding the internal mechanism and reaction principles of the ZNFB involves employing numerical simulations of multi-physical field coupling. Optimization methods are utilized in designing the battery, while recent studies using LMB methods have explored the effect of porous electrode structures and dendrite growth mechanisms within ZNFB performance.

2. There is a need to further develop novel battery structures and establish precise physical models to depict internal battery reactions and integrate external characteristics. Multi-scale investigations into the influences of battery materials, internal structures, and external operational parameters on the entire battery system aim to guide experimental and engineering design efforts and accelerate application progress.
3. To streamline calculations and enhance efficiency, the current ZNFB numerical model adopts the homogeneity hypothesis for the porous structure in positive. However, this hypothesis introduces a margin of error, as the positive porous structure significantly influences mass transfer and electrolyte flow processes at the interface. During late-stage charging of the ZNFB, oxygen evolution from the positive side reaction occurs, necessitating further investigation into its impact.
4. Addressing the growth of negative zinc dendrites and the implications of HER on battery operation are ongoing areas of study. Developing numerical models that consider hydrogen evolution bubble flow and negative zinc dendrite growth is crucial for accurately comprehending dendrite growth mechanisms in the ZNFB and the mass transfer mechanisms in the negative electrode.
5. The potential of high-performance batteries designed using biomimetic concepts, such as biomimetic lung fuel cells, flexible lithium-ion batteries prepared with a biomimetic backbone structure, and high-performance batteries utilizing an "ant nest" structure solid electrolyte to mitigate lithium dendrite formation, suggests a promising avenue for future development in ZNFBs by combining battery technologies with bionics.

REFERENCES

1. J. Nijnens, P. Behrens, O. Kraan, B. Sprecher, R. Kleijn, Energy transition will require substantially less mining than the current fossil system, *Joule*, 7 (2023) 2408–2413.
2. G. Luderer, S. Madeddu, L. Merfort, F. Ueckerdt, M. Pehl, R. Pietzcker, M. Rottoli, F. Schreyer, N. Bauer, L. Baumstark, C. Bertram, A. Dirnaichner, F. Humpenöder, A. Levesque, A. Popp, R. Rodrigues, J. Strefler, E. Kriegler, Impact of declining renewable energy costs on electrification in low-emission scenarios, *Nature Energy*, 7 (2022) 32–42.
3. F. Guo, B.J. van Ruijven, B. Zakeri, S. Zhang, X. Chen, C. Liu, F. Yang, V. Krey, K. Riahi, H. Huang, Y. Zhou, Implications of intercontinental renewable electricity trade for energy systems and emissions, *Nature Energy*, 7 (2022) 1144–1156.
4. S. Potrč, L. Čuček, M. Martin, Z. Kravanja, Sustainable renewable energy supply networks optimization–The gradual transition to a renewable energy system within the European Union by 2050, *Renewable and Sustainable Energy Reviews*, 146 (2021) 111186.
5. X. Huang, R. Zhou, X. Luo, X. Yang, J. Cheng, J. Yan, Experimental research and multiphysical modeling progress of Zinc-Nickel single flow battery: A critical review, *Advances in Applied Energy*, (2023) 100154.
6. S. Fleischmann, J.B. Mitchell, R. Wang, C. Zhan, D.-E. Jiang, V. Presser, V. Augustyn, Pseudocapacitance: From fundamental understanding to high power energy storage materials, *Chemical Reviews*, 120 (2020) 6738–6782.
7. P. Tan, W. Kong, Z. Shao, M. Liu, M. Ni, Advances in modeling and simulation of Li–air batteries, *Progress in Energy and Combustion Science*, 62 (2017) 155–189.

8. H. Zhang, W. Lu, X. Li, Progress and perspectives of flow battery technologies, *Electrochemical Energy Reviews*, 2 (2019) 492–506.
9. S. Li, K. Li, E. Xiao, J. Zhang, M. Zheng, Real-time peak power prediction for zinc nickel single flow batteries, *Journal of Power Sources*, 448 (2020) 227346.
10. S. Yao, Y. Zhao, X. Sun, Q. Zhao, J. Cheng, A dynamic model for discharge research of zinc-nickel single flow battery, *Electrochimica Acta*, 307 (2019) 573–581.
11. Z. Yuan, X. Li, Perspective of alkaline zinc-based flow batteries, *Science China Chemistry*, 67 (2024) 260–275.
12. S. Li, K. Li, E. Xiao, C.-K. Wong, Joint SoC and SoH estimation for Zinc–Nickel single-flow batteries, *IEEE Transactions on Industrial Electronics*, 67 (2019) 8484–8494.
13. S. Yao, P. Liao, M. Xiao, J. Cheng, W. Cai, Study on electrode potential of zinc nickel single-flow battery during charge, *Energies*, 10 (2017) 1101.
14. S. Yao, R. Zhou, X. Huang, D. Liu, J. Cheng, Three-dimensional transient model of zinc-nickel single flow battery considering side reactions, *Electrochimica Acta*, 374 (2021) 137895.
15. J. Cheng, L. Zhang, Y.-S. Yang, Y.-H. Wen, G.-P. Cao, X.-D. Wang, Preliminary study of single flow zinc–nickel battery, *Electrochemistry Communications*, 9 (2007) 2639–2642.
16. J. Cheng, Y.-H. Wen, Y. Xu, G.-P. Cao, Y.-S. Yang, Effect of matrix on electrodeposition of zinc in flowing potassium zincate lye, *Chemical Journal of Higher Education*, 32 (2011) 2640–2644.
17. L. Zhang, J. Cheng, Y.-S. Yang, Y.-H. Wen, X.-D. Wang, G.-P. Cao, Study of zinc electrodes for single flow zinc/nickel battery application, *Journal of Power Sources*, 179 (2008) 381–387.
18. L. Zhang, J. Cheng, Y. Yang, Y. Wen, X. Wang, Z. Xie, Preliminary study on zinc anode performance and battery performance of single flow zinc-nickel battery, *Electrochemistry*, 14 (2008) 248.
19. J. Cheng, Y.-H. Wen, G.-P. Cao, Y.-S. Yang, Influence of zinc ions in electrolytes on the stability of nickel oxide electrodes for single flow zinc–nickel batteries, *Journal of Power Sources*, 196 (2011) 1589–1592.
20. Y. Wen, T. Wang, J. Cheng, J. Pan, G. Cao, Y. Yang, Lead ion and tetrabutylammonium bromide as inhibitors of the growth of spongy zinc in single flow zinc/nickel batteries, *Electrochimica Acta*, 59 (2012) 64–68.
21. Y. Cheng, H. Zhang, Q. Lai, X. Li, D. Shi, L. Zhang, A high power density single flow zinc–nickel battery with three-dimensional porous negative electrode, *Journal of Power Sources*, 241 (2013) 196–202.
22. S. Xing, Q. Wang, Z. Ma, Y. Wu, Y. Gao, Effect of additives on the structure and electrochemical performance of mesoporous nickel hydroxide, *Ionics*, 19 (2013) 651–656.
23. S. Song, J. Pan, Y. Wen, J. Cheng, J. Pan, G. Cao, Effect of electrolyte flow rate on performance of Zinc-nickel single flow battery, *Journal of University Chemistry*, 35 (2014) 134–139.
24. Y. Cheng, Q. Lai, X. Li, X. Xi, Q. Zheng, C. Ding, H. Zhang, Zinc-nickel single flow batteries with improved cycling stability by eliminating zinc accumulation on the negative electrode, *Electrochimica Acta*, 145 (2014) 109–115.
25. Y. Cheng, X. Xi, D. Li, X. Li, Q. Lai, H. Zhang, Performance and potential problems of high power density zinc–nickel single flow batteries, *RSC Advances*, 5 (2015) 1772–1776.
26. J. Meng, Z. Yang, L. Liu, F. Cui, Y. Jiang, The in-situ growth of zinc-aluminum hydrotalcite on hollow carbon spheres and its application as anode material with long cycle life for zinc-nickel secondary battery, *Journal of Alloys and Compounds*, 809 (2019) 151842.
27. W. Kang, Y. Sun, B. Xu, J. Li, X. Kong, D. Huang, X. Zhang, H. Yang, B. Lin, Novel aqueous nickel-bismuth batteries using NiMoO4@ NiCo-layered double hydroxide heterostructure nanoarrays and $Bi_2O_2CO_3$ microspheres as advanced electrode materials, *Electrochimica Acta*, 323 (2019) 134819.
28. M. Xiao, F. Dou, S. Yao, R. Xing, J. Cheng, Y. Yang, Preparation and electrochemical performance of manganese-doped nickel hydroxide cathode materials, *International Journal of Electrochemical Science*, 15 (2020) 6024–6034.

29. J. Li, H. Zhang, C. Wu, X. Cai, M. Wang, L. Li, Q. Li, Z. Chang, E. Shangguan, Novel application of CoAl-layered double hydroxide/reduced graphene oxide nanocomposite as a highly efficient cathode additive for nickel-based secondary batteries, *Electrochimica Acta*, 330 (2020) 135242.
30. D. Fan, R.E. White, A mathematical model of a sealed nickel-cadmium battery, *Journal of the Electrochemical Society*, 138 (1991) 17.
31. Z. Mao, R.E. White, A finite-difference method for pseudo-two-dimensional boundary value problems, *Journal of the Electrochemical Society*, 141 (1994) 151.
32. W.B. Gu, C.Y. Wang, Thermal-electrochemical modeling of battery systems, *Journal of The Electrochemical Society*, 147 (2000) 2910.
33. Y. Song, Y. Wang, M. Xiao, S. Yao, J. Cheng, K. He, Optimization analysis of zinc-nickel single-flow battery stack structure based on internal flow field analysis. *Proceedings of the 21st National Academic Conference of the Engineering Thermophysics Committee of the Higher Education Association*, 2015.
34. M. Xiao, Y. Wang, S. Yao, Y. Song, J. Cheng, K. He, Analysis of internal reaction and mass transfer of zinc-nickel single flow battery, *Journal of Renewable and Sustainable Energy*, 8 (2016) 064102.
35. S. Yao, W. Liu, J. Cheng, W. Cai, Pipeline design optimization of modular system for zinc-nickel single flow battery, 2 (2018) 83–87.
36. S. Yao, Y. Zhao, X. Sun, D. Ding, J. Cheng, Numerical studies of cell stack for zinc-nickel single flow battery, *International Journal of Electrochemical Science*, 14 (2019) 2160–2174.
37. S.G. Yao, L.K. Xu, Z.Y. Sun, J. Cheng, Electrochemical mechanism in porous electrode of zinc–nickel single-flow battery based on lattice Boltzmann method, *International Journal of Heat and Mass Transfer*, 138 (2019) 903–915.
38. R. Liu, S. Yao, L. Xu, Z. Sun, J. Cheng, Transient simulation of porous cathodes of zinc-nickel single-flow batteries based on lattice Boltzmann method, *Journal of Energy Storage*, 32 (2020) 101937.
39. R. Zhou, S. Yao, Y. Zhao, J. Cheng, Tab design based on the internal distributed properties in a Zinc–Nickel single-flow battery, *Industrial & Engineering Chemistry Research*, 60 (2021) 1434–1451.
40. S. Yao, X. Huang, X. Sun, R. Zhou, J. Cheng, Structural modification of negative electrode for zinc–nickel single–flow battery based on polarization analysis, *Journal of The Electrochemical Society*, 168 (2021) 070512.
41. X. Huang, S. Yao, X. Yang, X. Sun, R. Zhou, X. Liu, J. Cheng, Polarization analysis and optimization of negative electrode nickel foam structure of zinc-nickel single-flow battery, *Journal of Energy Storage*, 55 (2022) 105624.
42. X. Huang, S. Yao, R. Zhou, X. Yang, X. Kan, J. Cheng, Study on the effect of hydrogen evolution reaction in the zinc-nickel single flow battery, *Journal of Energy Storage*, 50 (2022) 104246.
43. S.G. Yao, L.K. Xu, Y. Li, J. Cheng, Pore-scale simulation of internal reaction mechanism of positive electrode for zinc-nickel single-flow battery, *Journal of Solid State Electrochemistry*, 24 (2020) 915–928.
44. S. Yao, X. Kan, R. Zhou, X. Ding, M. Xiao, J. Cheng, Simulation of dendritic growth of a zinc anode in a zinc–nickel single flow battery using the phase field-lattice Boltzmann method, *New Journal of Chemistry*, 45 (2021) 1838–1852.
45. J. Luo, S. Yao, R. Liu, X. Kan, Y. Yang, J. Cheng, Study on ion transport mechanism of zinc-nickel single-flow battery with different porous electrode structures based on Lattice Boltzmann Method, *Journal of The Electrochemical Society*, 169 (2022) 050518.
46. Y.-X. Li, M.-C. Wong, W.-F. Ip, P.-C. Zhao, C.-K. Wong, J. Cheng, Z.-Y. You, *Modeling of Novel Single Flow Zinc-Nickel Battery for Energy Storage System*, IEEE, pp. 1621–1626.

47. J. Wang, X. Xu, Q. Ding, J. Zhu, Y. Ma, L. Zhao, X. Liu, Application and prospect of zinc-nickel battery in energy storage technology, *Energy Storage Science and Technology*, 8 (2019) 506.
48. D.E. Turney, M. Shmukler, K. Galloway, M. Klein, Y. Ito, T. Sholklapper, J.W. Gallaway, M. Nyce, S. Banerjee, Development and testing of an economic grid-scale flow-assisted zinc/nickel-hydroxide alkaline battery, *Journal of Power Sources*, 264 (2014) 49–58.

CHAPTER 17

Current Progress and Perspective of Rechargeable Zinc-Bromine Flow Batteries

Jeevanantham Balasubramaniam,
Abhinav Kalathum Padikkal,
and Shobana Mummoorthi Kanagarajan

17.1 INTRODUCTION

The increasing utilization of renewable energy sources such as solar and wind has raised concerns about the reliability and stability of the electrical grid infrastructure. Large-scale electrochemical energy storage technologies are therefore regarded as a crucial solution to improve grid reliability and power quality. Energy storage systems play a significant role in electrical grid-scale applications that offer consistent and dependable power; they have emerged as a prominent area of research interest. Among numerous energy storage technologies, redox flow batteries (RFBs) are regarded as realistic power sources due to their scalability, high efficiency, and long life cycles [1–6]. Compared to other RFBs, zinc-bromine flow batteries (ZBFBs) have received considerable interest and offer relatively high theoretical specific energy (440 Wh kg^{-1} at 298 K) and low material costs. The ZBFB was developed by Exxon in the early 1970s; the concept was patented more than a century ago [7]. However, two innate characteristics prevented the battery's evolution into a commercial battery: zinc's propensity to generate dendrites during deposition and the high bromine (Br_2) solubility in the aqueous zinc bromide electrolyte. ZBFBs can be divided into two main groups: flow and non-flow batteries. Flow batteries, such as those developed by Redflow (Australia) and Primus Power (US), use a solution of zinc bromide stored in two tanks. During charging and discharging, the electrolytes are pumped through a reactor stack from one tank to the next. Non-flow systems, on the other hand, are being developed

DOI: 10.1201/9781003506379-17

by companies like Gelion (Australia) and EOS Energy Enterprises (US). The high volatility of Br_2 permits diffusion and direct reactivity with the zinc electrode, resulting in the cell's self-discharge. Dendritic zinc deposits can cause the cell to short-circuit rapidly. The ZBFB is a modular system that consists of a cell stack with functional electrodes connected to pipes, electrolyte storage tanks, delivery pumps, and current collectors (with membranes separating them). To accomplish charge transfer and generate electrical current, the RFB depends on the electrolyte circulation system to supply electrochemically active species to electrode surfaces. Zinc bromide mixed in water to make an aqueous solution is the primary electrolyte in zinc/bromine batteries. The formulation is utilized in circulatory loops that service the anode and cathode during operation.

The main electrochemically active species that engages in charge-transfer processes with the electrodes to enable the system to operate as an energy storage device is $ZnBr_2$. Zinc is deposited at the negative electrode, while Br_2 is generated at the positive electrode during charging. At the corresponding electrodes, zinc and bromide ions are created during discharge. The reduction of direct chemical reaction and the corresponding self-discharge of the cell are attributed to the microporous separator between the electrode surfaces shown in Figure 17.1, which hinders the diffusion of Br_2 to the zinc deposit. The leading potential application for ZBFBs is stationary energy storage, either for the grid or domestic/stand-alone power systems. Their aqueous electrolyte makes them less prone to

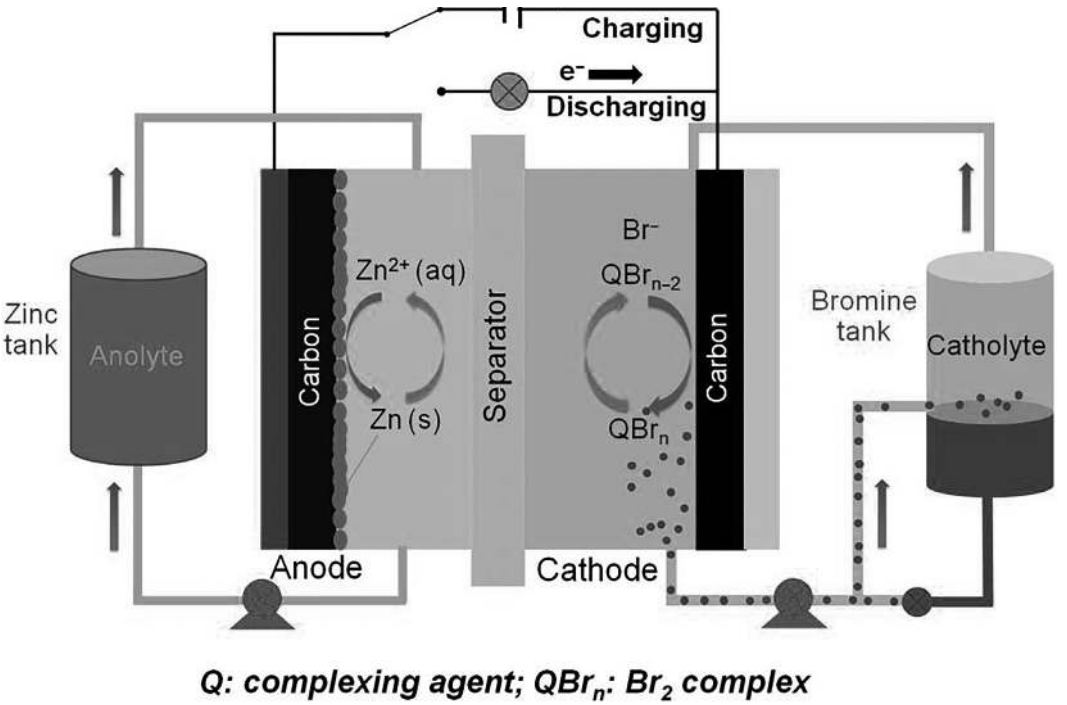

FIGURE 17.1 Schematic diagram of the ZBFB. (Adapted from [6], Copyright (2023), John Wiley & Sons.)

overheating and fire compared to lithium-ion battery systems. ZBFBs have also shown suitable properties for large-scale stationary energy storage applications, such as raw material availability and low battery costs [7]. ZBFBs incorporate several safety features to mitigate risks during operation. To avoid the corrosion and toxicity caused by free Br_2 generated during charging, ZBFBs use Br_2 complexing agents (BCAs) that create safe, chemically complex organic phases. The BCAs greatly reduce the chemical reactivity and evaporation rate of Br_2 compared to the pure element. For example, at 20°C, the vapor pressure of Br_2 over the complex is more than 20 times lower than for elemental Br_2. Several barriers are implemented to enhance electrolyte containment and minimize leakage in case of a breach. To guarantee that electrolyte circulation stops in the event of an accident, impact, or leak sensors with shut-down controls might be included. These modifications, however, can result in a decrease in the specific energy density and an increase in battery weight. The zinc and polybromide complexes are stored separately, away from each other. Even if the zinc electroplate were flooded with polybromide complex, the reaction rate would be relatively slow due to the low zinc surface area available for reaction.

Br_2 is present as polybromide ions dissolved in the aqueous electrolyte or bound with complexing agents in a second phase. Any remaining Br_2 is dissolved in the aqueous electrolyte. In the complex condition, the chemical reactivity and evaporation rate are reduced compared to pure Br_2. ZBFB falls under the category of hybrid flow batteries, meaning that while charging, part of the energy is stored on the anode by plating it with zinc metal, and the remaining portion is stored in the electrolyte. Two aqueous electrolytes function as the battery's electrodes and charge storage components in a $ZnBr_2$ battery. Reversible electrochemical reactions occur in the electrolyte solutions, which contain the reactive elements zinc and Br_2. As a result, energy is either charged into the battery or released. During battery charging, elemental zinc forms the anode by adhering to the carbon-plastic electrodes that connect each battery cell, whereas Br_2 forms at the cathode. The electrodes are made of carbon plastic because Br_2 is a very corrosive material. The battery's architecture incorporates a selective barrier to keep the electrolytes apart while enabling ion transfer to preserve charge neutrality [8,9]. Many benefits of flow batteries are lengthy lifespans, modular design, and nearly zero energy loss over the technology's storage life. However, the intricate design of these battery systems may result in higher expenses and more challenging development [10,11]. Compared to most other battery storage systems, ZBFB also has stricter operating parameters and poor efficiency [9]. Despite the positive attributes of the ZBFB, there are few comprehensive investigations into various facets of its electrochemistry. Furthermore, due to zinc's quick reaction kinetics, more research has been done on Br_2 electrochemistry and its application than on zinc [12]. Zinc has quick reaction kinetics compared to the Br_2 reaction, although its reversibility is debatable and believed to be a determining element in the overall features of cell performance. To achieve an improvement in the performance of the cell, research has been concentrated on the zinc electrochemical deposition/dissolution reaction in the ZBFB flow cell in the current work. Initially, they carried out basic quantitative investigations regarding the capacity of zinc deposition and dissolution.

17.2 HISTORY AND PRINCIPLE OF ZINC-BROMINE FLOW BATTERIES

Exxon created the ZBFB, a hybrid flow battery system, in the early 1970s. When the battery is charged, solid zinc is placed on the anode to store energy. Consequently, the total size of the electrolyte storage reservoirs and the anode surface area affect the ZBFBs' energy production. The energy ratings of ZBFBs are not completely decoupled, in contrast to other flow batteries that rely solely on changes in redox states in a single phase. ZBFBs have been successfully adapted for kW- to MW-scale applications and have been commercially implemented after a few decades of development [13]. For instance, Ensync Energy installed a 500 kWh ZBFB assembly at the Illinois Institute of Technology in the United States for microgrid applications. In 2016, Vionx Energy (formerly Premium Power) installed a 0.5 MW/3 MWh ZBFB system in Massachusetts, USA. Redflow International Pty Ltd. has deployed 180 active ZBFBs worldwide, installing 2053 MWh of energy capacity. Primus Power installed a 1 MWh energy storage system in South Africa, and Redflow installed a 2 MWh system in California [14]. Even though ZBFBs have had more success thus far, there are still a few real-world problems that need to be resolved to boost performance [15]. For instance, self-discharge may result from the diffusion of aqueous Br_2, and high-power density is negatively impacted by the relatively sluggish kinetics of the polybromide conversion reactions [16]. There is a chance that the solid zinc deposited on the negative electrode will form a dendritic material that will pass through the separators and produce short circuits. Moreover, maintaining an appropriate acid-base balance is crucial for controlling the pH of the electrolyte [11]. Zinc corrosion brought on by an excessively low pH depletes the electrolyte's protons, resulting in self-discharge in the ZBFB. Conversely, a pH greater than 4 will lead to inadequate zinc deposition and the production of a bromate product, such as solid $Zn(OH)_2$ /ZnO, which clogs membranes [17,18].

17.2.1 Mechanism of ZBFB's

A microporous separator divides the positive electrode (Br_2) and negative electrode (zinc) in a single cell of the traditional ZBFB. The electrochemically active zinc and bromide species are present in two tanks of aqueous electrolyte solutions, together with other salts for high conductivity, such as KCl and $ZnCl_2$, and a complexing agent to keep the Br_2 generated during the charging process in a solution [19]. The electrolyte solutions are identical in both tanks and are pumped across the surfaces of both electrodes, storing and releasing electrical energy as the condition of charge and discharge changes. Here, bromide (Br^-) ions release electrons and create Br_2 at the positive electrode during charging, ionic zinc receives electrons from the external circuit, and metallic zinc is plated on the negative electrode. The discharge process is when the opposite responses take place [20].

In addition to preventing unintentional short circuits in the cell, the microporous separator between the two electrode surfaces maintains ion diffusion during charge/discharge [21]. Additionally, the microporous separator lowers the Br_2 passage to the anode, preventing a direct chemical reaction and the ensuing self-discharge. As the electrode surfaces charge, the zinc and Br^- ions diffuse through the separator to their corresponding negative and positive half-cells. Although they pass over the electrodes, the other species in

the electrolyte do not react at the electrode surfaces. Self-discharge is caused by Br_2(aq)'s strong propensity to diffuse from the positive half-cell to the zinc metal [16]. Br_2 is held in a complex phase with low vapor pressure via Br_2 complexation with various quaternary ammonium bromides (QBr) to prevent the diffusion of Br_2 from the positive to negative half-cell and to lessen environmental concerns [22].

The behavior of the chemical compounds present in the electrolyte is more complex. $ZnBr_2$ is the primary electrolyte species that enables the zinc-bromine ($ZnBr_2$) battery to work as an energy storage system. The concentration of $ZnBr_2$ ranges from 1 to 4 M [23,24]. Furthermore, at 25°C, Br_2 (aq) has a high vapor pressure of 28.26 kPa and can have negative effects on the environment and human health [11]. Br_2 is held in a complex phase with low vapor pressure via Br_2 complexation with various quaternary ammonium bromides (QBr) to prevent Br_2 from diffusing from the positive to negative half-cell and to lessen environmental risks [22,25]. N-methyl ethyl-pyrrolidinium bromide (MEPBr) is the QBr complexing agent most frequently utilized [11]. According to Bajpal et al., Br_2 vapor can be reduced by over a hundred times by adding quaternary ammonium bromide complexes [26]. The polybromide species is likewise held in this quaternary ammonium bromide complex, which creates a distinct thick layer in solution that lessens Br_2 transport to the negative electrode [27].

17.3 CHALLENGES ASSOCIATED WITH RECHARGEABLE ZBFB

17.3.1 Hydrogen Evolution

One of the main problems with ZBFBs is the evolution of hydrogen gas. This is because the evolution of hydrogen gas consumes H^+ and raises the electrolyte's pH, which significantly affects the quality of the zinc deposited on the negative electrode [28]. Battery failure and the compound of solid zinc oxide or hydroxide are eventually caused by the elevated pH. pH ranges of 1–3.5 are normally maintained for the ZBFBs to function [29]. Electrolytes that are basic and mildly acidic can reveal deposited zinc that resembles moss. Therefore, to have good zinc plating in the ZBFB, the ideal pH range of the electrolyte must be maintained. Significant zinc corrosion is typically caused by an acidic electrolyte, which speeds up the development of hydrogen gas. As electrons are lost ($H^+ + e^- \rightarrow H_2$) to protons during charging instead of being received by the Zn^{2+} on the negative electrode, more hydrogen gas is anticipated. Zinc can be plated at high current and low pH with coulombic efficiencies of more than 90% since the kinetics of this type of corrosion response are slower than those of zinc deposition. The produced H_2 (g) would ideally recombine with Br_2 in the positive half-cell to produce H^+ according to the equation $H_2 + Br_2 \rightarrow 2HBr$ [30]. However, the significant proton reduction in the electrolyte raises the pH, and solid $Zn(OH)_2$ forms at a specific pH, which could have a high impact on the ZBFBs' flow capillary. However, when charging, the hydrogen evolution side reaction (HER) is also brought on by the water (H_2O) splitting process at the high negative electrode potential (−0.83 V). Additionally, $Zn(OH)_2$ and an increase in the electrolyte's pH are the outcomes of this [31]. The water-splitting process and zinc corrosion both increase the pH of the electrolyte and have an active effect on the zinc

deposition in the ZBFBs, a crucial technical problem that needs to be resolved. Zinc can be plated in aqueous acidic solutions even though the reaction potential for zinc reduction is more negative than that of proton reduction, making it thermodynamically more favorable. This is because zinc has a large hydrogen overvoltage, which causes a kinetically delayed reduction of protons. Chemical and electrochemical reactions can be used to explain the H_2 gas evolution reaction on the negative electrode.

17.3.2 Self-discharge

Br_2 is thermodynamically corrosive to zinc and will induce severe self-discharge in ZBFBs. The ZBFB's self-discharge mechanism is caused by a reaction between zinc metal and aqueous Br_2, with Br_2 being transferred to the negative half-cell across the membrane [32]. Thus, minimizing Br_2's diffusion to Zn is essential in the ZBFB system. By simply placing a well-mixed standard electrolyte solution on one side of a separator and the same solution without Br_2 on the other, the Br_2 transfer rate may be determined using the H-cell test. By measuring the Br_2 content on the opposite side and expressing it in terms of a pseudo-current, the transfer rate can be computed. Naresh et al., in 2021, introduced an effective pore-filling agent into a microporous Daramic membrane to inhibit Br_2 diffusion in ZBFB. The multiwalled carbon nanotube (MWCNT) with polyacrylonitrile (PAN) composite Daramic membrane shows 90% coulombic efficiency compared to the pristine Daramic membrane (68.53%) and PAN composite Daramic membrane (71.20%) at 160 mA cm^{-2}. After 500 cycles at 60 mA cm^{-2}, as shown in Figure 17.2a, the Daramic membrane shows uniform growth of interconnected zinc walls with large voids that promote Br_2 and water transfer, as shown in Figure 17.2b. Figure 17.2c and d shows the field emission scanning electron microscope (FESEM) images of PAN and MWCNT-Daramic membranes. In which the zinc nanowalls are not grown on these membranes and are responsible for prohibiting Br_2 transfer [33].

17.3.3 Dendrite Growth

Dendritic development on the zinc electrode during charging and discharging is another major problem with ZBFBs, similar to other metal-based rechargeable batteries. Uneven current density and a non-uniform electric field in a small area of the zinc surface lead to dendritic development [34]. It is a cycle-long process divided into three stages: initial growth, dissolution, and renewal. In essence, the remaining dendrites from earlier cycles act as sites for the deposition, resulting in denser dendrites. The region experiences an increase in electric field and consumes more Zn^{2+} to create dendrites due to the non-uniform deposition of zinc. Dendrites have the potential to break through the membrane and result in short circuits as they proliferate. Dendrite development can lead to flow channel blockage and reduced battery efficiency. Additionally, internal heating from short circuits carries the risk of battery fires. Dendrite development is influenced by zinc plating thickness, current density, and electrolyte flow rate to the electrode. To reduce the uneven deposition of zinc on the electrode, ZBFBs must have a thorough understanding of the fundamentals of the plating/stripping process at the zinc anode [35].

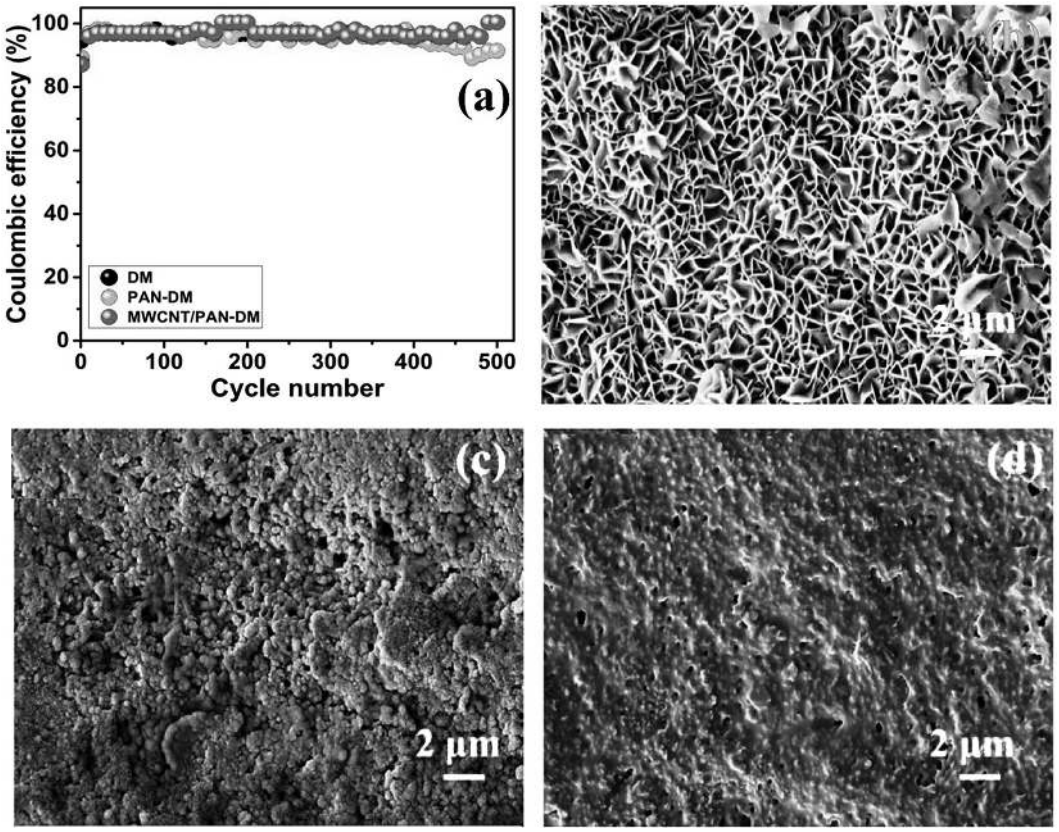

FIGURE 17.2 (a) Coulombic efficiency plot; FESEM images of (b) Daramic membrane; (c) PAN-Daramic membrane; (d) MWCNT/PAN-Daramic membrane after 500 cycles at 60 mA cm^2. (Adapted with permission from [33], Copyright (2021) American Chemical Society.)

17.4 BROMINE CONFINEMENT AND COMPLEXING AGENTS

Bromine is highly corrosive in nature, which deteriorates the other battery components. Over time, self-discharge and performance loss may result from this corrosion. Especially in systems without continuous electrolyte flow, there are not enough fresh electrolytes available to counteract these effects [6,36]. Unwanted reactions may arise when Br_2 species cross over from the cathode to the anode, further degrading the anode and decreasing battery efficiency. Retaining battery performance and preventing this crossover requires effective confinement techniques. The battery's overall efficiency may be impacted by the sluggish redox reactions involving Br_2. This slowdown is even worse in flowless setups, where the reaction kinetics may be further hampered by the absence of a new electrolyte [36]. As Br_2 is volatile, its containment can become highly tough, and there is a possibility of leakage due to higher internal pressures within the battery. Flowing electrolytes add complexity that may reduce efficiency, even if they can aid in reactant and heat management. Although essential, pumps and flow control systems can use more energy and eventually cause component deterioration [37].

Quaternary amines are an essential BCA that is stored safely, forms an oily phase, and remains immiscible with the rest of the aqueous electrolyte. The molar ratio between the complexing agent and the ZBFB active materials is 1:3, in which the complexing agent should contain 1 M [38]. Further, to design a battery, a suitable BCA is required. Fast kinetics is one of the most essential requirements to avoid the escape of Br_2 formed on the surface when the mechanism occurs between the salt and Br_2, which could reduce the self-discharge [39]. Although the diffusion of Br_2 via the separator is not controllable, that causes the primary self-discharge in the system. Thus, adding BCA to both sides of the electrode-electrolyte rectifies these effects. However, the deposition of zinc at the anode would take place because the organic phase formed is immiscible with the aqueous electrolyte and failed to deposit at the bottom of the storage tank [40]. Kim et al. in 2019 stabilized Br_2 during charging using 1-ethyl-1-methyl-pyrrolidinium (MEP. Br) as BCA in the electrolyte. Figure 17.3a and b show the dendrite growth of electrodeposited zinc, in which the electrode exhibits a stronger electric field at the tips; thus, zinc is preferentially deposited around the tips rather than the smooth regions. Figure 17.3c–f shows that the MEP cations repel the zinc ions closing to the surface of the zinc protuberance and induce zinc deposition in the adjacent regions. In this case, the MEP cations are complexed with polybromide (Br_3^-) and generate a slight amount of polybromide complex ($MEPBr_3$). Figure 17.3g and h shows the FESEM images of the performance comparison of zinc dissolution tests.

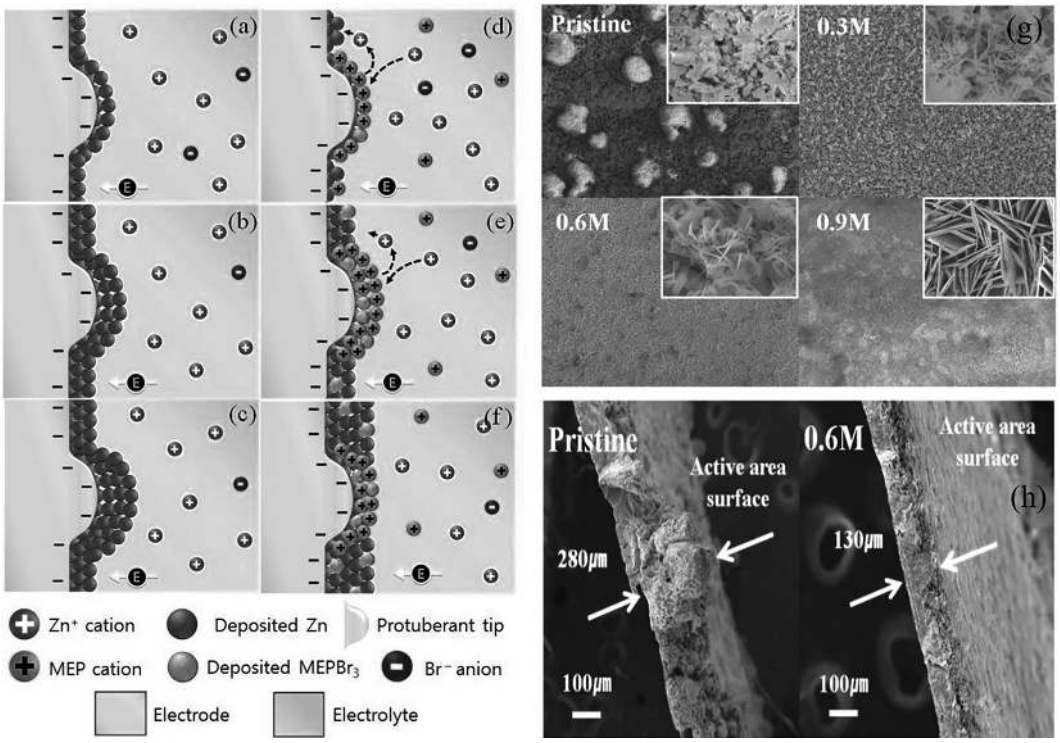

FIGURE 17.3 (a–c) Zinc dendrite deposition process; (d–f) electrostatic shielding process by MEP cations; (g) SEM images of zinc dissolution due to MEP.Br concentration; (h) cross-section of zinc dissolved surface. (Adapted with permission from [40], Copyright (2019) Elsevier.)

In addition, the BCA is an additive for Br_2 stability, and their chemical and structural characteristics affect the overall performance of ZBFBs [40]. In this case, studying the complexing agent is necessary and capable of improving the properties of the currently used [41]. In general, ionic liquids are low-temperature molten salts consisting of a large inorganic or organic anion with a melting point of less than 100°C. It makes them very interested in the use of BCAs in ZBFBs. Also, it is characterized by a wide range of liquids, nonflammability, nonvolatility, and excellent thermal and chemical stability [42,43]. These properties make them alternatives to classical organic solvents and they are used in catalysis, liquid-phase extraction, electrochemistry, and the polymerization process [44]. Further, the ionic liquids have different cation structures; each compound is obtained from the Menshutkin reaction (in a polar medium, the alkylation occurs between the tertiary amines and alkyl halides) [41].

17.5 DEVELOPMENT OF ZBFBs

ZBFBs are becoming more popular as a viable energy storage option because of their high energy density, affordability, and security features. The sophisticated materials used in ZBFBs, such as membranes, electrodes, and electrolytes, have recently drawn more attention. It has not only significantly accelerated the development of these batteries but also encouraged the creation of novel ZBFB systems. ZBFB systems vary so much that the advanced materials used in these batteries also range in structural makeup to hasten the development of the batteries. For example, the ZBFB system's initial electrodes were metal-plated substrate electrodes or carbon-plastic electrodes [45]. However, these types of electrodes also provide several issues for ZBFBs. For example, a battery operating at a relatively low current density is caused by the electrode's poor electrochemical activity toward redox couples, and the problems related to zinc dendrite/accumulation at these electrodes are significantly more noticeable. As a result of technological advancements and ZBFBs' strict requirements for electrodes, a series of highly advanced electrode materials with complex architectures and excellent performance have been created [46]. The advancement of materials is essential to improving their longevity, effectiveness, and performance. The electrodes used have a high impact on how well ZBFBs work. The creation of carbon materials doped with nitrogen is one recent development that has improved battery overall efficiency by demonstrating significant catalytic activity for the Br_2 redox process. Additionally, by enabling better electron transport and zinc deposition, the fabrication of composite electrodes like those composed of carbon nanotubes and expanded graphite has enhanced the electrochemical performance.

It is crucial to carefully select the membrane to minimize the crossover of active materials and enhance ionic conductivity. The objective of the research has been to create highly selective porous membranes that permit efficient ion transport while efficiently capturing Br_2. Additionally, research is being done on membrane material innovations that improve stability and lessen degradation under operating conditions. The performance of ZBFBs is significantly influenced by the electrolyte composition. To increase solubility and decrease viscosity, which can improve the flow properties and battery performance overall, efforts are being undertaken to optimize electrolyte compositions. Research is also being done on the application of additives to improve the cycle stability of the zinc electrode and stabilize the electrolyte. Several challenges remain in the development of ZBFBs. Key issues

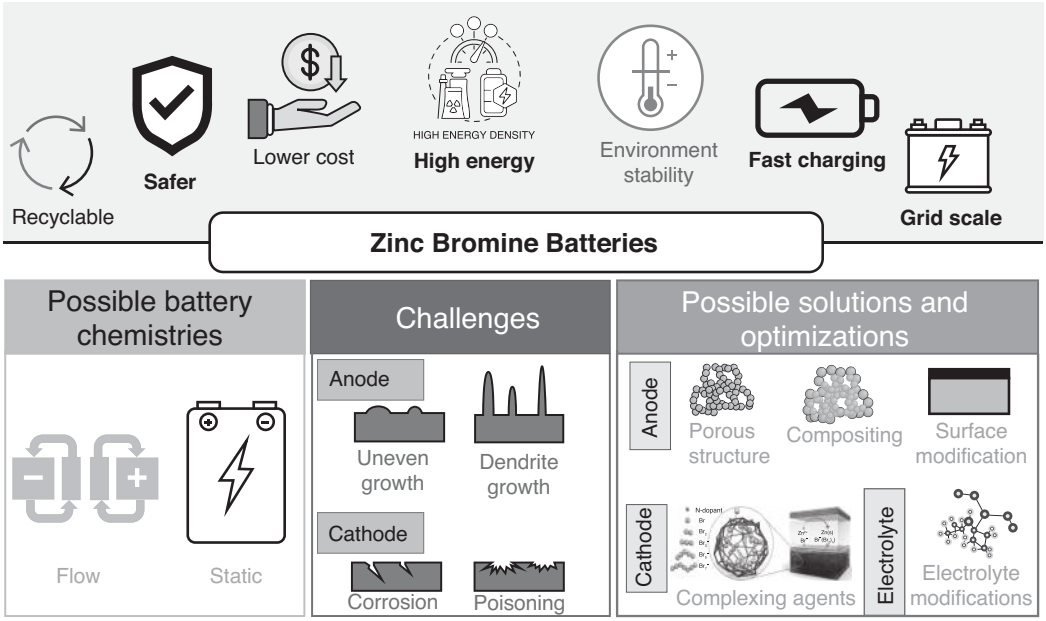

FIGURE 17.4 Illustration of ZBFB key advantages, possible chemistries, and challenges. (Adapted from [36], Copyright (2023) John Wiley & Sons.)

include the Br_2 shuttle effect, which can lead to reduced efficiency, and the need for materials that can withstand the corrosive nature of Br_2. The subject of advanced material research for ZBFB is constantly evolving and shows potential for enhancing energy storage technologies. To overcome current obstacles and realize ZBFB technology's full potential, more research into electrode materials, membranes, and electrolytes is necessary. Figure 17.4 shows the critical advantages of ZBFBs, their challenges, and possible challenges.

17.6 OVERVIEW AND FUTURE PERSPECTIVES

ZBFBs are a promising technology for large-scale energy storage due to their high energy density, low cost, and safety advantages compared to other battery systems. ZBFB offers versatility in their application for grid storage and renewable energy integration, as they can be easily scaled from small to large systems. In comparison to some other flow battery technologies, the use of zinc, which is abundant and reasonably priced, helps to keep the entire cost of the battery system cheaper. However, the overall cost may vary depending on the price of Br_2 and system parts. In general, ZBFB has good chemical stability and safety characteristics. Despite being harmful, Br_2 is controlled within the system to reduce danger. For applications that need frequent cycles of charging and discharging, these batteries exhibit good round-trip efficiency and a long cycle life. Compared to certain other battery technologies, ZBFBs have a relatively low environmental impact, especially due to the controlled use of Br_2 and the potential for zinc recycling. Optimizing the fabrication of cell designs is necessary. To compete with other energy storage technologies, it is essential to develop innovative cell designs that solve the dendritic growth of zinc, the area restriction of the anode, and the low energy density of the battery. In terms of electrolyte additives, it improves the Br_2 complexing capacity and increases efficiency. Also, the additives alter the properties of the electrolyte, such as high and

low temperature tolerance, ionic conductivity, and kinetics. Similarly, conductive anodes play a vital role in zinc deposition during charging. The dendrite deposition affects the coulombic efficiency and cyclic stability of the batteries. Thus, optimizing the uniform zinc deposition by functionalizing the anode surface and designing the anode with sufficient junction and space to store the zinc. Additionally, designing and synthesizing membranes with good chemical and mechanical stability is a prerequisite to resist zinc dendrite and Br_2 corrosion. It possesses excellent resistance to polybromide crossover and high ionic conductivity.

Addressing some safety and environmental concerns, advancements in Br_2 handling and containment could increase the technology's viability for widespread application. ZBFBs, which store energy from sporadic sources like solar and wind, could be extremely important in stabilizing the grid as the globe moves toward renewable energy sources. ZBFBs may become more cost-competitive with other energy storage technologies if materials and manufacturing techniques continue to improve. A wider market's acceptance could result from increased adoption of commercial and industrial applications, which could spur additional research and development. Continued research and development are necessary to overcome existing constraints and investigate novel uses, which may yield discoveries that completely reinterpret the possibilities of ZBFBs. In conclusion, although ZBFBs now have a lot going for them in terms of cost, scalability, and energy density, more progress has to be made in the areas of safety, cost-cutting, and material science before their full potential can be realized. Further, these issues are resolved, and new energy systems will probably determine their place in the energy landscape of the future. ZBFBs appear to have a bright future overall, with the potential for significant breakthroughs that might position them as a major player in the energy storage industry. Their innate benefits, like affordability and scalability, along with continuous advancements, point to their expanding importance in both broad and specialized applications.

REFERENCES

1. M. K. Shobana, Metal oxide coated cathode materials for Li ion batteries–A review. *Journal of Alloys and Compounds* 802 (2019): 477–487.
2. B. Jeevanantham and M. K. Shobana. Enhanced cathode materials for advanced lithium-ion batteries using nickel-rich and lithium/manganese-rich LiNixMnyCozO_2. *Journal of Energy Storage* 54 (2022): 105353.
3. C. Wang, G. Gao, Y. Su, J. Xie, D. He, X. Wang, Y. Wang, and Y. Wang. High-voltage and dendrite-free zinc-iodine flow battery. *Nature Communications* 15, no. 1 (2024): 6234.
4. M. K. Shobana, M. K. Self-supported materials for battery technology-A review. *Journal of Alloys and Compounds* 831 (2020): 154844.
5. Q. P. Jian, M. C. Wu, H. R. Jiang, Y. K. Lin, and T. S. Zhao. A trifunctional electrolyte for high-performance zinc-iodine flow batteries. *Journal of Power Sources* 484 (2021): 229238.
6. M. Rana, N. Alghamdi, X. Peng, Y. Huang, B. Wang, L. Wang, I. R. Gentle, S. Hickey, and B. Luo. Scientific issues of zinc-bromine flow batteries and mitigation strategies. *Exploration* 3, no. 6 (2023): 20220073.
7. P. C. Butler, P. A. Eidler, P. G. Grimes, S. E. Klassen, and R. C. Miles. Zinc/bromine batteries. *Handbook of Batteries* 1 (2001): 37–01.
8. A. A. Akhil, G. Huff, A. B. Currier, B. C. Kaun, D. M. Rastler, S. B. Chen, A. L. Cotter, D. T. Bradshaw, and W. D. Gauntlett. *DOE/EPRI Electricity Storage Handbook in Collaboration with NRECA*. No. SAND2015-1002. Sandia National Lab. (SNL-NM), Albuquerque, NM, 2015.
9. A. R. Abele, E. Elkind, J. Intrator, and B. Washom. *2020 Strategic Analysis of Energy Storage Technology*. CEC, 2011.

10. X. Luo, J. Wang, M. Dooner, and J. Clarke. Overview of current development in electrical energy storage technologies and the application potential in power system operation. *Applied Energy* 137 (2015): 511–536.
11. R. H. Byrne, T. A. Nguyen, D. A. Copp, B. R. Chalamala, and I. Gyuk. Energy management and optimization methods for grid energy storage systems. *IEEE Access* 6 (2017): 13231–13260.
12. M. Beaudin, H. Zareipour, A. Schellenberglabe, and W. Rosehart. Energy storage for mitigating the variability of renewable electricity sources: An updated review. *Energy for Sustainable Development* 14 (2010): 302–314.
13. S. Suresh, T. Kesavan, Y. Munaiah, I. Arulraj, S. Dheenadayalan, and P. Ragupathy. Zinc–bromine hybrid flow battery: effect of zinc utilization and performance characteristics. *RSC Advances* 4 (2014): 37947–37953.
14. A. Khor, P. Leung, M. R. Mohamed, C. Flox, Q. Xu, Liang An, R. G. A. Wills, J. R. Morante, and A. A. Shah. Review of zinc-based hybrid flow batteries: From fundamentals to applications. *Materials Today Energy* 8 (2018): 80–108.
15. USDo Energy. *Energy Storage Grand Challenge: Energy Storage Market Report*. *USDo Energy, Editor*, 2020.
16. Z. Li and Y. C. Lu. Material design of aqueous redox flow batteries: Fundamental challenges and mitigation strategies. *Advanced Materials* 32 (2020): 2002132.
17. S. S. Dosanjh, Sandia National Laboratories, *IEEE Computational Science and Engineering* 2, no. 2 (Summer 1995): 10–15.
18. X. Yuan, J. Mo, J. Huang, J. Liu, C. Liu, X. Zeng, W. Zhou, J. Yue, X. Wu, and Y. Wu. An aqueous hybrid zinc-bromine battery with high voltage and energy density. *ChemElectroChem* 7 (2020): 1531–1536.
19. M. Wang, Y. Zhou, Y. Zhang, S. Hong Hahn, and E. Jung Kim. From Zn (OH) 2 to ZnO: A study on the mechanism of phase transformation. *CrystEngComm* 13 (2011): 6024–6026.
20. H. R. Jiang, M. C. Wu, Y. X. Ren, Wei Shyy, and T. S. Zhao. Towards a uniform distribution of zinc in the negative electrode for zinc bromine flow batteries. *Applied Energy* 213 (2018): 366–374.
21. X. Li, T. Li, P. Xu, C. Xie, Y. Zhang, and X. Li. A complexing agent to enable a wide-temperature range bromine-based flow battery for stationary energy storage. *Advanced Functional Materials* 31 (2021): 2100133.
22. P. Xiong, L. Zhang, Y. Chen, S. Peng, and G. Yu. A chemistry and microstructure perspective on ion-conducting membranes for redox flow batteries. *Angewandte Chemie International Edition* 60 (2021): 24770–24798.
23. G. P. Rajarathnam, M. E. Easton, M. Schneider, A. F. Masters, T. Maschmeyer, and A. M. Vassallo. The influence of ionic liquid additives on zinc half-cell electrochemical performance in zinc/bromine flow batteries. *RSC Advances* 6 (2016): 27788–27797.
24. K. J. Cathro, P. M. Hoobin, and D. C. Constable. *Zinc-Bromide Batteries for Energy Storage Applications*. Department of Resources and Energy, 1987.
25. K. Cedzynska. Properties of modified electrolyte for zinc-bromine cells. *Electrochimica Acta* 40 (1995): 971–976.
26. S. N. Bajpai. Vapor pressures of bromine-quaternary ammonium salt complexes for zinc-bromine battery applications. *Journal of Chemical and Engineering Data* 26 (1981): 2–4.
27. M. Küttinger, J. K. Wlodarczyk, D. Daubner, P. Fischer, and J. Tübke. High energy density electrolytes for H 2/Br 2 redox flow batteries, their polybromide composition and influence on battery cycling limits. *RSC Advances* 11 (2021): 5218–5229.
28. G. P. Rajarathnam and A. M. Vassallo. *The Zinc/Bromine Flow Battery: Materials Challenges and Practical Solutions for Technology Advancement*. Springer, 2016.
29. T. Egami, B. H. Toby, W. Dmowski, J. D. Jorgensen, D. G. Hinks, M. A. Subramanian, J. Gopalakrishnan, A. W. Sleight, and J. B. Parise. Local atomic displacements in high T c oxides studied by pulsed neutron scattering. In *Oxygen Disorder Effects in High-T c Superconductors*. Boston, MA: Springer US, 1990, pp. 47–54.

30. S. Biswas, A. Senju, R. Mohr, T. Hodson, N. Karthikeyan, K. W. Knehr, A. G. Hsieh, X. Yang, B. E. Koel, and D. A. Steingart. Minimal architecture zinc–bromine battery for low cost electrochemical energy storage. *Energy & Environmental Science* 10 (2017): 114–120.
31. M. Kirch, J. M. Lehn, and J. P. Sauvage. Hydrogen generation by visible light irradiation of aqueous solutions of metal complexes. An approach to the photochemical conversion and storage of solar energy. *Helvetica Chimica Acta* 62 (1979): 1345–1384.
32. Y. Shiancherng. An approximate model for estimating the faradaic efficiency loss in zinc/bromine batteries caused by cell self-discharge. *Journal of Power Sources* 50 (1994): 343–360.
33. R. P. Naresh, P. Ragupathy, and M. Ulaganathan. Carbon nanotube scaffolds entrapped in a gel matrix for realizing the improved cycle life of zinc bromine redox flow batteries. *ACS Applied Materials & Interfaces* 13 (2021): 48110–48118.
34. M. Wang, Y. Meng, K. Li, T. Ahmad, N. Chen, Y. Xu, J. Sun, M. Chuai, X. Zheng, Y. Yuan, and C. Shen. Toward dendrite-free and anti-corrosion Zn anodes by regulating a bismuth-based energizer. *Escience* 2 (2022): 509–517.
35. Y. Huyan, J. G. Wang, S. Tian, L. Ren, Huanyan Liu, and B. Wei. Assembling metal-polyphenol coordination interfaces for longstanding zinc metal anodes. *EcoMat* 4 (2022): e12173.
36. A. Mahmood, Z. Zheng, and Yuan Chen. Zinc–bromine batteries: Challenges, prospective solutions, and future. *Advanced Science* 11 (2024): 2305561.
37. N. S. Alghamdi, M. Rana, X. Peng, Y. Huang, J. Lee, J. Hou, I. R. Gentle, L. Wang, and B. Luo. Zinc–bromine rechargeable batteries: From device configuration, electrochemistry, material to performance evaluation. *Nano-Micro Letters* 15 (2023): 209.
38. U. Jiménez-Blasco, E. Moreno, M. Cólera, P. Díaz-Carrasco, J. C. Arrebola, A. Caballero, J. Morales, and Ó. A. Vargas. Enhanced performance of Zn/Br flow battery using N-methyl-N-propylmorpholinium bromide as complexing agent. *International Journal of Molecular Sciences* 22 (2021): 9288.
39. L. Tang, P. Leung, Q. Xu, M. R. Mohamed, S. Dai, X. Zhu, C. Flox, and A. A. Shah. Future perspective on redox flow batteries: Aqueous versus nonaqueous electrolytes. *Current Opinion in Chemical Engineering* 37 (2022): 100833.
40. M. Kim, D. Yun, and J. Jeon. Effect of a bromine complex agent on electrochemical performances of zinc electrodeposition and electrodissolution in Zinc–Bromide flow battery. *Journal of Power Sources* 438 (2019): 227020.
41. U. Jiménez-Blasco, J. C. Arrebola, and A. Caballero. Recent advances in bromine complexing agents for zinc–bromine redox flow batteries. *Materials* 16 (2023): 7482.
42. B. Ghalami-Choobar and T. N. Fallahkar. Thermophysical properties of 1-ethyl-3-methylimidazolium bromide ionic liquid in water+ ethylene carbonate mixtures at T=(298.2, 308.2 and 318.2) K. *Fluid Phase Equilibria* 496 (2019): 42–60.
43. N. I. Malek and S. P. Ijardar. Binary mixtures of ([C4mim][NTf2]+ molecular organic solvents): Thermophysical, acoustic and transport properties at various compositions and temperatures. *The Journal of Chemical Thermodynamics* 93 (2016): 75–85.
44. G. Kaur, H. Kumar, and M. Singla. Diverse applications of ionic liquids: A comprehensive review. *Journal of Molecular Liquids* 351 (2022): 118556.
45. J. McBreen. Rechargeable zinc batteries. *Journal of Electroanalytical Chemistry and Interfacial Electrochemistry* 168 (1984): 415–432.
46. C. Wang, Q. Lai, P. Xu, D. Zheng, X. Li, and H. Zhang. Cage-like porous carbon with super-high activity and Br2-complex-entrapping capability for bromine-based flow batteries. *Advanced Materials* 29 (2017): 1605815.

CHAPTER 18

Organic Solar Flow Batteries

Prospect, Feasibility, and Challenge

Jiarui Wang, Yanmei Xu, Yinghui Han, and Xiaotao Hao

18.1 INTRODUCTION

At present, the global energy crisis and environmental pollution problems are mainly due to the excessive dependence on fossil energy. Fossil fuels such as coal, oil, and natural gas, as the main energy sources in the past few centuries, have driven the industrial revolution and the rapid development of the global economy. However, their widespread use has also led to serious carbon dioxide emissions and environmental pollution problems, which have become one of the important causes of global climate change. In addition, fossil energy resources are limited to meet the growing energy demand for a long time, making it urgent to seek cleaner and more sustainable energy sources. In this context, clean energy has become the core direction of future energy development. Renewable energy, including wind energy, solar energy, geothermal energy, and hydropower, has gradually replaced fossil energy as an important part of the energy structure. Solar energy, in particular, has become a star in the field of renewable energy with its inexhaustible resource advantages and wide global applicability [1]. Solar cell has developed rapidly in recent years, but it also faces challenges of intermittency and instability, as shown in Figure 18.1. Therefore, in order to realize the efficient use of renewable energy, it is crucial to develop efficient energy storage technology [2–6]. The progress of electrochemical energy storage technology has provided strong support for the wide application of clean energy, among which liquid flow batteries have become the main force in the field of energy storage. Compared with other energy storage technologies, flow batteries are especially suitable for large-scale energy storage and can effectively respond to power supply fluctuations in renewable energy systems. Flow batteries store energy in liquid electrolyte through REDOX reaction, which has a long life, high efficiency, and flexible scale-adjustable characteristics. Solar flow batteries (SFBs) are an innovative technology that combines solar photovoltaic conversion with flow battery storage, enabling the direct conversion of solar energy into electricity

DOI: 10.1201/9781003506379-18

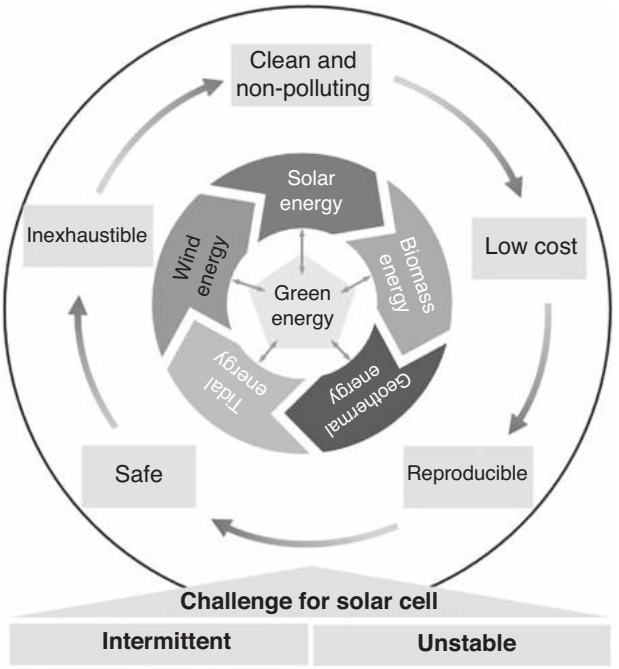

FIGURE 18.1 Characteristics and challenges of solar cells.

while simultaneously storing it [7–13]. This integrated design not only ensures the efficient utilization of clean energy but also addresses the critical issue of the instability of renewable energy, promoting large-scale storage and application of clean energy in the future. Organic solar flow batteries (OSFBs) refer to systems where the photovoltaic conversion component is realized through organic photovoltaic (OPV) cells, which are then integrated with organic redox flow batteries. OPV cells exhibit exceptional performance in flexibility, adaptability, and environmental friendliness. When combined with organic flow batteries, they offer even broader potential, making them suitable for a wide range of applications.

18.2 PROSPECTS OF ORGANIC SOLAR FLOW BATTERIES

Photovoltaic solar flow batteries consist of photovoltaic solar cells, positive and negative redox components, current conductors, membranes, and the structure of SFB in Figure 18.2. At the core of the battery's storage system are two liquid electrolyte tanks, which store electrolytes at the positive and negative electrodes. When solar panels generate electricity, it drives chemical reactions in the electrolytes, converting electrical energy into chemical energy for storage. When electricity is needed, these chemical reactions reverse, releasing the stored chemical energy and converting it back into electrical energy. About existing SFBs, the devices used to convert solar energy into electricity can be categorized into two types: semiconductor-liquid junction cells [14,15] and photovoltaic cells [16]. Semiconductor-liquid junction cells achieve photoelectric conversion through the

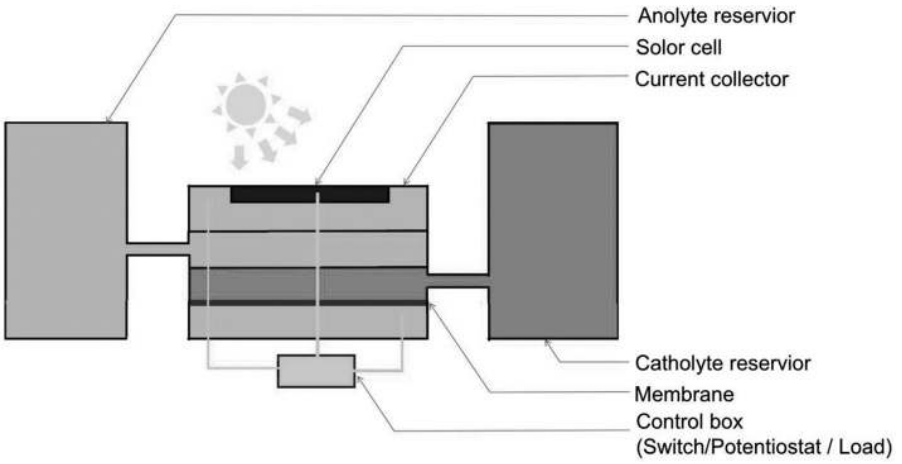

FIGURE 18.2 Basic structure diagram of solar flow batteries.

interface formed between semiconductor materials and electrolyte solutions. The key to semiconductor-liquid junction cells lies in the energy level alignment between the semiconductor and the redox materials, as this alignment directly determines the photovoltage generated by the battery [17]. A larger energy level difference results in higher photovoltage, thereby improving conversion efficiency. Thus, it is critical to find suitable semiconductor materials and redox materials.

In contrast, photovoltaic cells generate photovoltage through an internal PN junction rather than through reactions with external redox species. In other words, they do not require precise energy level matching like semiconductor-liquid junction cells. This characteristic simplifies the overall design of photovoltaic cells, reducing the need to account for external environmental influences on voltage matching. In photovoltaic solar flow battery systems, photovoltaic cells play the role of converting solar energy into electricity, while the flow battery component is responsible for energy storage and release. The combination of these two components enables efficient utilization of solar energy and ensures a stable energy supply.

Solar flow battery has a series of advantages: (1) *High safety*: the electrolyte is liquid, so there is no risk of explosion or combustion; (2) *Long life*: the charge and discharge process of the battery has little impact on the chemical properties of the electrolyte; (3) *Strong scalability*: the energy storage capacity of the battery can be easily expanded by increasing the amount of electrolyte; (4) *Low cost*: especially for large-scale energy storage applications. However, SFBs have some limitations, such as a relatively low energy density, which means they require plenty of space to store the same amount of electricity. Moreover, their efficiencies are limited by the electrolyte flow and the reaction rate. Therefore, it is necessary to further optimize the various parts of the solar flow battery to promote its large-scale application in the field of solar power stations and grid-connected energy storage. Usually, the efficiency of SFBs can be optimized by the following aspects: (1) *Improvement of the electrolyte*: the use of higher concentration and higher conductivity electrolyte can improve the electrochemical performance of the battery; (2) *Electrode materials*: develop and use

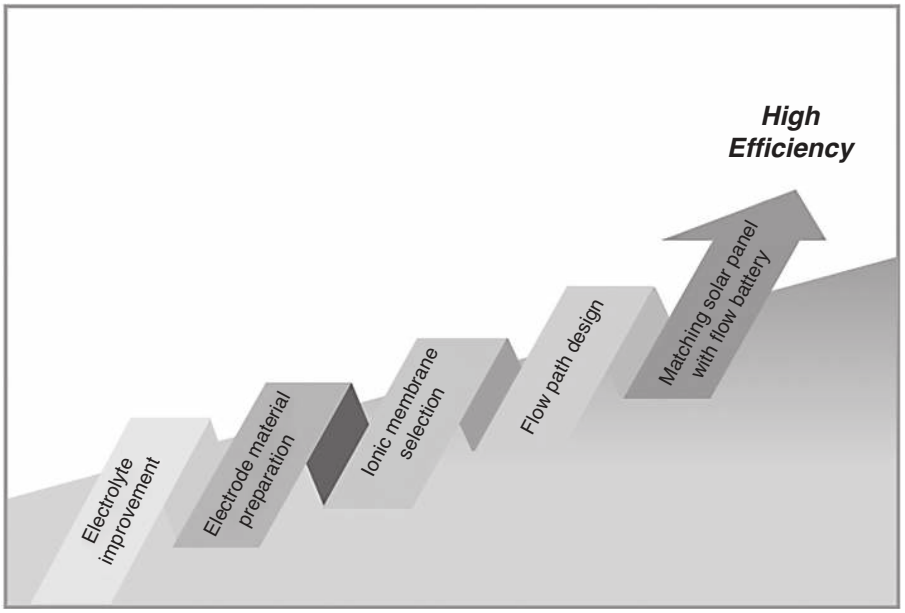

FIGURE 18.3 Optimization approach of solar flow battery.

electrode materials with high catalytic activity and stability to reduce the overpotential and increase the reaction rate; (3) *Membrane material*: select the membrane material with high ionic selectivity and low resistance to reduce the electrolyte cross-contamination and improve the charge and discharge efficiency of the battery; (4) *Battery design*: to optimize the flow channel design of the battery, ensure the uniform flow of the electrolyte, reduce the internal resistance, and increase the reaction area; (5) *System integration*: by optimizing the matching of solar cells and flow cells, improve the energy conversion efficiency of the overall system. Through the comprehensive optimization of these aspects, the final efficiencies of SFBs can be effectively improved. The optimization approach is summarized in Figure 18.3.

It is evident that optimizing the compatibility between solar cells and flow batteries can enhance overall performance by integrating suitable solar cells without altering the flow battery. In 2018, Jin et al. proposed a highly efficient single-chip integrated SFB device that combined III–V tandem solar cells with a low-cost organic redox pair, 4-hydroxy-2,2,6,6-tetramethylpiperidinyloxy (4-OH-TEMPO) and methyl viologen (MV), as the flow battery component. This system achieved a record-breaking solar-to-output efficiency (SOEE) of 14.1%. This research demonstrated that the rational matching of solar cells with flow batteries is critical for achieving high-efficiency SFBs [18]. In 2020, the same research group utilized a $(FAPbI3)_{0.83}(MAPbBr3)_{0.17}$ (MA, methylammonium; FA, formamidinium) perovskite/silicon tandem solar cell as the photovoltaic layer, coupled with a redox flow battery using bis-(trimethylammonium)-propyl viologen (BTMAP-Vi) and 4-trimethylammonium-TEMPO (NMe-TEMPO) as the redox pair, achieving an impressive SOEE of 20.1% [19]. These studies highlight the critical role of photovoltaic cells in single-chip integrated SFBs. Among them, third-generation thin-film solar cells provide

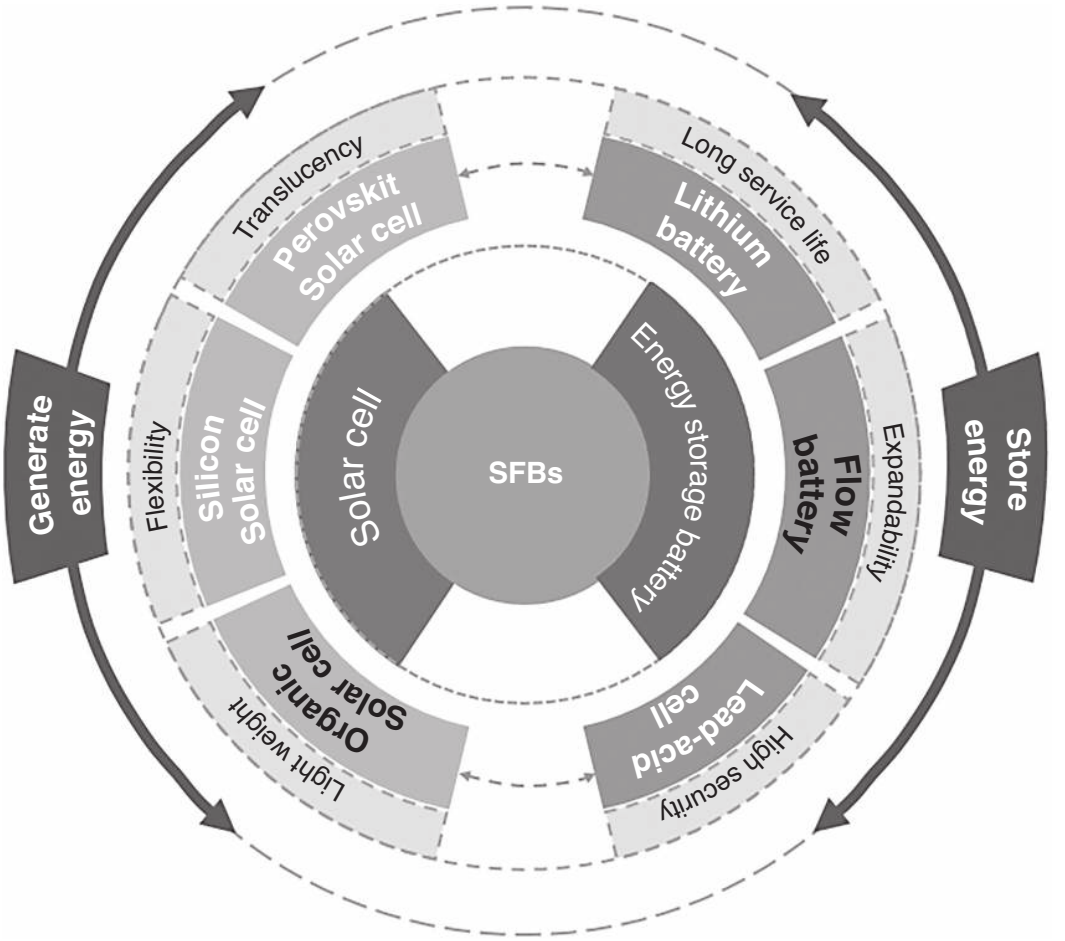

FIGURE 18.4 Combination of the power generation unit and the energy storage unit of SFBs.

vital support for efficient and long-lasting clean energy solutions. As a representative of third-generation solar technologies, organic solar cells exhibit unique advantages and vast application potential. Compared with traditional inorganic solar cells, organic solar cells stand out with their lightweight, flexible structure, low manufacturing cost, high tunability of materials, and environmental friendliness.

These characteristics make organic solar cells ideal for various innovative applications and offer new possibilities for future solar energy conversion and storage technologies. To better understand the tremendous potential of organic solar cells, the following sections will elaborate on their specific advantages in aspects such as lightweight and flexible design, low-cost manufacturing processes, tunable bandgaps, and environmental sustainability. The schematic diagrams of the energy generation part and the energy storage part are shown in Figure 18.4. These benefits not only drive innovation in solar technology but also inspire new strategies for their integration with energy storage systems like flow batteries.

18.3 INSPIRATION FOR OSFBs FROM THE ADVANCE OF OSCs

The progress of OSFBs is due to the development of organic solar cells. Although there is still a long way to go from cell to batteries, and the research is still in the embryonic stage, compared with traditional inorganic solar cells, OSFBs have excellent performance in lightweight, flexible, low manufacturing costs, strong material adjustability, and environmental friendliness. These characteristics make it stand out in many innovative application scenarios and offer new possibilities for future solar conversion and energy storage technologies. The following sections introduce the lightweightness and flexibility design of solar cells, low-cost manufacturing processes, bandgap adjustability, and environmental friendliness, aiming to inspire advancements in organic solar flow battery technology.

18.3.1 Improvement of Mechanical Properties of OSFBs Inspired by Flexible OSCs

Flexible organic solar cells (F-OSCs) have become a hot research field due to their high-power conversion efficiency (PCE), light weight, wearability, portability, compatibility with solution manufacturing, and applications in self-powered e-skin and various medical applications [20–26]. The flexible organic solar cell is composed of an active layer sandwiched between the flexible transparent bottom electrode and the top metal electrode (Figure 18.5).

The portability of flexible organic solar cells makes them more promising for outdoor products. However, extreme weather conditions are often encountered during outdoor operations, leading to insufficient solar power supply and causing solar devices to fail. Therefore, combining organic solar cells with energy storage devices can address this critical issue. Flow batteries, which offer a long lifespan, deep discharge capacity, high safety, low maintenance cost, and environmental friendliness, are our preferred choice for preparing organic energy storage solar cells. The combination of flexible solar cells and flow storage batteries has great potential for future outdoor applications. The portability of flexible organic solar cells is feasible. Although flow battery technology has a range of advantages and has been widely applied in the energy storage field, its large size and weight prevent it from achieving ideal lightness and portability. Currently, some research is focused on micro-flow batteries. Micro-flow batteries can be as small as the size of a hand, ranging from a few cubic centimeters to tens of cubic centimeters, and are typically used in portable or embedded device fields. Although the capacity of micro-flow batteries

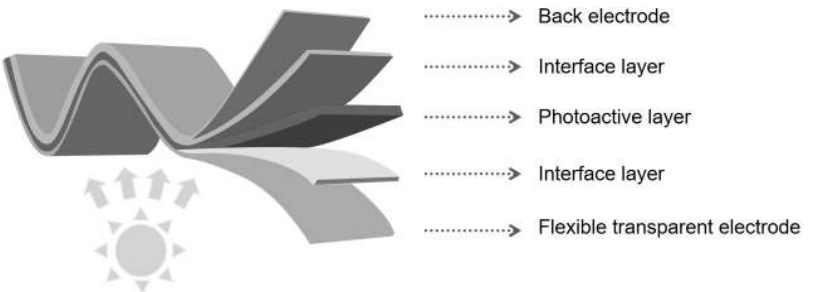

FIGURE 18.5 Structure schematic diagram of flexible organic solar cells.

is generally less than a few watt-hours, they are sufficient for emergency use in outdoor portable devices. Researchers at Georgia Tech have developed a miniaturized flow battery using sub-millimeter micro-tube membranes, reducing the battery size by 75% [27]. This design increases the volume power density, making it a strong candidate for residential energy storage or small-scale applications. At present, flow batteries urgently need to address issues such as optimizing flexible electrodes and designing active layer materials for flexible organic solar cells, in addition to achieving miniaturization and portability. Traditional transparent conductive electrodes commonly use metal oxides such as indium tin oxide (ITO) and fluorine-doped tin oxide. These materials are widely used in rigid optoelectronic devices, especially ITO electrodes, which are favored for their high transmittance (80%–90%) and low sheet resistance on glass substrates. However, when ITO electrodes are deposited on plastic substrates, their conductivity decreases significantly, and their conductivity deteriorates under mechanical stress, limiting their application in flexible optoelectronic devices. ITO alternatives as flexible transparent electrodes (FTEs) have received significant attention, requiring high optical transparency, excellent electrical performance, appropriate work function (WFs), excellent mechanical strength, and good wettability. FTEs play a key role in determining the performance of flexible photovoltaic cells (such as efficiency, flexibility, and stability) [28–34]. Currently, many potential FTE materials, such as metal nanowires (NWs), metal grids, graphene, poly(3,4-ethylenedioxythiophene)/poly(styrenesulfonate) (PEDOT), and MXene, have been extensively studied. Although these new materials have shown some promising preliminary results, each material still has different degrees of limitations, such as insufficient flexibility, weak adhesion, moderate conductivity, less than ideal transparency, high surface roughness, poor wettability, and stability issues. These problems hinder the development of flexible OSCs without ITO. In addition to optimizing flexible electrodes, many active layer material design strategies have been applied to regulate the PCE and mechanical stability of F-OSCs. Hydrogen bonding is a weak intermolecular interaction, but it can form a reversible crosslinked structure in materials, improving the film's ductility and durability. For example, introducing molecules that can form hydrogen bonds in the active layer helps rearrange molecules during strain or stretching, relieving accumulated mechanical stress, thus increasing the elongation at break and crack strain (COS) of the film. In view of the addition of flexible fragments, long-chain alkyl or ether groups can reduce the rigidity of materials, thus increasing flexibility. These fragments can be embedded into the main chain or side chains of NF-SMA or donor polymers, forming flexible molecular chains that buffer stretching forces when stress is applied. This flexible design improves the device's bending and cracking resistance [35,36]. About the application of single-component materials, the design of single components integrates donor and acceptor units into the same molecule, reducing the number of phase separations and microscopic interfaces, which can enhance the material's stability and reduce the likelihood of mechanical failure. The concept of single-component materials helps control the microscopic morphology of the active layer, preventing strain concentration, and improving mechanical ductility and overall performance. About the application of polymer acceptors, due to their inherent chain structure, polymer acceptors possess excellent mechanical flexibility. Compared to rigid small

molecule acceptors, polymer acceptors can absorb and disperse stress through segmental motion during application, significantly improving COS and tensile strength. In addition, polymer acceptors are better compatible with polymer donors, forming more uniform phase separation structures, which helps improve the photovoltaic conversion efficiency. The efficiency of the entire polymer solar cell reached 19.50% [37]. About the insertion of flexible or conductive interface layers, buffering stress and preventing interface delamination during bending or stretching. For example, inserting interface layers with flexible long chains can provide some buffering effect in stress concentration areas, preventing the formation and propagation of cracks, thus improving the mechanical ductility of the film [38]. About the use of self-healing materials, by introducing self-healing materials into the active layer or interface layer, the device can self-repair when slightly damaged. For example, materials containing dynamic covalent bonds (such as disulfide bonds) can re-bond when exposed to external stimuli such as heat or light, repairing the damaged area and extending the device's lifetime. The development of miniaturized flow batteries and flexible organic solar cells, combined, offers a range of advantages. High customization: Miniaturized flow batteries can be designed in different sizes and capacities according to needs. Combined with the flexibility of organic flexible solar cells, they can meet the specific needs of different application scenarios; Good environmental adaptability: Organic flexible solar cells have strong environmental adaptability, able to withstand multiple bending and folding, while flow batteries can operate stably across a wide temperature range, ensuring good performance under different environmental conditions; Easy maintenance: Flow batteries are relatively simple to maintain, as replacing the electrolyte restores capacity, and organic flexible solar cells are easy to install and replace due to their lightweight and flexible characteristics; Low-cost benefit: With technological advancements, the cost of organic flexible solar cells and flow batteries is gradually decreasing, making their combination more cost-effective in commercial and residential fields. Therefore, the integration of both can provide an efficient, stable, safe, and environmentally friendly energy solution.

18.3.2 Exploring the Synergy between OSCs and Flow Batteries through Bandgap Engineering

In SFBs, the voltage of the solar cell must exceed the potential difference of the redox pair to drive the electrochemical reaction. Matching the open-circuit voltage with the redox potential can maximize charging efficiency, while excessively high voltage can lead to significant energy losses and side reactions such as electrolyte decomposition. Therefore, it is crucial to find an organic solar cell with a suitable open-circuit voltage and relatively high-PCE. Compared to silicon-based solar cells, the bandgap of organic solar cells is easier to adjust. By introducing different conjugation lengths, modifying the substituent groups of molecules, or utilizing intermolecular interactions, it is possible to fine-tune the bandgap of organic semiconductor materials. Through rational design of suitable materials, parameters matching the flow battery (open-circuit voltage and solar cell efficiency) can be achieved. The following discussion takes the acceptor materials in organic solar cells as an example to explore the impact of molecular design on these parameters.

The development of organic solar cells (OSCs) has been largely due to the revolution of non-fullerene acceptors, especially the fusion ring electron acceptors (FREAs) of acceptor-donor-acceptors (A-D-A) structures. This technique was first proposed in 2015 by Zhang et al. [39]. Subsequently, in early 2019, Zou et al. introduced a generation of novel FREAs of A-DA′D-A structures (e.g., Y6 in Figure 18.6) containing electron defect units in the fusion ring core. These unique structural features make the FREAs generally have excellent absorption properties and tight intermolecular π-π stacking. Through continuous molecular optimization and device engineering advances, the state-of-the-art single-junction OSCs have a PCE of over 20%.

Despite the excellent performance of FREAs, their highly fused conjugate backbones make the synthesis methods complex and costly, limiting the possibility of large-scale applications. To address this issue, the researchers propose a low-cost non-fused ring electron acceptor (NFREAs) as an alternative. The design concept is to simplify the structure of the central core to make the synthesis process more efficient. Their structures are usually not fused (or simply fused, or even completely unfused), thus providing significant

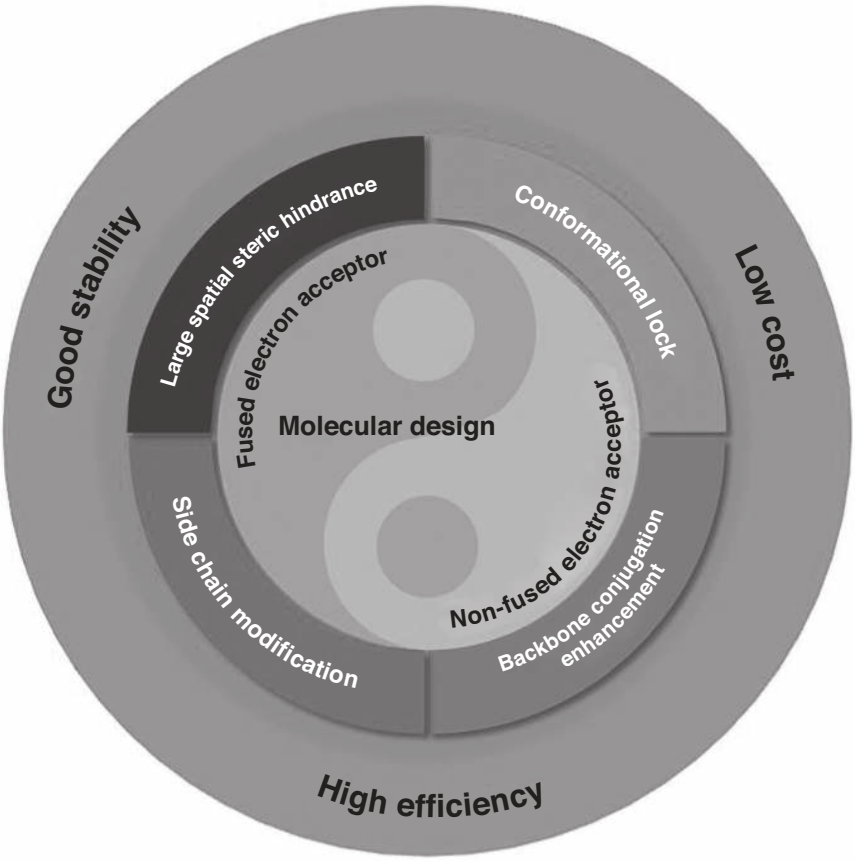

FIGURE 18.6 Diagram of the optimization strategy of the non-fused ring.

advantages in synthesis and molecular regulation. Despite the advantages of NFREA's structure and cost, their single-bond connecting units are rotatable, which may lead to more conformational isomers that affect charge transport and molecular reorganization energy. Therefore, researchers usually introduce a non-covalent conformational lock (NoCL) strategy [40] and a large steric hindrance strategy in non-thick ring acceptors to optimize the planarity of non-thick ring acceptors. Among them, the NoCL strategy introduces intramolecular non-covalent interactions such as F···H, N···S, and S···O to lock the conformation of NFREAs and form a rigid and coplanar structure, thus improving the electron mobility and promoting the charge transfer. The introduction of NoCLs can effectively improve the performance of NFREAs, making it close to FREAs in PCE, while significantly reducing the synthesis complexity. The large steric aromatic group construction of the new NFREAs structure strategy also greatly reduces the distortion of the molecule [41,42]. The summary of the non-fused ring optimization strategy is shown in Figure 18.6.

Non-fused ring acceptor materials are usually further optimized by increasing the conjugate length. Compared with IDT-IC (Figure 18.7a), the effective conjugation length of SMA ITIC (Figure 18.7b) by replacing thiophene in IDT as a unit D with thiophene [3, 2-b] thiophene (TT) and using 3-(1,1-cyanomethyl)-1-indanone (INCN) as unit is extended by improving the planarity of the molecule, significantly red-shifting the absorption spectrum, and extending the λ onset to about 800 nm [43]; heteroatoms are introduced into the fused ring: the Se atoms have a larger atomic radius and a more polarized d orbit compared with the S atoms. The π electrons in the Se-substituted heterocycle tend to adopt more quinone features and exhibit enhanced planarity, resulting in a decrease in the optical energy gap and a red shift of the absorption spectrum. For instance, Lin and Yan et al. introduced benzoselenadiazole into ADA'DA-type SMA, and Y6-Se (Figure 18.7d) was synthesized [38,44]. Y6-Se-based OSC shows higher short-circuit current density (Jsc) compared with Y6-based OSC under the same conditions (Figure 18.7c). Using different

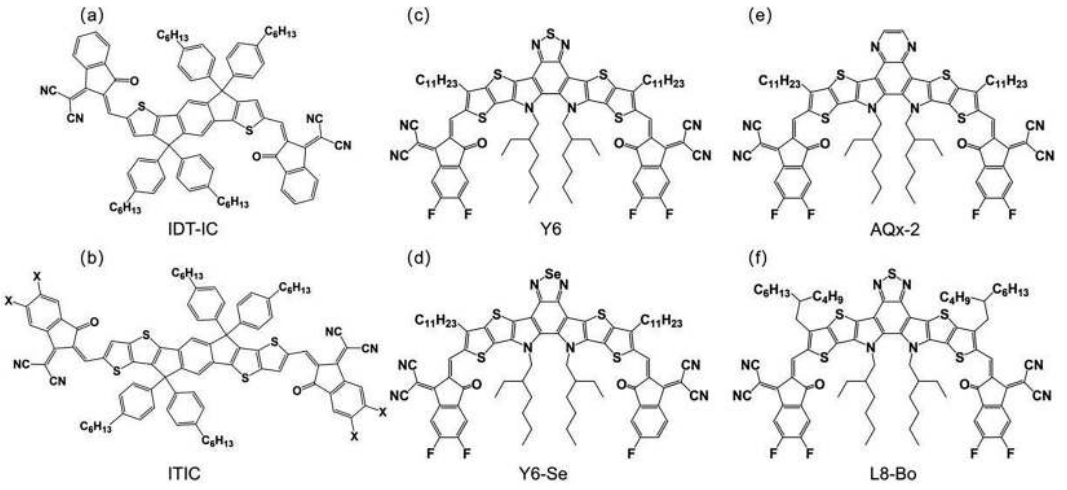

FIGURE 18.7 The chemical construction of (a) IDT-IC, (b) ITIC, (c) Y6, (d) Y6-Se, (e) AQx-2, and (f) L8-BO.

A-terminal groups, Qx units can provide quinone resonance and can also be used as an A' unit for the synthesis of ADA'DA-type SMA. The resultant AQx-2 (Figure 18.7e) shows a slightly larger Eg opt of 1.35 eV, slightly larger than the 1.33 eV of Y6, and has balanced electron and hole mobility [45]. The PM6-based OSC produced a photoelectric conversion efficiency of 16.64%; Side chain engineering: side chain engineering can optimize the performance by modifying the head, shoulder, and tail of the molecule. For example, the L8-BO (Figure 18.7f) developed by the Sun group modified the shoulder alkyl chain of the Y6 skeleton, changed the molecular filling behavior of non-fullerene acceptors, and improved the structural order and charge transport of the film, with an efficiency of 18% [46]. The ability of blue-shifted light absorption, reduced band gap, and upshifted LUMO levels is shown.

18.3.3 Green and Sustainable of OSFBs

Flow batteries are well-known for their scalability and long cycle life. The flow battery also has a striking green environmental protection. Usage of liquid electrolytes: these electrolytes are usually composed of aqueous solutions and soluble salts, compared to traditional batteries used heavy metals and harmful chemicals, flow battery materials are more environmentally friendly; Renewable and recyclable: the electrolyte in the flow battery can be recycled and recycled, reducing environmental pollution. At the end of the battery's life, electrolytes and electrode materials can be recycled, reducing waste generation; Non-toxic materials: the electrolyte and electrode materials of the flow battery are usually non-toxic or low-toxic substances, reducing the potential harm to the environment and human health; Long life and high stability: the flow battery has a long service life and high stability, reducing the environmental burden caused by frequent battery replacement. Therefore, flow batteries are particularly suitable for use in combination with renewable energy systems such as solar energy and wind energy, helping to improve the energy storage efficiency and stability of these systems, and promoting the wide application of renewable energy.

At present, green organic solar cells are also being widely studied. OSCs are a kind of solar cell that uses organic conjugated materials as a photoactive layer. Its photoactive layer is usually composed of two conjugated materials, an electron donor and an electron acceptor. These materials are usually dissolved in organic solvents, such as chloroform (CF), chlorobenzene (CB), and o-dichlorobenzene (o-DCB). During processing, these donor and acceptor materials are mixed in solution and deposited onto the substrate by spin coating technology (for small area equipment) or printing technology (for large area equipment) to form a photoactive layer. Optimizing the photoactive layer, especially the microphase separation between donor and acceptor materials, is key to achieving high photovoltaic performance. However, conventional organic solvents such as chloroform, chlorobenzene, and o-dichlorophenes contain halogens and aromatic compounds that pose significant threats to human health and the environment. Therefore, the use of these solvents has been limited industrially. To address this issue, it is crucial to develop and use non-halogen and non-aromatic solvents to achieve green processing. This shift will not

only help to reduce the environmental impact but will also help to improve the sustainability of organic solar cells.

In terms of specific applications, THF is used as a traditional non-halogen and non-aromatic solvent. A ternary OSC system based on PM1 acting as a donor polymer and L8-BO acting as an acceptor was reported by Min et al. [47]. The introduction of BTP-3Cl improves the absorption spectrum, extends the exciton lifetime, and enhances the charge transport. The ternary mixture was dissolved in THF and coated to form a film, and the final OSCs reached a high PCE of 18.8%, which is comparable to the device manufactured using chloroform (CF). Furthermore, the OSC of 1 cm^2 demonstrated 17.8% PCE, while the PM1-based two-component solar cells significantly reduced PCE to 15.5%. These results suggest that the introduction of the third component helps to alleviate the PCE gap between small and large areas of OSC. Woo et al. designed two conjugated polymers used as electron donors, in which the benzothiophene (BDT) segment with a fluorothiolene side group was synthesized [27,48,49]. The position of the fluorine atom on the thiophene unit has significant effects on the microstructure and photovoltaic properties of OSCs. After optimizing the polymer structure and making the photoactive layer using THF, the PCE reached 13.86%, which is comparable to the PCE manufactured by CF. These advances suggest that the development of conjugated materials compatible with environmentally friendly solvents and addressing phase separation issues are critical for achieving more sustainable OSCs, promising to significantly improve OSC performance and reduce environmental impact.

The greening of OSFBs not only contributes to environmental protection but also promotes the transformation of the energy structure, which is of great significance for achieving the Sustainable Development Goals. Actively promote the green of organic solar cells and flow cells, and realize green and portable organic solar flow cells will be around the corner.

18.4 CONCLUSION

This chapter explores the unique advantages of OSFBs, and their potential. By detailing the feasibility and future prospects of the fusion of organic solar cells and flow batteries to form OSFBs, it will greatly promote the development of clean energy technology and energy storage. As a representative of the third generation of solar technology, organic solar cells not only have low manufacturing costs with their lightweight and flexible design but also can optimize the photovoltaic performance by adjusting the material band gap. These advantages give organic solar cells wide applicability in a wide range of application scenarios, including providing sustainable energy solutions under high-demand environmental conditions. Moreover, the environmentally friendly nature of organic solar cells makes them an important part of future clean energy technologies.

In addition, flow batteries have shown great potential to cope with the intermittent supply of renewable energy with their superior energy storage capacity and high efficiency. By storing energy in liquid electrolyte, flow batteries can provide long-term stable power support, and their adjustable scale makes them suitable for large-scale energy storage requirements. The combination of solar photovoltaic conversion and flow battery energy

storage technology not only improves energy efficiency but also reduces the dependence on external power electronic equipment, which provides a feasible technical path for future large-scale clean energy storage and application. There is reason to believe that the combination of organic solar cells and flow cells will bring breakthroughs in the future of clean energy technologies. Such integrated solutions can not only contribute to tackling the global energy crisis but can also play an important role in achieving the Sustainable Development Goals.

Overall, OSFBs, as the combination of organic solar cells with flow batteries provide new perspectives and solutions for driving innovation in clean energy technologies. Future research should continue to explore how to optimize the combination of these two technologies to achieve a more efficient, economical, and environmentally friendly energy system and contribute to the global energy transition.

ACKNOWLEDGMENTS

This work was supported by the National Natural Science of China (Grant No. 52320105003) and the Fundamental Research Funds for the Central Universities (No. E3ET1803).

REFERENCES

1. Lewis, N. S. (2016). Research opportunities to advance solar energy utilization. *Science. 351*, aad1920.
2. Hou, Y., Vidu, R., and Stroeve, P. (2011). Solar energy storage methods. *Ind. Eng. Chem. Res. 50*, 8954–8964.
3. Crabtree, G. W., and Lewis, N. S. (2007). Solar energy conversion. *Phys. Today. 60*, 37–42.
4. Kamat, P. V. (2007). Meeting the clean energy demand: Nanostructure architectures for solar energy conversion. *J. Phys. Chem. C. 111*, 2834–2860.
5. Lewis, N. S. (2007). Toward cost-effective solar energy use. *Science. 315*, 798–801.
6. Fritz, S. (1960). Some solar radiation data presentations for use in applied solar energy programs by an international group of authors - Introduction. *Sol. Energy. 4*, 1–1.
7. Yu, M., McCulloch, W. D., Beauchamp, D. R., Huang, Z., Ren, X., and Wu, Y. (2015). Aqueous lithium–iodine solar flow battery for the simultaneous conversion and storage of solar energy. *J. Am. Chem. Soc. 137*, 8332–8335.
8. Liao, S., Zong, X., Seger, B., Pedersen, T., Yao, T., Ding, C., and Li, C. (2016). Integrating a dual-silicon photoelectrochemical cell into a redox flow battery for unassisted photocharging. *Nat. Commun. 7*, 11474.
9. Li, W., Fu, H. C., Li, L., Cabán-Acevedo, M., He, J. H., and Jin, S. (2016). Integrated photoelectrochemical solar energy conversion and organic redox flow battery devices. *Angew. Chem. 128*, 13298–13302.
10. Wedege, K., Azevedo, J., Khataee, A., Bentien, A., and Mendes. (2016). A direct solar charging of an organic-inorganic, stable, and aqueous alkaline redox flow battery with a hematite photoanode. *Angew. Chem. Int. Ed. 55*, 7142–7147.
11. Cheng, Q., Fan, W., He, Y., Ma, P., Vanka, S., Fan, S., and Wang, D. (2017). Photorechargeable high voltage redox battery enabled by Ta3N5 and GaN/Si dual-photoelectrode. *Adv. Mater. 29*, 1700312.
12. McKone, J. R., DiSalvo, F. J., and Abruna, H. D. (2017). Solar energy conversion, storage, and release using an integrated solar-driven redox flow battery. *J. Mater. Chem. A. 5*, 5362–5372.
13. Zhou, Y., Zhang, S., Ding, Y., Zhang, L., Zhang, C., Zhang, X., and Yu, G. (2018). Efficient solar energy harvesting and storage through a robust photocatalyst driving reversible redox reactions. *Adv. Mater. 30*, 1802294.

14. Fujishima, A., and Honda, K. (1972). Electrochemical photolysis of water at a semiconductor electrode. *Nature. 238*, 37–38.
15. Grätzel, M. (2001). Photoelectrochemical cells. *Nature. 414*, 338–344.
16. Branker, K., Pathak, M. J. M., and Pearce, J. M. (2011). A review of solar photovoltaic levelized cost of electricity. *Renew. Sust. Energ. Rev. 15*, 4470–4482.
17. Zhou, Y., Zhang, S., Ding, Y., Zhang, L., Zhang, C., Zhang, X., Zhao, Y., and Yu, G. (2018). Efficient solar energy harvesting and storage through a robust photocatalyst driving reversible redox reactions. *Adv. Mater. 103*, 1802294–1802297.
18. Li, W., Fu, H. C., Zhao, Y., He, J. H., and Jin, S. (2018). 14.1% efficient monolithically integrated solar flow battery. *Chem. 4*, 2644–2657.
19. Li, W., Zheng, J., Hu, B., Fu, H. C., Hu, M., Veyssal, A., and Jin, S. (2020). High-performance solar flow battery powered by a perovskite/silicon tandem solar cell. *Nat. Mater. 19*, 1326–1331.
20. Li, W., Kerr, E., Goulet, M. A., Fu, H. C., Zhao, Y., Yang, Y., and Jin, S. (2019). A long lifetime aqueous organic solar flow battery. *Adv. Energy Mater. 9*, 1900918.
21. Hu, H., Li, Y., Zhang, J., Peng, Z., Ma, L. K., Xin, J., and Yan, H. (2018). Effect of ring-fusion on miscibility and domain purity: Key factors determining the performance of PDI-based nonfullerene organic solar cells. *Adv. Energy Mater. 8*, 1800234.
22. Tamai, Y., Ohkita, H., Benten, H., and Ito, S. (2015). Exciton diffusion in conjugated polymers: From fundamental understanding to improvement in photovoltaic conversion efficiency. *J. Phys. Chem. Lett. 6*, 3417–3428.
23. Lin, Y., and Zhan, X. (2014). Non-fullerene acceptors for organic photovoltaics: An emerging horizon. *Mater. Horiz. 1*, 470–488.
24. Lin, Y., and Zhan, X. (2015). Designing efficient non-fullerene acceptors by tailoring extended fused-rings with electron-deficient groups. *Adv. Energy Mater. 5*, 1501063.
25. Yuan, J., Zhang, Y., Zhou, L., Zhang, G., Yip, H. L., Lau, T. K., and Zou, Y. (2019). Single-junction organic solar cell with over 15% efficiency using fused-ring acceptor with electron-deficient core. *Joule. 3*, 1140–1151.
26. Zhu, L., Zhang, M., Zhou, G., Wang, Z., Zhong, W., Zhuang, J., and Liu, F. (2024). Achieving 20.8% organic solar cells via additive-assisted layer-by-layer fabrication with bulk pin structure and improved optical management. *Joule. 8*, 3153–3168.
27. Cho, H. W., Jeong, S. Y., Wu, Z., Lim, H., Park, W. W., Lee, W., and Woo, H. Y. (2023). A newly designed benzodithiophene building block: tuning of the torsional barrier for non-halogenated and non-aromatic solvent-processible photovoltaic polymers. *J. Mater. Chem. A. 11*, 7053–7065.
28. Yang, W. S., Noh, J. H., Jeon, N. J., Kim, Y. C., Ryu, S., Seo, J., and Seok, S. I. (2015). High-performance photovoltaic perovskite layers fabricated through intramolecular exchange. *Science. 348*, 1234–1237.
29. Poorkazem, K., Liu, D., and Kelly, T.L. (2015). Fatigue resistance of a flexible, efficient, and metal oxide-free perovskite solar cell. *J. Mater. Chem. A 3*, 9241–9248.
30. Chen, L., Xie, X., Liu, Z., and Lee, E.-C. (2017). A transparent poly(3,4-ethylenedioxylenet hiophene):poly(styrene sulfonate) cathode for low temperature processed, metal-oxide free perovskite solar cells. *J. Mater. Chem. A 5*, 6974–6980.
31. G. Yang, Chen, C., Yao, F., Chen, Z. L., Zhang, Q., Zheng, X. L., Ma, J. J., Lei, H. W., Qin, P. L., Xiong, L. B., Ke, W. J., Li, G., Yan, Y. F., and Fang, G. J. (2018). Effective carrier-concentration tuning of SnO_2 quantum dot electron-selective layers for high-performance planar perovskite solar cells. *Adv. Mater. 30*, 1706023.
32. Yang, D., Yang, R., Zhang, J., Yang, Z., Liu, S., and Li, C. (2015). High efficiency flexible perovskite solar cells using superior low temperature TiO2. *Energy Environ. Sci. 8*, 3208–3214.
33. Zhou, L., Yu, M. J., Chen, X. L., Nie, S. H., Lai, W. Y., W. M. Su, Cui, Z., and Huang, W. (2018). Screen-printed poly(3,4-ethylenedioxythiophene):poly(styrenesulfonate) grids as ITO-free anodes for flexible organic light-emitting diodes. *Adv. Funct. Mater. 28*, 1705955.

34. Zhang, Q., Li, B., Huang, S., Nomura, H., Tanaka, H., and Adachi, C. (2014). Efficient blue organic light-emitting diodes employing thermally activated delayed fluorescence. *Nat. Photonics*. *8*, 326.
35. Song, W., Chen, Z., Lin, C., Zhang, P., Sun, D., Zhang, W., Ge, J., Xie, L., Peng, R., Yang, D., et al. (2024). An in situ crosslinked matrix enables efficient and mechanically robust organic solar cells with frozen nano-morphology and superior deformability. *Energy Environ. Sci. 17*, 7318–7329.
36. Li, C., Zhou, J., Song, J., Xu, J., Zhang, H., Zhang, X., Guo, J., Zhu, L., Wei, D., Han, G., and Sun, Y. (2021). Non-fullerene acceptors with branched side chains and improved molecular packing to exceed 18% efficiency in organic solar cells. *Nat. Energy 6*, 605–613.
37. Luo, Z., Liu, T., Ma, R., Xiao, Y., Zhan, L., Zhang, G., Sun, H., Ni, F., Chai, G., Wang, J., and Yang, C. (2020). Precisely controlling the position of bromine on the end group enables well-regular polymer acceptors for all-polymer solar cells with efficiencies over 15. *Adv. Mater. 32*, 2005942.
38. Lin, Y., Wang, J., Zhang, Z. G., Bai, H., Li, Y., Zhu, D., and Zhan, X. (2015). An electron acceptor challenging fullerenes for efficient polymer solar cells. *Adv. Mater. 27*, 1170–1174.
39. Liu, M., Han, X., Chen, H., Peng, Q., and Huang, H. (2023). A molecular descriptor of intramolecular noncovalent interaction for regulating optoelectronic properties of organic semiconductors. *Nat. Commun. 14*, 2500.
40. Wang, X., Lu, H., Liu, Y., Zhang, A., Yu, N., Wang, H., and Bo, Z. (2021). Simple nonfused ring electron acceptors with 3D network packing structure boosting the efficiency of organic solar cells to 15.44%. *Adv. Energy Mater. 11*, 2102591.
41. Zeng, R., Zhang, M., Wang, X., Zhu, L., Hao, B., Zhong, W., and Liu, F. (2024). Achieving 19% efficiency in non-fused ring electron acceptor solar cells via solubility control of donor and acceptor crystallization. *Nat. Energy. 9*, 1–12.
42. Wang, W., Yan, C., Lau, T. K., Wang, J., Liu, K., Fan, Y., and Zhan, X. (2017). Fused hexacyclic nonfullerene acceptor with strong near-infrared absorption for semitransparent organic solar cells with 9.77% efficiency. *Adv. Mater. 29*, 1701308.
43. Huang, C., Liao, X., Gao, K., Zuo, L., Lin, F., Shi, X., and Jen, A. K. Y. (2018). Highly efficient organic solar cells based on S, N-heteroacene non-fullerene acceptors. *Chem. Mater. 30*, 5429–5434.
44. Yu, H., Qi, Z., Zhang, J., Wang, Z., Sun, R., Chang, Y., and Yan, H. (2020). Tailoring nonfullerene acceptors using selenium-incorporated heterocycles for organic solar cells with over 16% efficiency. *J. Mater. Chem. A*. *8*, 23756–23765.
45. Li, Z., Li, X., Xue, J., Zhang, J., Zhu, C., Li, J.,... Li, Y. (2023). A-DA′ DA type acceptor with a benzoselenadiazole A′-unit enables efficient organic solar cells. *ACS Energy Lett. 8*, 2488–2495.
46. Shi, Y., Chang, Y., Lu, K., Chen, Z., Zhang, J., Yan, Y., and Wei, Z. (2022). Small reorganization energy acceptors enable low energy losses in non-fullerene organic solar cells. *Nat. Commun. 13*, 3256.
47. Zhang, Y., Liu, K., Huang, J., Xiao, X., Cao, J., Zhao, G., and Li, G. (2021). Graded bulk-heterojunction enables 17% binary organic solar cells via nonhalogenated open air coating. *Nat. Commun. 12*, 4815.
48. Wan, J., Wu, Y., Sun, R., Qiao, J., Hao, X., and Min, J. (2022). An alloy small molecule acceptor for green printing organic solar cells overcoming the scaling lag of efficiency. *Energy Environ. Sci. 15*, 5192–5201.
49. Wu, Y., Zhang, F., Wang, T., Huang, P. W., Filippas, A., Yang, H., and Liu, N. (2023). A submillimeter bundled microtubular flow battery cell with ultrahigh volumetric power density. *Proc. Natl. Acad. Sci. 120*, e2213528120.

CHAPTER 19

Other Flow Battery Chemistry

James Friday Amaku, Fanyana M. Mtunzi,
and Jesse Greener

19.1 INTRODUCTION

The ever-rising worldwide fossil energy consumption raises worries about the safety of the environment for humanity [1]. To address climate change, it is imperative to decarbonize a sustainable energy system. Hence, utilizing clean energy, especially renewable energy, becomes crucial for the transition of energy. The main barrier to the broad deployment of renewable energy sources is the intermittent, volatile, and cyclical nature of renewable energy sources [2]. To circumvent the challenges associated with the utilization of renewable energy, energy storage systems with extended durations were proposed. An intensive effort has been channeled into the design and modification of energy storage facilities with user and environmental friendliness, flexible design, and long cycle life. Hence, stakeholders admire the application of flow batteries (FBs) as an alternative energy storage device [3].

The flow battery is classified into two main categories, namely the novel flow battery systems, which include organic-based FBs with tremendous potential for energy storage applications, and traditional FBs, like vanadium, zinc, and iron-chromium FBs [4]. A flow battery consists of an electrochemical cell stack, pumps, electrolytes, and connectors (pipelines). Meanwhile, bipolar plates, electrodes, and a membrane are the primary components of an electrochemical cell. The overall process of a flow battery is governed by a power conversion system (PCS), energy management system (EMS), and battery management system (BMS) [5]. It is interesting to know that the energy storage capacity of a flow battery is dependent on the volume and concentration of the electrolyte [6]. The power of the system (FB) is a function of the number of cells in a stack and the nature of the electrodes employed [7]. The aforementioned factors are also known to influence the electrochemical performance (energy density, power density, coulombic efficiency, voltage efficiency, energy efficiency, and durability) of a flow battery system [8]. Hence, the judicious use of renewable energy is largely dependent on the availability of effective large-scale energy storage devices. Chemical energy produced by renewable energy sources can be stored in

DOI: 10.1201/9781003506379-19

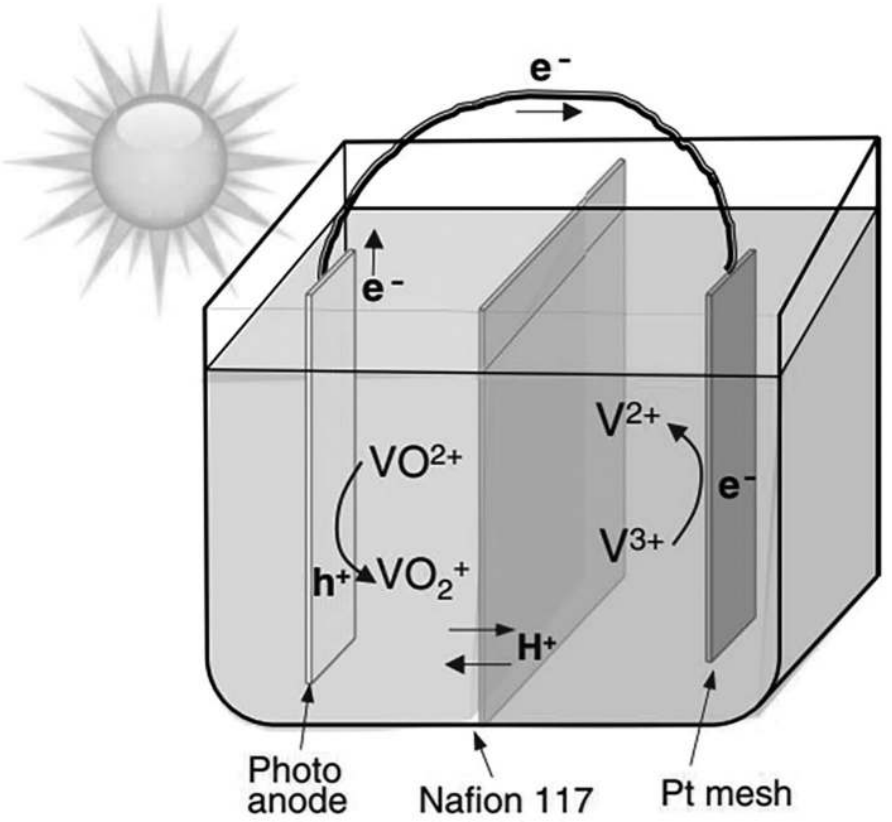

FIGURE 19.1 Schematic illustration of the all-vanadium redox PEC storage cell. (Adapted with permission [10], Copyright (2014) Elsevier. Distributed under a Creative Commons Attribution License 4.0 (CC BY).)

batteries, which can then convert that chemical energy into electric energy when needed. This demonstrates the key role of flow battery technologies in sustainable energy utilization. Hence, the recent advances in flow battery chemistry for the design of cost-effective, environmentally benign, and high-capacity batteries are essential for energy sustainability.

19.1.1 Research Overview of Flow Batteries

Before now, the need to design energy storage systems with excellent capacity for usage has been a major setback for most electrical devices. A major finding was reported at the National Aeronautics and Space Administration (NASA) in 1974 in which a valence state change approach was used for a reversible redox reaction that resulted in energy generation [9]. The findings demonstrated a huge difference in the design and existing perception of the battery. This ushered in redox flow batteries (RFBs) such as iron-chromium flow batteries (FB), vanadium flow batteries (VFBs), zinc-based flow batteries (ZFBs), and sodium polysulfide-bromine flow. As discussed in the previous chapters, this class of batteries has

shown a promising capacity for application and good market prospects. This could be attributed to high energy efficiencies, large storage capacities, lack of geographical condition limitations, deep discharging, long working lifespans, and environmental benignity among others. However, extensive investigations have been directed toward the development of novel flow battery systems based on innovative design and electrochemical kits for the purpose of improving power and energy densities and decreasing costs.

Meanwhile, many research articles have been published in this regard. Based on this, our study will provide basic insight into the chemistry of other flow battery systems. Wei and a coworker demonstrated the application of vanadium in the design of a photoelectrochemical storage cell (see Figure 19.1). The study revealed the release of hydrogen and oxygen via the photolysis of water as the light energy is converted into chemical energy. The electrochemical process was quite promising, as it demonstrated a 25 h photocharging with a 95% Faradaic efficiency that is void of external voltage bias at a conversion rate of 0.0042 μmol h^{-1} for a VO^{2+}, having ~12% photon-to-current efficiency at 350 nm. The excellent kinetics of vanadium redox couples of VO^{2+}/VO^{2+} and V^{3+}/V^{2+} may be attributed to the observed phenomenon [10]. On the other hand, the application of $ATiO_2/WO_3$ electrodes using the same experimental condition yielded much higher photocurrents [11]. In strict terms, this technique converts radiant energy to chemical energy and cannot be exhaustively considered a battery; however, the output energy is simply an electrochemical process.

19.2 TITANIUM POLYHALIDE REDOX FLOW BATTERIES

Another interesting application of a variety of halide and titanium halide redox couples has been assessed in the capacity of redox flow cells for flow battery systems by Skyllas-Kazacos and Milne [12]. In order to determine the reversibility of the redox couplings as well as the anticipated cell voltage and performance in a redox flow cell, cyclic voltammetry and cell cycling measurements were utilized. Due to insoluble iodine deposits formed inside the cell, causing cell obstruction, they suggested that an iodine cell was not feasible. However, it was demonstrated that a titanium polyhalide cell with an open circuit voltage of 0.93 V and significant current efficiencies (97%–98%) could be achieved by using 4 M HBr, 3 M HCl, and 0.56 M $TiCl_4$ as the supporting electrolyte in both half-cells at 40 $mAcm^{-2}$.

19.2.1 Single-Flow Acid Cu–Pbo_2 Battery

Worthy of note is the single-flow battery (SBF) for distributional energy storage designed by Pan and co-researchers. The SBF consists of an anode (PbO_2), cathode (copper), and electrolyte (H_2SO_4–$CuSO_4$) solution (see Figure 19.2). The SBF system was reported to have a superior long-lasting capacity for energy storage. It was also perceived to sustain an average coulombic efficiency of 97%, an energy efficiency of 83%, and a discharge voltage of 1.29 V [13]. The design is anticipated to be the perfect combination of low cost and optimal performance for power generation using renewable energy sources for energy storage. It's a cutting-edge battery solution that deserves more study.

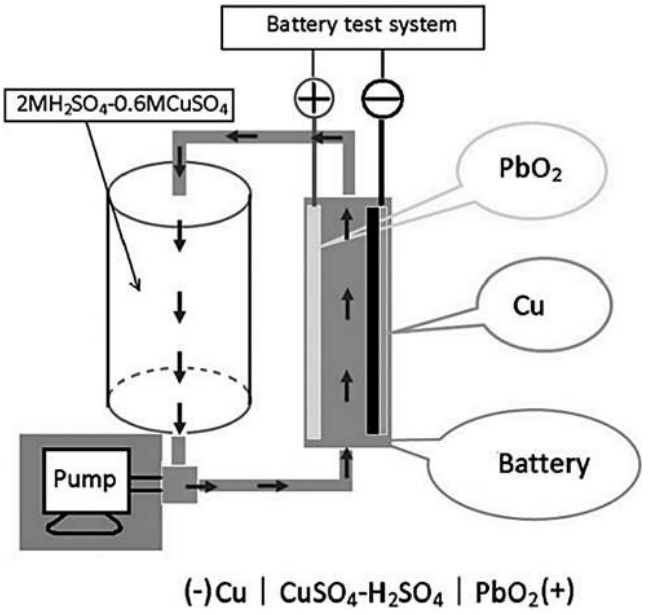

FIGURE 19.2 Schematic diagram of single-flow acid Cu-PbO_2 battery. (Adapted with permission [13], Copyright (2008) Elsevier. Distributed under a Creative Commons Attribution License 4.0 (CC BY).)

19.2.2 Polysulfide/Bromine Redox Flow Battery

Another approach to the design of RFBs involves the application of carbon felt, activated carbon, sodium polysulfide (anolyte), and sodium bromide solution (catholyte) for the fabrication of a laboratory-scale battery. The application of carbon felt, and activated carbon as electrodes was an electrochemical process in the negative half-cell reactions due to catalyst coating. The implication of catalytic coating also resulted in a more uniform discharge voltage curve and stable cycling performance. Hamad and colleagues reported the fabrication of cost-effective elemental-sulfur sodium polysulfide/sodium bromide aqueous electrolytes for RFBs. The study aimed at the design of a low-cost aqueous flow battery system with enhanced energy density. Owing to the ubiquitous nature and cost efficiency of sulfur and bromine salts, elemental added sulfur sodium polysulfide (EASSP) was fabricated at a ratio of 1:4 and is utilized as an anolyte. A bromine–polysulfide redox flow battery (BPRFB) containing a 1.4 M EASSP anolyte and 8 M NaBr catholyte is charged and discharged for 5 min, which results in a capacity of 17 mAh (3.4 mAh cm^{-2}) at a current density of 40 mA cm^{-2}. The cyclic performance of the BPRFB is characterized by a capacity of 17 mAh at 40 mA cm^{-2}, which is retained over 150 cycles with a 98% coulombic efficiency. The assembled BPRFB cell with the optimized electrolyte composition (1.4 M EASSP: 8 M NaBr) exhibits constant current (without leakage) and potential. These findings demonstrate a potential application of the novel anolyte with the optimal catholyte concentrations, which is inexpensive, economical, and can be scaled up to implement a required energy storage capacity for grid-scale applications [14]. Zhou and coworker reported an average energy efficiency of up to 81% over 50

cycles (about 600 h) using a current density of 40 mA cm^{-2}. On the contrary, activated carbon-based electrodes exhibited an energy efficiency of 64.7% within 16 cycles with a rapid decline due to surface area loss that was attributed to sulfur deposition. The contrast in the performance of the two types of materials in the sodium polysulfide/bromine redox flow battery is associated with the structural differences of the materials [15–17].

19.2.3 Cd-Fe Redox Flow Battery

To enhance the electrochemical process and cost reduction, researchers and stakeholders have employed the Cd/Fe system in the quest for a durable and efficient flow battery. Cheng and fellow researchers reported the design of a Cd/Fe system with regulated ion diffusion across the membrane. The system was observed to have a swift electrochemical reaction. Meanwhile, hydrogen overvoltage was noticed to allow Cd^{2+} to be seamlessly extracted from 0.5 M H_2SO_4 solutions; also the noninteraction of Cd^{2+} with Fe^{2+} or Fe^{3+} aided its easy removal from the acid. The electrolytes are composed of 1.5 M $CdSO_4$ in 1 M H_2SO_4 for the negative half-cell and 0.5 M $FeSO_4$ and 0.25 m $Fe_2(SO_4)_3$ in 1 M H_2SO_4 for the positive half-cell. The NAFION membrane was employed for the process. At 0.99 V, the battery's discharge voltage was 10 $mAcm^{-2}$, and its energy and current efficiencies were 71% and 91%, respectively. However, during the first 50 cycles of charge and discharge, the efficiency was noticed to drop [18].

19.2.4 Np^{V}/Np^{IV} Redox Flow Battery

Actinides such as americium, neptunium, plutonium, and uranium have been theoretically deemed to be useful as redox couples for FBs. These noble materials are often sourced from spent fuel rods. These materials exist in varied oxidation states, and this confers on them isostructural (An^{4+}/An^{3+}) benefits given room for high electron transfer rates. Owing to the higher rate constants of Np, Np-based batteries could attain high efficiencies up to 99.1% at 70 mA cm^{-2}. Hence, it is possible to charge and discharge a battery based on 0.05 M Np in 1 M HNO_3. On the other hand, the disproportionate nature of some actinides (U^{V}, Pu^{V}, and Am^{IV}) makes them unfit for aqueous electrolytes, as they exhibit a slow electrochemical process [19–21].

19.2.5 Aqueous Organic Redox Flow Batteries

Wang and colleagues synthesized a novel viologen derivative, 1,10-bis(4,40-dime thylpiperidiniumyl)-4,40-bipyridinium tetrachloride $(DBPPy)Cl_4$, as a stabilizer of organic active molecules in the aqueous organic redox flow batteries (AORFBs) system. The authors also revealed the long-duration and scalability implications of novel negolyte. The storage capacity of the battery is shown in Figure 19.3. The stabilizer demonstrated superior solubility (1.84 M) and redox potential (−0.52 V vs. Ag/AgCl). Interestingly, the steric impediment to the OH^- nucleophilic attack was provided by the grafted N-cyclic quaternary ammonium groups in $(DBPPy)Cl_4$. Aside from the basic assessment of negotiate $(DBPPy)Cl_4$, the authors reported a superior specific capacity (22.43 Ah L^{-1}), retention rate (99.99% per cycle at 60 mA cm^{-2}), and energy efficiency (78.35%) for a 1.0 M flow battery when paired with a posolyte $(TPABPy)Cl_3$ [22].

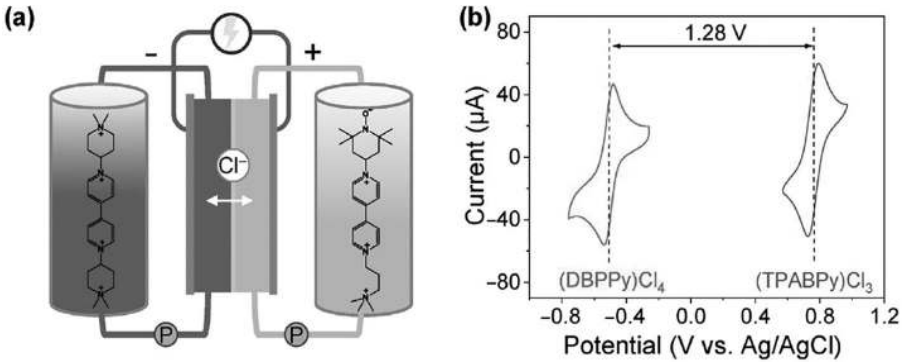

FIGURE 19.3 (a) Schematic illustration of $(DBPPy)Cl_4/(TPABPy)Cl_3$ AORFB; (b) CVs of 5.0 mM $(DBPPy)Cl_4$ and 5.0 mM $(TPABPy)Cl_3$ in 1.0 M KCl solution. (Adapted with permission [22], Copyright (2024) Elsevier. Distributed under a Creative Commons Attribution License 4.0 (CC BY).)

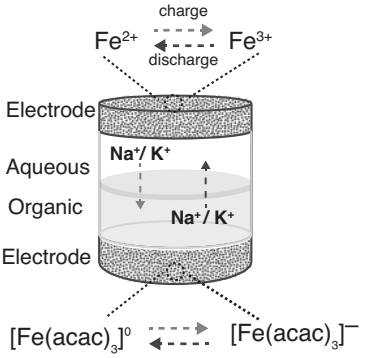

FIGURE 19.4 Schematic of battery operation, showing redox reactions and accompanying ion transport. (Adapted with permission [23], Copyright (2018) Elsevier. Distributed under a Creative Commons Attribution License 4.0 (CC BY).)

19.2.6 Membraneless All-Iron Redox Flow Battery

A membraneless all-iron redox flow battery capable of recharging and recirculating the same electrolyte streams for multiple cycles maintains the advantages of decoupled power and energy densities. Briefly, two immiscible solvents were employed as both aqueous anolyte (iron(II) sulfate ($FeSO_4$)) and organic catholyte (iron(III) acetylacetonate ($Fe(acac)_3$)) liquids.

To ensure the effectiveness of this system, water-immiscible ionic liquid (IL) 1-butyl-1-methylpyrrolidinium bis(trifluoromethylsulfonyl)imide and polar salts (NaCl and K_2SO_4) were used as the supporting electrolyte for the organic and aqueous phases, respectively (see Figure 19.4). The system was noticed to exhibit over 60% of initial discharge potential that was sustained, and over 80% of coulombic efficiency was retained after 25 circles [23].

19.2.7 $Pb^{2+}/Pb//PbO_2/Pb^{2+}$

In 2004, Hazza and co-authors proposed a lead-based redox flow battery. The electrochemical process was noticed to solid Pb and PbO_2, respectively. However, this challenge was controlled by introducing methanesulfonic acid (CH_3SO_3H). The solvent (2M CH_3SO_3H) aided a fast electrochemical process, and the insolubility of the solid deposition led to the deposition and dissolution of lead on glassy carbon electrodes. The design of this cell births the idea of a membrane-free RFB. The study revealed the diffusion coefficient of $6.1 \times 10^{-6} cm^2 s^{-1}$ for Pb^{2+} in 2 m CH_3SO_3H. Meanwhile, due to the higher viscosity of the electrolyte at high Pb^{2+} concentrations, the conductivity decreased and increased with increased acid concentration [24]. Another study reported a current efficiency of >85% at 20–100 mA cm^{-2} and a cell voltage of 1.78 V using an electrolyte combination of 1.5 M $Pb(CH_3SO_3)_2$ solution in 0.9m CH_3SO_3H [25]. Owing to the promising nature of this class of FB, several researchers have modified the electrolyte concentration, nature of additives, and operating conditions to improve the overall output.

19.2.8 Bromine-Manganese Flow Battery

Owing to the high redox potential, solubility, and outstanding kinetics of Mn^{2+}/Mn^{3+}, its redox pair has been considered to be a promising cathode for high-energy-density batteries. However, the disproportionation side reaction of Mn^{3+}, which results in the accumulation of MnO_2, limits its reversibility and further density [26]. Aside from the conventional catholyte, the authors proposed the application of Mn^{2+} and Br^- as catholyte in a flow battery system due to its long cycle life and energy density. Finally, the researchers observed that the bromine-manganese flow battery exhibited a high energy efficiency of 76% at 80 mA cm^{-2} with an energy density of 360 Wh L^{-1} [26].

19.2.9 Hydrogen/Bromine RFBs

This class of RFBs has gained massive attention due to their high energy capacity, inexpensive redox materials, and high conversion rates [27]. Besides, bromine is known to have good water solubility, quick reaction kinetics, and high surface area carbon electrode characteristics with distinct durability. In the general setup of these FBs, the hydrogen redox pair can serve as the negative electrode, hence necessitating the application of a platinum-based precious metal catalyst due to hydrogen evolution and oxidation [28]. However, the effectiveness of the setup with time is a function of its catalyst activity. Meanwhile, factors such as temperature, pH, bromine concentration, and crystal structure impact bromine chemisorption. The deterioration catalyst is a major challenge to this class of battery. However, it was conceived that by replacing the spent electrolyte, the battery's cycle span would be enhanced with undiminished initial energy capacity [29], as though this may sound, it is limited due to catalyst deterioration. To prevent the interaction of platinum with hydrogen when a battery is in use, a coating of the catalyst was introduced. However, the act of coating tends to prevent crossover but hinders conductivity. By reducing the ohmic resistance, Tucker et al. found that covering the membrane with a catalyst layer on the negative side enhances performance and results in a power density of 1,250 mW cm^{-2} at 2.5 A cm^{-2} [30]. Thick, multi-layered electrodes were used by Cho et al. to achieve energy densities of 6.5

Wh L^{-1} and power densities of 1300 mW cm^{-2} by pretreating them in sulfuric acid [31]. Hydrogen/bromine RFBs have high power densities with economic benefits, but the application of platinum as catalysts tends to make their cost implication unattractive. Hence, to design effective and robust hydrogen/bromine RFBs, it is imperative to explore the chemistry's cycle life and the catalyst modification that will prevent the absorption of bromine on the negative electrode.

19.2.10 Aqueous Flow Battery Systems

The application of bromine and 9,10-anthraquinone-2,7-disulphonic acid as the active species in the design of novel aqueous flow battery systems has provided a novel system with room for improvement [32]. The system exhibited a working current density of 500 mA cm^{-2} when hydrobromic acid and sulfuric acid were employed as positive and negative supporting electrolytes, respectively. Interestingly, a setback to the application of this battery is the ease of bromine oxidation, poor resistance to corrosion, and poor open circuit voltage (0.7 V) [33]. Owing to the shortcomings of this class of battery, a twist to its composition was invoked. The modification involved the replacement of bromide with nontoxic ferricyanide ions involving $K_4Fe(CN)_6$ and 2,6-dihydroxyanthraquinone as active cathodic and anodic species, respectively. About 84% energy efficiency, an open circuit voltage of 1.2 V, a current density of 100 mA cm^{-2}, and steady processes of over 100 charge/discharge cycles were achieved when bromine was replaced by ferricyanide ions. The ferrocene/ferrocenium ion ($Fc/FcBF_4$) redox couple was investigated as a model chemistry for a non-aqueous redox flow battery system. Voltammetry, flow-cell battery cycling, and UV–vis spectroscopy were used to validate the performance of the system. Regardless of the poor solubility of the $Fc/FcBF_4$ redox couple in acetonitrile, the stability of its oxidation and facile kinetics makes the couple a value-added system for FBs. The high-capacity retention of ferrocene at 10 mM concentration showed 80% capacity retention after 200 cycles (7.8 days). The feasibility of the process was observed to depend on $FcBF_4$ decomposition in the electrolyte. Worthy of mention is that this class of battery sustains good safety and excellent environmental friendliness, reduced electrolyte resistance, lower costs, and robust power density. Notwithstanding the benefit of this system, its power and energy density need to be improved.

19.2.11 Non-aqueous Flow Battery Systems

In the quest to design a superior battery system, Singh and colleagues investigated the application of metals such as V and Ru and organic ligands as active species in non-aqueous flow battery systems [34]. The results from this study revealed a working poor current density owing to the low ionic conductivity of the supporting electrolytes [35]. Worthy of note is the fabrication of a lithium/2,2,6,6-tetramethylpiperidine-1-oxyl (Li/TEMPO) flow battery system in which the radical reaction of TEMPO (cathode reaction) and dissolution of Li (anode reaction) were used. The study engaged TEMPO, which served as the electroactive material on the positive side, lithium hexafluorophosphate ($LiPF_6$) acted as the supporting charge carrier. Nevertheless, drawbacks to the application of this system are attributed to its low current densities (5 mA cm^{-2}) [36]. Aside from the application of the Li/ferrocene

(Li/Fc) flow battery system, which exhibited a low solubility that posed a safety challenge [37], the modification of ferrocene via the inclusion of quaternary ammonium groups demonstrated a good solubility and enhanced current density of only 3.5 mA cm^{-2} [38]. Finally, a remarkable success of 85% energy efficiency, over 99% capacity, and coulombic efficiency of more than 95% was reported for the study involving a non-aqueous all metallocene-based lithium-based flow battery [39–42]. Kunlong and colleagues investigated the use of naphthol green B (NGB), as a catholyte material for AORFBs. Naphthol green B and Fe(III)/Fe(IV) were used to design an electroredox couple. The couple was noticed to have a high redox potential of 0.73 V. On the other hand, a limited transmembrane crossover, enhanced electrochemical performance, and high stability were observed when hydroxypropyl-β-cyclodextrin (HP-β-CD) was employed as the outer coordination sphere of naphthol green B. Interestingly, when used as an anolyte with 1,1′-bis(3-sulfonato propyl)-4,4′-bipyridinium (Spr)2V, the NGB/(Spr)2V system with HP-β-CD proved exceptional cycling potential at current rates ranging from 5 to 30 mA cm^{-2} and maintained above 99% of its total capacity or experienced less than 0.00125% capacity decay per cycle, with an average coulombic efficiency of almost 100% over 800 cycles at 10 mA cm^{-2} [43].

19.2.12 Hybrid Systems/Protic Electrolytes

The hybrid system gives room for the innovative design of robust flow battery systems with superior output and good scalability for industrial applications. Protic solvents are known to have a limited electrochemical working potential due to their poor solubility tendencies. However, specific modification of these solvents makes them adaptable in flow battery systems.

19.2.12.1 V/Glyoxal and V/l-Cysteine Flow Battery Systems

A system consisting of the combination of a VOFC with a cell for the electrosynthesis of organic materials accompanied by simultaneous energy storage was used to investigate the oxidation of glyoxal to glyoxylic acid and L-cysteine to L-cysteic acid [16,44,45]. The V/Glyoxal and V/l-cysteine flow battery system is made up of a conventional VOFC, which used oxygen to oxidize V^{2+} to V^{3+} and water, and a subsequent cell, where glyoxal was oxidized with water by V^{3+}. The vanadium solution was distributed through both cells. The electrosynthesis was proposed to act as the energy storage, while the energy consumption was to be performed by the VOFC. The use of Fe^{3+}/Fe^{2+} with separate oxidation by oxygen as the oxidant in the VOFC for bypassing the ORR has also been proposed [16,45].

19.2.12.2 Anthraquinone/Bromine

Huskinson and coworkers designed a metal-free redox flow battery system [32]. The study used 9,10-anthraquinone-2,7-disulfonic acid (AQDS) and $Br_2/Br¢$ in H_2SO_4 or HBr. A rate constant of 7.2×10^{-3} cm s^{-1} and a diffusion coefficient of 3.8×10^{-6} cm^2s^{-1} were obtained for the reduction of AQDS via the cyclovoltammetric analysis. The system was observed to have a standard potential of +0.213 V and a theoretical electrochemical reversibility value of 59 mV n^{-1} having a peak difference of 34 mV. The benefit of this hybrid system is

the possibility of attaining higher cell voltages, higher solubility, and thus higher energy densities. A cell with 9,10-anthraquinone-2,7-disulfonic acid achieved a maximum power density of 3.3 W cm^{-2} using a catalyst-free carbon electrode [32].

19.3 CONCLUSION

The design of novel flow battery systems has gained the attention of stakeholders. Hence, extensive studies that are geared toward establishing novel electrochemical/photochemical systems with the capacity to generate high-power and energy-density batteries have been reported. Interestingly, the new class of flow battery systems showcases the platform for a complete power grid that is void of fossil fuels. Battery systems such as titanium halide, SFB, PRFBs, Cd-Fe redox flow battery, actinides redox flow battery, AORFBs, membraneless all-iron redox flow battery, bromine-manganese flow battery, hydrogen/bromine redox flow battery, aqueous redox flow battery, and non-aqueous flow battery were discussed. The aforementioned SBF demonstrated the possibility of industrial scale-up. Surprisingly, the favorable cost implications of aqueous batteries and bromine-based batteries present these classes of batteries as models for the future. However, the toxicity of bromine and other hazardous by-products that are generated from the electrochemical process of some of the discussed FBs limits their application. Another issue that needs to be taken into account when thinking about the chemistry of future FBs is corrosion in carbon-based electrodes. Therefore, it is essential to develop FBs in a novel manner with the goal of improving their stability, durability, energy density, and power density with the potential for industrial application.

REFERENCES

1. Ertugrul, N., *Reinventing the Power Grid: Renewable Energy, Storage, and Grid Modernization*. 2024, CRC Press.
2. Medina, C., C.R.M. Ana, and G. González, Transmission grids to foster high penetration of large-scale variable renewable energy sources–A review of challenges, problems, and solutions. *International Journal of Renewable Energy Research (IJRER)*, 2022. 12(1): pp. 146–169.
3. Zhang, C., Z. Yuan, and X. Li, Designing better flow batteries: An overview on fifty years' research. *ACS Energy Letters*, 2024. 9(7): pp. 3456–3473.
4. Park, M., J. Ryu, W. Wang, and J. Cho, Material design and engineering of next-generation flow-battery technologies. *Nature Reviews Materials*, 2016. 2(1): pp. 1–18.
5. Wang, H., S.A. Pourmousavi, W.L. Soong, X. Zhang, and N. Ertugrul, Battery and energy management system for vanadium redox flow battery: A critical review and recommendations. *Journal of Energy Storage*, 2023. 58: p. 106384.
6. Kosswattaarachchi, A.M. and T.R. Cook, Concentration-dependent charge-discharge characteristics of non-aqueous redox flow battery electrolyte combinations. *Electrochimica Acta*, 2018. 261: pp. 296–306.
7. Ke, X., J.M. Prahl, J.I.D. Alexander, J.S. Wainright, T.A. Zawodzinski, and R.F. Savinell, Rechargeable redox flow batteries: Flow fields, stacks and design considerations. *Chemical Society Reviews*, 2018. 47(23): pp. 8721–8743.
8. Sankaralingam, R.K., S. Seshadri, J. Sunarso, A.I. Bhatt, and A. Kapoor, Overview of the factors affecting the performance of vanadium redox flow batteries. *Journal of Energy Storage*, 2021. 41: p. 102857.

9. Bockris, J.O.M. and A.K. Reddy, Conversion and storage of electrochemical energy. In *Modern Electrochemistry 2B: Electrodics in Chemistry, Engineering, Biology, and Environmental Science*, 2000: pp. 1789–1901.
10. Wei, Z., D. Liu, C. Hsu, and F. Liu, All-vanadium redox photoelectrochemical cell: An approach to store solar energy. *Electrochemistry Communications*, 2014. 45: pp. 79–82.
11. Liu, D., Z. Wei, C.-J. Hsu, Y. Shen, and F. Liu, Efficient solar energy storage using a TiO_2/WO_3 tandem photoelectrode in an all-vanadium photoelectrochemical cell. *Electrochimica Acta*, 2014. 136: pp. 435–441.
12. Noack, J., M. Skyllas-Kazacos, L. Thaller, G. Tomazic, B. Jonshagen, and P. Morrissey, History of flow batteries. *Flow Batteries: From Fundamentals to Applications*, 2023. 1: pp. 29–52.
13. Pan, J., Y. Sun, J. Cheng, Y. Wen, Y. Yang, and P. Wan, Study on a new single flow acid Cu–PbO_2 battery. *Electrochemistry Communications*, 2008. 10(9): pp. 1226–1229.
14. Ahmad, A., T.A. Aldawood, M. Mansha, S. Ali, M.N. Tahir, M. Khan, I.A. Khan, and S.A. Khan, Optimized and cost-effective elemental-sulfur sodium polysulfide/sodium bromide aqueous electrolytes for redox flow batteries. *Journal of Power Sources*, 2024. 614: p. 235013.
15. Price, A., S. Bartley, S. Male, and G. Cooley, A novel approach to utility-scale energy storage. *Power Engineering Journal*, 1999. 13(3): pp. 122–129.
16. Noack, J., N. Roznyatovskaya, T. Herr, and P. Fischer, The chemistry of redox-flow batteries. *Angewandte Chemie International Edition*, 2015. 54(34): pp. 9776–9809.
17. Price, A., Recent developments in energy storage. *Power Engineering Journal*, 1999 13(3): p. 179.
18. Cheng, J., H.M. Zhang, Y.H. Wen, G.P. Cao, and Y.S. Yang, Study on a Cd-Fe redox flow battery in a sulphuric acid electrolyte. *Advanced Materials Research*, 2012. 399: pp. 1519–1523.
19. Shiokawa, Y., H. Yamana, and H. Moriyama, An application of actinide elements for a redox flow battery. *Journal of Nuclear Science and Technology*, 2000. 37(3): pp. 253–256.
20. Shiokawa, Y., T. Yamamura, and K. Shirasaki, Energy efficiency of an uranium redox-flow battery evaluated by the Butler–Volmer equation. *Journal of the Physical Society of Japan*, 2006. 75(Suppl): pp. 137–142.
21. Yamamura, T., N. Watanabe, and Y. Shiokawa, Energy efficiency of neptunium redox battery in comparison with vanadium battery. *Journal of Alloys and Compounds*, 2006. 408: pp. 1260–1266.
22. Wang, L., K. Wan, X. Yuan, Z. Xiang, Z. Fu, and Z. Liang, Steric hindrance shielding viologen against alkali attack in realizing ultrastable aqueous flow batteries. *Journal of Energy Chemistry*, 2024. 97: pp. 529–534.
23. Bamgbopa, M.O., Y. Shao-Horn, R. Hashaikeh, and S. Almheiri, Cyclable membraneless redox flow batteries based on immiscible liquid electrolytes: Demonstration with all-iron redox chemistry. *Electrochimica Acta*, 2018. 267: pp. 41–50.
24. Hazza, A., D. Pletcher, and R. Wills, A novel flow battery: A lead acid battery based on an electrolyte with soluble lead (II) Part I. Preliminary studies. *Physical Chemistry Chemical Physics*, 2004. 6(8): pp. 1773–1778.
25. Pletcher, D. and R. Wills, A novel flow battery: A lead acid battery based on an electrolyte with soluble lead (II) Part II. Flow cell studies. *Physical Chemistry Chemical Physics*, 2004. 6(8): pp. 1779–1785.
26. Liu, Y., C. Xie, and X. Li, Bromine assisted MnO_2 dissolution chemistry: Toward a hybrid flow battery with energy density of over 300 Wh L^{-1}. *Angewandte Chemie*, 2022. 134(51): p. e202213751.
27. Iwakiri, I., T. Antunes, H. Almeida, J.P. Sousa, R.B. Figueira, and A. Mendes, Redox flow batteries: Materials, design and prospects. *Energies*, 2021. 14(18): p. 5643.
28. Hughes, A.E., N. Haque, S.A. Northey, and S. Giddey, Platinum group metals: A review of resources, production and usage with a focus on catalysts. *Resources*, 2021. 10(9): p. 93.

29. Saadi, K., P. Nanikashvili, Z. Tatus-Portnoy, S. Hardisty, V. Shokhen, M. Zysler, and D. Zitoun, Crossover-tolerant coated platinum catalysts in hydrogen/bromine redox flow battery. *Journal of Power Sources*, 2019. 422: pp. 84–91.
30. Tucker, M.C., K.T. Cho, A.Z. Weber, G. Lin, and T. Van Nguyen, Optimization of electrode characteristics for the Br_2/H_2 redox flow cell. *Journal of Applied Electrochemistry*, 2015. 45: pp. 11–19.
31. Cho, K.T., P. Ridgway, A.Z. Weber, S. Haussener, V. Battaglia, and V. Srinivasan, High performance hydrogen/bromine redox flow battery for grid-scale energy storage. *Journal of The Electrochemical Society*, 2012. 159(11): p. A1806.
32. Huskinson, B., M.P. Marshak, C. Suh, S. Er, M.R. Gerhardt, C.J. Galvin, X. Chen, A. Aspuru-Guzik, R.G. Gordon, and M.J. Aziz, A metal-free organic–inorganic aqueous flow battery. *Nature*, 2014. 505(7482): pp. 195–198.
33. Lin, K., Q. Chen, M.R. Gerhardt, L. Tong, S.B. Kim, L. Eisenach, A.W. Valle, D. Hardee, R.G. Gordon, and M.J. Aziz, Alkaline quinone flow battery. *Science*, 2015. 349(6255): pp. 1529–1532.
34. Singh, P., Application of non-aqueous solvents to batteries. *Journal of Power Sources*, 1984. 11(1–2): pp. 135–142.
35. Gong, K., Q. Fang, S. Gu, S.F.Y. Li, and Y. Yan, Nonaqueous redox-flow batteries: Organic solvents, supporting electrolytes, and redox pairs. *Energy & Environmental Science*, 2015. 8(12): pp. 3515–3530.
36. Wei, X., W. Xu, M. Vijayakumar, L. Cosimbescu, T. Liu, V. Sprenkle, and W. Wang, TEMPO-based catholyte for high-energy density nonaqueous redox flow batteries. *Advanced Materials*, 2014. 26(45): pp. 7649–7653.
37. Ding, Y., Y. Zhao, and G. Yu, A membrane-free ferrocene-based high-rate semiliquid battery. *Nano Letters*, 2015. 15(6): pp. 4108–4113.
38. Wei, X., L. Cosimbescu, W. Xu, J.Z. Hu, M. Vijayakumar, J. Feng, M.Y. Hu, X. Deng, J. Xiao, and J. Liu, Towards high-performance nonaqueous redox flow electrolyte via ionic modification of active species. *Advanced Energy Materials*, 2015. 5(1): p. 1400678.
39. Ding, Y., Y. Zhao, Y. Li, J.B. Goodenough, and G. Yu, A high-performance all-metallocene-based, non-aqueous redox flow battery. *Energy & Environmental Science*, 2017. 10(2): pp. 491–497.
40. Zhang, C., L. Zhang, Y. Ding, X. Guo, and G. Yu, Eutectic electrolytes for high-energy-density redox flow batteries. *ACS Energy Letters*, 2018. 3(12): pp. 2875–2883.
41. Zhang, L., C. Zhang, Y. Ding, K. Ramirez-Meyers, and G. Yu, A low-cost and high-energy hybrid iron-aluminum liquid battery achieved by deep eutectic solvents. *Joule*, 2017. 1(3): pp. 623–633.
42. Zhang, C., Z. Niu, Y. Ding, L. Zhang, Y. Zhou, X. Guo, X. Zhang, Y. Zhao, and G. Yu, Highly concentrated phthalimide-based anolytes for organic redox flow batteries with enhanced reversibility. *Chem*, 2018. 4(12): pp. 2814–2825.
43. Yang, K., T. Zhang, Q. Li, Z. Peng, J. Ning, R. Sun, S. Jiang, and B. Li, Assembling-induced redox property adjustment of Fe (III)/Fe (IV) electroredox couple-based commercial dye catholyte via bio-inspired multicoordination sphere construction strategy for stable aqueous redox flow batteries. *Energy Storage Materials*, 2024. 71: p. 103648.
44. Wen, Y., J. Cheng, Y. Xun, P. Ma, and Y. Yang, Bifunctional redox flow battery: 2. V (III)/V (II)–l-cystine (O_2) system. *Electrochimica Acta*, 2008. 53(20): pp. 6018–6023.
45. Wen, Y., J. Cheng, P. Ma, and Y. Yang, Bifunctional redox flow battery-1 V (III)/V (II)–glyoxal (O2) system. *Electrochimica Acta*, 2008. 53(9): pp. 3514–3522.

CHAPTER 20

Emerging Applications of Flow Batteries

Arpana Agrawal

20.1 INTRODUCTION

To meet today's energy demands, several energy storage systems (metal-air batteries, metal-ion batteries, fuel cells, supercapacitors, flow batteries, etc.) have been invented and studied to improve their efficiency [1–6]. Among the various energy systems, flow batteries have nowadays gathered immense attention. Flow batteries are a type of rechargeable battery where energy storage and conversion occur in two separate components: the electrolyte-containing storage tanks and the electrochemical cell [7]. Unlike conventional batteries, such as lithium-ion batteries, where the energy is stored within the electrode materials themselves, flow batteries store energy in liquid electrolytes that flow through the electrochemical cell during charging and discharging cycles. The basic structure of a flow battery consists of two electrolyte solutions, each containing dissolved active materials (typically metal ions), separated by a membrane or separator. During operation, these electrolytes are pumped from their respective storage tanks into the electrochemical cell, where they undergo redox (reduction-oxidation) reactions. These reactions either store or release electrical energy, depending on whether the battery is being charged or discharged. The most common types of flow batteries include vanadium redox flow batteries (VRFBs) and zinc-bromine-flow batteries, each characterized by the specific redox pairs used in the electrolytes. Among these, VRFBs are much more popular.

One of the distinguishing features of flow batteries is their scalability. The energy capacity of the system is determined by the volume of the electrolyte storage tanks, while the power output is governed by the size and number of electrochemical cells. This decoupling of energy and power allows for flexible design and optimization based on specific application needs. Additionally, flow batteries have a long cycle life, as the electrode materials typically do not degrade as they do in solid-state batteries. Flow batteries have evolved significantly over the past fifty years, driven by extensive research focused on improving

DOI: 10.1201/9781003506379-20

their design, performance, and applicability across various sectors, including industrial, residential, and commercial loads, scalable flow batteries, and renewable energy sources, as shown in Figure 20.1 [8].

According to Li et al. [9], the development of advanced materials for battery separators has played a crucial role in enhancing the efficiency and longevity of flow batteries. Zhang et al. [10] provide an overview of the key advancements in flow battery technology, emphasizing the importance of innovative design strategies in achieving better energy storage solutions. Additionally, Daniel et al. [11] highlight the growing potential of redox flow batteries in industrial applications, pointing to future opportunities that could further expand their usage. The work of Tomazic and Skyllas-Kazacos [12] underscores the vital role of redox flow batteries in renewable energy integration and grid balancing, a field where these systems continue to show promise due to their scalability and flexibility.

Flow batteries offer notable advantages in scalability, allowing for independent scaling of energy capacity through increased electrolyte volume and power output by adding or

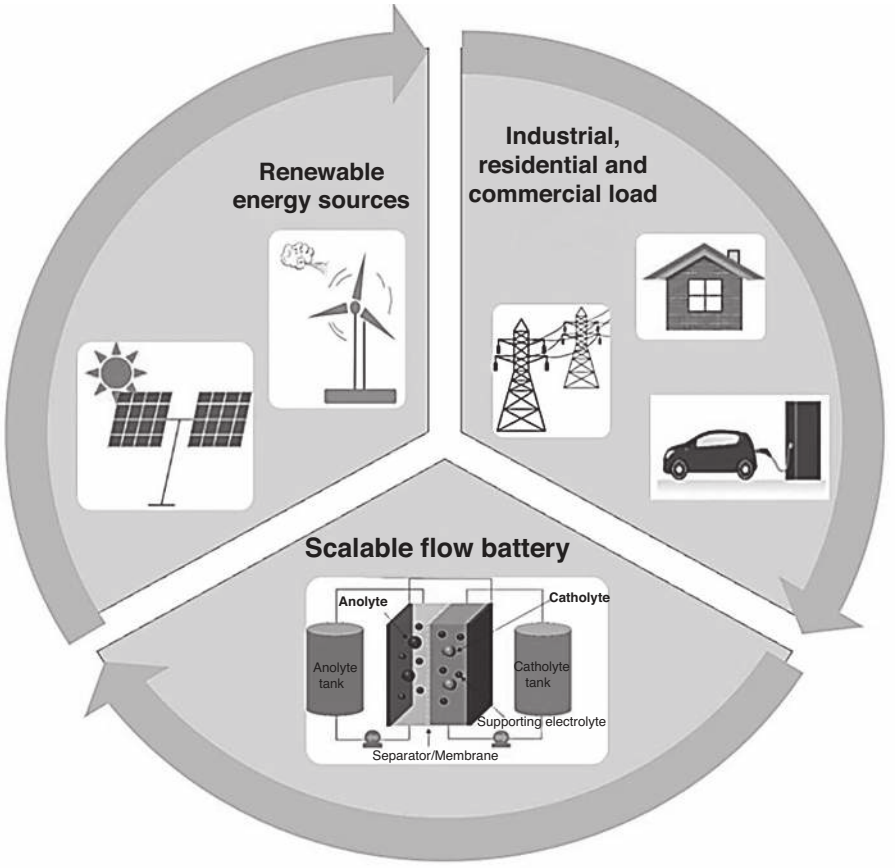

FIGURE 20.1 Emerging applications of flow batteries include industrial, residential, and commercial loads, scalable flow batteries, and renewable energy sources. (Adapted with permission from ref [8]. Copyright The Authors, some rights reserved; exclusive licensee [MDPI]. Distributed under a Creative Commons Attribution License 4.0 (CC BY) https://creativecommons.org/licenses/by/4.0/.)

enlarging electrochemical cells, making them ideal for large-scale energy storage applications like grid integration and renewable energy storage [8–10]. They also feature a long cycle life, often exceeding 10,000 cycles, due to the separation of electrolyte and electrode materials, which reduces degradation over time. Additionally, flow batteries enhance safety by operating at lower temperatures and using aqueous electrolytes, which minimize the risk of thermal runaway and fire. Their modular design facilitates easier maintenance and upgrades, enabling component replacement and system enhancements without the need for a complete overhaul, thus extending operational life and accommodating future technological advancements. Despite several advantages, there exist a few limitations, including lower energy density compared to other energy storage systems like lithium-ion batteries (LIBs), which necessitate larger storage tanks and make them less suitable for space-constrained applications such as electric vehicles. Their complexity and higher initial costs, due to the need for pumps, tanks, and additional components, can be a barrier to adoption, especially for smaller-scale applications, despite their lower long-term operational costs. The commercialization of flow batteries is also limited, with challenges in scaling production, a lack of standardized designs, and fewer established suppliers compared to more mature technologies like lithium-ion. Additionally, flow batteries typically have lower round-trip efficiency due to losses from electrolyte pumping, internal resistance, and other inefficiencies, presenting ongoing challenges for optimizing their overall performance.

This chapter examines the various applications of flow batteries, highlighting their significant contributions to stabilizing energy grids, integrating renewable energy sources, and improving industrial energy management. Their potential also spans transportation and mobility, including uses in heavy-duty vehicles, electric vehicles, and uninterrupted power supply (UPS). Despite challenges such as lower energy density and higher initial costs, materials science and system design advancements are driving their progress. Additionally, supportive market trends and policy frameworks are expected to boost the adoption of flow batteries. Looking ahead, the technology is set to play a vital role in the shift toward a sustainable, low-carbon energy future, fueled by innovations in hybrid systems, smart grid integration, and new materials.

20.2 ENERGY GRID INTEGRATION

Flow batteries play a crucial role in integrating renewable energy into the grid, stabilizing the grid, and optimizing grid operations through peak shaving and load leveling. Their ability to store and dispatch energy flexibly and reliably makes them an essential component of the modern, renewable-powered grid. Alotto et al. [13] provide a comprehensive review of flow batteries as a promising technology for renewable energy storage, highlighting their scalability, flexibility, and long cycle life, which make them suitable for large-scale applications. The review discusses the key components of flow batteries, including the electrolyte, membrane, and electrode materials, and analyzes the challenges related to energy density, cost, and system complexity. Leung et al. [14] examine the progress made in flow battery development, focusing on technological advancements, the challenges that remain in optimizing performance and cost-effectiveness, and their potential applications in grid-scale energy storage.

20.2.1 Role in Stabilizing the Electrical Grid

The electrical grid is a complex and dynamic system that requires a constant balancing of supply and demand to ensure reliable power delivery [7–9]. Traditional power generation methods, such as fossil fuel plants, can adjust output relatively easily to match demand. However, as renewable energy sources like solar and wind become more prevalent, the grid faces new challenges due to the intermittent and variable nature of these energy sources. Flow batteries offer a solution to these challenges by providing a reliable, flexible, and scalable energy storage system that can stabilize the grid in several key ways, including balancing supply and demand, frequency regulation, voltage support, grid resiliency, and deferring grid upgrades. Emmett and Roberts [15] discussed recent advancements in alternative aqueous redox flow batteries, emphasizing their suitability for grid-scale energy storage due to their safety, scalability, and environmental friendliness. Doetsch and Pohlig [16] provide an overview of the role of flow batteries in national grid energy storage, underscoring their potential to support the energy transition by offering reliable and flexible storage solutions. García-Quismondo et al. [17] detailed the operational experience of a 5 kW/5 kWh all-VRFB used in photovoltaic grid applications and provided insights into the performance, efficiency, and practical challenges of integrating VRFBs with solar power systems. Figure 20.2a provides a schematic representation of a vanadium battery, where two electrolyte solutions are stored in separate tanks and pumped through manifolds into half-cells separated by an ion-selective membrane, illustrating its operation during discharge. Figure 20.2b shows the voltage-time profile as a current of 100 A is applied to charge the battery. The current was held constant until a specific voltage level was reached, after which it was gradually reduced until the desired charge level was attained.

The research highlights how these batteries can effectively support photovoltaic grids by storing and stabilizing renewable energy, offering valuable data on their reliability and operational benefits in real-world scenarios. Flow batteries play a crucial role in energy grid integration by addressing multiple key challenges. They balance supply and demand by storing excess energy during periods of low demand or high renewable output and releasing it when demand increases or renewable generation drops, ensuring grid stability. Muñoz-Cruzado-Alba et al. [18] have presented a use-case study focused on the integration of acid-base flow battery technology into power grids, demonstrating the potential of this technology for enhancing grid stability and supporting renewable energy integration. Flow batteries also support voltage stability by supplying reactive power, which is essential for maintaining proper voltage levels and ensuring efficient operation of electrical equipment, especially in areas with significant renewable penetration or weak grid infrastructure. Behabtu et al. [19] review various energy storage technologies, including flow batteries, highlighting their application potential in enhancing the integration of renewable energy sources into power grids, with a focus on their ability to improve grid resilience and sustainability. Economic factors that influence the viability of flow batteries in grid applications have also been investigated [20]. The utilization of VRFBs for the integration of wind power into the grid has been explored, showcasing their potential to facilitate the smoother integration of intermittent renewable energy sources [21]. Kebede et al. [22] offer a comprehensive review of stationary energy storage devices, including flow batteries,

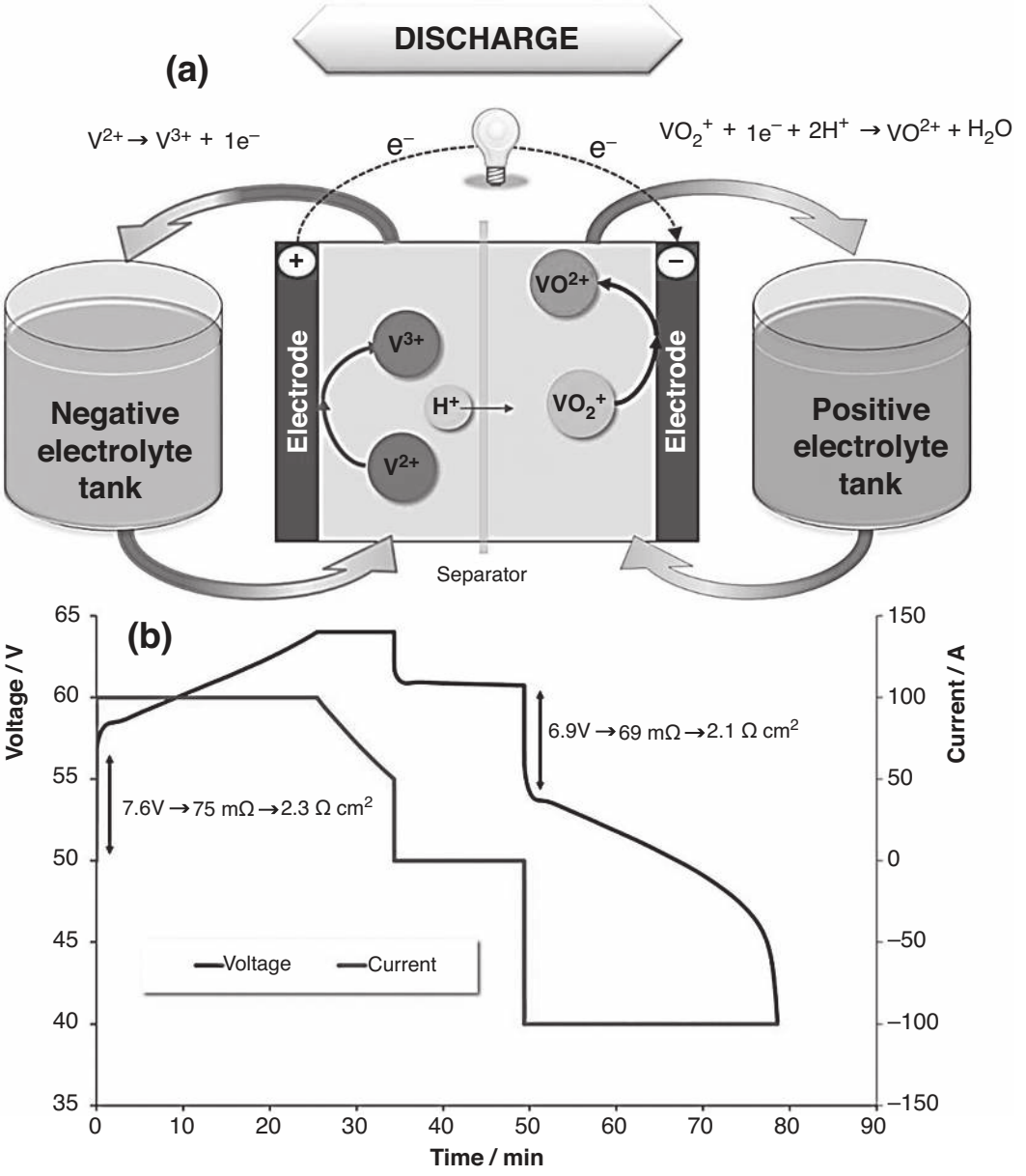

FIGURE 20.2 (a) Vanadium battery utilizing two electrolyte solutions stored in separate tanks, which are pumped through manifolds into half-cells separated by an ion-selective membrane, illustrating its discharge function. (b) Voltage-time profile during battery charging with a 100 A current. The current was kept constant until a specific voltage was reached, after which it was gradually reduced to achieve the target charge level. (Adapted with permission from ref [17]. Copyright The Authors, some rights reserved; exclusive licensee [MDPI]. Distributed under a Creative Commons Attribution License 4.0 (CC BY) https://creativecommons.org/licenses/by/4.0/.)

and their role in supporting large-scale renewable energy grid integration. Cho et al. [23] have investigated the optimization of hydrogen/bromine-flow batteries, another promising technology for grid-scale energy storage, focusing on their high-power capabilities and potential for enhancing grid reliability.

Additionally, flow batteries enhance grid resiliency by providing reliable backup power during outages, thanks to their long-duration storage capabilities, which help prevent blackouts and ensure a continuous power supply to critical infrastructure. Furthermore, they can defer the need for costly grid upgrades by managing peak loads and balancing supply and demand locally, thus reducing strain on aging infrastructure and extending its operational lifespan.

20.2.2 Applications in Renewable Energy Storage (Solar, Wind)

Renewable energy sources like solar and wind are key components of the transition to a low-carbon energy system. However, their intermittent nature presents significant challenges for grid integration. Flow batteries offer a promising solution for storing and managing renewable energy, enabling a more reliable and efficient use of these resources [24]. Flow batteries also play a pivotal role in optimizing the integration of renewable energy by addressing several key challenges. They smooth renewable energy output by storing excess energy from variable sources like solar and wind during periods of high generation and releasing it when generation drops, thus ensuring a more consistent and predictable power supply and reducing reliance on fossil fuel backup. This capability enables higher renewable penetration by providing long-duration storage that absorbs large amounts of energy when generation is high and discharges it during low generation periods, which is crucial for balancing the intermittency of sources such as wind power, which may generate more energy at night.

Li and Jin [24] discussed the design principles and recent advancements in integrated solar flow batteries, focusing on the integration of solar energy harvesting with flow battery technology to create a sustainable and efficient energy storage solution. They explore various approaches to optimize the integration of photovoltaic cells with flow batteries, highlighting the potential for these systems to enhance energy storage efficiency and reduce reliance on conventional power sources. Lu et al. [25] provide a mini-review that examines the materials, performance, and system design considerations for integrated solar flow batteries and emphasize the importance of material selection and system architecture in improving the overall performance and durability of these energy storage systems. Parmeshwarappa et al. [26] have focused on the practical aspects of integrating flow batteries with solar photovoltaic systems and residential loads. They discussed power and energy rating considerations, underscoring the importance of properly sizing and configuring these systems to meet the dynamic demands of residential energy consumption while maximizing the benefits of renewable energy integration. Li et al. [27] present a monolithically integrated solar flow battery comprising an III-V tandem cell photoelectrode paired with 4-OH-TEMPO/MVCl2 redox couples (as shown in Figure 20.3a) with an efficiency of

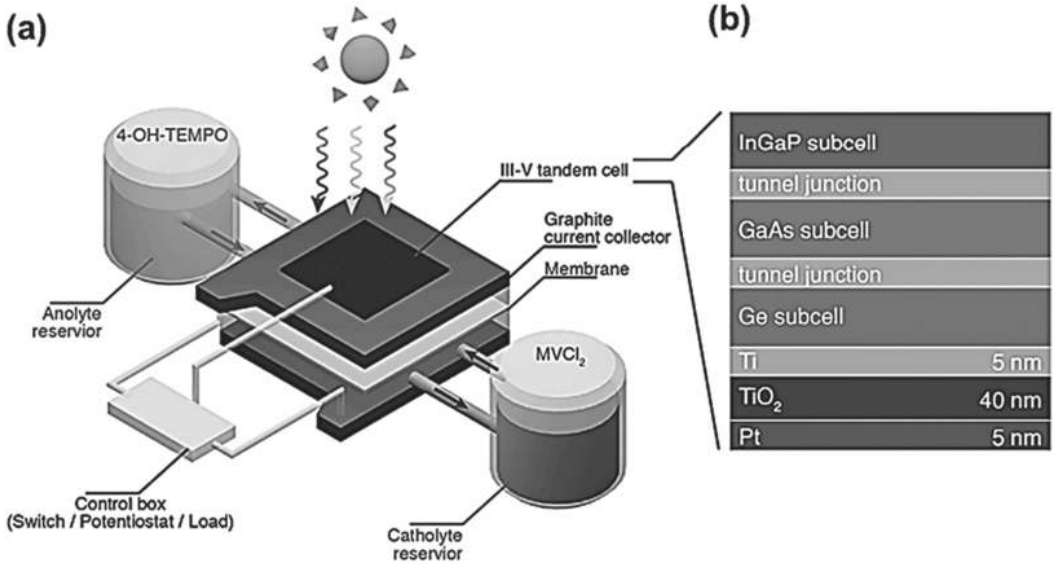

FIGURE 20.3 (a) Design of integrated solar flow battery device utilizing an III-V tandem cell photoelectrode paired with 4-OH-TEMPO/MVCl2 redox couples. (b) Structure of the photoelectrode, featuring an InGaP/GaAs/Ge tandem solar cell with Ti/TiO_2/Pt protective layers on the Ge bottom cell. (Adapted with permission [27], Copyright (2018), Elsevier.)

14.1% and explore the innovative integration of solar and flow battery technologies into a single system. The structure of the photoelectrode, featuring an InGaP/GaAs/Ge tandem solar cell with Ti/TiO_2/Pt protective layers on the Ge bottom cell, has been illustrated in Figure 20.3b. This approach aims to optimize energy conversion and storage efficiency by combining photovoltaic cells with flow battery technology, resulting in a more efficient and compact energy storage solution.

In remote or off-grid areas, flow batteries enhance the reliability and sustainability of power systems by storing energy from renewables and providing continuous power when generation is low, which is essential for microgrids. Additionally, they facilitate renewable energy trading by allowing energy to be stored and dispatched at optimal times, thus maximizing its economic value.

Banham-Hall et al. [28] have explored the use of flow batteries to enhance the integration of wind power into the electrical grid and examined the variability and intermittency of wind energy by providing reliable energy storage that can balance supply and demand. They highlighted the potential of flow batteries to improve grid stability, reduce curtailment of wind power, and enable higher penetration of renewable energy sources. Moreover, flow batteries help mitigate curtailment, which occurs when renewable energy generation exceeds grid capacity, by storing excess energy that would otherwise be wasted and making it available for future use, thereby improving the efficiency and return on investment of renewable energy projects.

20.2.3 Peak Shaving and Load Leveling

Peak shaving and load leveling are two critical applications of flow batteries that help optimize grid operations and reduce costs for both utilities and consumers. Flow batteries are highly effective in peak shaving, load leveling, and enhancing demand response programs, offering significant economic and operational benefits. In peak shaving, flow batteries help reduce grid electricity consumption during high-demand periods by storing energy during off-peak hours when electricity is cheaper and discharging it during peak times. This not only lowers electricity costs but also reduces the necessity for additional, often less efficient, power plants, leading to more efficient grid operations. For load leveling, flow batteries balance the grid load by storing excess energy during periods of low demand and discharging it during high-demand periods. Their ability to store and release large amounts of energy over extended durations helps alleviate stress on the grid, reduces the need for peaking power plants, and improves overall grid efficiency.

Ouyang et al. [29] explore the use of flow battery energy storage systems in microgrids, demonstrating how predictive control algorithms can optimize peak shaving to enhance energy efficiency and reliability. Lucas and Chondrogiannis [30] developed a smart grid energy storage controller using VRFBs to achieve both frequency regulation and peak shaving.

Their study presents a MATLAB/Simulink model that demonstrates how a VRFB-based storage system can deliver multiple ancillary services, specifically focusing on frequency regulation and peak shaving. Figure 20.4a illustrates the schematic diagram of the proposed vanadium flow battery system. The model is designed for a medium-voltage substation and considers a load profile from a residential neighborhood along with a demand

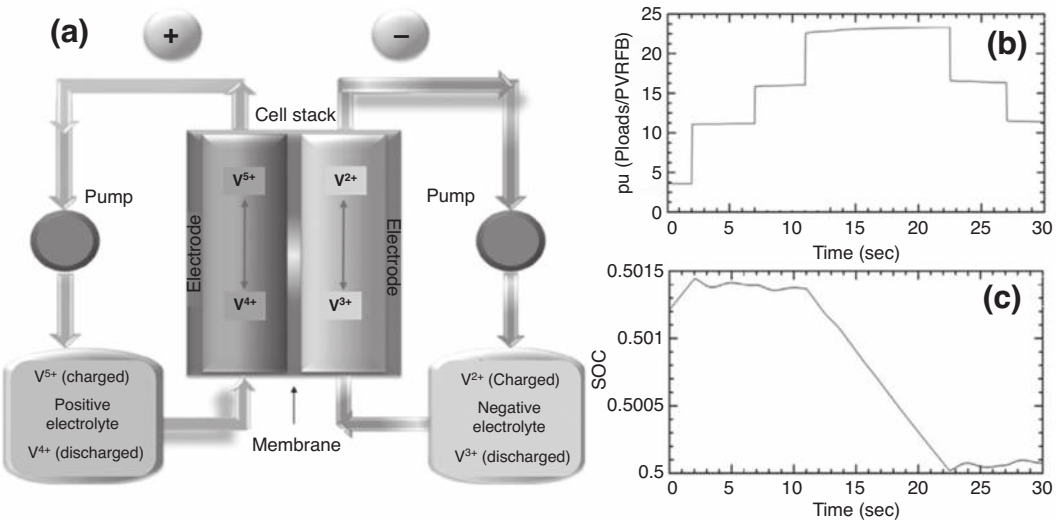

FIGURE 20.4 (a) Schematic representation of a vanadium flow battery system. (b) System power per unit (pu), showing the ratio of load power demand to the storage system's nominal power. (c) Charging and discharging behavior of the storage system throughout the simulation. (Adapted with permission [30], Copyright (2016), Elsevier.)

from fast charging stations. An integrated inverter controller is included to manage the net power output of the battery system, enabling the simultaneous provision of both services. Figure 20.4c illustrates the battery's charging behavior in response to the load power demand shown in Figure 20.4b. In this case, the battery's power supply or demand has minimal impact on the state of charge (SOC) due to the short duration of the simulation (30 s). However, two main trends in power output can be observed. The first trend occurs during the initial 12 s of the simulation when the battery is instructed to charge. The second trend begins after 12 s, when the battery starts supplying energy to the system, thereby reducing power output from the grid and effectively performing peak shaving.

Economically, these applications lead to cost savings for utilities by reducing the reliance on expensive peaking power plants and minimizing wear on infrastructure, while consumers benefit from lower electricity bills, especially in time-of-use pricing markets. Additionally, flow batteries support demand response programs by providing a reliable source of stored energy that enables consumers to adjust their usage without compromising comfort, thereby assisting utilities in managing demand more effectively and reducing the need for additional generation capacity.

20.3 INDUSTRIAL APPLICATIONS

Flow batteries offer significant benefits for industrial applications, from large-scale energy storage and cost management to providing reliable backup power and integrating with microgrids. Their flexibility, scalability, and long-duration storage capabilities make them an ideal choice for industries seeking to enhance energy efficiency, reduce costs, and ensure continuous operation.

20.3.1 Backup Power for Critical Infrastructure

Critical infrastructure, such as hospitals, data centers, and water treatment plants, requires a reliable and UPS. Power outages or fluctuations can lead to catastrophic failures, significant financial losses, or even endanger lives. Flow batteries offer a robust solution for providing backup power to these essential facilities. Flow batteries offer significant advantages for UPS systems by providing extended backup durations during grid failures, unlike traditional UPS solutions that rely on lead-acid or LIBs with limited capacity. They excel in delivering long-duration backup power, making them ideal for critical facilities that need to remain operational for several hours or even days during emergencies such as natural disasters or cyberattacks. Kuzmin et al. [31] investigate the application of flow batteries as a source for autonomous power supply systems, emphasizing their potential to provide reliable and consistent energy for off-grid applications. The study highlights the adaptability of flow batteries in maintaining power stability in isolated settings. Similarly, Trovò [32] discusses the battery management systems (BMS) tailored for industrial-scale VRFBs, focusing on their critical role in ensuring the efficient operation and longevity of the system. Panwar et al. [33] have explored the integration of flow batteries into advanced distribution grids, demonstrating the contribution of these batteries in enhancing grid resilience, particularly in response to disruptions and peak demand scenarios.

Flow batteries can enhance grid independence by storing energy from on-site renewable sources or alternative power supplies, allowing critical infrastructure to operate without

relying on external grids, which is especially valuable in remote or disaster-prone areas with unreliable grid connections. Additionally, flow batteries offer reduced maintenance and lifecycle costs compared to other battery technologies due to their lower maintenance needs and longer operational lifespans. Their modular design facilitates easy upgrades and component replacements, further extending their useful life. Moreover, flow batteries help ensure compliance with stringent regulatory standards for power reliability and emergency preparedness, making them particularly relevant for sectors like healthcare and finance, where uninterrupted operations are essential.

20.3.2 Integration with Microgrids

Microgrids are localized energy systems that can operate independently or in conjunction with the main grid. They are increasingly being used in industrial settings to improve energy reliability, integrate renewable energy sources, and reduce dependence on the central grid. Flow batteries significantly enhance the stability and efficiency of industrial microgrids by addressing several key challenges. They stabilize microgrids by storing excess renewable energy and discharging it when needed, ensuring a consistent and reliable power supply, which is essential for maintaining production and operational efficiency in industrial settings. Their ability to integrate with renewable energy sources like solar or wind supports the transition to sustainable operations by maximizing renewable utilization and reducing reliance on fossil fuels, thereby helping achieve environmental goals. Xiong et al. [34] have focused on a two-stage control strategy designed for VRFBs, optimizing their performance for grid applications by ensuring efficient energy management and grid stability. Tang et al. [35] have evaluated the capital costs of both conventional and emerging redox flow batteries, providing insights into the financial feasibility of deploying these technologies for grid storage. Additionally, flow batteries are crucial for enabling islanded operation, allowing microgrids to function independently from the main grid during outages or disturbances, which is especially valuable in preventing costly downtime or equipment damage. Serban and Marinescu [36] presented a control strategy for three-phase battery energy storage systems, aimed at providing frequency support in microgrids while ensuring an UPS to local loads. Their work underscores the importance of robust control mechanisms in optimizing the performance of battery systems in complex grid environments.

Flow batteries also contribute to demand response and load management by adjusting power output based on grid signals and smoothing demand spikes, thus enhancing overall microgrid efficiency and providing potential financial benefits through energy market participation. The scalability and modular design of flow batteries make them adaptable to varying energy needs within microgrids, allowing for expansion as energy demands increase. Furthermore, flow batteries bolster energy resilience and security by providing a reliable backup power source during grid failures, equipment malfunctions, or emergencies, ensuring uninterrupted industrial operations and minimizing financial losses.

20.4 TRANSPORTATION AND MOBILITY

20.4.1 Potential Use in Electric Vehicles (EVs)

EVs are at the forefront of the transition to sustainable transportation, driven by the need to reduce greenhouse gas emissions and decrease reliance on fossil fuels [37]. While LIBs have become the standard for EVs due to their high energy density and established supply chains, flow batteries are being explored as a potential alternative or complement in specific use cases. They enable range extension by allowing EVs to combine the steady, long-duration driving capabilities of flow batteries with the high-power performance of traditional LIBs, thus extending driving range without the need for larger, heavier LIBs. Additionally, flow batteries could revolutionize rapid refueling by enabling quick exchanges or replenishment of liquid electrolytes at refueling stations, akin to current gasoline or hydrogen refueling processes, which could significantly reduce downtime and make EVs more practical for long-distance travel [38]. Their longer cycle life, often reaching tens of thousands of charge/discharge cycles without significant degradation, is advantageous for fleets or high-utilization scenarios where battery longevity is crucial for reducing overall costs.

Cunha et al. [37] have assessed the feasibility of using VRFBs for energy storage and fast charging of EVs at gas stations, highlighting the potential of VRFBs to support the growing demand for EV infrastructure. The study emphasizes the advantages of VRFBs, such as their scalability, long cycle life, and ability to provide high-power output, making them suitable for both energy storage and rapid charging applications. Mohamed et al. [39] have explored the challenges and progress in adapting redox flow batteries for hybrid electric vehicles (EVs), addressing issues like system integration, energy density, and cost-effectiveness. Barelli et al. [40] have studied the application of VRFBs for electric bus propulsion and also examined the performance of hybrid energy storage systems. They highlighted the integration of VRFBs with other energy storage technologies for improving electric buses' efficiency and operational capability. They have modeled a hybrid $LiFePO_4$/VRFB battery based on available experimental data and tested it with an active area of 12 cm^2. Figure 20.5 presents a schematic diagram of a modeled hybrid battery, featuring a layered structure that includes aluminum plates, a copper plate serving as the current collector, a graphite plate, a Teflon gasket, a carbon felt, and a Nafion 115 membrane. By analyzing various performance metrics, the study assesses the potential benefits of VRFBs in providing reliable and sustained power for electric bus fleets, focusing on aspects such as energy density, cost-effectiveness, and overall system performance in real-world applications.

Tolmachev et al. [41] have discussed the potential of high-specific-energy aqueous flow batteries for fully EVs, proposing their use not only for vehicular applications but also for direct solar-to-chemical energy conversion. Katsoudas et al. [42] further explore the integration of flow batteries into EVs, discussing the feasibility and future potential of this technology in advancing sustainable transportation solutions.

Flow batteries also enhance thermal management and safety, operating at lower temperatures and being less prone to thermal runaway, which mitigates risks of fires in vehicle accidents and boosts consumer acceptance and regulatory compliance. However,

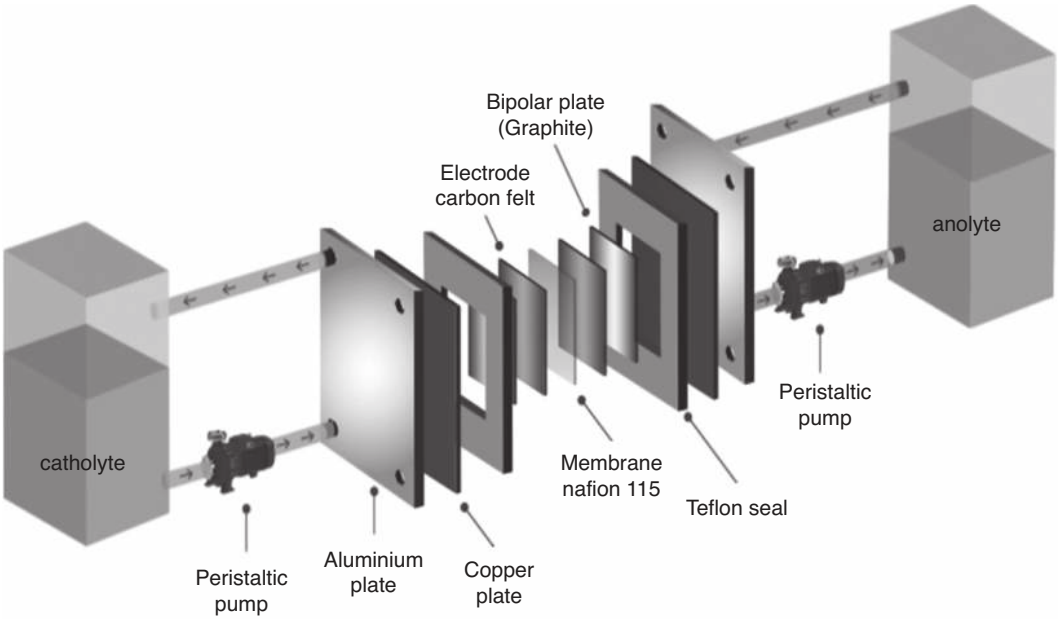

FIGURE 20.5 Exploded view of a VRFB. (Adapted with permission [40], Copyright (2019), Elsevier.)

challenges persist, particularly due to their lower energy density compared to LIBs. The current size and weight of flow battery systems, including tanks and pumps, make them less suitable for passenger vehicles, where space and weight are critical. Ongoing research is focused on improving their energy density and simplifying their systems to enhance their viability for future EV applications.

20.4.2 Hybrid Systems for Heavy-Duty Vehicles

Heavy-duty vehicles, such as trucks, buses, and construction machinery, have different energy demands compared to passenger cars. These vehicles require high power for acceleration and load carrying, as well as long-range capabilities, making them prime candidates for hybrid energy storage systems that combine the strengths of different battery technologies. Wang et al. [43] have explored the integration of lithium-based redox flow batteries with hybrid electrolytes, highlighting their position at the intersection of lithium-ion and traditional redox flow technologies. This hybrid approach seeks to combine the advantages of both technologies, potentially enhancing performance and application versatility. Ventosa et al. [44] have also presented a study on aqueous mixed-cation semi-solid hybrid-flow batteries, emphasizing their innovative design and the benefits of combining various cation types to improve battery performance and stability. Khor et al. [45] have reviewed zinc-based hybrid-flow batteries, detailed their fundamental principles and various applications, and assessed their potential to address key challenges in energy storage. Schubert et al. [46] have discussed the latest developments in hybrid energy storage systems based on redox flow batteries, outlining the ongoing challenges and future

directions for these systems, including improvements in efficiency, cost, and integration with other energy storage technologies.

In heavy-duty vehicles, integrating flow batteries with high-power LIBs offers a hybrid system that optimizes both power and energy flexibility. The flow battery can manage energy-intensive tasks such as long-distance driving and high auxiliary power demands during idle periods, while the lithium-ion battery provides the high power needed for acceleration and dynamic load management. This synergy enhances vehicle performance and efficiency across various driving conditions. Campillo et al. [47] have investigated the potential applications of flow batteries in heavy vehicles, focusing on their use in enhancing energy storage solutions for large-scale transportation systems.

Additionally, flow battery systems facilitate the electrification of heavy-duty vehicles, contributing to significant reductions in fuel consumption and emissions, which is crucial for sectors like freight, public transit, and construction, which are major contributors to greenhouse gas emissions. The extensive energy storage capacity of flow batteries supports extended range and operating hours, making them ideal for long-haul trucks and equipment operating in remote areas with limited charging infrastructure. Their durability and low maintenance requirements, due to their long operational life and reduced degradation, offer considerable advantages in demanding environments, minimizing downtime and operational costs. However, challenges persist due to their lower energy density and the additional weight and space required for components like pumps and tanks, which could impact payload capacity and efficiency. Despite these issues, flow batteries present a promising solution for enhancing the performance and sustainability of heavy-duty vehicles, particularly where space and weight constraints are less critical.

20.5 REMOTE AND OFF-GRID POWER SOLUTIONS

Flow batteries offer significant potential for remote and off-grid power solutions, providing reliable and sustainable energy storage for remote communities, off-grid renewable energy systems, and critical applications in military and disaster relief operations. Their scalability, durability, and ability to integrate with renewable energy sources make them an ideal choice for powering areas and operations where access to the grid is limited or nonexistent. Remote communities, often located in isolated or hard-to-reach areas, face significant challenges in accessing reliable and affordable energy. These areas are typically disconnected from centralized power grids, relying instead on diesel generators or other conventional energy sources that are costly, environmentally damaging, and logistically difficult to maintain. Flow batteries offer a promising solution for providing sustainable and reliable energy storage in these remote settings.

Flow batteries offer a robust solution for providing reliable power to remote communities, significantly improving their energy security by storing energy from local renewable sources like solar or wind and ensuring availability even during periods of low generation. Their modular design allows for scalability, making it possible to customize the size of the system to fit the specific needs of various community sizes—from small villages to larger,

industrialized areas. Economically, flow batteries help reduce the operating costs associated with diesel generators, cutting fuel and maintenance expenses while also decreasing environmental impact by promoting the use of clean energy. Their long lifespan and low maintenance requirements are particularly advantageous for remote locations where technical support is limited, ensuring continuous service with minimal intervention. Additionally, by providing a stable power supply, flow batteries can stimulate local economic development, supporting small businesses, agricultural activities, and essential services like healthcare and education, while reducing reliance on external fuel sources and keeping more economic resources within the community.

Off-grid renewable energy systems are also becoming increasingly important as the world seeks to expand access to clean energy while reducing greenhouse gas emissions. Flow batteries play a critical role in these systems by providing the necessary energy storage to ensure that renewable energy can be used even when the sun isn't shining or the wind isn't blowing. Flow batteries are exceptionally well-suited for integration with solar and wind power systems in off-grid settings, as they can store surplus energy generated during peak renewable production and release it when demand exceeds supply, thus ensuring a stable and reliable power supply even amidst variable renewable output. This capability allows off-grid renewable systems to deliver consistent electricity without relying on fossil fuels or external grid connections. In hybrid off-grid applications, flow batteries enhance energy management by balancing the energy mix, ensuring efficient use of various sources like small-scale hydropower, biomass, or diesel generators, and reducing reliance on less sustainable options. The inclusion of flow batteries in off-grid systems provides greater energy independence and resilience, crucial for communities and critical infrastructure in remote areas, as it mitigates vulnerabilities to external supply disruptions. Environmentally, these systems significantly lower greenhouse gas emissions by replacing fossil fuel-based generators, improving air and water quality, and supporting sustainable development by delivering clean energy to underserved populations while preserving local ecosystems. Despite these benefits, challenges such as high initial capital costs, material availability, and technical expertise for installation and maintenance persist. Addressing these challenges through collaborative efforts from governments, NGOs, and the private sector—by providing financing, training, and support services—can make flow battery systems more accessible and affordable for off-grid communities, facilitating broader adoption and impact.

20.6 CHALLENGES AND FUTURE PROSPECTS

While flow batteries offer many advantages in energy storage, several limitations and technical challenges must be addressed to fully realize their potential across various applications. The relatively low energy density compared to technologies like LIBs limits their suitability for space-constrained applications such as EVs and portable power solutions. Their initial capital costs are also high due to the expense of large tanks, pumps, and other components required for electrolyte storage and circulation, making them less attractive for projects with short-term financial constraints despite their lower operating costs and longer lifespans. The complexity of flow battery systems, involving numerous components

such as pumps and valves, results in increased maintenance requirements and operational challenges, potentially adding to the overall cost and complexity of managing the system. Material availability and sustainability issues, particularly concerning vanadium used in VRFBs, pose challenges due to fluctuating supply and environmental impacts. Additionally, managing the electrolyte in flow batteries is complex, with issues like degradation, cross-contamination, and the need for precise flow control affecting system efficiency and longevity. Ongoing research aims to address these challenges by developing advanced materials and management techniques to improve flow battery performance and viability.

The adoption and expansion of flow battery technology are also influenced by various market and policy drivers that shape the energy storage landscape. The increasing global demand for renewable energy integration is a primary driver for flow battery technology, as these systems provide reliable, long-duration storage essential for balancing the intermittent nature of solar and wind power. Supportive policy and regulatory frameworks, including tax credits and subsidies, further enhance the attractiveness of flow batteries by reducing financial barriers and fostering investment. The ongoing grid modernization and decentralization efforts also create opportunities for flow batteries to offer crucial storage and balancing services in evolving grid systems and microgrids, especially in remote areas. Growing emphasis on decarbonization and sustainability is driving interest in flow batteries, given their low environmental impact and capability to facilitate high renewable energy penetration, aligning with ambitious carbon reduction targets. Additionally, corporations and industrial sectors are increasingly incorporating flow batteries into their energy strategies to reduce costs, enhance resilience, and meet sustainability objectives, solidifying their role in large-scale energy storage solutions.

The future of flow battery technology is shaped by ongoing research, technological advancements, and evolving market dynamics. Several key trends and research directions are expected to influence the development and adoption of flow batteries in the coming years. Advancements in materials science are poised to significantly enhance flow battery technology by exploring alternative, cost-effective, and environmentally friendly electrolytes, such as organic and aqueous solutions, while innovations in membrane and electrode materials promise higher energy densities and longer lifespans. The development of hybrid-flow battery systems that combine flow batteries with high-energy-density technologies like LIBs could offer both rapid power bursts and long-duration storage, broadening their application range and enhancing flexibility. Scaling up production and reducing costs through economies of scale, improved designs, and manufacturing innovations are crucial for making flow batteries more competitive. Integration with smart grid technologies and digital energy management systems will optimize performance, providing valuable grid services and increasing their appeal to grid operators. Expansion into new markets, including transportation, data centers, and residential storage, alongside the development of compact, portable systems, will diversify flow battery applications. Collaboration between industry, academia, and government, supported by policy incentives and research funding, is essential for accelerating innovation and adoption. Addressing environmental and social considerations, such as sustainable raw material sourcing, minimizing manufacturing

impacts, and enhancing accessibility for developing regions, will be critical for the technology's global impact and sustainability.

20.7 CONCLUSION

Flow batteries are a versatile and promising energy storage technology with significant potential across various sectors. They offer long-duration storage, high cycle life, and scalability, making them ideal for grid stabilization, renewable energy integration, and industrial applications. Their ability to provide reliable backup power and support for microgrids further enhances their appeal, especially in sectors like transportation, where they could contribute to the electrification of heavy-duty vehicle applications. Despite current challenges like energy density and initial costs, ongoing research and supportive policies are driving advancements, positioning flow batteries as a key technology in the transition to a sustainable, low-carbon energy future.

Looking ahead, the future of flow batteries in emerging applications is bright, driven by continuous innovation and a growing demand for sustainable energy solutions. As research addresses current technical challenges, such as improving energy density and reducing costs, flow batteries are expected to become more competitive and accessible across a wider range of applications. Market trends, such as the increasing focus on renewable energy integration and grid modernization, will further drive the adoption of flow batteries, particularly in large-scale energy storage, industrial settings, and grid services. Additionally, as the world moves toward decarbonization and net-zero emissions, flow batteries are poised to play a crucial role in enabling a more resilient and sustainable energy infrastructure. Their potential for integration with smart grids, hybrid systems, and new materials will continue to expand their use cases, making them an integral part of the future energy landscape.

REFERENCES

1. A.C.M. Hussain, Green and sustainable metal-air batteries for powering flexible wearable electronics: Current status and future prospects, *Sustain. Energy Fuels*, *8* (2024) 4687–4708.
2. A. Agrawal, Multi-atom catalysts for metal-air batteries, in *Atomically Precise Electrocatalysts for Electrochemical Energy Applications*, R. Gupta (Ed.) (pp 365–381). Springer Nature, 2024.
3. A. Agrawal, C.M. Hussain, Metal-air batteries for wearable electronics: A case study for modern society, in *Next-generation of Human Resources and Technologies*, C.M. Hussain, A. Petrillo & S.U. Islam (Eds.) (15 pages). CRC Press, 2023.
4. A. Agrawal, Polymer materials for metal-air battery, in *Recent Advancements in Polymeric Materials for Electrochemical Energy Storage*, R. Gupta (Ed.) (pp. 367–381). Springer Nature, 2023.
5. A. Agrawal, C.M. Hussain, Wearable metal-air batteries, in *The Handbook of Metal-Air Batteries: Principles, Progresses and Perspective*, R. Gupta (Ed.) (12 pages). CRC Press, 2023.
6. A. Agrawal, Graphene-based nanomaterials for battery applications, in *Handbook of Energy Applications of 2D Nanomaterials*, R. Gupta (Ed.) (17 Pages). CRC Press, 2022.
7. T. Nguyen, R.F. Savinell, Flow batteries. *Electrochem. Soc. Interface*, *19*(3) (2010) 54.
8. A.G. Olabi, M.A. Allam, M.A. Abdelkareem, T.D. Deepa, A.H. Alami, Q. Abbas, A. Alkhalidi, E.T. Sayed, Redox flow batteries: Recent development in main components, emerging technologies, diagnostic techniques, large-scale applications, and challenges and barriers, *Batteries*, *9*(8) (2023) 409.

9. J. Li, M. Al-Yasiri, H. Pham, J. Park, Redox flow batteries. In *Adv. Mater. Battery Separators*, Sabu Thomas, Didier Rouxel, Nandakumar Kalarikkal, Bicy Kottathodi, Hanna J. Maria (Eds.) (pp. 327–347). Elsevier, 2024.
10. C. Zhang, Z. Yuan, X. Li, Designing better flow batteries: An overview on fifty years' research. *ACS Energy Lett.*, *9*(7) (2024) 3456–3473.
11. M. Daniel, N.P. Byron, C.M. Krowne, Harnessing redox flow batteries for industrial applications: Opportunities and future directions. *J. Power Sources*, *591* (2024) 233889.
12. G. Tomazic, M. Skyllas-Kazacos, Redox flow batteries, in *Electrochemical Energy Storage for Renewable Sources and Grid Balancing*, Patrick T. Moseley, Jürgen Garche (Eds) (pp. 309–336). Elsevier, 2015.
13. P. Alotto, M. Guarnieri, F. Moro, Redox flow batteries for the storage of renewable energy: A review. *Renew. Sust. Energy Rev.*, *29* (2014) 325–335.
14. P. Leung, X. Li, C.P. De León, L. Berlouis, C.J. Low, F.C. Walsh, Progress in redox flow batteries, remaining challenges and their applications in energy storage. *RSC Adv., 2*(27) (2012) 10125–10156.
15. R.K. Emmett, M.E. Roberts, Recent developments in alternative aqueous redox flow batteries for grid-scale energy storage. *J. Power Sources*, *506* (2021) 230087.
16. C. Doetsch, A. Pohlig, The use of flow batteries in storing electricity for national grids, in *Future Energy* Trevor M. Letcher (Ed.) (pp. 263–277). Elsevier, 2020.
17. E. García-Quismondo, I. Almonacid, M.A. Cabañero Martínez, V. Miroslavov, E. Serrano, J. Palma, J.P. Alonso Salmerón, Operational experience of 5 kW/5 kWh all-vanadium flow batteries in photovoltaic grid applications. *Batteries*, *5*(3) (2019) 52.
18. J. Muñoz-Cruzado-Alba, R. Musca, J. Ballestín-Fuertes, J.F. Sanz-Osorio, D.M. Rivas-Ascaso, M.P. Jones, A. Catania, E. Goosen, Power grid integration and use-case study of acid-base flow battery technology. *Sustainability*, *13*(11) (2021) 6089.
19. H.A. Behabtu, M. Messagie, T. Coosemans, M. Berecibar, K. Anlay Fante, A.A. Kebede, J.V. Mierlo, A review of energy storage technologies' application potentials in renewable energy sources grid integration. *Sustainability*, *12*(24) (2020) 10511.
20. S. Ha, K.G. Gallagher, Estimating the system price of redox flow batteries for grid storage. *J. Power Sources*, *296* (2015) 122–132.
21. B. Türker, *Modeling and utilizing a vanadium redox flow battery for easier grid and market integration of wind power* (Doctoral dissertation, Universität Bremen), 2014.
22. A.A. Kebede, T. Kalogiannis, J. Van Mierlo, M. Berecibar, A comprehensive review of stationary energy storage devices for large scale renewable energy sources grid integration. *Renew. Sust. Energy. Rev*, *159* (2022) 112213.
23. K.T. Cho, P. Albertus, V. Battaglia, A. Kojic, V. Srinivasan, A.Z. Weber, Optimization and analysis of high-power hydrogen/bromine-flow batteries for grid-scale energy storage. *Energy Technol.*, *1*(10) (2013) 596–608.
24. W. Li, S. Jin, Design principles and developments of integrated solar flow batteries. *Acc. Chem. Res.*, *53*(11) (2020) 2611–2621.
25. P. Lu, P. Leung, H. Su, W. Yang, Q. Xu, Materials, performance, and system design for integrated solar flow batteries–A mini review. *Appl. Energy*, *282* (2021) 116210.
26. P. Parmeshwarappa, R. Gundlapalli, S. Jayanti, Power and energy rating considerations in integration of flow battery with solar PV and residential load. *Batteries*, *7*(3) (2021) 62.
27. W. Li, H.C. Fu, Y. Zhao, J.H. He, S. Jin, 14.1% efficient monolithically integrated solar flow battery. *Chem*, *4*(11) (2018) 2644–2657.
28. D.D. Banham-Hall, G.A. Taylor, C.A. Smith, M.R. Irving, Flow batteries for enhancing wind power integration. *IEEE Trans. Power Syst.*, *27*(3) (2012) 1690–1697.
29. T. Ouyang, M. Zhang, P. Qin, X. Tan, Flow battery energy storage system for microgrid peak shaving based on predictive control algorithm. *Appl. Energy*, *356* (2024) 122448.

30. A. Lucas, S. Chondrogiannis, Smart grid energy storage controller for frequency regulation and peak shaving, using a vanadium redox flow battery. *Int. J. Electr. Power Energy Syst.*, *80* (2016) 26–36.
31. I. Kuzmin, A. Loskutov, E. Osetrov, A. Kurkin, Source for autonomous power supply system based on flow battery. *Energies*, *15*(9) (2022) 3027.
32. A. Trovò, Battery management system for industrial-scale vanadium redox flow batteries: Features and operation. *J. Power Sources*, *465* (2020) 228229.
33. M. Panwar, S. Chanda, M. Mohanpurkar, Y. Luo, F. Dias, R. Hovsapian, A.K. Srivastava, Integration of flow battery for resilience enhancement of advanced distribution grids. *Int. J. Electr. Power Energy Syst.*, *109* (2019) 314–324.
34. B. Xiong, J. Tang, Y. Li, C. Xie, Z. Wang, X. Zhang, H.B. Gooi, Design of a two-stage control strategy of vanadium redox flow battery energy storage systems for grid application. *IEEE Trans. Sustainable Energy*, *13*(4) (2022) 2079–2091.
35. L. Tang, P. Leung, M.R. Mohamed, Q. Xu, S. Dai, X. Zhu, C. Flox, A.A. Shah, Q. Liao, Capital cost evaluation of conventional and emerging redox flow batteries for grid storage applications. *Electrochim. Acta*, *437* (2023) 141460.
36. I. Serban, C. Marinescu, Control strategy of three-phase battery energy storage systems for frequency support in microgrids and with uninterrupted supply of local loads. *IEEE Trans. Power Electron.*, *29*(9) (2013) 5010–5020.
37. Á. Cunha, F.P. Brito, J. Martins, N. Rodrigues, N., Monteiro, V., Afonso, J. L., & Ferreira, P. Assessment of the use of vanadium redox flow batteries for energy storage and fast charging of electric vehicles in gas stations. *Energy*, *115* (2016): 1478–1494.
38. J. Jorné, Flow Batteries: Rechargeable batteries with circulating electrolyte are being developed for use in electric vehicles and to meet fluctuating demand at power stations. *American Scientist*, *71*(5) (1983) 507–513.
39. M.R. Mohamed, S.M. Sharkh, F.C. Walsh, Redox flow batteries for hybrid electric vehicles: Progress and challenges. In *2009 IEEE Vehicle Power and Propulsion Conference* (pp. 551–557), 2009, September. IEEE.
40. L. Barelli, G. Bidini, P.A. Ottaviano, D. Pelosi, Vanadium redox flow batteries application to electric buses propulsion: Performance analysis of hybrid energy storage system. *J. Energy Storage*, *24* (2019) 100770.
41. Y.V. Tolmachev, A. Piatkivskyi, V.V. Ryzhov, D.V. Konev, M.A. Vorotyntsev, Energy cycle based on a high specific energy aqueous flow battery and its potential use for fully electric vehicles and for direct solar-to-chemical energy conversion. *J. Solid State Electrochem.*, *19* (2015) 2711–2722.
42. J.P. Katsoudas, E.V. Timofeeva, C.U. Segre, D. Singh, Integration of flow batteries into electric vehicles: Feasibility and the future. *NTSINanotech*, *3* (2014) 435–438.
43. Y. Wang, P. He, H. Zhou, Li-redox flow batteries based on hybrid electrolytes: At the cross road between Li-ion and redox flow batteries. *Adv. Energy Mater.*, *2*(7) (2012) 770–779.
44. E. Ventosa, O. Amedu, W. Schuhmann, Aqueous mixed-cation semi-solid hybrid-flow batteries. *ACS Appl. Energy Mater.*, *1*(10) (2018) 5158–5162.
45. A. Khor, P. Leung, M.R. Mohamed, C. Flox, Q. Xu, L. An, R.G.A. Wills, J.R. Morante, A.A. Shah, Review of zinc-based hybrid flow batteries: From fundamentals to applications. *Mater. Today Energy*, *8* (2018) 80–108.
46. C. Schubert, W.F. Hassen, B. Poisl, S. Seitz, J. Schubert, E. Oyarbide Usabiaga, P.M. Gaudo, K.H. Pettinger, Hybrid energy storage systems based on redox-flow batteries: Recent developments, challenges, and future perspectives. *Batteries*, *9*(4) (2023) 211.
47. J. Campillo, N. Ghaviha, N. Zimmerman, E. Dahlquist,. Flow batteries use potential in heavy vehicles. In *2015 International Conference on Electrical Systems for Aircraft, Railway, Ship Propulsion and Road Vehicles (ESARS)* (pp. 1–6), 2015, March. IEEE.

CHAPTER 21

Challenges and Limitations

Navid Nasajpour-Esfahani, Marissa Bailey Reichelscheimer, Hamid Garmestani, and Steven Y. Liang

21.1 INTRODUCTION

Energy storage is becoming increasingly important as the reliance on electric vehicles and sustainable power sources increases. The current leading form of energy storage is in the form of lithium-ion batteries [1]. Other energy storage options are harder to produce and implement on a wide scale, increasing the cost of energy storage to anywhere from three to ten times that of the national United States Department of Energy goal (5 cents per kilowatt-hour stored) [2,3]. The goal of modern energy storage methods is to store large amounts of energy (on the terawatt-hour scale) for long periods of time (around 12 hours to solve energy storage needs within the United States). The goal of energy storage manufacturers is to have a perfectly efficient battery, or one that has perfect (100%) renewable energy utilization. While renewable energy is becoming increasingly popular due to its sustainable nature, it is highly intermittent. For example, solar energy is only harvested in sunny conditions; when the day ends, no solar energy will be provided. Similar properties can be applied to wind turbine energy sources as well. Thus, developing viable energy storage techniques is also crucial to improving the viability of renewable energy sources by storing energy in times when energy can be harvested by the renewable source and providing constant energy during times when the source is not available [3,4]. An optimal energy storage device should store 5.5 terawatt-hours of energy for a period of 12 hours to meet 80% or more of the energy demand within the United States, given that the energy source used is either solar or wind. One of the main areas for improvement lies in the charging and discharging of electric vehicles. Furthermore, the overall cost of energy storage devices should be decreased, and cycle stability should be increased to improve the viability of energy storage devices. Currently, lithium-ion batteries are being developed and improved to establish these goals [4]. Lithium-ion batteries are commonly used in energy storage applications due to their high efficiency. Despite their optimal performance, lithium-ion batteries are detrimental, as they can pose a safety concern under heat; this is due to a

DOI: 10.1201/9781003506379-21

combustion reaction of the oxygen from the metal oxide compounds [5]. Even with the addition of preventive measures to lithium-ion batteries, these energy storage means still pose a significant risk. Thus, aqueous solutions of electrolytes have been proposed as a safer alternative to energy storage components. In particular, a system of zinc and bromine is proposed to act within a battery device [6]. Electrochemical reactions at each electrode are separated by a membrane, and ions are moved throughout the entire cell to control reactant and product concentrations. In a battery system, this could be seen when zinc reduces and coats an electrode as it is charged. As the battery discharges, the zinc is oxidized and re-enters the solution as an ion. While this process can lead to efficient battery charging and discharging, there is a capability of zinc dendrite to form; zinc dendrite can result in broken batteries by ripping the membrane separating the electrodes and creating short circuits that inhibit battery function. An alternative method for producing electrolytic batteries is proposed in the introduction of flowless battery systems [7]. In a flowless battery there is no membrane or pumping system. Energy is stored when zinc metal is formed at the negative electrode of the battery. This should reduce the cost of storing energy to less than half of traditional energy storage methods. Thus, a flowless battery could come closer to meeting the United States Department of Energy's goal of storing energy at a lower cost. Flowless Zn-Br battery systems experience problems such as the mixing of charged materials that are able to be dissolved, removal of metal, and degradation of electrolytic materials. While these issues can be resolved in certain ways, solving one problem often opens the door to another. To give an example, making the battery system simpler by making it flowless can increase the prevalence of charged materials crossing over and self-discharging. To combat this, there are two proposals. The first involves removing the membrane and introducing a thicker electrolyte phase on one end; this is more economical, but it produces lower energy storage capabilities. The other involves applying a thin membrane and complexation agents; this yields the opposite result as the former [8]. Another significant issue that lithium-ion batteries face is that they are unable to perform optimally in reduced-temperature environments; specifically, they experience a loss of power, loss of ability to charge, loss of stability, and hazardous conditions. One of the ways that this issue can be mediated while continuing to implement lithium-ion batteries is by raising the inherent reactivity of the battery through altering the organization of the cell (by adding electrolytes, altering the boundary between anode and cathode, and altering the materials that participate in the reaction) to promote a more optimal temperature for the external reaction to occur. Charging and discharging of batteries requires lithium ions to transfer as a liquid, dissolve into the reaction, move along with solid electrolytes at the interfacial area, and diffuse as a solid [9]. At conditions of reduced temperatures, the lithium reactions occur at a slower pace. The kinetics of the reaction should be altered by changing the thickness of the electrolyte applied, altering the solvation abilities of the material, and choosing specific materials to act as electrodes [10]; this would shift the factor of low-temperature performance to rely on the diffusion of liquid lithium ions or solid lithium ions [11]. One of the reasons that the low temperature of the environment can hinder battery performance is that the greatest effect occurs by reducing the phase window of liquid electrolytes; thus, a drop in temperature could cause solidification of lithium or precipitation of

lithium-based salts, as well as a rise in the viscosity of the electrolytic solution. This overall process has the effect of reducing the conduction of liquid ions and drops the ability of electrodes to wet within the battery [12]. In addition, cooler temperatures hinder the charging process within the lithium-ion batteries. A study suggests that a drop in temperature results in slower charging than discharging for the anode component, posing a threat to the performance and longevity of energy within the battery. This is due to the fact that solid lithium will easily coat the graphite anode when the external temperature is cool enough. One of the major safety concerns of lithium-ion batteries comes from the fact that lithium can often deposit on the graphite components within the battery if the temperature is low enough or current is less homogenous. This can result in the breakdown of the battery by causing a short circuit that passes current directly through without much resistance, raising temperatures to the point where the battery explodes [13]. Thus, the safety of the battery should be prioritized by implementing controls to prevent the temperature within the battery from deviating too much from the working value. This problem has been resolved by implementing heat sources within and outside of the battery. Heat sources applied are in the forms of materials of liquid or gaseous phases, as well as materials with variable phases (phase change materials) [14]. These materials are exposed to convection heating techniques. However, adding heat to the battery can result in overheating of the battery, which hinders performance. Internal heating methods are highly attractive, as they are able to work under optimal performance and heat relatively uniformly when compared with external heat applications. Batteries can be heated by passing current through (either direct current or alternating current) and by applying pulses of energy. Direct current is the most optimal of these internal heating methods when considering speed, as it can heat the quickest of the three; however, adding a direct current to the battery is known to degrade the battery and reduce its working life [15].

21.2 COST

Flow batteries containing aqueous compounds that can undergo redox reactions are gaining traction as safe and effective batteries. The cost of the materials required to produce these batteries is analyzed, as the economic feasibility of this battery form is crucial to indicate its ability to be used in widespread applications. The cost of manufacturing and the price the battery would retail for are crucial components to determine if this is a viable long-term solution to energy storage needs. Of the materials used, the electrolytes and water are of negligible cost compared to battery materials; thus, these costs can be disregarded, as they do not have a significant impact on the economic viability of flow batteries. The material whose cost is to be analyzed is the active material within the battery. The United States Department of Energy has set a goal of reducing the cost of energy storage devices to be less than $150 per kilowatt-hour of energy stored and increasing the capacity of the battery to be over 4 hours for discharge. In order to meet this goal, it has been determined that the active material within the battery should be purchased at a cost of $5 or less per kilogram of material. This would mean that theoretically, energy could be stored for $25 per kilowatt-hour (or less). However, accounting for usable energy discharged means that this value should be $37 per kilowatt-hour of energy stored [16]. Of the

material groups analyzed, quinones are a type that would function in these flow batteries; within the group of quinones, 2,6-anthraquinone disulfonic acid is one that is relatively simplistic. Fortunately, 2,6-anthraquinone disulfonic acid is also projected to meet the cost standard set by the United States Department of Energy. Despite these economic promises, however, 2,6-anthraquinone disulfonic acid may not function as optimally within the redox flow battery as other materials [17]. Thus, less simplistic quinones are proposed to act within redox flow batteries, providing stability, cost-effectiveness, and high energy storage density [18]. Ferrocyanide is another material commonly proposed as a reactant within redox flow batteries and thus, should be cost-analyzed [19]. The price of a material used is typically provided in dollars per kilogram of material. The cost of manufacturing includes the cost of the raw materials, the cost to treat waste from processing, the cost of operating manufacturing plants, and the depreciation of value for the manufacturing center. The price is defined as the price that the material would be sold for produce a redox flow battery or the price at which the final redox flow battery would be sold. On the other hand, the cost is defined as the price that the material manufacturer pays to produce said product. The sales price is the total profit that a materials manufacturer makes and the expenses required to sell the product. The least expensive materials analyzed were 2,6-anthraquinone disulfonic acid or sodium ferrocyanide posolyte. These are considered relatively inexpensive due to their low cost to obtain and high yield when processed. However, even for these materials, the United States Department of Energy's cost goal is still exceeded by about two times (to 50 dollars per kilowatt-hour of energy stored). Other materials that have been analyzed have energy storage costs that exceed those of the aforementioned materials. In order to improve the costs associated with producing redox flow batteries, several steps can be taken. For one, couples should be produced with the goal of having a high potential. Otherwise, active materials that are capable of undergoing redox reactions could be developed to have a low equivalent weight. Alternatively, if current materials are unchanged, the processing required in each step should be made as efficient as possible to reduce overall costs. Lastly, organic solvent usage should be reduced as much as possible, as these comprise a significant portion of overall manufacturing costs. One specific proposal offered is to use negolytes or posolytes that are independent of the solution. One example of a solvent that has been examined for this purpose is propylene carbonate [8].

21.3 DESIGN

An aqueous flow battery includes similar features to proton exchange membrane-based cells. Each individual proton exchange membrane-based cell can balance the charge within itself by moving protons throughout. Non-acidic cells do not contain protons as a primary ion, but they do contain cations of electrolyte in solution; thus, for these cells, the cation is exchanged throughout to balance the overall charge of the battery. One of the main issues associated with cation transport batteries is that resistance can be promoted through inefficiently transporting cations. If resistance increases, more energy is required to charge the battery. Therefore, the battery would discharge with less power than a more optimized cell. In addition to facing more resistance, these batteries could also undergo undesired reactions that break down the cell further [20]. A common cation exchange membrane that is

used in acidic batteries is a type of perfluorinated sulfonic acid material known as Nafion™ 212. This type of membrane utilizes differences in hydrophilicity to cause phase separation within, providing structure (from materials like polytetrafluoroethylene) to the hydrophilic regions that are able to absorb water and grow. Within the swollen hydrophilic regions, solutions containing cations are able to flow, moving efficiently through the cell [21]. Therefore, more hydrophilic materials are preferred, as they can absorb more water to facilitate ion transport. A greater hydration of cations also isolates cations from other anions within the solutions, further facilitating efficient transport [22]. Several hydrates are used within this study; specifically, potassium hexacyanoferrate (II) trihydrate ($K_4Fe(CN)_6 \cdot 3H_2O$), chromium (III) chloride hexahydrate ($CrCl_3 \cdot 6H_2O$), cobalt (II) acetate tetrahydrate ($Co(CH_3COO)_2 \cdot 4H_2O$), and lithium hydroxide monohydrate ($LiOH \cdot H_2O$) are used. Additionally, compounds including NaOH, KOH, Rb_2CO_3, Cs_2CO_3, choline chloride, choline bitartrate, 1-ethyl-3-methylimidazolium chloride, 1-ethyl-1-methylpyrrolidinium, and CsCl are used. Solutions of 1,3-ethylenediaminetetraacetic acid, 6 normal ammonia, 40% methyl ammonia solution, 40% dimethyl ammonia solution, 45% trimethyl ammonia solution, and a quarter tetramethylammonium solution are used. $[CrPDTA]^{-1}$ is produced by following standard techniques established in a previous study [23]. The 21.3 g of chromium (III) chloride hexahydrate (which translates to 0.080 mol of compound) are dissolved in 30 mL of DI water, along with 24.502 g of H_4PDTA (which translates to an equal molar amount of 0.080 mol). The solution is heated for 16 hours, and then 10 g of potassium hydroxide in its solid phase (0.018 mol) is added in amounts of half a gram every 15 seconds. The solution stays at an elevated temperature for 24 hours total and is then reduced to 80°C. One milliliter of 5 molar potassium hydroxide solution is added at a time to the resulting mixture until the pH has reached a value of 5. Then, the solution is heated at reflux for a total of 16 hours. The pH of the final solution should be between four and five, and the temperature of the final mixture should be reduced to room temperature before the mixture is passed through a filter. The products of the mixture can be cleaned by adding ethanol at a temperature of 25°C. The final product is displayed in the form of red-colored crystals, which are combined with a small amount of DI water (just enough to produce a solution that is saturated). The final solution is named $X^+[Cr(1,3\text{-}PDTA)]^{-1}$ and remains at room temperature during the night to then be characterized with a UV-Vis technique. This process is repeated for compounds lithium hydroxide, sodium hydroxide, Rb_2CO_3, Cs_2CO_3, ammonium hydroxide, $(CH_3)NH_3OH$, $(CH_3)_2NH_2OH$, and $(CH_3)_3NHOH$ to replace the cation in the compound containing $[Cr(1,3\text{-}PDTA)]^{-1}$ with the respective cation of each of the aforementioned compounds. For the salt containing choline, a chilled solution of choline bitartrate is combined with chilled KCrPDTA to leave choline CrPDTA in solution form as potassium bitartrate is precipitated out [24]. To produce $NaCoPDTA \cdot 3H_2O$, a different procedure is utilized. A solution of 4.98 g or 0.020 mol of $Co(OAc)_2 \cdot 4H_2O$ and 136.08 g or 0.120 mol of NaOAc is made in 100 mL of DI water. Then, 2 grams of activated charcoal and 4 mL of a 30% solution of hydrogen peroxide are put into the solution. After being bubbled for 2 days with regular air, filtered, condensed in oil, and left at a temperature of 0°C during the night, purple-colored crystals of the product are obtained. These crystals are rinsed with both ethanol and diethyl ether and recrystallized

as ethanol is added at 0°C. This procedure can be repeated with various cations replacing the Na^+ with the anion of $[Co(1,3\text{-}PDTA)]^{-1}$ by using different compounds containing the relevant cation [25]. Compounds with an anion of $[FePDTA]^{-1}$ can be produced using pre-existing methodology. To give an example of producing LiFePDTA, 2.78 g or 0.010 mol of $FeSO_4{\cdot}7H_2O$ is added to 20 mL of deionized water and bubbled for half an hour. Separately, 3.06 g or 0.010 mol of H_4PDTA is combined with 0.719 g or 0.030 mol of lithium hydroxide in a small amount of heated water. These two solutions are combined in the beaker containing the bubbled $FeSO_4{\cdot}7H_2O$ and stirred vigorously to combine. The resulting mixture is heated for at least 16 hours at a temperature of 95°C and then cooled and evaporated to produce a concentrated 10 mL solution. The solution is left at room temperature to evaporate the liquid and precipitate crystals of the product, which are then removed by a vacuum filtration technique and rinsed with chilled water. Adding a small amount of hot water to these crystals allows them to recrystallize and produce a saturated LiFePDTA solution, which is cooled to room temperature and 0°C to form crystals. This procedure can be repeated to replace the lithium cation with a desired cation by varying the compound included [26]. Another procedure is used to produce compounds containing $(X^+)_4Fe(CN)_6$, where X^+ is one of the following substances: lithium ion, ammonium ion, $MeNH_3^+$, $Me_2NH_2^+$, Me_3NH^+, or Me_4N^+. Hydroxides containing ion X^+ are added in excess of 50% to a column, which is then mixed with water until a pH considered neutral is obtained. For compounds containing Rb^+ or Cs^+ as the element X^+, carbonate salt is also added in excess. After water is added, saturated $K_4Fe(CN)_6$ is added. More water is added to follow. Reducing the pressure of the solution and heating the temperature to 50°C, as well as using a rotary evaporator device, allows the product to become dehydrated. The resulting product is also kept in vacuum conditions during the night to further ensure the removal of excess water. For ferrocyanides containing NH_4^+ or alkyl ammonium, the water added to the compound should be purged with nitrogen gas to remove any dissolved oxygen within the water. After measuring the solubilities of resulting compounds, there is no distinct pattern that can be determined; the measured solubilities vary significantly for salts of varying cations. Thus, more research should be done to examine electrolytes based on regular cell shapes. Additionally, it can be determined that a material such as Nafion™ 212 has properties that vary significantly depending on which cation is used to produce the material; specifically, the resistance within the material is found to increase as the cation added increases in ionic radius size. These properties can be expanded to determine broader overall battery characteristics when these materials are used. When designing a redox flow battery that is efficient, has a high energy storage, and can be used for long periods of time, it is necessary to consider the solubility of the cation within the compounds included in the material, the resistance of the membrane included in the battery, and the compatibility of materials when combined [27]. Redox flow batteries are attractive in that they can be scaled to store large amounts of energy, be designed variably for different applications, and remain decoupled to promote efficiency. Despite their potential in energy storage uses, redox flow battery usage is inhibited by the fact that they utilize materials that can undergo redox reactions, which are often hard to obtain and expensive. Thus, there is a push to design alternative materials to be used in redox flow batteries to mitigate this

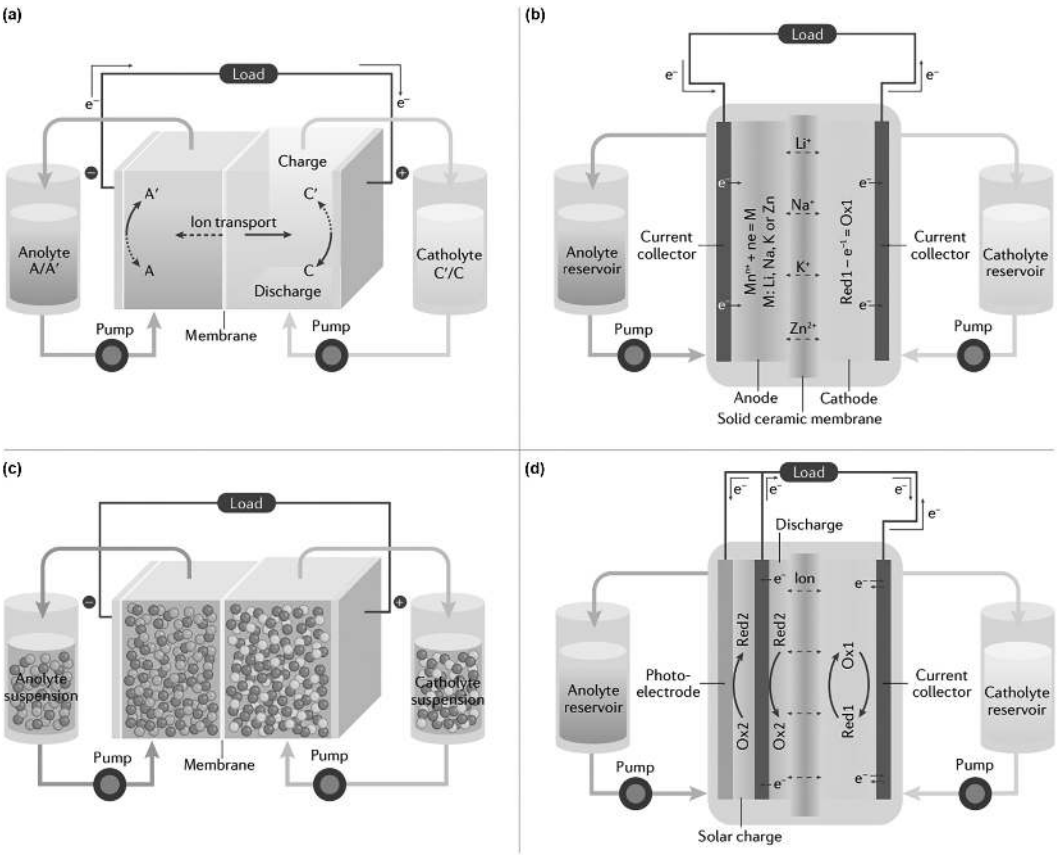

FIGURE 21.1 Various redox flow battery designs. (Adapted with permission from [29], Copyright (2022), Nature)

problem [28]. Figure 21.1 displays various redox flow battery designs that can be implemented. Figure 21.1a is a traditional redox flow battery, where electrolytes in solution undergo redox reactions to transport charge throughout the battery. Reduction and oxidation occur upon discharge of the battery at the catholyte and anolyte, respectively. The membrane between the catholyte and anolyte permits the movement of substances capable of neutralizing charge buildup. Figure 21.1b highlights a battery that incorporates hybrid techniques to increase the capacity of the battery while reducing the redox potential of the reactions occurring. These reactions occurring at the cathode within the battery are similar to those of a traditional redox flow battery in principle. On the anode side, metal is stripped or deposited reversibly. Figure 21.1c displays a semi-solid flow battery that has solid powder and conductive particles in a suspension of electrolytic material to allow for flow without having to incorporate a limit to the amount of material dissolved. Despite these benefits, a semi-solid flow battery is prone to slowing down the rate of reaction by interfering with the flow of fluid and thus reducing the efficiency of the resulting battery. A solar redox flow battery is shown in Figure 21.1d, which uses solar harvesting materials to provide energy to charge the battery. This type of battery uses a photoelectrode to take in

energy from sources of sunlight and uses this energy to allow for redox reactions to occur. Solar redox flow batteries are useful in that they are more affordable and efficient batteries that can cool environments by absorbing heat. The main difficulty scientists developing these battery types face is that there is often degradation that can happen at the photoelectrode, which can reduce the functionality of the battery [29].

Aqueous redox flow batteries are an economical energy storage system. The components are derived from inexpensive materials and are not intensive to manufacture, and these batteries do not require much surveillance when in operation. The electrolytic materials and water required for redox flow batteries are much less expensive than components that are typically used to produce lithium-ion batteries. However, electrolytic solutions could be combined with cosolvents, increasing their price in redox flow battery applications. Additionally, some aqueous redox flow batteries do require some specific manufacturing conditions (such as low fluctuation in oxygen and low moisture content). Another issue that should be considered is the ability of aqueous batteries to explode upon experiencing issues while performing. Some traditional aqueous batteries do not experience this concern, as they can undergo reactions that allow for some degree of overcharging [30]. Aqueous batteries can conduct electrons more efficiently than other types of batteries due to the fact that they are not incredibly viscous and allow ions to fully separate from one another. This increased conductivity allows the battery to charge and discharge at a quicker rate, efficiently act at lower temperatures, and work with larger electrodes instead of those on a micron scale [31]. Lithium-ion batteries are more beneficial than aqueous redox flow batteries regarding their electrochemical stability; aqueous batteries are only stable within a narrow range, as they may oxidize or reduce to form oxygen or hydrogen, respectively, outside of this range. Additionally, using water in a battery may result in the degradation of components that are intended to remain intact. This limits the ability of researchers to choose components that will not dissolve in water [32]. To combat this issue, one component that can be added to a battery to prevent the unwanted degradation of specific components is a semi-permeable selective membrane. These membranes act as selective gates, permitting the flow of certain components while preventing others from being subjected to degradation by harsh conditions. However, implementing these membranes is known to increase the cost of producing a battery. To give an example, applying a Nafion layer to a vanadium flow battery has been determined to constitute 27%–44% of the entire cost of the battery [33]. The type of electrode implemented into a redox flow battery should be established based on the reaction that occurs within that electrode. This would prevent researchers from analyzing two of the same reactions that have been applied to different electrodes. Insertion reactions include an intercalation reaction, which requires a host material that can undergo redox reactions to allow for the release of ions. This reversible process is described in Figure 21.2a. Figure 21.2b highlights a conversion reaction, which requires the electrode to destruct and re-establish itself as a different structured material during charging and discharging. This type of reaction allows for the use of simplistic materials such as electrodes, as they do not have to remain intact during charging and discharging. Figure 21.2c displays a deposition reaction, also known as a plating reaction, when the electrode is a metallic element. In one part, there are only ions

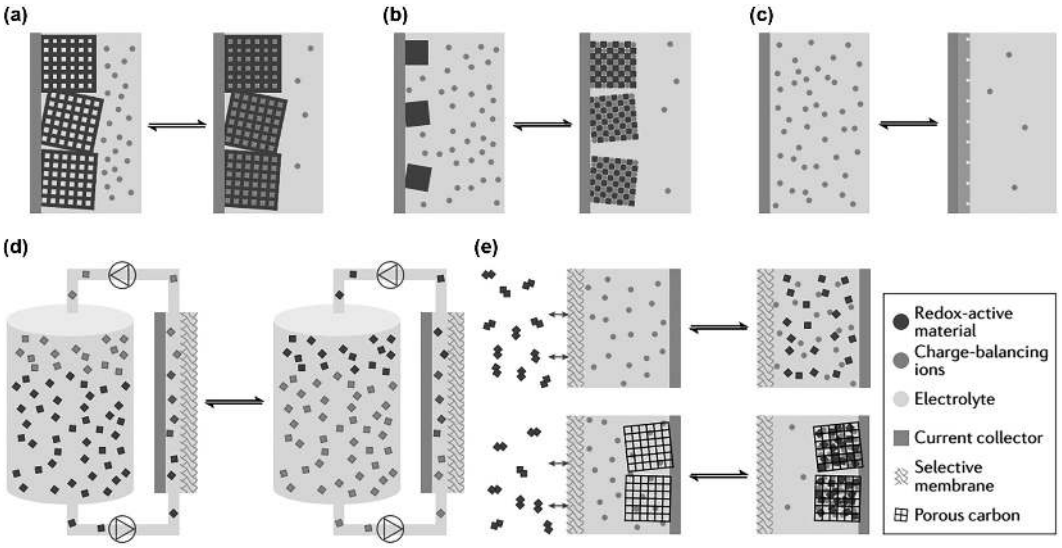

FIGURE 21.2 Different electrode chemistries in aqueous batteries. (Adapted with permission from [30], Copyright (2022), Nature)

of the active material present. On the other side, the active material has been deposited to form a solid structure. This process is common for the reaction of zinc ion and solid, lead oxide and lead ion, and manganese oxide and manganese ion. Flow reactions are shown in Figure 21.2d. This type of reaction occurs within a redox flow battery and allows for the flow of any material of fixed charge. A storage tank is used to provide free charge, further decoupling the energy within the battery. An air reaction is highlighted in Figure 21.2e. This allows for the free flow of gaseous active materials. Thus, no storage component is necessary, and it is assumed that the component has an unlimited energy density available. The limit of this type of reaction lies in the ability of gaseous components to flow and deposit themselves [30].

21.4 MACHINE LEARNING

Organic flow batteries are composed of organic redox-active species such as C, H, O, N, and S. These elements are readily available, making them potentially inexpensive materials to form batteries. Certain characteristics, such as potential and reaction rate, can also be altered through molecular modification of the aforementioned elements. To streamline the development process of new materials, simulators and computers are able to assist by organizing and analyzing data; while computational models provide high potential to assist in materials science research, these are limited in their inability to quickly perform complicated calculations [34]. Thankfully, machine learning and artificial intelligence have emerged in recent years, providing streamlined ways to determine relationships between and among data entries. Machine learning techniques have been proposed to assist with the development of flow batteries, particularly being applied in the production of organic flow batteries and vanadium flow batteries [35]. To begin, data is placed into a set to be analyzed using machine learning programs. Then, the major features of the data set are established

using mathematical analyses and used to define the data. These filtered data sets are then randomly split into two categories: data to be trained and data to be tested. For the training set, the data is subjected to a machine learning-developed model that fits the features of the data to a function. This model can be tested in its accuracy by comparing it with the test data. If the model is accurate, it is used to predict characteristics of data points that are not yet established. Databases used to advance machine learning technologies are established through large-scale sample experiments or calculations, pre-existing studies, and open databases consisting of material properties [36]. Of the algorithms employed within machine learning technologies, the main ones are Bayesian methods, decision tree analysis, support vector machine, random decision forest analysis, and cluster techniques. To describe several of these techniques, support vector machines classify data and use regression to determine a hyperplane that can distinguish between data. Decision tree models pass data through different tests that sort each piece. Machine learning technologies are more accurate when more data comprises each set; thus, growing the amount of data in the dataset over time improves the quality of the results obtained with these methods. Within the development of efficient flow batteries, machine learning technology has been used to determine the optimal design of a flow battery by taking into consideration factors such as electrolyte solubility, potential of active components, and stability of substances. The most optimal organic redox-active species used in a flow battery would be very soluble, have a rational potential to undergo a redox reaction, and be highly stable. Typically, this type of material would be determined through experimental trial-and-error methods or computations. However, those processes can be costly in time and money. Thus, machine learning provides an efficient shortcut to determining optimal materials for flow battery applications based on specific properties. Machine learning models are also applicable in flow battery development, as they can be used to determine optimal operating conditions for batteries, such as temperature and current passing through the battery. This would help optimize the life of the battery and improve its efficiency. While providing high potential in materials science applications, among many others, machine learning is still a relatively new development. Thus, more work should be done to further improve its accuracy. One of the ways that this can be improved is by fostering collaboration among those in possession of data sets and individual algorithms. Combining data sets or increasing access to data allows the machine learning algorithm to have more references to base off and provide a more accurate result [37].

21.5 MODELING AND SIMULATION

Vanadium redox flow batteries have emerged as useful redox flow batteries due to the fact that they can easily regenerate energy from vanadium ions that are present throughout the battery; this reduces the negative impact from cross-contamination of components and degradation of energy capacity that the battery can store [38]. Most notably, these models can be used to control and monitor battery systems, design batteries, and estimate loss of capacity to optimize vanadium-based redox flow batteries. Of the models tested, only those of the zero dimension have been tested for industrial wide-scale applications [39]. The ability of the models examined throughout the study to accurately

describe the functionality of a vanadium redox flow battery is determined by comparing results to those obtained by experimental means. A 10-cell vanadium redox flow battery stack with an active area of 20 cm^2 for each cell in the stack is analyzed to obtain experimental data. Each tank contained a total of 0.400 L of a 1.6 M concentrated vanadium solution. The "8×8" model includes four forms of vanadium ion ranging from V^{2+} to V^{5+}. There are thus eight totally different concentrations of ions divided between the cell and the tanks. The "2×2" model describes an idealized version of the battery where there is one concentration of ions split evenly between the cell and the tank. The "1×1" model is also known as the Coulomb counter method. This involves the amount of charge at any specified time based on an integral of the current passing through the battery. While this is the most simplistic method of analyzing a vanadium redox flow battery, it does not reveal any information regarding the loss of state of charge as crossover occurs within the battery [40]. The effectiveness of a redox flow battery in sustainable energy storage applications is highly dependent on the characteristics of the porous electrode contained within it. A porous electrode is made of various microparticles composed of carbon, felt, or other material with an active surface. The goal of the porous electrode is to efficiently undergo redox reactions. While a greater porosity is ideal in that it can facilitate reaction through liquid and mass transfer capabilities to allow reactants to efficiently transfer throughout the cell, increasing the amount of pore space within the electrode will reduce the effective surface area and thus reduce the conductance of the electrode. Current production techniques to create porous electrodes for use within redox flow batteries employ methods such as aerogel production through direct ink writing; this has been used to produce porous electrodes that are composed of carbon and graphene and can act within supercapacitive applications [41]. Computer-aided simulators are useful in materials science applications, as they are able to assist with designing efficient flow batteries and define parameters for use. This study uses computer-based models to effectively decide what the most-efficient distribution of the cell porosities is, analyze the ability of the battery to perform, and find ways to improve upon performance. This computer model should be able to assist with future flow battery applications by expanding upon their use and effectiveness. After using computer simulators to redesign porous electrodes for flow battery applications, it can be determined that the efficiency of the computer-aided design increased by 13.5%–310%. This is due to the fact that the computer model is able to identify sources of energy loss and assist with the process of reducing their impact. For example, adding more channels with a low hydraulic resistance can help to increase the ability of liquid to flow through the battery and thus increase its efficiency. Another way the battery is modified after undergoing computational analysis is by the addition of a system of distributed liquids that can improve upon these fluid paths even more. Through the analysis of reaction kinetics and electrolytic concentration, these conclusions can be observed. The computational model is also used to design a larger electrode with greater efficiency, which is 40.3% more efficient than the current most-efficient electrode. Thus, computational models are incredibly useful in determining the features of redox flow batteries to further optimize their performance and allow them to be used in more applications [42].

21.6 ORGANIC SPECIES

The ability of a redox flow battery to perform efficiently is due to many factors, one being the electrolyte in solution that undergoes reactions. For organic redox flow batteries, the solubility of organic components can be increased as more chains with soluble groups are added. Additionally, the potential of the organic species is important to determine the properties of the battery constructed. The potential of an organic substance is defined by molecular orbital theory: the energy associated with the highest occupied molecular orbital and lowest unoccupied molecular orbital defines the capability of the species to oxidize or reduce, respectively [43]. The redox potential of the organic species can even be altered by adding groups that are capable of donating or pulling excess electrons. The redox flow battery can also be made more stable by a specific choice of organic species; one of the ways an organic component is made more stable is by altering functional groups of the substance. Anthraquinone, ferrocene, alloxazine, phenazine, phenothiazine, fluorenone, 2,2,6,6-tetramethylpiperidin-1-yl oxyl, and 2-phenyl-4,4,5,5-tetramethylimidazoline-1-oxyl-3-oxide are some examples of the organic species applied to redox flow batteries throughout the study. The stability, cost, solubility, and potential of various components are analyzed and compared in Figure 21.3 [44].

While organic species provide great potential to improve the availability and sustainability of redox flow batteries, they are not as soluble or energy-rich as vanadium in these applications. For example, in sulfuric acid, vanadium is soluble up to concentrations of 2.5 M. In this same solvent, organic species are only soluble up to concentrations of 1.5 M. Compared with the ferrocene organic redox species, anthraquinone has a higher energy density of over 25 Wh per liter, a decent capacity, and a lower voltage potential. Of the organic redox species analyzed, phenazine, fluorenone, and alloxazine do not have optimal operation. However, alloxazine and phenazine can be enhanced to yield energy densities of 20 watt-hours per liter. Within the realm of non-aqueous organic redox flow batteries, the lithium 2,2,6,6-tetramethylpiperidin-1-yl oxyl redox flow battery yields the highest energy density and voltage values of 126 Wh per liter and 3.5 V, respectively. These batteries can also be improved to become even more efficient and stable through the operation of cycles. Non-aqueous organic redox flow batteries can also prevent cross-contamination of various components within the cell to improve operation. However, these organic components

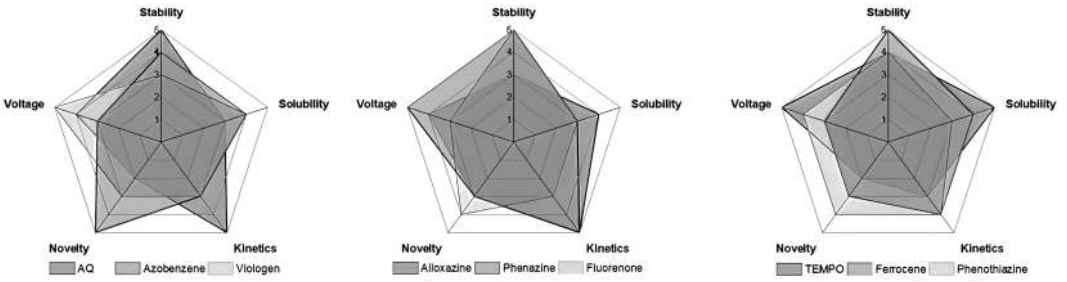

FIGURE 21.3 Characteristics of various types of molecules. (Adapted with permission from [44], Copyright (2022), Elsevier)

require low current densities to operate effectively. Many of the components examined can only function at current densities less than or equal to 20 mA per square centimeter. Aside from these drawbacks, the improvement of organic redox species has drastically improved the potential to enhance redox flow batteries. In the future, the price of these batteries is expected to drop as their efficiency increases, enabling them to be used in a greater variety of applications [44]. Bipolar redox-active molecules are substances derived from a single component that can be oxidized or reduced depending on whether a redox flow battery is charging or discharging. Thus, a symmetric redox flow battery composed of bipolar redox-active molecules has two identical half-cells. This allows for the elimination of a gradient, preventing any negative side reactions [45]. Additionally, crossover is almost entirely prevented; in the case of an accidental crossover, the battery would also self-discharge, rather than becoming contaminated and unusable [46]. A radical is capable of undergoing both oxidation and reduction, as they are singly occupied molecular orbitals. Radicals are also capable of decaying themselves, leading to their destruction before they are able to react to store energy. Thus, it is important to stabilize the radical before utilizing it as a component in the redox flow battery. One of the most commonly used neutral radicals is 2,2,6,6-tetramethylpiperidine-1-oxyl. Unaltered spin-paired molecules are rarely able to undergo oxidation or reduction. Thus, they should be functionalized with electron-accepting or -donating groups by covalent bonding or producing a eutectic mixture. 1,4-diaminoanthraquinone is a molecule consisting of both electron-donating species and electron-accepting species in the amine and quinone components, respectively. The molecule is able to both oxidize and reduce because of the existence of these two functional groups. Organic complexes can facilitate oxidation on a larger scale, as they have larger pi-bonding and electron-donating species. However, these molecules are hardly soluble in even organic solutes. Thus, a suspension of organic molecules in 5% Ketjen Black solvent by weight is produced for use in flow battery research, achieving a final solubility of 200 mg of solute per mL of solvent. However, utilizing a suspension instead of a solution did increase the viscosity of the mixture. In the future, organic redox flow batteries should be improved in solubility to over 1.0 M concentration, voltage output to 2–3 volts, and stability to 10,000 cycles. It can be challenging to measure the solubility of certain species, as adding electrolytes to the solution can reduce the solubility of the organic molecule in question. Additionally, the charge of the substance in solution impacts its solubility. Thus, the solubility of a species at its varying charge states is important to fully understand the solubility of the species [47].

21.7 CONCLUSION

The rapid growth of electric vehicles and renewable energy sources has made energy storage technologies increasingly important. Lithium-ion batteries, the current standard for energy storage, offer high energy density and efficiency but are not without drawbacks. Issues such as safety risks due to thermal runaway, high production costs, and limited performance in extreme temperatures necessitate the exploration of alternative storage technologies. Aqueous zinc-bromine batteries, flow batteries, and other emerging technologies show promise due to their potential for lower costs, enhanced safety, and scalability for large-scale energy

storage applications. Aqueous zinc-bromine batteries offer a safer alternative to lithium-ion batteries by reducing the risk of combustion, but they face challenges such as dendrite formation, which can lead to short circuits and reduced battery life. Flow batteries, particularly redox flow batteries, provide an opportunity for scalable and flexible energy storage. Their design allows for the decoupling of energy capacity and power, which makes them ideal for large-scale energy storage applications. However, they are often limited by the high cost and availability of materials that can undergo redox reactions. The integration of machine learning and advanced modeling techniques in the development of new battery materials and designs is a promising approach to overcoming these challenges. Machine learning can optimize the selection of materials and predict the performance of new battery chemistries, thereby accelerating the development of more efficient and cost-effective energy storage solutions. Additionally, computer simulations can help in designing more efficient battery architectures by identifying areas of energy loss and suggesting modifications to improve performance. Despite the potential of these emerging technologies, significant research and development are still needed to address their limitations and make them commercially viable. For instance, improving the stability and solubility of organic compounds in redox flow batteries could enhance their performance and reduce costs. Similarly, advancements in membrane technology could mitigate issues related to cross-contamination and improve the overall efficiency of flow batteries. Ultimately, achieving the United States Department of Energy's goal of reducing the cost of energy storage to below $150 per kilowatt-hour will require continued innovation in both materials and design. The focus should be on developing batteries that are not only efficient and safe but also economically feasible for widespread adoption. By addressing these challenges, we can create energy storage solutions that are capable of supporting a more sustainable and reliable energy future, enhancing the integration of renewable energy sources and reducing dependence on fossil fuels. In conclusion, while lithium-ion batteries remain the cornerstone of current energy storage systems, the exploration of alternative technologies such as aqueous zinc-bromine and redox flow batteries is crucial. These technologies, coupled with advancements in machine learning and materials science, could pave the way for the next generation of energy storage solutions. As we continue to innovate and refine these technologies, we move closer to a future where energy storage is safe, cost-effective, and capable of meeting the global demand for sustainable energy.

REFERENCES

1. G. Zubi, R. Dufo-López, M. Carvalho, and G. Pasaoglu, "The lithium-ion battery: State of the art and future perspectives," *Renew Sustain Energy Rev*, vol. 89, pp. 292–308, 2018, doi: 10.1016/j.rser.2018.03.002.
2. DOE, *Energy Storage Grand Challenge*. Department of Energy (https://energy-storage-grant-challenge/energy-storage-storage-grant-challenge).
3. T. M. Gür, "Review of electrical energy storage technologies, materials and systems: Challenges and prospects for large-scale grid storage," *Energy Environ Sci*, vol. 11, no. 10, pp. 2696–2767, 2018, doi: 10.1039/C8EE01419A.
4. Z. Yang et al., "Electrochemical energy storage for green grid," *Chem Rev*, vol. 111, no. 5, pp. 3577–3613, 2011, doi: 10.1021/cr100290v.
5. D. Ouyang, J. Weng, J. Liu, M. Chen, and J. Wang, "Influence of current rate on the degradation behavior of lithium-ion battery under overcharge condition," *J Electrochem Soc*, vol. 166, no. 12, pp. A2697–A2706, 2019, doi: 10.1149/2.1441912jes.

6. R. Kim et al., "Modulated Zn deposition by glass fiber interlayers for enhanced cycling stability of Zn–Br redox flow batteries," *ACS Sustain Chem Eng*, vol. 9, no. 36, pp. 12242–12251, 2021, doi: 10.1021/acssuschemeng.1c03796.
7. S. Biswas et al., "Minimal architecture zinc–bromine battery for low cost electrochemical energy storage," *Energy Environ Sci*, vol. 10, no. 1, pp. 114–120, 2017, doi: 10.1039/C6EE02782B.
8. K. Shin, J.-H. Lee, J. Heo, and H.-T. Kim, "Current status and challenges for practical flowless Zn–Br batteries," *Curr Opin Electrochem*, vol. 32, p. 100898, 2022, doi: 10.1016/j.coelec.2021.100898.
9. N. Piao et al., "Challenges and development of lithium-ion batteries for low temperature environments," *eTransportation*, vol. 11, p. 100145, 2022, doi: 10.1016/j.etran.2021.100145.
10. M. F. Hasan, C.-F. Chen, C. E. Shaffer, and P. P. Mukherjee, "Analysis of the implications of rapid charging on lithium-ion battery performance," *J Electrochem Soc*, vol. 162, no. 7, pp. A1382–A1395, 2015, doi: 10.1149/2.0871507jes.
11. Y. Xia et al., "Thickness-independent capacitance of vertically aligned liquid-crystalline MXenes," *Nature*, vol. 557, no. 7705, pp. 409–412, 2018, doi: 10.1038/s41586-018-0109-z.
12. J. Wang, Y. Yamada, K. Sodeyama, C. H. Chiang, Y. Tateyama, and A. Yamada, "Superconcentrated electrolytes for a high-voltage lithium-ion battery," *Nat Commun*, vol. 7, no. 1, p. 12032, 2016, doi: 10.1038/ncomms12032.
13. I. J. Fernández, C. F. Calvillo, A. Sánchez-Miralles, and J. Boal, "Capacity fade and aging models for electric batteries and optimal charging strategy for electric vehicles," *Energy*, vol. 60, pp. 35–43, 2013, doi: 10.1016/j.energy.2013.07.068.
14. S. Wu, R. Xiong, H. Li, V. Nian, and S. Ma, "The state of the art on preheating lithium-ion batteries in cold weather," *J Energy Storage*, vol. 27, p. 101059, 2020, doi: 10.1016/j.est.2019.101059.
15. X. Wu, Z. Cui, E. Chen, and J. Du, "Capacity degradation minimization oriented optimization for the pulse preheating of lithium-ion batteries under low temperature," *J Energy Storage*, vol. 31, p. 101746, 2020, doi: 10.1016/j.est.2020.101746.
16. R. M. Darling, K. G. Gallagher, J. A. Kowalski, S. Ha, and F. R. Brushett, "Pathways to low-cost electrochemical energy storage: A comparison of aqueous and nonaqueous flow batteries," *Energy Environ Sci*, vol. 7, no. 11, pp. 3459–3477, 2014, doi: 10.1039/C4EE02158D.
17. Q. Chen, L. Eisenach, and M. J. Aziz, "Cycling analysis of a quinone-bromide redox flow battery," *J Electrochem Soc*, vol. 163, no. 1, pp. A5057–A5063, 2016, doi: 10.1149/2.0081601jes.
18. D. G. Kwabi et al., "Alkaline quinone flow battery with long lifetime at pH 12," *Joule*, vol. 2, no. 9, pp. 1894–1906, 2018, doi: 10.1016/j.joule.2018.07.005.
19. X. Wei et al., "An aqueous redox flow battery based on neutral alkali metal ferri/ferrocyanide and polysulfide electrolytes," *J Electrochem Soc*, vol. 163, no. 1, pp. A5150–A5153, 2016, doi: 10.1149/2.0221601jes.
20. A. Trovò, W. Zamboni, and M. Guarnieri, "Multichannel electrochemical impedance spectroscopy and equivalent circuit synthesis of a large-scale vanadium redox flow battery," *J Power Sources*, vol. 493, p. 229703, 2021, doi: 10.1016/j.jpowsour.2021.229703.
21. A. Kusoglu and A. Z. Weber, "New insights into perfluorinated sulfonic-acid ionomers," *Chem Rev*, vol. 117, no. 3, pp. 987–1104, 2017, doi: 10.1021/acs.chemrev.6b00159.
22. M. A. Izquierdo-Gil, V. M. Barragán, J. P. G. Villaluenga, and M. P. Godino, "Water uptake and salt transport through Nafion cation-exchange membranes with different thicknesses," *Chem Eng Sci*, vol. 72, pp. 1–9, 2012, doi: 10.1016/j.ces.2011.12.040.
23. W. Cr, "Complexes of chromium (III), 3d 3," vol. 7, no. iii, pp. 114–116, 1968.
24. S. E. Waters, J. R. Thurston, R. W. Armstrong, B. H. Robb, M. P. Marshak, and D. Reber, "Holistic design principles for flow batteries: Cation dependent membrane resistance and active species solubility," *J Power Sources*, vol. 520, p. 230877, 2022, doi: 10.1016/j.jpowsour.2021.230877.
25. N. Tanaka and H. Ogino, "A cobalt (III) complex with trimethylenediaminetetraacetate," *Bull Chem Soc Jpn*, vol. 37, no. 6, pp. 877–879, 1964, doi: 10.1246/bcsj.37.877.

26. K. Kanamori, H. Dohniwa, N. Ukita, I. Kanesaka, and K. Kawai, "The Raman spectral study on the solution structure of iron(III)-edta complexes," *Bull Chem Soc Jpn*, vol. 63, no. 5, pp. 1447–1454, 1990, doi: 10.1246/bcsj.63.1447.
27. J. Luo et al., "Unprecedented capacity and stability of ammonium ferrocyanide catholyte in pH neutral aqueous redox flow batteries," *Joule*, vol. 3, no. 1, pp. 149–163, 2019, doi: 10.1016/j.joule.2018.10.010.
28. M. Park, J. Ryu, W. Wang, and J. Cho, "Material design and engineering of next-generation flow-battery technologies," *Nat Rev Mater*, vol. 2, no. 1, p. 16080, 2016, doi: 10.1038/natrevmats.2016.80.
29. L. Zhang, R. Feng, W. Wang, and G. Yu, "Emerging chemistries and molecular designs for flow batteries," *Nat Rev Chem*, vol. 6, no. 8, pp. 524–543, 2022, doi: 10.1038/s41570-022-00394-6.
30. Y. Liang and Y. Yao, "Designing modern aqueous batteries," *Nat Rev Mater*, vol. 8, no. 2, pp. 109–122, 2022, doi: 10.1038/s41578-022-00511-3.
31. F. Ai, Z. Wang, N.-C. Lai, Q. Zou, Z. Liang, and Y.-C. Lu, "Heteropoly acid negolytes for high-power-density aqueous redox flow batteries at low temperatures," *Nat Energy*, vol. 7, no. 5, pp. 417–426, 2022, doi: 10.1038/s41560-022-01011-y.
32. S. Gheytani, Y. Liang, Y. Jing, J. Q. Xu, and Y. Yao, "Chromate conversion coated aluminium as a light-weight and corrosion-resistant current collector for aqueous lithium-ion batteries," *J Mater Chem A Mater*, vol. 4, no. 2, pp. 395–399, 2016, doi: 10.1039/C5TA07366A.
33. V. Viswanathan et al., "Cost and performance model for redox flow batteries," *J Power Sources*, vol. 247, pp. 1040–1051, 2014, doi: 10.1016/j.jpowsour.2012.12.023.
34. L. Cheng et al., "Accelerating electrolyte discovery for energy storage with high-throughput screening," *J Phys Chem Lett*, vol. 6, no. 2, pp. 283–291, 2015, doi: 10.1021/jz502319n.
35. B. Sanchez-Lengeling and A. Aspuru-Guzik, "Inverse molecular design using machine learning: Generative models for matter engineering," *Science (1979)*, vol. 361, no. 6400, pp. 360–365, 2018, doi: 10.1126/science.aat2663.
36. K. A. Severson et al., "Data-driven prediction of battery cycle life before capacity degradation," *Nat Energy*, vol. 4, no. 5, pp. 383–391, 2019, doi: 10.1038/s41560-019-0356-8.
37. T. Li, C. Zhang, and X. Li, "Machine learning for flow batteries: Opportunities and challenges," *Chem Sci*, vol. 13, no. 17, pp. 4740–4752, 2022, doi: 10.1039/D2SC00291D.
38. O. C. Esan, X. Shi, Z. Pan, X. Huo, L. An, and T. S. Zhao, "Modeling and simulation of flow batteries," *Adv Energy Mater*, vol. 10, no. 31, 2020, doi: 10.1002/aenm.202000758.
39. T. Wang, J. Fu, M. Zheng, and Z. Yu, "Dynamic control strategy for the electrolyte flow rate of vanadium redox flow batteries," *Appl Energy*, vol. 227, pp. 613–623, 2018, doi: 10.1016/j.apenergy.2017.07.065.
40. S. Bogdanov et al., "Dynamic modeling of vanadium redox flow batteries: Practical approaches, their applications and limitations," *J Energy Storage*, vol. 57, p. 106191, 2023, doi: 10.1016/j.est.2022.106191.
41. C. Zhu et al., "Supercapacitors based on three-dimensional hierarchical graphene aerogels with periodic macropores," *Nano Lett*, vol. 16, no. 6, pp. 3448–3456, 2016, doi: 10.1021/acs.nanolett.5b04965.
42. V. A. Beck et al., "Computational design of microarchitected porous electrodes for redox flow batteries," *J Power Sources*, vol. 512, p. 230453, 2021, doi: 10.1016/j.jpowsour.2021.230453.
43. J. Luo, B. Hu, M. Hu, Y. Zhao, and T. L. Liu, "Status and prospects of organic redox flow batteries toward sustainable energy storage," *ACS Energy Lett*, vol. 4, no. 9, pp. 2220–2240, 2019, doi: 10.1021/acsenergylett.9b01332.
44. Z. Li, T. Jiang, M. Ali, C. Wu, and W. Chen, "Recent progress in organic species for redox flow batteries," *Energy Storage Mater*, vol. 50, pp. 105–138, 2022, doi: 10.1016/j.ensm.2022.04.038.
45. R. A. Potash, J. R. McKone, S. Conte, and H. D. Abruña, "On the benefits of a symmetric redox flow battery," *J Electrochem Soc*, vol. 163, no. 3, pp. A338–A344, 2016, doi: 10.1149/2.0971602jes.

46. K. Lourenssen, J. Williams, F. Ahmadpour, R. Clemmer, and S. Tasnim, "Vanadium redox flow batteries: A comprehensive review," *J Energy Storage*, vol. 25, p. 100844, 2019, doi: 10.1016/j.est.2019.100844.
47. M. Li, J. Case, and S. D. Minteer, "Bipolar redox-active molecules in non-aqueous organic redox flow batteries: Status and challenges," *ChemElectroChem*, vol. 8, no. 7, pp. 1215–1232, 2021, doi: 10.1002/celc.202001584.

Index